Terms and Conditions of Use of Digitised Theses from Trinity College Library Dublin

Copyright statement

All material supplied by Trinity College Library is protected by copyright (under the Copyright and Related Rights Act, 2000 as amended) and other relevant Intellectual Property Rights. By accessing and using a Digitised Thesis from Trinity College Library you acknowledge that all Intellectual Property Rights in any Works supplied are the sole and exclusive property of the copyright and/or other IPR holder. Specific copyright holders may not be explicitly identified. Use of materials from other sources within a thesis should not be construed as a claim over them.

A non-exclusive, non-transferable licence is hereby granted to those using or reproducing, in whole or in part, the material for valid purposes, providing the copyright owners are acknowledged using the normal conventions. Where specific permission to use material is required, this is identified and such permission must be sought from the copyright holder or agency cited.

Liability statement

By using a Digitised Thesis, I accept that Trinity College Dublin bears no legal responsibility for the accuracy, legality or comprehensiveness of materials contained within the thesis, and that Trinity College Dublin accepts no liability for indirect, consequential, or incidental, damages or losses arising from use of the thesis for whatever reason. Information located in a thesis may be subject to specific use constraints, details of which may not be explicitly described. It is the responsibility of potential and actual users to be aware of such constraints and to abide by them. By making use of material from a digitised thesis, you accept these copyright and disclaimer provisions. Where it is brought to the attention of Trinity College Library that there may be a breach of copyright or other restraint, it is the policy to withdraw or take down access to a thesis while the issue is being resolved.

Access Agreement

By using a Digitised Thesis from Trinity College Library you are bound by the following Terms & Conditions. Please read them carefully.

I have read and I understand the following statement: All material supplied via a Digitised Thesis from Trinity College Library is protected by copyright and other intellectual property rights, and duplication or sale of all or part of any of a thesis is not permitted, except that material may be duplicated by you for your research use or for educational purposes in electronic or print form providing the copyright owners are acknowledged using the normal conventions. You must obtain permission for any other use. Electronic or print copies may not be offered, whether for sale or otherwise to anyone. This copy has been supplied on the understanding that it is copyright material and that no quotation from the thesis may be published without proper acknowledgement.

Field tests on single piles subjected to lateral and combined axial and lateral loads

By

Declan T. P. Phillips

Doctor of Philosophy

Submitted to

University of Dublin, Trinity College.

2002

I declare that this thesis, in whole or in part, has not been submitted to any University as an exercise for a degree. I further declare that, except where reference is made in the text, the contents are entirely my own work. The author agrees that the library may lend or copy the thesis upon request for study purposes, subject to normal conditions of acknowledgement.

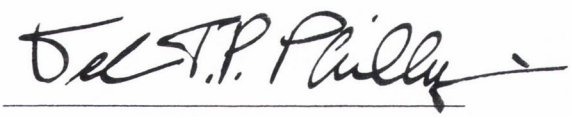

May 27, 2002

Declan T. P. Phillips

SUMMARY

This thesis describes the results of full-scale instrumented field studies on laterally loaded piles embedded in a layered soil. The research centred around tests on (i) 350mm square reinforced concrete piles driven through a surface layer of granular fill into a deep deposit of soft clay and (ii) 203mm wide steel H-piles driven into a stiff glacial till. The piles were subsequently subjected to a series of static loading tests. The thesis examines a number of topical items in regard to the design of laterally loaded piles; these include the influence of soil layering, pile head restraint, and pile width. The effects of soil ageing and the presence of an axial load on the lateral pile response are also examined. The latter has also been investigated via centrifuge tests on a pile embedded in a calcareous sand and subjected to lateral and combined loading.

The results of the field tests were used to derive *p-y* curves or non-linear 'soil springs' that characterise the soils at each test site. These results are compared with the *p-y* response derived from cone pressuremeter tests and cone penetration tests performed in the vicinity of the load tests at the soft clay site. The *p-y* response is also compared with the recommendations of the American Petroleum Institute (API).

The research illustrates the importance of accurate interpretation of instrumentation data particularly in the case of piles that experience a reduction in flexural rigidity as the pile bending moment develops under increasing lateral load. The results emphasise the need to determine the structural response of the pile from first principles rather than the design approach customarily used by structural engineers. The load tests revealed that the presence of an axial load had no significant effect on the soil's lateral response although axial load eccentricity should be given careful consideration. The degree of pile head restraint was also shown to have minimal effect on the lateral soil response. Although the *p-y* approach to lateral pile design has its limitations, these are shown to be second order effects - even in a strongly layered soil stratigraphy. Retesting the piles nineteen months after the initial tests revealed that soil ageing did not enhance lateral performance of the piles at the test site. The use of CPM and CPT in-situ testing techniques were shown to provide useful correlations with the measured pile response and with proper calibration, these techniques can be applied in the design of laterally loaded piles. From a practical standpoint, the benefit to be gained from the densification of a relatively shallow depth of the near surface soils may lead to considerable economies in the design of laterally loaded piles.

ACKNOWLEDGEMENTS

Since embarking on this research I have had to good fortune of meeting and working with some wonderful people. Firstly, I would like to extend a special thanks to my supervisor Dr. Barry Lehane for his technical advice and guidance and in particular his words of encouragement (when they were most needed!) over the duration of my work. It was a privilege to work with such a talented and enthusiastic engineer.

To the staff at Trinity College in particular the gifted George Jones and Gerard McGranaghan who assisted with the fabrication and load testing and Martin Carney in the soils laboratory. The assistance of Dave McAulay and Chris O'Donovan in the site investigation and project planning respectively is also acknowledged.

To the staff at Lowry Piling in particular Eddie Horkan and Michael Troughton, for giving their time and expertise to make this research possible. The financial contribution of John Barnett and Associates towards the purchase of instrumentation is gratefully acknowledged, as is the permission of the Waterworks Department of Belfast for the use of the site for research purposes.

To my employers, Waterford Institute of Technology, who provided financial assistance and accommodated my research over the years and in particular John Wall, Dr. Kieran Murphy, Dr. Séan Connor, Con Casey and Denis Moran.

To my friend Dr. Bryan McCabe who undertook parallel research at the Kinnegar test site and provided many of the more humorous moments over the years, not to mention his ability to make a good cup of tea!

Finally to my wife, Sarah and children Caoimhe, Cillian, Muireann and Áine who have made sacrifices and altered plans many times over the years, I am eternally grateful. It is now time to go on that long overdue family holiday! Special thanks also to our parents and family who provided much appreciated backup over the years.

LIST OF SYMBOLS

Chapter 2

ρ	Density of soil (mass/length^3)
ε	Linear normal strain
ν	Poisson's ratio
β	Pressuremeter reduction factor within the critical depth
ζ	Strength reduction factor
Θ	The complement of the angle β_m
γ	Unit weight of soil (force/length^3)
ϕ'	Effective angle of soil friction (°)
ρ'	Effective density of soil (mass/length^3)
γ'	Effective unit weight of soil (mass/length^3)
σ_1,σ_2, σ_3	Principle stresses (force/length^2)
ε_a	Axial strain
ε_h	Horizontal soil strain
σ_{h0}	In-situ horizontal stress (force/length^2)
σ_{h0}'	In-situ effective horizontal stress (force/length^2)
β_m	Angle defining the slope of the wedge in the SW method
ϕ_p'	Effective plane strain angle of soil friction (°)
σ_r	Pressuremeter stress (force/length^2)
ε_r	Radial strain
ε_v	Volumetric strain
σ_v'	Effective overburden pressure (force/length^2)
σ_{v0}	In-situ vertical stress (force/length^2)
σ_{v0}'	In-situ effective vertical stress (force/length^2)
ε_x, ε_y, ε_z	Orthogonal strains
σ_y'	Preconsolidation yield pressure (force/length^2)
a & b	Pore pressure coefficients and curve fitting parameters in the p-y method for stiff submerged clays
B	Pile width or diameter (m)
BEF	Beam on an elastic foundation
CPM	Cone pressuremeter
CPT	Cone penetration test
c_u	Undrained shear strength of soil (force/length^2)
D	Width of pile section in the SW method
D_c	Critical depth of pile determined from the pressuremeter tests
D_{PMT}	Diameter of pressuremeter
D_r	Relative density of soil
e	Void ratio
E	Young's modulus (force/length^2)
E_c	Young's modulus for concrete (force/length^2)
E_h	Young's modulus for soil measured in the horizontal orientation (force/length^2)
EI	Flexural rigidity of pile (force x length^2)

E_s	Young's modulus of soil (force/length^2)
F	Pile resistance due to side friction (force/length^2)
F_1	Wedge body force
F_2	Force acting along the sloped face of the wedge
F_3 & F_4	Forces acting along the sides of the wedge
F_5	Force acting along the vertical face of the wedge
F_6	Force acting normal to the sloped face of the wedge
F_7	Passive force acting normal to the vertical face of the wedge
f_{cu}	Characteristic compressive strength of concrete (force/length^2)
f_y	Yield strength of reinforcing steel (force/length^2)
F_z	Axial pile load
G	Shear modulus (force/length^2)
h	Depth of the passive wedge formed in front of a laterally loaded pile
H_{0u}	Ultimate horizontal capacity of soil (force)
I	Second moment of area (length^4)
$i_{e\alpha}$	Inclination factor
k	Coefficient of subgrade reaction (force/length^3)
K	Modulus of subgrade reaction [p/y] (force/length^2)
k_h	Coefficient of horizontal subgrade reaction (force/length^3)
K_i	Initial soil modulus (force/length^2)
K_R	Soil pile interaction factor
K_s	Modulus of subgrade reaction in the SW method [p/y] (force/length^2)
K_{ult}	Soil modulus at ultimate load (force/length^2)
k_v	Coefficient of vertical subgrade reaction (force/length^3)
L	Pile length
l_e	Effective pile length
M	Slope of critical state line in p'-q space
M_u	Ultimate moment of resistance of the structural section (force x length)
n	Porosity of soil
n_h	Coefficient of subgrade reaction for soil with a modulus that increases in approximately linearly with depth (force/length^3)
P	Soil pressure (force/length^2)
p	soil reaction (force/length)
$p_{(max)}$	Maximum horizontal reaction provided by the soil
p'	Mean effective stress (force/length^2)
p_0	In-situ horizontal pressure measured by the pressuremeter
p_a	Suction pressure equivalent to one atmosphere
p_l	Limit pressure measured in a pressuremeter test (force/length^2)
p_L*	Pressuremeter net limit pressure within the critical depth
p_{ult}	Ultimate lateral soil resistance (force/length)
q	Deviator stress (force/length^2)
Q	Frontal pile resistance (force/length)
Q_0	Ultimate axial load capacity
R	Soil-pile interaction factor for overconsolidated clays OR the pressuremeter radius
r_0	Pile radius
RR	A relative rigidity factor between the pile and p_L*
SL	Horizontal stress level in the soil as defined in the SW method

SPT 'N'	The standard penetration test 'N' value corresponds to number of blows required to drive a split spoon sampler 300mm into the ground. The blows are delivered from a 62.5kg hammer falling 760mm.
SW	Strain wedge method of analysis for laterally loaded piles
T	Soil-pile interaction factor for normally consolidated soils
u	Pore water pressure (force/length^2)
u_0	In-situ pore water pressure (force/length^2)
w_L & w_P	Liquid and plastic limits respectively
y	Soil displacement (length)
z	Depth below ground level
z_c	Pressuremeter critical depth
α	Multiplication factor to transform the pressuremeter curve into a *p-y* curve for a laterally loaded pile (Robertson et al. 1982) OR Strength reduction factor within the critical pile depth for the *Q-y* curve (Smith, 1983).
ΔR	Change in pressuremeter radius
Δu	Change in pore water pressure
$\Delta\sigma_h$	Change in the horizontal soil stress (force/length^2)
δ	Linear displacement angle of the pile in the SW method
φ_m	Mobilised angle of friction
φ'_m	Mobilised effective stress angle of friction
μ	Coefficient of friction at interface between soil and pile
θ	Rotation
$\tau_{r\theta(max)}$	Maximum circumferential shear stress (force/length^2)

Chapter 3

AC/DC	Alternating current/Direct current
AL1	Pile subjected to axial and lateral load
ALT	Axial pile load test
CLT	Combined axial and lateral load test
DAS	Data acquisition System
DG	Dial gauge
DMT	Dilatometer test
EL	Electro-level
ERS	Electrical resistance strain (gauge)
L1	Pile subjected to lateral load only
LT	Lateral load test
LVDT	Linear variable displacement transformer
RT	Re-test
STC	Self-temperature-compensated
VW	Vibrating wire

Chapter 4

Note – only terms not previously defined or having a different meaning than in previous chapters are included in this chapter

API	American Petroleum Institute

c'	Soil cohesion intercept (force/length^2)
x	Depth below ground level
c_c	Compression index measured in an oedometer test
c_h	Horizontal coefficient of consolidation
c_α	Creep coefficient
c_v	Vertical coefficient of consolidation
c_{utc}	Undrained shear strength in triaxial compression
ε_{50}	Strain at half the maximum deviator stress measured in UU triaxial tests
C_c^*	Compression index for reconstituted soil
G	Shear modulus (force/length^2)
G_{sec}	Secant shear stiffness
p'_i	Isotropically consolidated mean effective stress
σ'_{vy}	Yield stress in the vertical direction (force/length^2)
ϕ_{cv}'	Constant volume friction angle
ϕ_{pres}'	Peak residual friction angle
ϕ_{res}'	Ultimate residual friction angle
w	Natural moisture content
UU	Unconsolidated undrained triaxial test
CK_0U	Anisotropically consolidated undrained triaxial test
CIUC	Consolidated isotropically undrained triaxial compression test
ICL	Intrinsic compression line
OCR	Overconsolidation ratio
YSR	Yield stress ratio
TP	Trial pit
PM	Pressuremeter
q_c	CPT end resistance

Chapter 5

Note – only terms not previously defined or having a different meaning than in previous chapters are included in this chapter

α	Shaft adhesion factor
A_c	Area of concrete
A_s	Area of steel
E_c	Young's modulus for concrete
E_s	Young's modulus for steel
F_{NSF}	Force due to negative skin friction or downdrag on a pile
N_q	Bearing capacity factor
N_{60}	SPT 'N' value at 60% energy efficiency
$\Delta\varepsilon$	Change in strain
ΔL	Movement measured by a change in slope over a monitored length, L
L	Length monitored between adjacent ELs
β	Burland's (1973) effective stress shaft friction factor
γ_{sat}	Saturated unit weight
K_c	Ratio of radial effective stress to vertical effective stress
PC	Total pressure cell

Chapter 6

Note – only terms not previously defined or having a different meaning than in previous chapters are included in this chapter

d	Distance from applied lateral load to strain gauge
e	Distance between the pin joint and the strain gauge where the bending moment is measured
EI_{cr}	Flexural rigidity of the cracked pile section pile
F_c and F_s	Forces in concrete and steel respectively due to an applied moment
f_{cu}	Characteristic strength of concrete
f_r	Concrete cracking stress
h	The mobilised frictional force between the test beam and the loading mechanism
H	Applied lateral load
H_R	The resultant horizontal load applied to pile AL1
I_g	Gross second moment of area
l_a	Distance between the pin joint and the point of horizontal load application
l_b	Distance between the test beam and the pin joint
L_c and L_s	Respective lever arms for the concrete and steel about the neutral axis.
M	Bending moment
$M_{applied}$	Applied bending moment
M_{cr}	Cracking moment for a concrete section
V	Axial compressive load applied to the pile
x	Distance between the LVDT and the applied horizontal load, H
z	Depth below pit level at pile L1 & AL1
Δ	Horizontal displacement of the pin joint relative to the uppermost electro-level
β	The angle of rotation of the loading mechanism between the test beam and the pin joint
δ	Horizontal pile displacement measured by the LVDT
ε	Strain
ε_c	Strain in the concrete
ε_s	Strain in the steel
ϕ	Pile curvature

Chapter 7

Note – only terms not previously defined or having a different meaning than in previous chapters are included in this chapter

B	Pile width
c_u	The undrained shear strength of the soil
CY	Cyclic load test
DBC	Dublin boulder clay
DT	Displacement transducer
LT	Lateral load test
P	Applied horizontal load
p	Soil reaction in units of force/length
P_{max}	The predicted ultimate horizontal load

y	Soil displacement in units of length
δ	Horizontal displacement measured at the pile head
ε_{50}	Strain at half the maximum deviator stress in an UU triaxial test
κ	Slope of the unloading-reloading line in *v-ln p'* plane for reconstituted, intact soil
λ	Slope of the normal compression line in *v-ln p'* plane for reconstituted, intact soil
K	Modulus of subgrade reaction or 'spring' stiffness of the soil (=p/y) in units of force/length^2

Chapter 8

Note – only terms not previously defined or having a different meaning than in previous chapters are included in this chapter

a_0, a_1, a_2 etc	Curve fitting coeffieients
SF	Shear force
R	Soil reaction (force/length)

Chapter 9

Note – only terms not previously defined or having a different meaning than in previous chapters are included in this chapter

D	Depth
E_{pile}	Young's modulus for pile material
FE	Finite element (analysis)
FEA	Finite element analysis
P-Δ effect	Secondary bending moment induced due to eccentric loading
y_{max}	Maximum horizontal soil displacement

TABLE OF CONTENTS

TABLE OF FIGURES

TABLE OF PLATES

Chapter 1

Introduction

1. INTRODUCTION

1.1 Background

Piles have been used for many millennia as a means of transmitting loads from buildings and other structures to ground of higher bearing capacity located at some reasonable depth below ground level. Timber piles have been found in the remains of Neolithic structures (≈6500 years ago), while Fleming et al. (1992) note their first mention in history in the writings of the Greek historian, Herodotus, who lived and wrote of his travels in the year's c485 to c425 B.C. He described how lake dwellers in Paeonia built their houses on piles driven into a lakebed.

Historically, piling was required to transmit vertical load from relatively small structures to a suitable bearing stratum. The capacity and number of piles required was essentially based on previous experience and the degree of effort required during installation of the piles (Figure 1-1). With the commercial production of steel in 1760's and the mechanisation of industry, continued industrial development has spiralled to meet the ever-expanding needs of a modern civilisation. Today, these demands have necessitated the construction of larger (and increasingly lighter) structures such as, high-rise

buildings and offshore platforms in particular. Accordingly, the design of foundations to support such structures requires a more rational approach than that offered by the 'degree of effort' approach. Moreover, the demand to develop sites previously deemed unsuitable has further added to the need for improved methods for predicting the carrying capacity of piles.

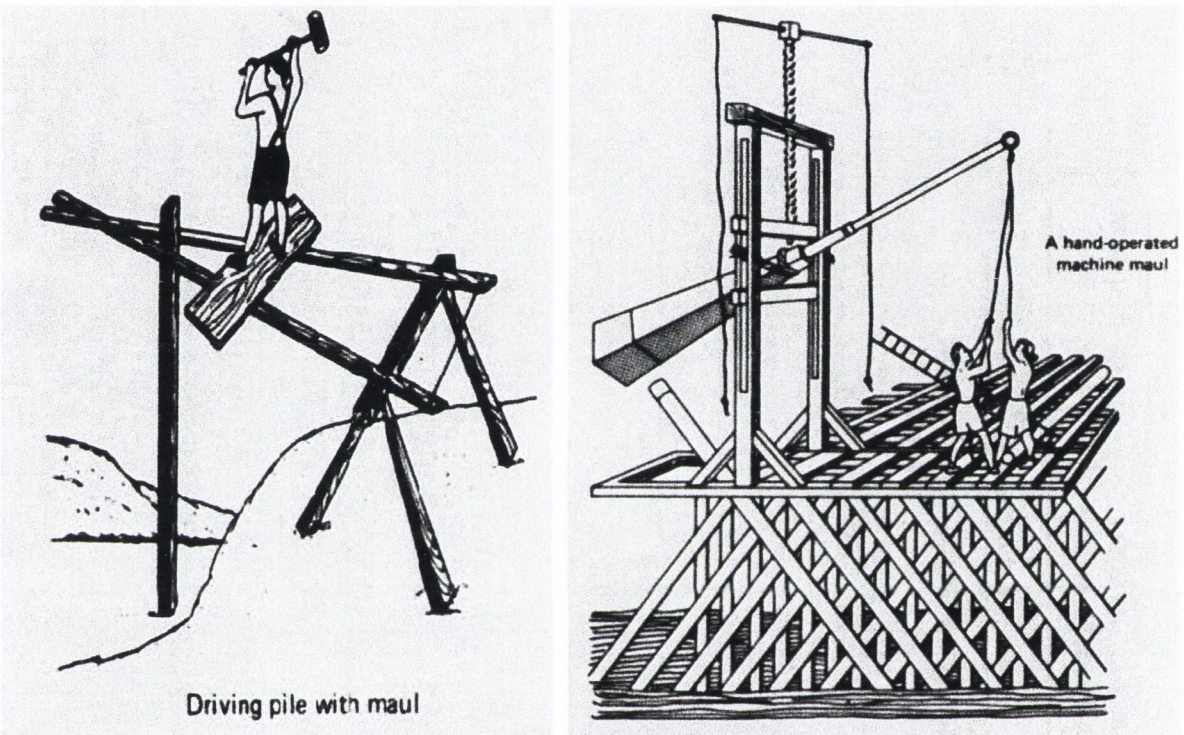

Figure 1-1: Early pile driving techniques (www.geoforum.com)

The first major advance in this regard resulted from the introduction of soil mechanics in the 1920's: the concept of effective stress provided a rational basis for understanding the factors controlling soil behaviour. This has led to a more soundly based approach to pile design, which incorporates soil strength and stiffness properties along with geological factors within a scientific framework.

Modern pile supported structures, because of their size and lightness, are frequently subjected to significant overturning and lateral forces that must be counteracted by the pile's ability to resist uplift and lateral load respectively. The uplift resistance is provided by the soil-pile shaft friction, which is influenced by a number of factors

including the soil-shaft interface properties, pile length and the soil type. The approach used to estimate the uplift resistance of a pile is similar to that used when calculating the skin friction developed for a pile loaded in compression. However, the approach to be adopted when designing laterally loaded piles is not so clear despite the existence of extensive research and numerous design approaches postulated since the early 1960's. In this regard, Reese (when discussing McClelland and Focht, 1958) stated:

> *'Of all the problems that are encountered in the design of offshore structures, the behaviour of laterally loaded piles is the least understood ……'*

Until the mid 1960's designers usually assumed piles could carry only axial load and batter piles were installed to cater for the lateral loads (Bowles, 1996). Graphical methods were used to find the individual pile loads in a group, and the resulting force polygon could close only if there were batter piles to resist the lateral loads. Around the same time, the offshore exploration industry experienced a surge in growth, leading to calls for more accurate predictive methods for assessing the lateral capacity of piles. The installation of battered piles through great depths of water was no longer a feasible option. Therefore, to improve the existing methods, a series of instrumented pile tests were undertaken along the Gulf of Mexico. The results of these tests have validated the ability of vertical piles to resist lateral loads[1] and led to the development of the semi-empirical design approach known as the *p-y* method. The method uses data from pile tests to derive a set of soil resistance (p) versus soil displacement (y) curves at various depths along the pile. These curves represent the soil's resistance to lateral load which is combined with the intrinsic resistance of the pile (using a beam-column analysis) to give the overall lateral response of the pile.

The *p-y* curves, which characterise the true non-linear response of the soil (and therefore extends Winkler's spring concept), were correlated with soil properties at each test site such that these correlations could be used to construct *p-y* curves for any site

[1] Vertical piles resist horizontal forces by deflecting laterally to mobilise their strength and that of the surrounding soil.

(Tomlinson, 1994 and others). However, research by Dunnavant and O'Neill (1989) and more recently Ashour et al. (1998) and Ashour & Norris (2000), suggest that such correlations are site and pile specific and therefore the generality of the method has not been fully validated. However, the method despite its semi-empirical basis provides good predictions of the measured pile behaviour for the (limited) conditions encountered at the test sites.

The current American Petroleum Institute (API) recommendations for *p-y* curve formulation (with modifications as the database of test results expands) are widely used in practice. However, none of the current *p-y* recommendations discusses the effect of combined vertical and lateral loading on the resulting *p-y* curves. Design guidance for combined loads suggests the assessment of the axial and lateral capacities of the pile independently followed by superposition of the results to compute the pile stresses under combined loading (Price and Wardle, 1988; Shahrour and Meimon, 1991; Bowles, 1996). The examination of piles subjected to simultaneous axial and lateral loads is the subject of this thesis.

Research Objective

One of the primary objectives of this research is to advance the *p-y* technique for evaluating the response of single piles subjected to lateral loads. In particular, the effect of simultaneous horizontal and vertical loading on the soil-pile reaction is investigated to determine if the existing analysis procedures require adjustment for combined loads. The contribution of instrumented in-situ testing techniques (e.g. the electric cone penetration test (CPT) and the cone pressuremeter test (CPM)) to the analysis of laterally loaded piles is also examined in this research.

1.2 Outline of the Thesis

1.2.1 Scope of Work Presented

This thesis examines the current recommendations for the analysis of laterally loaded single piles in cohesive soils and compares the findings to results from full-scale load

tests on two instrumented piles; one pile (AL1) was subjected to simultaneous axial and lateral loading while the second pile (L1) was loaded laterally. The primary experimental programme, undertaken at a soft clay test site at Kinnegar on the northeastern outskirts of Belfast city, also included re-testing the same piles under lateral load nineteen months after the initial tests. By re-testing, the effect of a previously applied axial load could be assessed from pile AL1, while the adjacent pile, L1 provided information on the effects of ageing after reloading. Table 1.1 outlines the programme for this series of experiments.

Test reference[2]	Axial load (kN)	Max Lateral load (kN)
ALT (October 17, 1997) pile AL1	170	-
CLT1 (October 18, 1997), pile AL1	168	59.75
LT1 (October 18, 1997), pile L1	-	59.75
CLT2 (October 19, 1997), pile AL1	133	89.75
LT2 (October 19, 1997), pile L1	-	89.75

Table 1.1: Programme of load tests performed at the Kinnegar test site

The thesis also presents the results from the author's lateral load tests on instrumented steel H-piles in stiff glacial till in addition to centrifuge tests commissioned by the author. Although some details regarding the lateral tests on the H-piles were reported by the author (Phillips 1995), this thesis presents the first detailed interpretation of the test results. All experimental data permit measured *p-y* curves to be compared with those recommended by the API for soft and stiff clays.

[2] ALT refers to the axial load test on pile AL1 carried out in advance of the CLT tests. CLT1 & CLT2 refer to first and second combined load tests respectively. LT and RT are the lateral load test and re-load tests respectively.

Note

It is acknowledged that piled foundations can be subjected to two general forms of lateral load:

1. *Active loading*, where external loads are applied to the pile, with the soil resisting the load, for example forces applied at the pile top resulting from wind and earthquake loads on tall buildings, wave and current forces on offshore structures.

2. *Passive loading*, where movement of the soil subjects the pile shaft to bending stresses, for example where piles support a bridge abutment with backfill overlying weak soils through which the piles penetrate.

This thesis is concerned primarily with the former although some of the concepts discussed are applicable to both categories of loading.

1.2.2 Contents of the Thesis

The contents of each chapter are summarised as follows:

Chapter 2: Reviews the current analysis procedures for laterally loaded single piles in cohesive soils. Traditional approaches, which were often graphically based due to the unavailability of computers, have been mentioned but not described in detail since they have essentially been superseded by non-linear computer based approaches (i.e., *p-y* method). The review concentrates on recent advances for obtaining and improving *p-y* curves.

Chapter 3: Describes the design and fabrication of the instrumented precast concrete piles and the field procedures followed during the load test programme. The chapter also briefly outlines the instrumentation and calibration procedures along with the structural properties of the piles.

Chapter 4: Summarises the geology of the Belfast area and the soil properties at the test site. Particular attention is focused on those properties relevant to the interpretation of laterally loaded pile behaviour. Special emphasis is placed on the results from CPT and CPM tests conducted in the vicinity of the load tests and include the derivation of *p-y* curves from the CPM tests.

Chapters 5: Presents the results from the instrumented load tests at Belfast, these include:

- Axial load test (ALT)
- Lateral (LT) and combined lateral and axial load tests (CLT) and
- Re-tests (RT) on the piles, involving lateral loads applied nineteen months after the initial tests.

Chapter 6: Provides structural analysis details of the combined load test set-up and the pile section response for the Belfast tests. A detailed analysis of the pile head condition at AL1 (the pile subjected to combined loading) is provided and the role of the pile head condition on the observed pile behaviour is discussed in detail.

Chapter 7: Presents details of laterally loaded pile tests in stiff glacial till as well as the *p-y* curves interpreted from the results. These curves are compared with the API recommended *p-y* curves for stiff clay and some general conclusions are drawn from the test results.

Chapter 8: Provides detailed interpretation of the Belfast tests. The curve fitting procedures adopted for the derivation of *p-y* curves from the instrumentation data are discussed in detail. The results from the RT are interpreted and the main findings presented.

Chapter 9: The main findings of the research are presented and their implications for the design of laterally loaded piles discussed. The results from the centrifuge tests commissioned by the author to investigate the effect of an axial load on the lateral pile response are also presented here.

Chapter 10: Presents the main research conclusions and suggests areas in which the findings of this research can be usefully employed in pile design.

Supplementary information is presented in the appendices:

Appendix to Chapter 2

- Appendix 2a: Relationship between Young's modulus E and the Spring Stiffness of the Soil K
- Appendix 2b: Summary of *p-y* curve formulations

Appendix to Chapter 3

- Appendix 3: Instrumentation Calibration

Appendix to Chapter 4

- Appendix 4: Pressuremeter Results

Appendices to Chapter 5

- Appendix 5a: Analysis of Axial Pile Capacity using;
  - Bustmante and Gianeselli Method
  - NTD Design Method
  - Conventional Soil Mechanics Approach using α-method
- Appendix 5b: Axial Load Distribution along Pile AL1 & Estimate of Negative Skin Friction

Appendices to Chapter 6

- Appendix 6a: Structural Analysis of Pile Section & Cracked and Uncracked Flexural Rigidity
- Appendix 6b: Finite Element Moment-Strain Relationship for Reinforced Concrete Pile Section

- Appendix 6c: Back-calculation of E_c from Lateral Load Tests
- Appendix 6d: Analysis of Head Restraint at Pile AL1

Appendices to Chapter 8

- Appendix 8a: Validation of Curve Fitting Equation
- Appendix 8b: Derivation of Curve Fitting Coefficients and Least Squares Optimisation
- Appendix 8c: Detailed Test Results

Appendices to Chapter 9

- Appendix 9: Interpretation of Instrumentation Data

Chapter 2

Literature Review

2. A REVIEW OF CURRENT ANALYSIS METHODS FOR LATERALLY LOADED SINGLE PILES

2.1 Introduction

This chapter presents an overview of the techniques currently adopted for the design of laterally loaded single piles. Numerous methods of analysis have been proposed during the last few decades, ranging from simple procedures using design charts, to the use of complex computer programs. In general, the procedures can be grouped into the following categories:

- Ultimate load analysis
- Continuum method
- Subgrade reaction models
- Finite element methods.

It is current opinion, particularly in the offshore industry, that methods based on the theory of elasticity (continuum method) are not generally applicable for design of single piles because of the difficulty in assigning single (representative) values to the soil's elastic properties (Young's modulus and Poisson ratio) especially when yielding of the soil

occurs[1]. Other methods based on the theory of subgrade reaction, incorporate simplifying assumptions, such as assuming a variation of the subgrade modulus with depth and linear elastic soil behaviour (Winkler, 1867; Hetenyi, 1946; Terzaghi, 1955; Broms 1964 a & b). These simplifying assumptions reduce the difficulty in obtaining a solution to the problem, but errors of an unknown magnitude are introduced since soil stratification, time effects, the effect of load intensity, and structural factors cannot be considered.

The elastic methods were initially developed before computers became readily available to engineers and hence the solutions were often presented in the form of non-dimensional charts or tables to permit designs to be completed with minimum computation (Broms, 1964 a & b; Matlock & Reese, 1960; Poulos, 1971; Randolph, 1981). On small projects with limited budgets, these methods can be successfully employed for final design provided the soil parameters required for the analysis are judiciously selected to ensure a conservative design. The methods may also be used for preliminary design purposes on larger projects.

However, in situations where lateral loads may govern the foundation design, for example; in the case of offshore structures where piles may stand freely in 100m of water or more (thus making full scale load testing impractical), there is a clear need to improve predictive methods for reasons of enhanced safety and performance. It is generally accepted that the most realistic predictions are obtained by modelling the soil as a series of non-linear non-interactive elastic springs (an extension of the Winkler foundation), with the pile modelled using beam-column theory. This approach, known as the *p-y* method, provides the most rational design approach since it permits the variability of the soil system, pile structural stiffness and head fixity to be modelled. Furthermore, the method can also account for the effects of cyclic loading, common in offshore structures, where repetitive loading causes softening of the soil resistance particularly in normally consolidated clays.

The *p-y* method despite some theoretical shortcomings, for which it has received criticism (Poulos, 1971; Randolph, 1981; Poulos and Davis, 1980; Scott, 1981; Davies and Budhu.,

[1] Poulos (1971) has suggested a modification to the general continuum approach to account for soil yield but the accuracy of this approach diminishes as the depth of yielding soil increases.

1986), has been shown, via back analysis of full scale field tests (Matlock, 1970; Reese, et al., 1974 and others), to accurately predict the measured pile bending moment and displacement profiles. As the original *p-y* database is extended; through further research, improved computer modelling facilities and in-situ test methods, so to are the accuracy and reliability of the predictions. Therefore, for these reasons, the *p-y* method is outlined in detail and will subsequently be used in the analysis of the test results presented in this thesis.

For the design of laterally loaded piles, two criteria need to be satisfied: first, an adequate factor of safety against ultimate lateral failure; and second, the displacement at working loads must be capable of being tolerated by the superstructure. As in other areas of soil mechanics, these criteria are generally treated separately, and the design is arranged to provide the required safety margins independently. Estimating the ultimate lateral resistance of single piles will be described section 2.2 and pile displacement will be discussed in section 2.3.

2.2 Ultimate Lateral Soil Resistance

2.2.1 Background

The ultimate soil resistance to lateral load is normally provided by three components; (a) the passive resistance offered by the soil in front of the pile, (b) side friction developed between the soil-pile interface and (c) in the case where the piles receive a pile cap, shear developing along the base of the pile cap. However, in the case of the latter, Davisson (1970) remarks that a slight settlement of the soil beneath the cap can essentially eliminate this resistance, hence skin friction between the pile cap and soil is usually ignored for design purposes.

The ultimate lateral resistance of a soil-pile system is governed by either the yield strength of the pile section or by the ultimate lateral resistance of the supporting soil. For an unrestrained pile head, failure is achieved in long piles by the formation of a plastic hinge in the section or in the case of a short pile rigid pile rotation takes place, both scenarios are

shown in Figure 2-1 a and b respectively. In the case of piles restrained at the pile head, failure depends on the length of pile embedded in the ground. Long piles (Figure 2-2a) fail by the formation plastic hinges in the pile section while piles of intermediate length (Figure 2-2b) generally fail by a combination of rotation and plastic hinge formation. Short rigid piles (Figure 2-2c) fail by translation.

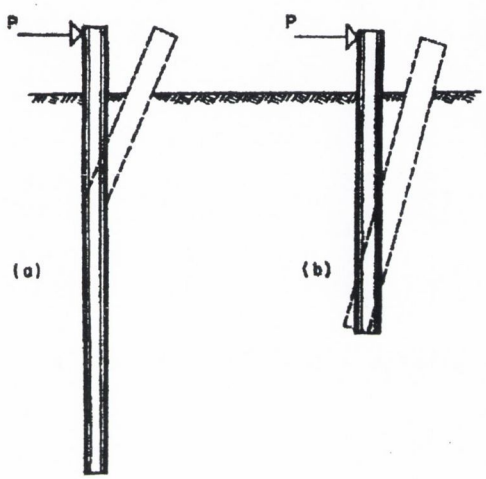

Figure 2-1: Modes of failure for unrestrained pile head (from Broms 1964a)

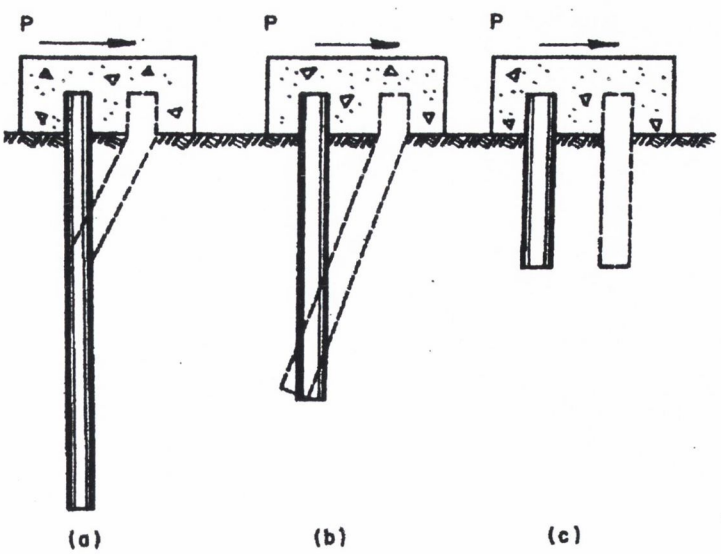

Figure 2-2: Modes of failure for restrained pile head (from Broms 1964a)

The first step therefore, in determining the ultimate lateral resistance of a pile is to decide whether the pile will behave as a short, intermediate or long member. The demarcation between short and long pile behaviour can be estimated in terms of a relative stiffness factor (R or T) given by Hetenyi (1946). The factors provide a relation between the flexural rigidity (EI) of the pile and soil stiffness (expressed as a modulus of subgrade reaction). For soil with a modulus that increases linearly with depth (a condition approximated by normally consolidated clays and cohesionless soils) the stiffness factor, T, is expressed as:

$$T = (EI/n_h)^{1/5}$$

were n_h is the constant of horizontal subgrade reaction measured in instrumented pile load tests[2].

For soils with constant modulus (an approximation often applied to overconsolidated clays), the stiffness factor, R, is expressed as:

$$R = (EI/k_hB)^{1/4}$$

where k_h = coefficient of subgrade reaction (kN/m^3)

B = pile diameter or width (m)

Woodward et al. (1972) defined short versus long members in terms of these stiffness factors as shown in Table 2-1

[2] Assuming a linear variation with depth z, $k_h = n_hz$ (kPa) or in terms of pile width, B, $k_h = n_hz/B$.

Pile type	Soil Modulus	
	Linearly increasing	**Constant**
Rigid (free head)	$L \leq 2T$	$L \leq 2R$
Flexible (free head)	$L \geq 4T$	$L \geq 3.5R$

Table 2-1: Classification of rigid or flexible piles

2.2.2 Ultimate Lateral Resistance of Cohesive Soil

The ultimate lateral resistance of cohesive soil has been well documented (Reese, 1958; Brinch Hansen 1961, Broms 1964; Randolph and Houlsby, 1984). Summaries of the main approaches are presented in following section.

Reese (1958)

In responding to McClelland and Focht's (1958)[3] seminal paper on laterally loaded piles, Reese presented an approximate analysis of the ultimate lateral resistance for saturated clay[4]. In the analysis, Reese considered the horizontal displacement of a vertical pile of square cross-section. The ultimate resistance was calculated using two models; one which assumes that the clay around the pile shaft fails as a group of sliding blocks (deep failure) and the other assumes failure is controlled by a passive soil wedge in front of the pile (shallow failure), the controlling mode of failure depends on the depth considered below the ground surface. Close to the ground surface there is a zone of reduced resistance due to

[3] The literature refers to two papers by McClelland and Focht bearing the title *Soil modulus for laterally loaded piles*. The papers, which were identical, are contained in issues of the Journal of the Soil Mechanics and Foundations Division of ASCE published in 1956 and 1958 respectively, it appears the original paper was reprinted in the 1958 Journal in order to set the context for a discussion by a number of contributors.

[4] The shear strength, c_u was obtained from UU triaxial tests with the initial angle of internal friction ϕ equal to zero.

the lack of vertical confinement, the soil located in front of the loaded pile moves upwards in the direction of least resistance to form a passive wedge. The soil below this zone is no longer directly influenced by the ground surface and flows horizontally around the pile giving plane strain conditions. There is general agreement with these idealisations (Brinch Hansen, 1961; Broms, 1964a; Matlock, 1970; Sullivan et al., 1980; Evans, 1982; Reese et al. 1984; Randolph and Houlsby, 1984; Fleming et al., 1992; Briaud, 1992; Ashour et al., 1998 and Ashour and Norris, 2000).

Deep or Flow around Failure

Figure 2-3a shows a vertical section through the pile and Figure 2-3b shows the blocks of soil that are assumed to be displaced horizontally when the pile is deflected. It is assumed that the stress, σ_1, on the side of block E next to the pile is equal to zero. If the soil strength in undrained conditions is defined by the expression $\tau = c_u$, the magnitude of σ_2 must be $\approx 2c_u$ in order to cause failure in block E. By a similar analysis if σ_2 is considered to be the confining stress on block D then the stress, σ_3, is $4c_u$. If block C, in moving relative to the pile and the adjacent soil, is assumed to develop full resistance along each side, the magnitude of σ_4 will be $6c_u$. If blocks B and A fail in a similar manner to blocks E and D, the value of σ_6, will be $10c_u$.

Having determined the stresses acting on the pile, the free body (Figure 2-4) shows that the ultimate (plane strain) soil resistance is given by Eq 2.2.

Eq. 2-1... $$p_{ult} = (\sigma_6 + 2c_u - \sigma_1)B = 12\, c_u B \quad (kN/m)$$

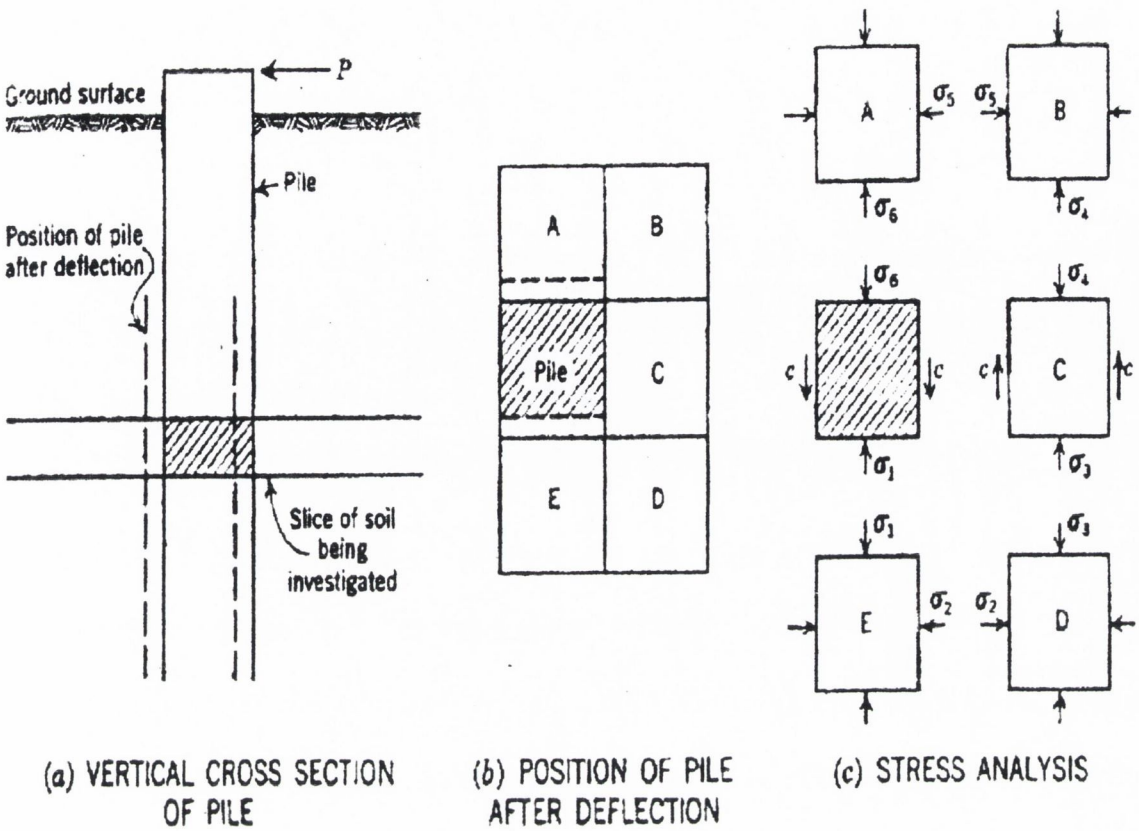

Figure 2-3: Model for ultimate resistance of clay at depth due to lateral displacement of a pile (from Reese, 1958)

Note: $c \equiv c_u$ in Figure 2.3(c)

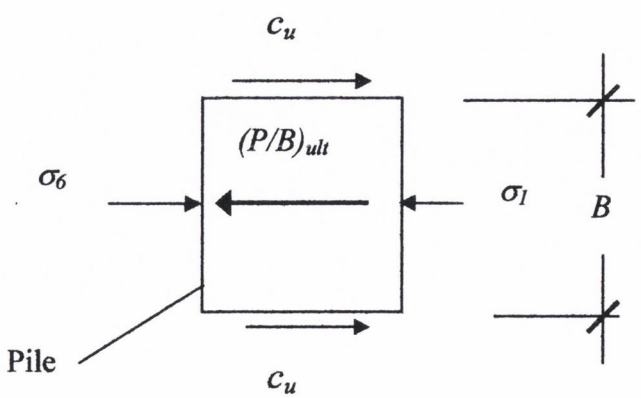

Figure 2-4: Free body diagram of stresses acting on the pile

Shallow or Passive Wedge Failure

Within the wedge the soil resistance decreases from the 'deep' resistance at the base of the wedge to a minimum resistance at the ground surface. Figure 2-5 shows that the wedge resists lateral movement by means of its weight and shear resistance along its sides and bottom. If it is assumed that the full shear resistance, c_u, of the soil is developed on planes ACE, BDF and ABFE, and that only part of the shear resistance, ζc_u, is developed on plane CDFE then the following equations can be written to represent the forces acting on these planes

$$F_1 = \tfrac{1}{2}\gamma B h^2 \tan\theta$$

$$F_2 = c_u B h \sec\theta$$

$$F_3 = \tfrac{1}{2} c_u h^2 \tan\theta$$

$$F_4 = \tfrac{1}{2} c_u h^2 \tan\theta$$

$$F_5 = \zeta c_u B h$$

Summing the forces in the vertical direction yields

$$F_6 = \tfrac{1}{2}\gamma B h^2 \sec\theta + \zeta c_u B h \operatorname{cosec}\theta + c_u B h \operatorname{cosec}\theta + c_u h^2$$

and summing the forces in the horizontal direction yields

$$F_7 = \tfrac{1}{2}\gamma B h^2 + \zeta c_u B h \cot\theta + 2 c_u B h \sec\theta \operatorname{cosec}\theta + c_u h^2 \sec\theta$$

The horizontal soil resistance offered by the wedge acting against the pile can be obtained by taking the derivative of F_7 with respect to h to give the result shown in Eq. 2-2.

Eq. 2-2... $$p_{ult} = \frac{dF_7}{dh} = \zeta c_u B \cot\theta + \gamma B h + c_u B \sec\theta \operatorname{cosec}\theta + 2 c_u h \sec\theta$$

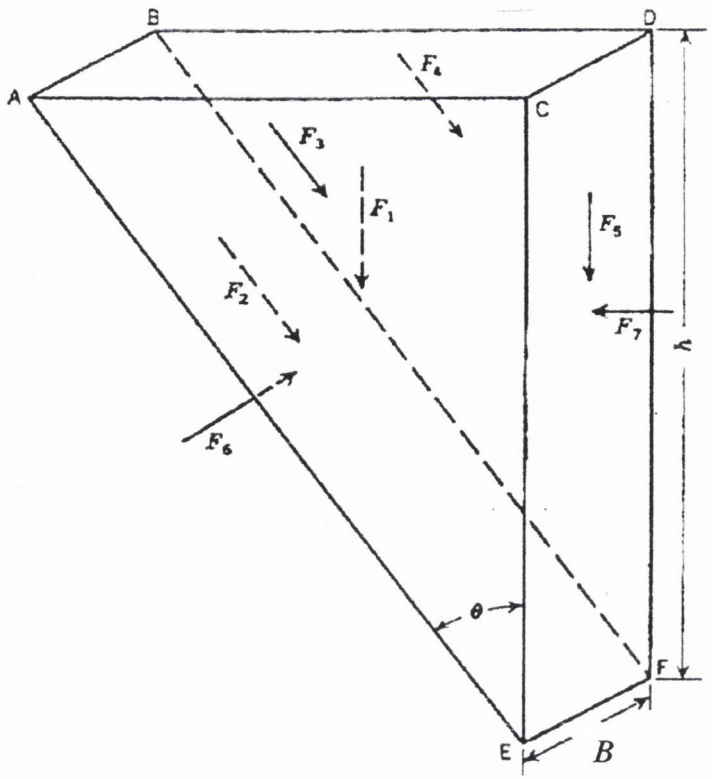

Figure 2-5: Assumed passive wedge type of failure for clay

and at the ground surface $h = 0$, and $p_{ult} = \zeta c_u B \cot\theta + c_u B \sec\theta \operatorname{cosec}\theta$

If the value of θ is assumed to be 45° and ζ is taken as 0, then

$$p_{ult} = 2c_u B$$

Eq. 2-1 and Eq. 2-2 can be solved simultaneously to find the depth at which the failure would change from the wedge type to the flow-around type. Broms (1964a) has shown the transition to take place at a depth of approximately three pile diameters below the ground surface.

Broms (1964a)

The probable distribution of soil resistance for cohesive soils is shown in Figure 2-6(b); this has been simplified by Broms (1964a) to a rectangular distribution as shown in Figure 2-6(c). Broms assumed that some soil shrinkage away from the pile would occur close to the ground surface and allowed for this by assuming a lateral soil reaction equal to zero to a depth of 1.5 pile diameters, below this depth the soil reaction was taken as $9c_uB$, where B is the pile diameter or the pile width.

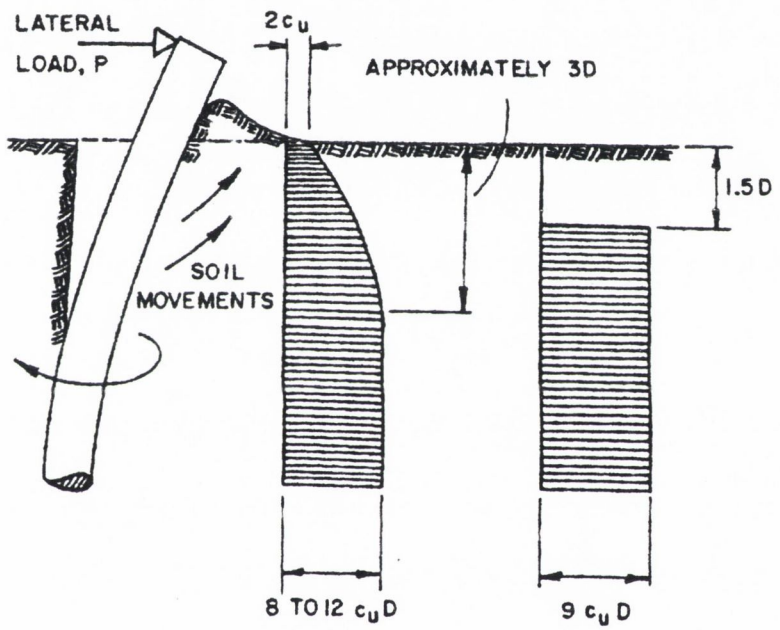

(a) Laterally loaded pile showing passive wedge (b) Probable distribution of soil reactions (c) Assumed distribution of soil reactions

Figure 2-6: Distribution of lateral earth pressures (after Broms, 1964a)

Broms applied this simplified soil reaction to both free and restrained pile heads assuming the failure modes for long and short piles shown in Figure 2-1 and Figure 2-2. Broms assumed the lateral resistance of the surrounding cohesive soil would govern failure of relatively short laterally loaded piles whereas the plastic or yield resistance of the pile

section would govern the lateral resistance of relatively long piles. In assessing the precision of the rectangular distribution of soil reaction {Figure 2-6(c)} Broms obtained ratios of measured maximum moment to calculated maximum moment of 0.84 to 1.13 for the cases analysed. Based on this, Broms concluded that the proposed method of analysis could be used with confidence to predict the maximum bending moments for both free and restrained piles but suggested additional test data was desirable to fully validate the method. The method is popular for preliminary design or for piled foundations whose design is not governed by lateral loading. Broms presented his findings for both free and restrained laterally loaded piles in graphical form, an example of one such chart is shown in Figure 2-7 for piles in clay.

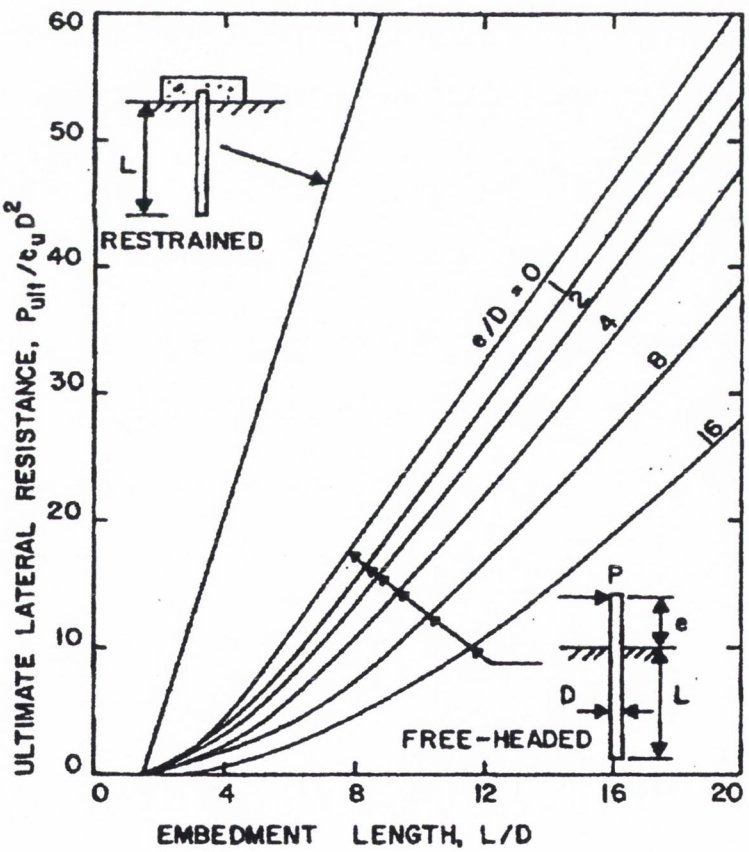

Figure 2-7: Typical design chart developed by Broms (1964a) for long piles in cohesive soils

Randolph and Houlsby (1984)

Randolph and Houlsby (1984) used the similarity between the soil deformation during a pressuremeter test[5] and the behaviour of soil surrounding a laterally loaded pile to present an approximate calculation of the lateral soil resistance at depth. The calculation was based on the observation of a mechanism of cavity expansion in front of the pile, the calculation also incorporated an allowance for the lateral resistance developed from side shear along the soil pile interface; the side shear contribution was estimated as being of the order of $1.0c_uB$.

When a pile is loaded laterally, the pressure in front of the pile increases from the in situ horizontal stress level, σ_{h0}, up to the limit pressure p_l obtained from a pressuremeter test. Behind the pile, the stresses will decrease. The lowest value obtainable under undrained conditions corresponds to a suction of one atmosphere p_a ($\approx$ 100kPa), above which cavitation is assumed to occur leading to a gap forming between the soil and the pile. After breakaway the pressure behind the pile will fall to zero, or, if there is free water available, to the pore water pressure u_0. Thus the ultimate resistance at depth will lie between $(p_l + p_a + c_u)\ B$ and $(p_l - u_0 + c_u)\ B$. From the analysis of the pressuremeter test Briaud, (1992) suggests the limiting pressure p_l for a cohesive soil may be written as

$$p_l = \sigma_{h0} + c_u\,[ln(G/c_u) + 1]$$

where G is the shear modulus of the soil also determined from the pressuremeter test. For typical values of G/c_u the above expression gives $p_l = 6c_u + \sigma_{h0}$. Therefore, substituting for p_l the ultimate resistance at depth will fall between the range given in Eq. 2-3[6].

Eq. 2-3… $$7 + \sigma_{h0}'/c_u < p_{ult}/c_uB < ([\sigma_{h0} + p_a]/c_u) + 7$$

[5] See section 2.5.1

[6] Note σ_{h0} on the left hand side of Eq. 2-3 is in terms of effective stress.

where the lower limit corresponds to the case of the ambient head of water behind the pile, and the upper limit is where a suction develops behind the pile. For normally or lightly overconsolidated clay, the ratio σ_{h0}/c_u will be ≈ 2. Thus the lower limit corresponds to the result for a smooth pile using plasticity theory. For stiff overconsolidated clay, the ratio σ_{h0}/c_u may be as low as 0.5 at shallow depths. Even allowing for suction between the pile and the soil the ultimate resistance may be below $9c_uB$. Thus for overconsolidated soils the ultimate resistance calculated from the cavity expansion considerations may be lower than that calculated for flow around failure using plasticity theory (Eq. 2-4).

Eq. 2-4... $$p_{ult}/c_uB = 10.5$$

As in previous analyses (Broms, 1964a; Reese, 1958) the reduced resistance near the ground surface was based on a passive wedge failure in front of the pile. At the ground surface, a passive pressure of $2c_u$ in front of the pile together with some allowance for side shear would yield an ultimate resistance of approximately $3.0c_uB$. Reese (1958) considered the failure of a 45° wedge in front of the pile and derived the expression for ultimate resistance given in Eq. 2-5 where z represents the depth considered.

Eq. 2-5... $$p_{ult} = c_uB(2+ \sigma_{v0}/c_u + 2\sqrt{2z/B})$$

Subsequent field tests by Reese and Cox (1975) showed that Eq. 2-5 overestimated the measured ultimate resistances by ≈ 1.7. Allowing for the factor of 1.7, Eq. 2-5 was found to exceed the ultimate lateral resistance estimated by Eq. 2-3 at depths of about 3 pile diameters. In soft clay, Matlock (1970) found from experimental results that the last term in Eq. 2-5 over predicted the lateral resistance and should be replaced by $1.5z/D$. However, in normally consolidated or lightly overconsolidated clay, the term $\gamma z/c_u$ will dominate. Therefore at about 3 pile diameters the ultimate resistance given by Eq. 2-5 will start to exceed that predicted by the cavity expansion mechanism (Eq. 2-3) and plasticity theory (Eq. 2-4). Hence, at shallow depth the following expression was tentatively suggested for the ultimate wedge resistance:

Eq. 2-6... $$p_{ult}/c_uB = 2 + \sigma_{v0}/c_u + 1.5z/B$$

When the piles are under water, the total stresses σ_{vo} and σ_{h0} should be replaced by effective stresses and where different failure mechanisms are anticipated, Eq. 2-3, Eq. 2-4 and Eq. 2-6, should be plotted with depth and the lowest value taken at any particular depth.

2.2.3 Simplified Pressuremeter Method

As with previous simplified methods (Broms, 1964a & b and Evans, 1982), Briaud (1997) has produced a simplified pressuremeter approach. The method known as 'Simple Approach for Lateral Loads On Piles,' (SALLOP) was developed as a "back of an envelope" check on the lateral pile performance using the results from preboring pressuremeter tests. The technique avoids having to employ the time consuming and cumbersome work of transforming the pressuremeter curve into a *p-y* curve and the subsequent application of the beam-column analysis. The method is based on the concept that the sinusoidal soil resistance-depth profile (Figure 2-8) tends to cancel itself out except for a shallow zone close to the ground surface, which contributes most of the lateral resistance. A Winkler analysis was used to determine the controlling depth of pile for the application of SALLOP (i.e., the depth at which zero shear force occurs).

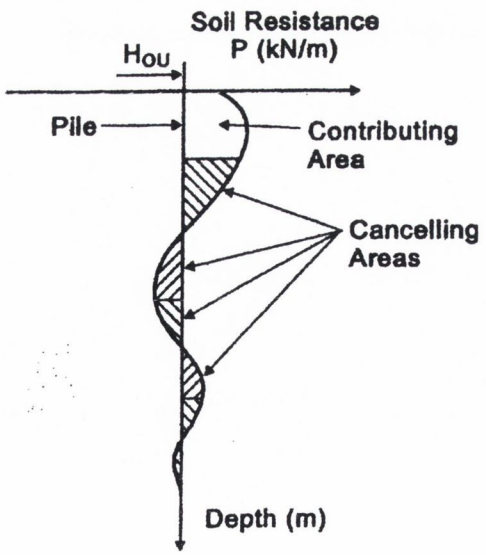

Figure 2-8: Conceptual soil resistance versus depth profile (Briaud, 1997)

The method is semi empirical, in that, the framework is theoretical but the factors in the theoretical equations are adjusted empirically by appropriate correlations developed from 20 full-scale load tests with corresponding pressuremeter test results. The database used to validate the method comprised piles varying in length from 4.6m to 36.6m, pile widths from 0.273 to 0.915m, for steel, concrete and timber piles for sand, clay and sand over clay. The method assumes that the soil is uniform with depth and the flexural stiffness (EI) of the pile is independent of the bending moment. Caution must therefore be exercised when applying the method to concrete piles, which may gradually crack and lead to excessive deflections. If it is known that the cracking moment, M, for a concrete pile occurs before a reference load (taken as one third of the predicted lateral capacity, $H_{0u}/3$) an alternative method must be used to allow for the nonlinearity in the relationship between EI and M. The reliability of the method can be judged by inspection of Figure 2-9 which illustrates the predicted ultimate capacity (H_{0u}) versus measured lateral capacity[7].

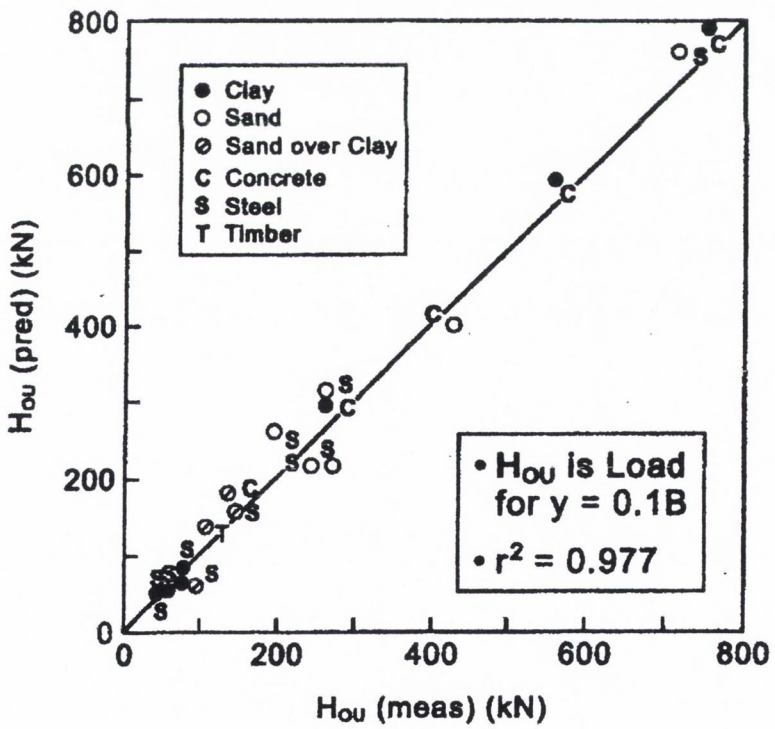

Figure 2-9: Predicted versus measured lateral capacity (H_{ou}) using SALLOP database

[7] SALLOP can also be used to estimate the lateral pile displacement at working loads (taken as $H_{0u}/3$) but the accuracy of the displacement predictions is not as good as that of lateral capacity predictions.

2.2.4 Summary on Ultimate Lateral Resistance in Cohesive Soils

The difference in shallow and deep resistance of laterally loaded soil is clearly acknowledged in the preceding references. Table 2-2 summarises the findings from this section along with the results of predictions by other researchers.

Reference	Analysis model	Soil resistance p_{ult}/c_uB (kN/m)		Comments
		Shallow resistance	Deep resistance	
Brinch Hansen (1961)	Active and passive soil pressure theory	-	8.3 –11.4	
Reese (1958)	Sliding blocks in plane strain & Passive wedge	2*	12+	Approximate rational analysis * passive wedge failure +flow around failure
Broms (1964a)	Ultimate active and passive soil resistance†	0*	9+	* to a depth of 1.5B +factor was found to vary from 8 to 12 †in the case of long piles the moment capacity of the pile section dictates ultimate failure
Poulos and Davis (1980)	Plasticity theory and limit analysis	-	8.18 –11.14	Smooth square pile loaded normal to the diagonal – depending on the pile aspect ratio
Poulos (1971)	Plasticity theory	2	11.41	
Randolph and Houlsby (1984)	Plasticity theory	-	9.14 11.94	Smooth pile Rough pile

Table 2-2: Summary of ultimate lateral soil resistance

2.3 *Elastic Methods*

2.3.1 Background

Theoretical methods for predicting displacements of laterally loaded piles generally adopt one of two approaches:

(a) The elastic approach, which assumes the soil to be an ideal elastic continuum and,

(b) The subgrade-reaction method, in which the continuous nature of the soil medium is ignored and the pile reaction at a point is simply related to the deflection at that point.

Only the subgrade reaction method is discussed in this section as it provides the necessary background for the development of the *p-y* method.

2.3.2 Subgrade Reaction Method or Beam on an Elastic Foundation

The method of subgrade reaction or beam on an elastic foundation has been used since about 1920 for computing displacement, bending moment and shear force profiles in piles acted upon by horizontal forces above the ground surface. The subgrade reaction concept, assumes a complete lack of continuity in the supporting soil, as if it consisted of a series of independent linear elastic springs that deflect when directly loaded, but do not induce movement in the adjacent springs (Winkler foundation). The spring concept is contrasted with that of a soil continuum in Figure 2-10.

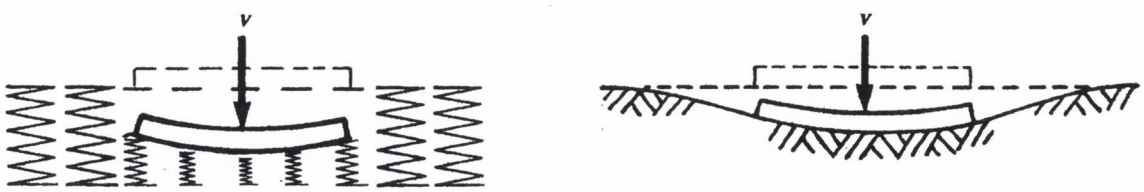

(a) Non-interactive Winkler springs (b) Elastic continuum

Figure 2-10: Foundation models (from Elson [1984])

In the case of a homogeneous soil the method assumes that the soil has a linear *p-y* curve and that the same *p-y* curve applies for all depths as shown in Figure 2-11 i.e., $p/B = ky$ where p is the soil reaction in load per unit length of pile (force/length) and y the displacement of the pile at the same point. The coefficient of proportionality k (force/length^3) became known as the coefficient of subgrade reaction.

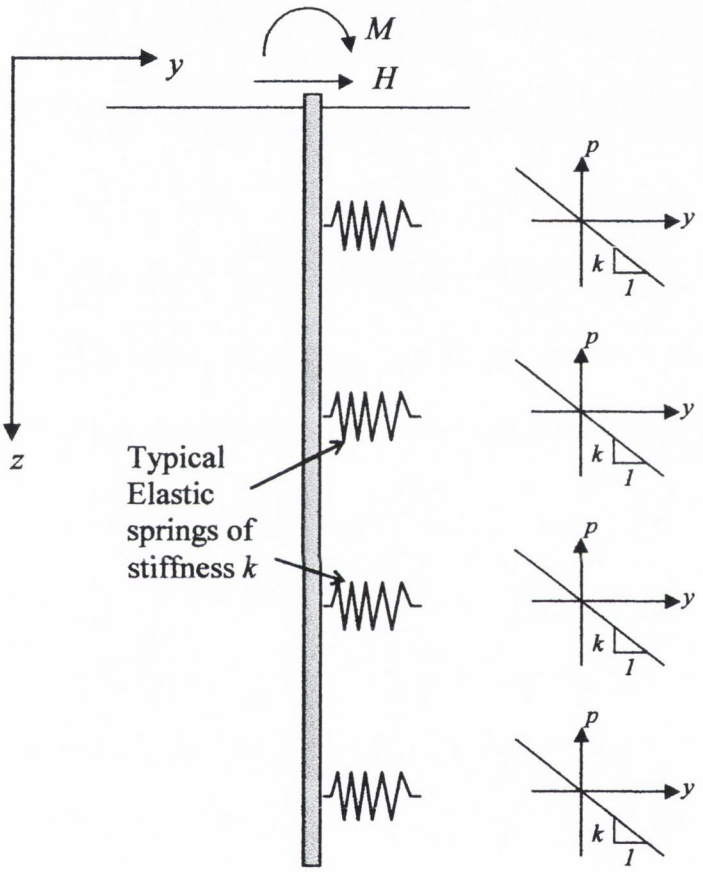

Figure 2-11: Assumptions for the subgrade reaction method

A long flexible pile can be treated as a beam-on-an-elastic foundation. Using beam-column theory, a fourth order differential equation (modified to include a term for the soil response) is solved to yield the displacement, shear and bending moment profiles required for pile design. The differential equation (Eq. 2-7[8] section 2.4.2) can be solved by hand

[8] Note in Eq. 2-7 k is replaced by K, the soil modulus, which is equivalent to kB where B is the pile width.

using either a closed form solution if k is assumed to be independent of depth (homogeneous soil) or in the case of a soil with k increasing with depth, a power series solution can be employed. Both methods further assume linearly elastic soil behaviour, and a pile of constant flexural stiffness. Hetenyi (1946) devoted an entire book to solving beam on elastic foundation problems subjected to various boundary conditions. Broms (1964a) also used the theory of subgrade reaction to analyse piles subjected to lateral load. These methods were only intended to be accurate at working loads and therefore will underestimate the pile displacements once the soil yields.

Concluding Comment

Typical results from the subgrade reaction method are presented in Figure 2-12. As the subgrade reaction method assumes linear elastic behaviour of both the soil and the pile, the accuracy of the solution is limited to predictions of displacements and bending moments at the lower stress levels encountered under working loads. Moreover, the non-linear response (even at low stress levels) and eventual plastic behaviour of the soil near the ground surface is not accounted for in this model. These limitations can be addressed by employing the *p-y* method outlined in the following section.

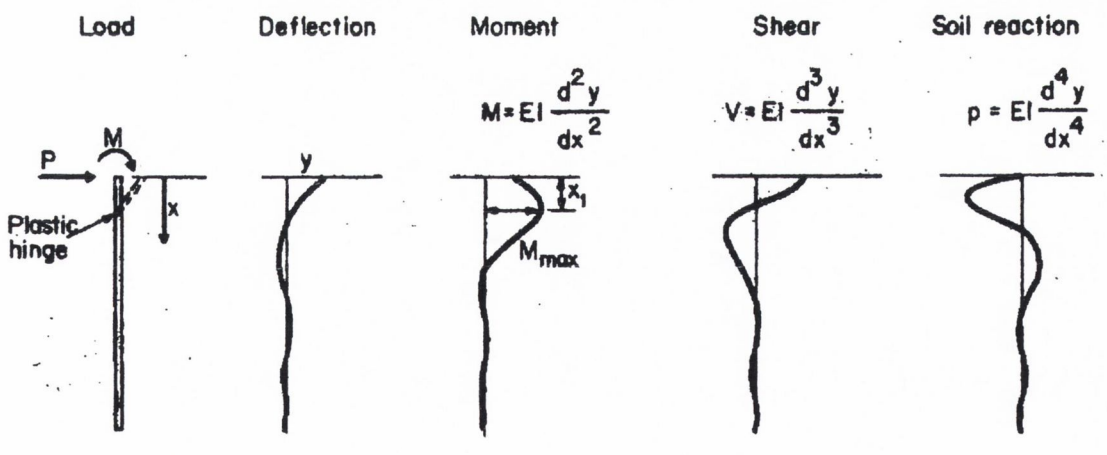

Figure 2-12: General results obtained from a laterally loaded flexible pile (from Hunt 1986)

2.4 *p-y Method*

2.4.1 Background

The *p-y* method can be considered as a Winkler foundation that extends the soil response beyond the linear elastic range to include yielding of the soil. This extension provides more realistic and accurate predictions of pile performance, particularly when yielding or degradation of the soil resistance due to cyclic loading needs to be considered.

Two problems must be solved to obtain the response of a laterally loaded pile: (1) the soil resistance must be known as a function of depth, pile deflection, pile geometry and the nature of loading; and (2) the equations that yield pile deflection, bending moment and shear must be solved.

2.4.2 *p-y* Concepts of Lateral Load Transfer[9]

When a pile (modelled as a beam-column) is inserted vertically into the ground, the supporting soil surrounding the shaft is considered as a series of non-linear elastic springs as depicted in Figure 2-13(b). It is generally acknowledged that such a soil model is not strictly true (Reese, 1977 and others) but experimental evidence indicates that the soil reaction at a point is dependant essentially on the pile displacement at that point, and not on pile displacements above and below. Therefore, for the purposes of simplifying the analysis, the soil can be removed and replaced by a set of discrete springs.

[9] The *p-y* curves generally employed by practitioners do not consider consolidation effects that would occur under sustained loading. Nor do they consider cases where the loadings are dynamic, as would occur during an earthquake. However, recent research by El Naggar and Bentley (2000) has proposed a model for obtaining dynamic *p-y* curves that relate the pile displacements to the non-linear soil reactions. These methods are beyond the scope of this research and therefore will not be discussed further.

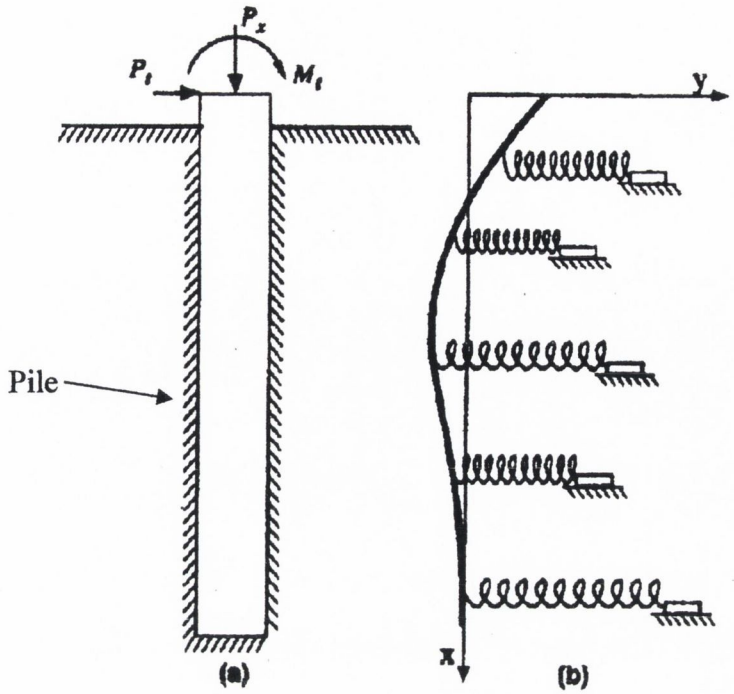

Figure 2-13: Idealisation of soil around pile (from Reese 1997)

The concept of a *p-y* curve can be defined graphically by considering a thin slice of pile and surrounding soil as shown at section x-x in Figure 2-14. When the pile is subjected to a lateral load it will move laterally until equilibrium is established between the stresses and displacements of both the soil and the pile at each point along its shaft. The earth pressures acting on the thin slice of pile considered prior to lateral loading (Figure 2-14b) are assumed to be uniform and the resultant soil reaction, *p*, (in units of kN/m) obtained by integrating the pressures, is zero. If the pile is then given a lateral displacement, *y*, as shown in Figure 2-14a, the state of stress around the pile changes to a non-uniform distribution resulting in a net soil reaction upon integrating the pressures over the depth of the thin slice.

This process can be repeated for a series of *y* values, resulting in a set of corresponding *p* values, these are combined to define a *p-y* curve for the soil at the depth considered. A number of these curves are necessary to describe the full soil-pile resistance profile. The spacing between the *p-y* curves is reduced within the relatively shallow depth of soil below the ground surface that controls the pile behaviour, this depth is referred to as the critical

depth[10]. Fewer curves are required below the critical depth in order to complete the profile. Because of the non-linear stress-strain behaviour of most natural soil deposits, the *p*-y curves are also non-linear as illustrated in Figure 2-15.

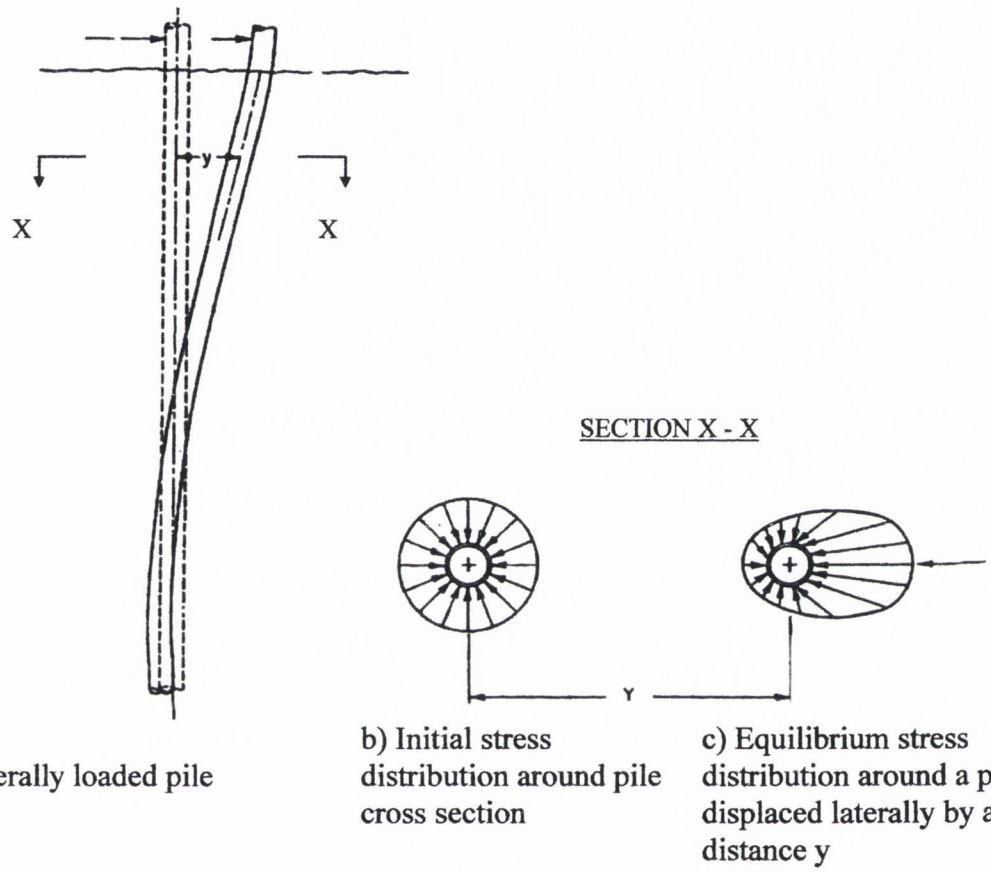

a) Laterally loaded pile

b) Initial stress distribution around pile cross section

c) Equilibrium stress distribution around a pile displaced laterally by a distance y

Figure 2-14: Graphical definition of *p* and *y* (from Yegian and Wright, 1973)

In the *p*-y method, the constant of proportionality k_h from the subgrade reaction method is replaced by the subgrade reaction modulus[11], K obtained from the secant of the *p-y* curve shown in Figure 2-16.

[10] The critical pile depth can be considered as the pile length beyond which the presence of additional pile length has negligible effect on pile-head behaviour.

[11] K has been given a variety of names. It is the foundation stiffness but it has been called the *coefficient of subgrade reaction* or *subgrade modulus*. In American literature, the coefficient is called a *soil modulus* and is denoted by the symbol E_s. This definition leads to confusion with Young's modulus of elasticity which also has units of stress. In this thesis, the symbol K will be used to avoid such confusion.

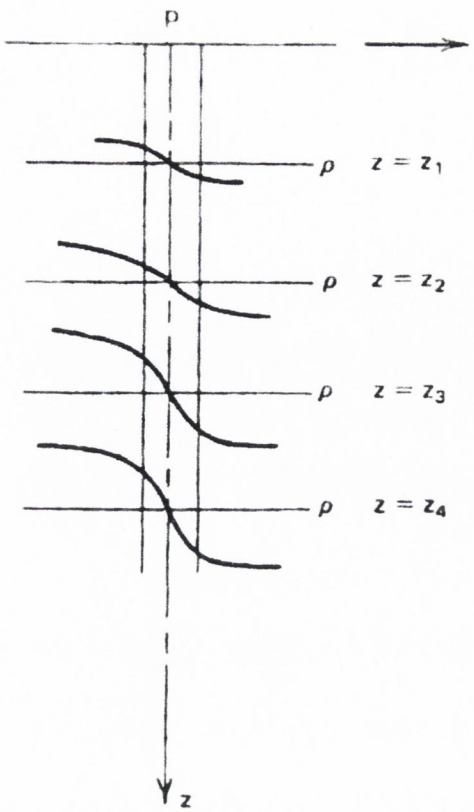

Figure 2-15: Possible family of *p-y* curves (from Poulos and Davis, 1980)

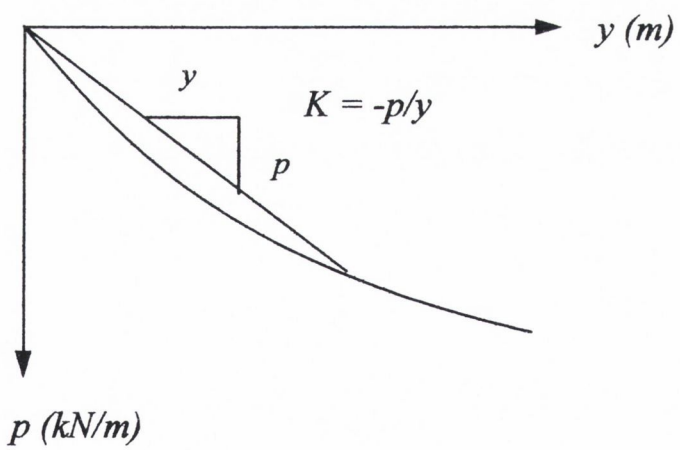

Figure 2-16: Illustration of secant soil modulus (spring stiffness)

The negative sign in the expression shown in Figure 2-16 indicates that the direction of pile displacement is opposite to the direction of the soil reaction. Because the curve is strongly non-linear and varies with depth, K is not a constant except for a small range of

displacements, the soil modulus[12] changes from an initial stiffness K_i to an ultimate stiffness $K_u = p_u/y_u$. Because p varies with both y and z a numerical method, normally the finite difference technique is employed to solve the differential equation shown in Eq. 2-7. The solution provides the displacement, moment and shear profiles for the loaded pile.

Eq. 2-7... $$EI\frac{d^4y}{dz^4} + F_z\frac{d^2y}{dz^2} + K\ y = 0$$

where

E = Young's modulus for the pile

I = Second moment of area of the pile

F_z = Axial load

y = Lateral deflection

z = Depth below the pile top

Before the advent of computers, the closed form analytical solutions were popular but imposed the restriction of a constant soil modulus. Series-type solutions (Hetenyi, 1946) were also available for a linear variation of soil modulus with depth however; both these methods were adopted for their mathematical convenience rather than their ability to represent the real soil behaviour. As these simplified soil models restrict the nature of the soil modulus variation, and hence the ability to accurately predict the pile behaviour, the *p-y* approach has been adopted as a more realistic representation of the soil modulus.

Criteria for constructing "generic" *p-y* curves in different soil media have been published on the basis of validation from full-scale pile load test. Meyer and Reese (1979) present a review of the *p-y* formulations that emanated from the original tests and illustrate the usefulness of the approach (a summary of these formulations is provided in Appendix 2b). However, the established *p-y* criteria are limited to soils of one type and therefore judgment

[12] The soil modulus K, has units of force per length squared, given by the soil reaction p at a point along the pile divided by the movement of the pile into the soil at the same point y, it can be considered as the spring stiffness of the soil i.e. $K = kB = p/y$.

and experience is required when selecting *p-y* curves for situations that deviate from those in the original database. The following section presents some recent advances in the derivation of *p-y* curves, which help make the method more accessible to designers.

2.5 Recent Advances in the p-y Method

2.5.1 *p-y* Curves from In-situ Tests

The work outlined in section 2.4 has represented a major step forward in the solution of laterally loaded pile problems. It is believed that in-situ tests such as the pressuremeter and DMT represent an additional advance by allowing the quality and range of applicability of the *p-y* curve approach to be improved. The pressuremeter offers the following advantages:

(1) The *p-y* curve is obtained point by point in situ with the pressuremeter. Utilising curves based directly on in-situ testing removes a level of uncertainty introduced by correlating, for example, SPT 'N' values with soil strength properties.
(2) The pressuremeter test can be performed in almost all soils and rocks and therefore is very versatile.
(3) The method of installation of the pile can be duplicated by the method of installation of the pressuremeter; for example in the case of a bored pile, preboring the hole for the pressuremeter seems to be appropriate; in the case of a closed-end driven pile, it may be more appropriate to drive the pressuremeter in place. Alternatively, for displacement piles the hole can be bored, the pressuremeter expanded a first time to simulate the driving of the pile and then expanded a second time.
(4) The type of loading can easily be simulated during the pressuremeter test including long-term sustained loads, cyclic loads and the rate of loading effects. Furthermore the incorporation of pressuremeters into CPT equipment as shown in Figure 2-17 (see Lunne et al., 1997) has led to the economic production of *p-y* curves at the SI stage thereby facilitating early design of laterally loaded piles.

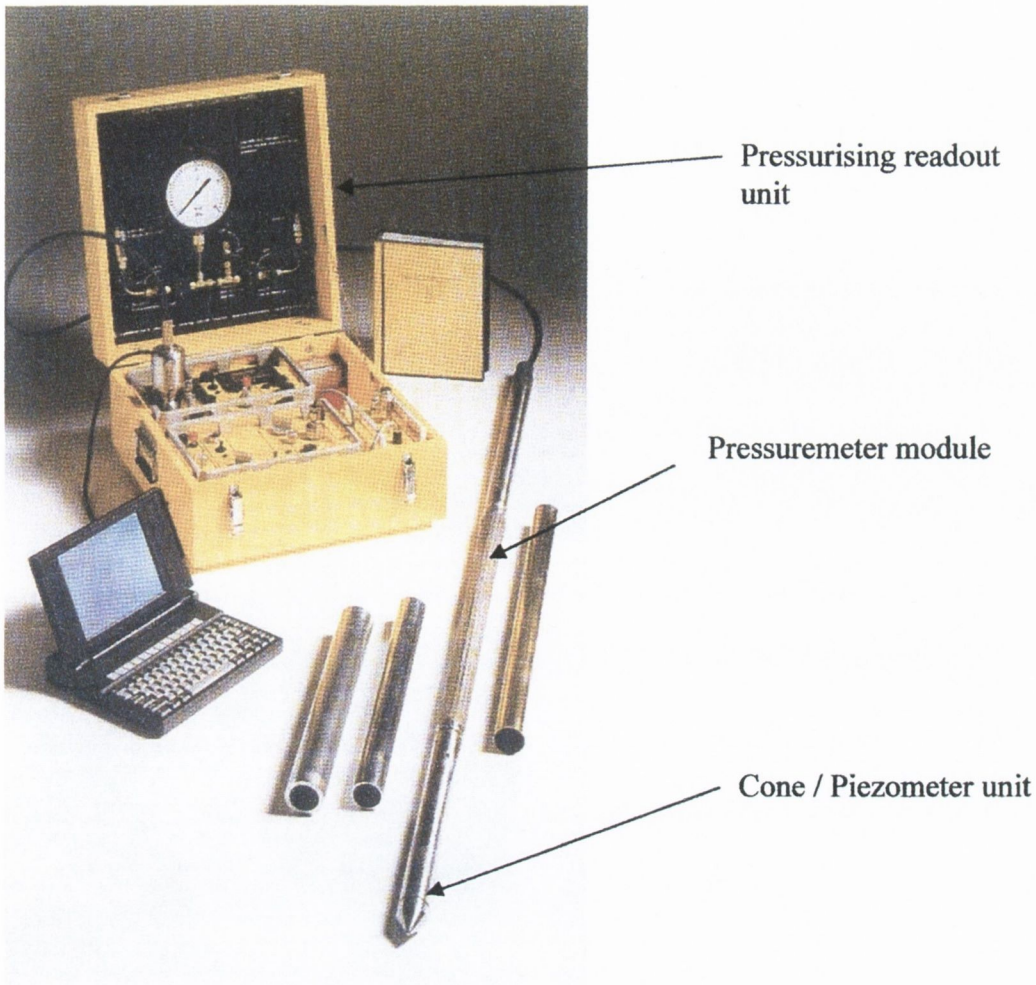

Figure 2-17: Cone pressuremeter equipment (from Dalton, 1997)

The dilatometer, unlike the pressuremeter, produces only a very small lateral displacement (≈1mm) plus there are no increments of pressure with which to develop a load-deformation curve. Therefore, the properties determined from the dilatometer indices are used in conjunction with a mathematical expression[13] to develop *p-y* curves.

Because of the availability of good quality pressuremeter results from the test site used in this research, the following section will outline in detail the technique used to develop *p*-y curves from pressuremeter tests. The analogy between the pressuremeter curve and the *p-y* curve can be seen in Figure 2-18.

[13] Gabr et al. (1994) and Anderson and Townsend (1999) used hyperbolic and parabolic functions respectively to develop *p-y* curves from dilatometer results.

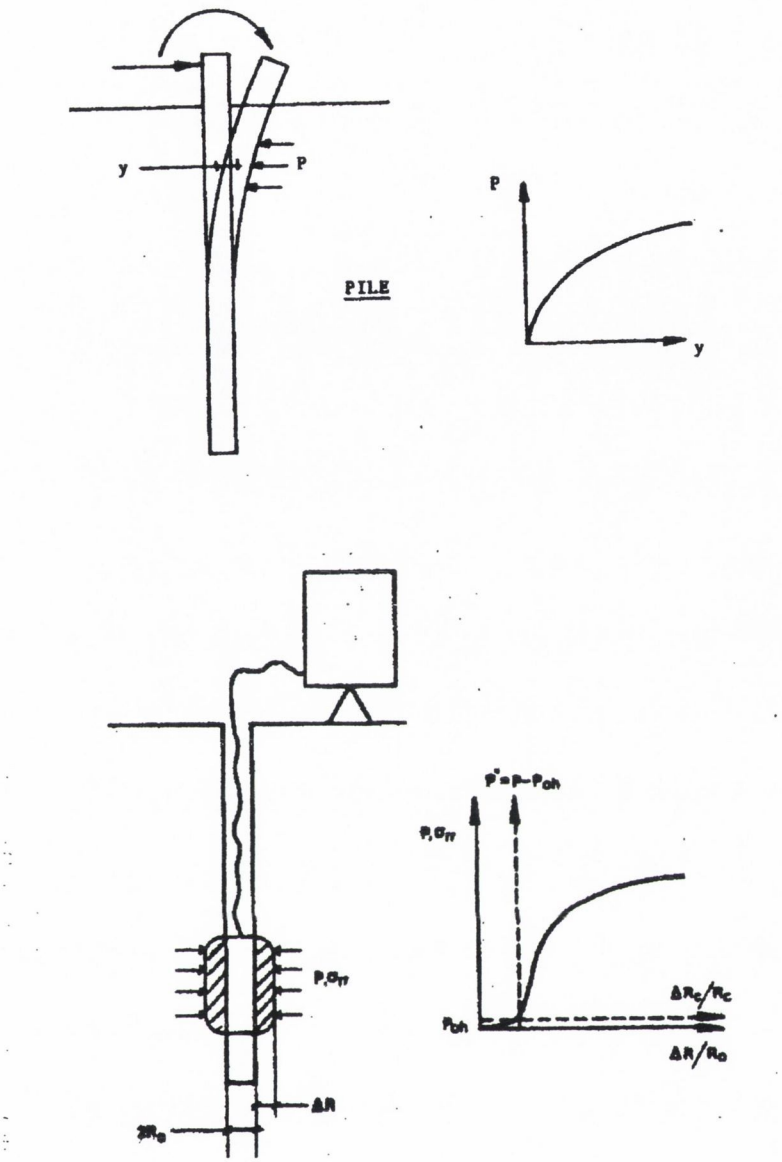

Figure 2-18: Pressuremeter-pile analogy (from Briaud, 1992)

The various types of pressuremeter, their operation and the interpretation of the test results have been described in detail by Clarke (1995), Clarke (1997) and Briaud (1992). Nine pressuremeter approaches for the design of laterally loaded piles have been identified in Briaud (1992). Of these, the approach for pushed-in (full displacement) pressuremeter tests proposed by Robertson et al. (1982 and 1986), is relevant to the research undertaken for this thesis since the probe installation models the soil disturbance caused by pile driving. The Robertson et al. (1986) *p-y* construction, utilising results from full displacement pressuremeter tests, have been validated via case histories by the authors and more recently by Anderson and Townsend (1999) and Anderson et al. (1999). The critical

depth phenomena, which accounts for the reduced soil resistance close to ground level, was incorporated into a method proposed by Smith (1983) and Briaud et al. (1985d) for preboring pressuremeter tests and was adopted by Robertson et al., (1986) in the full displacement pressuremeter method. Therefore the Briaud-Smith approach will also be reviewed in this section.

p-y Curves From Pressuremeter Tests

Robertson et al. 1982 and 1986

Robertson et al. (1986) suggested a method that used results from a pushed-in pressuremeter to evaluate *p-y* curves for a driven displacement pile. The pressuremeter was a conventional self-boring pressuremeter with a solid 60° cone at the tip but was pushed into the ground by jacking against a vehicle designed for conducting electric cone penetration tests. The instrument was 76mm in diameter with the membrane section having a length to diameter ratio for of six. Robertson et al. (1982) hypothesised that the initial displacement induced in the soil surrounding a driven pressuremeter faithfully represents the displacements in the soil surrounding a driven pile. Therefore, results from a series of pressuremeter tests performed at different depths, can be used to provide the *p-y* response of the soil at the test depths. In Robertson et al. (1982) *p-y* curves were obtained for a 300mm square precast concrete pile driven into the soil profile shown in Figure 2-19; piezocone results are also provided in the Figure.

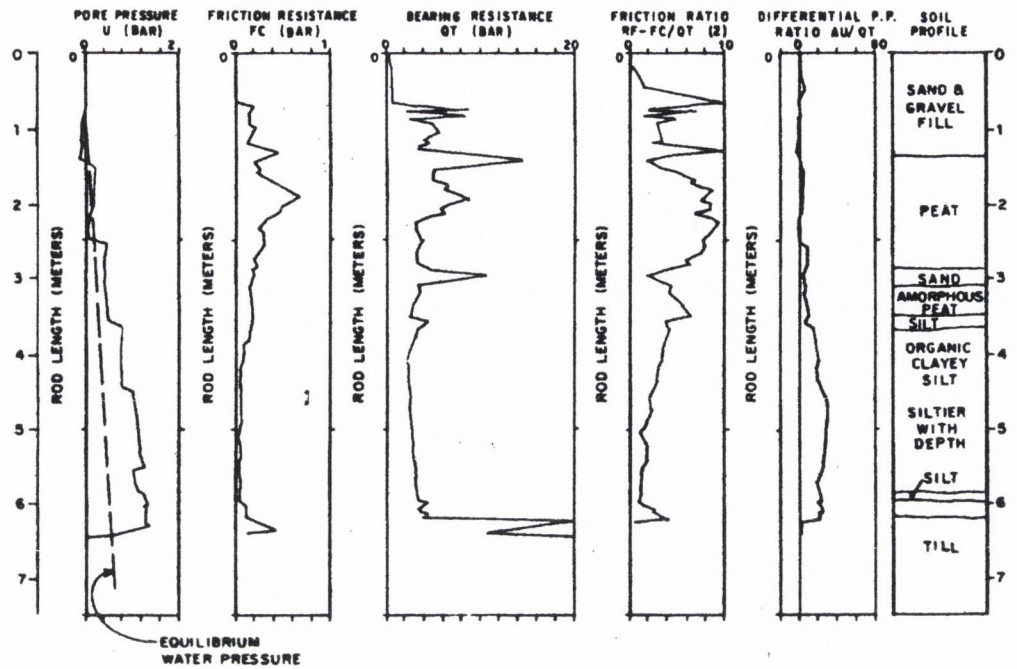

Figure 2-19: Soil profile at the Robertson et al. (1982) test site

According to Robertson et al. (1982), the soil deforms in a simple radial direction during a pressuremeter test, whereas the displacements in the soil surrounding a laterally loaded pile are far more complex, as the soil moves away from the front face of the pile and inwards towards the back face. It was suggested that the soil in the centre region of the pile (*A-B*) in Figure 2-20(a) would deform in a similar manner to that about a pressuremeter. It was therefore concluded that the geometric form of the pressure expansion curve obtained from the pressuremeter would be similar to the *p-y* curve for the soil acting in front of the pile, provided the pressuremeter was installed to model the soil disturbance during pile installation.

The curve p_0Ap_L shown in Figure 2-20(b) represents a typical test from a self-boring pressuremeter in which the probe was inserted into the soil with no disturbance where p_0 is the initial total stress, and p_L is the limit stress (at which indefinite cavity expansion occurs). Therefore the geometric form of the *p-y* curve is given by p_0Ap_L, that is, the origin for the pressure would be moved to p_0 (as shown in Figure 2-20(c)).

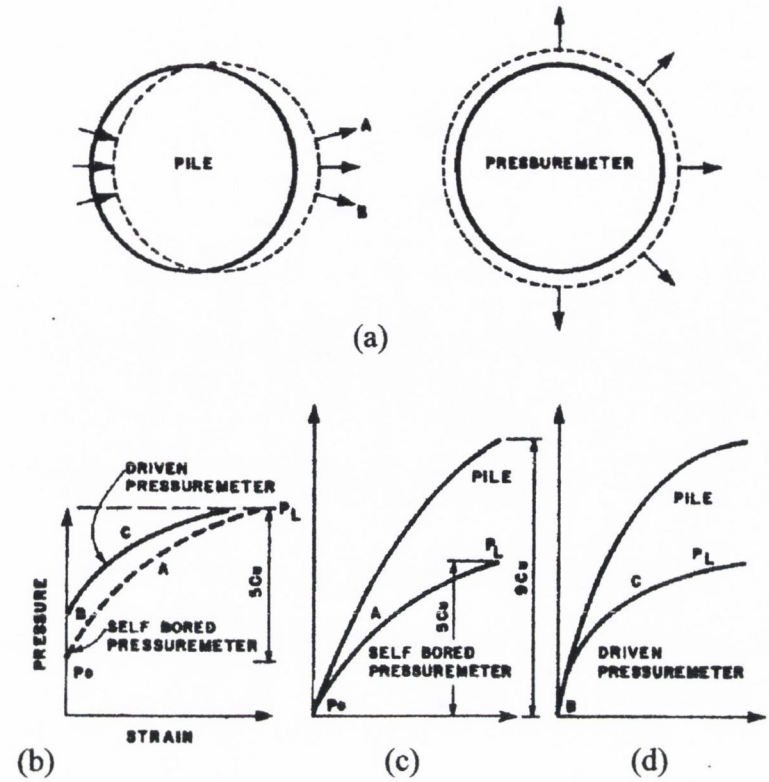

Figure 2-20: Schematic showing development of *p-y* curves from pressuremeter data (from Robertson et al., 1982)

TRANSFORMING PRESSUREMETER CURVES INTO *P-Y* CURVES

The limit pressure $(p_L\text{-}p_0)$ for the pressuremeter test is different from the limiting pressure required to push a pile sideways through the soil. If the section of the pile considered is at some distance remote from the surface i.e., where plane strain conditions exist, then the limiting lateral resistance is approximately $9c_u$, where c_u is the undrained shear strength. In the case of the pressuremeter, the limiting pressure[†] $(p_L - p_0)$ is approximately $5c_u$.

[†] The limit pressure for cohesive soil was defined in Briaud (1992) as $p_L = p_0 + c_u\,(1 + Ln[G/c_u])$ where p_0 is the total horizontal stress at rest, c_u is the undrained shear strength. This equation can be rewritten as $p_L^* = \beta c_u$, where p_L^* represents the net limit pressure $(p_L - p_0)$ and a value of $\beta = 5.5$ was purported in Briaud (1992) to have been suggested by Menard in 1970. However, Briaud notes that the value of β depends on ratio G/c_u which varies with the OCR of the clay. Briaud suggested reasonable limits between 100 and 600 for the ratio thus leading to values of β between 5.6 and 7.4 with an average value of 6.5. The foregoing analysis was based on an infinitely long pressuremeter i.e., the analysis is appropriate at depth where plane strain conditions apply. Briaud has shown that, in clays, the limit pressure for a sphere is 1.33 times the limit pressure for an infinitely long cylinder. Therefore Briaud concludes that the limit pressure for conventional pressuremeters are expected to be higher than that proposed by Menard and the average value of β needs to be higher than 6.5. Briaud's analysis suggests that the factor of 5 reported above should be increased to at least 6.5.

Non-displacement Piles

For non-displacement piles where the initial stress on the pile is ≈ the same as the initial stress in the ground, the pressuremeter curves obtained from self-boring pressuremeters have to be increased by some factor (α) to give the correct *p-y* curves for the pile. The multiplying factor α, accounts for the fact that laterally loaded piles have limiting soil reactions that are higher than those for radially expanding pressuremeters (due primarily to three dimensional effects). In recognition of this, the following multiplying factors were recommended in Robertson et al. 1982 and 1986:

$\alpha = 2$ for cohesive soils

$\alpha = 1.5$ for cohesionless soils

The multiplying factors were confirmed by Byrne and Atukorala (1983) using finite element analyses, but further research was recommended to refine these numbers for different soil types. The application of the multiplying factors to the pressure component of the pressure expansion curve is shown in Figure 2-21.

Displacement Piles

The above procedure has to be modified slightly for driven piles. It has been observed that the limit stress p_L in a pressuremeter test is almost independent of the method of installation of the probe. However, the initial stress before expansion is dependent on the method of insertion. The result of an idealised pushed-in pressuremeter curve is given by BCp_L in Figure 2-20(b). The initial stress on the probe (point B) is above the in-situ lateral stress p_0. If it is assumed that the shape of the *p-y* curve follows the pressuremeter curve, then the pressuremeter curve must be magnified further, such that the limiting pressure ($p_L - p_0$) still equals $9c_u$.

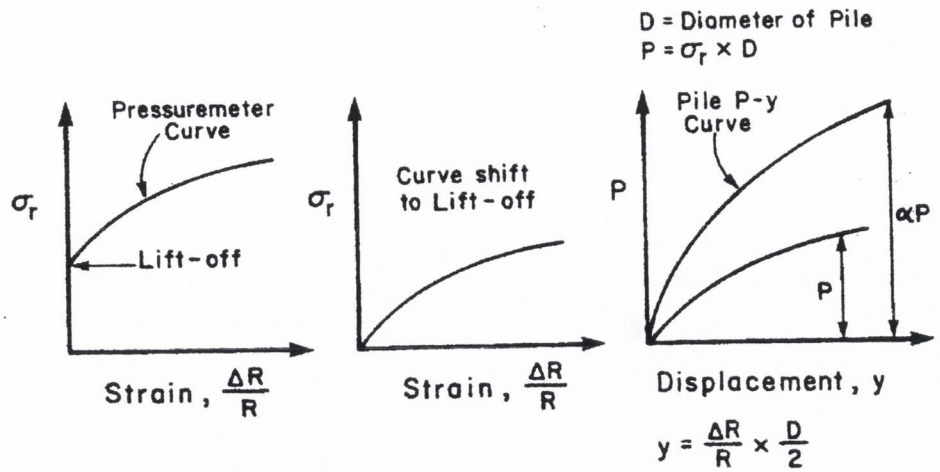

Figure 2-21: Schematic representation illustrating the transformation of pressuremeter curves to *p-y* curves (from Robertson et al., 1986).

Conditions Close to the Ground Surface

At shallow depths, the pressuremeter is subject to a reduction in the mobilised resistance near the ground surface. This reduction affects both the displacements of the laterally loaded pile and the expanding pressuremeter. The following critical depths (z_c) (within which a reduced resistance can be expected) have been proposed by Baguelin et al., 1978):

$$z_c = 15\ D_{PMT} \quad \text{for cohesive soil}$$

$$z_c = 30\ D_{PMT} \quad \text{for cohesionless soil}$$

where D_{PMT} = diameter of the pressuremeter

The pressure component of the near surface pressuremeter curve is then corrected using a reduction factor (β); the reduction factor will be discussed in the next section on *p-y* curves derived from preboring pressuremeter tests. Similarly, the soil displacement around a laterally loaded pile is also influenced by the ground surface. In the case of a pile the critical depth (D_c), to which resistances are reduced, depend on the pile load in addition to its diameter and stiffness. To account for the reduced resistance near the ground surface,

the α factor is progressively reduced as shown in Figure 2-22. Smith (1983) and Briaud et al. (1985) proposed a relative rigidity factor, RR from which D_c can be determined. A more detailed discussion on D_c will be provided in the next section. Robertson el al. (1982) suggested using a general critical depth D_c of four pile diameters, however, the relationship proposed by Briaud et al. (1985) (see Figure 2-24) is recommended in practice since it incorporates the influence of varying relative rigidities.

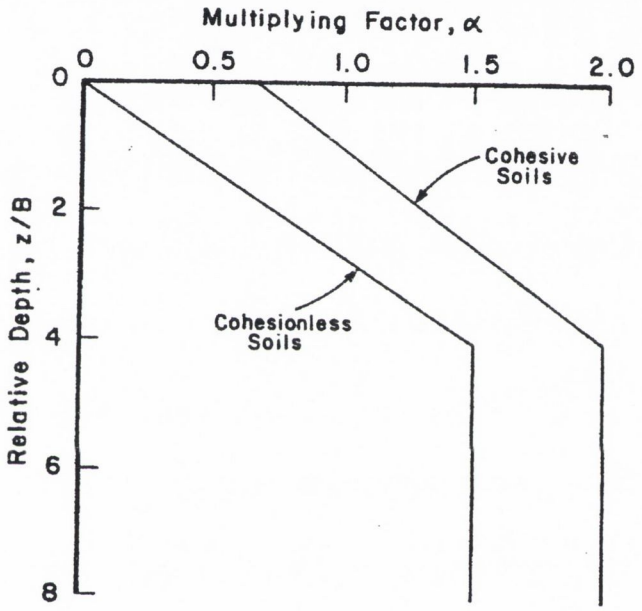

Figure 2-22: Variation of multiplying factor with relative depth (from Robertson et al., 1986)

p-y curves required for pile analyses were obtained by converting the pressuremeter stress (σ_r) by multiplying by the pile width and the α factor to give the soil resistance in units of force per unit length. The radial strain[14] measured by the pressuremeter, is multiplied by half the pile width to obtain the soil displacement *y*. The pressuremeter *p-y* curves were used by Robertson et al. to predict the lateral load-pile head displacement for a range of case histories, the results gave good agreement between the measured and calculated pile head displacement, indicating that the method may have applicability in other situations.

[14] The radial strain is given by ΔR/R where R is the initial radius of the probe and ΔR is the change in radius.

Smith 1983 and Briaud et al. 1985

Briaud et al. (1985) proposed a method using the results from a preboring pressuremeter to predict the behaviour of 17 laterally loaded piles of varying sizes and lengths, which underwent full scale testing at various sites. The piles included driven and bored piles ranging from 0.32m to 1.37m in diameter and from 3m to 21m in length. Soil failure was considered in terms of deep and shallow soil behaviour; at depth, plane strain or flow around conditions dictate. The authors suggested the overall soil resistance, p_{ult}, at depth is derived from two components; firstly, the dominant frontal component *Q (kN/m)* and secondly, *F (kN/m)* the frictional resistance along the pile soil interface.

Justification of the two component model was provided by back analysing experimental results from a lateral load test on a 0.9m diameter bored pile containing pressure cells on the passive side of the pile[15]. The free-headed pile was constructed in stiff clay (c_u = 100kPa measured in a UC triaxial test) and loaded 0.75m above ground level. The soil resistance due to the front resistance (Q) was calculated from the pressure cell readings. By considering front resistance only, Briaud et al. (1985) found horizontal and moment equilibrium could not be obtained for the pile. However, it was found that if frictional resistance on the soil-pile interface, corresponding to the full shear strength of the soil, were included, both horizontal and moment equilibrium were approximately satisfied[16]. This finding indicates: (1) the frictional resistance is an important part of the total resistance. Briaud et al. (1984) evaluated various pressuremeter approaches used to model the behaviour of laterally loaded piles, they concluded that the contribution from pile-soil interface friction might be as much as 50% of the total resistance at working loads, and (2) the frictional resistance is fully mobilised before the front resistance because it takes less displacement to mobilise friction than bearing resistance. Briaud et al. (1985) therefore

[15] The lateral soil pressures measured using pressure cells were correlated with the results from pre-bored pressuremeter tests. If however, the pile was driven into the soil and fully displaced it, Briaud et al. (1985) noted the resulting Q profile would be different from the one for a bored pile in the same clay. They suggested that the Q response for the driven pile be derived from the reload portion of the pressuremeter curve.

[16] The soil resistance due to friction was calculated as $F = \tau_{r\theta(max)}(2r_0)(I)$ where $\tau_{r\theta(max)}$, r_0 and I are the maximum shear stress, the pile radius and the shape factor respectively. This allowed enough frictional resistance to exist in the back of the pile to raise the shape factor from $\pi/4$ to 1. It was also assumed that $\tau_{r\theta(max)}$ was equal to one-half the unconfined compression strength i.e., full frictional resistance was mobilised at the soil pile interface.

concluded that a soil model that distinguishes between friction and front resistance is a proper model.

The difference between deep and shallow soil resistance was acknowledged by the Briaud et al. (1984). The transition from deep to shallow failure occurs at a depth known as the critical depth, D_c. If there was no weakening influence due to the close proximity of the stress free ground surface, the variation of resistance in a uniform soil would be as shown by the dotted line CD in Figure 2-23. Where there is a reduction in soil resistance towards the surface, the soil resistance distribution follows CBA with a maximum resistance $p_{(max)}$, at D_c. The shallow soil resistance for piles loaded laterally was obtained by multiplying the deep resistance by a reduction factor, α. Within D_c the soil resistance p is less than $p_{(max)}$ and the ratio $p/p_{(max)}$ defines the reduction factor α.

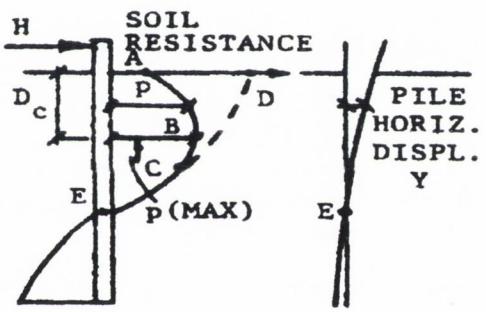

Figure 2-23: Definition of the pile critical depth.

The critical depth D_c is a soil-structure interaction phenomenon similar to that discussed previously in section 2.2.1. Smith (1983) defined an interaction factor (referred to as the relative rigidity) *RR* for the preboring pressuremeter method:

$$RR = \frac{1}{B}\sqrt[4]{\frac{EI}{p_L^*}}$$

where B is the pile diameter and p_L^* is the pressuremeter net limit pressure within the critical depth. In a study of ten different piles Briaud (1992) showed that piles of different rigidity in the same soil generate different relative critical depths, D_c/B (see Figure 2-24). Furthermore, the same pile generates different relative critical depths in different soils.

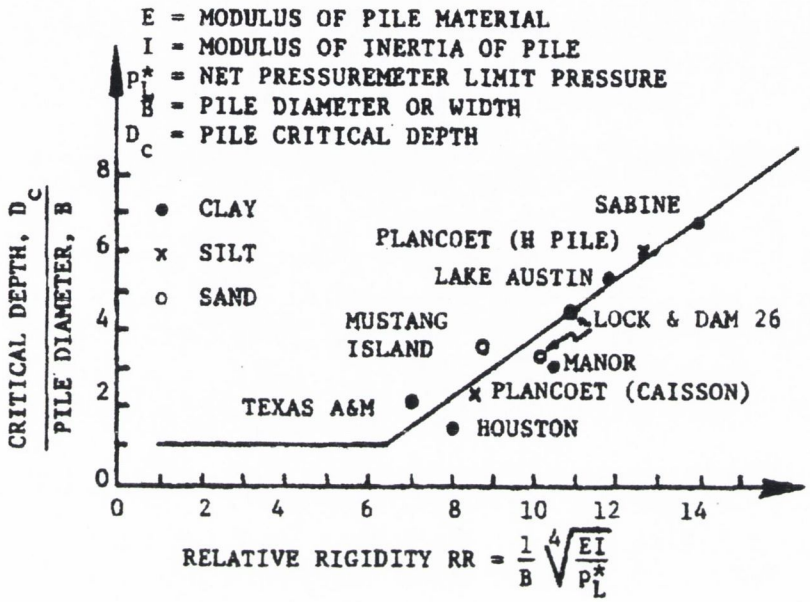

Figure 2-24: Pile critical depth versus soil pile relative rigidity

The recommended values of α which apply to the Q-y component of the p-y curve within the critical depth are shown in Figure 2-25a. The recommendations for α were based on experimental data collected for four piles in clay and two piles in sand. The α factor is not considered to apply to the F-y curve because the F-y curve is a very localised phenomenon as can be seen from Figure 2-26. It is interesting to note that the rate at which the load resistance mechanisms of skin friction and end bearing are developed in axially loaded piles, as outlined by Burland and Cooke (1974), are also evident in piles subjected to lateral loads. Figure 2-26 shows the initial frictional resistance along the sides of the pile provides resistance to lateral load at small displacements. At greater displacements the frontal resistance is mobilised and dominates the overall resistance to lateral load.

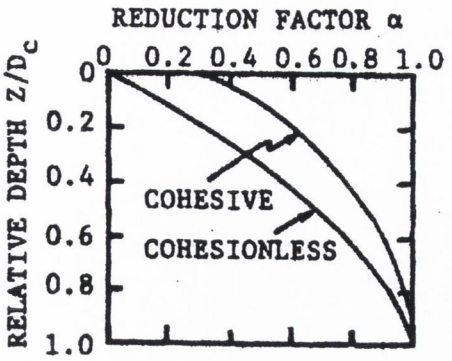

(a) Pile reduction factor, α

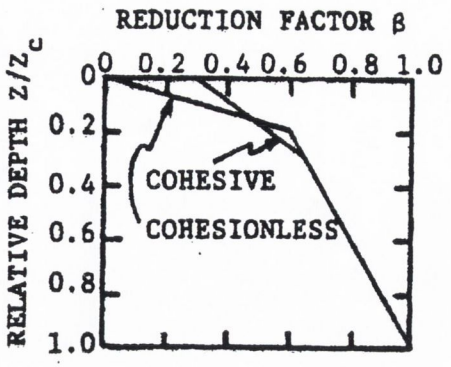

(b) Pressuremeter reduction factor, β

Figure 2-25: Pile reduction factor, α and pressuremeter reduction factor β

Pressuremeter Resistance Close to the Ground Surface

As the pressuremeter test replicates the behaviour of a laterally loaded pile at depth (Figure 2-18) it is reasonable to assume that the critical depth phenomenon also applies to the pressuremeter curve. Baguelin et al. (1978) stated that the pressuremeter appears to be below its critical depth z_c if it is one metre deep in clay and two metres deep in sand. For a conventional 35mm radius probe, z_c would correspond to 30 and 60 pressuremeter radii in clay and sand respectively. Briaud (1992) concluded that this finding referred to the limit pressure. Smith (1983) conducted a finite element study to investigate the pressuremeter critical depth (z_c) problem at small strain levels. The results from Smith's study in conjunction with that of Baguelin et al.'s (1978) critical depth observation has led to the pressuremeter critical depth and reduction factor β given in Figure 2-25.

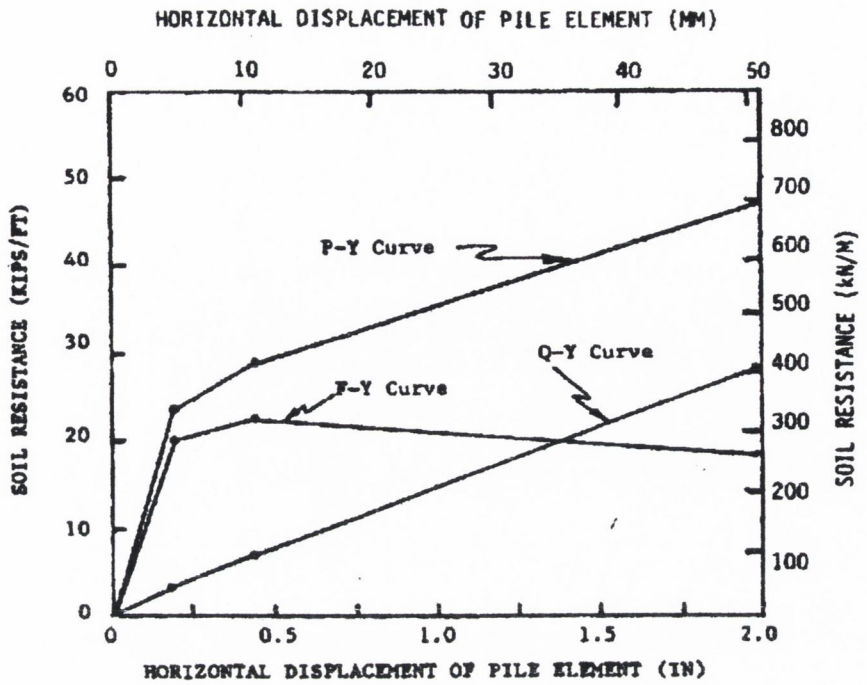

(a) Small displacements

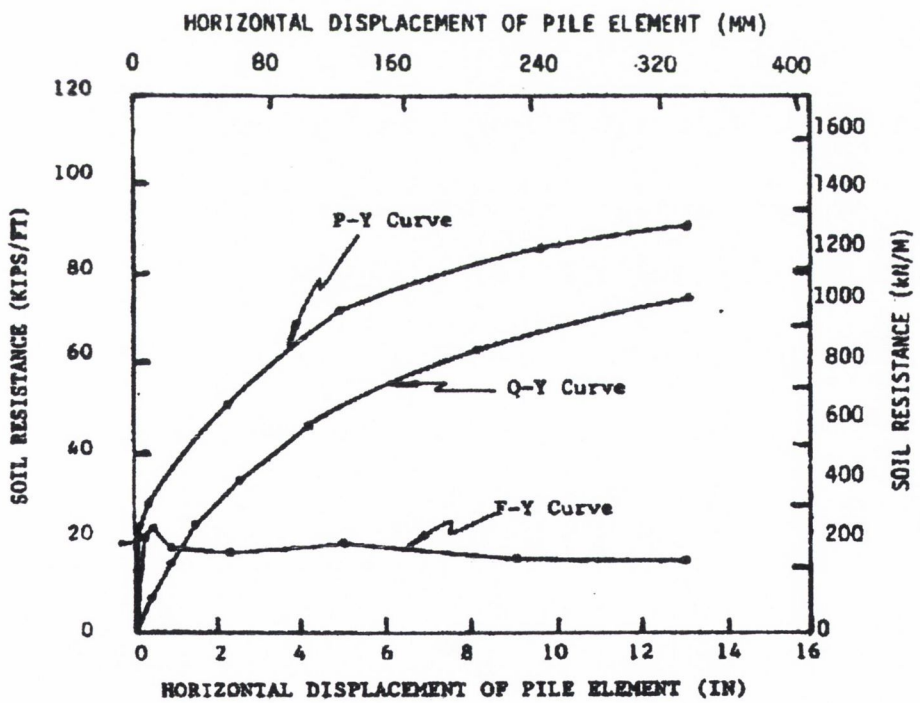

(b) Large displacements

Figure 2-26: Friction resistance, front resistance and total resistance for a typical pile element

Precision of the Preboring Pressuremeter Method for Establishing *p-y* Curves

Briaud (1992) used a database of pile load test data to determine the precision of the method. The piles in the database covered a wide range of pile types and pile insertion techniques including bored piles, pipe piles, H piles and precast concrete piles. The pile lengths varied from 3m to 25m and the diameters from 0.27m to 1.37m. The soils included sand, silt and clay as well as layered profiles. For each pile, preboring pressuremeter tests were performed next to the pile and the horizontal load-displacement curve at the pile top was predicted. On the same graph the measured curve obtained during the load test was plotted. In comparing the results, the loads obtained at a value of horizontal deflection equal to 10% (defined as ultimate) and 2% (small movements) of the pile diameter were compared in Figure 2-27 (a) and (b) respectively and shows that the method predicted the measured behaviour very satisfactorily.

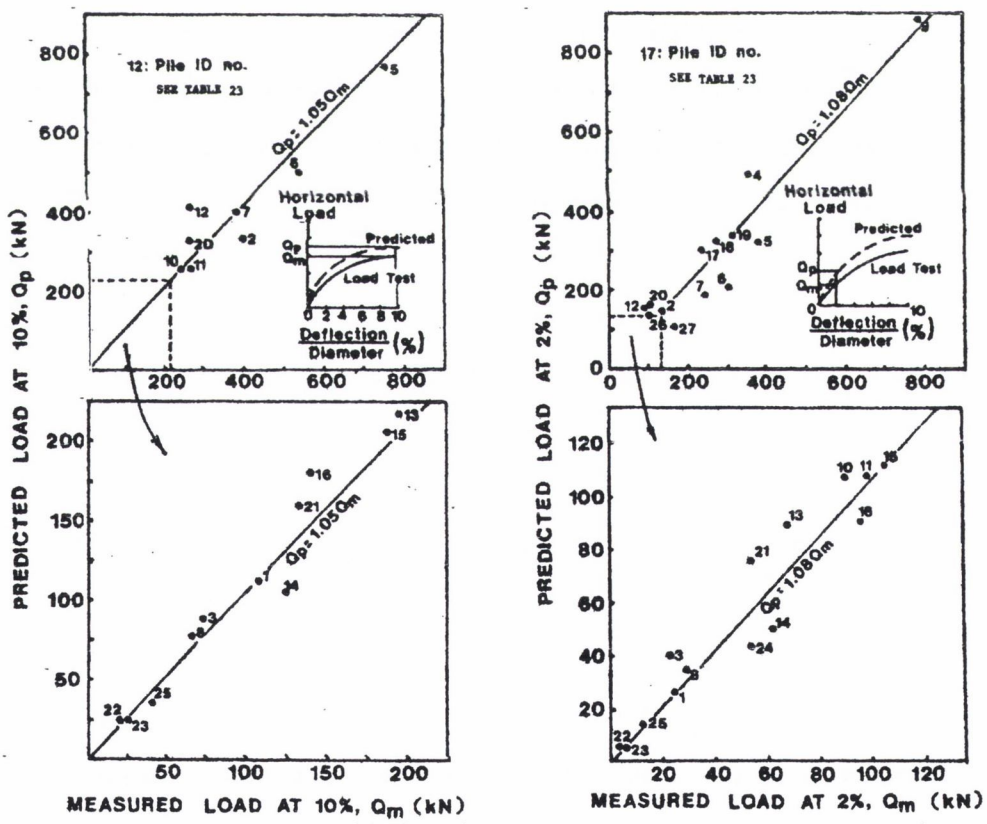

(a) Predicted vs. measured horizontal loads at a displacement equal to 10% of the pile diameter

(b) Predicted vs. measured horizontal loads at a displacement equal to 2% of the pile diameter

Figure 2-27: Precision of the pressuremeter method for predicting pile behaviour.

2.5.2 Strain Wedge Model

Although the traditional non-linear *p-y* characterisation provides reasonable assessment for a wide range of laterally loaded piles, Ashour et al. (1998) found that the *p-y* curve depends not only on the soil properties but also on the pile properties (width, shape, bending stiffness and pile head conditions). To cater for these parameters Ashour et al. (1998) proposed the strain wedge (SW) model, which permits the influence of the pile properties on the *p-y* response of the soil to be investigated.[17] The SW model employs an effective stress analysis (ES) for both sands and clays[18] and requires only soil properties that are readily attainable from standard laboratory tests.

These parameters are used to develop an envisioned three-dimensional (3-D) passive wedge of soil developing in front of the pile. The basic purpose of the SW model is to relate the stress-strain-strength behaviour of the soil in the wedge to one-dimensional (1-D) beam on elastic foundation (BEF) parameters. The model therefore provides a theoretical link between the more complex 3-D soil-pile interaction and the simpler 1-D BEF characterisation i.e., the soil-pile interaction is modelled through the modulus of subgrade reaction. The correlation between the SW response and BEF characterisation reflects the following interdependence:

- The horizontal soil strain (ε_h) in the developing passive wedge in front of the pile to the displacement pattern (y versus depth, x) of the pile

- The horizontal soil stress change ($\Delta\sigma_h$) in the developing passive wedge to the soil-pile reaction (p) associated with the BEF

- The non-linear variation in the Young's modulus ($E_h = \Delta\sigma_h/\varepsilon_h$) of the soil to the non-linear variation in the soil subgrade reaction ($K_s = p/y$) associated with the BEF characterisation.

---

[17] The SW model pertains only to the soil behaviour and no truncation due to the development of a plastic hinge forming in the pile is applied to the *p*-y curves presented in this section.
[18] Therefore, the mobilised angle of friction φ_m in clay is not zero.

The reason for linking the SW model to the BEF analysis was to allow the appropriate selection of BEF parameters to solve the governing fourth order differential equation presented in section 2.4.2 (Eq. 2-7). It should be noted that the SW model, although based on theoretical concepts, is a semi empirical approach because the stress-strain characterisation of the soil has been formulated from the observed behaviour during triaxial tests. The SW model yields successive points on the *p-y* curves caused by a change in the modulus of subgrade reaction, $K_s(x)$ profile with increasing soil strain ε (considered constant with depth in the wedge, hence the name strain wedge). The horizontal stress change $\Delta\sigma_h$ in a sublayer is taken equal to the deviatoric stress from a triaxial test at a strain ε and a confining pressure σ_3 equal to the effective overburden pressure σ'_{v0} acting on that sublayer. It is the resultant linear Young's modulus E $(=\Delta\sigma_h/\varepsilon)$ profile that yields the subgrade modulus ($K_s = p/y$) profile. The ES analysis for clay includes the development of excess pore-water pressure Δu with undrained loading based on Skempton's (1954) equation for pore pressure coefficients. By using an ES analysis with clay, the 3-D SW geometry (Figure 2-28a) can be defined based on the more appropriate mobilised ES friction angle φ'_m.

Soil Passive Wedge Configuration in Uniform Soils

The mobilised passive wedge in front of the pile is characterised by base angles, β_m and Θ_m; the current passive wedge depth, h; and the spread of the wedge fan angle, φ_m. These are shown in Figure 2-28a & b for uniform soil along with the horizontal stress change at the passive wedge face, $\Delta\sigma_h$, and the side shear, τ, at the soil pile interface.

One of the main assumptions associated with the SW model is that the displacement profile of the pile is linear over the controlling depth of the soil near the top of the pile[19]. This results in a constant displacement angle, δ, as shown in Figure 2-28b. This assumption allows uniform horizontal and vertical soil strains to be assessed. Changes in the shape and depth of the passive wedge, along with changes in the state of loading and pile deflection,

[19] The relationship between the actual (closed form solution) and linearised deflection pattern was established by Norris (1986).

occur with change in uniform strain in the developing strain wedge. The geometry of the wedge at any load increment is a function of the mobilised friction angle, φ_m and wedge depth h as shown by the following expressions (Figure 2-28 a & b):

$$\Theta_m = 45 - \varphi_m/2$$

or its complement

$$\beta_m = 45 + \varphi_m/2$$

The width BC of the wedge face at any depth is

$$BC = D + (h - x)\ 2\ tan\beta_m\ tan\ \varphi_m$$

where x denotes the depth below the top of the studied passive wedge and D is the width of the pile cross-section.

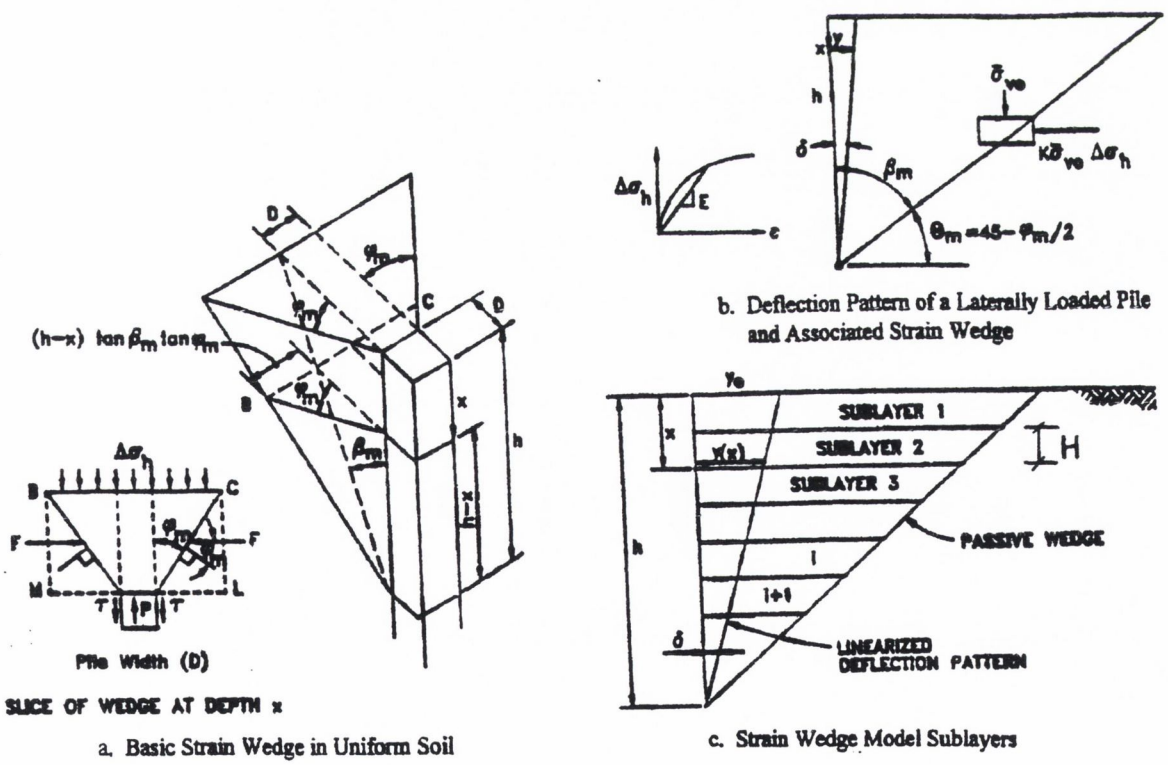

Figure 2-28: Basic configuration of strain wedge model (Ashour and Norris, 2000)

SW Model in Layered Soil

Ashour et al. (1998) extended the earlier work of Norris (1986) to account for the effect of layered soil on the response of a laterally loaded pile. The approach involved dividing up the soil profile and the loaded pile into sublayers and segments of constant thickness, respectively. Each sublayer is considered to behave as a uniform soil having its own properties according to the sublayer location and soil type while the deflection profile of the embedded pile is assumed to be continuous regardless of the variation in soil types (Figure 2-28c). The depth h of the passive wedge is controlled by the stability of the pile under the current pile-head load. This depth provides a means for distinguishing layers of different soil types as well as sublayers within each layer where conditions (ε_{50}, stress level[20] $\{SL\}$, φ_m) vary even though the soil and its properties (γ, e, or D_r, φ, etc.) remain the same. The geometry of the compound passive wedge (Figure 2-29) depends on the properties and number of soil types in the soil profile and the global equilibrium between the soil layers and the loaded pile. An iterative process is performed to satisfy the equilibrium between the mobilised passive wedge of the layered soil and the displaced profile of the pile for any level of loading.

The depth h, of the displaced portion of the pile can vary and its value at any time depends on the stability of the pile under the conditions of soil-pile interaction. The effects of the soil-pile properties are part of the soil-pile reaction along the pile length as reflected by the Young's modulus of the soil E, the SL in the soil, the pile deflection pattern (y versus x or δ), and the BEF modulus of subgrade reaction K_s between the pile segment and each soil sublayer. To account for the interaction between soil layers and between the soil and pile, the deflected length of the pile is considered to be a continuous beam of different short segments each with a uniform load resulting from the non-linear K_s supports from that sublayer (Figure 2-30).

[20] The horizontal stress level (SL) in the soil is defined in Ashour et al. (1998) as $SL = \Delta\sigma_h/\Delta\sigma_{hf}$ where $\Delta\sigma_h$ is the horizontal stress change in the passive wedge and $\Delta\sigma_{hf}$ is the horizontal stress change at failure. For clay $\Delta\sigma_{hf} = 2c_u$.

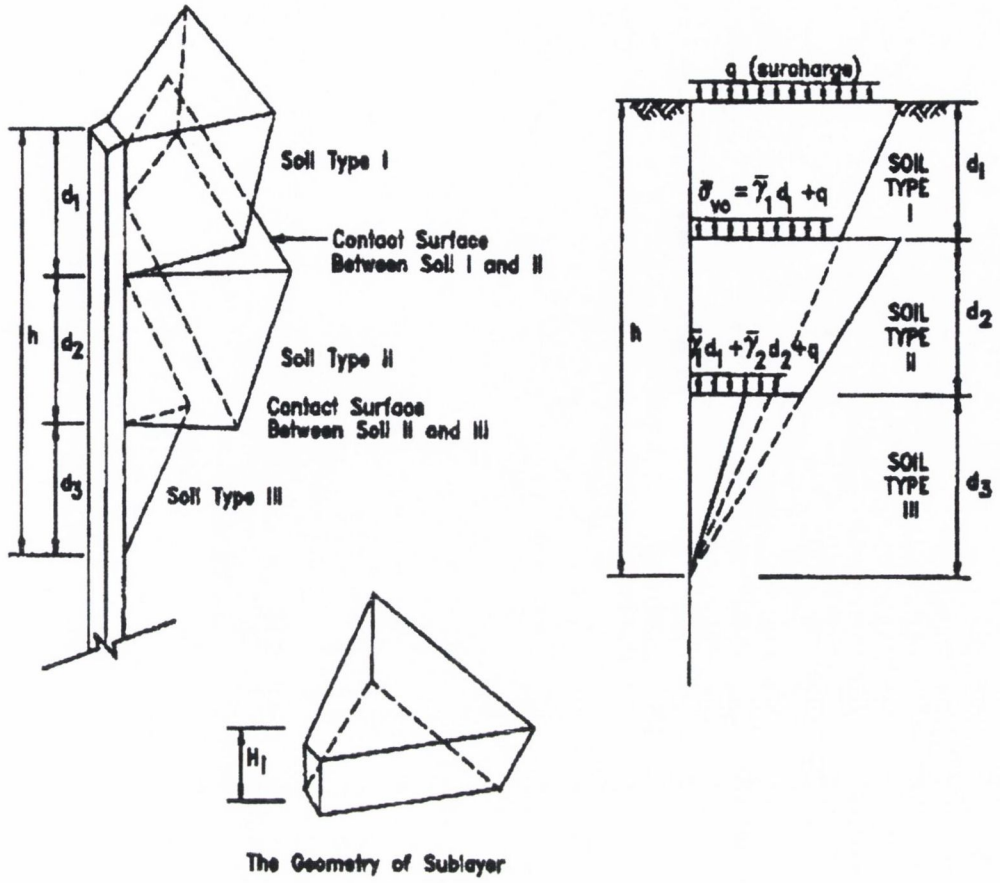

Figure 2-29: Proposed geometry of compound passive wedge (Ashour et al., 1998)

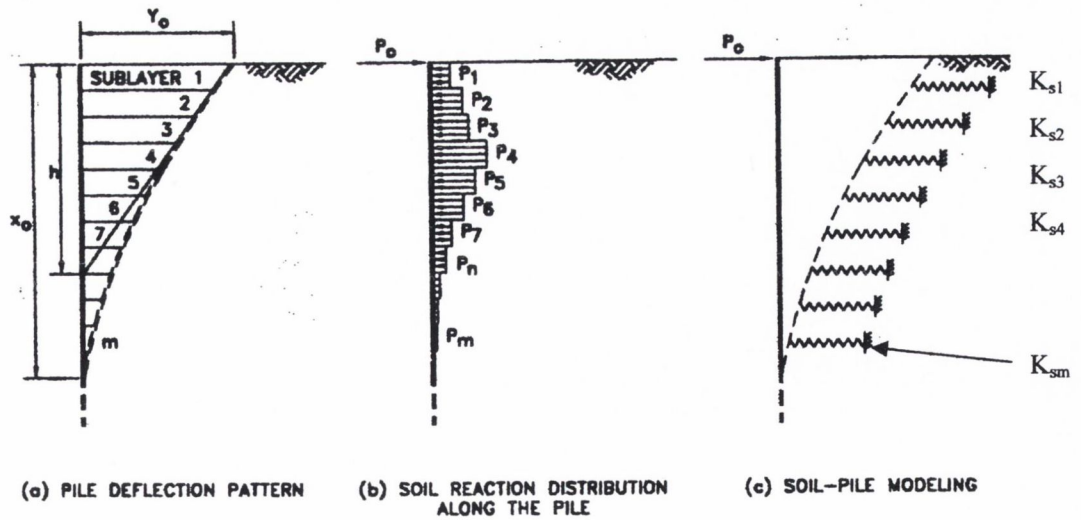

Figure 2-30: Distribution of soil-pile reaction along deflected pile (Ashour and Norris, 2000)

Effect of Soil and Pile Properties on *p-y* Curve

Ashour and Norris (2000) suggested that the traditional "Matlock-Reese" *p-y* curves required updating because they did not incorporate the influence of pile bending stiffness, pile cross-sectional shape, pile-head fixity, and pile head embedment along with changes in the neighbouring soil. These were investigated using the SW model and the findings are summarised in the following paragraphs:

Effect of Pile Bending Stiffness on p-y Curve

Based on the SW model analysis, the pile properties have a significant effect on the shape and geometry of the developing passive wedge and hence p_{ult} and A_{ult}. To illustrate this Ashour and Norris (2000) adopted the Matlock (1970) pile and soil properties for the load tests in soft clay at Sabine River. Employing the SW model, they derived the free-head *p-y* response for various pile stiffnesses at 0.915m below the pile head and compared the results with the *p-y* curve at the same depth derived using the Matlock criteria (Figure 2-31). It is noted that a very stiff pile (10EI) in the Sabine soft clay does not interact very well with the soil, and a deep and large passive wedge at higher stress levels (*SL* and SL_t[21]) quickly develops. Consequently, flow around failure occurs over the depth of the wedge and the soil-pile reaction *p* remains at a value less than p_{ult} below the wedge.

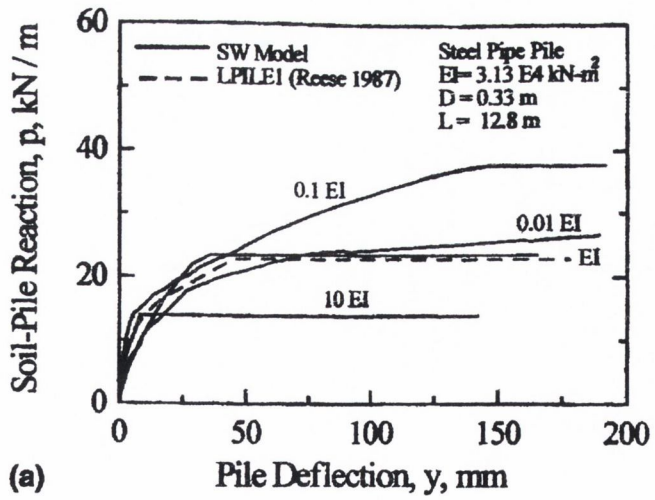

Figure 2-31: Effect of pile bending stiffness on p-y curve at 0.915m depth at Sabine River test site

[21] SL_t is the shear stress level along the sides of the pile and differs from that in the wedge (*SL*) in front of the pile.

Effect of Pile-Head Conditions on p-y Curve

The effect of the pile-head conditions (free and fixed head) is one of the significant factors that determines the depth of the passive wedge and therefore, the shape of the *p-y* curve as shown in Figure 2-32a and b for the piles in sand and clay respectively. Note that the fixed head *p-y* curve in stiff and soft clay (Figure 2-32b) reaches p_{ult} at a lower deflection (and pressure) than that of the free head *p-y* curve. This was found to be the result of the development of a larger passive wedge for the fixed head case at the same value of soil strain ε.

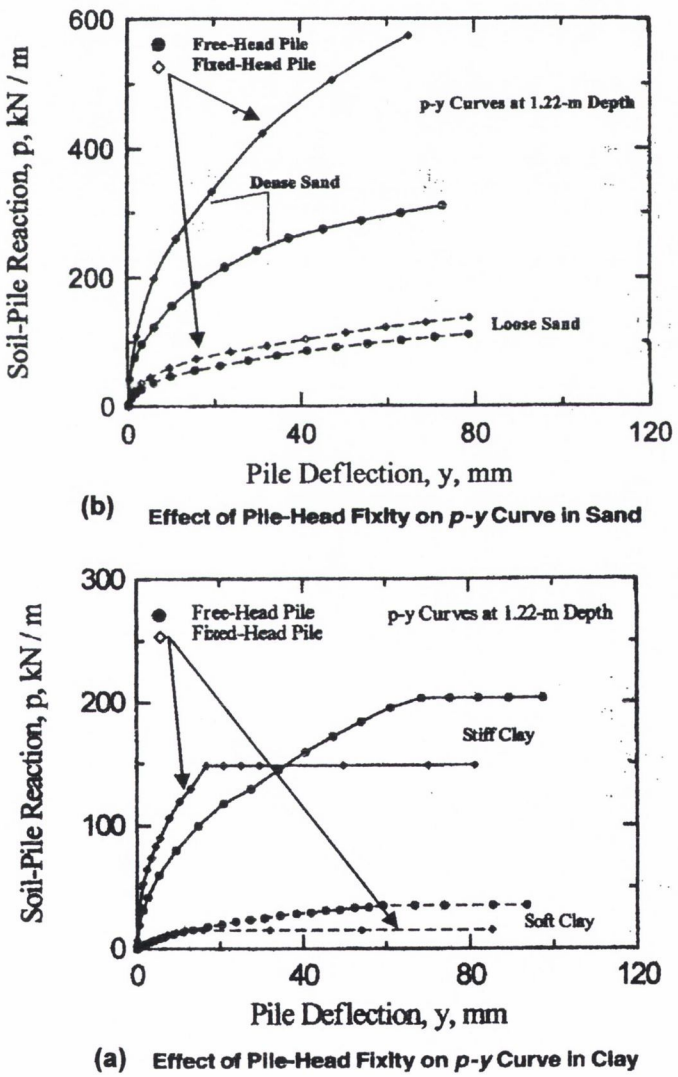

Figure 2-32: Effect of pile head fixity on *p-y* curve (a) sand and (b) clay

Effect of Pile Head Embedment Depth on p-y Curve

Embedding the pile head below the ground level (i.e., $x > 0$) was found to influence the resultant *p-y* curve. This was particularly the case for both loose and dense sands, where the soil-pile resistance increased significantly as the depth of pile head embedment was increased. This phenomenon occurred in sand because of the confinement provided by the overburden pressure along the top of the wedge of the embedded pile. To assess the effect of pile head embedment in clay, Ashour and Norris (2000) recommend that the undrained shear strength profile for the soil be specified rather than the average value to account for increased resistance with greater pile-head embedment.

Effect of Pile Cross-Sectional Shape on p-y Curve

The SW model considers the effect of the pile cross-sectional shape via shape factors S_1 and S_2. The SW model was used to assess the *p-y* curves at a 1.22m depth in sand and clay of two RC piles that were assumed to have the same bending stiffness of 11,500 kNm^2. The first pile had a square cross section of 305mm width, and the second pile had a circular cross-section of 305mm diameter. The only difference between the two piles was their cross-sectional shapes. Figure 2-33 shows the square pile in soft and stiff clay exhibits a soil-pile resistance higher than that of a circular pile. A similar effect relative to the *p-y* curves was observed in sand.

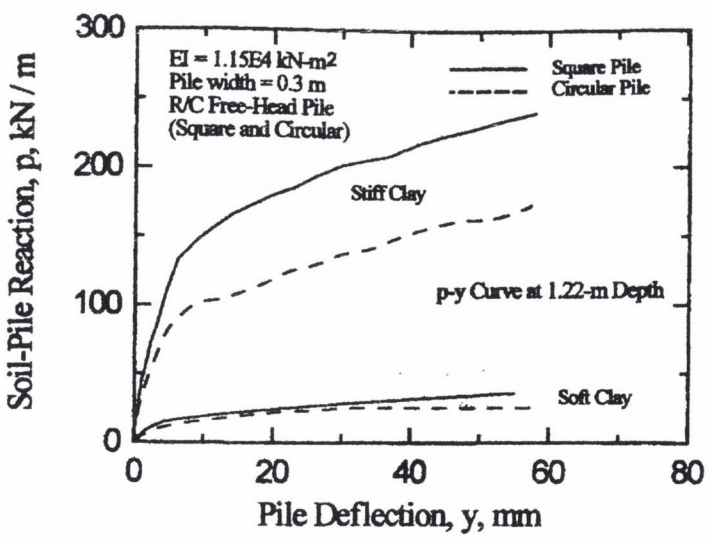

Figure 2-33: Effect of pile shape on *p-y* curve in clay

It is of interest to note that Robertson et al. (1986) found virtually all the soil displacements are radially away from or towards the pile in the case of a circular pile loaded laterally. They concluded that there was very little lateral slip along the side of the pile to generate lateral friction; this is consistent with the smaller shape factors recommended by Briaud et al. (1984) for circular piles.

Effect of Underlying and Overlying Layers of Soil on p-y Curve

Changing the soil immediately above or below the soil in which the *p-y* curve is sought will affect the nature of the *p-y* curve. Figure 2-34(a) and (b) show the SW model predicts this effect. As seen by the insert, changing the type of the lower layer of soil (from 1.83m down) in Figure 2-34(a) has some effect on the *p-y* curve in loose sand (upper layer) at 1.22m from the pile head. The same is true for the *p-y* curve in sand at a depth of 2.44m, where the upper 1.83m layer is changed as shown in Figure 2-34(b). It should be noted that all of the near-surface soil layers affect the resultant depth *h* of the mobilised wedge and, consequently, the *p-y* curve in the neighbouring soil layers.

Concluding Comments on the SW Method.

The SW model was found to provide *p-y* curves that were a good match with traditional *p-y* curves. It was concluded that the *p-y* curve for a given soil was not unique but depended on the neighbouring soil and pile properties and as such the soil reaction *p* is really a soil-pile reaction. The SW model therefore provides a means for evaluating such interdependence and the accompanying effects which influence the *p-y* curve. This in turn permits the engineer to take advantage of design variables that (s)he can influence to improve the efficiency of the design.

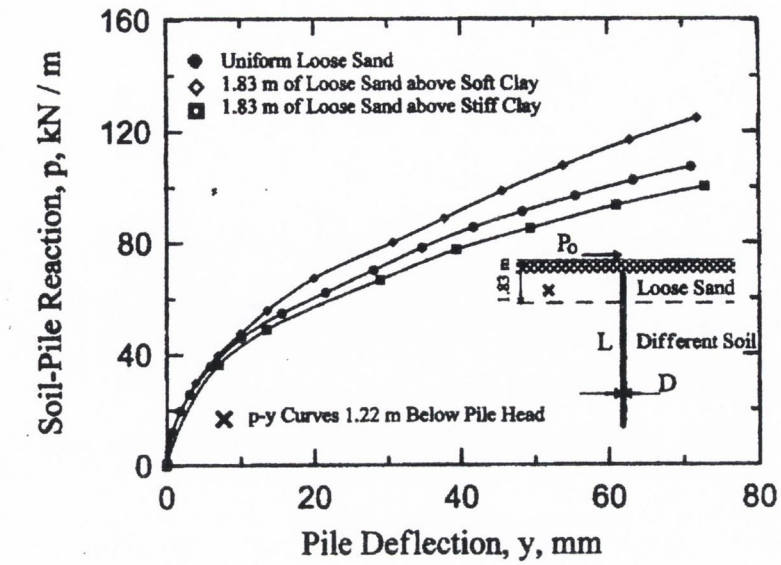

(a)

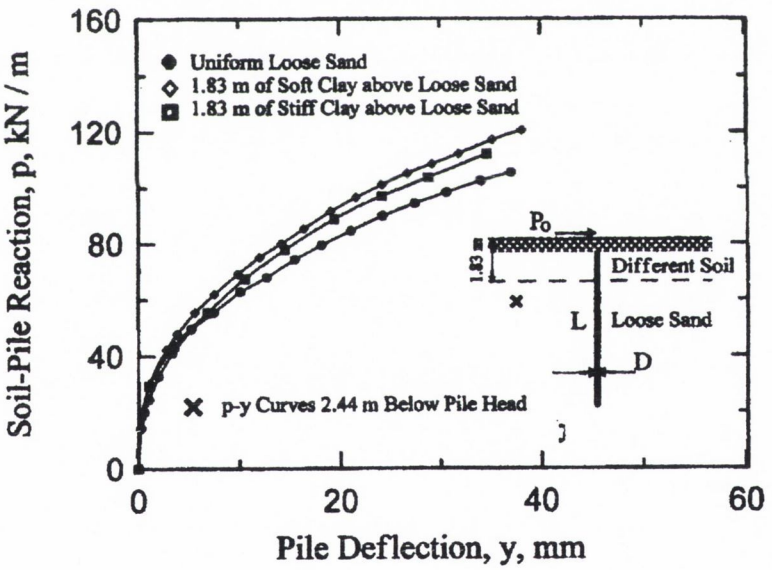

(b)

Figure 2-34: (a) Effect of underlying soil type on *p-y* curve in loose sand (b) Effect of overlying soil type on *p-y* curve in loose sand

2.5.3 Finite Element Method

The early development of *p-y* curves were limited by available theoretical procedures; however, the significant development of the finite element (FE) method in the late sixties has provided a powerful and relatively new tool in advancing the *p-y* method. The FE method appears well suited to the analysis of problems involving non-linear material properties, including the class of problems represented by laterally loaded piles, and specifically, their corresponding *p-y* relationships. In addition, the flexibility provided by the FE method for considering complex geometries and loading sequences offers almost unrestricted capabilities for evaluating pile group arrangements.

While computationally rigorous, the FE method relies on accurate modelling of the soil-structure interaction along with good quality soil parameters obtained from in-situ or laboratory tests on carefully retrieved piston samples. The key to good modelling comes from the findings of full-scale field tests, for example, Matlock's (1970) *p-y* curves for soft clay were based on a considerable amount of experience and experimental data and are believed to be among the most reliable and established procedures available for developing *p-y* curves Yegian and Wright, (1973). The FE method thus relies on a sufficient database of field tests against which results can be checked. Yegian and Wright (1973) compared FE predicted *p-y* curves for soft clay against Matlock's (1970) curves using 2-D plane strain analysis to model the soils response at depth and plane stress analyses to model the shallow response. Their results were found to under predict the ultimate pile resistance for a plane stress analysis and over predict the ultimate resistance when using a plane strain analysis. This suggests that neither of the idealised two-dimensional models (plane stress or plane strain) precisely represents the actual soil behaviour.

Randolph (1981) proposed a set of algebraic expressions for long flexible piles, which could be used to predict pile behaviour in an elastic continuum. The soil stiffness is characterised by an elastic modulus, rather than by a coefficient of subgrade reaction, thereby avoiding the problems that stem from the effect of pile size and stiffness on the appropriate choice of subgrade reaction coefficient. The expressions for the pile displacement are based on the results of elastic finite element (FE) studies using linear strain triangles to model the response of a laterally loaded cylindrical pile embedded in soil

with stiffness varying linearly with depth. The results were fitted using empirical power law expressions to relate p to the lateral displacement (y) and rotation (θ) at ground level. Randolph found that the FE method for analysis offered the ability to account for the heterogeneous nature of soil and the flexibility of descretising the pile into elements of varying size. The improved modelling facilities offered by the FE method resulted in improved accuracy over the integration solution used by Poulos (1971).

More recently, the benefit of FE analysis has been exploited with the availability of cheap powerful computers. It is now possible to model the real response of the piles using a three-dimensional FE model (Shahrour and Meimon, 1991; Trochanis et al., 1991; Bransby, 1999). Such models offer greater insight into and understanding of the behaviour of piles subjected to combined loading. The benefits of such techniques are offset against the time and difficulty encountered when developing the FE model.

2.6 Piles Subjected to Simultaneous Lateral and Axial Load.

Throughout this review, research addressing the behaviour of piles subjected to simultaneous axial and lateral loads was sparse and much of that reviewed was based on model tests conducted in soil chambers (Meyerhof and Gosh, 1989, Meyerhof and Sastry, 1985; Sastry and Meyerhof, 1990; Anagnostopoulos and Georgidis, 1993) or theoretical studies using numerical techniques such as the finite element method (Shahrour and Meimon, 1991 and Trochanis et al., 1991). The following is a brief summary of the findings contained within the above references.

Meyerhof and Ghosh, 1989

Meyerhof and Ghosh, 1989 investigated the ultimate capacity of flexible model piles and small pile groups, of varying relative stiffness, in loose sand and soft clay, under eccentric and inclined loads (the angle of inclination α was measured with respect to the vertical axis). The test results were compared with the ultimate capacity [22] based on the concept of

[22] Theoretical predictions of ultimate axial bearing capacity by Meyerhof and Ghosh were based on a conventional soil mechanics approach e.g. 'α' method for shaft friction in undrained conditions.

an effective embedment depth[23] in terms of the behaviour of equivalent rigid piles (Meyerhof and Sastry, 1985). The model piles were 12mm in diameter and embedded 190mm into soil confined by a stiffened test box 450mm square and 350 mm deep.

The following soil properties were reported: the loose sand had an average friction angle ϕ' of 32°, a unit weight γ of 14 kN/m^3 and a horizontal soil modulus K_h = 1.0 MPa at the pile tip. The soft clay had liquid and plastic limits of 43 and 21 respectively. The paper reported values for soil strength and average stiffness as c_u = 22kPa and K_s = 1.2 MPa where K_s is the average horizontal soil modulus for the clay.

The authors considered that scale effects between the model and the prototype were negligible under the soil and loading conditions adopted for the tests. The main conclusions from the tests were as follows:

- The results of the model tests on single flexible piles under eccentric inclined loads in clay and loose sand show that the eccentricity (e) and inclination (α) of the load significantly influence the ultimate bearing capacity of the piles.

- In the absence of structural pile failure, the ultimate lateral loads and ultimate moments of flexible piles can be expressed in terms of equivalent rigid piles using the concept of effective embedment depth.

- The vertical component of the ultimate bearing capacity of single flexible piles under eccentric inclined loads can be approximately obtained by multiplying the ultimate axial load capacity (Q_0) by an eccentric inclination factor $i_{e\alpha}$ defined as the ratio of the vertical component Q_{uv} (= $Q_u cos\ \alpha$) of central inclined load Q_u to the ultimate axial load Q_0.. A similar approach was also recommended for pile groups.

---

[23] Meyerhof and Ghosh (1989) provided approximate expressions for the effective depth ratio D_{eu}/D where D_{eu} is the effective embedment depth and D is the actual pile embedment. They found that the effective depth ratio was dependent on the soil-pile relative stiffness K_{rs} (= E_pI_p/K_hD^4) and to a lesser extent the D/B ratio.

Sastry and Meyerhof, 1990

Sastry and Meyerhof (1990) extended the previous research of Meyerhof and Ghosh (1989) on flexible model piles by subjecting a fully instrumented PVC model pile to inclined loads. The hollow pile was 1250mm long, had an outside diameter of 73mm and a wall thickness of 7.4mm, and was jacked (separately) into homogeneous sand and clay deposits. The instrumentation included strain gauges and pressure cells along the pile shaft with a load cell located at the base of the pile. Axial and lateral loads and displacements at the pile head were recorded using proving rings and displacement transducers respectively. The sand and clay were compacted into a steel drum, 1m in diameter and 1.6m long. The following properties were reported for the sand and clay:

Soil	Porosity, n %	ϕ', friction angle	ϕ_p', plane strain friction angle	Undrained shear strength, c_u	E_s, secant modulus of elasticity
Sand	47	30	35	_	0 – 2.5MPa*
Clay	_	_	_	15 (kPa)	3.1MPa (uniform)

* Increasing linearly from ground surface to a depth of 1135mm

The theoretical ultimate axial load was obtained using a conventional bearing capacity approach with the ultimate central load Q_u at an angle of inclination (α) estimated by multiplying Q_u by an inclination factor i_α to obtain the vertical component of Q_u. The theoretical pile capacity for soil failure of a flexible pile under horizontal load was obtained using the effective embedment depth concept discussed above in Meyerhof and Ghosh (1989). The results of the analyses were compared with the results of a limited number of field tests and show:

- The axial pile capacity of a flexible pile will be unchanged from that of a rigid pile, whereas under lateral load, the capacity of a flexible pile can be reasonably estimated using the concept of an "effective embedment depth" D_e of an equivalent rigid pile, where D_e is the depth of the location of zero lateral pressure on the pile.

- The concept of effective depth ratio for elastic loading (D_e/D) was also introduced along with the effective depth ratio at ultimate load (D_{eu}/D). These ratios were used to estimate the horizontal displacements at ground level (under working load, using the elastic theory approach of Banerjee and Davies, 1978) and the ultimate bending moments in flexible piles respectively with reasonable success.

- The ultimate lateral pressure in the upper part of the shaft of a flexible pile, above the point of zero pressure was closely estimated by using an ultimate effective embedment depth.

- The method also gave reasonable agreement with bending moment and displacement measurements recorded in a number of full scale instrumented pile load tests in sands and clays for a variety of pile types and sizes.

Anagnostopoulos and Georgidis (1993)

Anagnostopoulos and Georgidis (1993) undertook model tests to investigate experimentally the effects of lateral loading on axial pile displacements and stresses as well as the influence of axial loads on the lateral pile response. The interpretation of the measured pile behaviour was supported by the results from a non-linear 2-D FE analysis for the response of the axial response on a diaphragm wall embedded in an elasto-plastic soil. The paper reported results from six model tests performed on aluminium closed-ended piles (19 mm outside diameter and 1.5 mm wall thickness) subjected to a range of vertical, lateral and combined loads.

The piles were jacked 500 mm into a laboratory prepared soft clay bed (700 mm wide and 1000 mm long, the depth of the test bed was not provided in the paper) having the following properties w_L = 42, w_p = 24 and c_u = 28kPa (obtained from unconfined compression and vane tests). The piles were instrumented using a series of displacement transducers at the pile head and pairs of strain gauges positioned along the length of the shaft to measure the bending moment and axial load distributions during the test. Other than these general details specific test procedures were not provided in the paper. The

sequences of applying the vertical and horizontal loads were varied during the various tests the results of which are summarised in Figure 2-35. It is noteworthy that the experimental lateral load versus lateral pile head displacement relationships presented in Figure 2-35(b) indicates that the effect of an axial load on the lateral displacement is rather small.

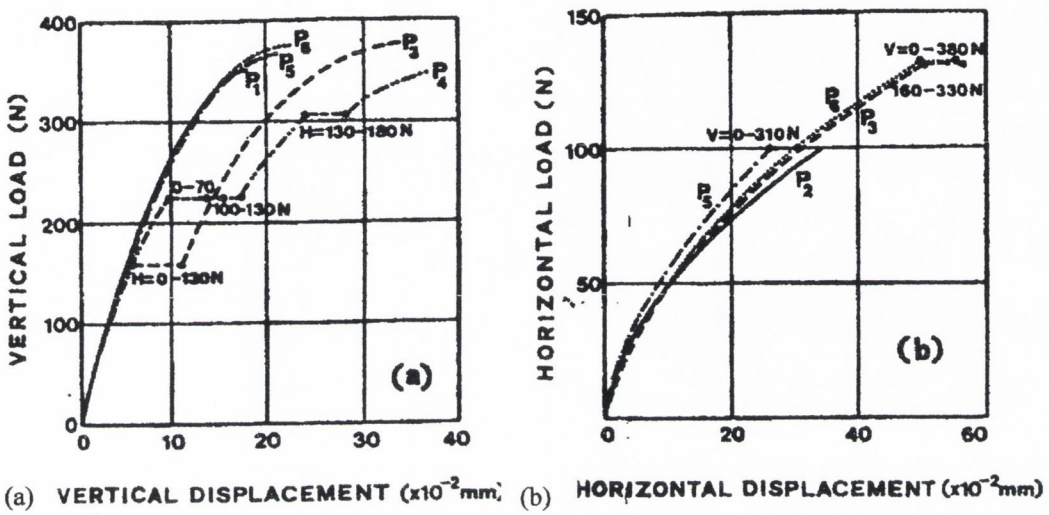

Figure 2-35: Experimental axial and lateral pile head displacements

Shahrour and Meimon, 1991

Shahrour and Meimon (1991) undertook a 3-D finite element (FE) analysis to study the behaviour of piles under inclined loads in sands. A non-associative Mohr-Coulomb law was assumed for the soil together with a Young's modulus that increased with depth. An elastic-plastic soil model was adopted for the analysis. After reviewing the results from laboratory tests on small model piles subjected to inclined loads by Meyerhof and Gosh, 1989; Sastry and Meyerhof , 1990 these authors recogonised the limitations of extrapolating the behaviour for full-scale piles from such tests. Shahrour and Meimon (1991) hypothesised that a 3-D FE analysis would account for the difference in scale between the model piles and real piles (which have lengths and stiffnesses many times greater than model piles). To this end, a 1m square reinforced concrete section (EI=3580 MNm^2) jacked 46m into sand and subjected to inclined loads (with inclinations $\alpha = 0°$, $30°$, 60^0 and $90°$) was analysed using a FE analysis. The sand had the following properties:

Young's modulus 15MPa, Poisson's ratio of 0.37, friction angle = 38° and dilatency angle of 5°. The results of the analysis revealed the following:

1. The lateral displacement and flexibility (i.e., the ratio of the lateral displacement to the lateral *component* (F_L) of the inclined load {F}) were found to be independent of the load's inclination (for inclinations of 0°, 30° and 60°). However the vertical displacement and flexibility (i.e., the ratio of the vertical displacement to the vertical *component* (F_v) of the inclined load {F}) were significantly influenced by the inclination of the load.

2. Under inclined loading, the distribution of axial force over the top 10 pile diameters increased; this was attributed to the development of frictional forces due to the upward movement of the soil in front of the pile. Below 10 pile diameters the axial load reduced steadily as the load was shed to the surrounding soil.

3. The horizontal soil reaction generated by the inclined load was independent of the inclination.

4. The *p-y* curves at various depths were unaffected by the inclination of the load. A similar finding was observed for the pile bending moment profile.

In conclusion the 3-D FE analysis indicated that the lateral behaviour of the pile, which included lateral stiffness, bending moment and *p-y* curves, was independent of the load inclination. Therefore, the authors concluded that the existing validated methods for the analysis of laterally loaded piles can also be employed to solve problems involving inclined loads.

Trochanis et al., 1991

Trochanis et al. (1991) investigated the non-linear response of pile foundations subjected to axial and lateral loads by means of 3-D FE analysis. An elastoplastic soil continuum was assumed with the soil-pile interface represented by a Coulomb friction model. Interface

elements were used to allow for slipping and separation between the pile and the soil. The interface elements could transfer only shear forces across their surfaces when a compressive normal pressure acts on them: otherwise a gap was assumed to open between the elements and the pile. The pile elements were assumed to remain elastic at all times. The validity of the 3-D model was tested by comparing its elastic predictions with those of previous studies i.e., Poulos and Davis (1980). Very good agreement existed between the results of 3-D model and those of the elastic theory. A limited parametric study which included single piles under axial, lateral or combined load was then undertaken to investigate pile-soil slippage and separation, soil yielding and coupling of axial and lateral load for piles of different geometric properties. The analysis employed an elastic-plastic soil model, using the properties given in the following table.

Pile	
Length	10m
Width (square pile)	0.5m
Young's modulus E_P	2×10^7 kPa
Poisson's ratio ν	0.3

Soil	
Elastic properties	
Submerged weight γ'_s	11.8kN/m^3
Young's modulus E_s	20,000kPa
Poisson's ratio ν	0.45
Plastic properties	
Friction angle ϕ	16.7^0
Cohesive strength c	34 kPa
Interface element properties	
Coefficient of friction μ	0.7
Elastic spring stiffness k	6,800 kN/m^3

The following findings in relation to lateral and combined lateral and axial loading were presented:

1. Adopting the soil and pile properties listed above the effect of soil-pile separation and soil yield on the lateral response of a single pile was examined. In the case of an elastic soil, the load-displacement curve predicted a considerable reduction in stiffness compared with the predictions made for a pile fully bonded to the soil once soil-pile separation occurred. The same behaviour was predicted for the more realistic case of an inelastic soil, in this case it was suggested that the non-linearity of the response was controlled by the soil plasticity. The effect of separation on the soil displacements in the vicinity of the laterally loaded pile is illustrated by contours in Figure 2-36.

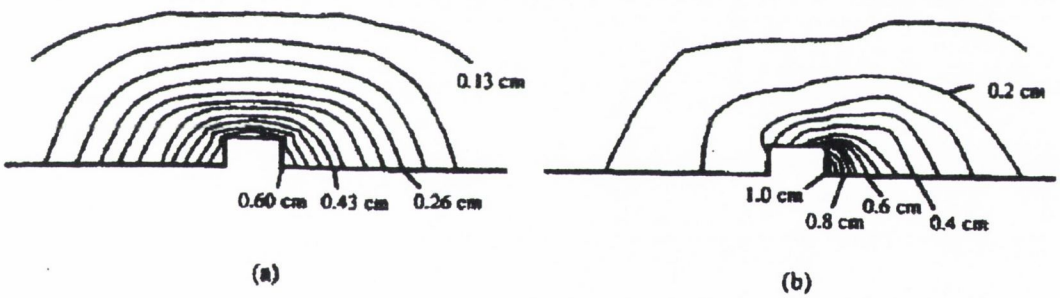

Figure 2-36: Effect of soil-pile separation on pattern of horizontal soil surface displacements around a pile loaded laterally (a) Pile and soil bonded (b) Pile and soil allowed to separate

2. The effect of simultaneous axial and lateral loading on a single pile was analysed for a constant axial load (V) of the order of 50% of the axial capacity followed by a cyclic lateral load with amplitude of 216kN. It was found that the lateral load-deflection curve was practically unaffected by the presence of an axial load. However, the interface shear stress at the leading face of the pile (Figure 2-37a) near the top of the pile was significantly greater with lateral loads than that predicted for pure vertical loading, confirming the earlier finding of Shahrour and Meimon (1991). Trochanis et al. suggested that the pile displacement induced significant normal pressure at the soil-pile interface close to ground level as the

lateral load increased, in contrast to the pressure midway down the pile, where the interface shear transmitted from the pile to the soil is approximately the same for various lateral loads.

3. The effect of the axial and lateral loads increasing simultaneously (monotonically) at the same rate to peak values of 600kN and 216kN respectively was also examined. While the lateral load-displacement curve for this case was found to be approximately the same as that corresponding to lateral loading alone, the vertical pile head movement under combined loading and under axial loading alone were quite different. Figure 2-37b shows that combined loading may result in *higher* ultimate axial load; it was suggested that this occurred because the shear resistance lost on the trailing face of the pile due to separation from the soil is exceeded by the increase in resistance on the leading face due to the increased normal pressure.

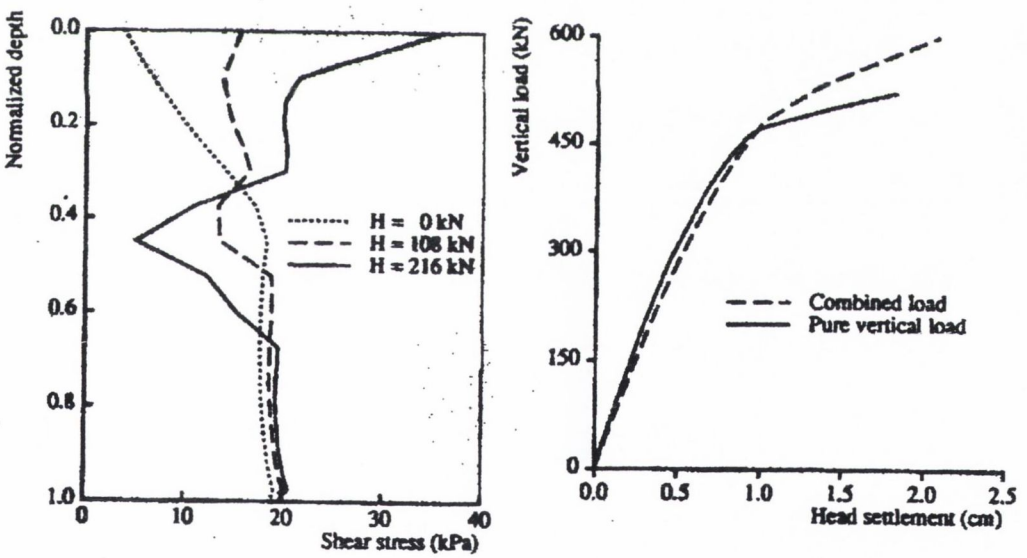

(a) (b)

Figure 2-37: Effect of combined axial and lateral loading: (a) Interface shear distribution with depth at leading face of pile (V =300kN) (b) Pile head load-displacement plot for simultaneous loading.

Chapter 3

Experimental Procedures

3 EXPERIMENTAL PROCEDURES

3.1 Introduction

This chapter outlines the details of four pile load tests carried out at a test site located on the Eastern shore of Belfast Lough. The chapter summarises the instrumentation, fabrication and installation of the piles in addition to describing the field set up and test procedures.

The events associated with the test programme are summarised in Table 3-1.

3.2 Test Pile Details

Two 350mm square and 10m long reinforced concrete piles L1 and AL1, were cast at the piling contractor's (Lowry Piling Ltd.) manufacturing facility. Both piles were instrumented with a selection of transducers, which will be described in the next section.

DATE	DESCRIPTION	COMMENT
June 9, 1997	Initial site assessment	Five standard CPT (E) tests performed
August 2, 1997	Casting of piles at the manufacturers facility	Concrete cube and cylinder specimens moulded
August 15-20, 1997	Installation of pneumatic piezometers	Monitoring pore water dissipation driving of adjacent pile group
September 4, 1997	Installation of two test piles	Junttan 5 tonne hydraulic hammer
October 3, 1997	Installation of electro-levels	
October 17, 1997	Axial load test	Performed on pile AL1
October 18 & 19, 1997	Combined axial and lateral load tests	
May 18, 1999	Re-test	Lateral loads only
June 1, 2000	Trial pit	Vane tests, bulk and piston samples retrieved.
August 2000 – June 2001	On-going site investigation	Sampling and Vane, CPM, DMT and CPTU tests

Table 3-1: Test programme details

Full-length reinforcement comprising eight 16mm diameter high yield steel bars was provided in each pile. One bar was placed in each corner and the remaining bars were placed at the midpoint of each face of the pile. The reinforcing bars were fabricated into a cage using 5mm diameter mild steel wire wrapped helically around the bars at a pitch of ≈200mm. A tighter pitch (≈50mm) was used at the ends of the pile to provide confinement of the concrete against driving stresses (Figure 3-1). Plastic chair spacers provided 35mm

concrete cover to all reinforcement and the concrete mix was designed to provide a compressive strength of 50 MPa at 28 days.

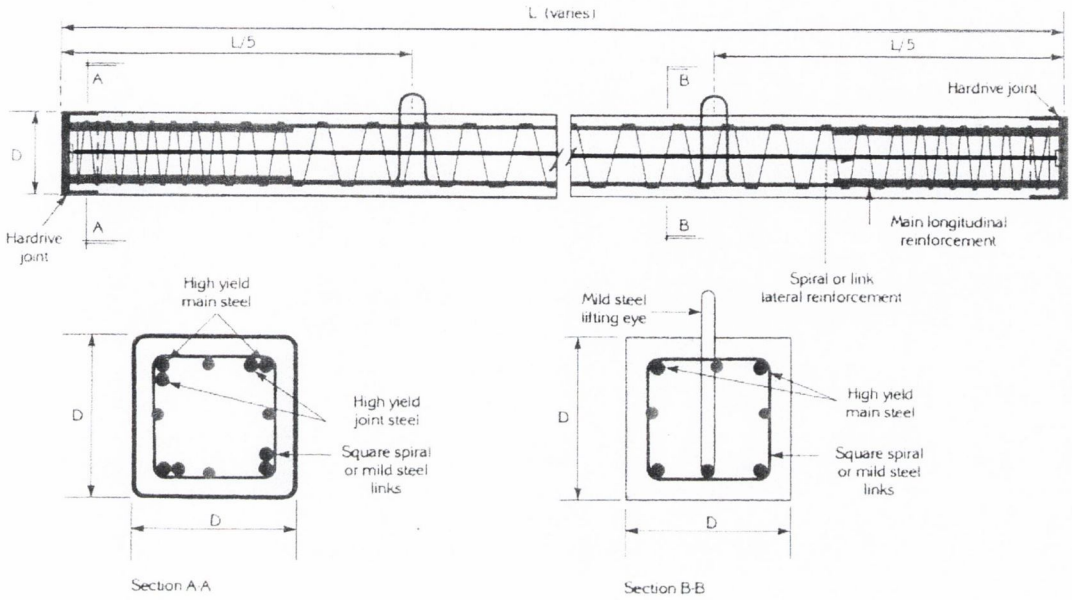

Figure 3-1: Typical section through pile unit

3.3 Instrumentation

The initial site investigation (June 1995) indicated that it would be feasible to adopt a single length of precast concrete pile, supported on the medium dense sand, located ≈ 9m below ground level. Both the piles were instrumented (see Figure 3-2 for details) to record the pile strain distribution profile, pile head movement and pile displacement profiles while pile AL1 was instrumented to record the lateral stress at various levels.

The majority of the laboratory work involved fixing electrical resistance strain (ERS) and vibrating wire (VW) strain gauges to the reinforcing bars and calibrating the various displacement, load and pressure measuring devices. The details of the laboratory work are summarised in the following sections with additional details on the instrumentation performance and calibration data provided in appendix 3.

3.3.1 Strain Gauges

Thirty ERS and six VW strain gauges were installed between the two piles. In pile AL1, two centre face bars both in the plane of applied lateral loading) were strain gauged. Pile L1, had one centre face bar, located on the opposite side to the applied lateral load, similarly instrumented (see Figure 3-2).

The capacity of the data acquisition system limited the number of ERS gauges that could be logged to thirty but the independently logged VW strain gauges, supplemented this by six. Twenty-four of the ERS gauges were installed in pile AL1 and the remaining six in pile L1. Four of the VW strain gauges were located in L1 with the remaining two positioned at the base of AL1. The strain gauges were concentrated in the upper region of the piles to gather data from the critical depth of soil controlling the lateral pile behaviour (typically assumed to be $\approx$ 10 pile diameters). Larger gauge spacing was adopted below this critical depth to complete the strain profile and to allow the axial load distribution to be determined.

ERS Gauges

In preparation for the application of ERS gauges to the reinforcing steel the deformations on the high yield bars were removed by grinding at the gauge locations. Surface preparation procedures recommended by the gauge manufacturer were carried out, followed by bonding the foil gauges[1] to the steel. After the adhesive had cured each gauge was energised by 10V DC and the gauge resistance checked against the manufacturers specifications[2]. Each gauge was subsequently waterproofed with a thick coat of silicone sealer and the bars were then placed in a specially fabricated box for transportation to the casting yard.

[1] Self–temperature-compensated type (reference number C-91114-M) composed of a thin Constantan foil (an alloy of 55% copper and 45% nickel) having a gauge factor of 2.1 and a resistance of 350 ohms.

[2] The gauges operate on the principal that an external force induces strain in the steel, which in turn causes the resistance of the gauge to change. As the gauge resistance changes so too does its output voltage. The change in output voltage can be calibrated against a known load or moment. Detailed information on strain gauge technology can be obtained in Window (1992).

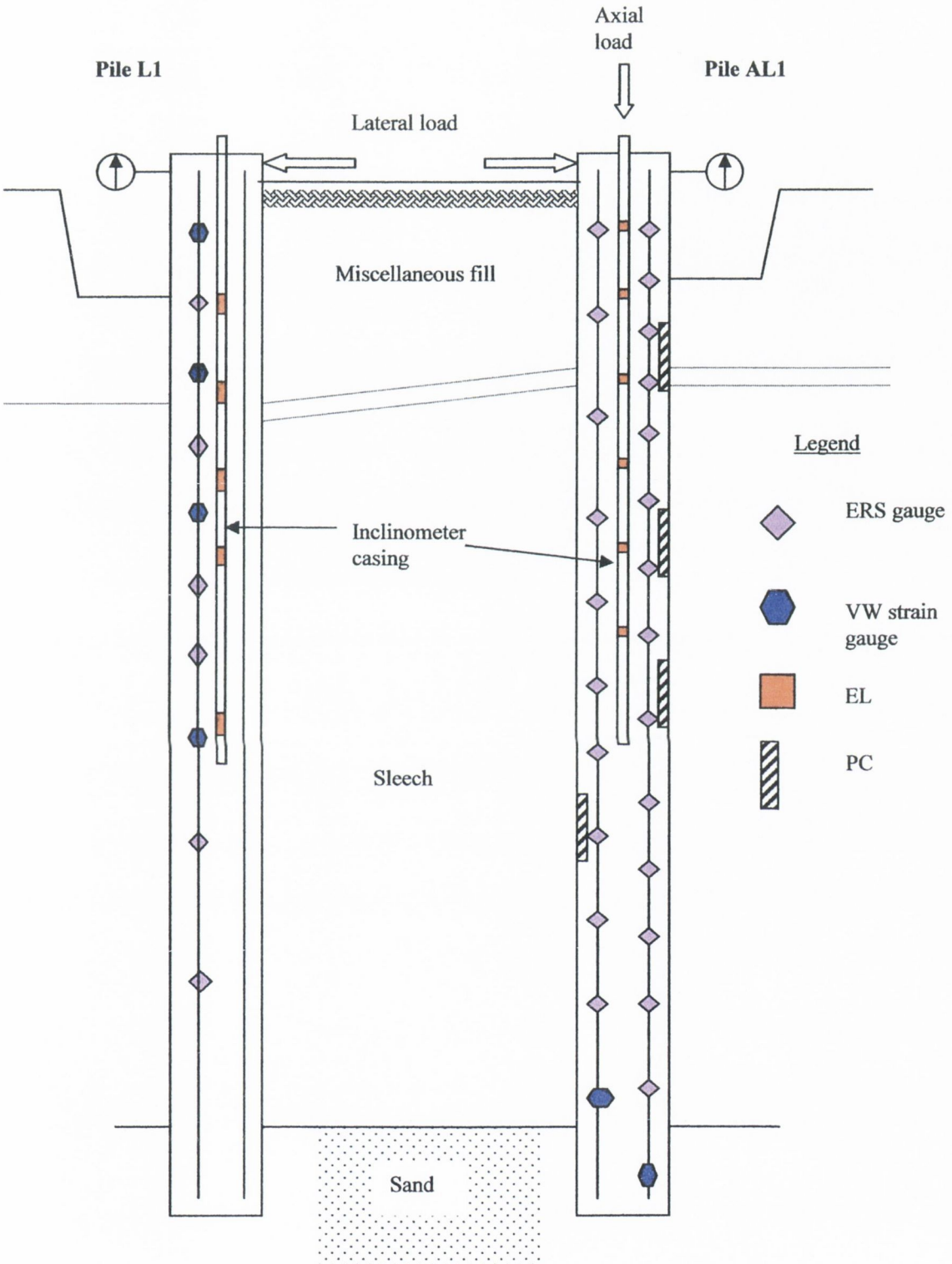

Figure 3-2: Schematic sketch of instrumentation layout

Self-temperature-compensated (STC) strain gauges were used in a quarter-bridge configuration due to the small diameter bar[3]. The gauges had a working strain range of ±5% with a digital output resolution of ±0.01με. The purchase cost for the ERS gauges and the associated cabling and adhesive was less than €127.

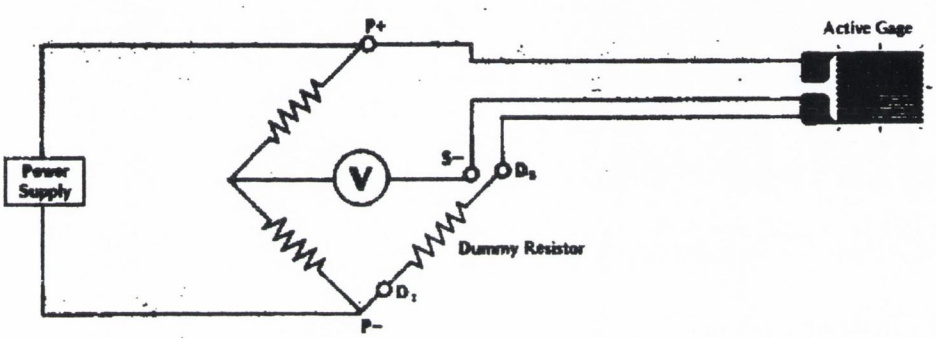

Figure 3-3: Three-wire circuit for single active gauge (quarter bridge)

VW Gauges

The VW gauges (type TSR/5.5/SB) were clamped to the reinforcing bars. Two gauges were located near the toe of pile AL1 and the remaining four in the top half of pile L1; the latter were placed alternately between the ERS gauges. Each VW gauge was potted in a PVC cylinder using a two part polyurethane compound, which acted as both a sealant and a damping material for the gauge (Figure 3-4).

[3] The STC gauges result in a marked improvement in compensation techniques for metal foil gauges subjected to resistance change resulting from fluctuating temperature. They employ a 'three-wire' circuit, which results in the temperature effects in the leads being cancelled, and the desensitisation of the active gauge is halved compared with the older half bridge system.

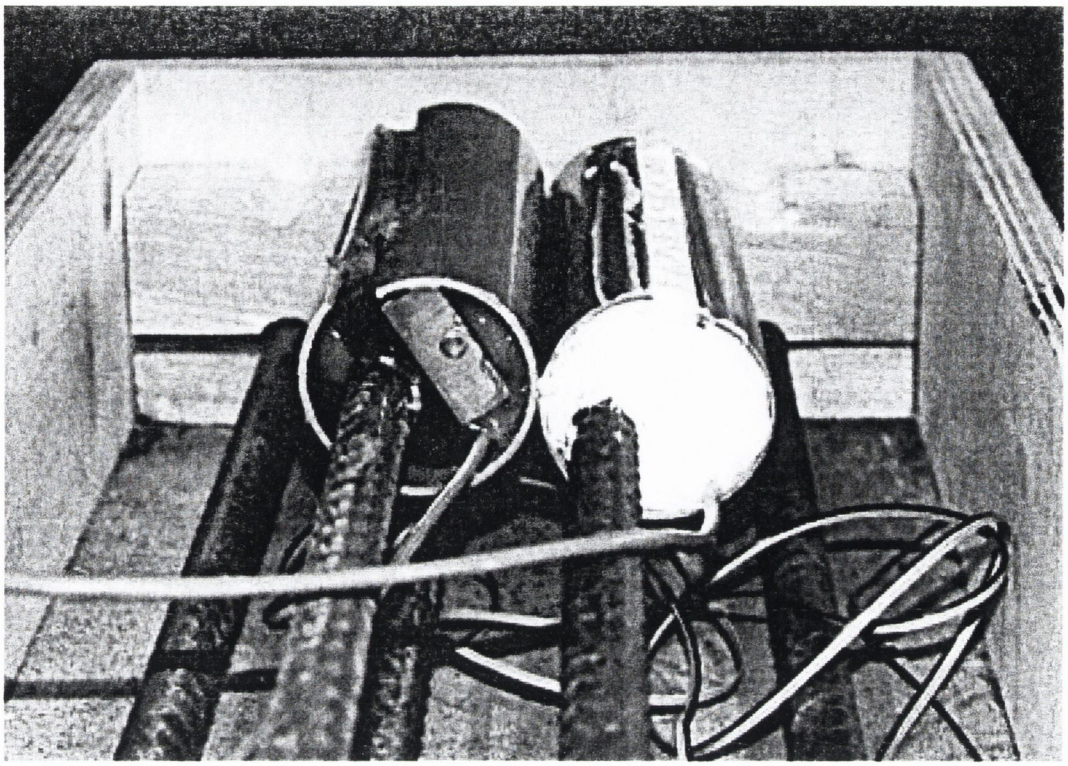

Figure 3-4: VW gauges at the toe of AL1

VW Gauge readings were recorded using the continuous excitation method employed by a strain meter (type GT1174). The VW gauges typically had a working strain range of 3000με and an approximate accuracy of ± 2με (Tyler, 1968). The 1997 unit cost per VW gauge, including the cabling and potting compound, was €115.

The strain history of the piles was traced by recording VW gauge readings at various stages of pile construction, notably, before and after casting, and prior to and immediately after installation. A similar monitoring programme using the ERS gauges was not practical due to their lack of robustness and inevitable schedule delays and zero drifts associated with connections and re-connections with the data logger.

3.3.2 Displacement Transducers

Both Linear Variable Differential Transformers (LVDT) and Dial Gauges (DG) were used to monitor the lateral and vertical movement at the pile heads and reference beams.

3.3.3 Pressure Cells

Four piezoresistive pressure transducers manufactured by Soil Instruments Ltd., were cast into pile AL1 (see section 3.6). The pressure cells (PCs) were 100mm x 200mm oil filled rectangular flatjacks connected to a 0-10 bar pressure transducer via a 200mm long steel tube. The pressure transducer employed (Figure 3-5) uses an integrated silicone strain gauge bridge, encapsulated within a stainless steel case by a thin welded isolating diaphragm. The transducer is finished with a cable gland and 5m of cable, which rendered the transducer waterproof. The instruments had a sensitivity of 1mV per 10kPa. The 1997 unit cost for each pressure cell was €760.

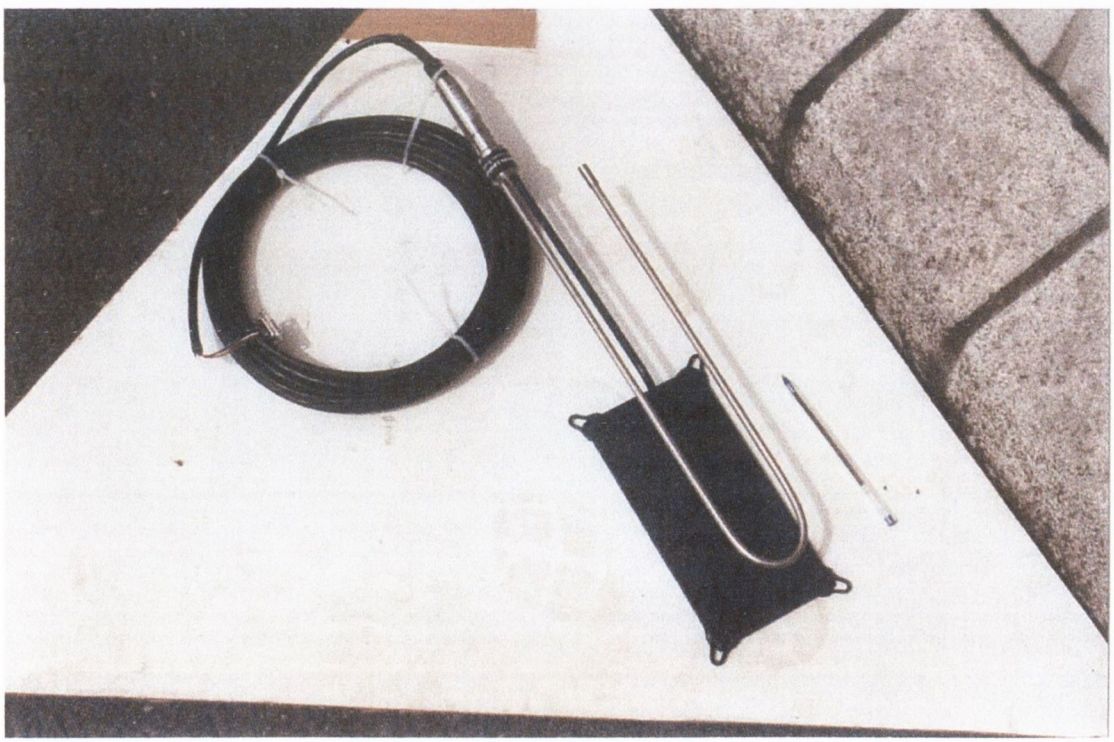

Figure 3-5: Typical pressure cell

3.3.4 Electro-levels (ELs)

The ELs are precise tilt monitors with a linear range of ± 3° and a potential resolution of greater than one second of arc. The electrolytic tilt sensor, shown in Plate 3-1 provides an output voltage proportional to tilt angle. The EL consists of a tubular glass vial partially filled with an electrolytic fluid in contact with two pairs of metal electrodes, one at either end of the vial. The innermost electrode of each pair is joined by a single wire (Figure 3-6). When the EL is connected to an AC power supply and levelled, equal impedance to the common electrodes will exist and the digital voltmeter (logger) will indicate a minimum output. Tilting the level will cause unbalanced impedance to the common electrode and an increase in the output voltage. This voltage is the useable output of the sensor and is proportional to the tilt angle. A signal conditioner remotely located from the EL is used to convert the DC supply voltage[4] to AC current and also protects the instrument in the event of fluctuations in the AC current.

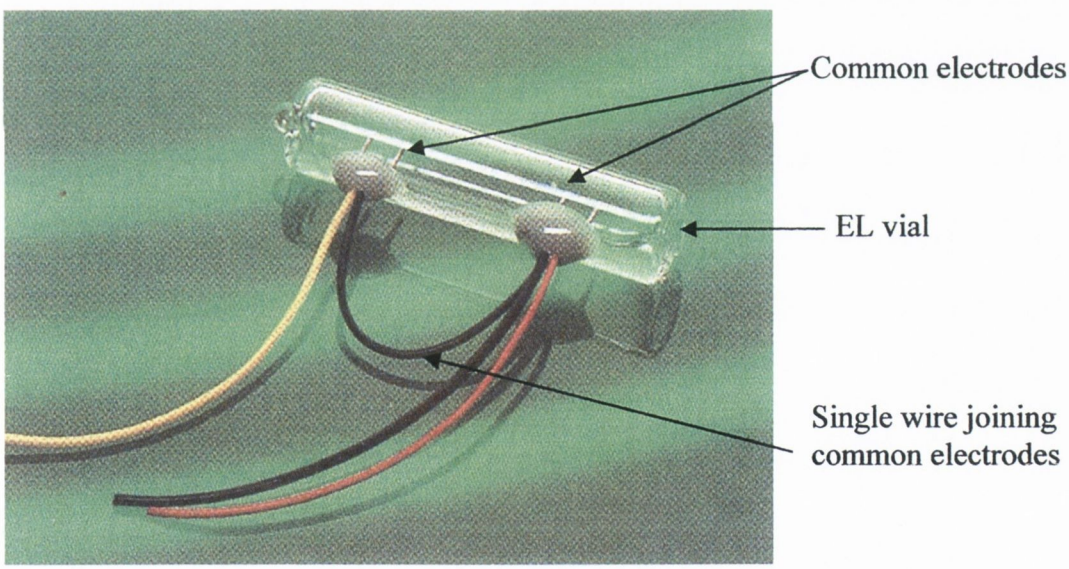

Figure 3-6: EL details

Electro-levels offer a number of distinct advantages over traditional instrumentation techniques; in this test programme the following advantages were notable:

[4] Direct current will damage the instrument and cause instability in the output voltage.

- The greatest risk of instrumentation damage in piles occurs during their manufacture and installation. Stresses developed, particularly during pile driving, are often responsible for the failure of pre-installed instrumentation. This risk is eliminated since the ELs are installed after the pile is in the ground.

- The high degree of accuracy that can be achieved using ELs is such that the displacement profiles derived from the EL data can be used in their own right to provide *p-y* curves for the analysis of laterally loaded piles (Price et al. 1985).

- The ability to instantaneously record the pile displacement profile is particularly advantageous. The traditional method for monitoring tilt using an inclinometer requires individual readings of tilt to be taken at various depths along the pile while the applied load remains constant; this procedure is time consuming and can lead to errors due to creep that inevitably occurs as the lateral load is sustained.

- ELs can be removed after the test and re-used in subsequent tests thereby reducing the cost of subsequent instrumented tests.

The unit cost of an EL and signal conditioner was €167 at the time of purchase (1997).

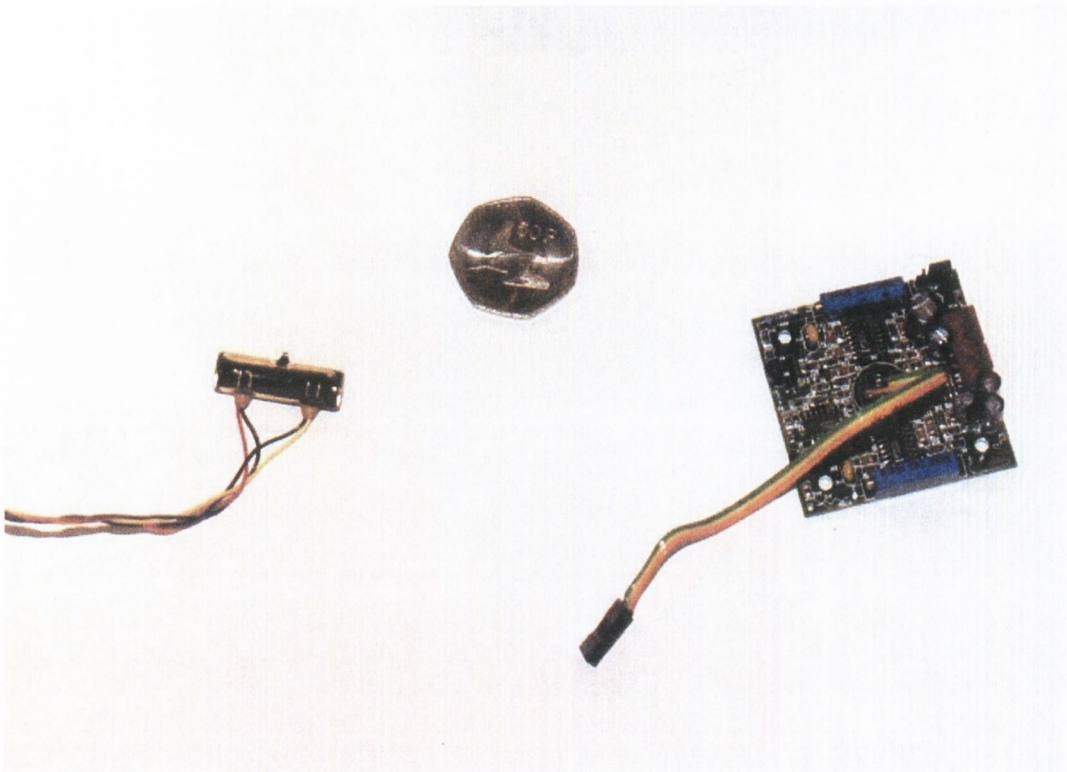

Plate 3-1: Electrolytic tilt sensor and signal conditioner

3.3.5 Load Cells

Standard load cells were used to measure both horizontal and vertical (axial) loads during the load tests. The load cells typically consist of a cylinder of steel with several ERS gauges bonded to the outer periphery of the cylinder at its midsection (see Figure 3-7). Half the gauges are orientated to measure hoop strains and half to measure axial strains. The gauges are connected to form a single full bridge network, thereby integrating individual strain gauge outputs and reducing errors that result from load misalignment and off-centre loading. The strain gauges were protected from mechanical and water damage by an outer protective steel cover, sealed at the ends with O-rings, and filled with waterproofing compound.

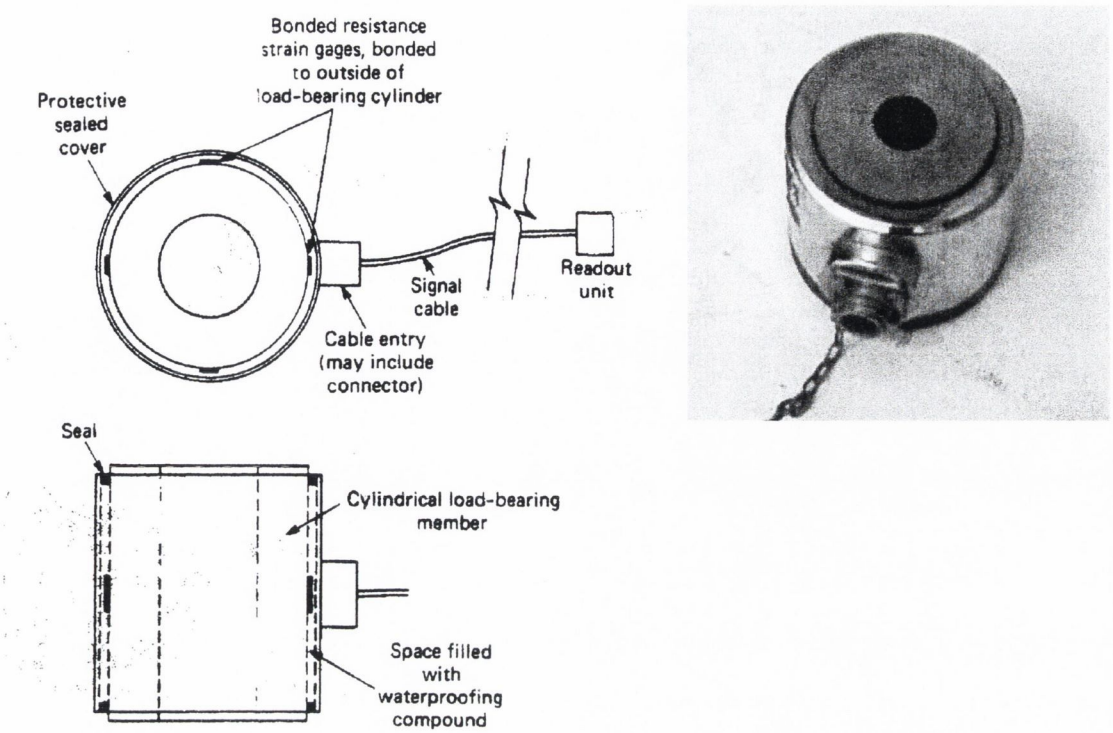

Figure 3-7: Schematic of electrical resistance load cell (from Dunnicliff and Green, 1988) alongside actual load cell

3.4 Calibration of Instrumentation

The strain gauges were calibrated during the field tests while the pressure cells, electro-levels and displacement transducers were calibrated in the laboratory in advance of the load tests. The following paragraphs give a brief summary of the procedures employed with additional details provided in appendix 3.

Strain Gauges

On-site calibration of strain gauges was performed using the top ERS gauge in pile L1. This gauge was located at pit level where the applied bending moment is known and given by the lateral load multiplied by the distance from the load to the gauge. As the lateral load was incremented, a field relationship for bending moment against bending strain was obtained. The accuracy of this relationship was checked against the

theoretical strain predicted under the applied bending moments, and was found to compare favourably with the theoretical strain.

Displacement Transducers

The displacement transducers were calibrated by observing readings when certified gauges of accurately known thickness were inserted under the tip of the transducer plunger. The electrical output in mV of the LVDT's was calibrated against the known displacement.

Pressure Cells

A manufacturer's calibration certificate accompanied each pressure cell. As a check, one pressure cell was re-calibrated in the laboratory by immersing the cell into a sealed chamber filled with water; see Plate 3-2. The pressure cell was connected to the data logger (used for the field tests) and the output voltage was monitored as the water in the chamber was pressurised. Increasing and reducing pressure cycles were used to check the linearity of the instrument output. The measured results provided an excellent match with the calibration data provided by the manufacturer and the response to the cyclic pressures was linear. The laboratory calibration pressure was limited to 400kPa by the hydraulic equipment, but this was adequate for any soil resistance anticipated during the load tests.

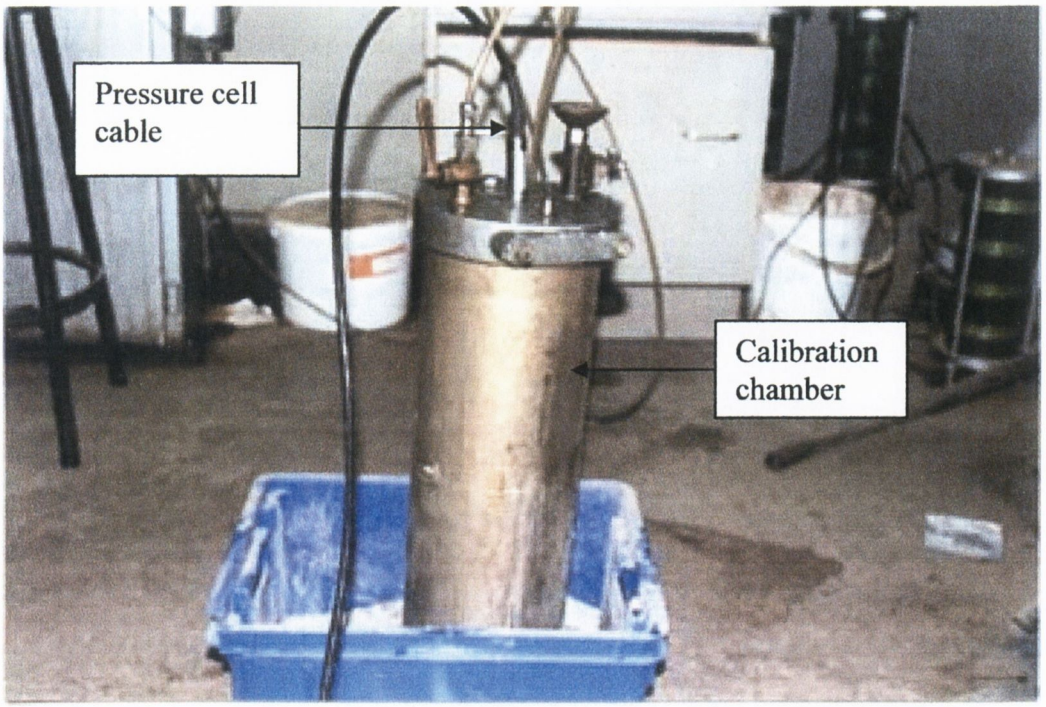

Plate 3-2: Calibration of the pressure cell

Electro-levels (ELs)

Since the ELs monitor tilt, calibration was carried out by determining the relationship between voltage output and changes in angle of tilt. Two methods of calibration were employed:

Method 1

In the first method, the EL vials were fastened to a machined mild steel block mounted on a Kern DKM2-AE theodolite (Plate 3-3) having a resolution of one-second of arc.

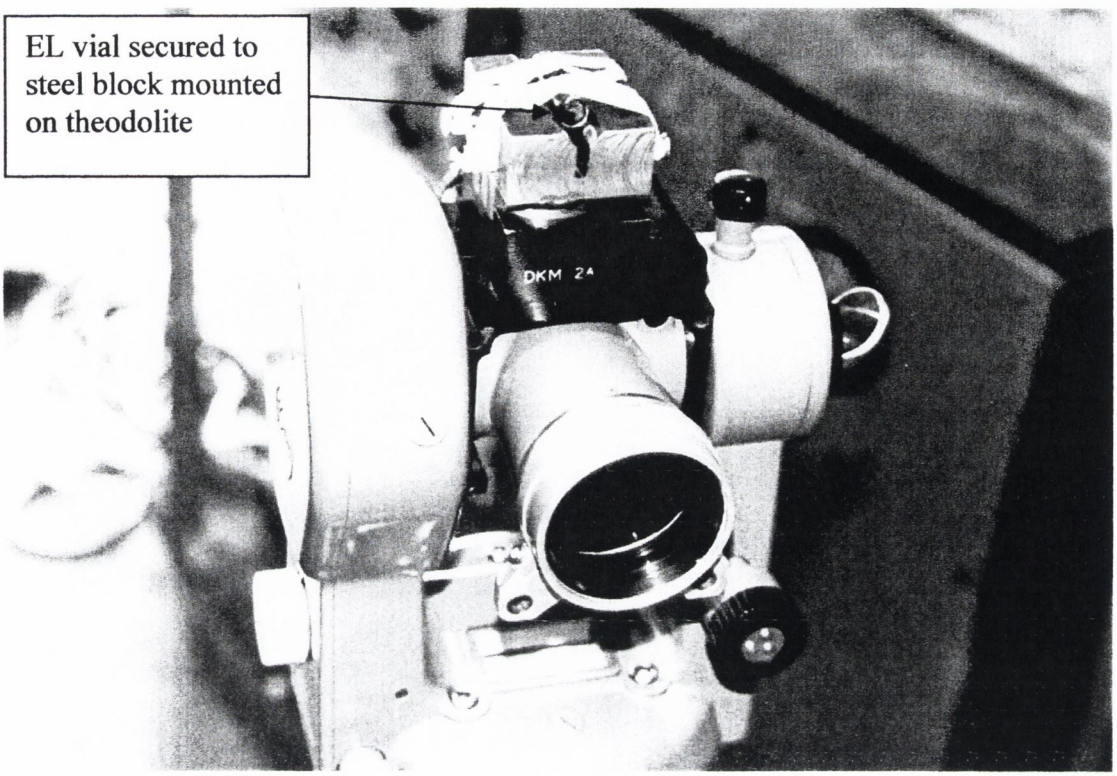

Plate 3-3: Theodolite calibration of electro-levels

As the theodolite was incrementally rotated through the working range of tilt (± 3°) the EL output (in millivolts) was recorded using the Datascan 7220 logger. Each EL in turn was calibrated in this manner and the complete set of calibration curves are presented in appendix 3a. The linear EL output yielded a calibration factor of 1mV ≈ 10 second of arc (1/20626.5 radians). The output range of 3° was considered suitable for the displacements anticipated during the load tests.

Method 2

As a check on the above, and to simulate conditions on site, readings from a set of ELs were obtained by placing five ELs, spaced 500mm apart, in a 3m vertical length of inclinometer tube. The tube was fastened to a rigid test frame as shown in Plate 3-4.

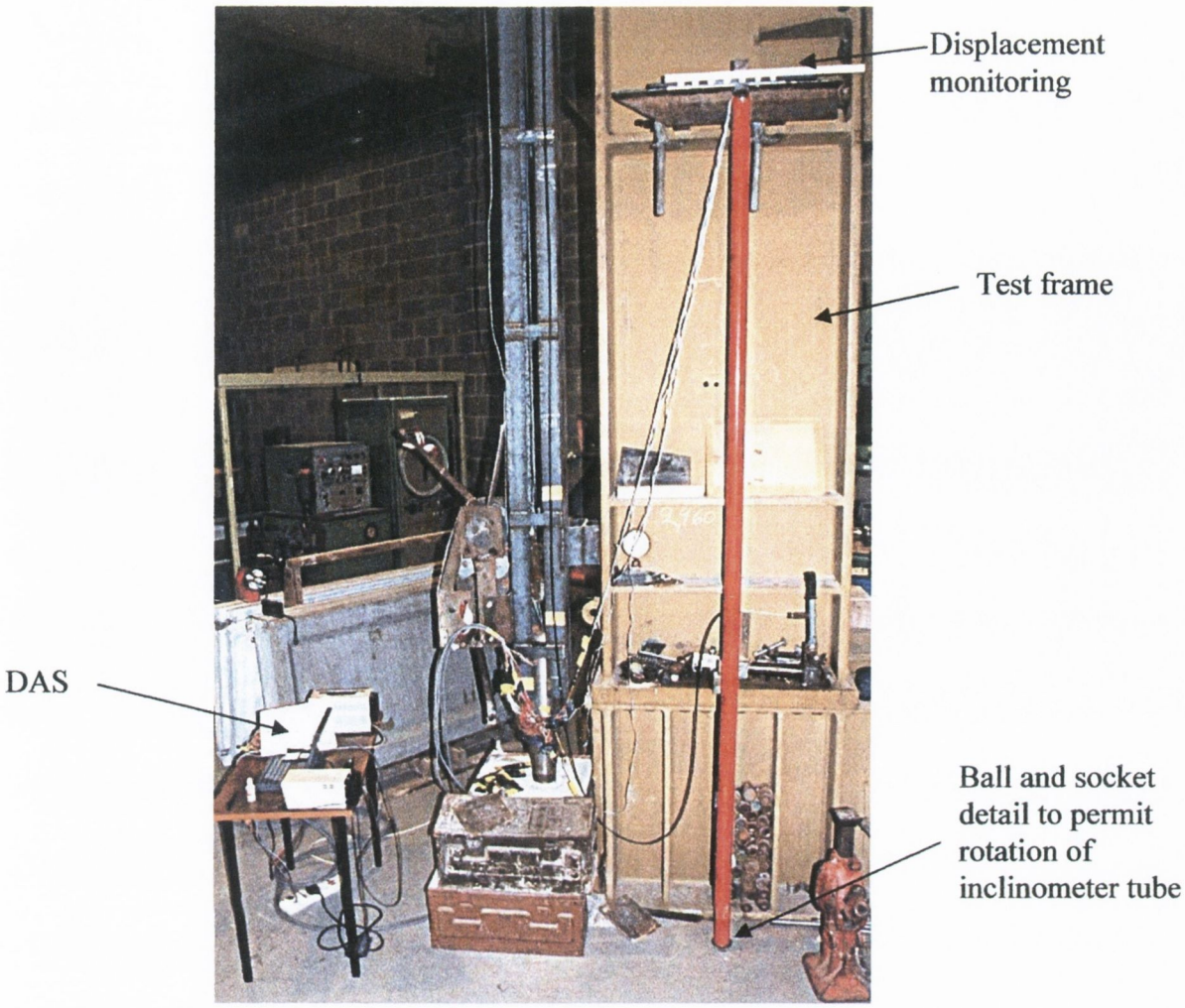

Plate 3-4: Calibration of a series of electro-levels in an inclinometer tube

The base of the tube was supported on a ball and socket arrangement to permit rotation of the tube. At the top, a pointer was moved across a graduated scale that permitted the controlled rotation of the tube. The tube was tilted in 50 mm increments to the left and right of the vertical position up to a maximum of ±150mm; the results of the calibration similarly showed 1mV of electrical output corresponded to a slope of 10 seconds of arc.

These results imply a displacement resolution of 0.024mm for ELs spaced 500mm apart, thus giving an overall resolution of lateral movement on site of 0.145mm for six ELs positioned over the top 3m of the pile.

On completion of the calibration, each of the fifteen ELs used in the field (and their corresponding signal conditioners) were given an identification mark to permit correct re-assembly on site.

Load Cells

Two electrical resistance type load cells were laboratory calibrated in advance of the field tests. The calibration was performed in compression using a Denison universal testing machine having a resolution of 0.1kN. The slope of the calibration curves indicated a 1:1 ratio between the output from the Denison and the readout units. The load cells monitoring the axial and lateral loads during the initial load test programme (CLT series) were logged directly to readout units[5], thus permitting the loads to be recorded to an accuracy of ± 0.1kN. For the re-test[6], the load cell was logged directly to the computer[5]. The result of the calibration in this case was again linear and indicated 1mV of electrical output corresponded to 0.2492kN.

3.5 Data Acquisition System

Two data acquisition systems (DAS) were available on site during the tests; these were Strain Measurement's System 5000 and Recorder's Datascan 7220. During the main test program in 1997, both DAS were employed in addition to a number of independent readout units to cater for instruments that could not be accommodated by the DAS. Only the Datascan DAS was required to monitor the instruments employed in the 1999 re-test as ERS gauges were not recorded during this test due to logistical restraints. The key features of the DAS are outlined in the following paragraphs.

3.5.1 Strain Measurements Incorporated System 5000.

The system 5000 is a flexible data logger with sophisticated data handling, storage and processing capability. The system can accommodate a large number of transducers; there was a facility for 30 electrical resistance strain (ERS) gauges, eight of which were logged

[5] The readout units and computer had a resolution of 0.01kN.
[6] See page 96.

to two six port high-level cards, while the remaining four ports were used to monitor the displacement transducers (Plate 3-5). The output to the computer included the scan number, date and time of logging in addition to the parameter being measured.

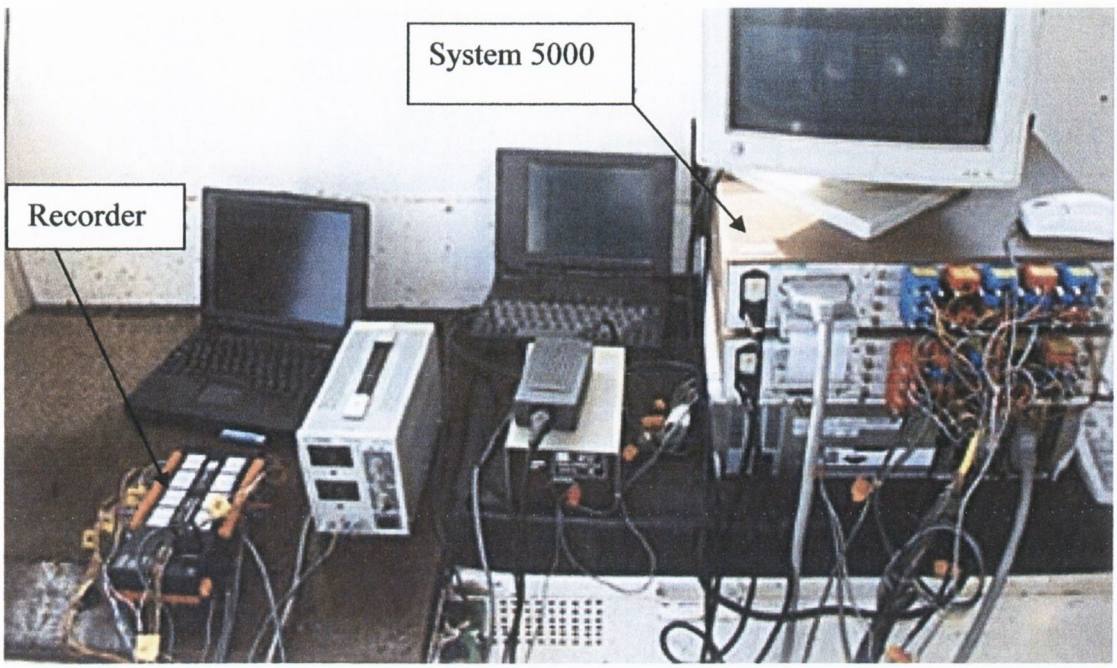

Plate 3-5: Data Acquisition Systems

3.5.2 Datascan Recorder

The Datascan Recorder was used to monitor the electro-levels and the pressure cells. This data logger was not as versatile as the System 5000 but nonetheless recorded time and the change in voltage registered by each instrument during the test.

3.5.3 Independent Read-out Units

During the 1997 (first time) load tests, the load cells were logged manually using digital read-out units. At specified time intervals during the tests the digital display was noted and subsequently converted to load using the load cell calibration factor.

In the case of the VW strain gauges, a GT1174 Miniature Strain Meter gave the period of vibration. The change in the period of the vibrating wire (due to varying stress conditions) was converted into strain using the calibration equation.

Dial gauges were used to supplement and check the LVDT's.

3.5.4 Power Supply

A mobile generator provided the power supply on site. 220 volt AC current powered the computers and DAS, and current converters were used to provide DC to most of the instruments with the exception of the electro-levels, which used signal conditioners to re-convert the DC to AC (Plate 3-1).

3.6 Casting of the Piles

The piles were cast in steel moulds that had been treated with a de-bonding agent. Prior to concrete placement, the reinforcing cage was placed in the mould and four pressure cells were located in AL1; three were placed flush with the bottom of the mould i.e. in the base of the pile, in the top 2.5m of pile length. The fourth was located flush with the top of the mould at a distance of about two-thirds the pile length from its head. The pressure cells were fastened to the reinforcing cage to prevent them from 'floating out' during concrete placement.

Finally, to accommodate the ELs, a 5m length of 58mm diameter inclinometer tube was located centrally in the top half of each pile. The tubes were positioned using wooden templates supported on the reinforcing cage and protruded ≈50mm through the top of the piles. The templates were removed once the tubes were securely tied in position and concrete placement commenced.

Particular attention was necessary during concrete placement (Plate 3-6). The standard procedure of cascading the concrete from above the top of the mould would have presented a significant risk of damaging the instrumentation, in particular the ERS gauges, which were not as robust as the other instrumentation. Concrete placement was achieved by initially placing the concrete close to the bottom of the mould and carefully working the concrete to the top surface. The process started at the toe of the pile and progressed

towards the pile head so that the ERS cables could be held in position during placement. Once cast, the piles were covered with an insulated tarpaulin and steam cured. The casting procedures employed proved successful with only three (one ERS and two VW strain gauges) of the thirty-six strain gauges malfunctioning after concrete placement.

Plate 3-6: Concrete placement

3.7 Pile Installation

The piles were installed using a PM20 piling rig with a 5 tonne Junttan hydraulic hammer employing a hammer drop of ≈450mm. The driving resistance varied, from tapping the pile through the initial 1.0m crust after which the weight of hammer was sufficient to push the pile ≈7.5m through sleech and onto the sand layer. The final seating required about 55 blows to achieve a half metre penetration into the medium dense sand layer (SPT N value =15). Driving to a predetermined set was not necessary as this research is primarily concerned with the performance of laterally loaded vertical piles. It was sufficient to ensure that the pile would not punch through the sand layer when the axial test load was applied. To guard against this, three estimates of the axial capacity of the piles were

performed in advance of the field tests; further details of these analyses are presented in chapter 5 (section 5.2.2) and appendix 5a. The minimum axial capacity of the pile was estimated at 117 tonnes thus, a factor of safety $\approx$ 2.2 was provided by limiting the maximum kentledge weight to 54 tonnes.

The instrumentation cables were protected during driving using a specially fabricated steel extension piece. The helmet like structure (Plate 3-7) was positioned on the head of the pile prior to pitching, and provided the transfer mechanism through which the pile could be driven. The helmet also formed part of the pile head detail, which was designed to transfer an axial load to pile AL1 (see section 3.9).

Plate 3-7: Helmet structure located over pile AL1

3.8 Installation of Electro-levels

Two weeks prior to carrying out the axial load test, eleven electro-levels (ELs) were installed between the two piles; six in pile AL1 and five in pile L1. Each EL vial was

placed in its PVC capsule, which in turn was located in a metal channel designed for locating ELs in the grooves of the inclinometer tube (Plate 3-8). The PVC capsules were custom made to protect and maintain the ELs in position after they had been inserted into the pile[7]. Each EL was located in the inclinometer tube and checked to ensure its output was within the linear calibrated range. Any necessary adjustments were performed at the pile head prior to sliding the EL to the desired position along the pile shaft. The device used to locate and retrieve the ELs is shown in Plate 3-9. The procedure of adjusting and positioning of thirteen ELs took approximately 3 hours to complete. During this period two EL vials were damaged because of over tightening the metal channel; the data from these instruments were ignored and the remaining eleven devices (see Figure 3-2) were used to derive the displacement profiles.

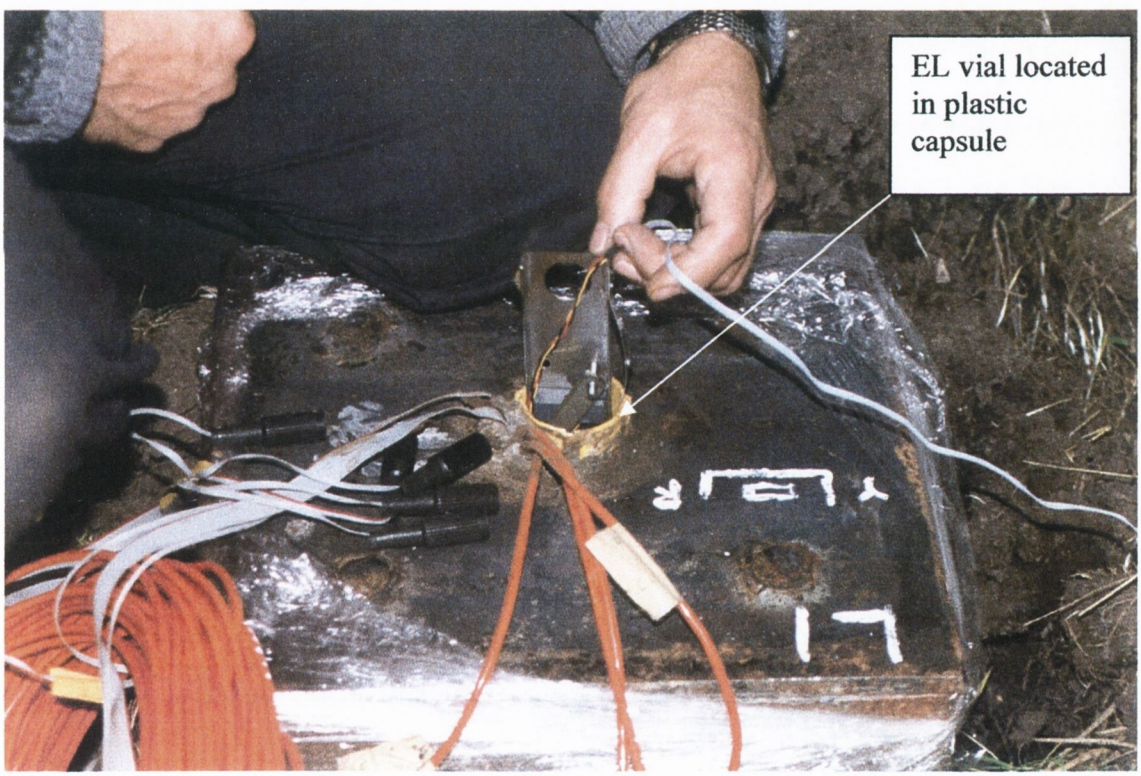

Plate 3-8: Installation of ELs in inclinometer tube using metal channel piece

[7] Any non-load related movement of the ELs would be detrimental to the results obtained during the load tests.

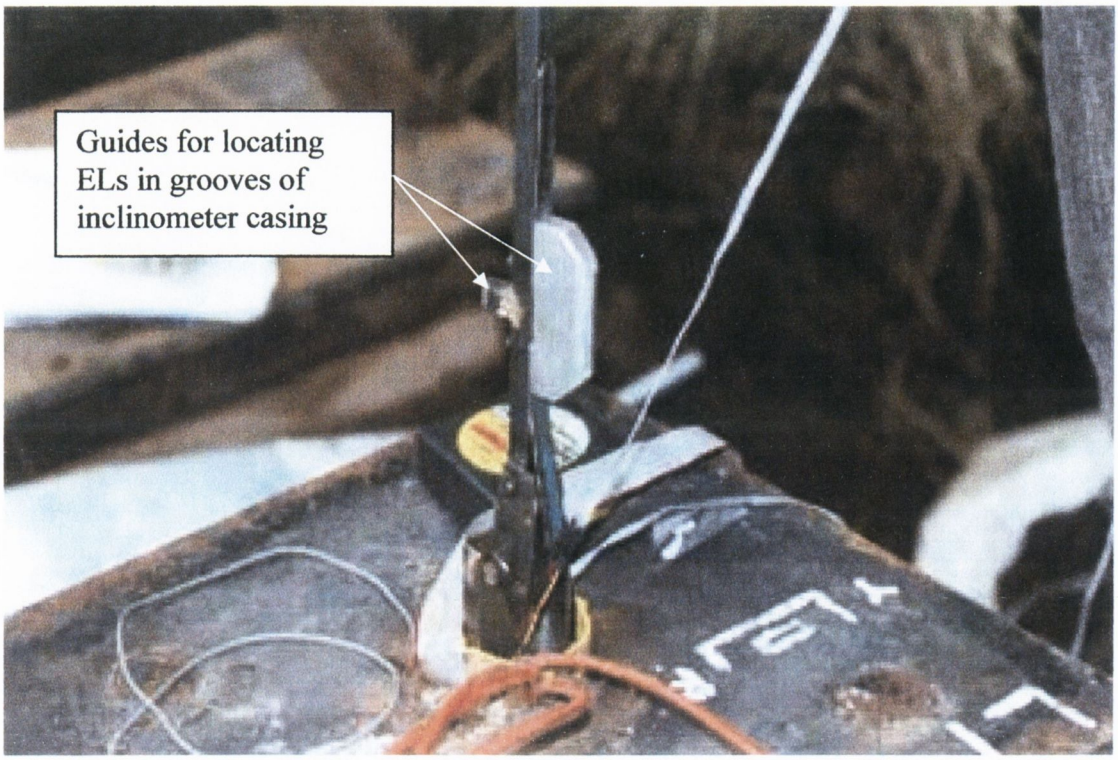

Plate 3-9: Device for installing and removing ELs

3.9 Lateral Loading Arrangement – Pin & Roller

The lateral loading was achieved by jacking the piles apart; steel collars, placed over each pile were connected in series to a jack, load cell and a rigid steel strut. The arrangement was levelled and its alignment maintained (by temporarily propping off the side excavation) until a small initial load was applied to stabilise the set-up.

The application of vertical and lateral load to pile AL1 necessitated the development of a special detail above the pile head (Plate 3-10). To permit translational movement of the pile, a roller mechanism, consisting of smooth hardened steel bars, was housed directly beneath the main test beam. A pin joint was positioned on top of the helmet and a load cell and jack were sandwiched between the pin joint and the roller. The instrumentation cables were connected to the DAS located in the cone truck via the open sided helmets (Plate 3-7).

3.10 Kentledge Details

The kentledge providing the axial load for the test was located centrally over pile AL1 (Plate 3-11). It consisted of a main test beam made up from four 457mm deep stiffened steel beams that supported a grillage of 254 mm deep structural steel beams. The test beam and grillage weighed 5 tonnes and supported fifteen 3.25 tonne concrete cubes, giving an overall dead weight of ≈54 tonnes. The kentledge was supported on timber cribbing and mass concrete blocks for a period of ≈ 2 hours prior to transferring the axial load to the pile. As the maximum axial load applied to pile AL1 was only 170kN, a factor of safety of 3.2 against kentledge uplift was provided.

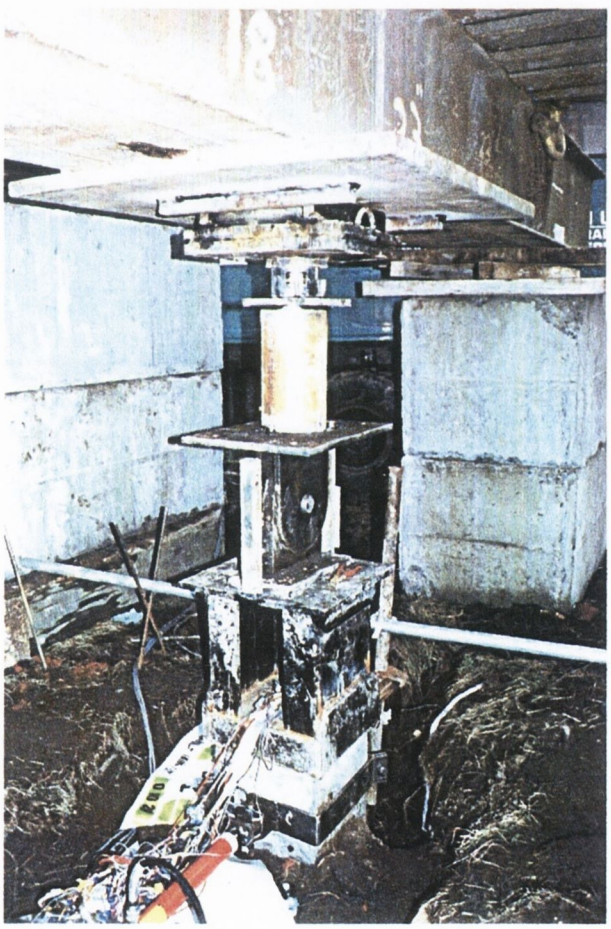

Plate 3-10: Mechanism used to apply axial and lateral loads to pile AL1

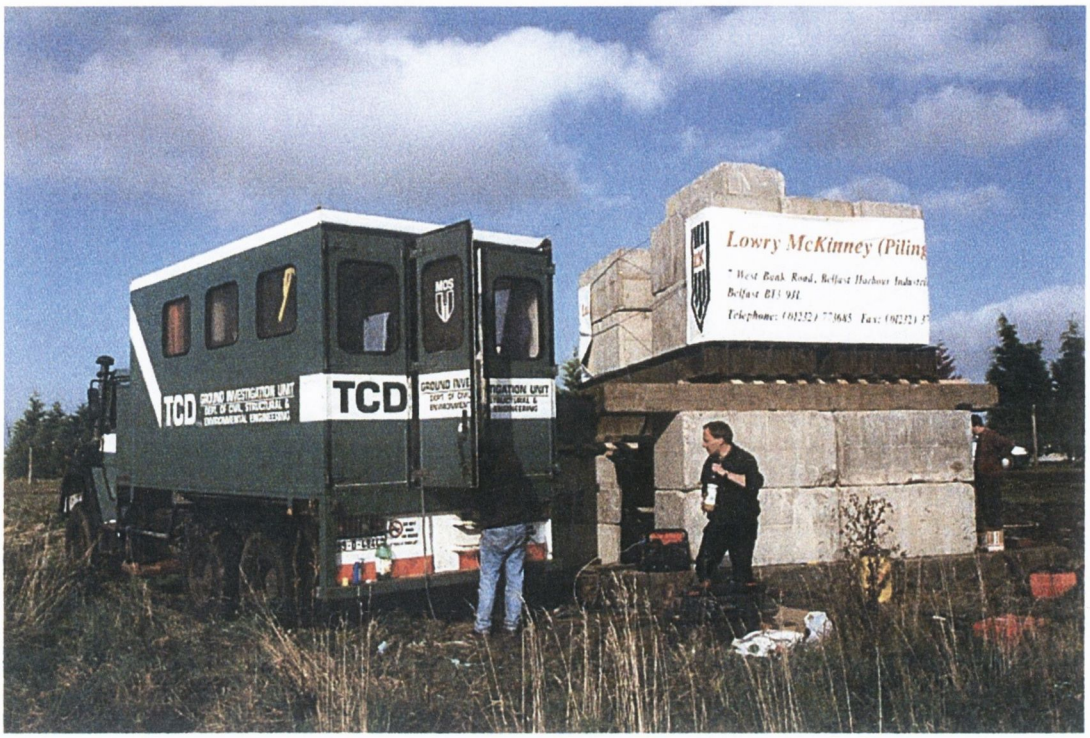

Plate 3-11: Kentledge set-up and CPT truck used to house the DAS

3.11 Details of Loading Tests

3.11.1 Axial Load Test

As one of the main objectives of this thesis was to assess the influence of an axial load on the performance of a laterally loaded pile, and not specifically to assess the performance of the pile under axial load; an accelerated axial loading procedure was adopted. The load was applied in eight quick succession increments by a hand operated hydraulic jack. An initial a load of 10 tonnes was applied in three steps followed by a series of 1.5 tonne increments up to a maximum load of 170kN. The pile head settlement was monitored using two dial gauges located on the diagonal edges of the pile (see Figure 5.1 in chapter 5) and supported on independent reference beams.

Load increments were maintained for a minimum of four minutes to permit a number of dial gauge and VW gauge readings to be obtained while the DAS monitored the ERS gauges every 10 minutes.

Secondary monitoring of the pile settlement was performed using a surveyor's level to record the movement of two vernier sighting cards. One vernier card was fitted to the pile and the second fitted to the reference beam support. The cards permitted vertical movements to be resolved to the nearest ±0.5mm and their location on the pile and referencing system meant that the measured data served as an approximate check on the settlement measured by the dial gauges.

3.11.2 Combined Axial and Lateral Load Tests

To avoid overlapping stresses between the piles, the lateral loads were applied by jacking the piles apart. The axial load of 170kN on pile AL1 had been in place for 20.5 hours in advance of starting the first combined load test, test CLT1. The load dropped over night to 168kN due to relaxation in the hydraulic jack or creep. The axial load was maintained at this level for the duration of CLT1 and once CLT1 had commenced no further monitoring of the vertical settlement of pile AL1 was performed.

The loading procedure involved increasing the lateral load in a series of small increments of ≈4.4kN. Each increment was held for a period of four minutes during which time the instrumentation was monitored at the following frequency; ERS gauges, ELs and PC's were logged every thirty seconds, VW gauges every two minutes and the load cell and displacement transducers at one-minute intervals.

The procedures adopted for CLT2 were identical to those in CLT1 except that the axial load on pile AL1 was reduced by ≈ 20% to 133kN about an hour before starting the test.

The stability of the kentledge was monitored during both tests using an engineer's level and a vernier-sighting card mounted horizontally on the main test beam. A benchmark reading was taken before starting the test and subsequent readings were taken at one-minute intervals during the tests.

3.11.3 Re-test

The piles were re-tested nineteen months after the initial tests using the test set-up shown in Plate 3-12. Only lateral loads were applied to the piles during the re-test.

Plate 3-12: Set-up during re-test

The test procedures were identical to those adopted for the earlier series detailed in section 3.11.2. The equipment employed to load and monitor the piles is shown in Plate 3-13. The initial tests (from October 1997), involved jacking the piles apart using a lateral force applied 140mm above ground datum[8]. The same loading arrangement was used for the re-test but with the jacking force (and the displacement transducers) located 300mm above datum. The application of lateral load at the higher elevation resulted in ground level bending moments ≈46% greater than those applied during the initial tests.

Data logging was performed using the portable 'Recorder' system connected to a laptop computer; the system was capable of accommodating the reduced number of instruments

[8] Ground datum refers to the ground level existing between the two piles

monitored during the test and thus provided a detailed record of the load and displacement history for the test. Logging to the computer was carried out at 30-second intervals with the manually recorded instruments (dial gauge and vibrating wire strain gauges) logged at one and two minute intervals respectively. The load increments and loading rates were similar to those applied during the initial test programme.

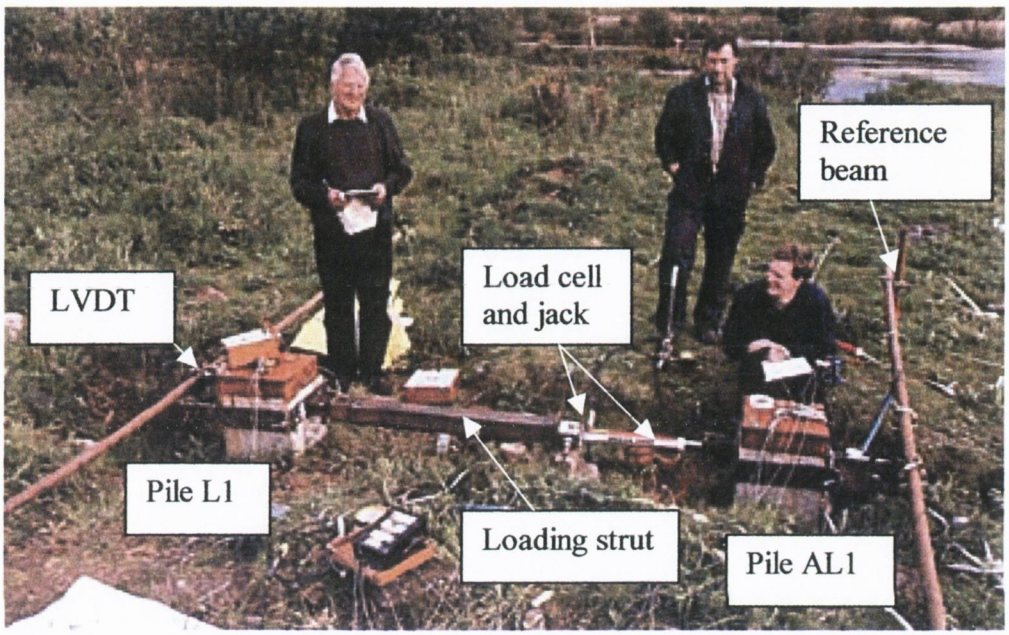

Plate 3-13: Load test set-up for re-testing

Chapter 4

Geology and Soil Properties at Kinnegar

4. GEOLOGY AND SOIL PROPERTIES AT KINNEGAR

4.1 Background

The geological and geotechnical properties from a designated test site at Kinnegar, Belfast are outlined in this chapter. The chapter summarises the results of parallel research under taken at the site by the author and McCabe (2002). In this thesis the geotechnical properties close to ground level receive special emphasis since they control the behaviour of laterally loaded piles.

4.2 Site description

Site location

The 'Kinnegar' site is located on the south side of Belfast Lough, 10km north east of Belfast city and 2km south east of Holywood village; see Figure 4-1. The site is located immediately south of Kinnegar sludge de-watering plant and is within 100m of the Tillysburn gate entrance to Belfast Harbour Industrial Estate. Permission to use the site as a geotechnical test bed was granted to TCD by the Dept. of the Environment (Northern Ireland) in 1996.

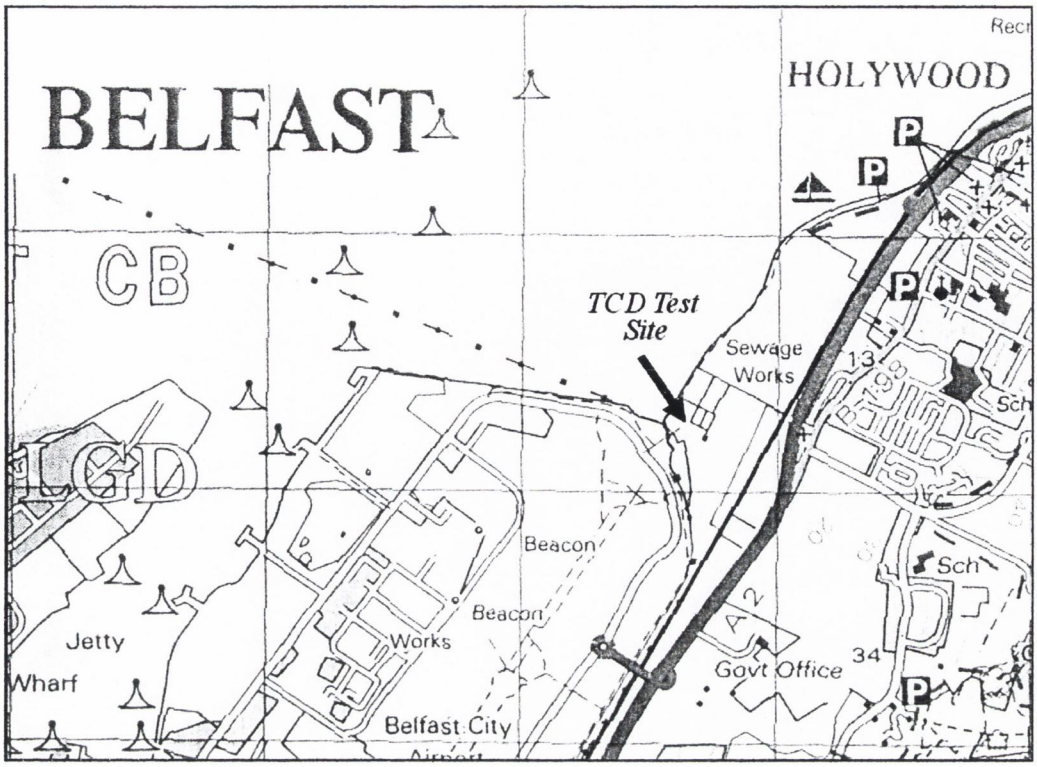

Figure 4-1: Test Site location (OSNI, 1:50000, Sheet 15 (20000), 175%

The site measures about 250m by 100m, is relatively level and lies just north of a 'pond', which is connected hydraulically to Belfast Harbour. The pond and its surroundings provide a habitat to a variety of wildlife. Only the southern half of the site (close to the pond) was used for pile testing and site characterisation studies.

4.3 Soil properties

4.3.1 Scope of site investigation

Investigations at a site close to the Kinnegar foundation test site have been reported by Crooks & Graham (1976) and Bell (1977) while specific investigations at the test site have been conducted or commissioned by Trinity College Dublin (TCD). The TCD investigations, which have been ongoing since 1997, include:

- Sampling using 100mm diameter piston samples (carried by the Northern Ireland Department of the Environment) and a 'Geonor' 54mm diameter samples (carried out by TCD)
- Trial pits conducted by TCD
- Piezocone, standard electric cone penetration tests and field vane tests (conducted by TCD)
- Seismic cone, cone pressuremeter and dilatometer tests conducted by BRE
- Classification testing at TCD, including X-ray diffraction and electron microscope analyses.
- Chemical analyses performed by Lutenegger and Cerato (2001)
- Parameter determinations at TCD in oedometer, shear box, ring shear, simple shear and triaxial tests.

The site plan shown in Figure 4-2 shows the borehole and in-situ test locations. The position of the test piles in relation to the borings and in-situ tests is shown in Figure 4-13.

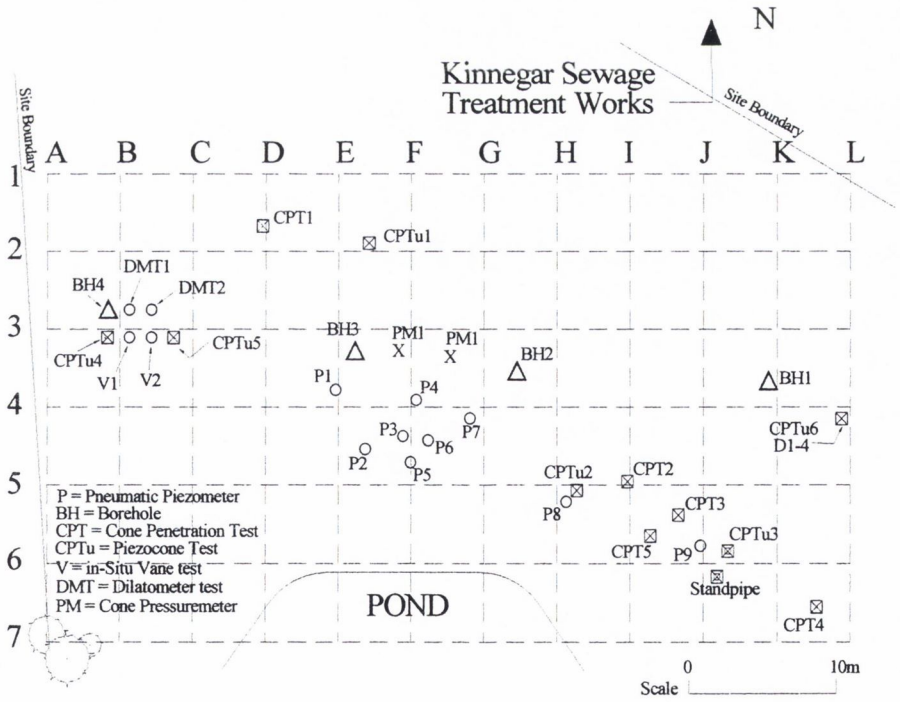

Figure 4-2: Site plan identifying borehole and in-situ test locations (from McCabe 2002)

4.3.2 Site geology

The geological succession of the drift deposits at the test site comprises glacial till underlying about 8.5m of estuarine clays, silts and sands. Deposition rather than erosion was the main feature of the glacial retreat. Extensive amounts of boulder clay were deposited in much of the Belfast area, with the exception of the central district and some zones in the north and east. This glacial deposit has been categorized into three distinct regions: (i) Upper Boulder Clay, (ii) Malone sands and (iii) Lower Boulder Clay. Dark, brown, silty, laminated clays have been found both at the base of the Malone sands and elsewhere in the lower boulder clay. Both the laminated clay and the Malone sands are believed to have formed in a glacial lake during the retreat of the main glacier. Some red marine clay has also been found, believed to be the result of the (geologically) sudden inundation of a large area of land by the sea.

The intermittent strata of sand and clay identified from DoE boreholes below the base of the soft clay at Kinnegar are broadly consistent with the chronology of glacial deposition described above. Late glacial deposits represent a product of erosion of the late-glacial land surface and are derived directly from the glacial deposits, and hence are composed of the same materials. They are inorganic fine sands and are readily distinguishable from the estuarine deposits; furthermore a layer of peat often separates the estuarine material from the fine sands. Doran (1992) has reported that these late glacial sands are considerably less compact than the Malone sands of the region.

The glacier retreat about 10,000 years ago was followed by considerable isostatic uplift (Figure 4-3) but also by a general rise in sea level (Crooks & Graham 1976). The estuarine materials were transported and deposited by the Lagan, Connswater and Blackstaff rivers, all of which confluence into Belfast Lough. The eustarine clays, known locally as *sleech*, were generally laid down on a peat layer and are estimated to be about 8000 years old. The clays underlie most of central Belfast, and have a maximum thickness of about 15m (Crooks and Graham, 1972). They are soft, with an average undrained shear strength of the order of 20kPa. They are very slightly overconsolidated, the preconsolidation load being consistently higher than the present overburden pressure by an amount equivalent to a fall in water table of approximately 1 to 2m (Doran, 1992).

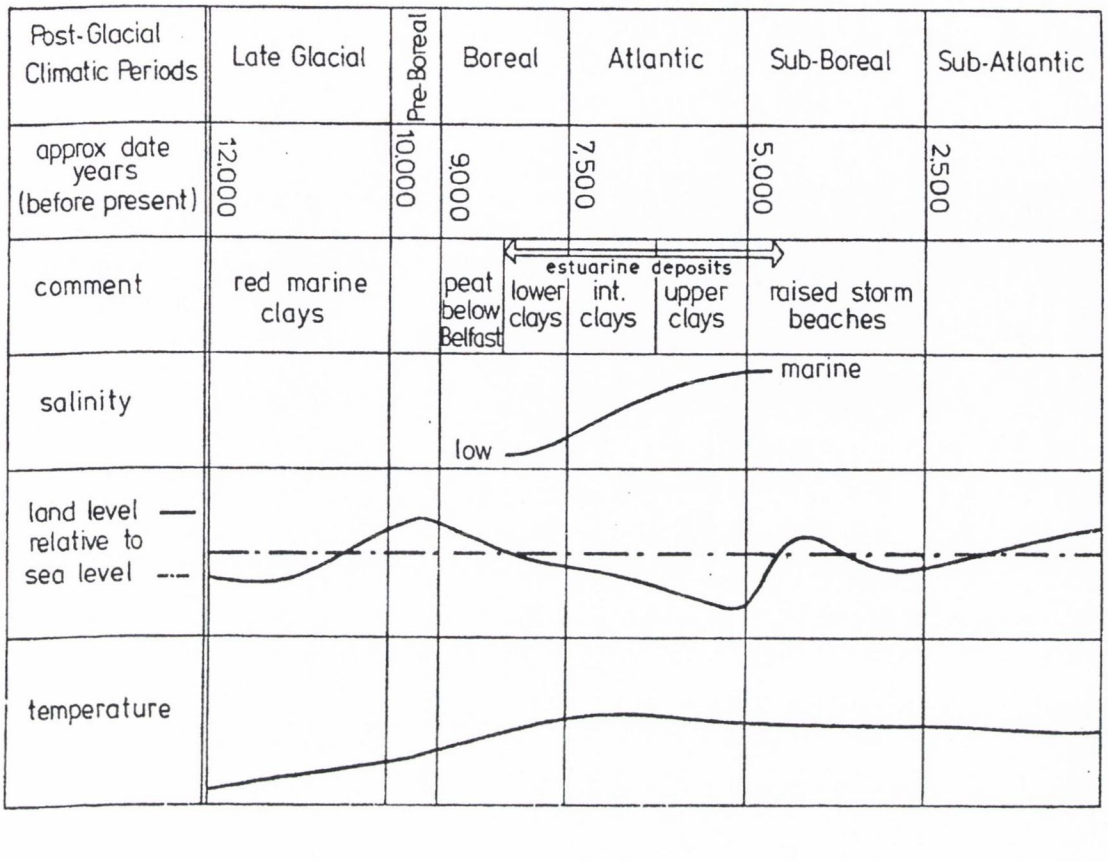

Figure 4-3: Suggested chronology of post-glacial geology of Belfast (Bell 1977)

Manning et al. (1972) subdivide the estuarine deposits into three phases (Figure 4-3). The Lower Estuarine clay was deposited under flat tidal conditions. Warm, low-salinity open water 5.5m deep facilitated the deposition of the Intermediate clay. The upper clays were deposited in marginally cooler conditions and laid down in 9m of salt water. This entire process took place over a period of 3000 years. This depositional environment is thought to be somewhat more energetic than that of the Bothkennar clay-silt (which has been the subject of extensive research, Hight et al., 1992).

Post-depositional processes are thought to include bonding, some leaching and groundwater fluctuations. Approximately 1m of sandy fill material was placed in the vicinity of the pile tests during construction of the nearby sewage treatment plant about 35

years ago (Glynn, 2001). This is consistent with borehole records from 1968 that note the presence of dense miscellaneous fill to a depth of 1m at the site.

4.3.3 Site stratigraphy

The boreholes, trial pits and Cone Penetration Tests performed in the general area of the pile tests revealed the stratigraphy summarised in Table 4-1.

Stratum	Approx. Depth (m)	Description
1	0-1.0	Matrix of building rubble with loose to dense silty sand and very silty gravel overlain by 0.1m of topsoil
2	1.0 to 1.3-2.5	Loose dark grey organic very silty SAND with some clayey silt lenses and shell fragments
3	1.3-2.5 to 8.5	Soft dark grey organic clayey SILT with shell fragments
4	8.5-11	Medium dense brown silty fine to medium SAND

Table 4-1: Stratigraphy in general area of pile tests

4.3.4 Soil composition

The particle size distributions, Atterberg limits and water content determinations are summarised in Figure 4-4 and Figure 4-5. Most of these determinations were performed on samples from Strata 2 and 3, which are estuarine deposits referred to earlier as 'sleech.'

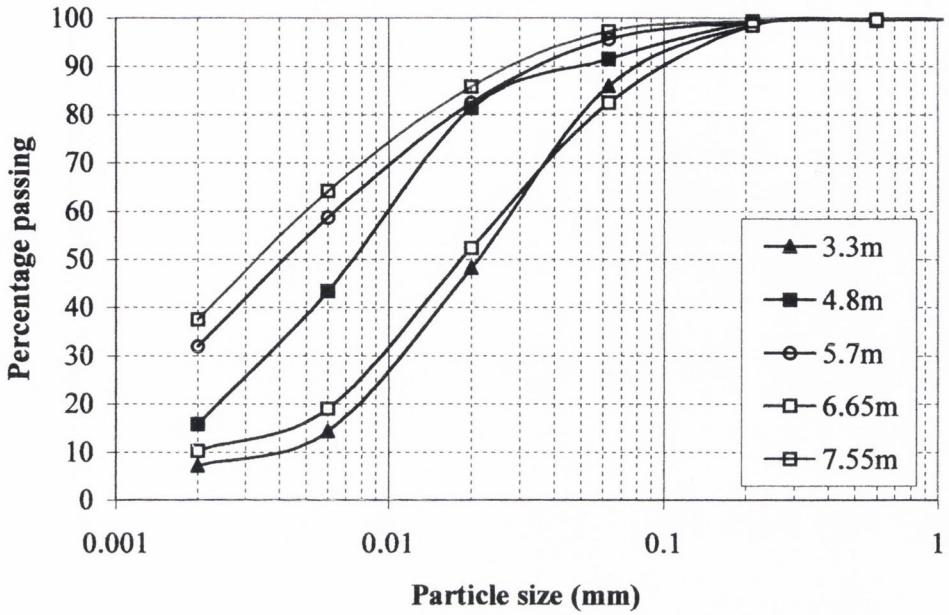

Figure 4-4: Particle size distribution results

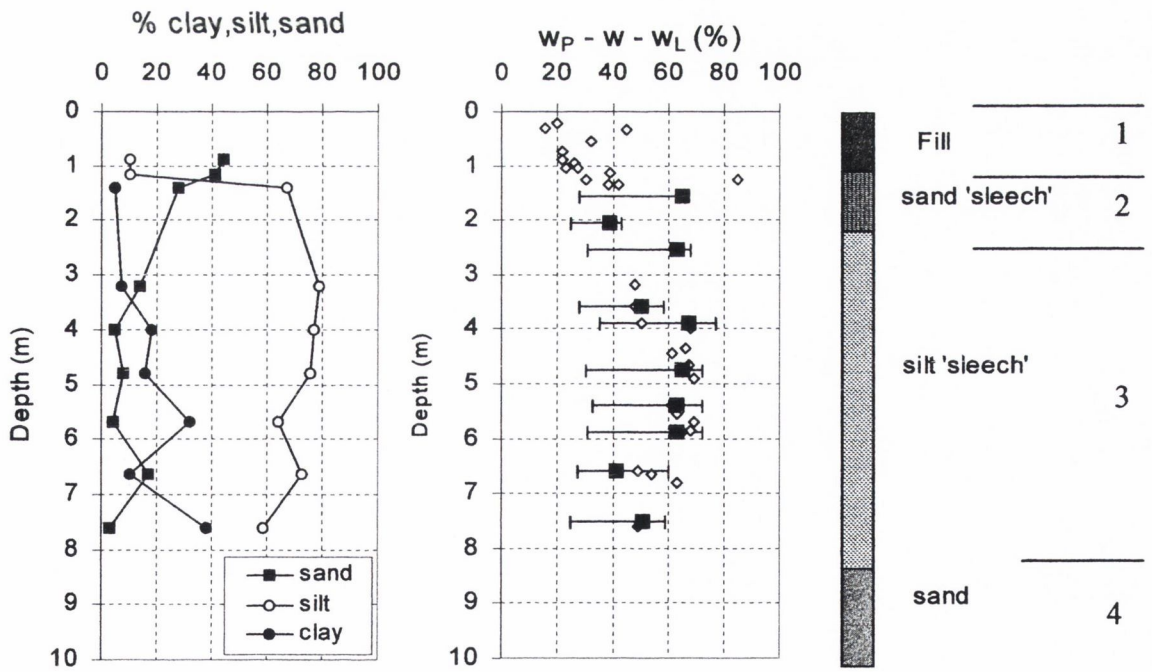

Figure 4-5: Index properties

Stratum 1

This stratum is highly variable and reduces in thickness towards the pond at the south of the site (see Figure 4-2). While it can be generally classified as sandy gravel or gravelly sand, topsoil was observed to extend to a depth of about 1m at a number of locations while poorly compacted brick and concrete rubble extended to 2.2m at other locations. A discontinuous 100mm thick vein of fibrous peat existed at the base of this layer in one trial pit.

Stratum 2

Although being of the same colour and containing similar quantities of organic matter and shells to Stratum 3, this stratum is generally non-plastic and contains a much higher percentage of coarse silt and fine sand. Observations made in trial pits and in the CPTs indicate that the stratum is primarily a silty sand but contains layers and lenses of sandy silt and occasional clayey silt.

Stratum 3

Stratum 3 may be generally described as a clayey organic silt, although clay fractions vary significantly from about 8% to 38%; such variability was not indicated by any of the in-situ tests (see Section 4.6). X-ray diffraction analyses indicated that the clay fraction is composed predominantly of illite and chlorite; quartz and calcite exist in smaller quantities and some traces of smectite were detected. Organic contents determined by the loss on ignition method at 450°C showed variability of less than 1% about the mean value of 11.5%. Chemical analyses reported by Luttenegger and Cerato (2000) on material smaller than 40μm (i.e. between ≈75 and 95% of the material) indicated a composition comprising about 50% quartz, between 15 and 20% dolomite and between 4 and 8% calcite. Electron microscope images, such as those shown on Figure 4-6, confirmed the presence of clay minerals and revealed a significant quantity of (siliceous) diatoms.

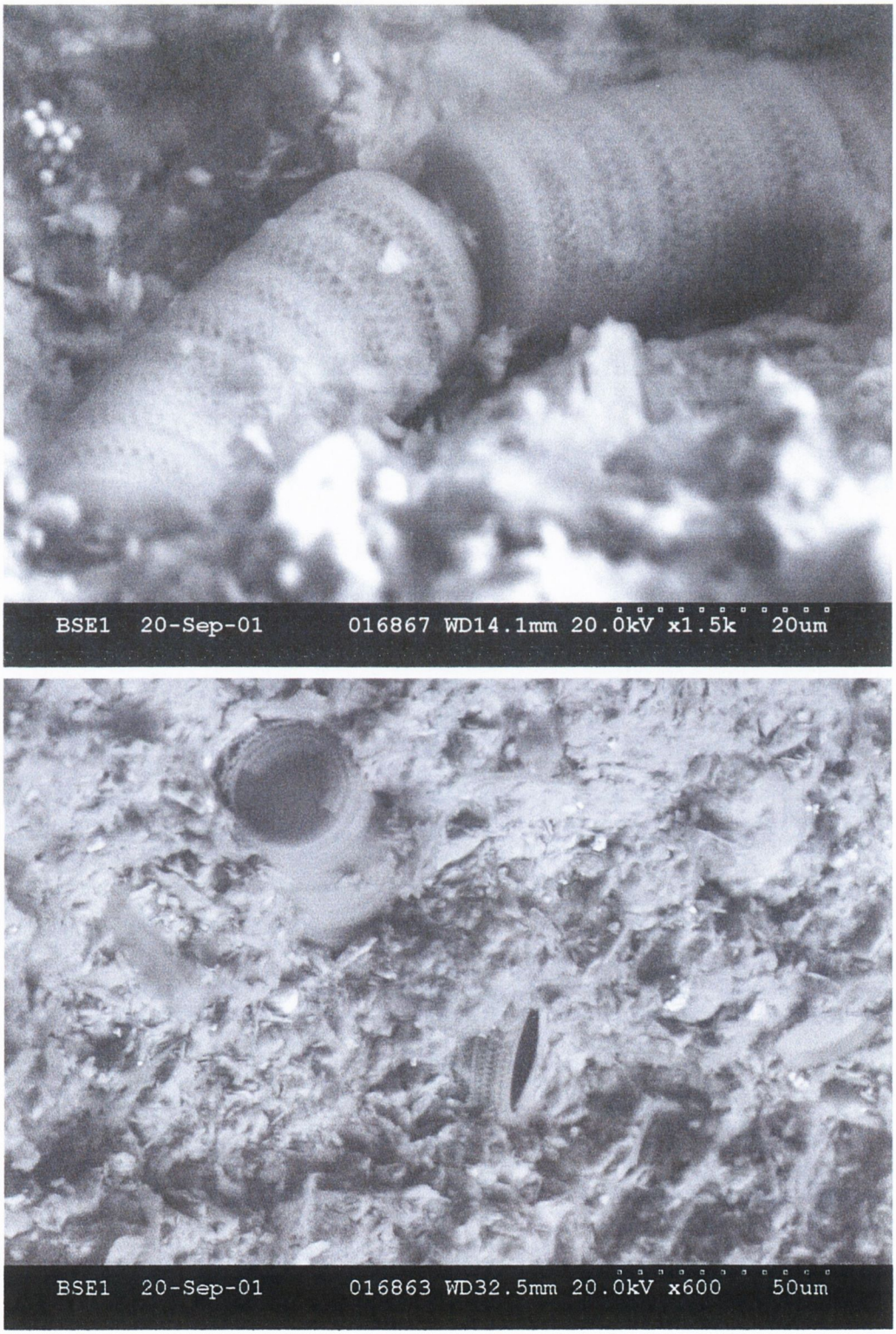

Figure 4-6: Electron microscope images of sleech showing diatoms

Water contents are typically 60 ± 10% and are generally consistent with an average liquidity index of ≈0.8 throughout the stratum. The mean liquid limit of 65 ± 10% and plasticity index of 35 ±5% plot in the high plasticity range of the Casagrande plasticity chart. However, a number of Atterberg limit determinations performed on samples with the organic fraction removed (by loss on ignition at 450°C) indicated that the liquid limit fell by about 20% and the plastic limit remained unchanged. The material with the organic fraction removed falls within the intermediate plasticity range; this plasticity, according to Hight et al. (1992), is likely to be more indicative of its mechanical characteristics. Sample inspections revealed that at least part of the organic fraction is composed of coarse fibrous plant material, which does not contribute to the high plasticity. As with the Bothkennar clay-silt, the organic fraction is therefore also likely to comprise the residue of marine organisms which have attached themselves to the clay.

Stratum 4

No laboratory tests have been performed on this stratum and reliance is placed on visual inspections, which describe it as a 'uniform fine to medium sand'.

4.3.5 Behaviour in 1-D compression

Compressibility

The response of the 'sleech' in standard 24-hour 1-D compression tests is shown for typical tests on Figure 4-7, which also plots the measured intrinsic compression line (ICL) of the same material after reconstitution at 1.3 times the liquid limit (w_L). The initial classical response of a natural (structured) soil is in evidence (i.e. a compression curve well above the ICL), which is followed by general convergence with the ICL at a stress of about 1 MPa. Measured compression indices for the reconstituted soil (C_c*) were in close agreement with those deduced from the Burland (1990) correlation between C_c* and the void ratio at the liquid limit. Use of this correlation for all oedometer tests indicated a relatively constant C_c/C_c* ratio of 1.3 ±0.1 (where C_c, which had a average value of 0.6, is the measured normal consolidation compression index of the intact soil up to σ'_v= 1MPa).

The ratio of the creep coefficient, C_α, to C_c was relatively constant at 0.04 ±0.01 in all the oedometer tests in the normally consolidated range.

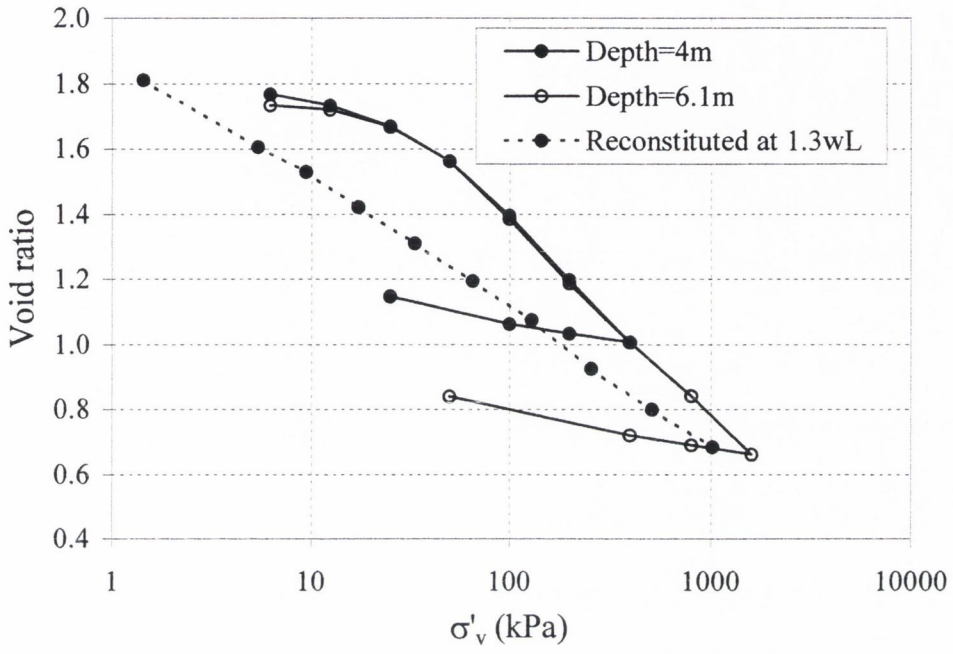

Figure 4-7: Typical oedometer results from tests performed on the sleech

Overconsolidation

Vertical yield stress ratios (YSR= $\sigma'_{vy}/\sigma'_{v0}$) inferred from oedometer tests on Stratum 3 varied from ≈1.6 at a depth of 3m to about unity a depth of 8m (McCabe 2002). Such a variation in YSR with depth arises as σ'_{vy} was found to be effectively constant at a value of 55 ±5 kPa. The tendency for a relatively constant σ'_{vy} value is compatible with fluctuating water levels at the site (as suggested by Crooks & Graham 1976), although better quality samples may well have indicated higher σ'_{vy} values at all depths within the stratum.

Although the soil in Stratum 2 is generally a silty sand, one sample of clayey silt was recovered from a depth of 1.4m. A standard oedometer test on this sample indicated a vertical yield stress of 60 kPa (≡ YSR of 2.7) and a C_c value of 0.28 which is less than half of the average of Stratum 3.

4.3.6 Permeability and coefficient of consolidation

Permeabilities estimated from oedometer tests on Stratum 3 reduced with increasing stress level but were typically in the range 1.5×10^{-10} to 5×10^{-10} m/s at in-situ stress levels.

Vertical coefficients of consolidation (c_v) determined in the same set of oedometer tests reduced from about $3m^2$/year in the overconsolidated region to $\approx 0.5m^2$/year at a vertical effective stress of 100 kPa. Piezocone dissipation tests performed in Stratum 3 indicated that the horizontal coefficient of consolidation, c_h (determined using the procedure of Houlsby and Teh, 1988) varied from $\approx 7m^2$/year to $\approx 12m^2$/year.

Overall, it appears that, despite the high silt content of Stratum 3, the clay fraction is sufficiently influential to lead to permeabilities and coefficients of consolidation which are more typical of a clay rather than a silt.

4.4 Strength determined from laboratory tests

4.4.1 Undrained strength in triaxial compression

A typical stress path[1] followed by a Geonor 54mm diameter piston sample sheared in undrained triaxial compression at an axial strain rate of 5%/day is shown on Figure 4-9a. The in-situ stress state of this sample (from 4.8m depth) was first recovered approximately by subjecting it to prescribed anisotropic consolidation, anisotropic swelling and a one day rest (or ageing) period. The undrained stress path is typical of lightly overconsolidated materials in CK_oU tests i.e. the deviator stress reaches a peak value at a low axial strain level (0.5% in this case) and subsequently drops sharply as the mean effective stress reduces and the mobilised friction angle increases.

[1] It should be noted that many of the stress paths shown by reconsolidated 100mm diameter piston samples recovered by DoE, Northern Ireland (and tested about 1 year after sampling) indicated a tendency to dilate at mobilised friction angles of $\approx 30°$. Following inspection by TCD and Queen's University Belfast, these samples were adjudged to have suffered gross disturbance. Arman and McManis (1975) found that the extended storage of thin walled tube specimens adversely affected the soil properties when compared to tests performed on identical specimens immediately after sampling. The authors suggested; relaxation of overburden stresses, changes in pore pressure and unavoidable migration of water within the sample as possible reasons for the changes measured in the soil characteristics.

The undrained strength ratio in triaxial compression (c_{utc}/σ'_v) of 0.41 exhibited in the test plotted on Figure 4-15a falls within the range of 0.4 to 0.45 measured in other similar tests performed at TCD and in CK_oU tests reported by Crooks & Graham (1976). Adopting the c_{utc} value of 17 kPa recorded in the test shown on Figure 4-9a and the average yield stress σ'_{vy} of 55kPa measured in oedometer tests yields a c_{utc}/σ'_{vy} ratio of 0.31. Better quality block or Sherbrooke samples are likely to give slightly higher c_{utc}/σ'_{vy} ratios (while also yielding higher c_{utc} and σ'_{vy} values).

The foregoing suggests that c_{utc} in Stratum 3 is likely to be in the range 17 to 22 kPa. As at the Bothkennar test site, this strength range forms an approximate lower bound to the undrained strength measured in field vane tests; see Figure 4-15.

The rate dependence of the undrained strength of normally consolidated 'sleech' was investigated in two undrained triaxial compression tests performed on 54mm diameter Geonor piston samples from between depths of 4m and 5m. These samples were isotropically consolidated to a mean effective stress (p'_i) of 100 kPa and each was then subjected to triaxial compression at an initial lower axial strain rate and at a final faster axial strain rate. The results from these tests are summarised on Figure 4-8, where it is evident that the c_u/p'_i ratios increase by a factor of 15% for each log cycle increase in strain rate[2].

[2]The 'extrapolated' c_u/p'_i ratios plotted on Figure 4-8b refer to ratios estimated from the initial slower rate adopted in each test.

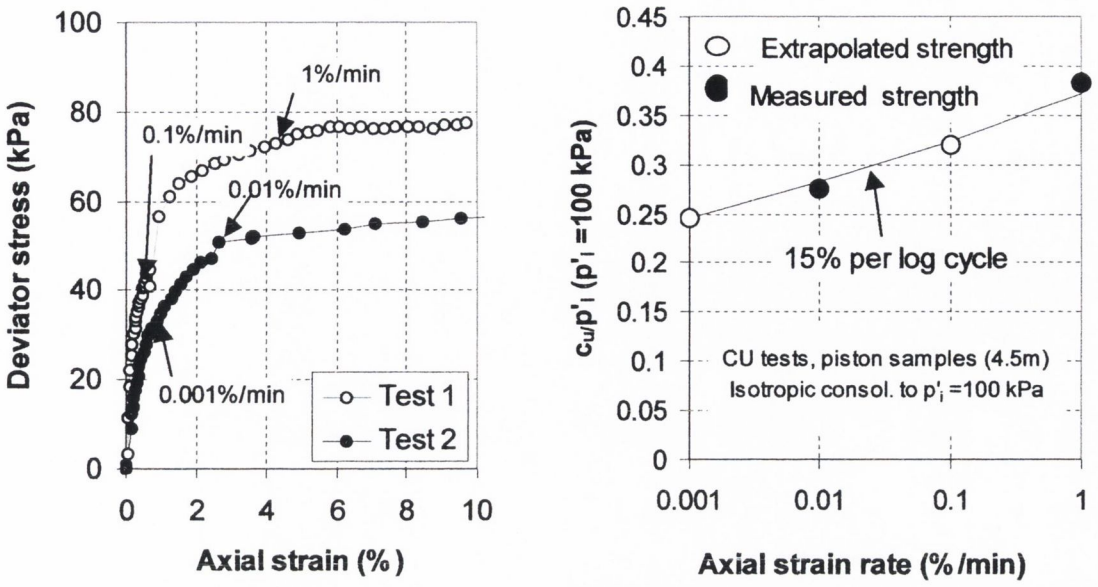

(a) (b)

Figure 4-8: Investigation of rate effects in sleech

4.4.2 ε_{50} from UU Triaxial tests

ε_{50} is defined as the strain at half the deviator stress, and is a reference strain for the development of *p-y* curves in cohesive soils. The value of ε_{50} is correlated empirically with the pile diameter to give a normalising parameter for the soil displacement (see appendix 2b). The API guidelines indicate that ε_{50} is determined from UU triaxial tests on good quality soil samples. The following table summarises the ε_{50} values measured at various depths in the sleech.

Depth below GL (i.e., x = 0m)	ε_{50}
3.6m	0.026
3.9m	0.035
5.5m	0.011
5.8m	0.014

4.4.3 Effective stress strength

The effective stress strength parameters of Stratum 3 were determined in a range of consolidated undrained triaxial compression tests on 38mm, 54mm and 100mm diameter piston samples. All samples were recovered from depths of between 3m and 7m and were tested in undrained compression after consolidation to the estimated in-situ mean effective stress, p'_0 (i.e. between about 29 and 45 kPa). Isotropic overconsolidation ratios of up to 5 were induced in some samples while samples subjected to anisotropic consolidation and swelling followed stress paths similar to those illustrated on Figure 4-9a.

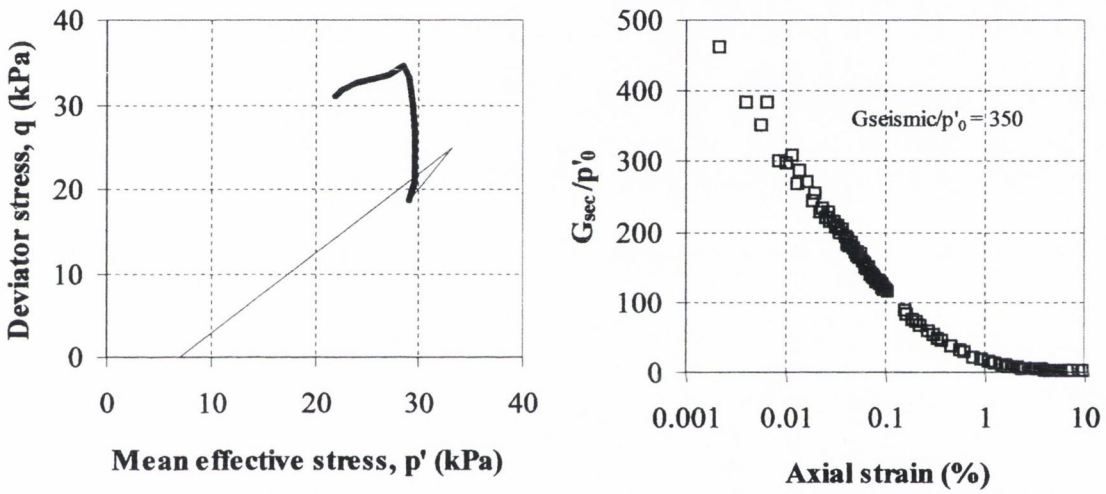

Figure 4-9: Typical (a) anisotropic consolidation and swelling stress path and (b) normalized shear stiffness for Belfast *sleech* (stratum 3)

The values of the t and s' stress invariants at ultimate conditions (i.e. ≈10-20% axial strain) are plotted on Figure 4-10 and indicate a relatively low sensitivity of the ultimate (or constant volume) friction angle (ϕ'_{cv}) to stress history, sample depth and sample quality. As indicated on Figure 4-10, the ultimate strength of this stratum in triaxial compression is well represented by the effective stress parameters, $c' = 0$ and $\phi'_{cv} = 33.5°$. This relatively high friction angle is comparable to that of the Bothkennar clay-silt, which has a slightly higher clay fraction but a lower percentage of clay minerals. It is also noteworthy that the variability in the particle size distributions within this stratum did not lead to a wide range in the ϕ'_{cv} angles.

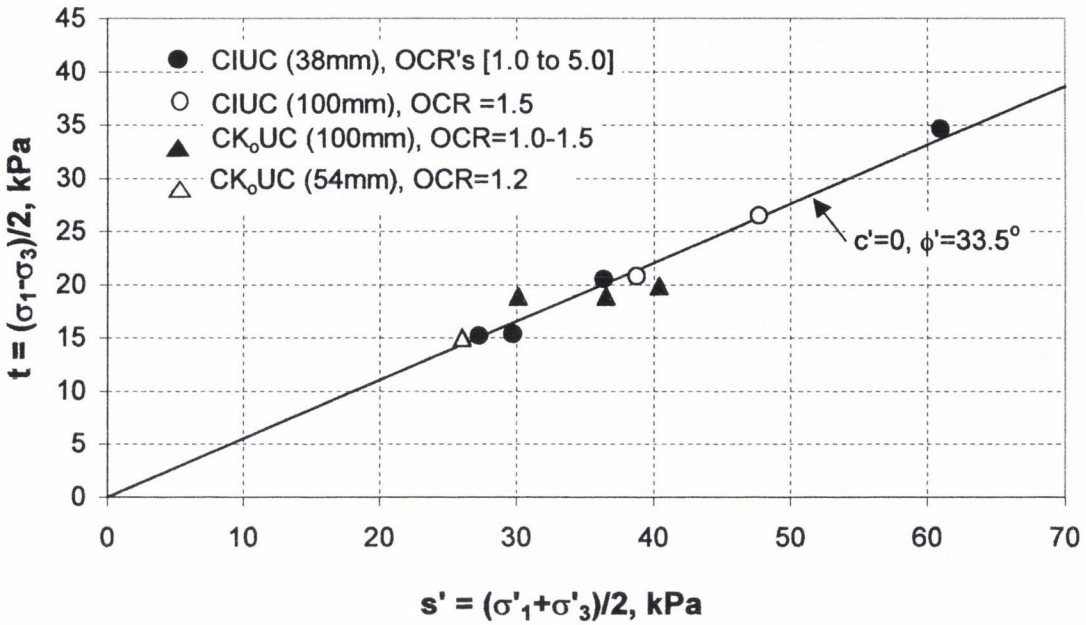

Figure 4-10: Constant volume friction angle for CU triaxial tests

Shear box tests were performed on recompacted samples of the Stratum 2 at normal effective stresses between 50 kPa and 200 kPa. These revealed best fit ultimate effective stress strength parameters of c'=0 and ϕ'_{cv}=35° for the stratum. Shear box tests performed on samples of Stratum 3 at the same stress levels indicated ϕ'_{cv} values of between 25° and 30° i.e. between 3.5° and 8.5° lower than the ϕ'_{cv} value measured in triaxial compression. The results of the shear box tests are plotted in Figure 4-11.

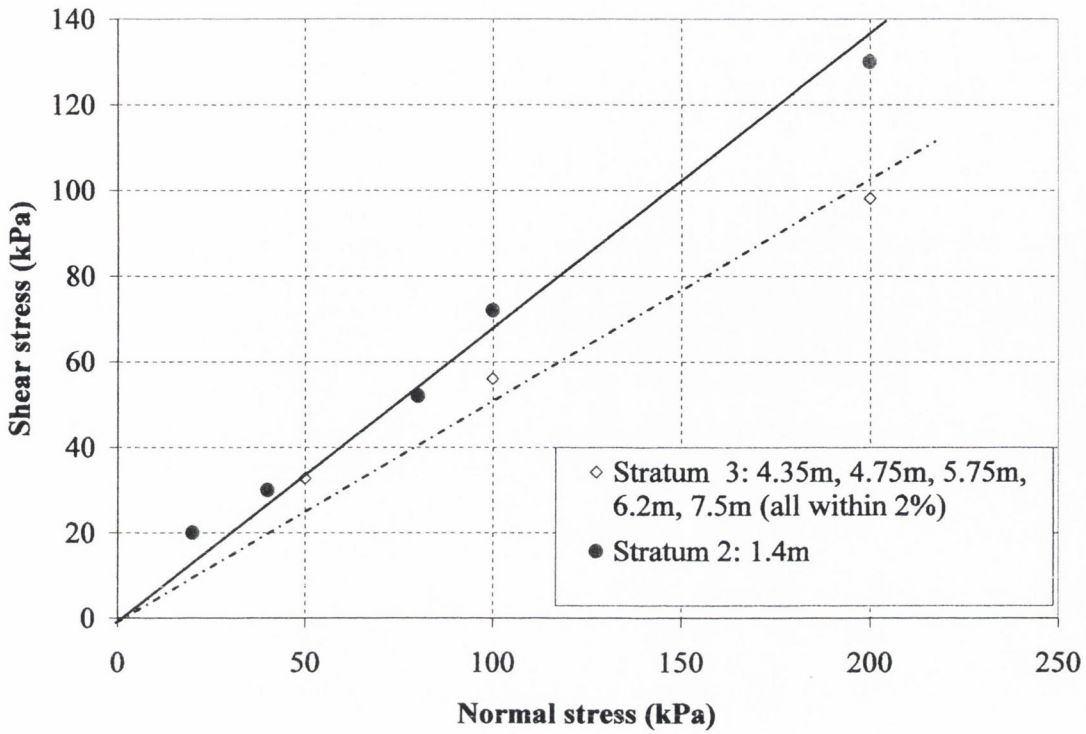

Figure 4-11: Shear box test results for strata 2 and 3

4.4.4 Stiffness

The secant shear stiffness normalised by the initial mean effective stress at the beginning of undrained shearing (G_{sec}/p'_0) measured in the CK_oU test (Figure 4-9a) is plotted against local axial strain[3] on Figure 4-9b. The observed variation of shear stiffness compares well with comparable data for Bothkennar clay-silt (e.g. see Hight et al. 1992), although the normalised stiffness values of Belfast 'sleech' are typically ≈15% lower.

4.4.5 Residual strength

Following the recommendations of Jardine et al. (1998) for ring shear testing performed for displacement pile design, samples tested in the TCD Bromhead ring shear apparatus after consolidation were first subjected to a large relative displacement (≈500mm) at a fast

[3] Measured using two Hall effect gauges

(undrained) rate of shearing. Samples were then sheared at a slow drained rate of displacement after a rest period of one day. The soil-soil peak and ultimate residual friction angles (ϕ'_{pres}, ϕ'_{res}) measured in this way and at normal effective stress of 100 kPa are plotted against depth on Figure 4-12. It is evident that the ϕ'_{res} down to a depth of ≈3m is comparable to ϕ'_{cv} measured in triaxial compression and that the shearing mode is 'turbulent' i.e. the soil particles are not aligned along the shearing zone. However, below this depth, ϕ'_{res} varies between 19.5° and 25.5°, indicating a 'transitional' sliding mode i.e. where both turbulent and sliding shear takes place in different parts of the shear zone. This shearing mode and the variability of the ϕ'_{res} angles measured is consistent with expectations based upon the composition described in Section 4.3.4.

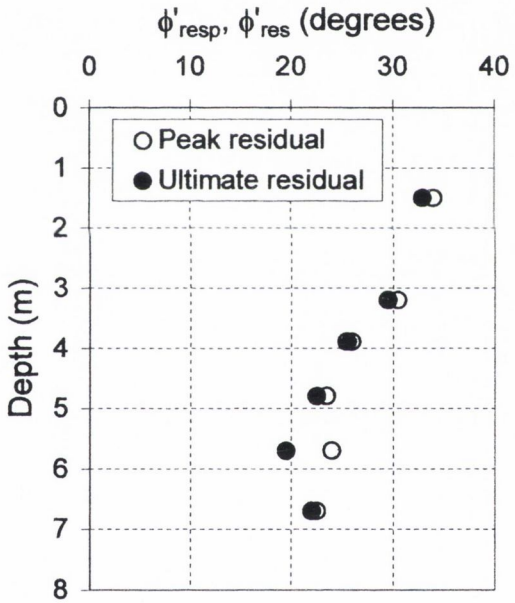

Figure 4-12: Residual friction angles for sleech

4.5 Trial Pit Investigation

In June 2000, three trial pits were excavated in the vicinity of the lateral load test area (see Figure 4-13). Trial pit 3 (TP3) was excavated initially to assess the depth and composition of stratum 1; no detailed logging or sampling was undertaken during the excavation of this

pit but visual examination and depth measurements revealed miscellaneous construction fill intermixed with a tan brown sand and gravel. The depth of fill extended to a depth of 2.2m (Figure 4-14). The thickness of stratum 1 decreased in a westerly direction to a depth of 1.0m at TP2. The test area had a gentle slope in the direction of the pond which is consistent with the variation in thickness of stratum 1. The sampling and in-situ test details for TP1 and TP2 are logged on the following pages. It is of interest to note that c_u values measured by shearing the soil in the vertical face of the excavation are consistent with the c_u values calculated from the pressuremeter tests (section 4.6).

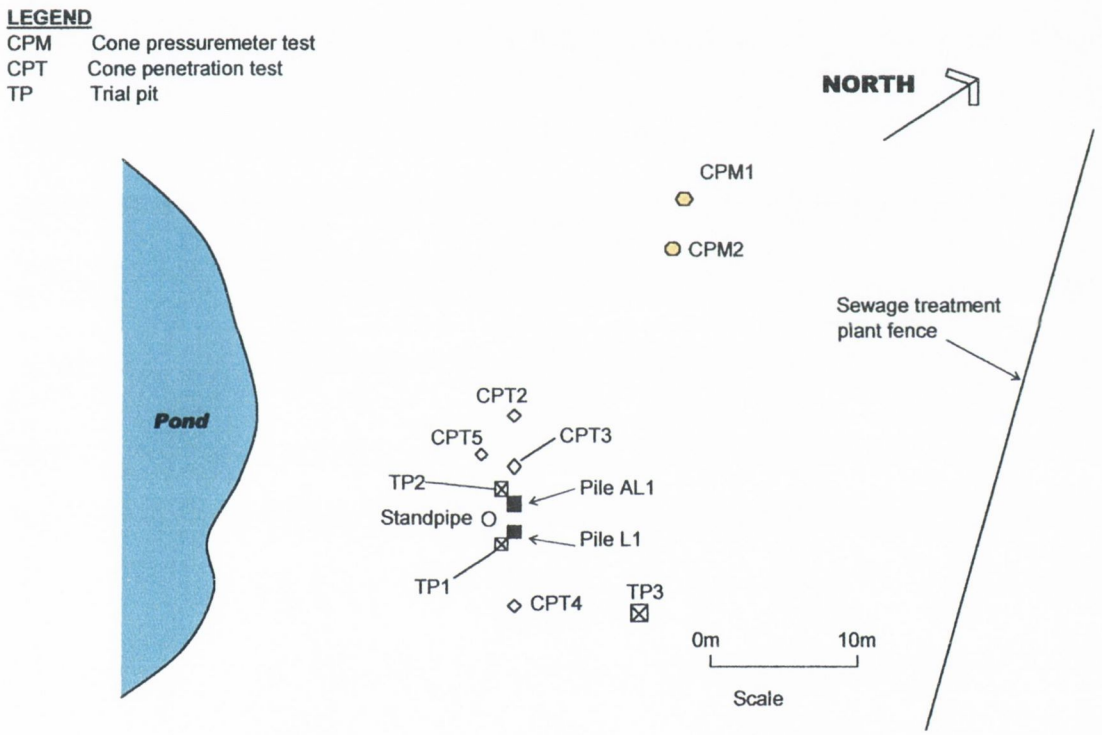

Figure 4-13: Location plan for trial pits and in-situ tests in relation to the test piles

Figure 4-14: Trial pit (TP3) excavated in the vicinity of load tests

Trial Pit 1 ***(Pile L1)***

Depth (m)	Description	Sample	$s_{u\ avg}$ (kPa)	Comments
0-0.1	Topsoil			
0.1-1.2	Misc fill;Brick, concrete wood, glass, fabric surrounded in a matrix of moist, loose to dense, grey to dark brown very silty SAND.	S1 (0.3m), S2 (1.15m), S3 (0.9m), SB1 (0.9m)		Soil excavated in front of pile to an elevation of 0.4m, hence 0.94m of misc fill in front of the pile
1.2-1.3	Soft, saturated black brown fiborous organic soil	S4 (1.25m)		Trickle of water
1.3-2.2	Soft, grey silty sand, strong odour on penetrating stratum.	V1 (1.39m) U-1 (1.39m) SB2(1.39m) S5 (1.8m)	15	Standing water at 1.36m after one hour. Tests performed on the vertical face of the TP using a hand vane). Undisturbed sample taken from the vertical face on the passive side of pile L1

End of trial pit at 2.2m

Note: All levels are referenced from the ground level between the test piles

S1 etc (bag sample for classification) U1 undisturbed sample

SB1 etc bulk sample V1 hand vane

Trial Pit 2 ***(Pile AL1)***

Depth (m)	Description	Sample	$s_{u\ avg}$ (kPa)	Comments
0-0.1	Topsoil			
0.1-0.98	Misc fill; Brick, concrete wood, glass, fabric, cast iron pipe, surrounded in a matrix of moist, loose to dense, grey to dark brown very silty SAND.	S1 (0.4m), S2 (0.95m), S3 (0.75m), S4 (0.55m), S5 (1.05m), S6 (1.10m), SB1 (0.9m)		Soil excavated in front of pile to an elevation of 0.5m, hence 0.5m of misc fill in front of the pile
0.98- 1.15	Soft, saturated black brown fiberous organic soil.	S7 (1.15m)		Trickle of water at 1.0m
1.15-3.4	Soft, grey silt (sleech), strong odour on penetrating stratum. Shells at top of stratum.	S7a (1.25m), S7b (1.35m), S8 (1.55m), S9 (2.05m), S10 (2.55m), V1 (1.39m) V2 (1.55m) V3 (1.75m) V4 (2.05m) V5 (2.55m) U-2 (1.25m) SB2(1.35m)	14 (1.25m) 10 (1.75m) 6 (2.05m) 8 (2.55m)	Standing water at 1.25m after one hour. Tests performed on the vertical face of the TP using a hand vane. Undisturbed sample taken from the vertical face on the passive side of pile AL1

End of trial pit at 3.4m

Note: All levels are referenced from the ground level between the test piles
S1 etc (bag sample for classification)
SB1 etc bulk sample
U1 undisturbed sample
V1 hand vane
The soil immediately adjacent to both piles was grey but as the trial pit was excavated towards the pond the material became dark brown in colour, this may indicate some oxidation of the soil minerals may have occured due to the pile installation and testing. The depth of misc fill reduced towards the pond

4.6 *In-situ tests*

CPT tests

The profiles of CPT end resistance (q_c), peak strengths from in-situ vanes (c_u-vane), shear wave velocities from seismic cone tests (v_s) and limit pressures in cone pressuremeter (CPM) tests (p_L) are summarised on Figure 4-15.

The q_c values provide a clear indication of the significant variability within the fill (Stratum 1) and the sandy 'sleech' (Stratum 2). For example, the lower bound q_c profile suggests a virtual total absence of Stratum 2 while the upper bound q_c profile indicates relatively competent soils to a depth of 2.5m. The stronger consistency of Stratum 2,

compared to Stratum 3, is confirmed by the higher vane strength and (slightly higher) shear wave velocities measured at 1.9m and the higher CPM p_L value at 2.3m.

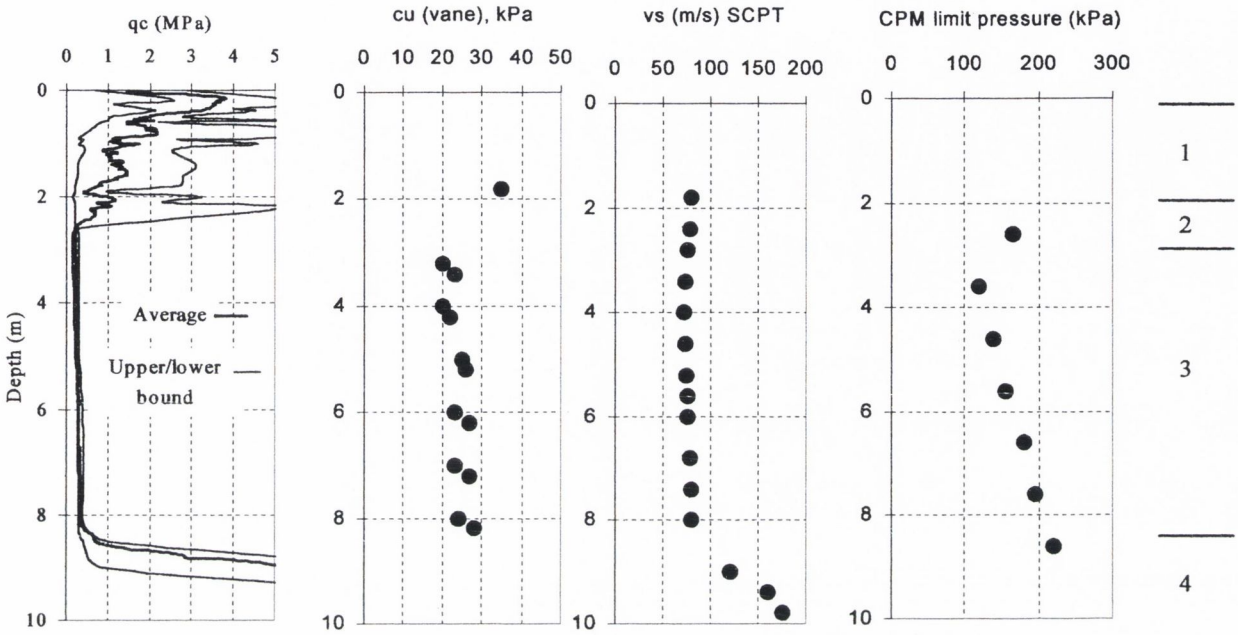

Figure 4-15: Summary profiles

The q_c profiles in Stratum 3 are remarkably uniform, despite the variations in composition indicated by Figure 4-5. Total cone resistances, q_t (i.e. q_c corrected for pore pressures acting on the cone's filter stone) increases linearly with depth from ≈200 kPa at 2.5m to 400kPa at 8m. Vane strengths increase over the corresponding depth interval from ≈20 kPa to 25 kPa and shear wave velocities increase from ≈72m/s to 80m/s.

Figure 4-16 provides individual q_c profiles from standard CPT soundings conducted in close proximity to the laterally loaded test piles: CPT4 was taken close to pile L1 while CPT3 and CPT5 were taken in the environs of pile AL1 (see Figure 4-13). The profiles highlight the variability in the soil over the first 2m below ground level. Prior to conducting the load tests, the top 0.55m of this material was excavated from in front of each pile to remove construction fill located near the ground surface. The q_c profiles shown in Figure 4-16 indicate that the remaining 1.5m of soil around pile L1 was, on

average, twice as strong as that measured over the corresponding depth in the neighbourhood of pile AL1. Retrieval of good quality 'undisturbed' samples for triaxial testing was not practical in stratum 1 given the granular[4] nature of the soil and the number of obstructions present, thus the measured q_c values provide the best indicator of soil strength within this material. These findings were subsequently confirmed by trial pit explorations around pile L1 and AL1.

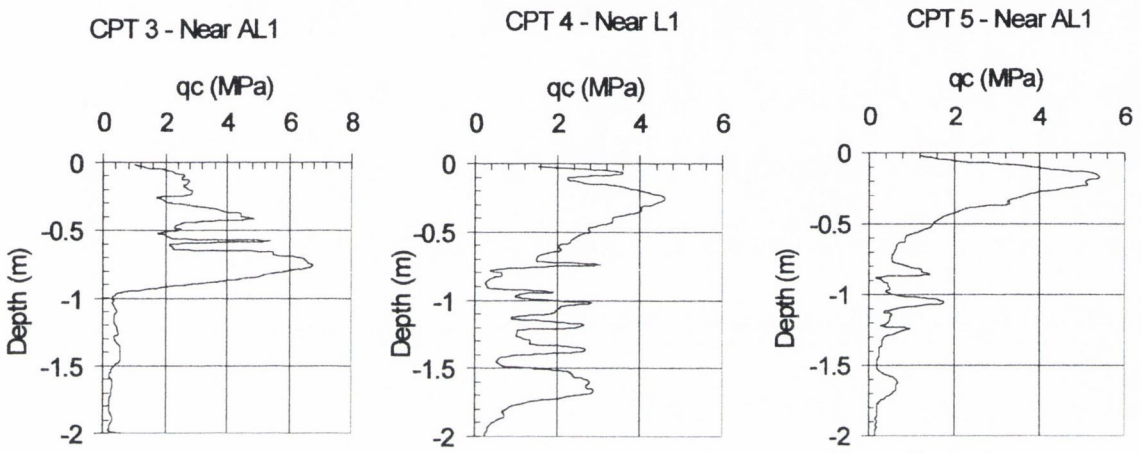

Figure 4-16: Near surface q_c profiles taken in the vicinity of the lateral pile tests.

4.7 Definitive CPT q_c Profiles for piles AL1 and L1

The profiles shown in Figure 4-17 were derived from the set of CPT soundings taken in the vicinity of the laterally loaded pile tests and represent the best estimate of ground conditions at pile L1 and AL1 respectively. These profiles are used subsequently in the interpretation and discussion of the Kinnegar pile tests in chapters 8 and 9.

[4] Particle distribution analyses indicate a silt and clay fraction less than 10% within this material.

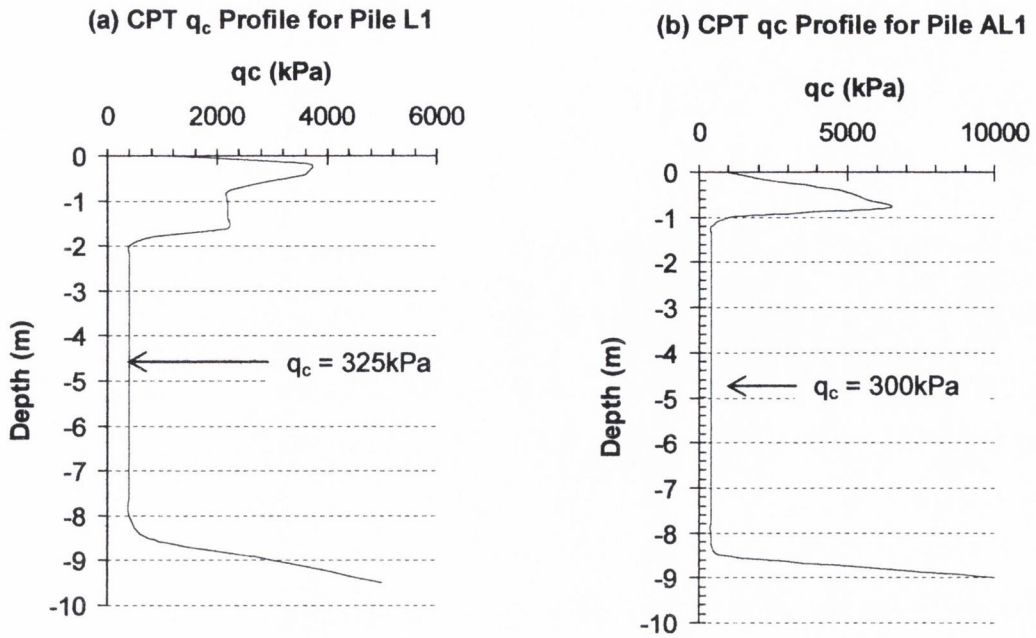

Figure 4-17: Definitive CPT q_c profiles adjacent to (a) pile L1 and (b) pile AL1

Cone pressuremeter (CPM) and Dilatometer (DMT) tests

CPM and DMT tests were performed at the locations shown in Figure 4-2. The results of these tests and the derived soil parameters are presented in the following sections.

Shear strength

Post peak strength is typically determined from the latter part of the pressuremeter curve; using the procedure recommended by Gibson and Anderson (1961)[5]. However, in the case of CPM tests, the method proposed Houlsby and Withers (1988) using cavity contraction theory is recommended. Both methods gave almost identical values[6] for c_u for the Kinnegar soils. The resulting profile is shown in Figure 4-18(a) along with the shear strengths measured by DMT and in situ vane tests. The peak strengths measured by the field vane (vane pk) are approximately twice the magnitude of the post peak strengths measured by the CPM. However, the residual strength (vane rm) at 4m, measured by

[5] In the Gibson and Anderson method, the pressuremeter pressure is plotted against the natural logarithm of the cavity strain. The slope of the straight-line portion of the plot is equal to twice the undrained shear strength ($2c_u$).

[6] Full details of the calculation of c_u are given in Appendix 4

rapidly rotating the vane is consistent with the post peak CPM strengths. Figure 4-18(b) also includes the estimated in-situ horizontal stress σ_{h0} profile calculated using Houlsby and Withers (1988).

Dilatometer tests (DMT)

Two locations (Figure 4-2) were selected for DMT testing using Marchetti's flat dilatometer; the undrained shear strength profiles determined from these tests are shown in Figure 4-18(a). The results were interpreted by the BRE using the method proposed by Powell and Uglow (1988); the DMT c_u profiles are remarkably consistent and display a similar strength trend observed in the CPT q_c and the vane profiles. Undrained strengths at about 2.5m below ground level are close to that measured by the CPM while at the bottom of the sleech the strength was approximately equal to the remoulded vane strength.

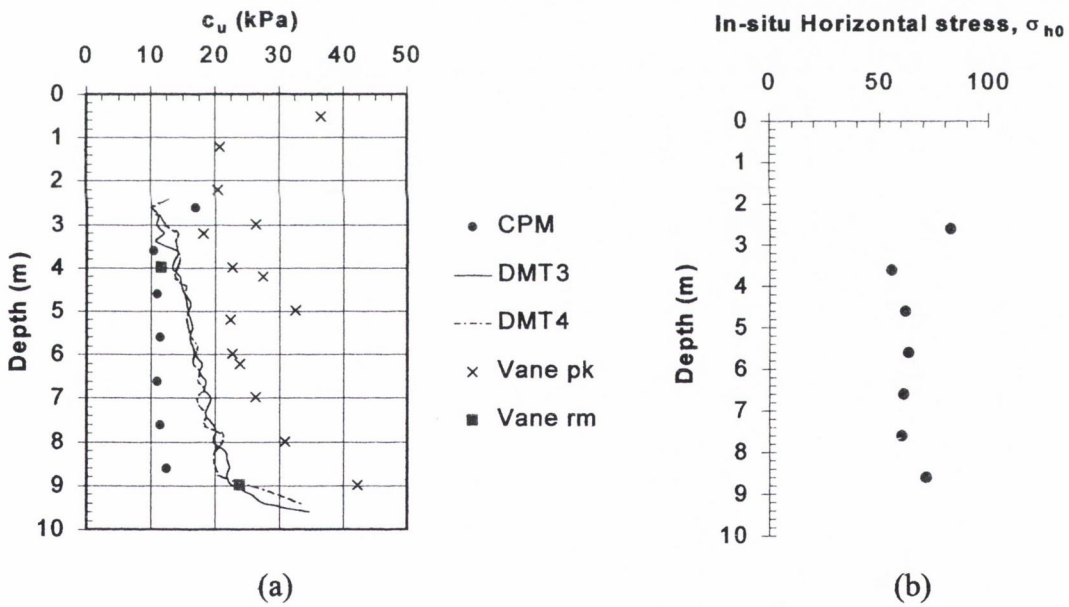

Figure 4-18: (a) c_u profiles determined from in situ tests (b) Estimated in-situ horizontal stress, σ_{h0}

CPM Tests

A total of seven CPM tests were performed in the sleech at the locations shown in Figure 4-13. Typical results for two of these tests are shown in Figure 4-19. It has been shown that the soil surrounding the CPM during installation is displaced and disturbed (in a manner that approximates a cavity expansion test from zero initial radius) by the passage

of the 60° cone. According to Dalton (1997) the CPM is inflated in a region of totally disturbed soil so the measured boundary for the test is the limit pressure[7] of the soil. The expansion phase of the test was used to determine two parameters; the horizontal shear modulus, G, and its variation with strain was one and the other was the limit pressure. Cavity contraction theory (Houlsby and Withers, 1988)[8] was then applied to the unloading portion of the test curve to obtain the undrained shear strength c_u and an estimate of the in situ horizontal stress, σ_{h0} shown in Figure 4-18b.

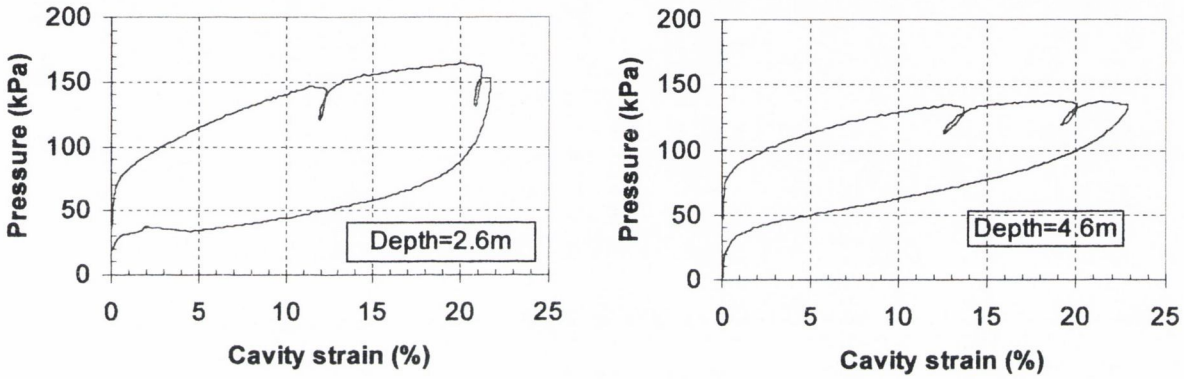

Figure 4-19: Typical cone pressuremeter test results

Shear Modulus

Since the pressuremeter test deforms the soil in pure shear, only the shear modulus is quoted. The modulus can be determined from the initial loading curve and/or from an unload-reload loop. The initial modulus is not normally used for design, as it is sensitive

[7] The limit pressure is defined as the pressure at which the expansion proceeds indefinitely without further increase in pressure.

[8] Houlsby and Withers (1988) noted that errors in modelling of the expansion and contraction phases of the test by cylindrical strain theory are due to the finite length of the pressuremeter in addition to the different stress paths involved by the penetration of a rod topped by a 60° cone compared to cavity expansion. However, the use of cavity expansion theory was justified on the basis of the stress distribution far behind the cone tip (where the pressuremeter module is located) being similar to the distribution created by the expansion of a cylindrical cavity from zero initial radius. Moreover, Houlsby and Withers (1988) found for the large strains experienced close to p_L, the volume of soil stressed plastically (during the inflation of the pressuremeter) may be a multiple of the pressuremeter length and thus may be more appropriately modelled using spherical expansion theory. However, during the initial phase of cavity contraction, the whole of the soil behaves elastically with elastic unloading of the previously plastic section, thus justifying the use of the cavity contraction theory to determine the parameters; G, c_u and σ_{h0}.

to disturbance caused by the installation process and is not as reliable and repeatable as the modulus derived from an unload-reload loop (Allan, 1994; Clarke, 1997).

The non-linear stiffness for the sleech was determined by taking a secant modulus from the shear stress-strain curve, with an origin at the minimum cavity strain in an unload-reload[9] cycle, to produce the variation in average stiffness with cavity strain. Typical non-linear variations in stiffness (normalised by the mean effective stress at the respective depths) with changes in cavity strain are shown in Figure 4-20. These values when multiplied by the appropriate normalising mean effective stress are consistent with Briaud's (1992) approximate values for G of 0 to 850kPa at the yield pressure (usually taken as the strain at about half the limit pressure) in clays.

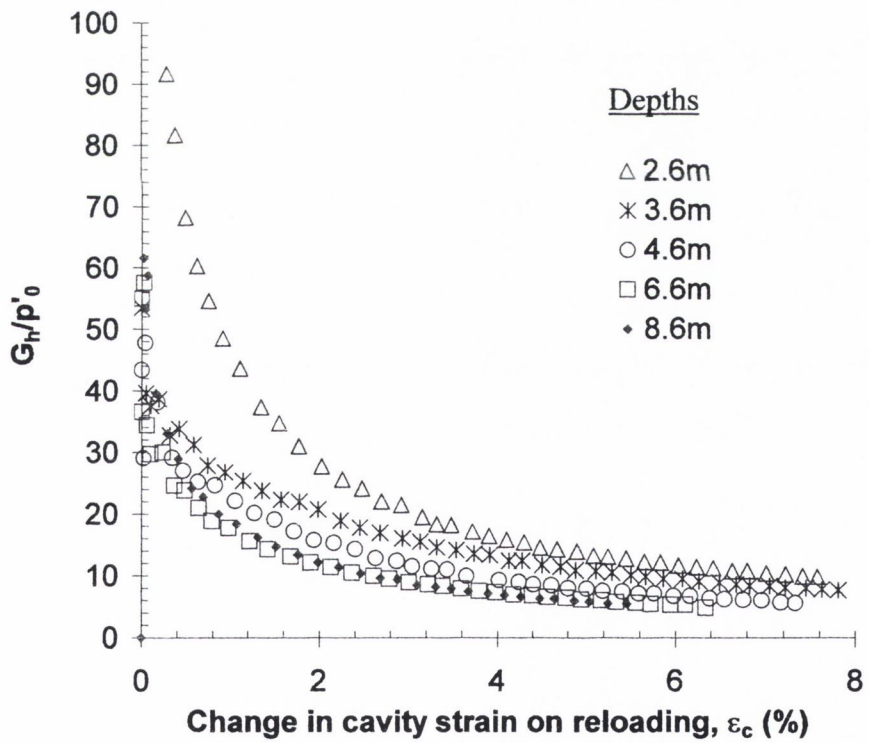

Figure 4-20: Typical Non-linear stiffness profiles from unload-reload cycle

[9] The results from the re-loading portion are typically quoted as these give more consistent stiffness values.

4.8 p-y Curves Derived from Cone Pressuremeter Tests

The use of pressuremeters in the analysis of laterally loaded piles was summarised in section 2.4.1 of chapter 2. In this chapter, the method proposed by Robertson et al. (1986) is employed to transform the results from the (pushed-in) cone pressuremeter (PM) into *p-y* curves for pile analysis. These provide a useful comparison with the *p-y* relationships derived from the pile load tests.

The *p* values for the *p-y* curves were obtained by converting the pressuremeter stress (σ_r) to soil resistance (in units of force per unit length) by multiplying σ_r by the pile width and a factor α. The α factor was described in chapter 2 as a magnification factor which transforms the PM limit pressure to the limiting lateral resistance for a laterally loaded pile ($\approx 9c_u$). To obtain the soil displacement or *y* component of the *p-y* curve, the radial strain ($\Delta R/R$) measured by the pressuremeter is multiplied by half the pile width.

In the case of the tests at Kinnegar, the first CPM test was performed in the sleech at a depth of 2.6m or 119 PM radii (7.4 pile diameters) below ground level (i.e., $x \approx 2.42$m and $z \approx 1.8$m in relation to the datum levels used at the test piles). Therefore, an α factor of 2 was appropriate since the initial CPM test was located below the zone of reduced resistance near the ground surface. A typical transformation from the PM curve to a *p-y* curve is shown in Figure 4-21. As can be seen from the inset, only the portion of the curve from the lift-off pressure up to the maximum cavity strain was utilised in the transformation. The recommendation of Anderson and Townsend (1999) to initiate the *p-y* curve from the start of the re-load sequence (to minimise the effect of installation disturbance) was not adopted, due to the large strain imposed on the soil before the first unload-reload sequence was performed. The unloading events which took place during the cavity expansion were ignored in the transformation process.

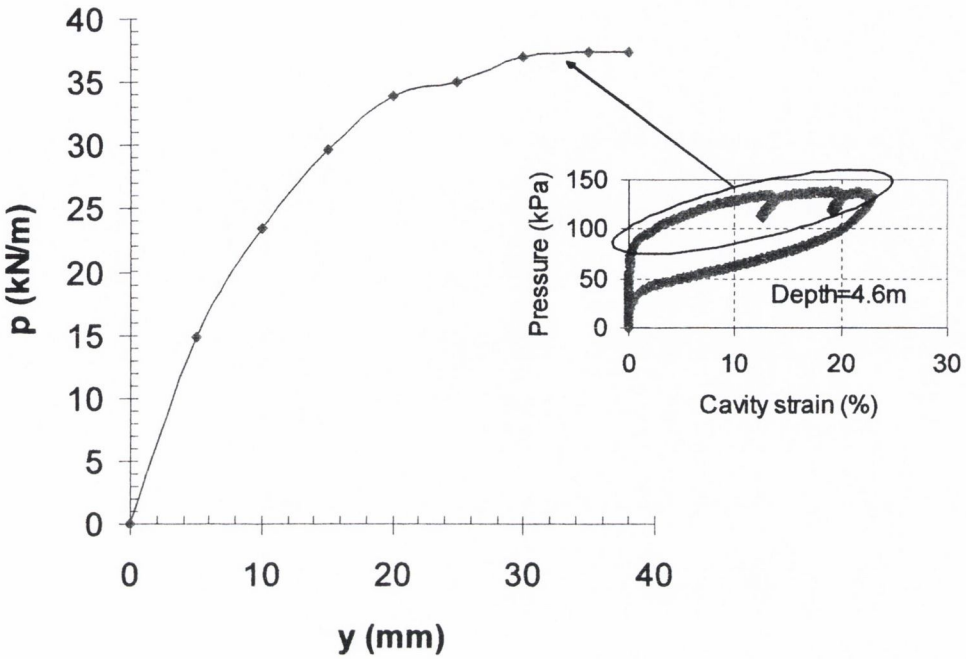

Figure 4-21: Transformation of pressuremeter curve to *p-y* curve at a depth of 4.6m below ground level (bgl)

The *p-y* curves for other PM tests in the sleech are presented in Figure 4-22. It can be seen that the *p-y* curves from the PM test are broadly compatible with the CPT q_c profiles[10] in that they also reflect the stiffer deposits present at ground level and beneath the sleech. The stiffer response exhibited by the PM test at 2.6m bgl is consistent with the sandy silt nature of the upper sleech observed during the post-test trial pit excavations. Similarly, the PM *p-y* curves between 3.6m and 7.6m exhibit a reduced but almost identical stiffness for each test; a feature which corresponds with the uniformity in the CPT q_c profiles over these depths.

[10] These tests were performed in the environs of the test piles see Figure 4-13.

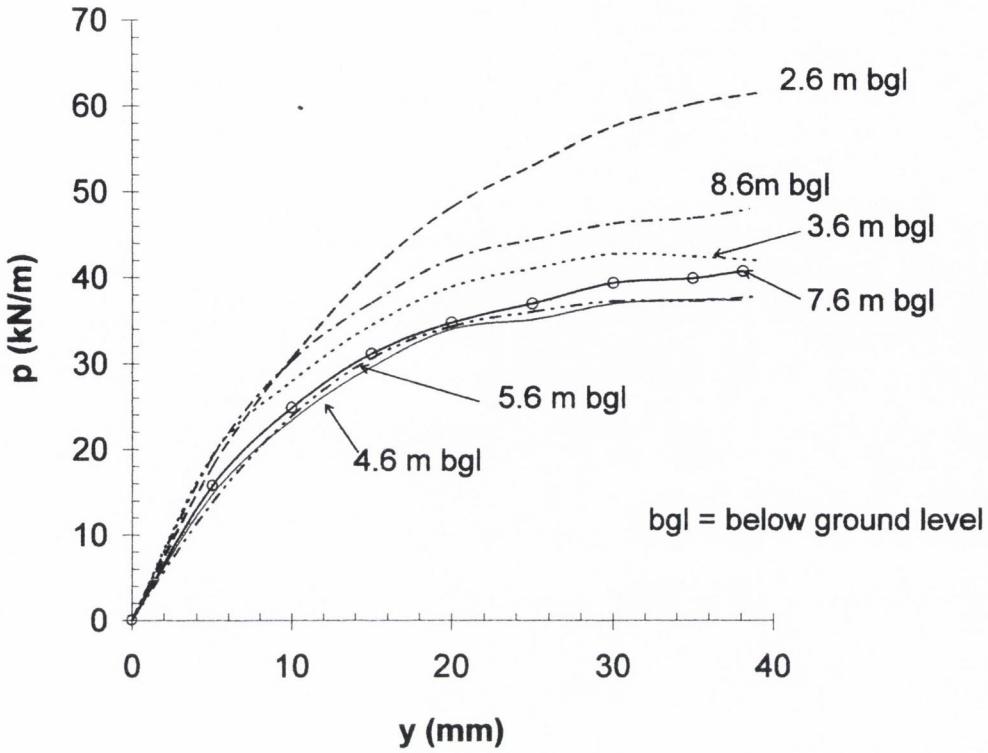

Figure 4-22: *p-y* curves derived from pressuremeter tests

Chapter 5

Load Test Results

5. LOAD TEST RESULTS

5.1 Introduction

This chapter presents the results from full-scale load tests described chapter 3. The tests involved two instrumented precast concrete piles driven side-by-side through a stiff fill underlain by soft clay and seated into medium dense sand located approximately 9m below ground level (see Figure 5-4). A single pile, designated as AL1, was subjected to a vertical load test and subsequently tested under lateral load with the vertical load in place. A second pile, designated L1, was subjected to lateral load. Both piles were re-tested under lateral load nineteen months after the initial test series had been completed. A summary of the test programme is provided in Table 5-1.

The test results are presented as load-pile head displacement plots for each test in addition to pile displacement profiles for the lateral load tests. A more detailed interpretation of these results and strain gauge data are presented in chapter 8. The axial load test (ALT) results will be interpreted in this chapter and will be presented prior to the combined load test (CLT) and re-test (RT) results. It is noteworthy that the results presented in this thesis

provide a (rare) opportunity to evaluate the influence of combined loading of a pile in a layered soil.

Test Series Designation[1]	Test Details	Axial load (kN)	Max Lateral load (kN)
ALT	October 17, 2001	168	-
CLT1	October 18, 1997, pile AL1	168	59.75
	October 18, 1997: pile L1	0	59.75
CLT2[2]	October 19, 1997: pile AL1	133	89.75
	October 19, 1997: pile L1	0	89.75
RT	May 18, 1999: piles AL1 & L1	0	74

Table 5-1: Summary of load test programme

5.2 *Axial Load Test*

5.2.1 Background

One of the primary research objectives of this thesis was to determine the behaviour of a laterally loaded single pile while supporting an axial load. In the field tests, pile AL1 was first loaded vertically to simulate the most likely loading sequence in practice i.e., all piles would be subjected to a superstructure load prior to being loaded laterally. After the vertical load had been in place for twenty-four hours, the pile was subjected to two lateral

[1] ALT refers to the Axial Load Test; CLT1 & CLT2 refer to initial and second Combined Load Tests respectively and RT is the Re-Test.

[2] Note that equilibrium between the soil and the pile was achieved for all load increments applied during this test except for the last increment. As the load was increased from 85.5kN the pin joint mechanism collapsed suddenly at a load of 89.75kN. Therefore any data presented for the 89.75kN load reflects the instantaneous results recorded by the DAS as attempts were made to reach the 94kN load increment. Because equilibrium was not obtained at 89.75kN these data were not used in the subsequent derivation of the *p-y* response of the soil.

load tests each supporting a different vertical load. The main findings of the axial load test are now presented.

5.2.2 Axial Pile Capacity

Three existing design methods were used to estimate the axial pile capacity in advance of the field tests. The top 1m of fill was ignored because of disturbance caused during pile installation and the partial removal of this material from in front of the piles prior to conducting the lateral load tests. The first estimate was based on the so called 'α–method' to calculate the skin friction (using $\alpha = 0.9^{\dagger}$ and $c_{u(ave)}$= 20kPa) along the 7.6m of sleech. The remaining shaft friction and end bearing in the sand was calculated using Berezantsev's N_q bearing capacity factor (= 89 for a ϕ' of 38° assessed on the basis of q_c (=12.5MPa) and SPT N (=15) values measured at the pile toe). This method yielded an ultimate pile resistance of 1113kN. The second approach involved Jardine and Chow's (1996) new design method for offshore piles which required CPT q_c data and laboratory test results (performed on good quality piston samples); an ultimate resistance of 1261kN was estimated using this method. The third method was that of Bustamante and Gianeselli (1982) which also utilised the CPT q_c data (obtained within 3m of the test piles), this approach gave an ultimate capacity of 1175kN. It was concluded that the Bustamante and Gianeselli[3] method, employing the direct use of in-situ test results provided the best estimate of the pile's axial capacity. Details of these calculations can be found in appendix 5a.

For this research, it was important to ensure that the pile was not overloaded vertically. For this reason the vertical load on pile AL1 was limited to 170kN, reflecting a minimum factor of safety of 7 on the lowest estimate of the axial capacity[4].

---

† API (1993) recommends α be taken as $0.5/(c_u/\sigma'_v)^{0.5}$ for $c_u/\sigma'_v \leq 1.0$. The ratio of c_u/σ'_v for the sleech was measured at 0.41 (see chapter 4).

[3] According to Lunne et al. (1997) the Bustamante and Gianeselli method (established from a database of 197-pile load tests) was found to give excellent results when compared to other prediction methods Lehane et al. (2000) provided recommendations for estimating the pile capacity provided piezocone data is available to correct q_c for the pore pressure acting on the filter stone.

[4] It was intended to apply an axial load in the region of 50% of the axial pile capacity. However, at the start of the test, the calibrated readout unit malfunctioned and a backup unit was employed. Subsequent calibration of this unit revealed that significantly less axial load had been applied to the pile; this was also confirmed by the strain gauge data.

5.2.3 Pile Installation

The pile installation was described in chapter 3 (section 3.7). To monitor pore water dissipation after pile installation, pneumatic piezometers were installed at various depths within the test bed two weeks prior to pile installation (see McCabe, 2002). The piezometer located closest to the test piles indicated that the pore water pressures generated by pile installation had essentially dissipated to hydrostatic conditions at the time of the ALT (six weeks after pile installation).

5.2.4 Load Settlement Behaviour

Details of the axial load test can be found in section 3.11.1. During application of the axial load, the pile head settlement was monitored using two dial gauges located at the edges of the pile along the diagonal (Figure 5-1). Additional settlement readings were taken to vernier sighting cards[5] attached to both the pile and the reference beam system. The sighting cards were read using an engineers level located ≈20m from the test area and the data served as an approximate check on the measurements recorded by the dial gauges.

The average load-settlement behaviour recorded by dial gauges (DG) and the adjacent vernier card are illustrated in Figure 5-1. The following are evident from the plot:

- Under the maximum applied axial load of 170 kN the pile settled by 2.48mm. The calculated elastic shortening of the pile accounts for ≈0.39mm (16%) of the settlement.
- The settlement recorded by the less accurate (as indicated by the error bars) vernier sighting cards was consistent with the dial gauge readings.
- The pile experienced negligible settlement up to a load of ≈100kN; in fact, the average dial gauge readings indicates that the pile rose upwards as the axial load increased close to this value, the vernier card measured a similar response. The upward movement (discussed later in section 5.2.5) was not significant registering only 0.1mm on the dial gauge.
- The majority of the settlement took place as the final 70 kN of load was applied. Since the CLT series immediately succeeded the ALT (after the vertical load had

[5] The vernier sighting cards had a reading accuracy of ±0.5mm

been in place for 24 hours) there was no unload-reload cycling of the axial load performed and hence no additional data were obtained relating to the axial performance of the pile. As expected, there was no evidence of pile failure at the levels of load applied during the test.

- It was noted that the vernier card revealed no discernable settlement of the reference system during the ALT thereby giving confidence in the accuracy of the pile settlement measurements.

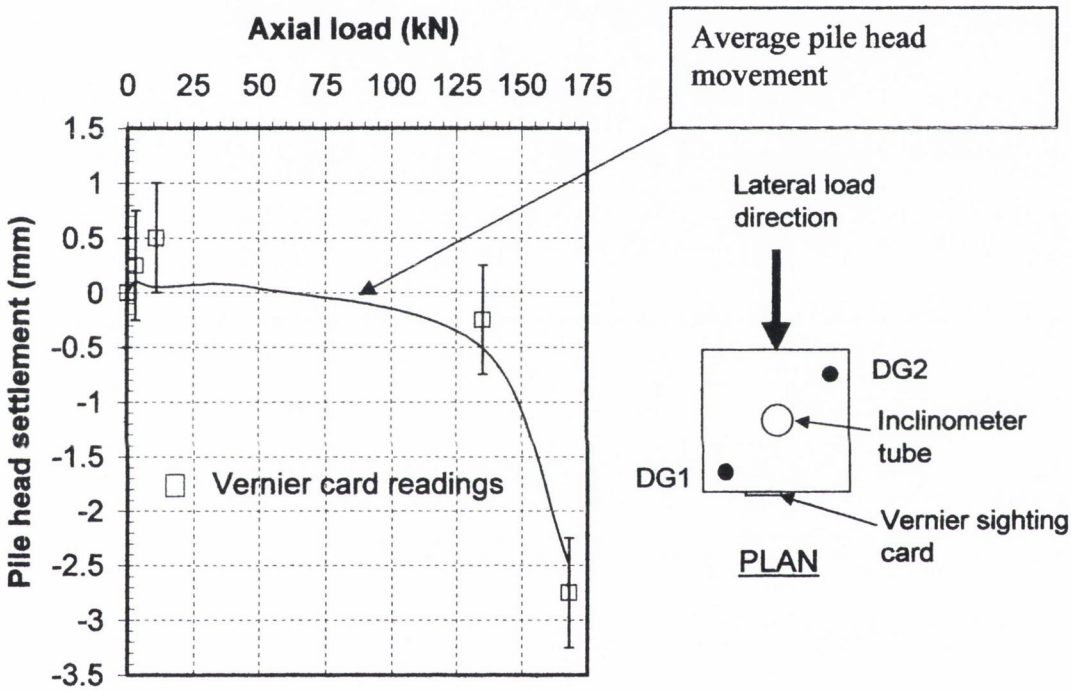

Figure 5-1: Load versus average pile head settlement for pile AL1

5.2.5 Pile Load Distribution Mechanism

A pile's resistance to applied load is derived from a combination of soil pile friction along the shaft and end bearing at the base of the pile. Results from pile tests in clay discussed by Burland and Cooke (1974) show that the two support mechanisms are mobilised at entirely different rates and are essentially independent of each other. The frictional resistance develops rapidly and linearly with increasing settlement and is generally fully mobilised when the settlement is about 0.5% of the shaft diameter or 5 to 10mm (Burland and Cooke, 1974). Thereafter the shaft resistance tends to remain constant regardless of

the settlement. The toe resistance on the other hand is seldom fully mobilised until the pile settlement reaches a value of 10 to 20% of the base diameter.

The above behaviour was not evident at the test site because the pile was seated into medium dense sand, which was considerably stiffer than the soft overburden of sleech. Estimates of soil stiffness based on empirical correlations[6] with q_c and SPT 'N' values suggest that the sand layer was over twelve times stiffer than the sleech. At the maximum vertical load, the strain gauge data indicated that 9kPa was developed in shaft resistance over the top 3.5m and this reduced to 2kPa at the base of the pile. The measured skin resistance along the upper section of the shaft is consistent with the ultimate shear resistance of 10.5kPa measured by McCabe (2002) for friction piles at the same site. This implies that the stiffer soil at the base prevented the movement necessary to mobilize further shaft friction and explains the absence of significant load shedding within the sleech (Figure 5-2). Moreover, the small pile-head settlement (<1% of the pile width) suggests that the pile's resistance was predominantly end bearing.

The profiles shown in Figure 5-2 were derived from the strain gauge transducers attached at various depths to diametrically opposite steel bars. The strains from each gauge were initially plotted against depth for a number of axial load increments. However, the resulting profiles revealed no clear evidence of the load reducing along the pile shaft. On further examination[7], the strain data from each instrumented bar indicated that the pile was not uniformly compressed; the larger strain measured on one side of the pile[8] was consistent with the axial load being applied at a small eccentricity (estimated at 8mm). Further confirmation of eccentric loading was provided by the load-settlement curve shown in Figure 5-1. The dial gauge (DG) readings indicated that the pile settled more on the compression side of the pile (DG1) than the opposite side (monitored by DG2) thereby indicating an eccentricity towards the compression side of the pile. Thus, the pile was undergoing bending in addition to compression during the ALT, which would explain the initial load settlement response for loads up to ≈100kN.

---

[6] The stiffness of the sand under typical working strains of 0.1 – 0.2% were estimated from $E'_v = 2500N_{60}$ or $5q_c$ (kPa) for OCR > 1. The stiffness of the sleech was estimated from $E'_v = 150c_{utc}$ (kPa).

[7] Strain versus load and strain versus time plots for each strain gauge revealed the gauges were responding sharply to changes in applied load.

[8] The side recording the higher strains will be referred to as the compression side of the pile in the subsequent lateral load tests

To correct for bending, the strain from pairs of gauges, located at ≈ the same depth on opposite reinforcing bars were averaged[9]. The average strain profile was then used to calculate the distribution of load shown in Figure 5-2. The calculations associated with Figure 5-2 are provided in appendix 5b.

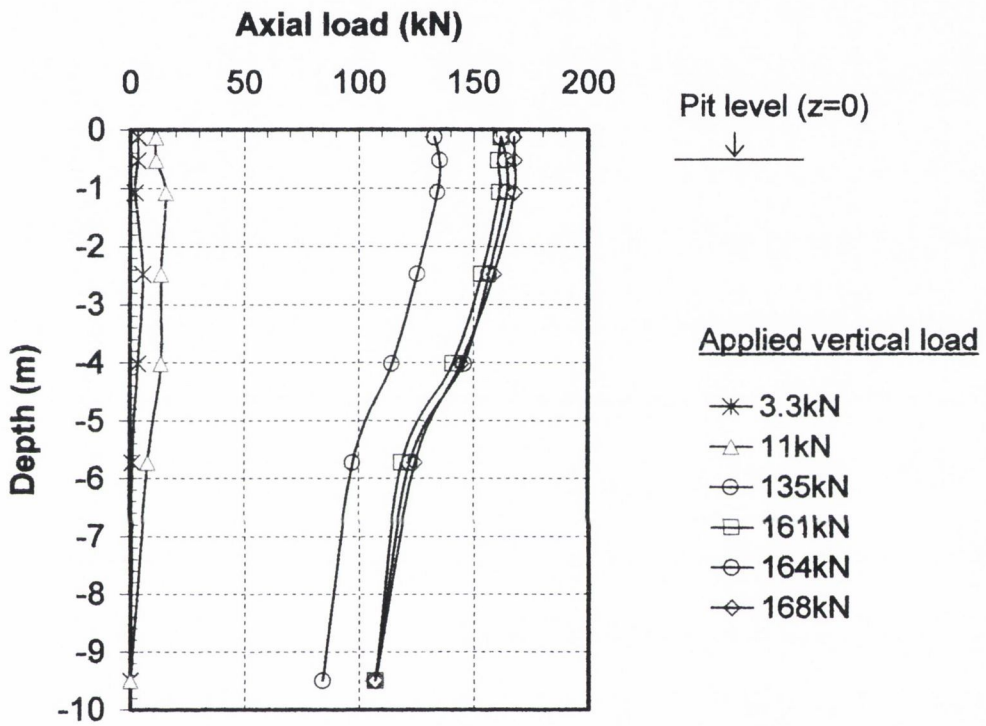

Figure 5-2: Load distribution profile for pile AL1 under increasing load

5.2.6 General Observations from Pile Toe Measurements

A number of general observations can be made regarding the strains monitored by the vibrating wire gauge (VW-B) located at the pile toe:

- The datum VW reading was recorded immediately after casting the pile in the mould. The next reading was taken five weeks later immediately before pile

[9] Data from single gauges were ignored in the analysis since single gauge measurements could not be corrected for bending effects.

driving. The VW gauge had registered a compressive strain due to shrinkage of $\approx 10\mu\varepsilon$.

- Immediately after pile driving the compressive strain measured by the VW strain gauge was $\approx 28\mu\varepsilon$. The next reading was taken before the axial load test (over six weeks after installation) and revealed a tensile strain of $-2.55\mu\varepsilon$, a net change of $30.55\mu\varepsilon$. Pneumatic piezometers (see McCabe, 2002) located in the vicinity of the test piles indicated that the increased pore pressure measured after pile installation had almost dissipated to hydrostatic conditions by the time the ALT was carried out. It is evident from these data that negative shear stresses have developed along the pile shaft in the intervening period.

- To assess the magnitude of pile downdrag or negative skin friction (NSF) mobilized along the pile, the shaft friction factor β (Burland, 1973)[10] was back calculated from the measured strain data and compared with typical values reported by Burland and Starke (1994). A load of 137kN due to NSF was inferred from the change in the measured strain as follows (see appendix 5b):

$$F_{NSF} = (E_c A_c + E_s A_s)\Delta\varepsilon$$

where F_{NSF} = the downdrag force due to negative skin friction
E_c = Young's modulus for the concrete, taken as $36kN/mm^2$
E_s = $205kN/mm^2$ Young's modulus for the reinforcing steel
A_c and A_s = the areas of concrete and steel respectively
$\Delta\varepsilon$ = change in strain recorded by the strain gauge at the base of the pile

The average shaft friction factor β, back calculated from the foregoing gave a value of -0.3. This value is consistent with the observations of Burland and Starke (1994)

[10] Burland (1973) defined $\beta = \tau_{sf}/\sigma_{v0}' = K \tan\delta'$ where β is the ratio of maximum shear stress (τ) divided by the vertical effective stress σ'_{v0}, K is the earth pressure coefficient and δ' is the effective angle of friction between the pile and the shaft. σ'_{v0} was evaluated from the site stratigraphy of 1m of fill ($\gamma_{fill} = 19kN/m^3$) surcharging 7.6m of submerged soft soil ($\gamma_{sat} = 16kN/m^3$) with the water table located at the interface between the fill and the soft clay.

who, after monitoring pile NSF measurements on numerous sites, for periods of a few months to seventeen years, found that average values for β in soft compressible sediment lay within relatively narrow limits of –0.25 to –0.35.

- Figure 5-3 illustrates that the application of lateral load (during the CLT series) had a negligible influence on the vertical load at the pile toe. The variation in axial load shown in Figure 5-3 can be attributed to the reading accuracy associated with the VW strain gauges. Tyler, (1968) suggested that VW readings were accurate to ±2με which equates to a load of ±9kN.

- The axial load was reduced by 20% at the start of CLT2, the reduction in load is consistent with the reduction measured by the VW strain gauge at the base of the pile (Figure 5-3).

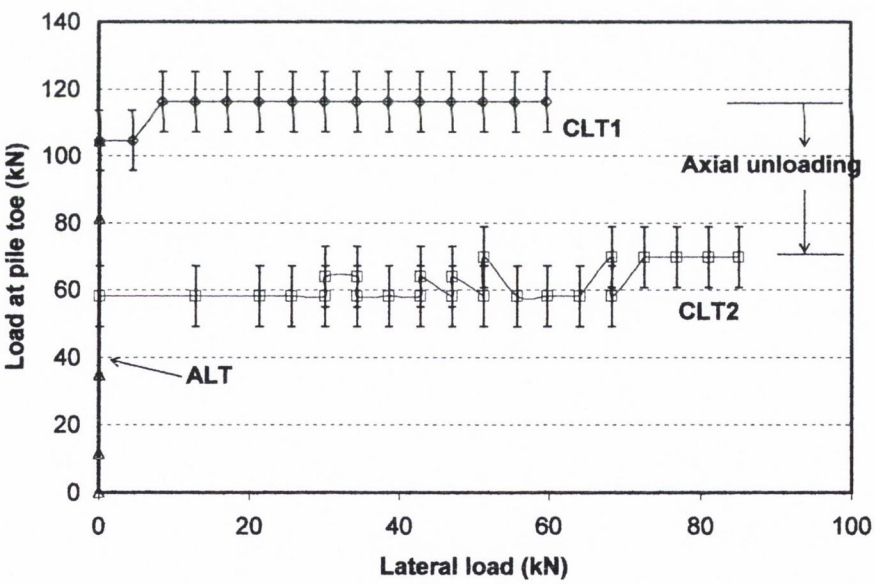

Figure 5-3: Variation in load at the pile toe load recorded by VW-B

5.3 Pressure Cell Results

Four pressure cells, to measure the horizontal earth pressure, were installed in pile AL1[11], the uppermost pressure cell (PC1) malfunctioned immediately after pile installation but the

[11] See Figure 3.2.

remaining three units (PC2, PC3 and PC4) continued to provide data for the duration of the tests. However, it must be emphasised that these sensors were located outside the critical pile length and so registered negligible pressures for the levels of load applied during the test. This may be justified by the displacement profiles presented in section 5.6 which show that movements at these depths were negligible and therefore it is likely that much of the lateral resistance was provided in side friction in this region rather than frontal resistance.

The Table 5-2 summarises the pressure cell details and the values for the coefficient of horizontal pressure (after equalisation)[12], K_c measured by the instruments. K_c was used in the pile design method proposed by Jardine and Chow (1996) for offshore structures; the values presented were calculated at the start of the ALT (43 days after pile installation). It can be seen that PC2 and PC3 give values that fall within the range for K_c reported in Jardine and Chow (1996).

Reference	**PC1**	**PC2**	**PC3**	**PC4**
Depth below GL	1.375 m	2.875 m	4.375 m	6.625m
Location in pile	Compression face	Compression face	Compression face	Tension face
Initial pressure, $P_{initial}$ = ΔmV x CF[13] (kPa)	_	54.4	75.9	82.8
Change in pressure due to ALT, $\Delta p_{ALT} = \Delta$mV x CF (kPa)	_	3.6	3.4	-6.4
Change in pressure 43 days after driving, $P_{43\ days}$ (kPa)	_	16.2	13.6	20.6
$\sigma_{rc} = P_{initial} - P_{43\ days}$	_	38.2	62.1	62.2
σ_v (kPa)	25.43	51.00	75.00	111.00
u_0 (kPa)	0	18.39	33.11	55.18
σ'_{v0} (kPa)	25.43	32.61	41.89	55.82
$K_c = (\sigma_{rc} - u_0)/ \sigma'_{v0}$	_	0.6	0.69	0.13 ?

Table 5-2: Total pressure cell results

[12] Jardine and Chow (1996) defined $K_c = \sigma'_{rc}/\sigma'_{v0}$ where σ'_{rc} is the radial effective stress = $(\sigma'_{rc} - u_0)$ and σ'_{v0} is the vertical effective stress.

[13] Note: Calibration factor (CF) for pressure cells - 10mV = 100kPa

5.3.1 Concluding Comments on the Axial Load Test

The results from the axial load test shown in Figure 5-2 indicate that the pile mobilised positive skin friction of 9kPa along the top 3.75m of the pile. The shear stresses along the shaft then drop significantly which suggests that the pile load was been transferred in end bearing to the stiffer sand at the base of the pile. Bearing pressures at the base of the pile are in the region of 980kPa, which is well below the bearing capacity of the sand determined using the methods discussed in section 5.2.2.

Since no further monitoring of the axial pile behaviour took place once the combined load tests commenced, no comment regarding creep and the subsequent pile behaviour can be offered.

5.4 Lateral and Combined Lateral and Axial Load Tests

5.4.1 Background

This series of tests designated as CLT1 and CLT2 involved loading pile L1 laterally while pile AL1 supported a sustained vertical load during the application of lateral loads. The vertical load was applied using the pin-jointed mechanism described in chapter 3.

Figure 5-4 schematically illustrates the test setup and includes the soil stratigraphy and the shallow pits excavated in front of each pile.

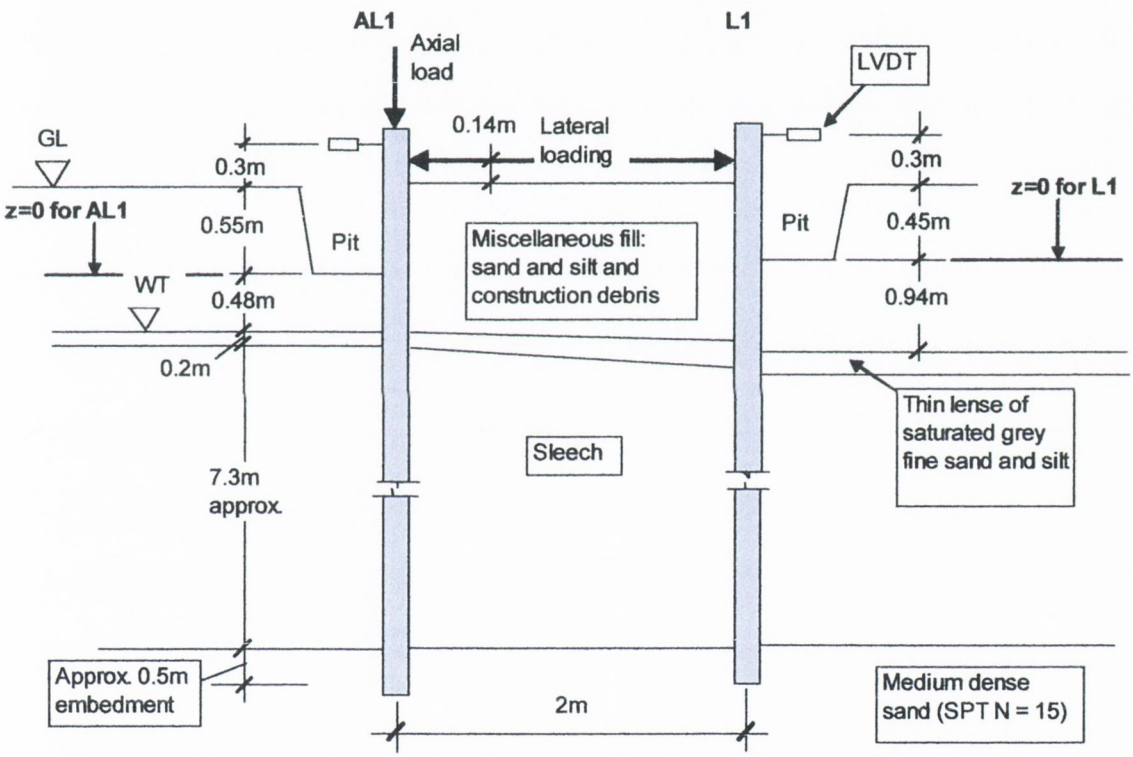

Figure 5-4: General test setup (not to scale)

5.4.2 Estimate of Maximum Lateral Test Load

Broms' (1964 a and b) empirical approach was employed to estimate the ultimate lateral resistance of the piles. This estimate was used to guide the loading sequence adopted for the field tests. The displacement profiles in section 5.6 suggest the piles were acting as flexible members, with fixity being achieved at a depth of ≈3m. Broms' presented separate approaches for calculating the ultimate lateral resistance in sands (Broms, 1964b)

and clays (Broms, 1964a) however; the soils at the test site involved a layered stratigraphy comprising both soil types. In chapter 4 the stratigraphy was described as ≈ 1m of sandy gravel or gravelly sand with some construction debris[14] followed by a thin band of silty sand containing layers and lenses of sandy silt and occasional clayey silt, this in turn overlayed a deep layer of clayey organic silt (sleech).

To determine the ultimate lateral resistance in a layered profile, judgment in the application of Broms' method was required. It was assumed that the critical depth of soil controlling the lateral behaviour of the piles was within the top 10 pile widths from ground level, thus 80% of soil within this depth is comprised of sleech having an average c_{utc} of 20kPa (see Figure 4-18a). The remaining 20% involves the upper strata of sandy gravel having q_c values of 3 ± 1 MPa. Therefore applying Broms' approach independently for sand (assuming $\phi' = 31°$)[15] and clay yielded to an ultimate lateral resistance $p_u \approx 74$kN in each case. Broms' considered the accuracy of the prediction to fall between (0.84 and 1.13) p_u thus giving a value of p_u between 64kN and 84kN.

5.5 Load-Displacement Behaviour at the Pile Head

CLT 1

Figure 5-5 compares the lateral load-displacement performance for pile L1 (subjected to no axial load) with that for AL1 (under constant axial load). There is a dramatic difference between the pile head displacement at a given load level. Pile AL1 was displaced only 5mm at the maximum lateral load compared to 25.8mm recorded by pile L1. The non-linear load-displacement behaviour is evident in both piles but with pile AL1 exhibiting a much stiffer response. It is clear from these observations that the axial load or the method of applying this load to pile AL1 had a significant influence on the pile response (see section 6.3).

Each pile displayed creep during the sustained loading period (≈ 6 minutes) for each increment. The recovery on unloading showed that pile AL1 rebounded to a residual displacement of 1.25mm and L1 to 7mm, representing ≈75% recovery in each case. Moreover, a noticeable gap developed behind pile L1 as the lateral load increased.

[14] 0.5m of this material was excavated from in front of the piles prior to the lateral load tests.
[15] Based on correlations with the average q_c values measured in CPT's 3, 4 and 5 (see Figure 4-13) and the vertical effective stress (Lunne et al., 1997)

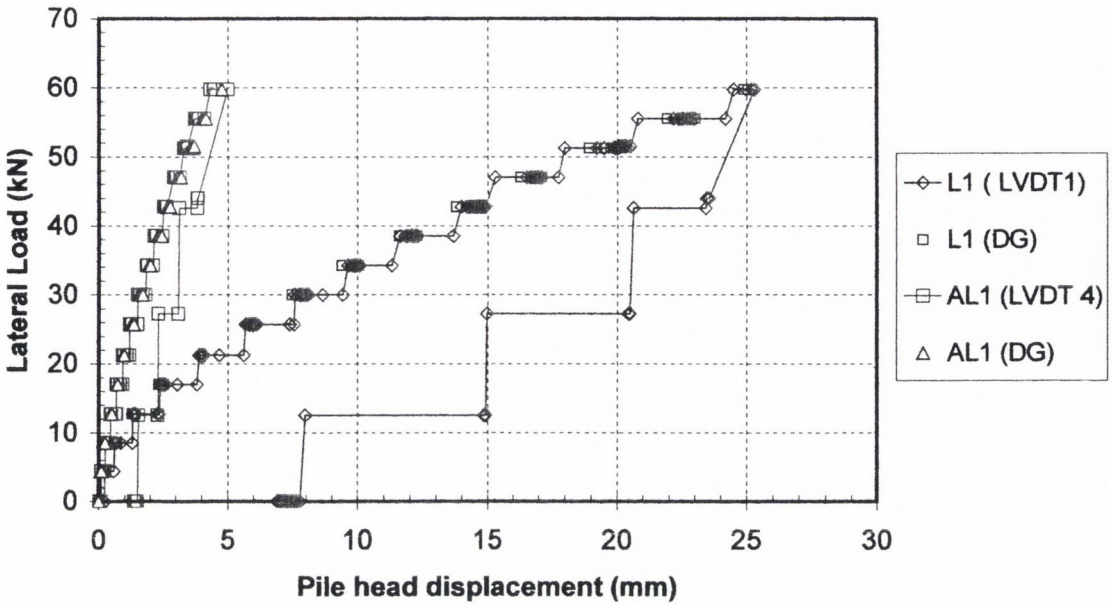

Figure 5-5: Load-pile head displacement behaviour for L1 and AL1 during CLT1

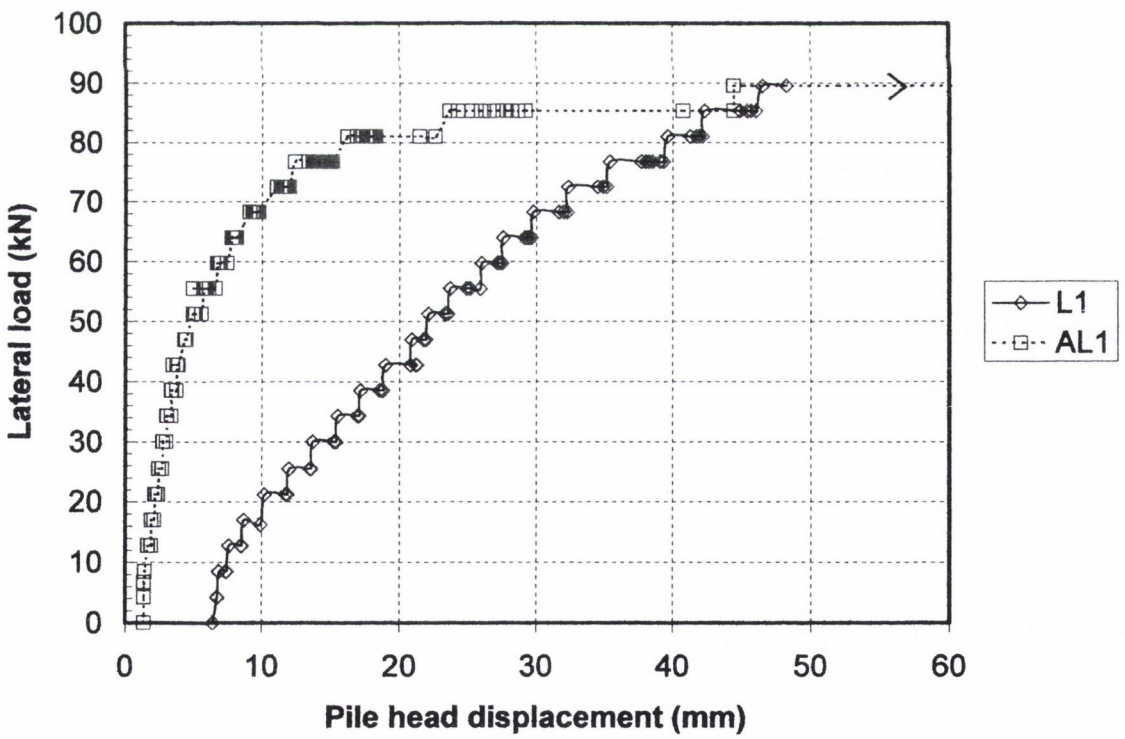

Figure 5-6: Load-pile head displacement behaviour for L1 and AL1 during CLT2

CLT2

Figure 5-6 shows the corresponding lateral load-displacement plot for CLT2. The displacements start from the residual measured at the end of CLT1 and again exhibit non-linear load-displacement behaviour for each pile. Despite the axial load on AL1 being reduced by 20% for CLT2, the pile displayed a very similar response up to the maximum load applied in CLT1. Furthermore, given the 75% recovery measured following unloading for each pile at the end of CLT1, it can be concluded that much of the soil surrounding AL1 had not yielded significantly. However, at load increments above 68kN, creep became prevalent in pile AL1 and at the 85.5kN load increment the soil could no longer resist the applied lateral load. Pile L1 on re-loading displayed a similar response as that measured in CLT1. Furthermore, as the pile L1 continued to resist load up to the failure at AL1, the creep rate was much less then that measured at AL1.

PILE L1 BEHAVIOUR DURING CLT1 AND CLT2

The load-displacement response for pile L1 during both CLT1 and CLT2 is shown in Figure 5-7. The slight increase in stiffness on reloading and the continued resistance to lateral load up to 90kN are clear from the graph.

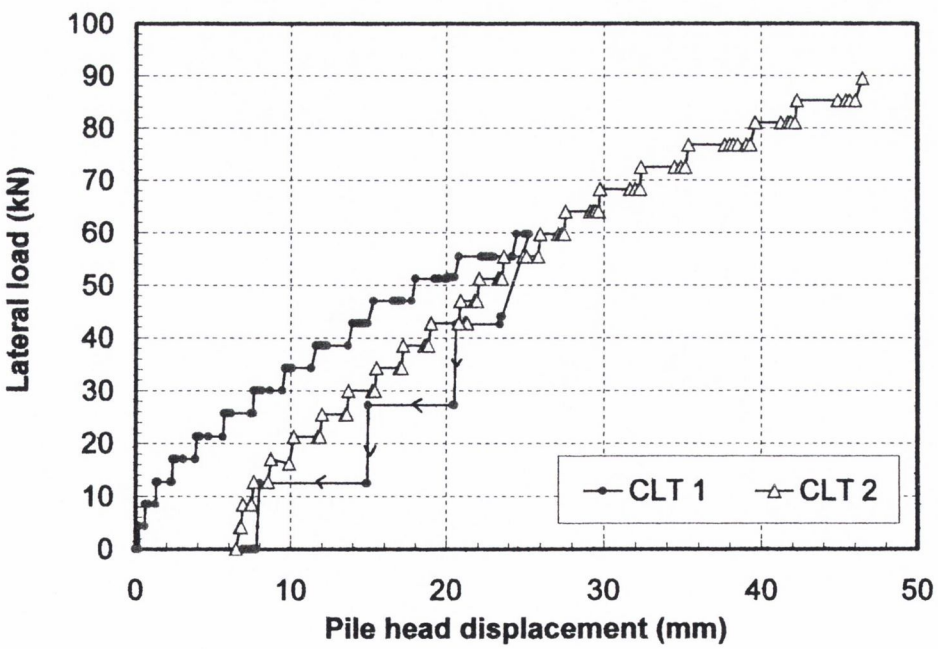

Figure 5-7: Load – pile head displacement performance for pile L1

PILE AL1 BEHAVIOUR DURING CLT1 AND CLT2

Figure 5-8 shows that pile AL1 started to undergo significant lateral displacement at lateral load levels of approximately 70kN. Significant yielding of the soil evidently took place above this load. The following observations are noteworthy for pile AL1:

- The reduction in axial load from 168kN in the first CLT to 133kN in the second test did not materially influence the lateral displacement at the pile head up to lateral loads of 60kN. This is consistent with the independent findings of Shahrour and Meimon (1991) and Anagnostopoulos and Georgiadis (1993) who observed that an axial load does not have a significant influence on the lateral displacement of the pile.

- At lateral loads above 60kN in CLT2, significant pile head displacement began to occur. The increased displacement was attributed to changes that took place in the loading mechanism; these will be evaluated in chapter 6.

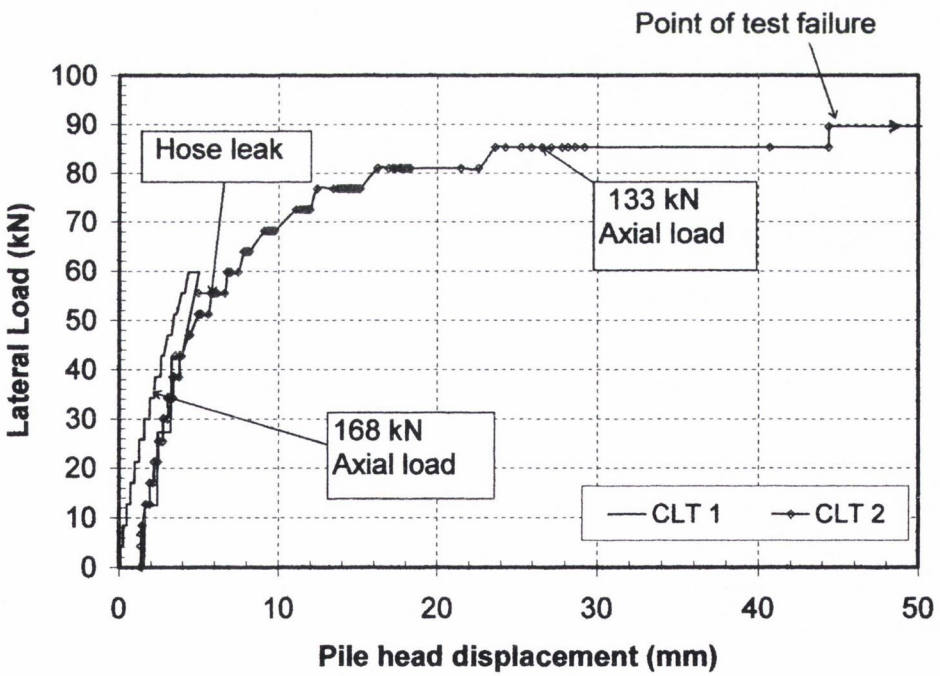

Figure 5-8: Load–pile head displacement performance for pile AL1

5.6 *Pile Displacement Profiles*

5.6.1 Background

The displacement profiles were calculated from the known pile head displacement and the slopes recorded by a series of electro-levels positioned at regular intervals along the pile shaft. Typical slope profiles for each pile are shown in Figure 5-9.

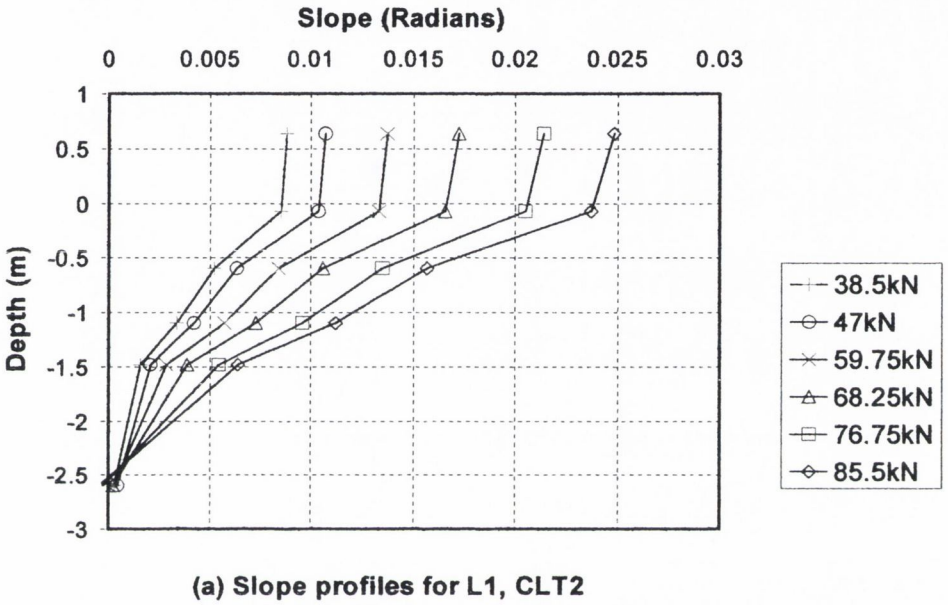

(a) Slope profiles for L1, CLT2

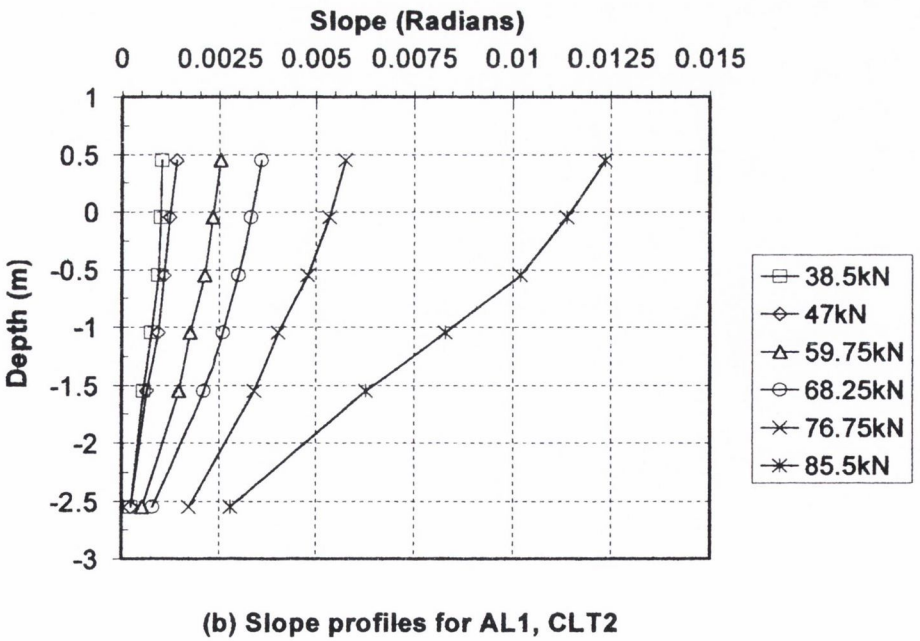

(b) Slope profiles for AL1, CLT2

Figure 5-9: Typical slope profiles measured by electro-levels

5.6.2 Profiles for CLT1

The pile displacement profiles were obtained using the displacement measured at the pile head as the reference datum. The profile was then determined by subtracting the lateral movement calculated from each electro-level (EL) along the shaft, starting from the reference datum. It was assumed that the change in slope (θ) monitored by each EL applies over a distance (L) halfway between adjacent ELs (see appendix 9 for commentary on EL interpretation). The movement (ΔL) over a distance L is then calculated as follows:

$$\Delta L = L \tan \theta$$

In chapter 8, an alternative method of determining the displacement profile by fitting a curve to the measured slopes is discussed. Figure 5-10 and Figure 5-11 present the displacement profiles for piles AL1 and L1 respectively. At the maximum load applied in CLT1, the displacement recorded for pile AL1 at pit level (z = 0) was 3mm. The profiles also illustrate that fixity is achieved at a depth of about -3m, as displacements at this level are negligible (≈0.5mm) and are close to the resolution achievable at the electro-level settings.

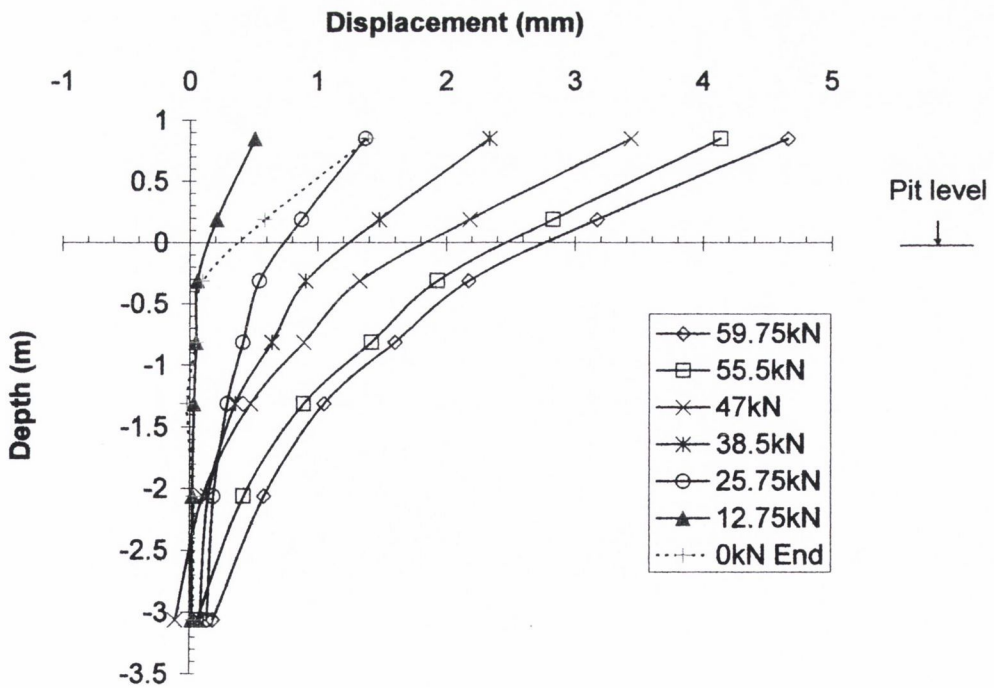

Figure 5-10: Displacement profiles for AL1 during CLT1

Contrasting these results with the profiles for pile L1 during CLT1 (Figure 5-11), the displacement at z = 0 was 17mm at the maximum lateral load. At a depth of 10 pile widths below z = 0, the displacement had reduced to 2.6mm. Negative displacements were not registered over the monitored depth of pile L1. The displacement profiles clearly indicate that the piles are flexible.

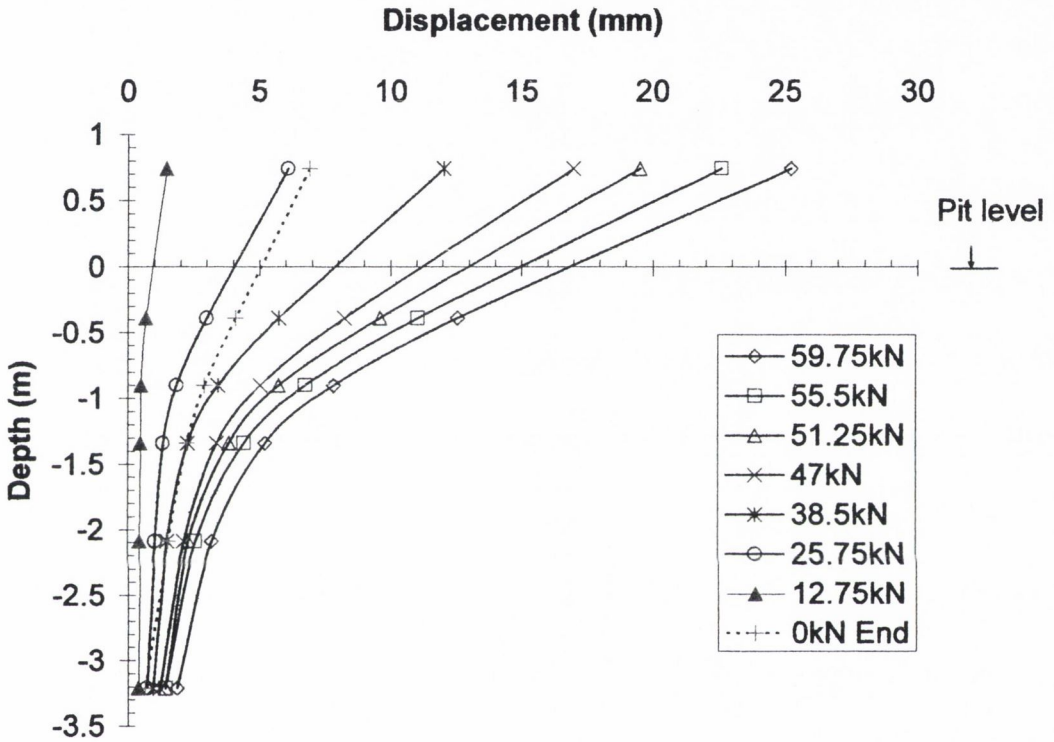

Figure 5-11: Displacement profiles for L1 during CLT1

5.6.3 Profiles for CLT2[16]

Figure 5-12 and Figure 5-13 present the CLT2 displacement profiles for pile AL1 and L1 respectively. After application of the 59.75kN load increment, the load was incremented in steps of 8.5kN until failure[17] occurred. At loads above ≈ 60kN in Figure 5-12, the disproportionate increase in displacement profile per load increment indicated that yielding

[16] Note: While the loading rates remained the same; the load increments applied during CLT2 did not, in some cases, correspond exactly with those applied during CLT1. However, the profile for the nearest load increment is plotted for comparative purposes.

[17] Failure is most commonly assumed to occur at a displacement equal to a certain percentage of the pile diameter (usually 10% although this can be reduced to as little as 2.5% in the case of offshore structures). However, for pile AL1 failure is taken to have occurred when the pin-jointed mechanism collapsed.

of the stiffer upper strata had taken place and may ultimately have resulted in a shallow wedge type of failure (as described in Matlock, 1970) of the soil in front of AL1. Once the soil resistance of the stiffer upper layer was exceeded the capacity of the underlying soft clay was insufficient to limit the pile translations that ensued over the subsequent load increments. The excessive translation ultimately led to the termination of the test.

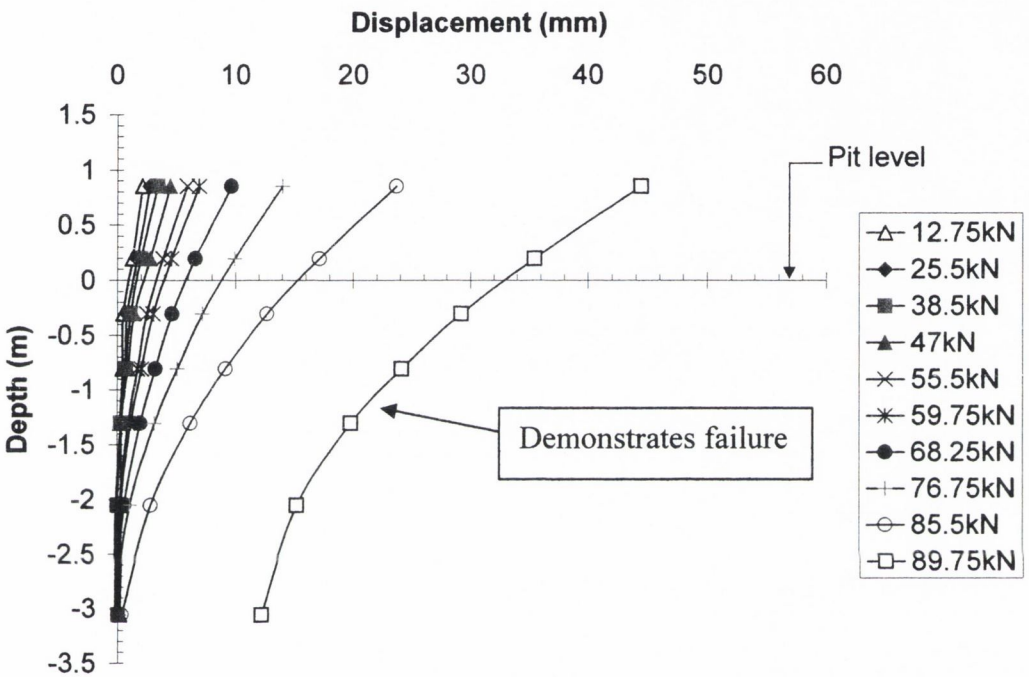

Figure 5-12: Displacement profiles for AL1 during CLT2[18]

The displacement profile for pile L1 (Figure 5-13) were also derived from the measured EL slopes; referenced to the datum displacement recorded at the pile head (see section 5.6.2). These profiles appear to indicate that the pile pivots about a depth of -1.4m which would explain the negative displacements being registered at a depth of -1.75m for all load increments between 59.75kN and 76.75kN. However, direct derivation of these profiles by fitting a curve to the measured slopes (or the strain gauge data both) reveal that negative displacements do not develop at any stage during CLT2 (see section 8.3.2). This finding is consistent with the calculated soil reactions and implies that displacement profiles

[18] The instantaneous displacement profile at 89.75kN is shown for pile AL1 to illustrate the dramatic increase in pile movement that occurred for the small increase in load above 85.5kN. Pile L1, as can be seen from Figure 5-13, did not exhibit the same trend at 89.75kN.

calculated from a displacement datum at the pile head may lead to small (but significant) changes in the displaced profiles if small errors exist in the instrumentation data.

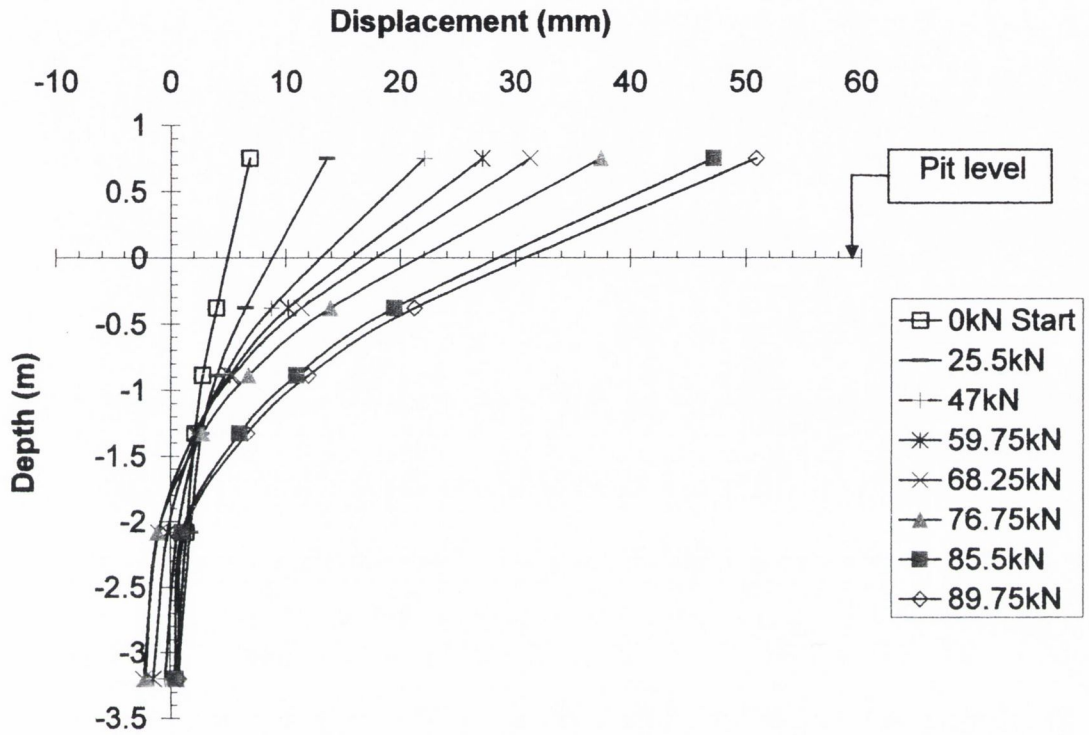

Figure 5-13: Displacement profiles for L1 during CLT2

To examine the behaviour of L1 more closely, the change in rotation for a series of short pile sections to a depth of 1.5m below the pit level were plotted in Figure 5-14. The plot reveals that the top half metre below pit level underwent a pronounced increase in pile rotation at a lateral load of 60kN (the maximum load applied during CLT1). A similar but less marked response can be observed at greater depths. Furthermore, it is noted that change in pile rotation is approximately constant between -0.5 and -1.5m. These findings confirm that initial soil yield also occurred close to pit level for pile L1 at a lateral load ≈60kN.

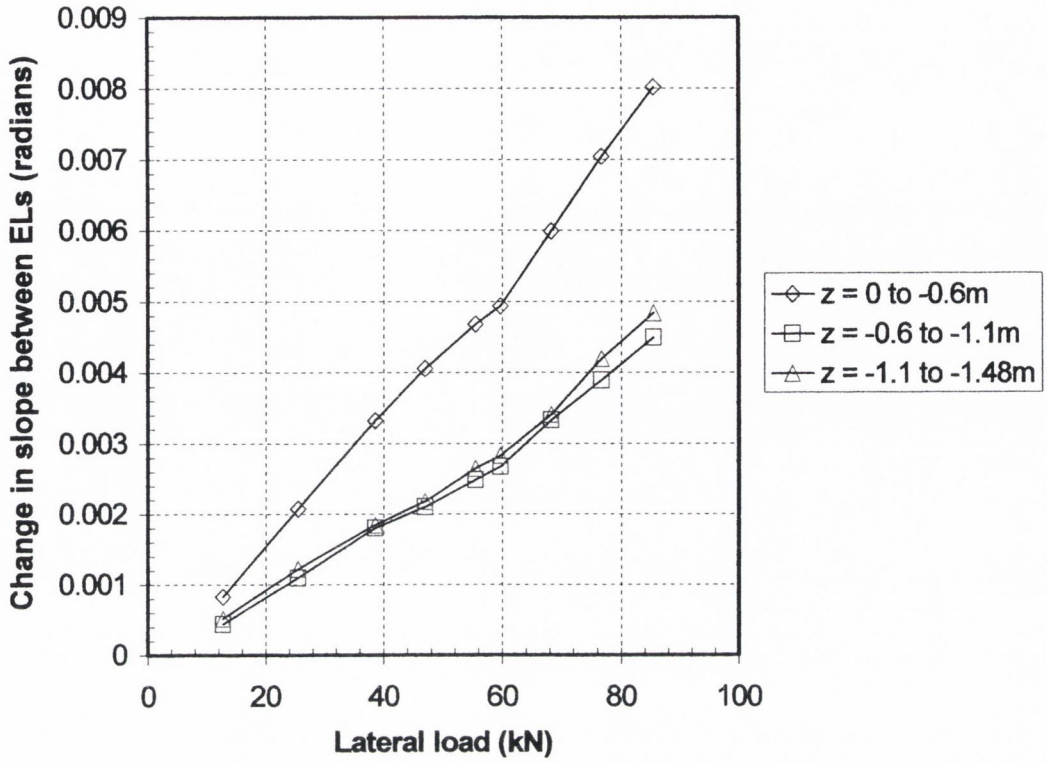

Figure 5-14: Change in pile rotation as pile L1 is re-loaded during CLT2

5.6.4 Analysis of Conditions at Test Failure

The 0.94m of fill (i.e. extending to a depth below the pit, z=0.94m) surrounding pile L1 contained large pieces of concrete slabs which, for the level of applied lateral loads, may have prevented the formation of a 'shallow-wedge' failure typically observed in uniform soils when the near surface bearing capacity has been exceeded. The post-test trial pit exploration (Figure 5-15) suggested that arching may have taken place between the slab segments; numerous air pockets were observed between the 'arched' slabs. The fill may therefore have acted more like a restraining 'strut' (capable of resisting the maximum test load) rather than a soil matrix.

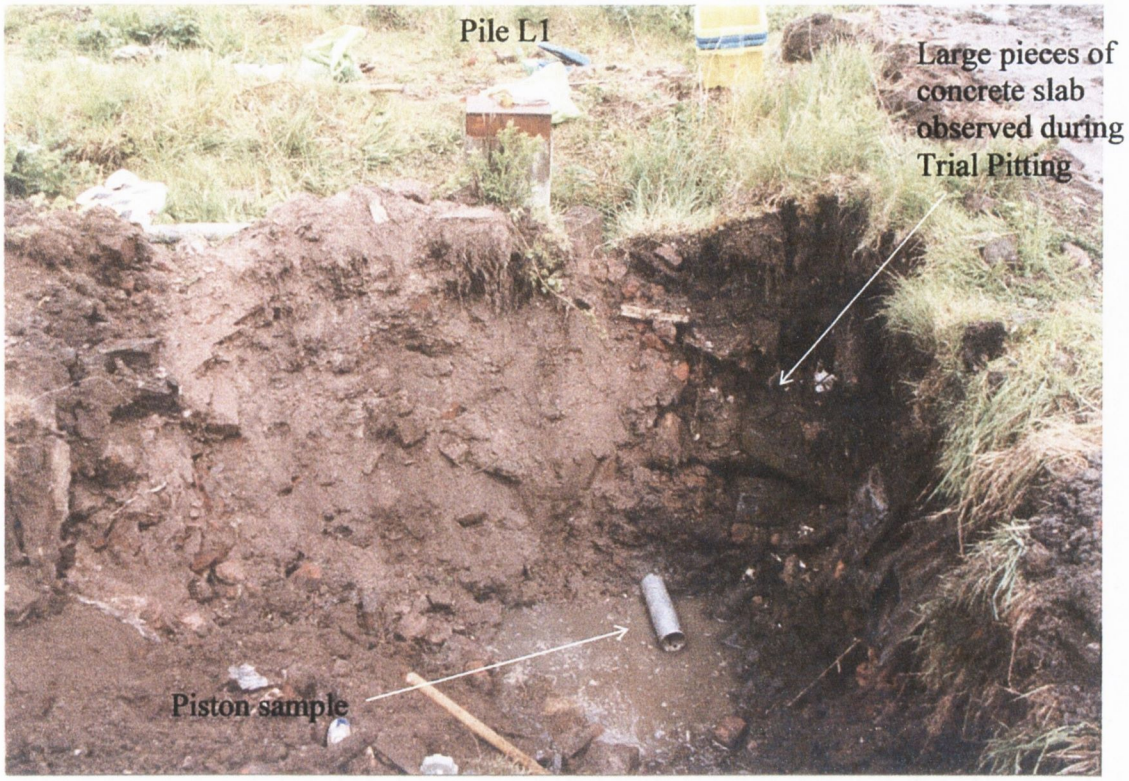

Figure 5-15: Trial pit excavated around pile L1 revealing large pieces of concrete slab

In contrast, the fill around pile AL1 was less than 0.5m thick (i.e. it extended to z= 0.48m) and contained only brick-sized construction debris embedded in a compact gravel[19]. Such a deposit is likely to exhibit a less stiff/strong response and allowed development of a shallow wedge failure discussed above. Confirmation that a shallow bearing capacity failure occurred around pile AL1 was provided during the re-test where pile head displacements for AL1 were greater than those measured at L1. In contrast, the continued resistance provided by stratum 1 around pile L1 was evident during the re-test (RT); where the pile head movements closely matched those measured during the initial load tests (see Figure 5-18).

[19] Similar to that observed in TP3, see Figure 4.14.

5.6.5 Concluding Comments on CLT Series

This series of tests served to illustrate the dramatic difference in lateral response for two identical piles, installed in close proximity to each other such that soil conditions are essentially identical. The piles differ only in pile head condition; the test setup employed to apply an axial load to pile AL1 also created a moment restraint at the pile head (see section 6.3). The second pile, L1 was only loaded laterally and therefore free to rotate at the pile head.

- At pile head displacements of say 10% of the pile diameter, (a value considered reasonable for typical piles employed for land based structures), the presence of the axial load did not adversely affect the lateral pile performance[20]. However, at larger pile head displacements the additional bending moment at the pile head (due to the eccentric axial load) may be significant and necessitate special consideration by the designer. Furthermore, if such movements have been manifested at the pile head, the superstructure is likely to have experienced structural damage.

- The smaller bending moments measured in pile AL1 compared to those measured in pile L1 were due to the restraining moment applied at the pile head. The gradual reduction of this restraint was observed as rotation of the pin joint released the moment at the pile head.

[20] It is well known that an axial compressive load on a reinforced concrete pile enhances the structural characteristics of the pile by increasing the stiffness of the section such that the onset of concrete cracking is delayed. Ignoring the influence of the surrounding soil, a stiffened pile subjected to the same lateral load as an unstiffened pile will register smaller lateral displacements for a period after the unstiffened pile has started to crack. This behaviour is attributed to the prestressing effect of the axial load.

5.7 *Re-Testing Piles under Lateral Load*

5.7.1 Background

The significantly different behaviour of two identical piles observed during the initial test programme resulted in speculation that the presence of an axial load on one of the piles may have strengthened the soil surrounding that pile (e.g. possibly due to dilation in the upper granular crust) and thus contributed to its stiffer response. While variations in soil properties exist within stratum 1, these alone could not explain the difference in stiffness observed between the two piles. Therefore, it was decided to re-test the piles under lateral loading to ascertain the influence of the axial load on pile AL1. Furthermore, re-testing pile L1 would provide information on the ageing effects (after initial loading) in the soil, a phenomenon known to contribute significantly to the axial capacity of piles when loaded for the first time (Lehane et al., 1999).

The additional test was performed on May 18, 1999; nineteen months after the initial test programme. The instrumentation for the test was limited to devices for measuring the load and pile head displacements in addition to recording the pile profiles using electro-levels (ELs). Readings from vibrating wire (VW) strain gauges on pile L1 were also recorded during the test. However, re-connection to the electrical resistance strain (ERS) gauges (severed following the initial load tests) was not established due to time and financial constraints. Details of the test procedure were outlined in chapter 3.
The findings from the re-test are compared with the results of the initial load tests in this chapter. The implications of the re-test on the lateral pile response will be discussed in chapter 9.

5.7.2 Pile Head Load-Displacement Behaviour

It can be seen from Figure 5-16 that the pile head displacement of pile AL1 was greater than that of pile L1[21]. At a lateral load of 74kN, AL1 registered a pile head displacement of 43.7mm compared to 35.4mm for pile L1. The variations in soil properties at the site

[21] The maximum test load was limited to 74kN (or 84% of the maximum load applied in the initial test programme) due to hydraulic fluid leaking from the jack. Because of the leaks a number of un-loading-reloading cycles were recorded during the test, for clarity these have been omitted from the plots shown in Figure 5-16

and the difference in pile diameters were not considered large enough to account for the observed disparity in behaviour. The recovery on unloading was also greater for L1 with 90% of the maximum displacement recovered at the end of the test compared to 71% for AL1.

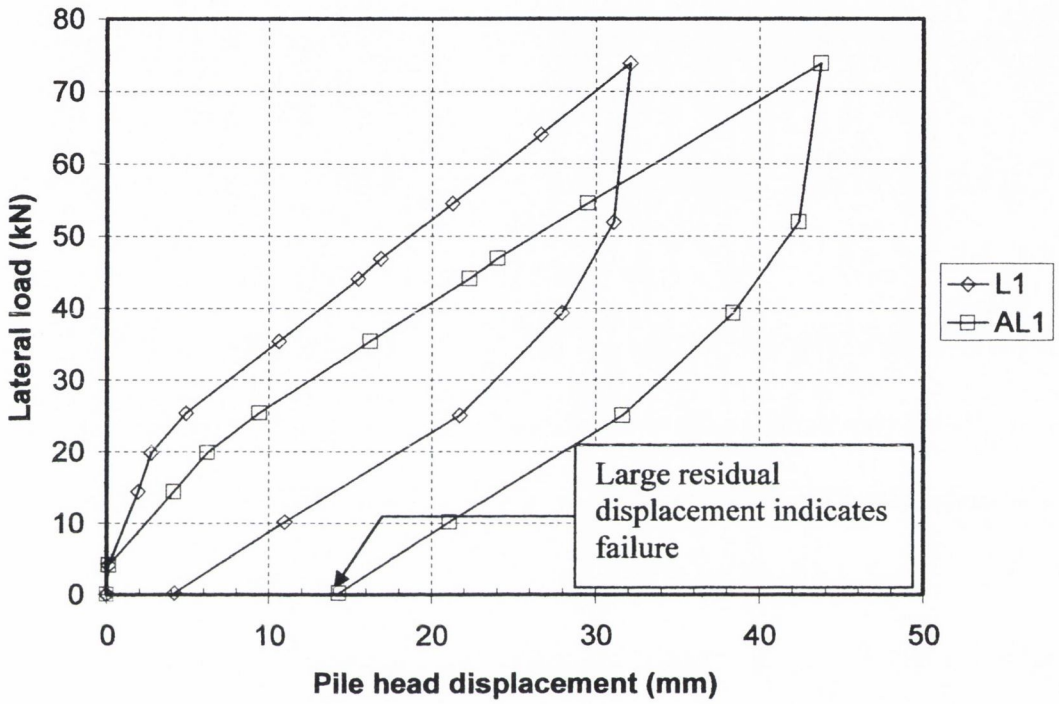

Figure 5-16: Load against pile head displacement during re-test

5.7.2.1 Load-Pile Head Displacement at Pile AL1

In Figure 5-17 the load-displacement response for pile AL1 is plotted in conjunction with the results from the initial tests. These profiles permit the assessment of the load-pile head displacement behaviour between the various tests. To facilitate direct comparison of the data, the curves have been plotted from an initial displacement of zero. The dramatic reduction in stiffness for pile AL1 during the RT indicates that the soil surrounding AL1 underwent a bearing capacity failure due to the loads applied at the end of CLT2.

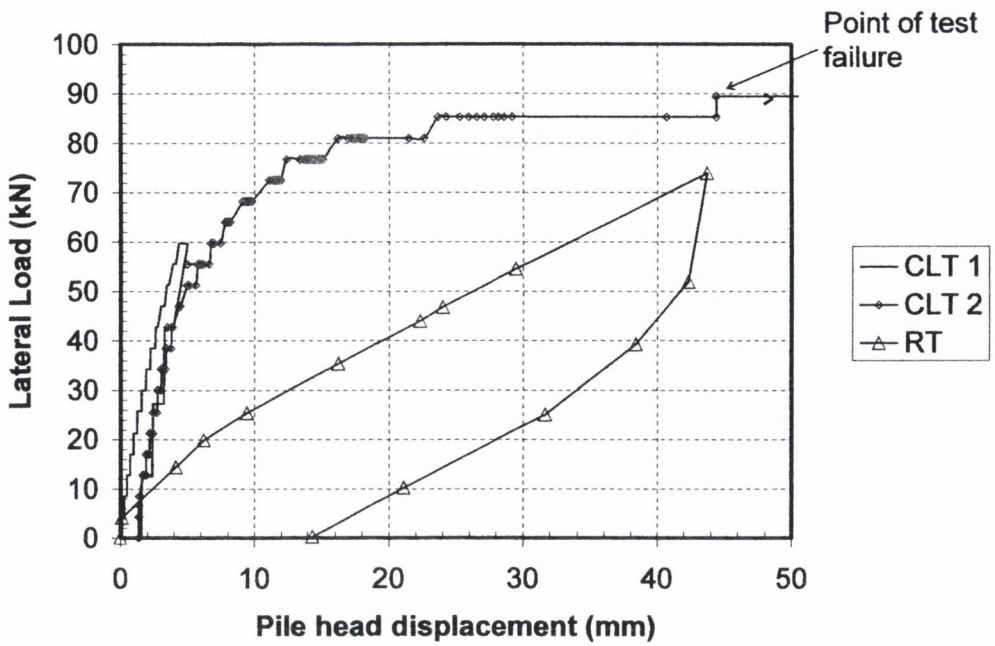

Figure 5-17: Pile AL1 displacements from initial tests and Re-test compared

5.7.2.2 Load-Pile Head Displacement at Pile L1

In Figure 5-18 the load-displacement response for pile L1 is plotted in conjunction with the results from the initial tests. These profiles permit the assessment of the load-displacement behaviour between the various tests. The following observations are noteworthy for pile L1:

- After the nineteen-month period, pile L1 exhibits a soil stiffness similar to that measured during CLT1 up to the maximum load. This behaviour indicates that the bearing capacity of the soil around L1 had not been exceeded during the initial test series.

- Pile L1 exhibited the more elastic response by rebounding to a residual displacement of 3.5mm fifteen minutes after unloading compared to 12.7mm for pile AL1. These results suggest that a bearing capacity failure of the soil around pile AL1 may have been responsible for the failure during the initial tests.

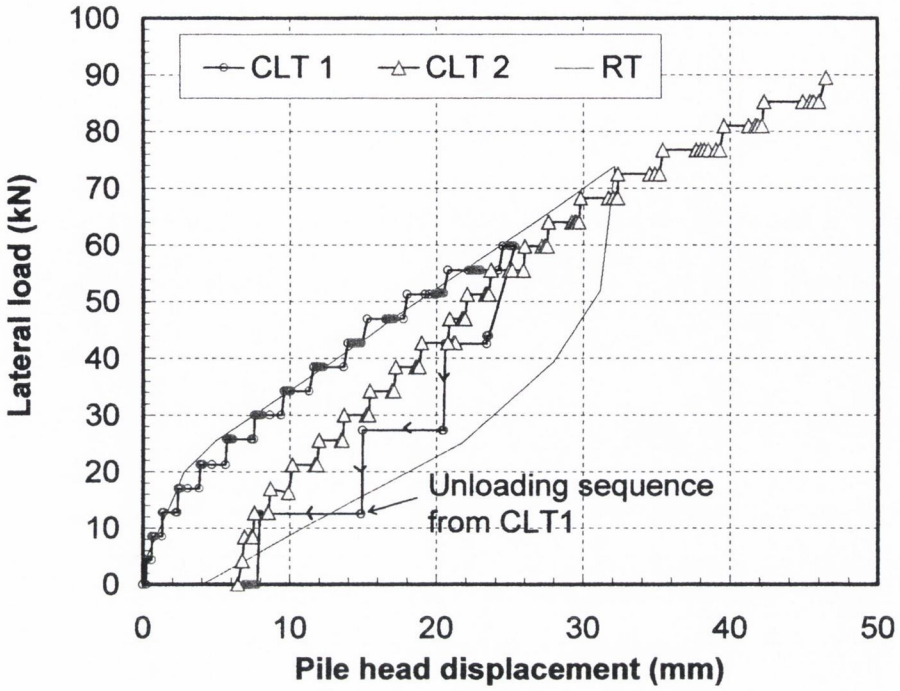

Figure 5-18: Pile L1 displacements from initial tests and Re-test compared

5.7.3 Displacement Profiles

The displacement profiles illustrated in the following sections were drawn using the procedure outlined in 5.6.2. For the re-test, each pile contained four ELs spaced a distance of 0.75m apart, the first EL was located 0.75m below the pile head displacement transducer. The ELs permitted the pile profile to be established over the depth of soil controlling the lateral response of the pile. At a depth of ≈2.5 metres below pit level, the displacements had reduced to negligible values.

5.7.3.1 Profiles for Pile AL1

The displacement profiles for pile AL1 during the re-load test are shown in Figure 5-19. The pile appears to rotate as a rigid unit up to loads of ≈30kN. Bending of the pile profile only became evident in the subsequent load increments.

The displacement profiles for a lateral load of ≈55.5kN are compared for each load test in Figure 5-20. The change in the pile profile for the re-test is evident from the graph; these profiles can be used to give an indication of the soil strain. The soil surrounding a laterally loaded pile generally experiences much higher strain than that experienced by the soil when the pile is loaded vertically. If the pile movement at pit level is related to half the pile width (i.e., B/2) then the normalised displacement of the soil adjacent to the pile, for a lateral load of 55.5kN, would be ≈ 1.4% during the initial tests, increasing to 10% for the same lateral load in the re-test.

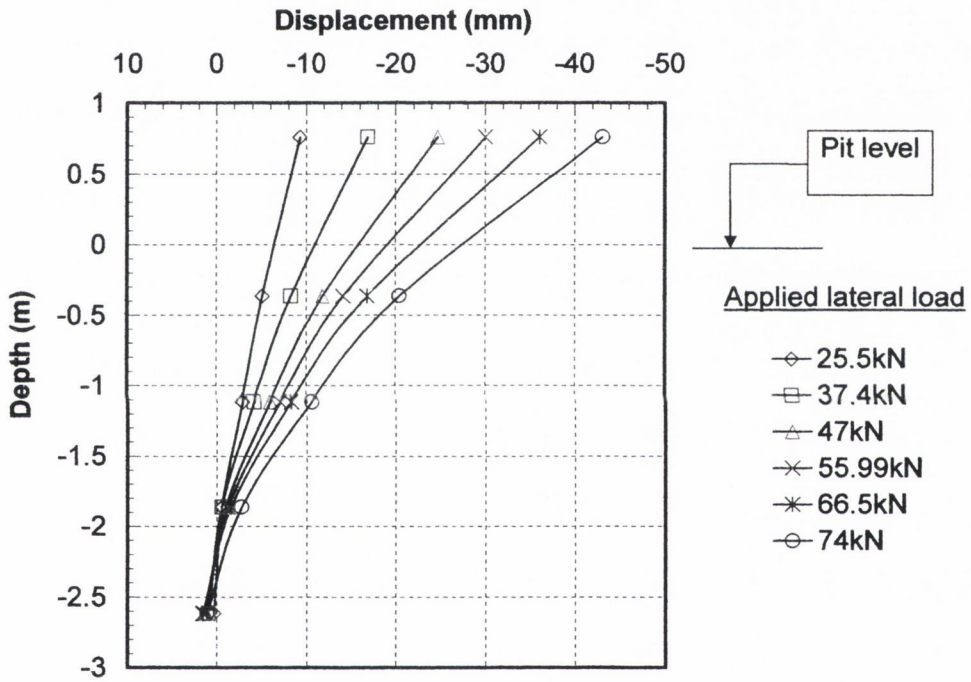

Figure 5-19: Re-test displacement profiles for pile AL1

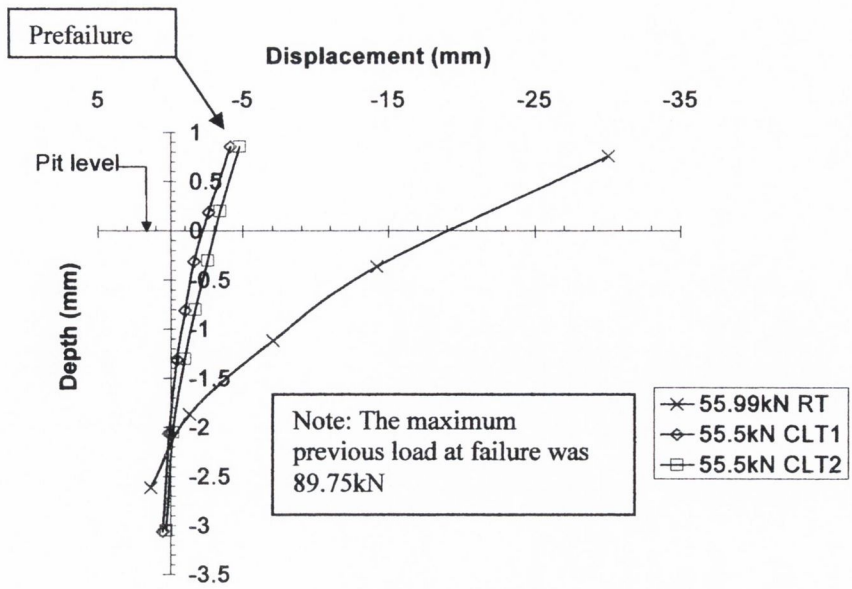

Figure 5-20: Comparison of displacement profiles for pile AL1 at ≈55.5kN

5.7.3.2 Profiles for Pile L1

The displacement profiles for pile L1 are shown in Figure 5-21. In contrast to pile AL1, pile L1 exhibits bending of the profile during each load increment. This suggests that on re-loading, the displacement necessary for the pile to re-engage with the soil was in the order of a few millimetres and evidence of a gap or post-hole around L1 was negligible.

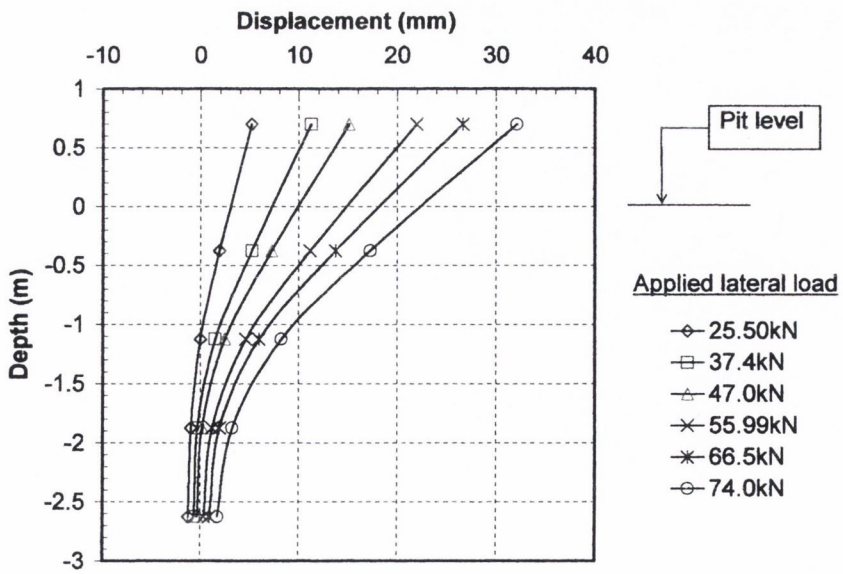

Figure 5-21: Re-test displacement profile for pile L1

In Figure 5-22 the 55.99kN displacement profile for pile L1 during the Re-test is compared with the 55.5kN displacement profile for CLT1. The results show the similarity between the profiles and imply that the bearing capacity of the soil around pile L1 had not been exceeded during the second combined load test. The results also show there has been no beneficial gain in strength over the intervening 19-month period. The maximum normalised displacement of the soil adjacent to the pile, again calculated in terms of half the pile width, approximates to 8.5% at pit level in both tests.

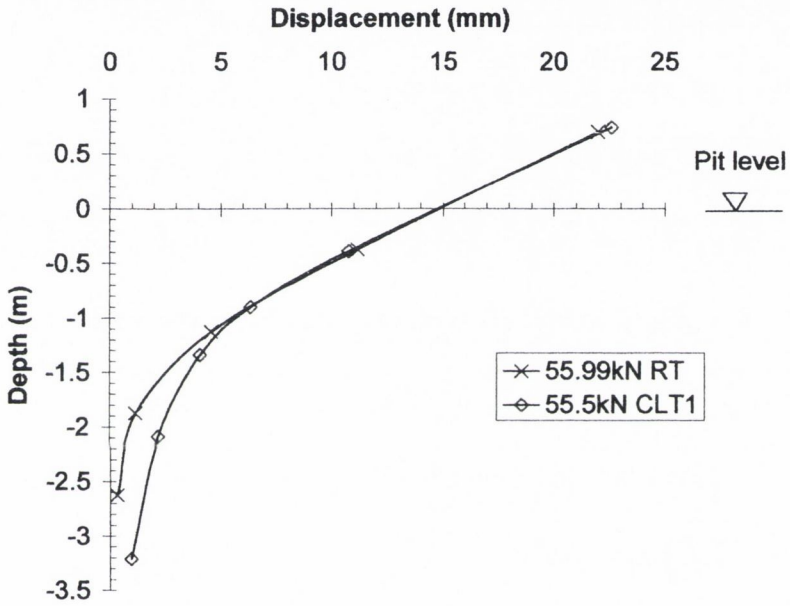

Figure 5-22: Comparison of displacement profiles for pile L1 at ≈55.5kN

Chapter 6

Structural Analysis of Test Setup and Pile Section Response

6. STRUCTURAL ANALYSIS OF TEST SET UP AND PILE SECTION RESPONSE

6.1 Introduction

In this chapter the interpretation of the combined loading on pile AL1 is presented. The load test setup at pile AL1 inadvertently applied a restraining moment at the pile head. The effect of the pile head restraint (induced by the loading mechanism) on the structural response of the pile is assessed from the displacement, rotation and load data measured at the pile head. The pile section response is evaluated using a moment-strain (M-ε) relationship established from a 2-D finite element (FE) analysis. To check the consistency of the relationship, the FE analysis results are compared with the in-situ M-ε relationship measured by a strain gauge located at pit level in pile L1. The factors controlling the structural design of the pile are discussed initially and measured bending moment distributions for each pile are presented at the end of the chapter.

6.2 Structural Design of the Pile Section

As the piles were used to measure the lateral resistance of the soil, structural design of the cross section was not dictated by the standard design considerations of moment capacity and deformation characteristics. However, the following factors influenced the selection of the pile size and its reinforcement:

(a) Under lateral loading, the piles required enough strength to stress a sufficient volume of soil to failure before a plastic hinge(s) is developed in the pile.

(b) The piles were to be of adequate size to accommodate the instrumentation.

(c) Sufficient reinforcement had to be provided to withstand bending stresses developed during hoisting and pitching of the piles.

(d) The piles were to remain uncracked during the handling and installation procedures. This would ensure that the flexural stiffness (EI) of the piles at the start of the first load test was that of an uncracked section, hence simplifying the subsequent interpretation of the load tests.

A 350mm square precast concrete section provided the desired characteristics. For condition (c), reinforced concrete theory was used to develop an interaction diagram for the piles based on the reinforcement arrangement and the compressive strength of the concrete. The analysis shows that the section had an ultimate bending moment capacity of 116kNm and under lifting conditions (see Figure 3-1 for lifting details) a maximum bending moment of 30kNm (or 26% of the bending capacity) would be induced due to the self-weight of the pile[1]. The moment capacity of the pile section varied with axial compressive load as shown in Table 6-1. Calculations associated with tabulated values can be found in appendix 6a.

Test reference	Axial load (kN)	Bending moment capacity (kNm)
CLT1 (October 1997), pile AL1	168	138
CLT2 (October 1997), pile AL1	133	132
L1 during CLT1 & 2 and both L1 & AL1 during the 1999 Re-test	0	116

Table 6-1: Results from the structural analysis of the pile section under various axial loads

[1] According to the American Concrete Institute (ACI 318) the cracking moment for normal density concrete is given by $M_{cr} = f_r I_g / y_t$ where the cracking stress $f_r = 0.7\sqrt{f_{cu}}$, I_g is the gross second moment of area for the section and y_t is the distance from the neutral axis to the extreme fibre. Therefore cracking in the pile section could be expected at bending moments above ≈35kNm.

In case (d), once the piles were cast, steam curing was carried out for a period of 24 hours and the piles were subsequently hoisted from the moulds two days later. Tests on cube specimens indicated the concrete had an unconfined compressive strength of 26 MPa after three days and 54 MPa at 28 days.

Assuming the concrete's flexural strength to be 10% to 15% of its compressive strength (ACI 1989) and its elastic stiffness[2], E as 37kN/mm^2 the ultimate flexural strain in the concrete is estimated to fall between 140με and 200με at its 28-day strength of 54MPa[3]. Calculations of strains due to pile handling indicated that the piles remained elastic throughout the handling process.

6.3 Modelling of Loading Mechanism at Pile AL1

The test configuration applying the vertical load to pile AL1 inadvertently provided a degree of restraint at the pile head; this was apparent from the large differences in the pile head displacements measured for each pile during CLT1 (see load-pile head displacement plots presented in chapter 5). To quantify the restraint, it was first necessary to understand the loading mechanism at the pile head.

Figure 6-1(a) schematically illustrates the test configuration while Figure 6-1 (b) shows the resolved forces acting on the displaced pile. Qualitatively these forces led to the structural model shown in Figure 6-2 (a) with a typical bending moment response shown in Figure 6-2(b). This model is consistent with the moment profiles measured during the tests.

The behaviour of AL1 can be explained through a combination of field observations, instrumentation data and the test beam movements recorded during the CLTs. These data confirm that translation of the rollers beneath the test beam did not occur during the load tests. Instead, the test beam moved with the pile in a series of steps corresponding with

---

[2] ENV 2 (1994) gives the static elastic modulus for concrete; $E_c = 9500(f_{cu} + 8)^{0.33}$ where f_{cu} is the characteristic compressive strength of the concrete.

[3] This is consistent with the findings of research cited by Neville (1981) and MacGregor (1992) who concluded that onset of flexural cracking in concrete is likely to be initiated at strain levels greater than 200με.

each load increment up to 59.75kN in CLT1. As the lateral loads were increased above this level in CLT2, the pin joint started to rotate noticeably.

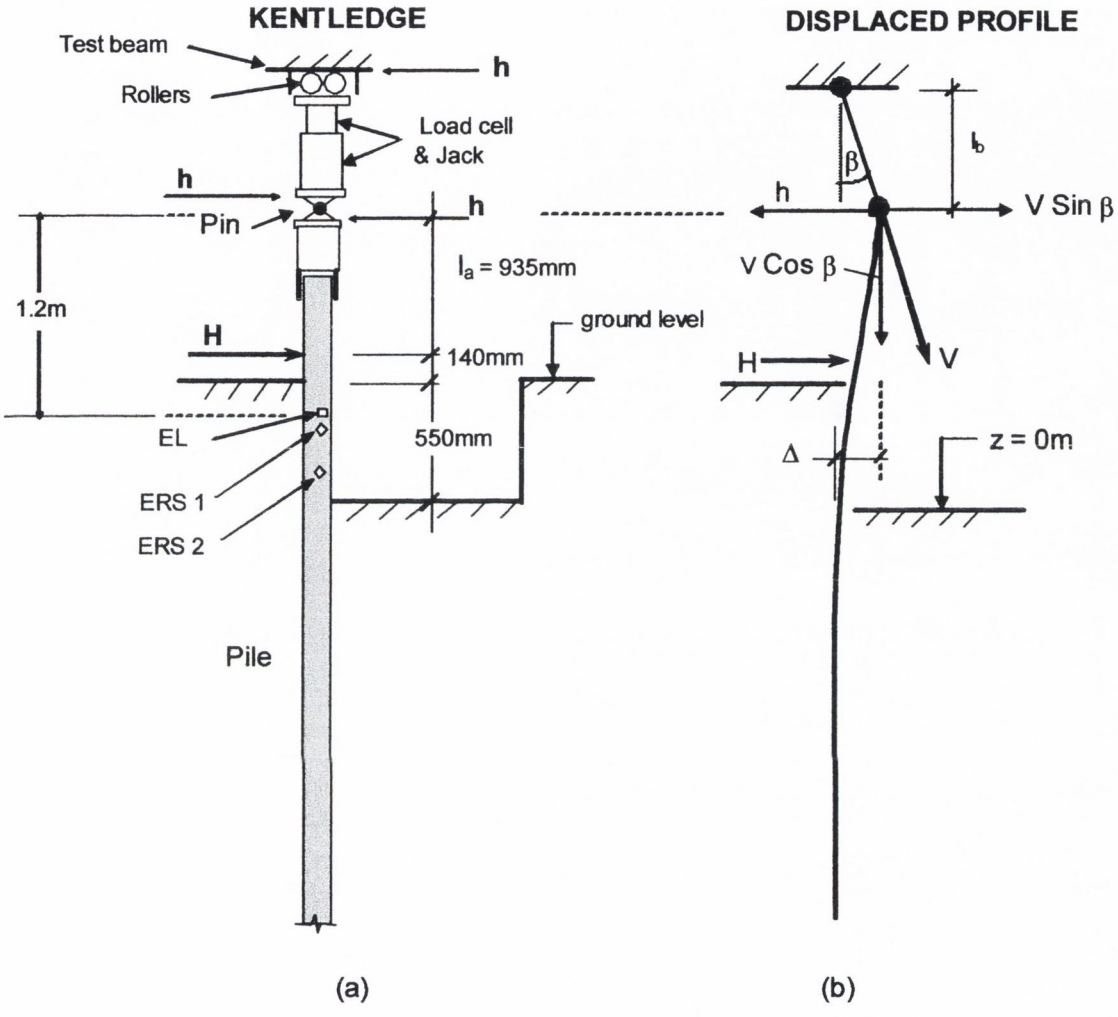

Figure 6-1: (a) Test configuration for pile AL1 (b) Resolved forces acting on AL1

It was therefore concluded that sufficient frictional force was mobilized between the 'rollers' and the test beam to cause the beam to move during the application of lateral loads. Taking a coefficient of friction[4] of 0.6 between the 'rollers' and the test beam, frictional forces up to 100kN and 80kN were estimated under the axial loads applied during CLT1 and CLT2 respectively. The mobilised frictional force, *h* shown in Figure 6-1 (a) had the effect of reducing the lateral load applied to AL1. Furthermore, as the frictional force was transferred across the pin joint (Figure 6-1a) it created a restraining

[4] Nash (1992)

moment, M at the point of lateral load application. These additional load effects were due to the test setup and clarify why, during CLT1 and much of CLT2, AL1 experienced smaller bending moments and displacements than pile L1.

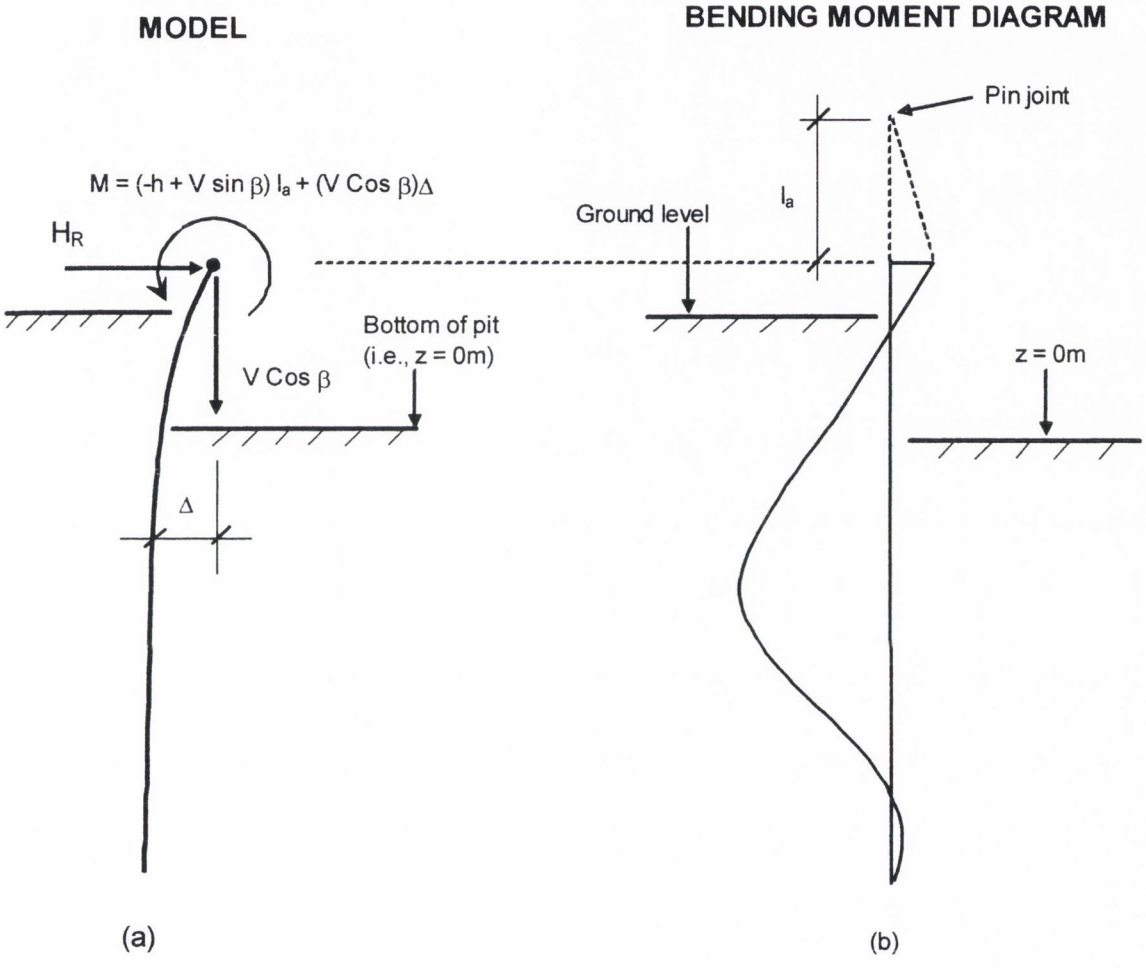

Figure 6-2: (a) Modelling of loads applied to AL1 (b) Typical bending moment profile

To quantify these effects, the shear (H_R) and applied moment ($M_{applied}$) at the point of lateral loading were back calculated using the bending moments inferred from strain gauges located above pit level and the slope measured by an electro-level (EL) located 240mm below the level of the applied lateral load (Figure 6-3). If it is assumed that the EL

slope θ is representative of the pile slope at the point of lateral loading[5], then the displacement at the pin joint Δ can be estimated as;

$$\Delta = \delta + (\theta)(l_a - x) \qquad \theta \text{ is in radians}$$

where δ = the displacement measured at the LVDT

$(l_a - x)$ = distance from the LVDT to the pin joint

The strain at any ERS gauge above the pit level[6] can be used in conjunction with the moment-strain relationship (section 6.4) to determine the bending moment ($M_{measured}$) resisted by the pile at that point. Therefore, having determined Δ and hence β ($= tan^{-1}\{\Delta / l_b\}$) (see Figure 6-1b and Figure 6-3), $M_{measured}$ at the ERS gauge level can be equated with $M_{applied}$ at the same level thus enabling h to be back calculated as follows for ERS 1:

Eq. 6-1... $h = [H(d) + V\sin\beta(e) + V\cos\beta(\Delta) - M_{measured}]/ e$ (kN)

where h = frictional force acting in the opposite direction to H

H = applied lateral load

V = the axial load measured by the load cell

d = distance from point of lateral loading to $M_{measured}$

$V \sin\beta$ = the horizontal component of the kentledge load due to pin joint rotation

e = distance from pin joint to $M_{measured}$

Δ = displacement of pin joint relative to EL (see Figure 6-3)

The horizontal component of the angled vertical load, $V \sin \beta$ (Figure 6-1b) was initially small but grew in magnitude as the joint rotation increased. The effect of the increasing

[5] This assumption is reasonable considering the inherent stiffness of the 350mm square reinforced concrete pile over the short distance between the EL and the point of horizontal loading. Adopting the EL slope for the slope at the loading point would result in negligible error in the calculated pin joint displacement.

[6] Note that at any point above the pit level, the net horizontal load multiplied by its distance to the point considered gives the applied moment.

joint rotation (β) on the magnitude of the restraining moment can be seen in Figure 6-4. It is noteworthy that rotation at the pin joint causes the initial restraining (negative) moment to undergo a change in direction at a rotation of $\approx 0.5°$. This trend continues and the moment eventually become a positive moment (i.e. an additional moment acting on the pile) once the pin joint rotation exceeds $\approx 2.6°$ (see also Figure 6-6).

The accuracy of the frictional force given by Eq. 6-1 was checked using data from a second ERS gauge (ERS 2, Figure 6-3) also located above pit level. The results from this gauge predicted the frictional force, h within 5% of the value predicted by the first gauge thus confirming the validity of the model. The average value for h calculated from the two ERS gauges was used in the subsequent analysis of the pile AL1 results. The details of these analyses for CLT1 and CLT2 are presented in appendix 6d.

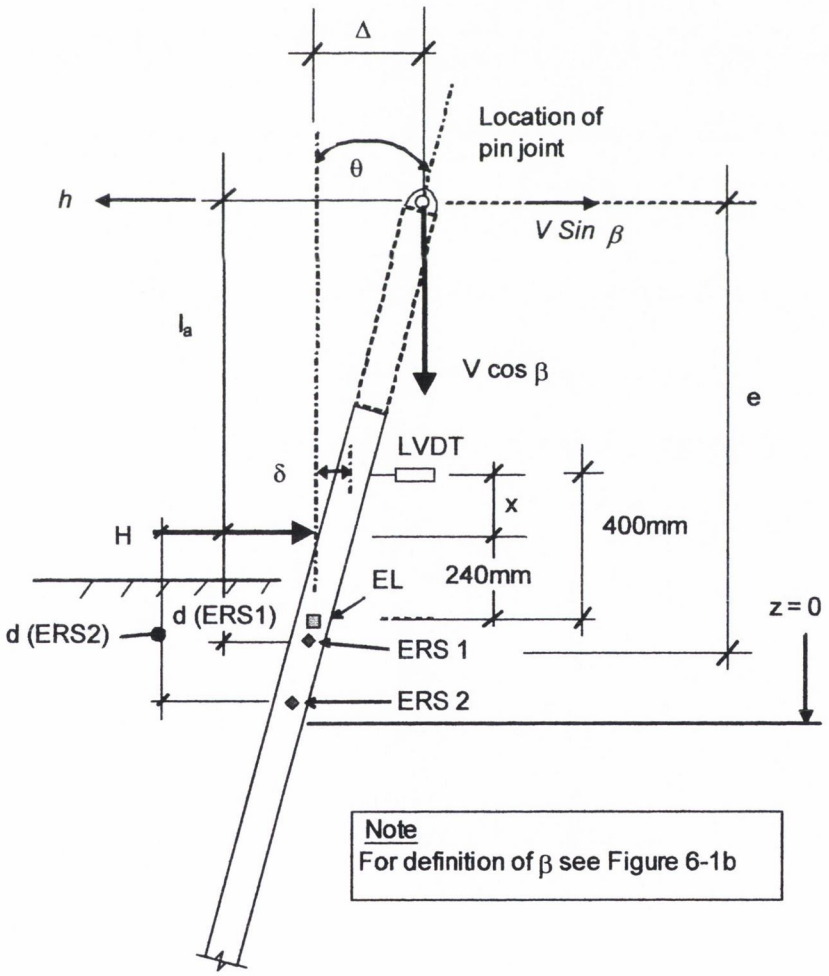

Figure 6-3: Geometry used to calculate the displacement at the pin joint, Δ

It should be noted that Eq. 6-1 ignores side friction above the strain gauge level which is considered negligible given the soil disturbance created during pile installation and the small horizontal stresses that exist close to the ground surface[7]. Furthermore, the absence of sustained consolidating forces at ground level means that any potential friction that may develop after installation would be minimal.

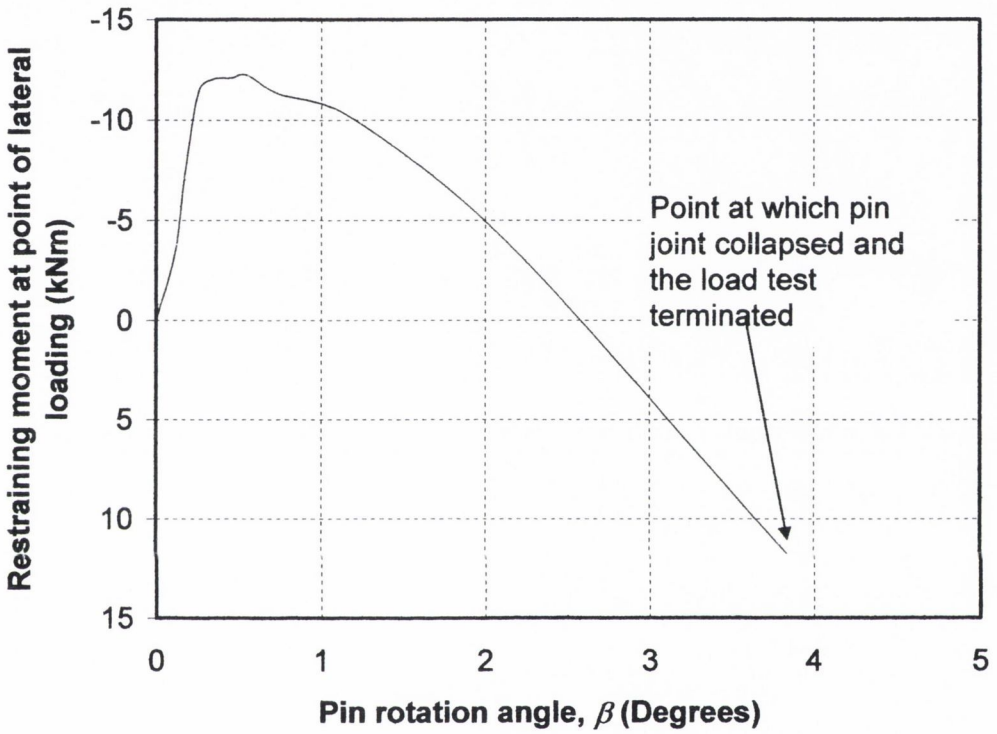

Figure 6-4: Variation in pile head restraining moment with pin joint rotation

Therefore, having determined h, the resultant horizontal load, H_R applied to AL1 is given by the algebraic sum of the horizontal forces as shown in Eq. 6-2.

Eq. 6-2... $$H_R = H - h + V \sin \beta$$

[7] At greater depth, where plane strain conditions exist, side friction can be a significant component in the lateral resistance of piles subjected to horizontal loading. Briaud et al. (1984) concluded that side friction might contribute up to 50% of the piles resistance at working load.

Hence, at ERS 1 for example, $M_{applied}$ can be calculated from the following:

Eq. 6-3... $$M_{applied} = (H_R)(e - l_a) + (V \cos \beta)(\Delta) \quad (kNm)$$

H_R and $M_{applied}$ are used to fit bending moment profiles to the measured bending moments (inferred from the strain gauges) for pile AL1. The influence of the load test setup on the variation in H_R, h and $M_{applied}$ with applied lateral load H is shown in Figure 6-5 and Figure 6-6 for CLT1 and CLT2 respectively. Details of these calculations are provided in appendix 6d.

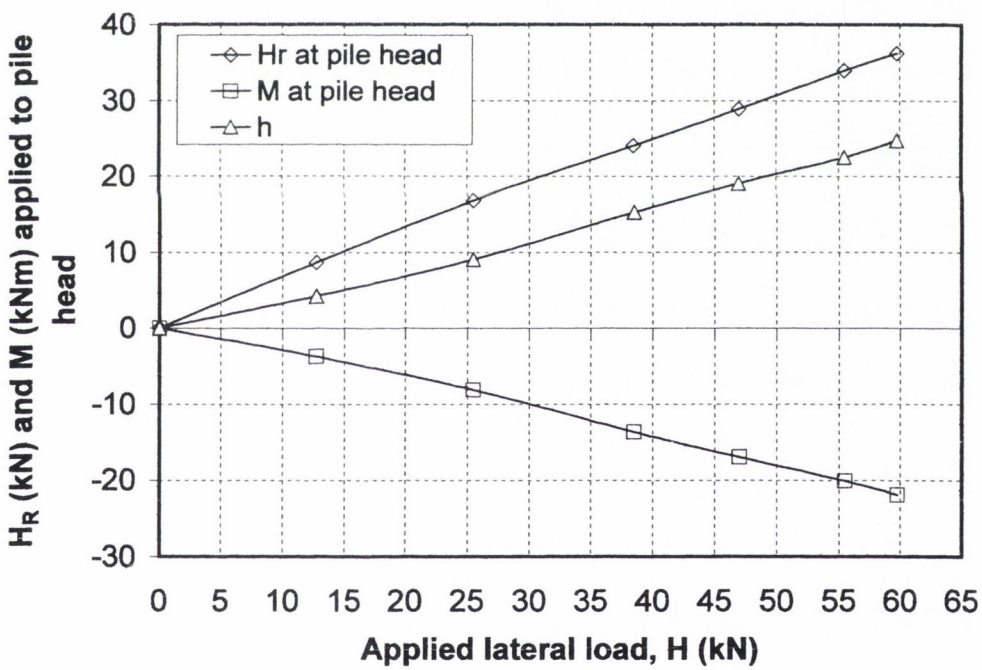

Figure 6-5: Resultant shear and moment acting at the pile head of AL1 during CLT1

Two points are worth noting from Figure 6-6:

1. At loads above H = 47kN the rate of gain in H_R increases and was found to surpass the applied lateral load in the final load increment. The increasing horizontal component due to the axial load rotation is the reason for this occurrence.

2. The magnitude of $M_{applied}$ was significantly less than that measured during CLT1 at the same load levels (Figure 6-5). Moreover, above lateral loads of H = 47kN the value of $M_{applied}$ started to reduce for subsequent loads and ultimately changed sign over the final load increment. This change of sign coincides with the increase in H_R.

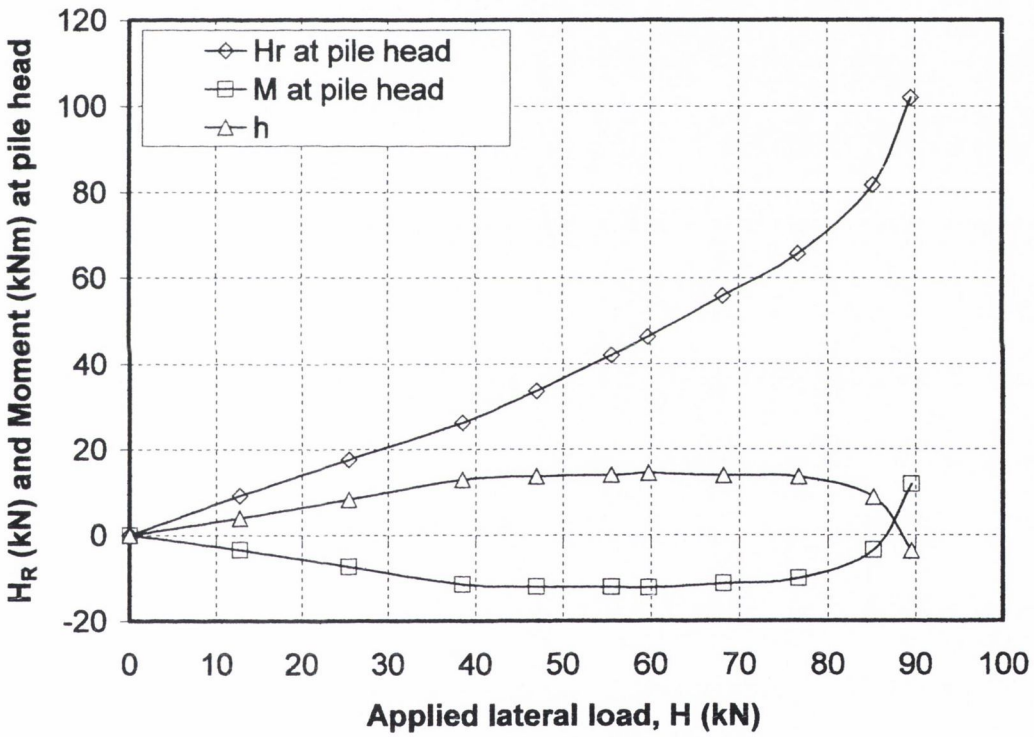

Figure 6-6: Resultant shear and moment acting at the pile head of AL1 during CLT2

Figure 6-7 shows how the pin joint displacement, Δ increases sharply above lateral loads of about 60kN. The variation in $M_{applied}$ (the restraining moment at the pile head) for CLT1 and CLT2 is plotted against the applied load, H on Figure 6-8. The divergence in the moments becomes obvious above H = 25kN. This may be due to rotation of the pin joint causing the gradual release of the restraint that was present during CLT1.

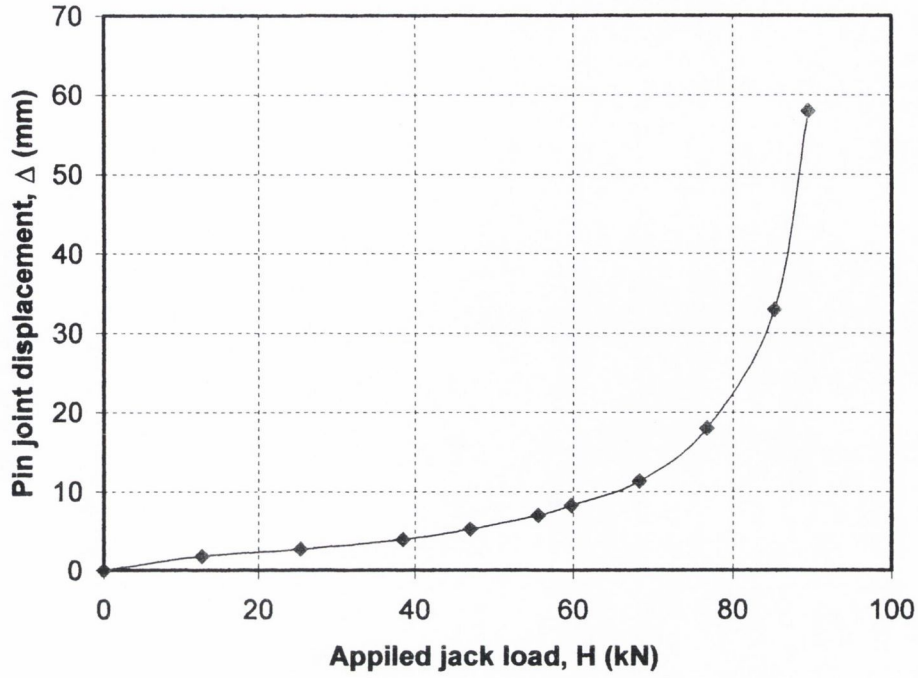

Figure 6-7: Pin joint displacement inferred from pile head displacements measured during CLT2

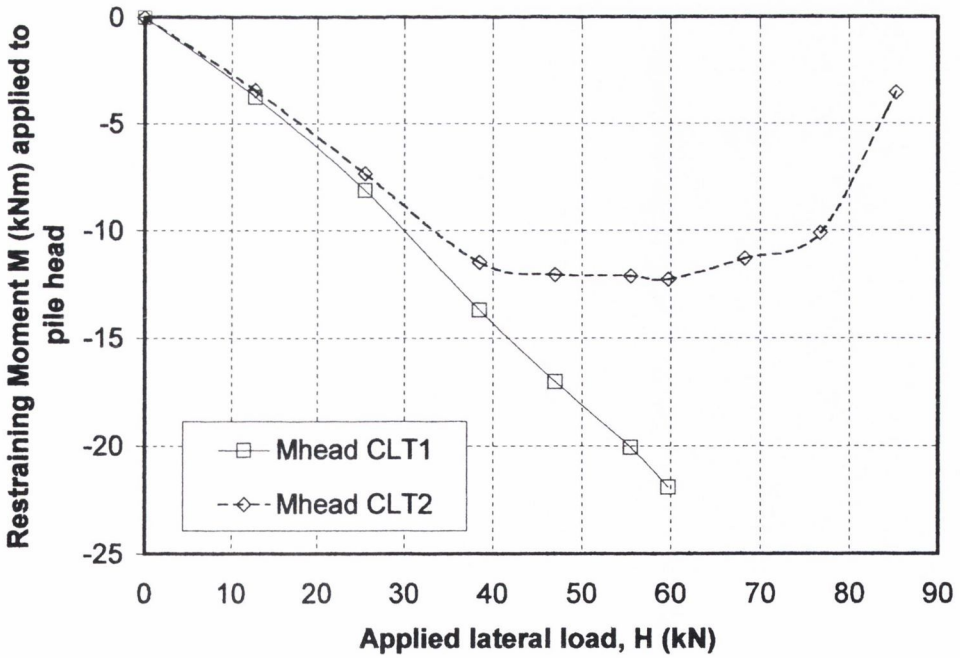

Figure 6-8: Pile head moment at AL1 during CLT1 and CLT2

6.4 Moment- Strain Relationship for the Precast Concrete Piles

It was necessary to establish a means of converting the measured strains into pile bending moments. Two methods were used to establish such a relationship; the first involved correlating known applied moments at pit level with strain gauge measurements obtained at the same level. The second approach used finite element analysis to determine the moment-strain response on the basis of strength tests performed on the pile concrete and reinforcing steel. These analyses will now be discussed in greater detail.

6.4.1 Pile Moment-Strain Relationship Using Strain Gauge Data and Finite Element (FE) Analysis

An in-situ moment-strain (M-ε) relationship was measured by pile L1. The data from a strain gauge[8] located close to pit formation on the compression side of the pile were correlated with the known applied moment at the same level. The resultant M-ε relationship was established as follows:

- The sensitivity, repeatability and linearity of the reference strain gauge were assessed and the results shown in Figure 6-9 and Figure 6-10. Both plots confirm that the gauge responds sharply to applied loads and is suitable for measuring the in-situ M-ε relationship.

- The pile bending moment at the reference gauge level was calculated from the lateral load multiplied by the distance from the load to the strain gauge. The measured strains were then plotted against the known bending moments to give the in-situ M-ε relationship. To check the accuracy of the relationship, an elastic analysis (discussed below) was performed to back calculate the theoretical strain in the pile under applied moments. This exercise was performed at the same load increments applied in CLT1 and CLT2 thereby allowing direct comparison between the measured and theoretical strains.

[8] ERS 30, subsequently referred to as the reference strain gauge, was located 0.765m below the applied lateral load on the compression face of pile L1. This depth approximately corresponds with the depth of the pit excavated in front of the pile, i.e., z = 0.

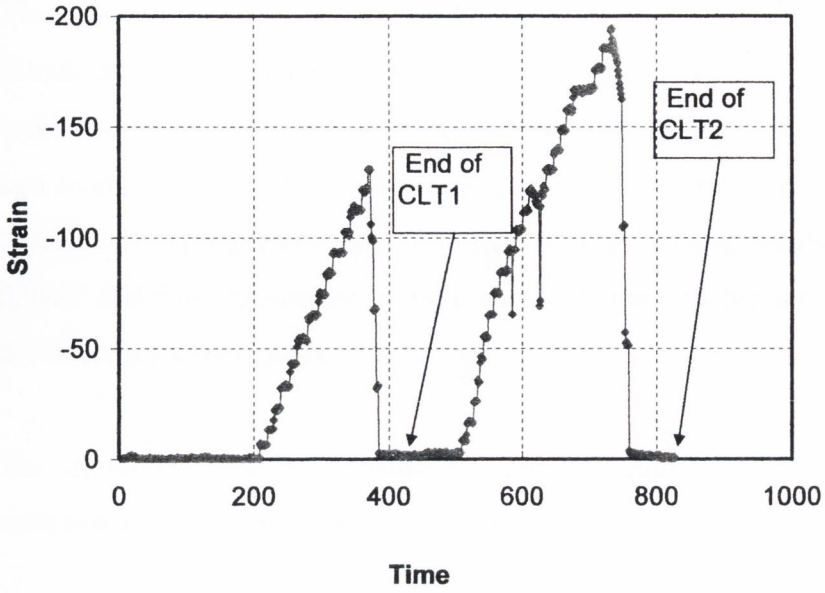

Figure 6-9: Strain versus Time for ERS 30 located on L1, 0.765m below the applied load

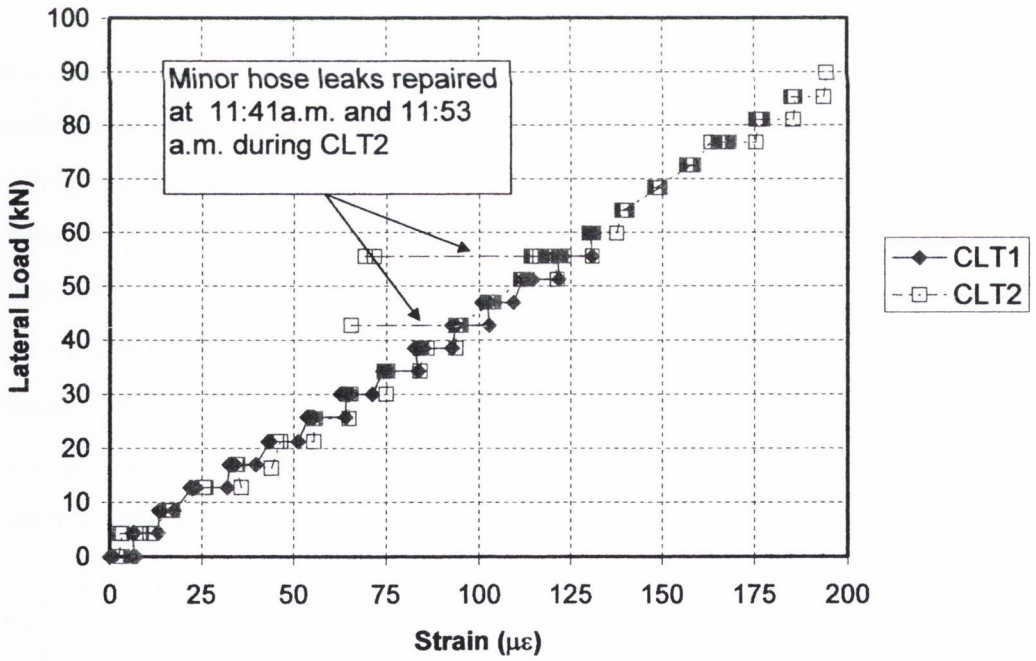

Figure 6-10: Strain versus load for ERS 30

Elastic analysis

The theoretical strain in an elastic beam due to an applied moment can be calculated as $\varepsilon = My/E_cI$, where Young's modulus (E_c) for the concrete was estimated from the equation recommended in Eurocode 2 (see footnote 2). The agreement between the elastic and measured M-ε relationship is evident from Figure 6-11. A regression analysis of the two sets of data resulted in an r^2 value of 0.9987 and thus confidence in the accuracy of the bending moments inferred from the reference strain gauge.

- The measured M-ε relationship for pile L1 could therefore be used to infer moments at other gauge locations along the pile shaft.

- The M-ε relationship could also be used to predict the bending moment profile for pile AL1 once the effect of axial compression had been accounted for.

However, the close proximity of the reference gauge[9] to the applied lateral load limits the maximum moment that could be inferred from the measured M-ε relationship to 68.5kNm. A review of the strain profiles measured during the tests revealed that bending moments of greater magnitude existed at depths below the reference gauge. Therefore an alternative means of inferring pile-bending moments at these locations was required. To facilitate this, a FE analysis was undertaken to extend the M-ε relationship beyond the strain levels recorded by the reference gauge. The results of the FE analyses (for the location corresponding to the reference ERS gauge) along with the ERS gauge M-ε relationship are shown in Figure 6-12. The details of the FE analysis are presented in appendix 6b.

[9] Appendix 9 presents a commentary on the lessons learned from the strain gauging of a reinforced concrete member and provides recommendations for future work.

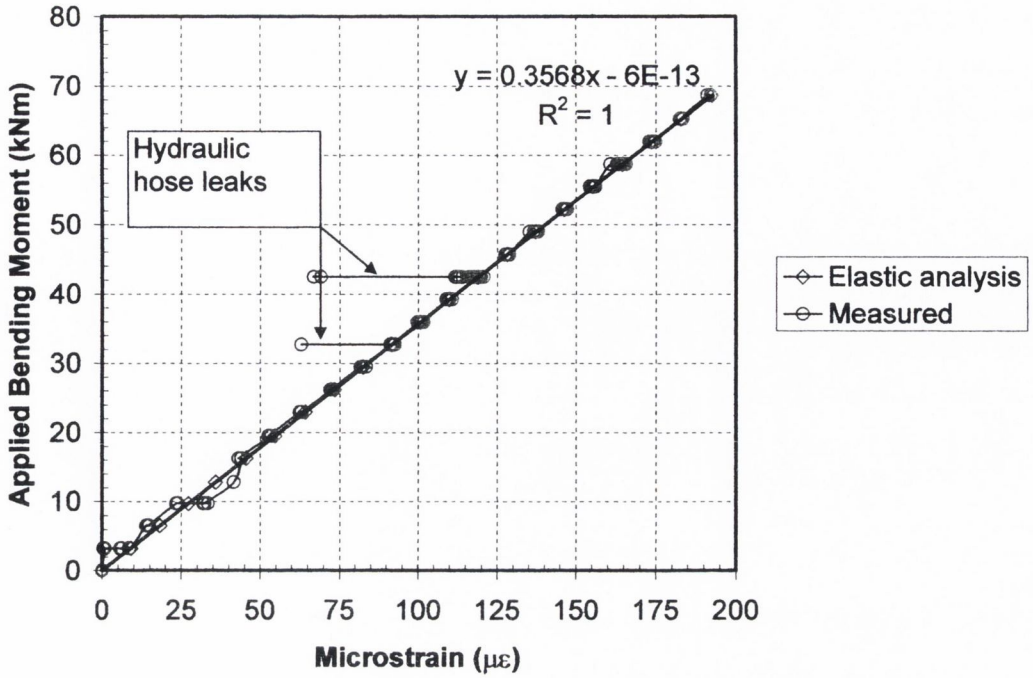

Figure 6-11: Comparison between M-ε relationships from elastic theory and that measured by the reference ERS gauge in pile L1

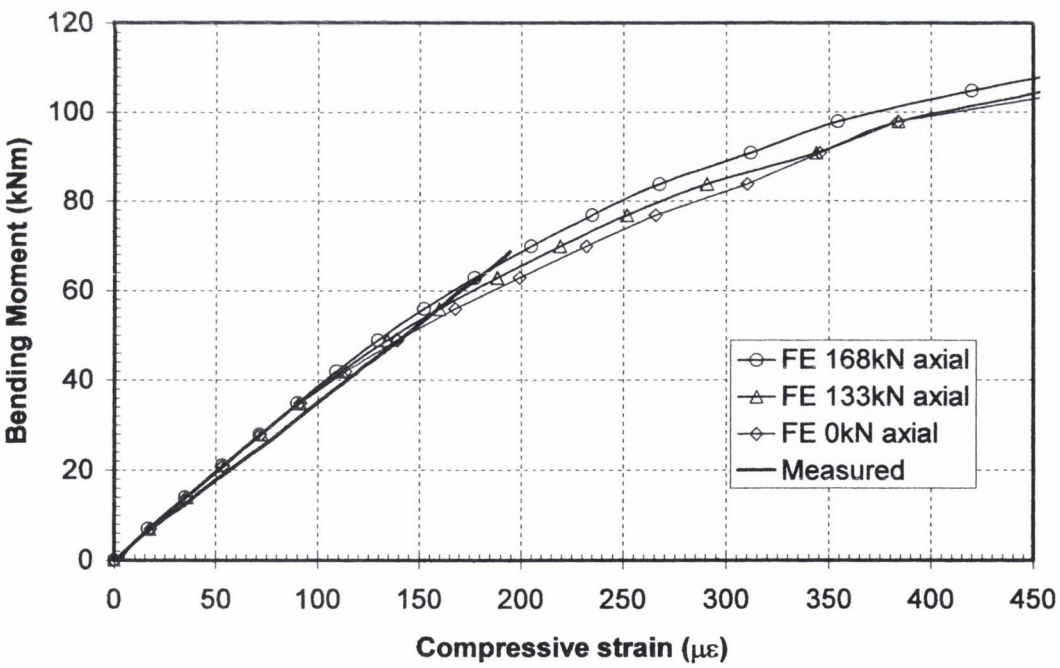

Figure 6-12: FE M-ε relationship for various axial loads compared with measured in-situ relationship

6.4.2 Back Calculated Young's Modulus (E_c) for Concrete from Lateral Load Tests

Employing the recommendations of EC 2 (see footnote 2) and the average cube strength of the concrete from the test piles (54 MPa); E_c was estimated as 37kN/mm^2. This value was used to provide an additional check on the accuracy of the strain gauges. Data from two opposite strain gauges, positioned at ground level and orientated along the plane of loading were used to locate of the neutral axis[9] and the bending moment at ground level. The latter was determined from the FE moment-strain relationship in Figure 6-12 and the strain data from the gauge located on the compression side of the pile. For static equilibrium, the applied moment (M_{meas}) must equal to the internal pile moment ($M_{conc} + M_{steel}$), and since the Young's modulus for the steel (E_s) is known, the equation can be solved to yield E_c i.e.

$$M_{meas} = M_{conc} + M_{steel} = F_c L_c + F_s L_s = (E_c \varepsilon_c A_c) L_c + (E_s \varepsilon_s A_s) L_s$$

where F_c and F_s are the forces in the concrete and steel and L_c and L_s their respective lever arms about the neutral axis.

Solving the equation gave E_c values over 36kN/mm^2 for a range of load increments applied during CLT1, which is in close agreement with the EC 2 value of 37kN/mm^2 and thus confirms the quality of the strain gauge data[10].

6.4.3 Influence of Flexural Rigidity on Pile Response

It should be noted that the changing flexural rigidity (EI) in a reinforced concrete section subjected to lateral load becomes important when the results from strain gauges are also used to back calculate the pile displacement profile i.e.,

$$y = \iint \left(\int \frac{M}{EI} dz \right) dz$$

[9] For CLT1, the strains on the tension and compression sides of the pile were approximately equal, thus confirming the location of the neutral axis of the section at the centroid of the pile. The nominally higher compressive strain suggests that the axial load was applied at a small eccentricity to the pile axis; this is consistent with previous findings (see chapter 5).

[10] See appendix 6c for details of the analysis.

In such cases, it is necessary to account for the reduction in stiffness that occurs when the concrete cracks. To illustrate the change in flexural rigidity during the test, the strains predicted by the FE analysis were used to establish a relationship between the applied bending moment (M) and the flexural stiffness (EI) of the pile. The pile curvature (ϕ) was calculated as the difference in strain ($\Delta\varepsilon$) between opposite elements (representing the tension and compression steel in the pile) divided by the distance between the elements[11] (L), i.e., $\phi = \Delta\varepsilon/L$. The reducing EI value as the test progresses can then be calculated by dividing the known moment by the curvature i.e., $EI = M/\phi$. The resulting relationship is presented in Figure 6-13 along with the theoretical values for the uncracked flexural rigidity (EI_u) and cracked flexural rigidity (EI_{cr}) (see Appendix 6a). The FE predictions are evidently consistent with these upper and lower bounds.

Figure 6-13 shows that flexural rigidity remains constant up to the cracking moment (M_{cr}), and then decreases sharply as the moment is increased[12]. If the loading were to continue beyond M_{cr}, the pile section would eventually reach a value equal to the fully cracked flexural rigidity (EI_{cr} = 9082kNm^2). However, in this thesis, it was not necessary to consider the changing flexural rigidity of the section as the displacement profiles were measured directly using electro-levels[13]. Nevertheless, the consistency of the electro level results were checked, against the profiles derived from the strain gauges (using Figure 6-13 to select an appropriate EI value), a typical result is shown in Figure 8-1 of chapter 8.

[11] The distance between the elements corresponds to the distance between the ERS gauges on the tension and compression reinforcing bars.
[12] M_{cr} was calculated using the recommendations of the American Concrete Institute (ACI 318-89).
[13] As a check on the strain gauge bending moments, estimates of bending moment were back calculated from the slopes measured by the electro-levels. For these estimates EI values were based on the relationship shown in Figure 6-13.

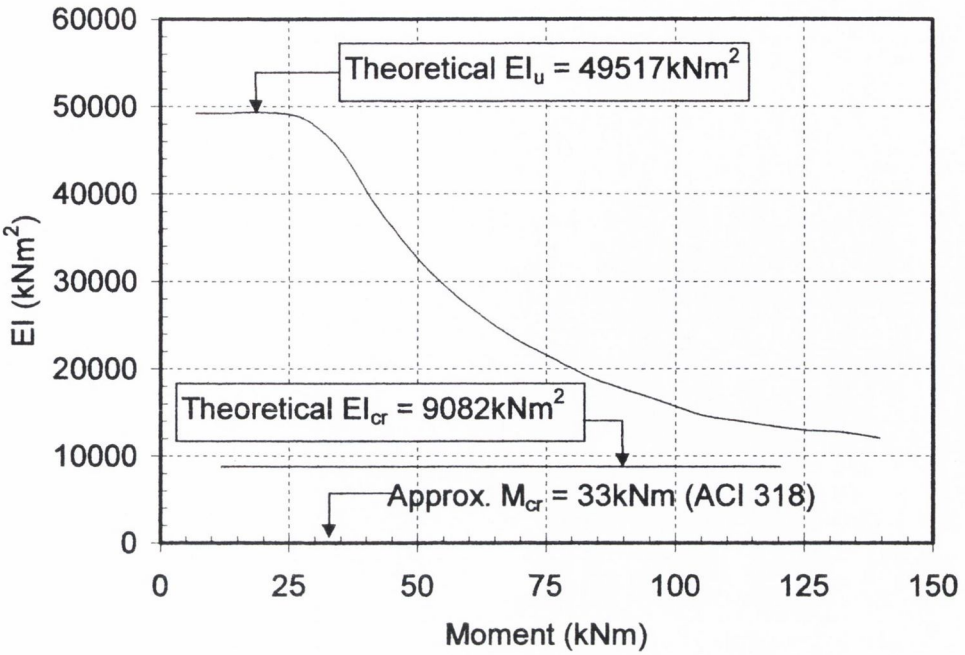

Figure 6-13: Variation in EI with increasing bending moment (as predicted by FEA)

6.5 Monitoring the Kentledge during the Load Tests

The stability of the kentledge over pile AL1 was monitored during both CLT's. A vernier sighting card, with a reading accuracy of ±0.5mm was mounted horizontally on the main test beam (see Plate 6-1). Readings to the sighting card were taken (at one-minute intervals) using a surveyor's level.

For CLT1, pile AL1 supported an axial load of 168kN and a maximum lateral load of 59.75kN. Figure 6-14 shows that the test beam translated 4.5mm in the direction of applied lateral load during CLT1. The incremental movements of the test beam were of the same order as the lateral movements at the head of AL1 (Figure 5-8) and also corresponded with the application of each load increment. This result suggests that frictional resistance developed between the 'rollers' and the beam flange caused the test beam to move in the direction of loading thus ensuring that the axial load applied to the pile remained vertical i.e., there was no significant rotation of the pin joint during CLT1.

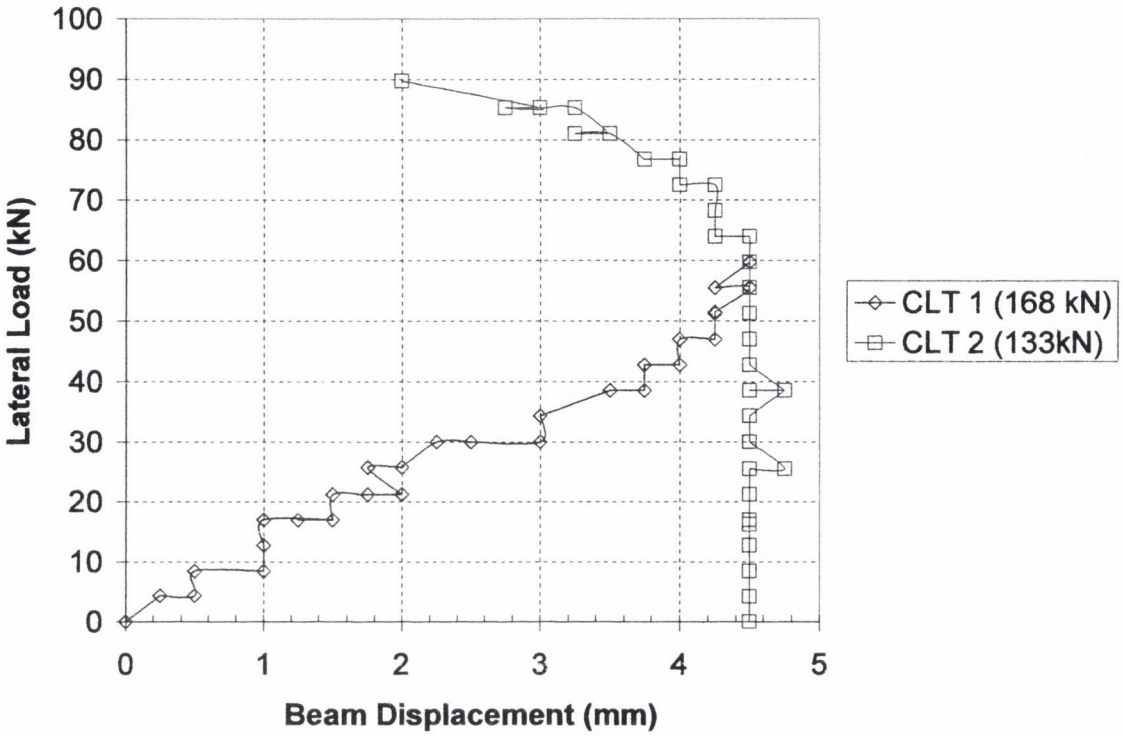

Figure 6-14: Movement of test beam during load tests

The beam movement recorded during CLT2 is also shown on Figure 6-14. With AL1 operating under a reduced axial load of 133kN, no significant movement of the test beam was recorded up to a lateral load of 60kN. Between 60kN and 85kN, the test beam moved ≈2.5mm in a direction opposite to the applied lateral load. This movement is consistent with the initial observation of pin joint rotation but the movement in itself accounts for only 0.12° of the total rotation of ≈4° measured at the joint. The measured strains at the maximum lateral load were well below that necessary for a plastic hinge to form in the pile, it is therefore concluded that yielding of the soil around the pile is the likely reason for the additional rotation. Further evidence of the soil yielding close to ground level is provided in Figure 6-15. The figure shows the change in rotation over the top 1m of pile as the lateral jacking load was increased. The dramatic increase in rotation at jacking loads above 47kN is indicative of yielding soil.

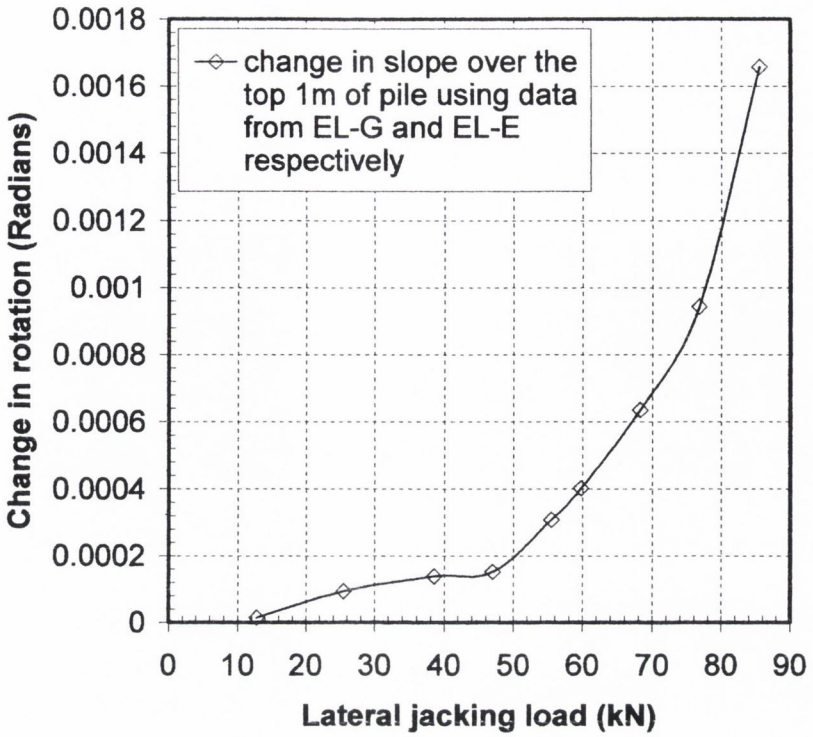

Figure 6-15: Pile rotation over the top metre below ground level

Plate 6-1 shows the pin joint rotation close to the end of the test. Increasing the lateral load above 85.25kN resulted in instability at the pin and this ultimately led to axial unloading of pile AL1. After axial unloading, the pile head displacement that ensued exceeded the travel capability of the displacement transducers and the test was terminated at this point.

This behaviour suggests that above a certain load level, translation of the test beam ceased as pin joint rotation grew in magnitude. At lateral loads above 68kN, rotation at the pin joint became noticeable and as the rotation increased so too did the horizontal component of the axial load created by its increased inclination from the vertical.

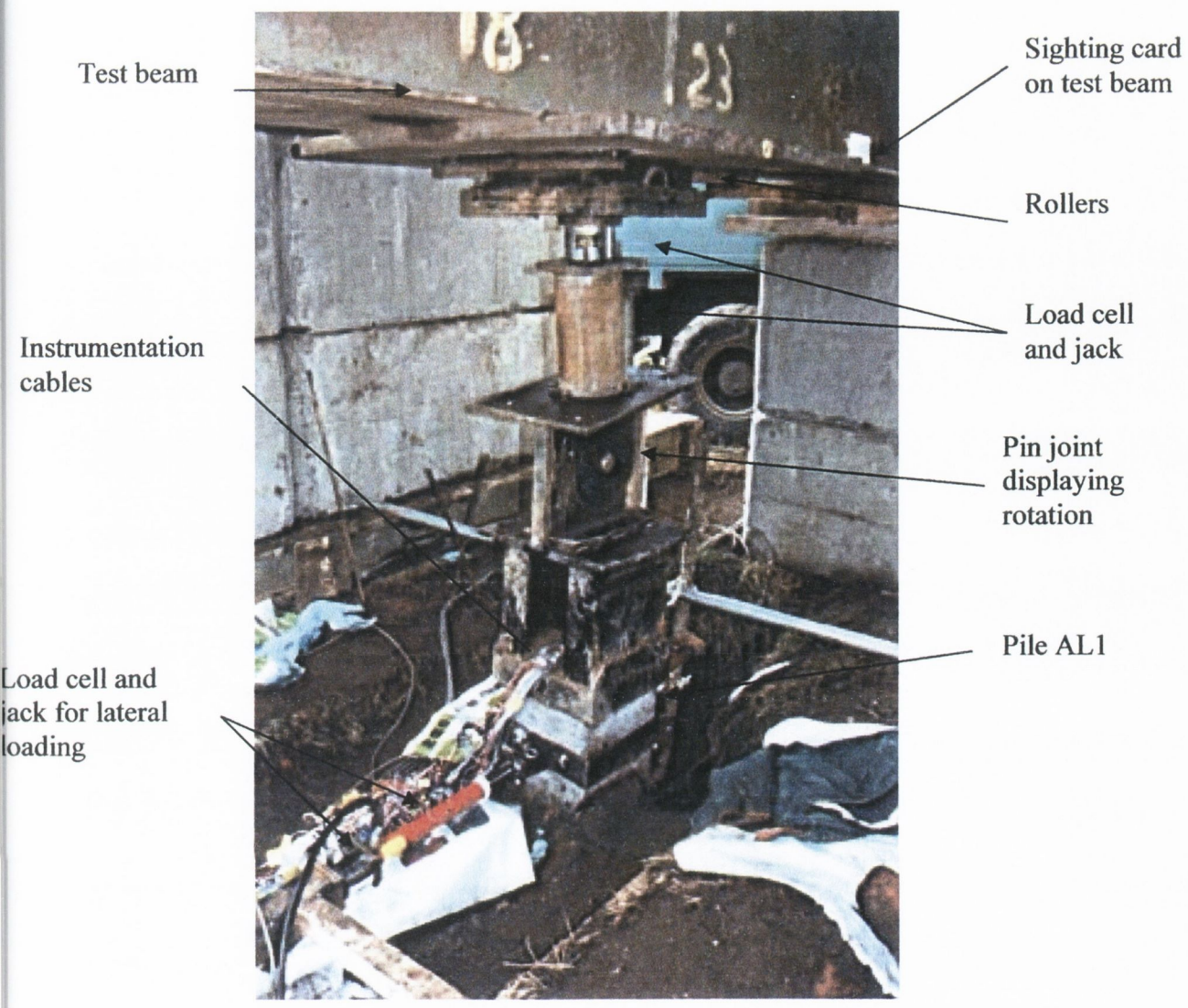

Plate 6-1: Pile AL1 prior to failure

6.6 Moment Profiles for Piles L1 and AL1

6.6.1 Introduction

The bending moment profiles derived from the strain gauge data exhibited the classic profile observed in laterally loaded piles; the initial increase in moment at relatively shallow depth due to the applied load is followed by a dramatic reduction in bending moment brought about by the soil reaction counteracting the moment applied by the lateral load. At approximately 10 pile diameters below ground level the bending moments had

reduced to negligible values thus confirming the critical length of pile is confined to a relatively shallow depth below ground level.

During the tests, equilibrium between the pile and soil was reached for all load levels except the final increment (89.75kN). Moment and displacement values determined for this increment are presented as part of the test results but are deemed unreliable for use in the derivation of the *p-y* response of the soil.

The moment profiles for pile AL1 incorporate the results of the pile head restraint analysis presented in section 6.3 .

6.6.2 CLT1

The measured bending moment profiles for CLT1 are shown in Figure 6-16 and Figure 6-17 for piles L1 and AL1 respectively. Any gauges that did not respond sharply to changes in applied load were ignored in determining these profiles.

PILE L1

The following can be observed from Figure 6-16:

- The depth of the maximum moment recorded by pile L1 did not appear to vary with load increment. The maximum moment occurred at a depth of ≈1.2m below the pit level. Others (including Matlock 1970, Reese and Welch 1975, Briaud et al., 1984) have found that the depth to the maximum moment tends to increase, as the lateral load is incremented upwards. The changing depth to maximum moment was due to yielding in the soil close to ground level and the subsequent transfer of the excess stress to soil at greater depth. These results show that significant yielding of the upper stiff layer did not occur at the loads applied during CLT1.
- It can be seen that the maximum pile moment at a lateral load of 25.75kN is close to the cracking moment M_{cr} (see Figure 6-13).

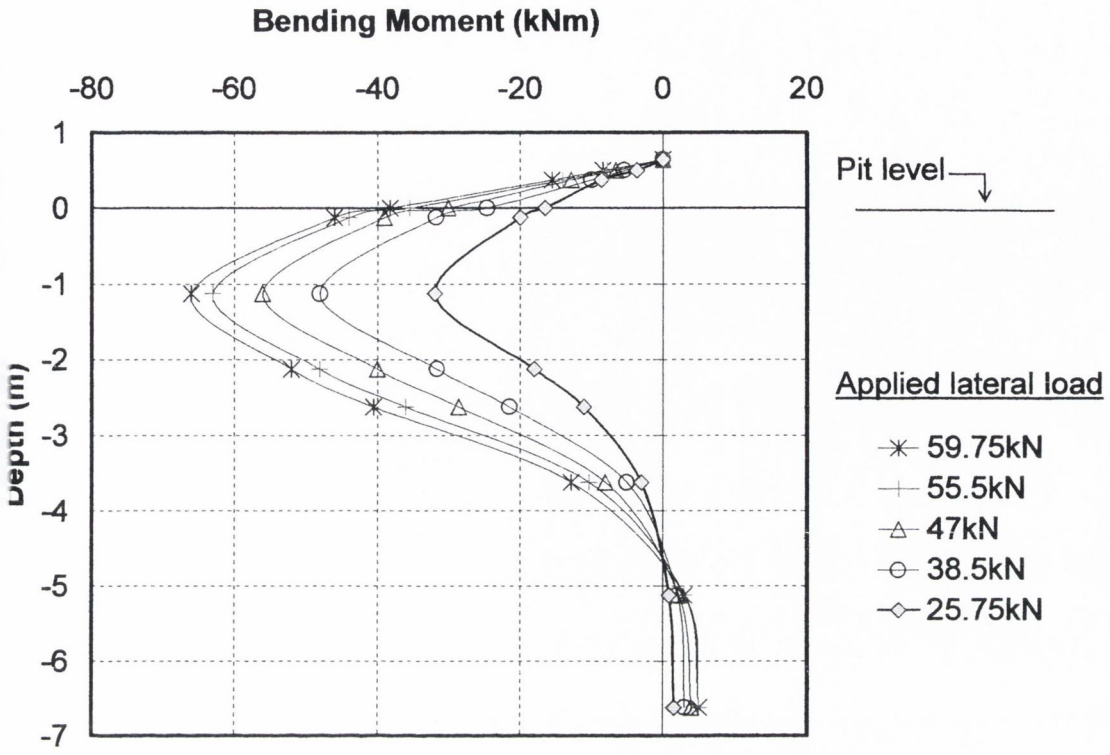

Figure 6-16: Moment profiles for pile L1 during CLT1

PILE AL1

The following observations for pile AL1 are noteworthy (see Figure 6-17):

- The shape of the bending moment diagram for pile AL1 is similar to that for pile L1. However, due to the test setup, pile AL1 was subjected to a restraining moment and a reduced lateral shear force at the pile head (as discussed in section 6.3).

- The overall magnitude of the 'free' bending moment (positive + negative) at the point of maximum moment is slightly less than the maximum moment measured in

L1 at the same load. The difference is due to the smaller shear force applied to pile AL1.

- Much smaller negative bending moments at depth occur compared to L1, presumably because of the application of a restraining moment at the pile head. Moreover, the application of a restraining moment at the pile head results in a re-distribution of the 'free' moment between the pile head and the pile shaft, thus resulting in a more economic use of the pile section.

- The bending moment profiles shown in Figure 6-17 indicate that the increase in bending moment is proportional to the applied load, thus implying that elastic conditions prevail in pile AL1 throughout CLT1.

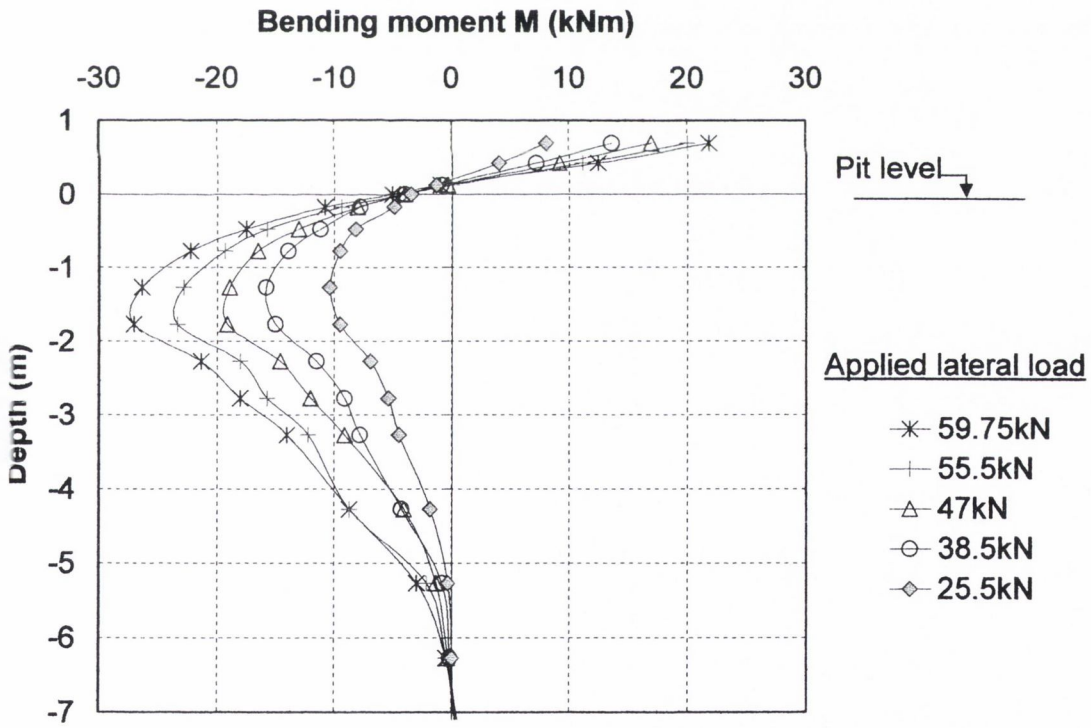

Figure 6-17: Moment profiles for pile AL1 during CLT1

6.6.3 CLT 2

The measured bending moment profiles for CLT2 are shown in Figure 6-18 and Figure 6-19 for piles L1 and AL1 respectively.

PILE L1

The following observations are drawn from the test results for pile L1:

- A comparison of Figure 6-16 and Figure 6-18 indicate that the bending moment profiles for the same load increment during CLT2 are about 6% less than those registered during CLT1. This is probably attributable to the increase in soil stiffness exhibited in the load-displacement re-loading curve (Figure 5-7 chapter 5).

- The bending moments can be seen to increase in direct proportion to the applied loads indicating that significant redistribution of the soil stresses to greater depths did not take place during this test.

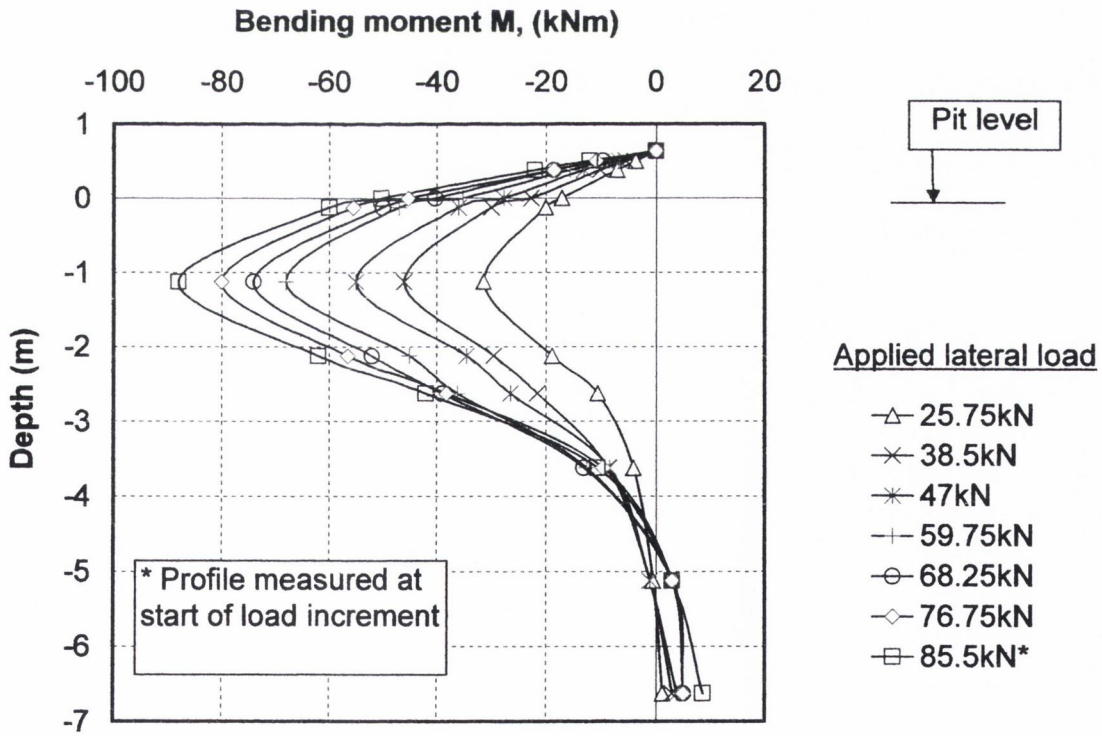

Figure 6-18: Moment profiles for pile L1 during CLT2

PILE AL1

The following can be observed from Figure 6-19:

- The positive bending moments measured at the pile head during CLT2 were, for the reasons discussed in section 6.5 less than those measured during CLT1 at the same load levels. The reduction in axial load may also have contributed to the reduced moment measured at the pile head.

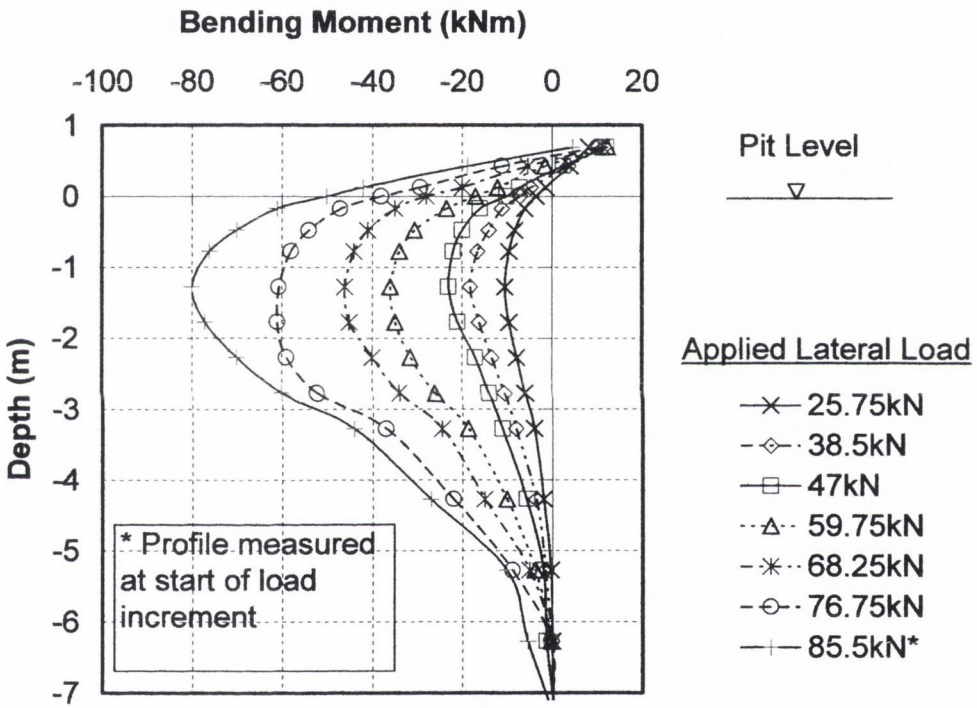

Figure 6-19: Moment profiles for pile AL1 during CLT2

- The magnitude of the positive bending moment at the pile head was negligible towards the end of the load test. The reduction was most likely due to the large rotations that occurred at the pin joint over the final load increments. The pin joint rotation (measuring $\approx 4°$) released the restraining moment and effectively reduced pile AL1 to free head pile subjected to lateral load.

- At the 85.5kN lateral load increment there were signs that pile AL1 was beginning to experience greater stress than pile L1. At the start of the 85.5kN lateral load increment, pile AL1 had to resist a maximum negative moment of 86kNm compared to a value of 80kNm for pile L1. This difference may be due to small variations in soil properties between the two piles but is most likely due to pile AL1 experiencing additional lateral load (due to the horizontal component of the vertical load) just before the pin joint collapsed

- Moreover, there was ≈20% increase in bending moment in pile AL1 over the 5.5-minute period while the lateral load was held constant at 85.5kN (Figure 6-20). This observation is indicative of impending failure at AL1.

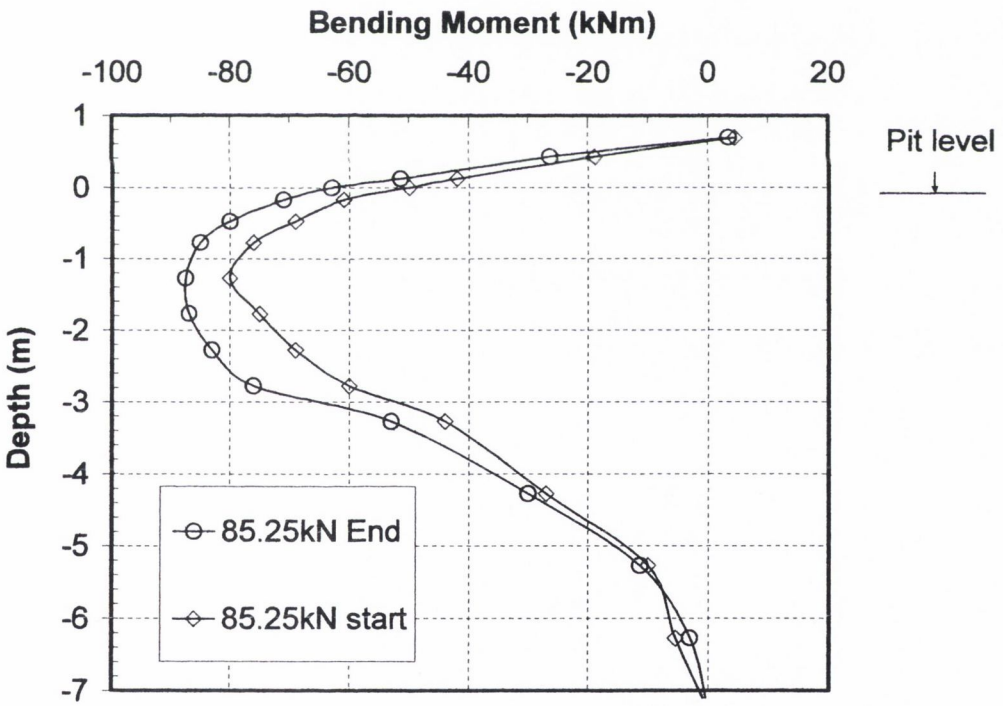

Figure 6-20: Increase in bending moment for AL1 during period of sustained loading at the 85.25kN load increment.

COMPARING THE MOMENT PROFILES FOR L1 AND AL1

Under the maximum applied load, the measured bending moment distributions revealed that each pile was operating below its ultimate moment capacity (see Appendix 6a). A comparison of bending moments from CLT1 and CLT2 shows that pile L1 had to resist a maximum bending moment of ≈65kNm during CLT1 compared to only 27kNm for pile AL1. In contrast, the bending moments induced in AL1 during CLT2 exceeded those of pile L1 at lateral loads above ≈80kN. A combination of soil yield and the reducing pile head restraint (due to creep) at the higher load levels are believed to be responsible for the increased bending moments in pile AL1.

Figure 6-21 illustrates that significant soil creep took place around pile AL1 in the final stages CLT2. The observed creep is consistent with the increase in bending moment within the 85.5kN load increment for pile AL1 (Figure 6-20). The increase in moment can be explained by the growing depth of soil experiencing yield and thus causing the excess load to be transferred to the pile section. From the approximately constant bending moment distributions during each load increment, it is evident that Pile L1 did not exhibit the same tendency to creep as pile AL1.

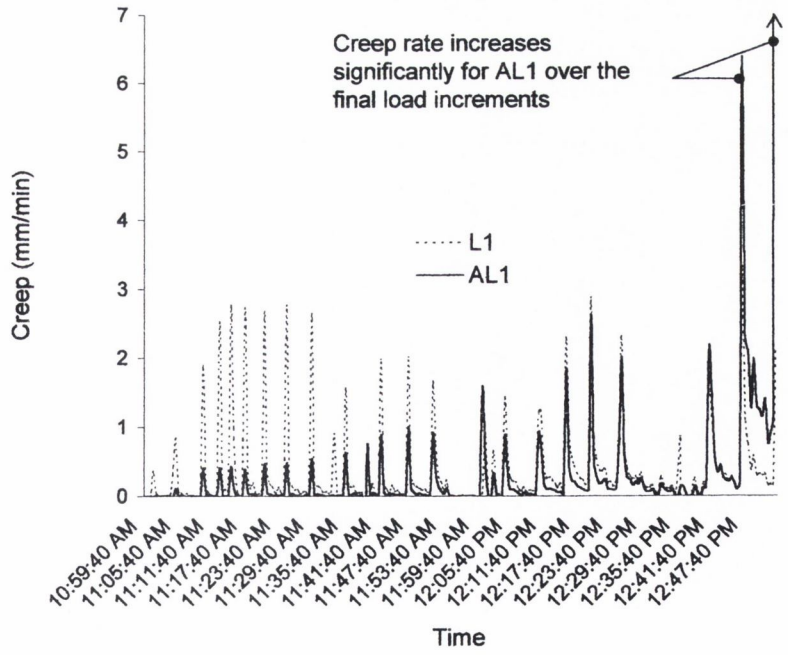

Figure 6-21: Creep rate measured by LVDTs during CLT2

The plots shown in Figure 6-22 indicate that there is no significant rate effects associated with the lateral loading of the piles. The figures indicate that for the different pile head restraint conditions, the overall load-displacement profiles are not affected by the loading rate. On the basis of the pressuremeter curves[14] and the results of laboratory tests on good quality soil samples (presented in chapter 4), it was concluded that undrained conditions prevailed during the load tests. However, the independent load-displacement behaviour shown in Figure 6-22 (a) and (b) may not result for a slow rate of loading (drained conditions) in the same material, since the soil stiffens as the effective stress increases during the application of load.

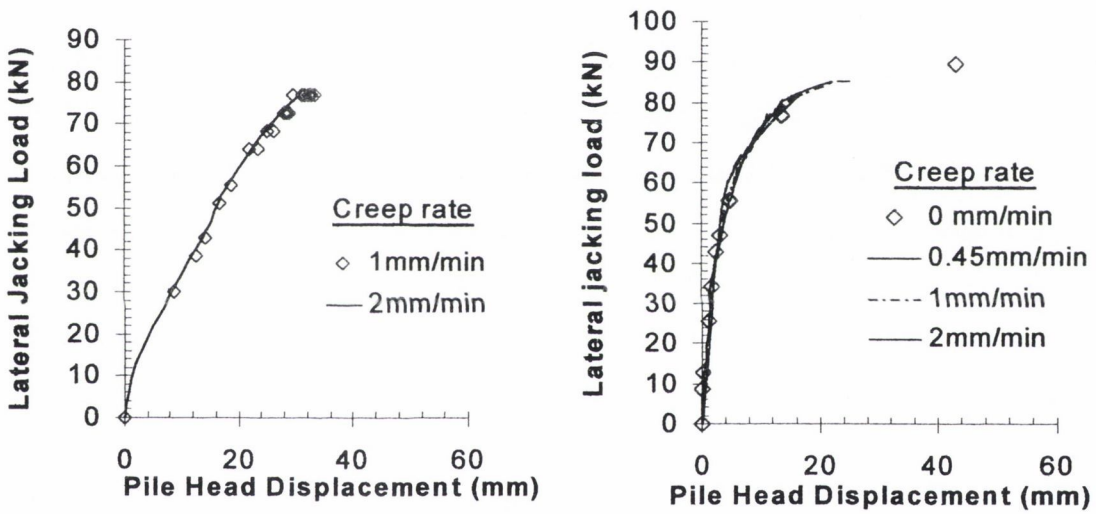

(a) Pile L1 (b) Pile AL1

Figure 6-22: Rate effects for L1 and AL1 during CLT2

6.7 Concluding Comments

In this chapter the quality of the instrumentation data was confirmed and the principal cause of the pile test failure was identified. In regard to the instrumentation, strain gauge data gave values for the Young's modulus of the concrete that were in keeping with those published in the literature, and pile head moments back calculated from the structural

[14] See also Clarke, 1997

model described in section 6.3 were consistent with the moments measured in the vicinity of the pile head.

The test failure was dictated by the behaviour of pile AL1 under combined loads. Towards the end of the test (lateral loads >85.5kN), the horizontal component of the sloped vertical load had become more significant. The combination of this along with the applied lateral load ultimately resulted in the formation of a mechanism at the pin joint. Therefore, the restraint observed at the pile head of AL1 during CLT1, and much of CLT2, was gradually eroded as the pin joint rotated to release the restraining moment. Ultimately, the resultant horizontal load H_R, applied to AL1 was increased above that applied by the jack H, by virtue of the additional horizontal component created by the rotation of the vertical load.

At the 68kN lateral load increment and above, the large displacement recorded at the pile head (Figure 5-8) compared to the previous increments gives a clear indication that CLT2 was approaching failure. Moreover, moment profiles plotted over these increments revealed an increase in bending moment of up to $\approx$ 20% over a 5.5-minute period of sustained loading (Figure 6-20). Thus in the final moments of the test, as efforts were made to increase the lateral load beyond 89.75kN, large lateral movements were recorded at each pile head as the jacking operation attempted to keep pace with the movements. The soil around pile AL1 could no longer provide the resistance necessary to sustain the pile loads and the pin-jointed mechanism collapsed.

It was evident from the measured bending moments that the pile had sufficient bending capacity to resist the applied moments. Therefore, the development of a plastic hinge in the pile is not considered to have contributed to the test failure. Consequently it was concluded that failure was being courted by a combination of instability within the test setup and the soil reaching its ultimate bearing capacity.

Creep measurements recorded at the pile head revealed that there was no significant rate effects recorded during the tests, despite the existence of different pile head restraint conditions at each pile. This result also suggests that undrained soil behaviour prevailed during the tests.

Chapter 7

Interpretation of lateral load tests in stiff glacial till – a Case History

7. INTERPRETATION OF LATERAL LOAD TESTS IN STIFF GLACIAL TILL - A CASE HISTORY

7.1 Introduction

This chapter presents a review and extension of earlier work on laterally loaded driven piles undertaken by the author as part of an M.Sc. dissertation[†] at Trinity College (Phillips, 1995). Detailed interpretation of the test results is presented for the first time in this thesis with supplementary information on the test programme available in Phillips (1995). The research involved two-instrumented steel H-piles driven 2m apart and subsequently loaded (one week later) by jacking the piles apart. The piles were driven 4.5m into a stiff glacial till at a site located in Coolock, 5km north east of Dublin's City Centre. At the time of the tests, a single storey framed structure supported on shallow pad and strip foundations was under construction at the site. A small area, remote from construction activity, was devoted to the lateral load tests. Instrumentation on the piles included inclinometer tubes (to measure the pile deformed shape) and electrical resistance strain gauges (to allow bending moment distributions to be calculated).

The test results include pile head load-displacement plots in addition to moment and displacement profiles. The latter profiles were used to construct *p-y* curves for the glacial till which are subsequently compared with the API recommended *p-y* curves for stiff clay. The interpreted *p-y* curves are also used to deduce conclusions regarding the lateral stiffness of the glacial till found in the greater Dublin area.

[†] The duration of this work was limited to 4 months.

7.2 Site Location and Geology

The stratigraphy comprised stiff glacial till (known locally as Dublin boulder clay [DBC]) which was underlain by relatively intact, homogeneous limestone. DBC was deposited beneath an ice sheet that covered much of Ireland during the Pleistocene period. The grinding action of this sheet as it eroded the underlying carboniferous limestone coupled with its preconsolidation effect resulted in the formation of a very dense or hard, low permeability deposit that contains occasional pockets and lenses of coarse gravel, particularly at depth. DBC is often found at or close to ground level and is typically 10-15 m in thickness. No significant chemical weathering has taken place other than in the top 2-3m of the stratum where oxidation of the iron content has resulted in a change in colour from black to brown (Lehane and Simpson, 2000).

A trial pit excavated near the test area revealed boulder clay beneath approximately 0.2m of granular fill. The water table was encountered at a depth of 1.7m below ground level and the characteristic separation between the brown and black strata occurred at a depth of 1.2m. Undrained shear strengths in the brown clay (measured using a hand vane) were in the order of 100kPa. In contrast, the black clay typically provides triaxial undrained strengths of between 350kPa and 600kPa. Lehane and Simpson (2000) reported the following typical properties for DBC (Table 7-1).

Bulk density (kN/m^3)	21.5 ± 0.5
Global water content (%)	11 ± 3
Liquid limit (%)	25 ± 4
Plastic limit (%)	14 ± 2
Plasticity index (%)	11 ± 2
Liquidity index	-0.2 ± 0.03
Clay fraction (%)	15 ± 5
Gravel fraction (%)	30 ± 5
Permeability (m/s)	1×10^{-11} to 1×10^{-8}
Coefficient of consolidation c_v (m^2/year)	40 ± 20
Preconsolidation stress, σ'_{vy} (MPa)	1.3 ± 0.3
In-situ OCR	8 – 30
λ (reconstituted, intact)	$0.04, 0.03 \pm 0.005$
κ (reconstituted, intact)	$0.008, 0.04 \pm 0.001$

Table 7-1: Typical properties of Dublin black boulder clay (from Lehane and Simpson, 2000).

7.3 Pile Configuration

The steel test piles employed were 203mm x 203mm UC sections having a mass of 46 kg/m. The well-defined physical and geometric properties of these piles meant that bending moments could be interpreted from strain measurements with a good level of accuracy. Both piles were instrumented over their full length of 5m with a total of 20 electrical resistance strain (ERS) gauges applied to the inside flange of each pile. The gauges were located in pairs, one on either side of the web and distributed along the pile shaft with a greater concentration of gauges provided in the region close to ground level. The ERS gauges were protected against damage during driving by metal plates welded to the flange[1]. The displacement profiles for the piles were recorded using an inclinometer torpedo which was passed down inclinometer tubes fixed to the inside flange of piles. Load cells and displacement transducers allowed the applied lateral loads and movements to be recorded at the pile heads.

7.4 Site Works

Pile Installation

A double acting pneumatic hammer was used to drive the piles, the energy from which was controlled by adjusting the air pressure from the compressor so as to minimise potential damage to the instrumentation. The centre lines of the two piles (referred to as pile A and B) were located 2m apart. A steel guide frame assisted in locating and aligning the piles. Considerable driving resistance was experienced at approximately 2m shortly after penetrating the black boulder clay. Pile B was driven with a rake of one percent in both directions. The verticality of Pile A could not, however, be maintained and a deviation of ten percent from the vertical was recorded at right angles to the direction of loading. Fortunately, the guide frame maintained the verticality at one percent in the direction of the applied lateral load. A summary of the events associated with the test programme is provided in Table 7-2.

[1] The metal plates were welded intermittently between the ERS gauges to avoid inducing thermal stresses in the gauges. The entire perimeter of each plate was subsequently sealed to prevent water ingress.

REFERENCE	ABBREVIATION	DATE
Pile installation	PI	July 18 & 19, 1995
Trial Pit Excavation	TP	July 20, 1995
Load Test 1	LT1	July 21, 1995
Load Test 2	LT2	July 26,1998
Cyclic Test 1	CY1	July 27,1995
Cyclic Test 2	CY2	July 28,1995
Load Test 3	LT3	August 1, 1995
Pile Removal	PR	August 4, 1995

Table 7-2: Summary of load testing programme

Testing Arrangement

Lateral loads were applied by jacking the piles apart using a hydraulic jack in series with a steel strut, load cell and loading platens at the strut-flange connections as shown in Plate 7-1. The platens were positioned 0.18m above ground level and the pile heads were free to rotate. The relatively high rake of Pile A normal to the direction of loading made it impossible to keep the webs of both piles collinear with the applied load. Consequently, a stiff transfer girder (Plate 7-1) was employed to impart the lateral loads to Pile A; this girder reacted off two four tonne concrete cubes situated about 4m away from the pile. The girder arrangement resulted in a slightly higher load (≈4%) being applied to pile A during jacking.

Digital readouts from the load cell and displacement transducers (DT's) allowed good on-site control of the tests. The DT's and dial gauges were fixed to reference beams supported on blocks bedded into the ground surface at a minimum distance of 7 pile widths from the test piles.

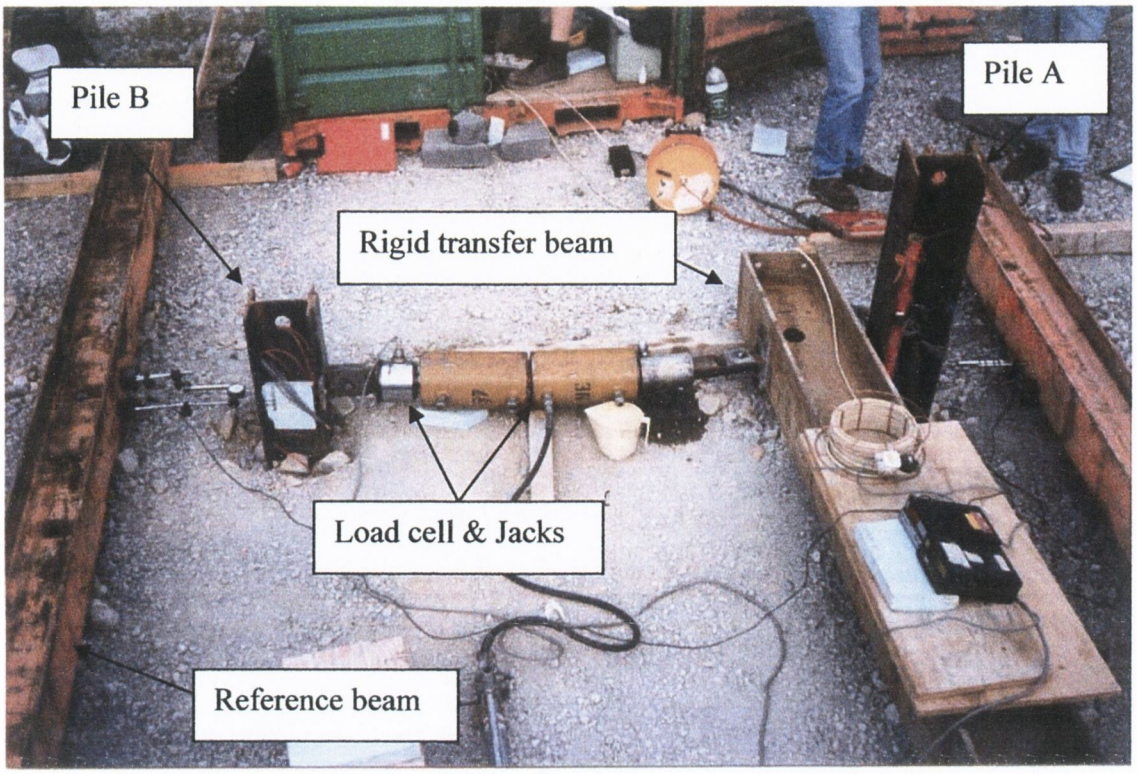

Plate 7-1: Typical load test setup (from Phillips, 1995)

Testing Programme

A total of three static and two cyclic loading tests were performed. Two initial static loading tests (LT1 and LT2) were scheduled to impart lateral loads of approximately one third and two thirds of the estimated lateral pile capacity respectively. The cyclic load tests were then performed within 24 hours of each other, the first test (CY1) consisted of 50 cycles (from zero to 50kN) while the second test (CY2) employed 100 cycles (from zero to 75kN). The third static test (LT3), intended to load the piles to the ultimate condition using a series of large load increments, was carried out three days after CY2. During LT3, excessive twisting of pile B (Plate 7-2) resulted in the termination of the test at a load of 210 kN.

.

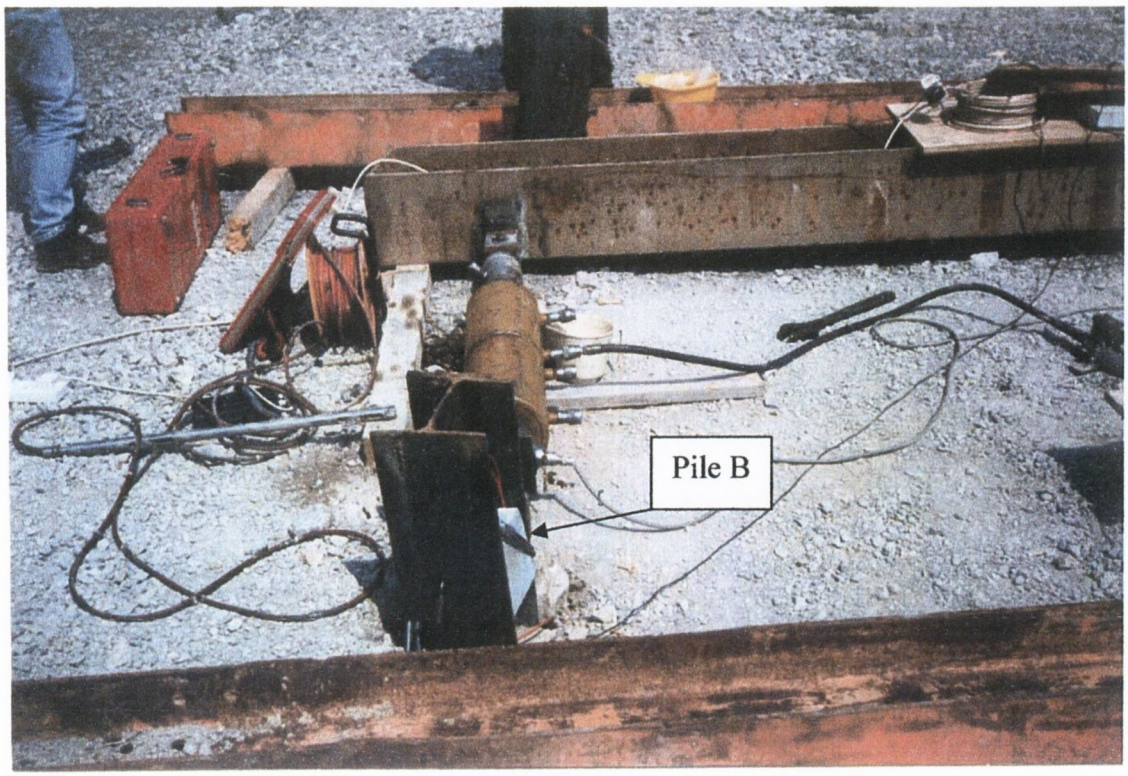

Plate 7-2: Twisting of pile B at a lateral load of 210kN

Test Procedure

Lateral loads were applied to the piles in increments of 10 kN during LT1 and 25kN in LT2. Load increments were held in position for periods ranging from 8 minutes when creep rates were below 0.35mm/min and 12 minutes at creep rates of less than 0.2mm/min. A minimum of two sets of strain gauge readings, one set of inclinometer measurements (involving both readings descending and ascending with the torpedo) and six sets of pile head displacement readings were obtained during each load increment. Records were also taken at the start and completion of each test.

7.5 Results

Overall Load Displacement Behaviour

The variation in the applied lateral load (P) with pile head displacement (δ) measured in LT1 and LT2 are shown for piles A and B in Figure 7-1. As the final static test (LT3) was undertaken after the cyclic tests, the P vs. δ response for this test will be discussed after the

cyclic test results are presented. Some observations from LT1 and LT2 are summarised below.

(i) The lateral load versus pile head displacement curves for LT2 show that the lateral capacity of both piles tends[2] towards a value of 225kN at lateral displacements of approximately 55mm (or ≈ quarter the pile width). This load of 225kN will be referred to as P_{max} in subsequent sections of the chapter.

(ii) The P vs. δ characteristic is non-linear and non-elastic, even at very low levels of load. For example, at an applied load of approximately 44% of P_{max}, the pile recovered only about two thirds of the pile head displacement. This 'permanent strain' is attributed to failure within the soil mass.

(iii) Strain hardening is apparent from the stiffer response shown by reload P vs. δ curves of LT2.

(iv) A comparison of the load–displacement plots in Figure 7-1 shows pile A (despite having a slightly larger load) to be about 15% stiffer than that of pile B in LT1 and LT2. Natural variability in the ground stiffness adjacent to each pile is believed to be the primary reason for this difference.

(v) From field observations the depth of post-holing[3] that developed during the tests were estimated to be in the order of 500mm to 700mm.

---

[2] This tendency can be clearly seen in Figure 7-11 for pile A once the residual displacements at the end of each load test have been incorporated into the load displacement behaviour.
[3] The formation of a gap or 'post-hole' around the pile.

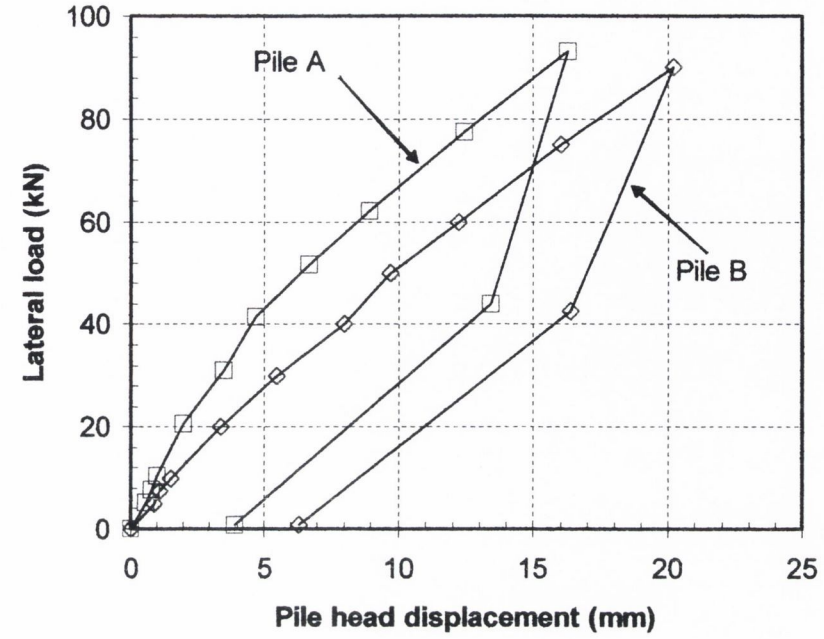

(a) LT1

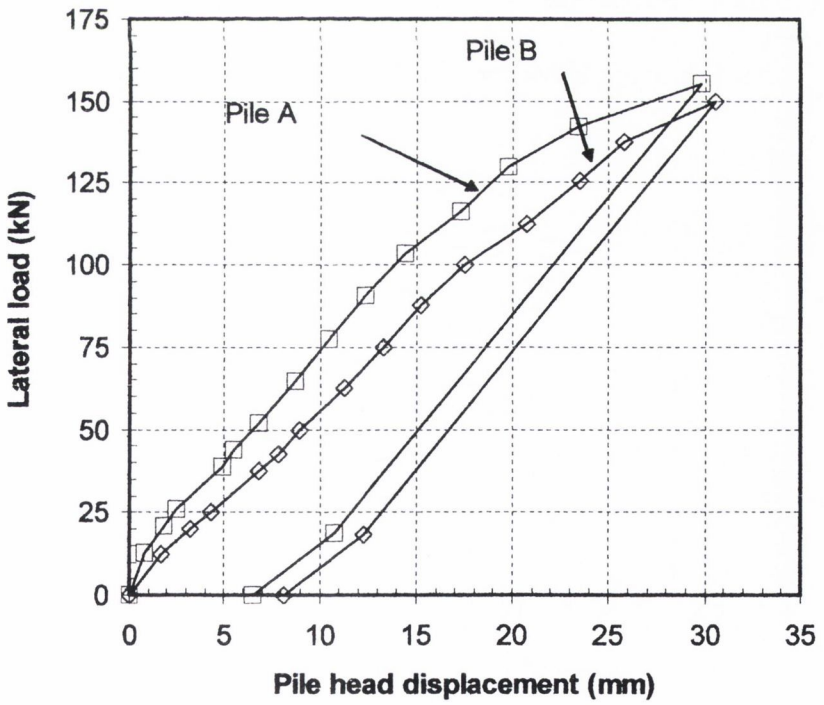

(b) LT2

Figure 7-1: Lateral load versus pile head displacement for LT1 and LT 2.

Displacement Profiles

The displacement profiles were obtained from the inclinometer measurements and the displacements recorded at the pile head; results for pile B during LT2 are shown in Figure 7-2. The displacement profile for each load increment was drawn by subtracting the torpedo displacement per gauge length, initially from the displacement at the pile head, and subsequently from each preceding profile position as the torpedo moves along the pile shaft. It is evident from the resulting profiles that lateral displacements generally reduce to less than 20% of the maximum value at a depth of 2m (or 10 times the pile width). Figure 7-2 also shows that the piles reached virtual fixity at a depth of 2.7m. It can therefore be concluded that the piles were acting as 'long' flexible members with their maximum lateral load capacity controlled solely by the ultimate moment of resistance of the pile section.

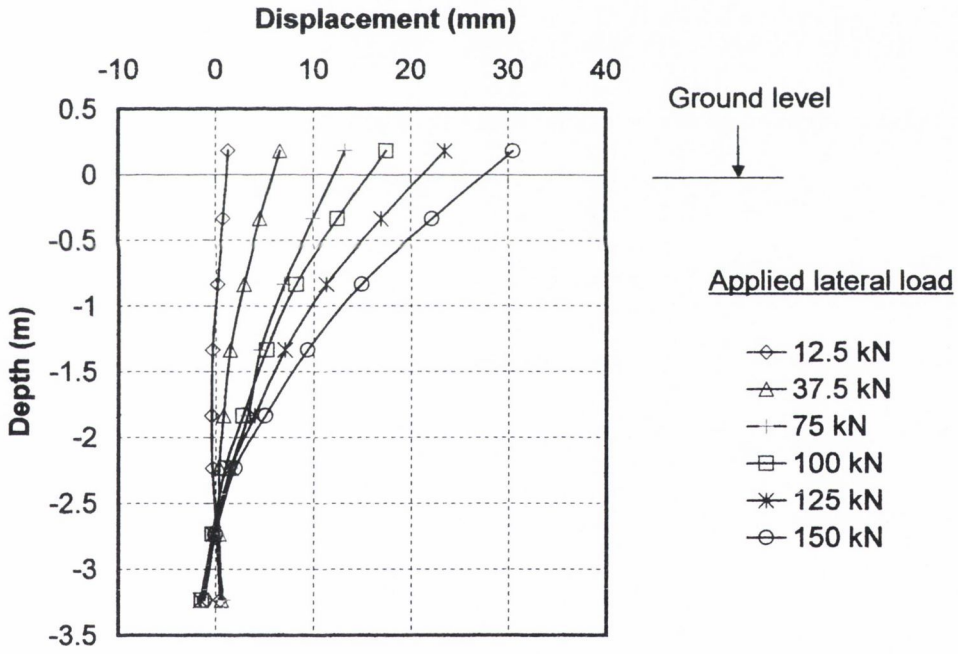

Figure 7-2: Displacement profiles measured by inclinometer for LT2, Pile B

As a result of exhuming the piles after LT3, it was discovered that the inclinometer tube attached to pile A had been severed 1.0m below ground level, presumably in response to the friction forces imposed on it during driving. This finding explains the poor quality inclinometer data obtained from pile A. Furthermore the displacement profiles measured for pile B during LT3 indicated that the accuracy of the inclinometer data was questionable.

Therefore, to supplement the limited displacement profiles obtained from the inclinometer readings (especially for pile A) it was decided to compare the displacement profiles of Figure 7-2 with those obtained from double integration of the measured bending moment distributions at the same load levels. The results for three of the load increments are shown in Figure 7-3.

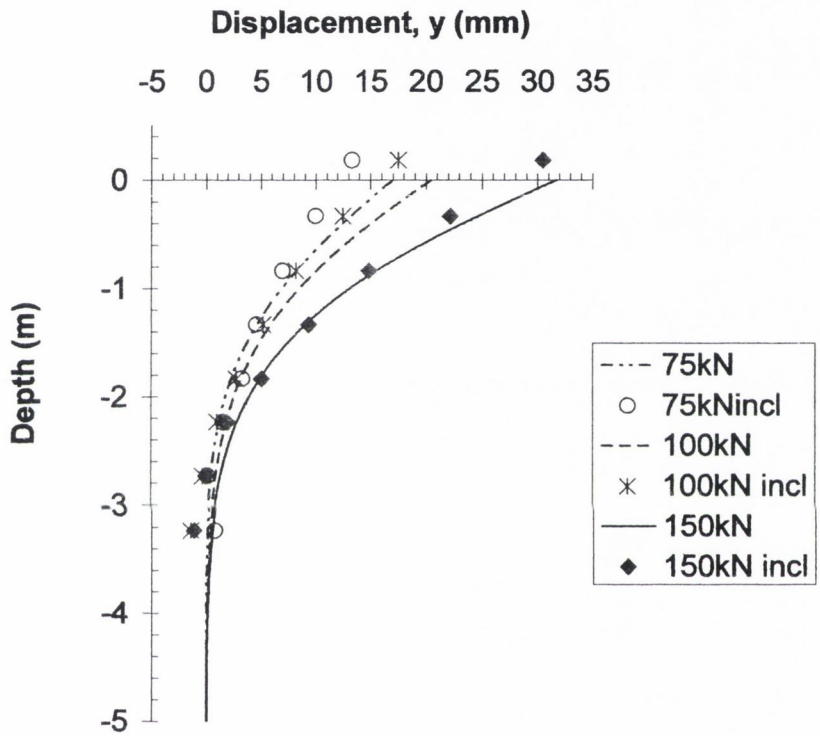

Figure 7-3: Comparison of displacement profiles obtained by direct measurement and indirectly by double integration of the bending moment distributions

At depths greater than 1m the measured and predicted displacements are in good agreement although the profiles indicate that the fit may be in error (attributed to the curve fitting procedure coupled with small errors in the strain data) by up to 24% at ground level for the 75kN load but this error reduces to less than 10% at the higher load level. Moreover, pile head displacements measured in LT3 (see Figure 7-16b) show a marked improvement in the quality of fit at ground level. It was therefore decided to adopt the double integration method to yield the displacement profiles for each test. The consistency

of the resulting profiles in addition to the known pile head displacements were used as a check on the accuracy of the method.

Bending Moment Profile

After pile installation, 70% of the 40 strain gauges remained operable; most of the gauges that malfunctioned were located at depth on pile B. The success of the instrumentation was considered reasonable, in light of the extremely hard driving conditions encountered on site. Figure 7-4 shows a series of strain vs. time records for pairs of gauges located as described previously; the records are positioned in the order in which they were located on the pile (shown schematically adjacent). The quality of the data produced was good; the consistent response between adjacent gauges over the depth of the pile is evident. Moreover, strain gauges located at ground level, where the free moment was known, gave bending moments within 5% of the theoretical value[4]. The bending moment profiles for a series of load increments in LT1 and LT2 are presented in Figure 7-5 to Figure 7-8. These were derived using elastic beam theory[5] and reveal the classic rapid increase in pile moment, with a maximum value close to ground level followed by a rapid reduction to negligible values at 3m. This trend arises because of the transition from the initial dominant effect of the moment induced by the applied load to the situation when the soil resistance becomes significant enough to outweigh this applied moment. The maximum moment (measured in pile A) at an applied load of 157kN (or 70% of P_{max}) was 80% of the calculated ultimate moment capacity of the pile.

[4] The piles were also subjected to cantilever loading in the laboratory prior to the site works. These calibration exercises confirmed the accuracy of the ERS gauges by showing that their strain outputs were consistent with the calculated second moment of area of the pile section and the applied bending moment.

[5] As strains measured up to lateral loads of 190kN were elastic, the pile bending moments (M) were derived from the equation $M = \varepsilon EI/y$ where ε is the average strain measured by adjacent gauges, EI is the flexural rigidity of the pile and y is the distance from the neutral axis to the gauge location.

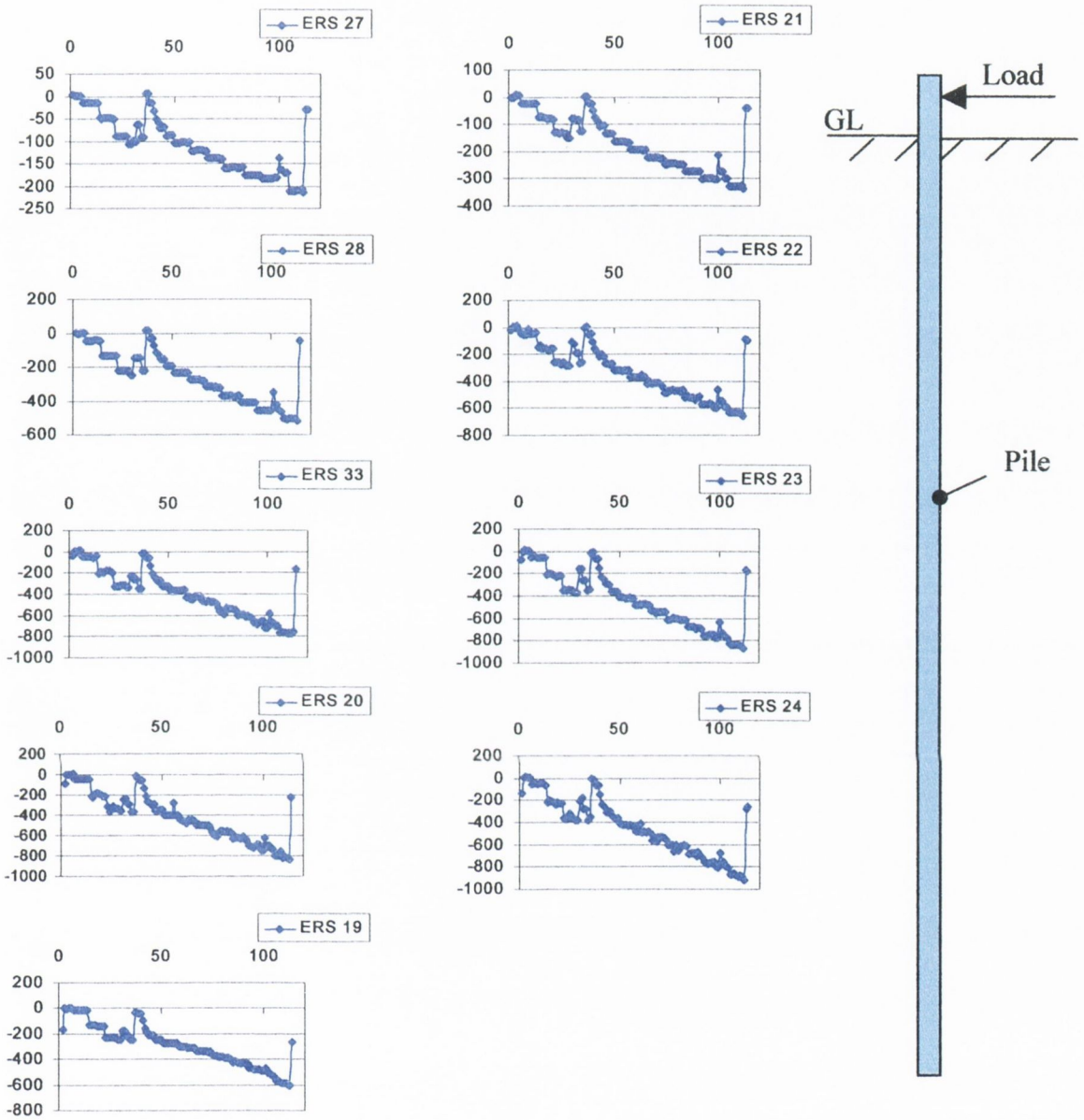

Figure 7-4: Strain (vertical axis) in με Vs Time (Horizontal Axis) plots for ERS gauges positioned along pile B (LT2)

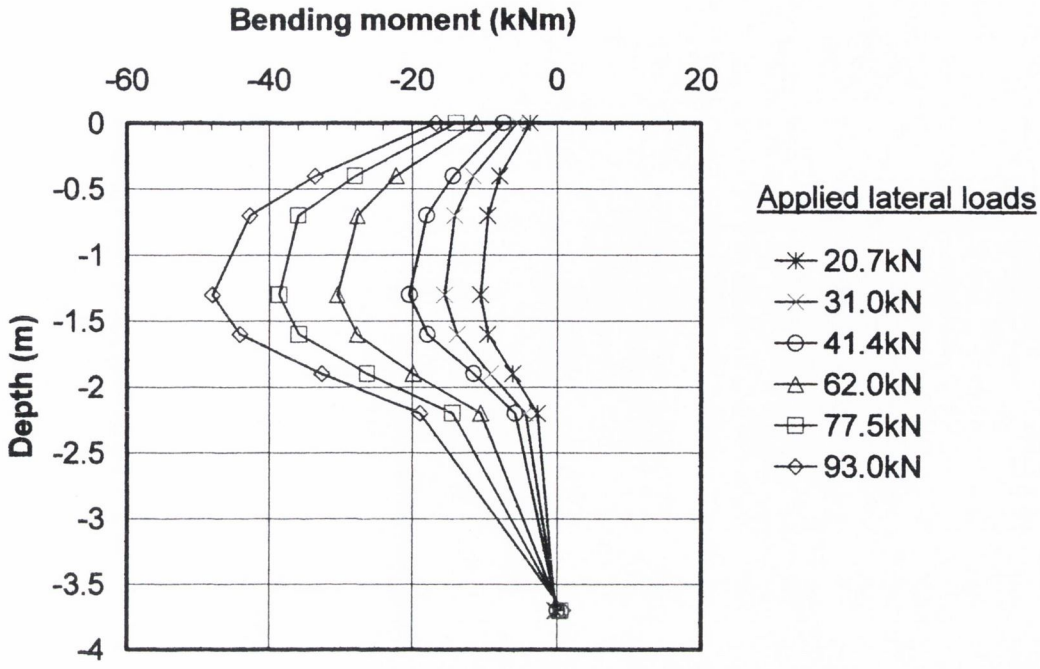

Figure 7-5: Bending moment profiles for pile A, LT1

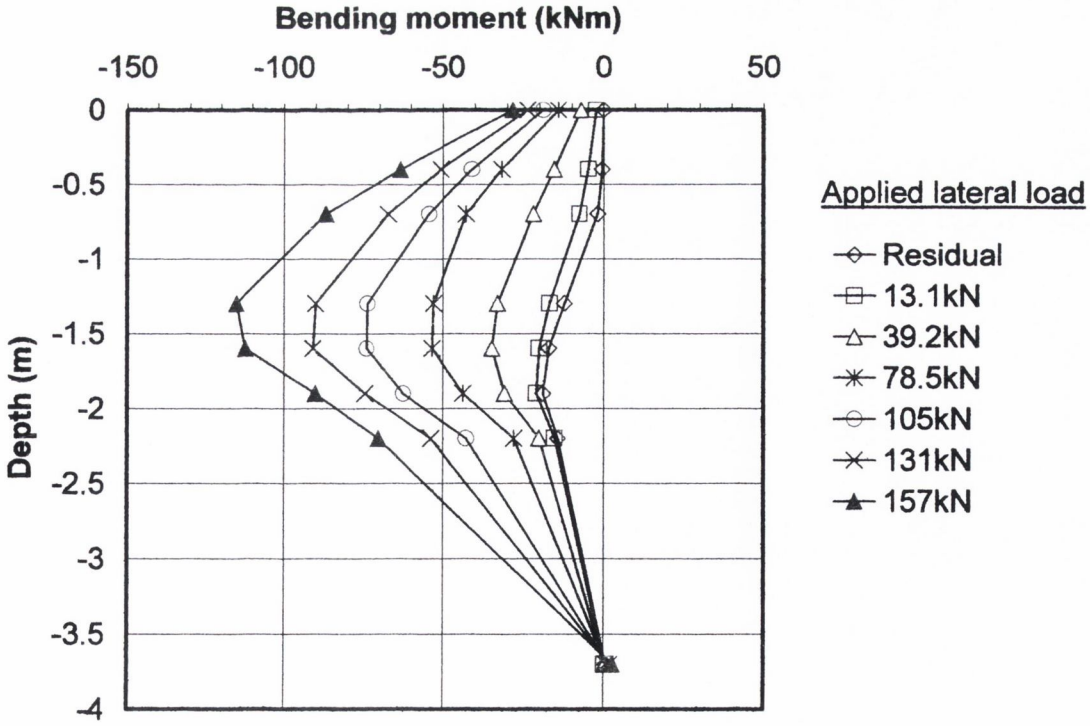

Figure 7-6: Bending moment profiles for pile A, LT2

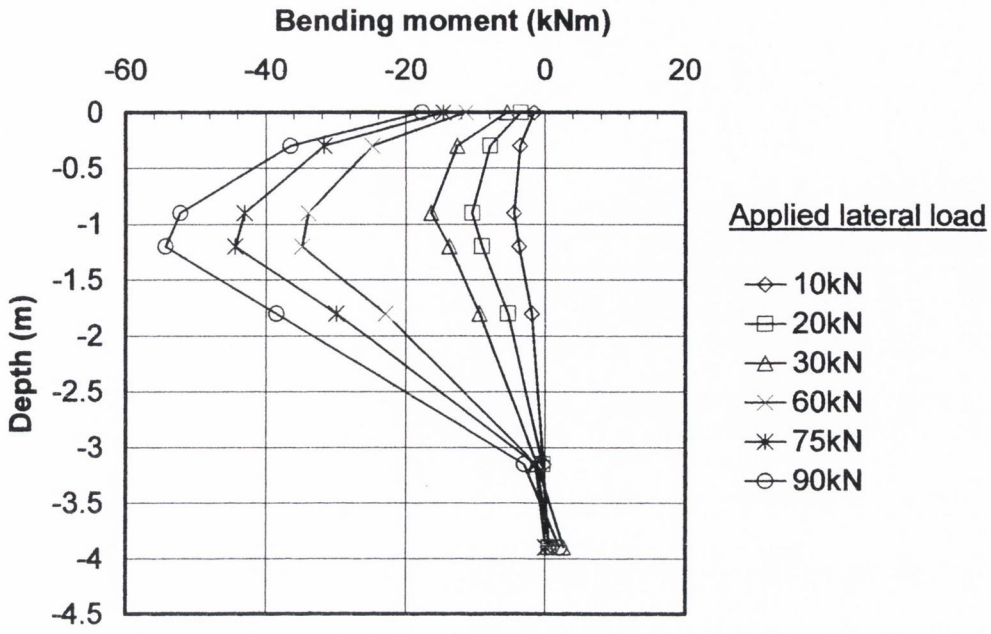

Figure 7-7: Bending moment profiles for pile B, LT1

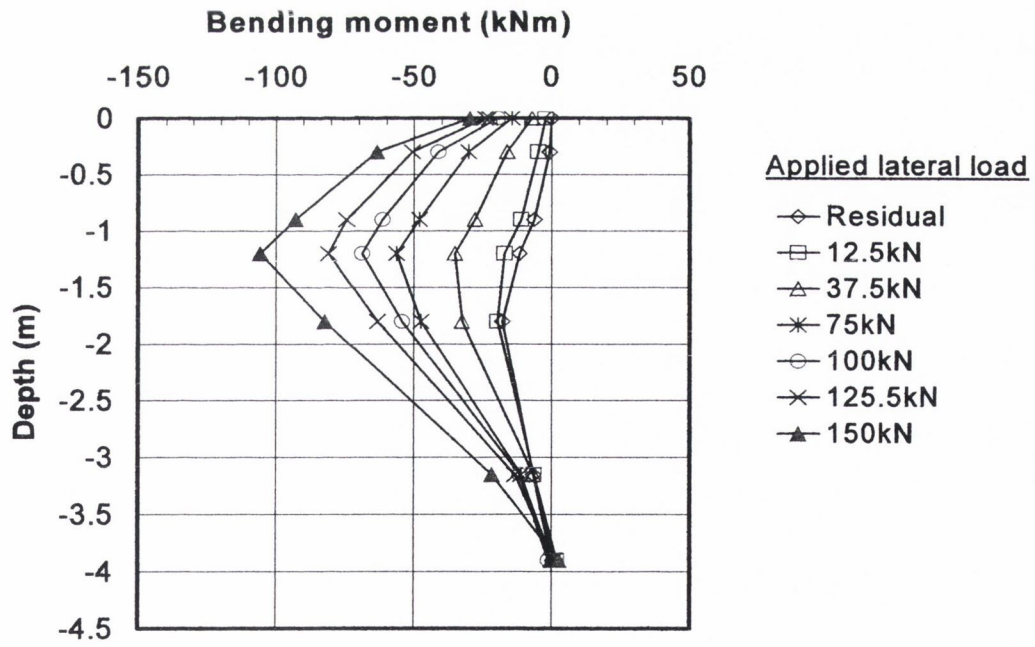

Figure 7-8: Bending moment profiles for pile B, LT2

Cyclic Loading (CY)

The cyclic testing was restricted to load and pile head displacement measurements at each pile. The purpose of these tests was to ascertain if significant degradation of the soil resistance resulted from the cyclic loading. The CY tests involved the application of 50kN and 75kN loads (equivalent to 23% and 35% of P_{max} respectively). The loading period per cycle lasted about one minute (to permit the reading of the dial gauges). Figure 7-9 illustrates that some fluctuation in the pile head displacement under the constant cyclic load occurred during the tests. Furthermore, the results indicate that the effects of the cyclic loading were more prevalent for pile A which exhibited an overall pile head displacement increase of 3.7mm after a hundred cycles of 75kN (CY2) compared to 1.5mm for pile B. A similar trend was also observed during CY1.

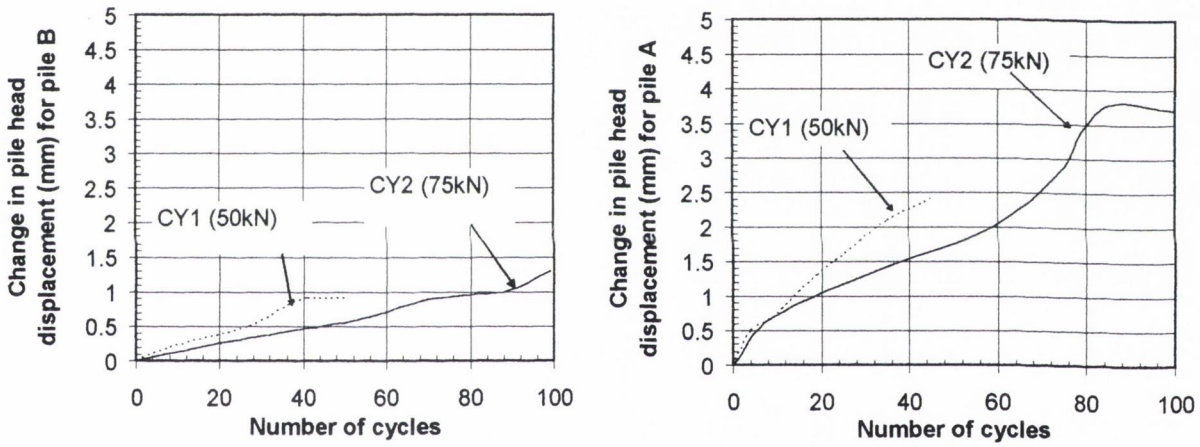

(a) Pile B (b) Pile A

Figure 7-9: Pile head movement during cyclic load tests

Load Test 3 (LT3)

Figure 7-10 illustrates the pile head load-displacement results for LT3. Note that LT3 started with an initial lateral load of 23.5kN. This was due to the insertion of steel packer pieces during LT2 to increase the stroke of the jack for the higher load increments. When the piles were unloaded at the end of LT2 the packing pieces remained in position thus preventing full recovery of the piles. The initial strain hardening behaviour of LT2 was not observed in LT3, notably, pile A now exhibited a less stiff response than pile B. This is consistent with the larger pile head displacement measured for pile A during the cyclic load

tests. Pile B also exhibited a less stiff response in LT3 compared to that measured during LT2. The reduced stiffness observed in each pile may have resulted from the CY tests but overall these tests are not considered to have appreciably affected the soil resistance. Only final recovery readings were obtained for LT 3 due to the sudden rotation of pile B. To illustrate the overall pile head displacement and the consistency of the projected ultimate capacity, the load–displacement response for pile A over the entire suite of tests is shown in Figure 7-11.

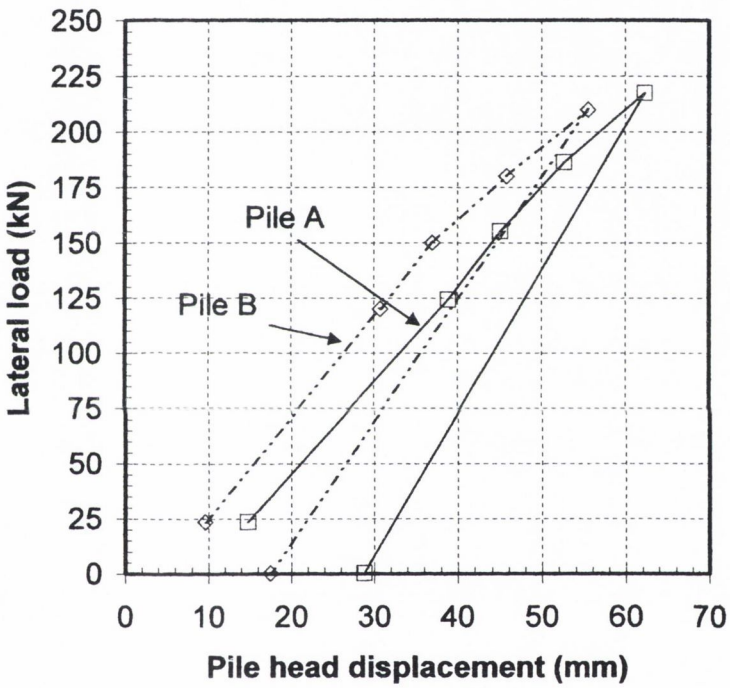

Figure 7-10: LT3 performed three days after two cyclic load tests.

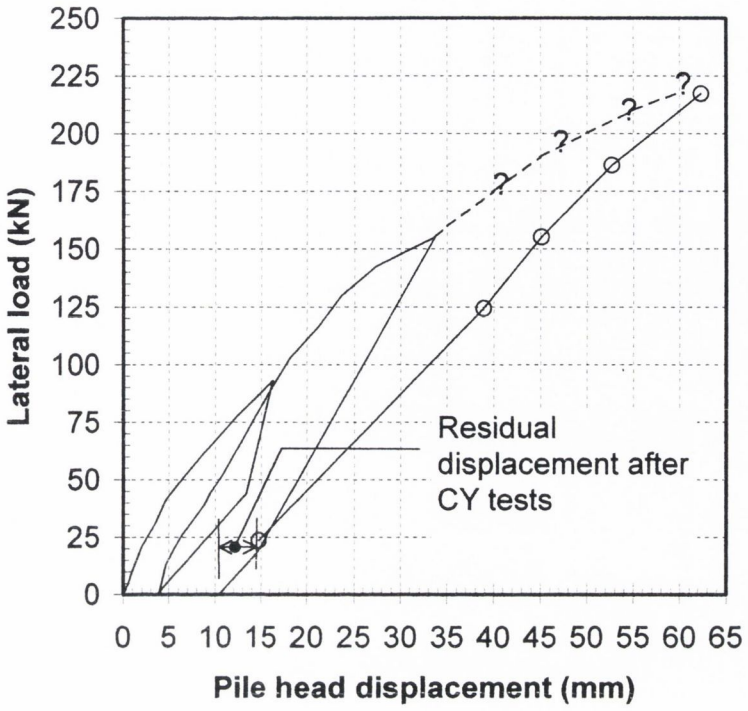

Figure 7-11: Cumulative test displacements for pile A

The bending moment profiles for piles A and B are shown in Figure 7-12 and Figure 7-13 respectively and account for the residual strains measured at the end of the CY tests. Strain gauge data was recorded in pile B up to a maximum lateral load of 180kN; under this load pile B registered a maximum bending moment of 123kNm, (85% of the pile section capacity, M_{cap}). It is estimated that the moment in pile B probably approached the section capacity as the lateral load reached 217kN. Pile A, despite being subjected to a slightly higher lateral load (188kN) only registered a maximum moment of 109kNm; this is in keeping with its less stiff response observed following the CY tests.

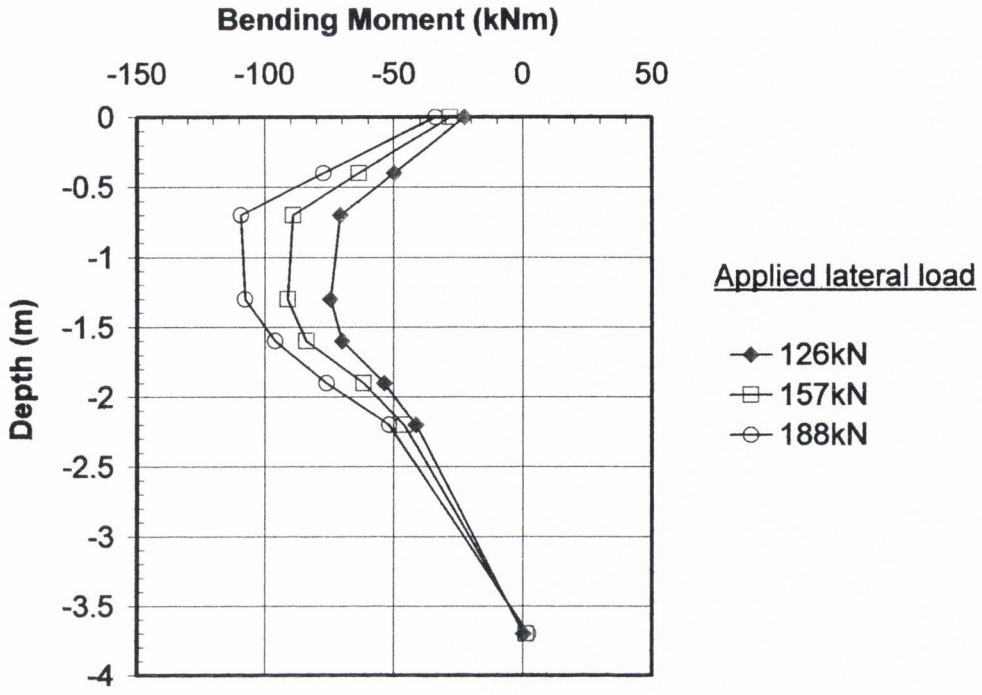

Figure 7-12: Bending moment profiles for pile A, LT3

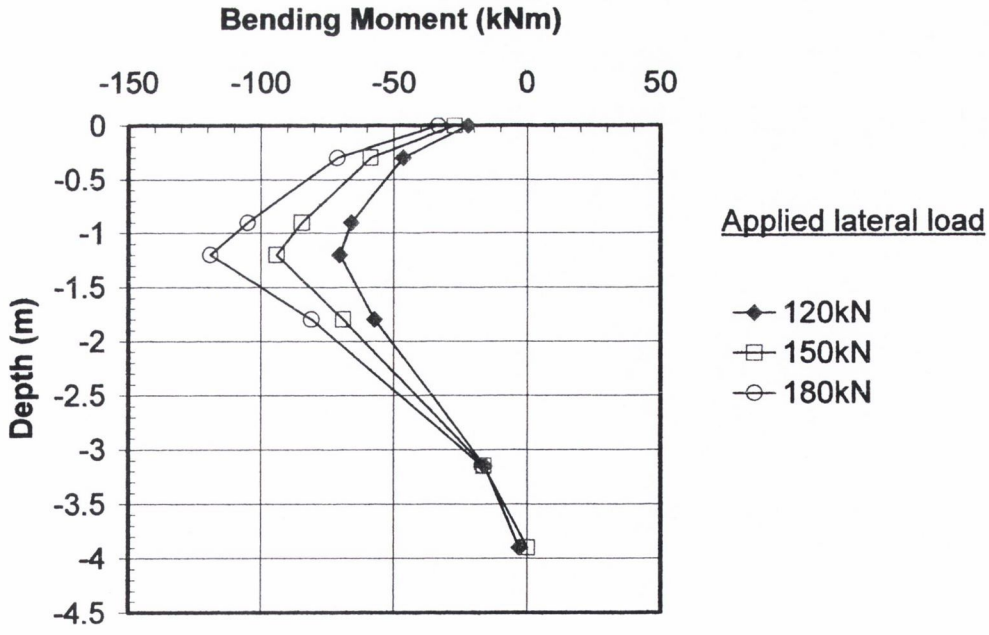

Figure 7-13: Bending moment profiles for pile B, LT3

7.6 Analysis of Results

Derivation of *p-y* Curves

The measured displacement and bending moment profiles from each pile were used to derive *p-y* curves for Dublin boulder clay. The curve fitting procedure employed for the Belfast tests (described in detail in the next chapter) was adopted to obtain an equation describing the measured pile bending moments; the fit quality was assessed by the measured r^2 value which consistently gave results above 0.95 for pile B and 0.85 for pile A. The resulting equation was differentiated twice to provide the soil reaction, p in units of force/length. Typical results from the curve fitting exercise are shown in Figure 7-14(a).

Because of the difficulties encountered with the inclinometer data, the displacement profiles were obtained by double integration of the best-fit moment equation, yielding the results shown in Figure 7-14(b). The derived displacement profiles result in a slight under prediction of the displacement at the pile head but overall the predictions are consistent with the values measured in the field and observations during pile exhumation.

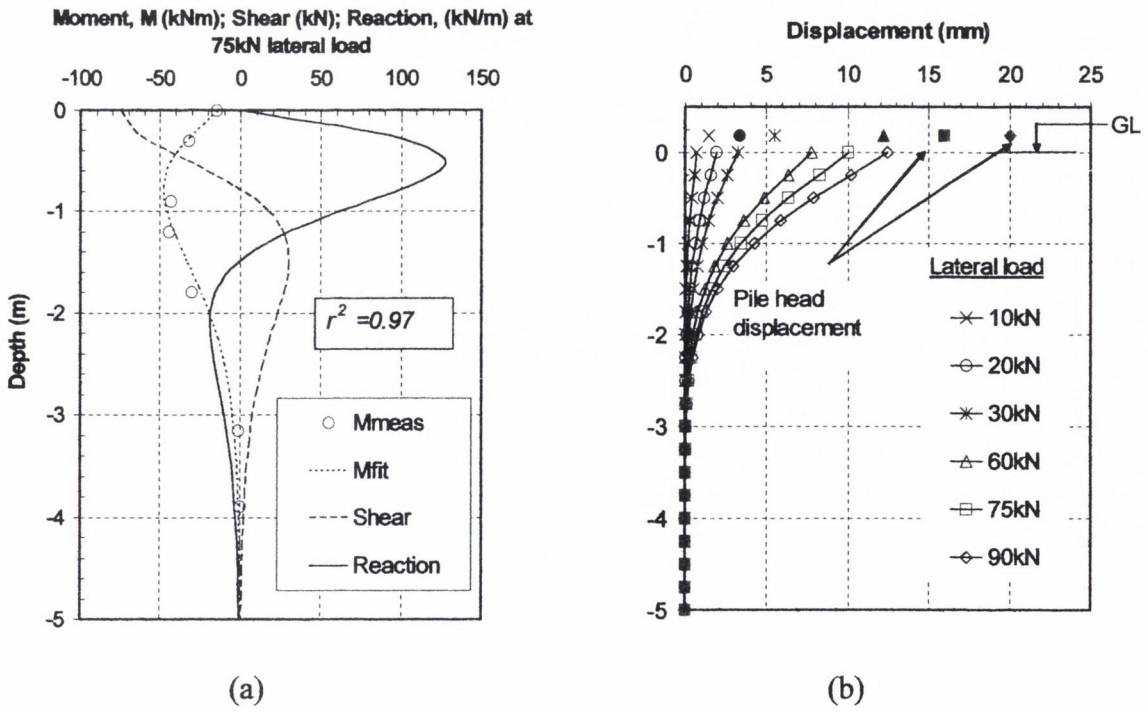

Figure 7-14: Typical curve fitting results for pile B at 75kN during LT1

The resulting p and y values at discrete depths along the pile were then combined over a series of load increments to provide p-y curves. Meaningful p-y curves could only be obtained to a depth of 1.5 m below ground level. Below this level the soil resistance underwent a sign change and the displacements were very small. Dunnavant and O'Neill (1989) have reported similar difficulty in accurately measuring displacements at depth for lateral pile tests in stiff clay.

Review of Measured p-y Curves from Static Load Tests

p-y curves, normalised by the pile width, are shown in Figure 7-15 (the resulting curves represent a plot of soil pressure against the normalised displacement, which gives an indication of the strain in the soil at the applied loads). The p-y curves up to 1.0m characterise the response of the brown boulder clay. The p-y stiffness increases up to $\approx$ 1m and no evidence of soil yield was apparent at the induced displacements. These curves suggest that the undrained strength of the soil mass is stronger than indicated by the in-situ 'hand' vane tests.

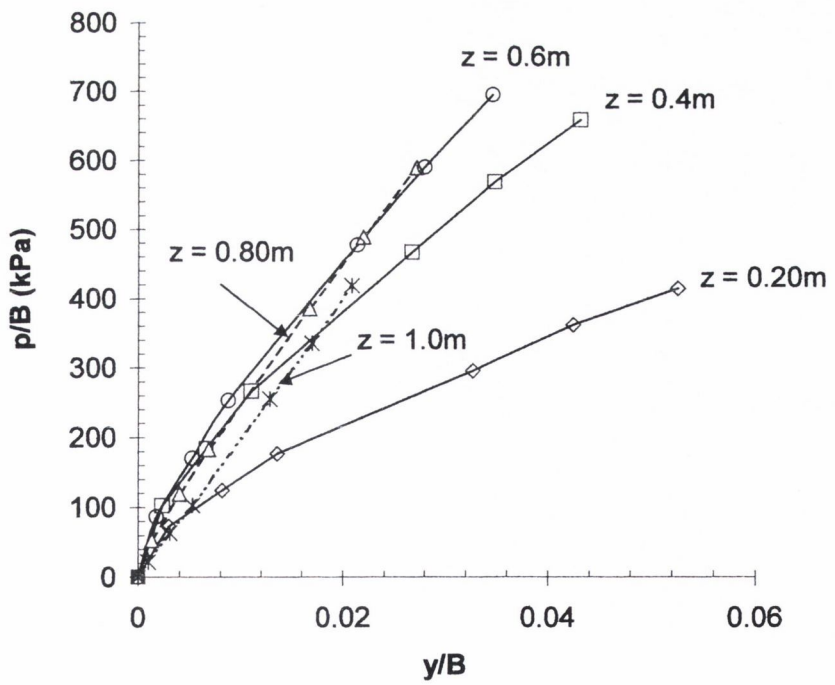

Figure 7-15: p-y curves for Dublin boulder clay derived from LT1

Typical results for static LT3 are shown in Figure 7-16. The agreement between the pile head movement and the displacement profiles obtained from the strain gauge data is evident and represents an improvement on the results presented for LT1 in Figure 7-14(b). The displacements at the pile head shown in Figure 7-16(b) are the displacements measured during LT3 and therefore do not include the residual displacement at the end of the previous test. The implication of this can be seen in the 'perceived' increase in the stiffness of the *p-y* curves for LT3 (Figure 7-17).

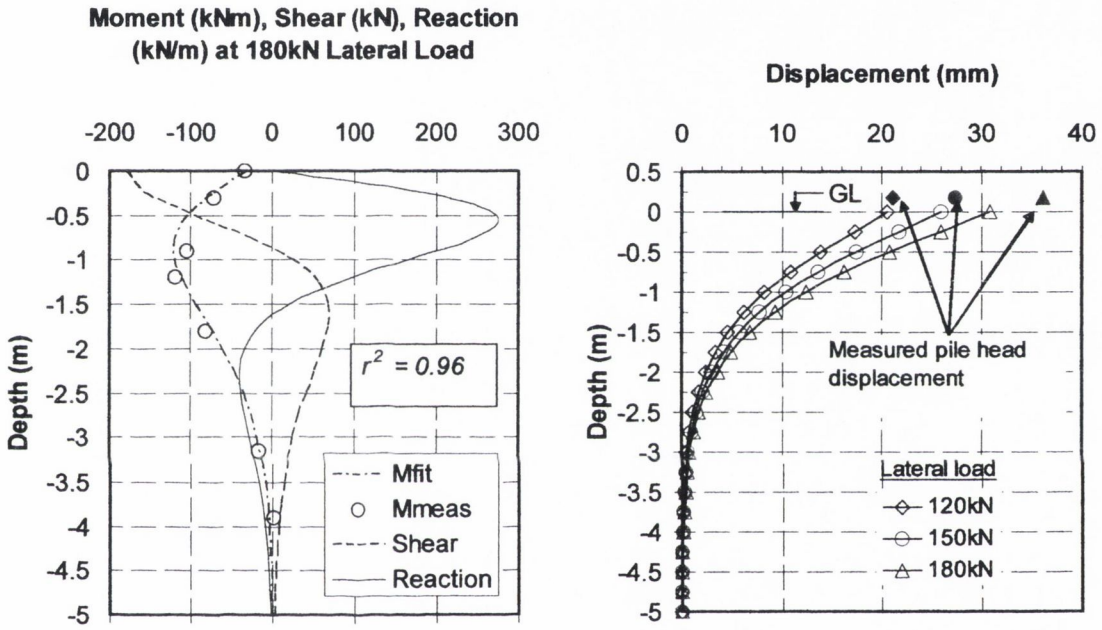

(a) Curve fitting results

(b) Displacement profiles

Figure 7-16: Typical test results for bending moments and displacements in LT3 for pile B

Normalised *p-y* curves for the three static load tests are shown in Figure 7-17. The figure indicates that a less stiff *p-y* response was measured in LT2, which was carried out within 16 hours of LT1. In LT3, the initial load increment was 120kN and therefore the *p-y* response up to this load level could not be assessed. However, as the higher loads extend the soil "pressure bulb" into previously un-stressed soil, there was no evidence of the reduced stiffness observed in LT2. Normally, a less stiff *p-y* response would be expected following the application of cyclic loads. However, on this occasion the cyclic loads represented a relatively low level of soil stress (35% of P_{max}) well below the yield strength of the soil. The test data therefore indicate that appreciable cyclic degradation of the soil

strength (as reported by Reese and Welch, 1975 and Dunnavant and O'Neill, 1984 for stiff clays) had not occurred at the pile head displacements induced by the CY tests. This result may be due to:

- The pile head movement apparently did not exceed a so-called 'threshold displacement' (Dunnavant and O'Neill, 1989) necessary before significant degradation of the soil resistance due to cyclic loading could occur.
- The approximately constant depth to the maximum pile moment observed in the pile tests is a further indication that a significant proportion of the soil within the critical depth was in a pre-yield condition. Significant yielding of the soil is characterised by the formation of a gap or 'post-hole' around the pile. As the post-hole depth increases, the applied load is transferred to the soil at greater depth thus causing a corresponding shift downwards in the location of the maximum moment. The post-holing depths at the Coolock site were estimated to be in the order of 500mm to 700mm which is consistent with the constant depth to the maximum pile moment
- The high ε_{50} values[6] exhibited by DBC in UU triaxial tests (3% ± 0.5%, see later) suggest that greater displacements are required to mobilise the peak soil strength of DBC compared to the API stiff clay. These displacements did not materialise at the applied load levels.

Figure 7-18 shows the consistency in the *p-y* relations between piles A and B measured during LT3; a similar correlation also existed in the other two static load tests. The American Petroleum Institute [API] (1993) gives the ultimate bearing capacity for stiff clay, subjected to static loading, as varying between $3c_u$ and $12c_u$ (≡ 300 to 1200kPa) depending on the depth below ground level considered; these limits are in keeping with the soil pressures inferred from LT3.

[6] ε_{50} is the strain at half the deviator stress at failure measured in UU triaxial tests.

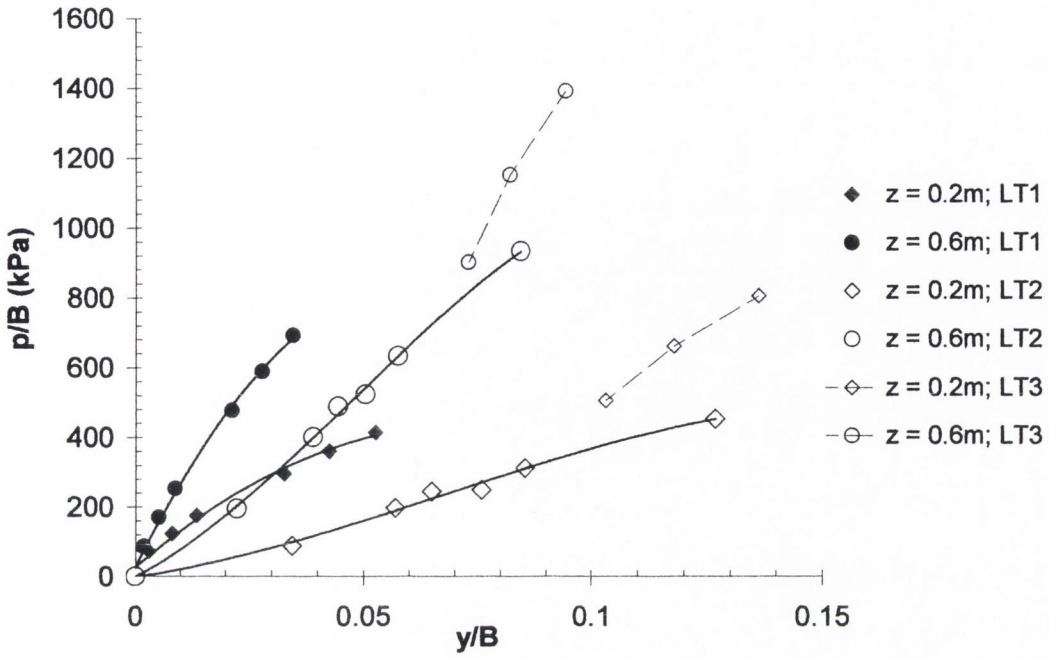

Figure 7-17: *p-y* curves for LT1, LT2 and LT3

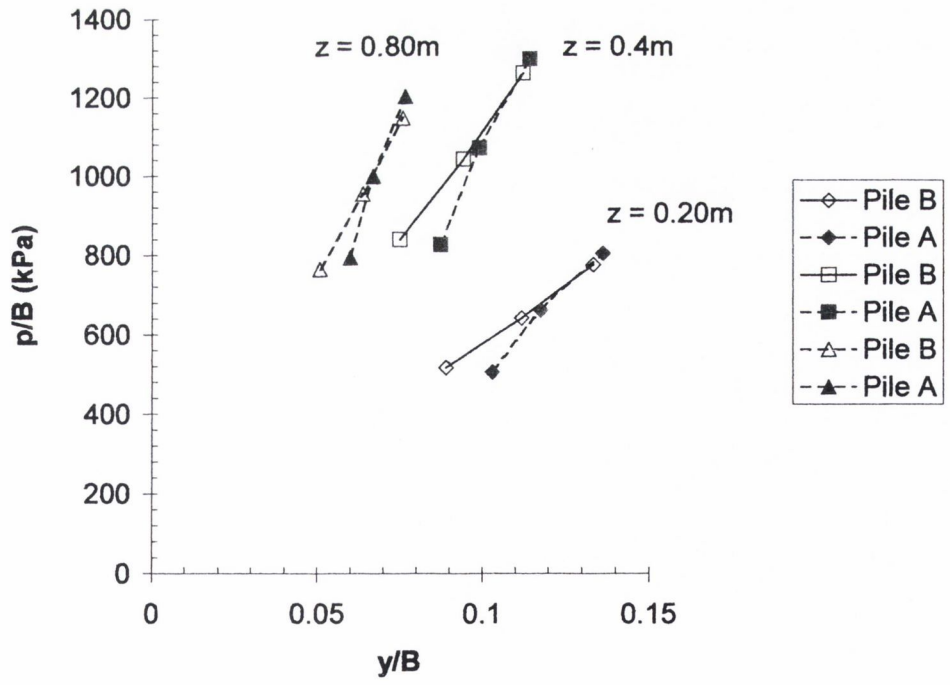

Figure 7-18: p-y curves for piles A and B derived from LT3

Comparison of Measured *p-y* Data with API (1993)

Figure 7-19 shows the *p-y* curves derived for DBC compared with the API recommended *p-y* curves for stiff clay. The *OASYS* software package ALP was used to generate the API *p-y* curves. The input parameters required to create these curves include the unit weight of the soil, the undrained shear strength profile and ε_{50} measured in UU triaxial tests; see Chapter 2. The short duration available to complete the research did not permit detailed analysis of the geotechnical properties of the site soils. Therefore the interpretation of the load tests was based on typical soil properties for DBC determined from on going research at Trinity College; Farrell (1989), Farrell and Wall (1990), Treacy (1996), Lehane and Simpson (2000), Carney (2002) and others. Site-specific undrained strength, c_u values were obtained in the brown boulder clay from in situ vane tests performed in a shallow trial pit excavated in the environs of the test piles. These results were consistent with values reported in the above references.

The API recommended values for ε_{50} were used to produce the *p-y* curves shown in Figure 7-19. The discrepancy between the measured and API predicted *p-y* response is obvious and suggests that the API recommendation for ε_{50} tends to over predict the initial stiffness response of DBC below depths of 1.0m. The discrepancy reflects the difference between the mass properties of DBC and the properties of the stiff clays used in the formulation of the API recommendation for ε_{50} values. The API suggested values for ε_{50} are based on two well instrumented field tests on piles (Reese and Cox, 1975 and Reese and Welch, 1975). The dramatic difference between the ultimate resistances predicted by the API (following the recommendations of Reese and Welch, 1975) and those measured at Coolock may be due to differences in the soil structure. The API stiff clay *p-y* criteria was derived from pile lateral load tests in a very stiff, heavily overconsolidated fissured and jointed clay of high plasticity; conditions which are unrepresentative of DBC. While the presence of fissures has been reported in DBC, these usually take the form of micro-cracks and are not considered to have an important influence on the mass behaviour of the material (Lehane and Simpson, 2000). Long et al. (1992) found[7] that better fits to measured *p-y* data are obtained if laboratory (rather than API recommended) values of ε_{50} are used to develop the curves[8]. Typical ε_{50}

[7] For piles tested in stiff glacial till at Tilbrook Grange, U.K.

[8] ε_{50} values determined from isotropically consolidated undrained (CIU) triaxial tests gave less scatter than those measured in unconsolidated undrained (UU) triaxial tests.

values for DBC based on a database assimilated over the past 20 years are 3% ± 0.5% (Carney, 2002); the tests also reveal that ε_{50} does not vary significantly over the critical depth for the piles at Coolock.

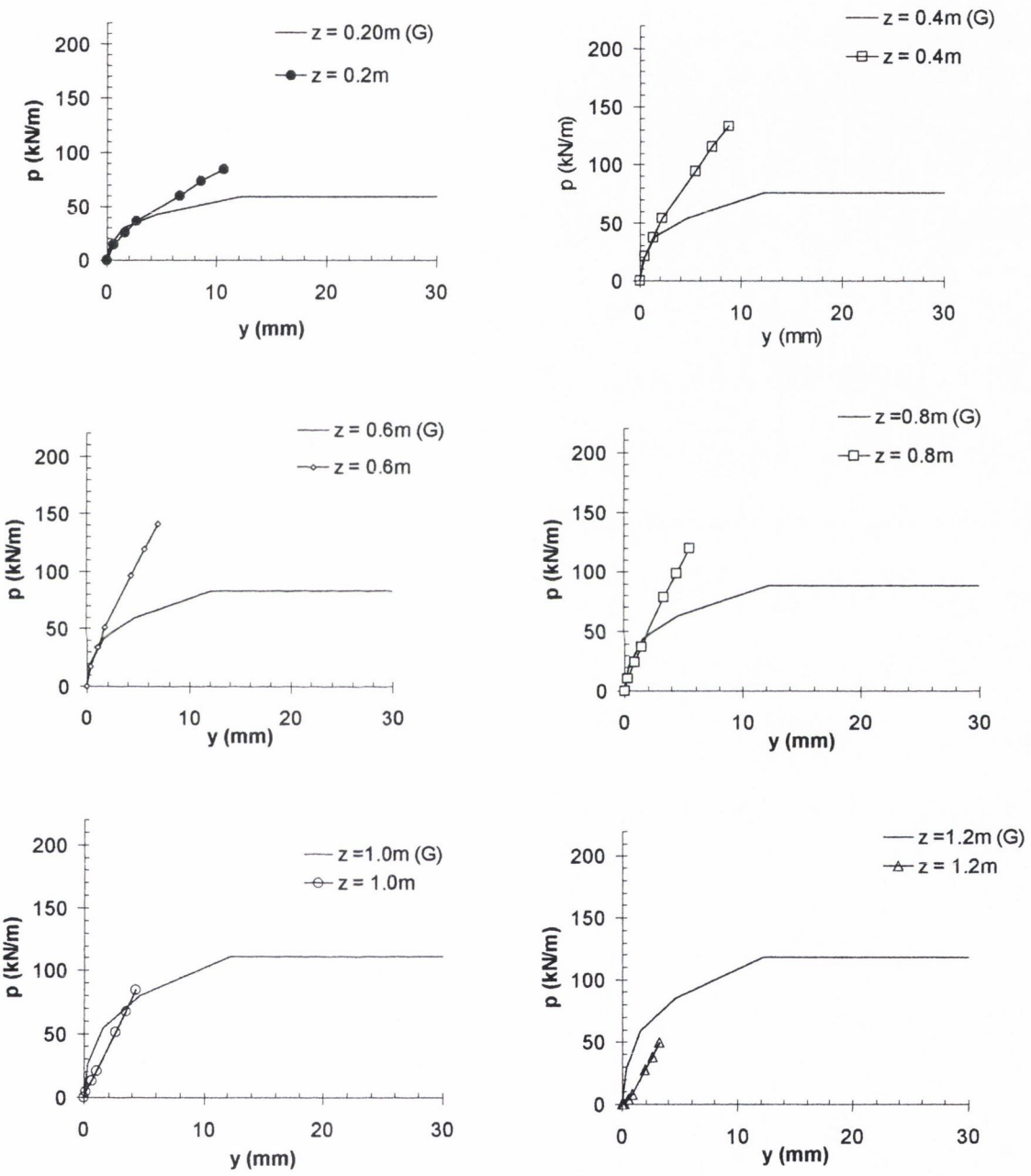

Figure 7-19: *p-y* curves for Dublin boulder clay compared with API p-y curves for stiff clay.

(Note: z =1.0m refers to the measured *p-y* curve at that depth and z = 1.0m (G) refers to the API generated *p-y* curve at the same depth)

To validate the measured pile response the derived *p-y* curves were specified in ALP in order to back predict the bending moment (M_{bc}) and displacement (y_{bc}) profiles for the piles. This exercise yielded good fits to the measured bending moment (M_m) and displacement profiles (y_m) as shown in Figure 7-20.

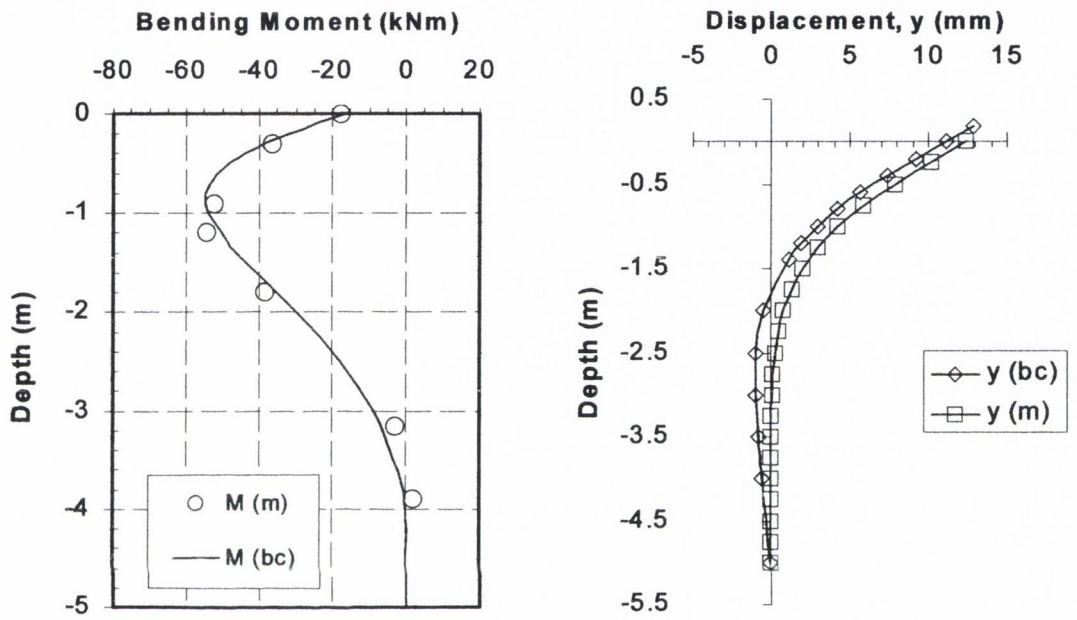

Figure 7-20: Moment and displacement profiles for LT1 at a lateral load of 90kN for pile B

Variation in Modulus of Subgrade Reaction

The measured *p-y* curves were used to determine the equivalent modulus of subgrade reaction or 'spring' stiffness (K) over the initial metre of soil. The results are shown in Figure 7-21 in terms of the equivalent 'cavity strain' (i.e. the ratio of pile displacement (y) to the half the pile width, B/2). The results indicate a significant reduction in K as the strain is increased.

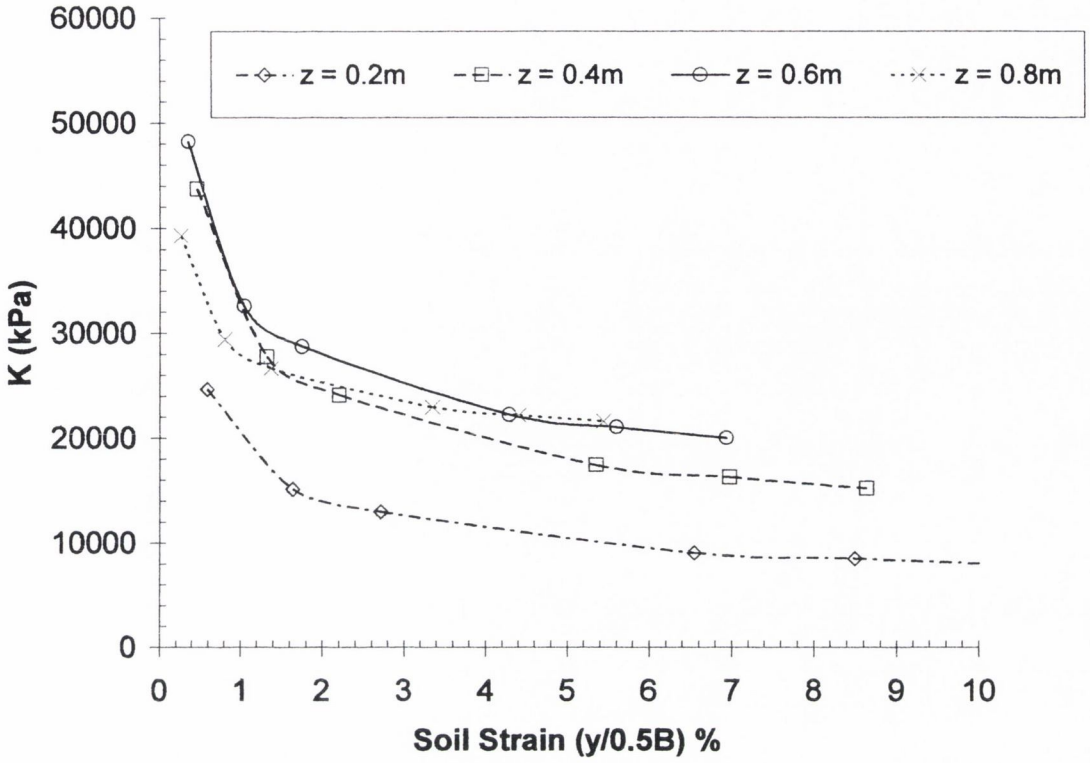

Figure 7-21: Variation of K with increasing soil strain for DBC

7.7 Concluding Remarks

- DBC has a higher ultimate lateral capacity but lower stiffness than predicted by the API (1993) recommendations. The API stiff clay had a high plasticity and contained joints and fissures which dominated the strength of the soil mass. The absence of such features in the structure of DBC is considered the principal reason for the higher resistances measured at Coolock.

- Pile bending moment (and displacement profiles) back-calculated from the measured *p-y* curves are in good agreement with the measured moment profiles.

- The pile displacement and bending moment profiles show that lateral response of the pile is controlled by the pile bending stiffness and the soil's resistance to a depth of approximately ten pile dimensions (10B).

- The *p-y* curves presented for DBC accurately predicted the measured pile behaviour. However, as these are the first *p-y* curves presented for DBC (to the author's knowledge), further investigation is necessary in order to fully validate the curves. In particular, the high soil pressures measured at relatively shallow depth during LT3 require further study. These may well have occurred due to high suction pressures in the near surface material

- Typical values for the spring stiffness (K) within the critical pile depth are much lower than the typical soil stiffness (E) adopted for the design of shallow foundations in DBC; this is due to the high strains imposed on the soil during laterally loaded pile tests. (Note that E/K is typically ≈1.25; see appendix 2a).

8. INTERPRETATION OF LATERAL LOAD TESTS AT KINNEGAR, BELFAST

8.1 Introduction

In the absence of site-specific *p-y* relations, API guidelines are used to specify appropriate design *p-y* curves that are related empirically to soil properties at the specific site. As outlined in chapter 2, considerable experience has been obtained using these procedures and, in many instances, predictions have been found to be satisfactory for design purposes. The API guidelines are based on field tests on laterally loaded piles installed in predominantly uniform soil conditions and have been found to be consistent with simplified analytical studies. The adoption of the guidelines to site conditions that differ significantly from those used in their derivation is questionable and is investigated in this chapter by derivation of *p-y* curves for the Belfast pile tests.

Although being typical of many situations encountered in practice, the stratigraphy in the vicinity of the lateral pile tests at Belfast is not uniform and essentially consists of a near-surface stiff clayey sand underlain by a soft clay. Furthermore, the combined loading of pile AL1 is typical of the loading on the vast majority of real structures. The varying depths of the stiff near-surface material surrounding pile L1 and AL1 in Belfast coupled with the contrasting restraints at their pile heads therefore allow for a thorough examination of the API guidelines.

The *p-y* curves are derived in this chapter using the data presented in chapter 6. A comparative analysis is undertaken between these *p-y* curves and the *p-y* curves established using the API guidelines.

In general the *p-y* curves are presented in their conventional form although a number of curves have been presented in terms of pile pressure P against normalised displacement y/B, which is a direct scaling (by B) of the *p-y* form. The normalised form gives a better indication of expected strain levels in the soil, while presenting the soil resistance in terms of pressure helps eliminate confusion often associated with the concept of *p-y* curves.

8.2 Assessment of Pile Displacements and Soil Reactions

It was concluded that pile displacements calculated from the EL slopes and the soil reaction derived from the strain gauge data provided the most accurate means of establishing reliable *p-y* curves. This conclusion was based on the following:

- As the displacement profiles can be calculated directly by integrating the measured slopes, the need to accurately calculate the pile's flexural rigidity (EI) is eliminated. Moreover, the profiles derived using this method were in good agreement with the displacements measured by the transducers at the pile head. The consistency between EL profiles and the displaced shape obtained from the double integration of the strain gauge bending moment profiles is shown in Figure 8-1. Reasonable agreement exists between the profiles with the main difference likely to be associated with the selection of an appropriate EI value in the case of the strain gauge profile[1]. The phenomena of a reducing EI in a reinforced concrete section (once the cracking moment is exceeded) has been well documented in the literature (Price and Wardle, 1987a and b; MacGregor, 1992; Reese and Wang, 1994: O'Brien and Dixon, 1995; Reese, 1997) and was illustrated again in the finite element results presented in Figure 6-13.

[1] The influence of EI on the pile displacement can be observed in Figure 8-2a

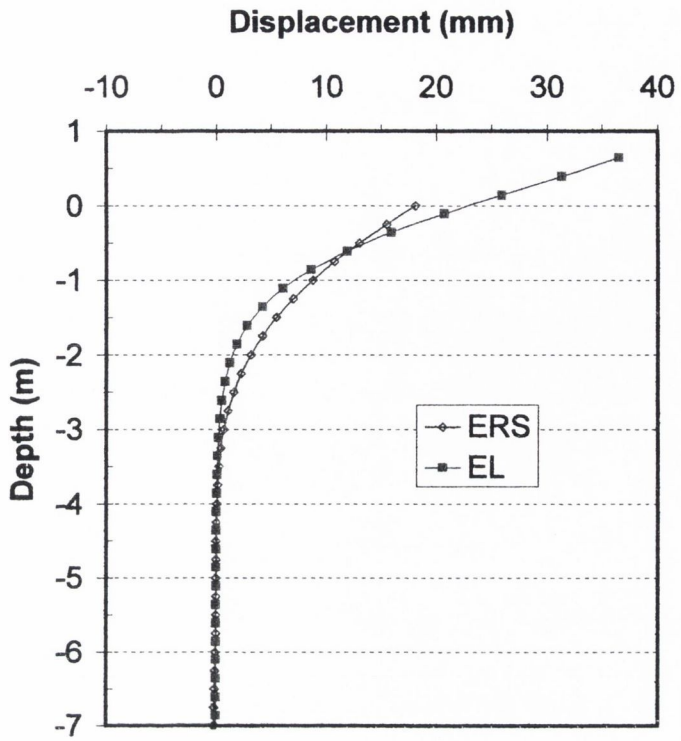

Figure 8-1: Comparison of displacement profiles for pile L1 at 76.75kN

- The selection of the correct value of EI is critical to the assessment of pile displacements from bending moment/strain gauge data. To illustrate this point, the computer program *OASYS* ALP was used to generate API *p-y* curves for soft clay. The soil properties and the test pile details from the Kinnegar site were input and the effect of varying the pile EI value between 150%EI and the fully cracked value was assessed. The results of this analysis are shown in Figure 8-2a; these illustrate the benefit of deriving displacement profiles from the measured pile slopes and their value in the subsequent derivation of the *p-y* relationships.

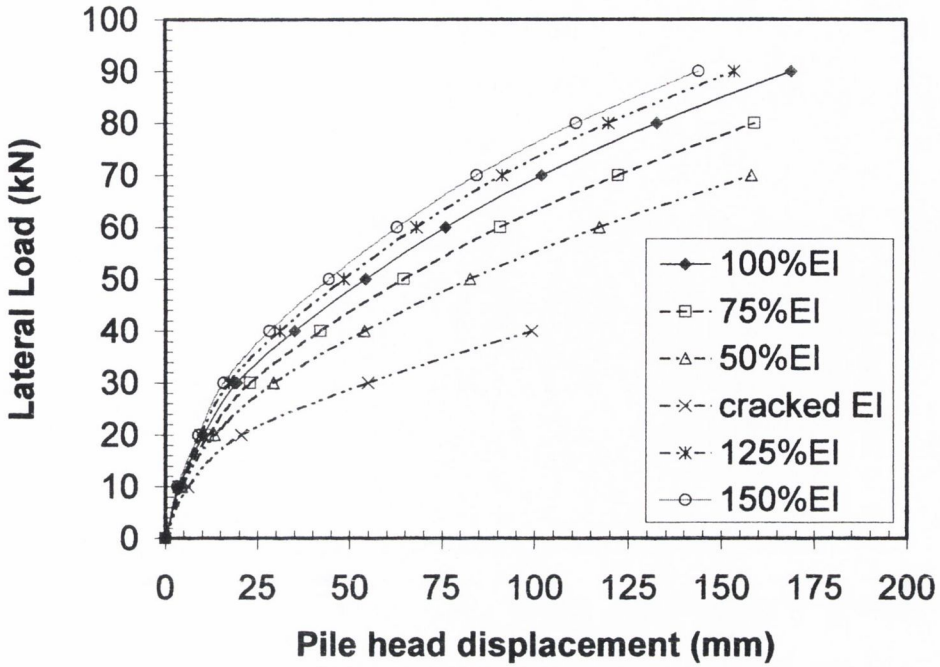

(a) Effect of changing EI on the pile head displacement

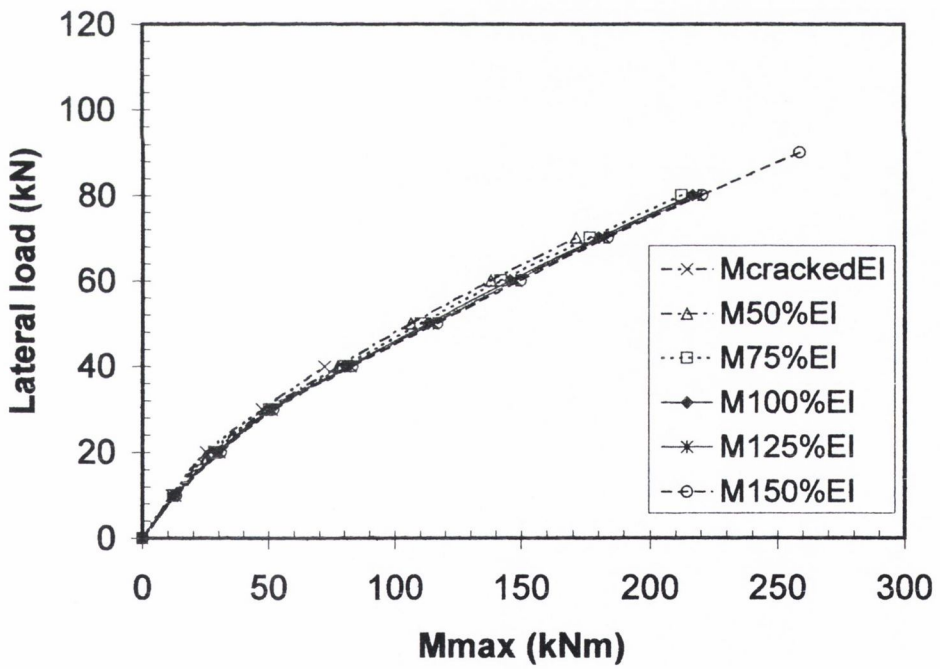

(b) Effect of changing EI on the maximum pile moment

Figure 8-2: Effect of varying pile flexural rigidity on the pile response

- The soil resistance p was determined from the distribution of bending moment along the pile. The moments, calculated from the measured strains, gave excellent agreement with the known free moment at the gauge level (chapter 6). A

comparison of the free moment with the measured values suggests the moments are accurate to better than 10%. Moreover, the agreement exhibited between the measured M-ε relationship and that of the FE analysis (Figure 6.12) gave confidence in the accuracy of the measured moments. It is of interest to note that the magnitude of the pile moment is not sensitive to the value of EI chosen; this was illustrated using *OASYS* ALP program (as outlined above) and the results are shown in Figure 8-2b.

8.3 Curve Fitting

8.3.1 Curve Fitting of Strain Gauge Bending Moment Data

The algebraic equation given in Eq. 8-1 accurately represented the measured bending moment profiles recorded during the tests[2]. A sixth order polynomial, multiplied by an exponential component (to ensure that the bending moment did not increase without bound over the pile depth) provided satisfactory results. As different constraints existed at the pile heads, the curve fitting procedure will be described separately for each pile.

Eq. 8-1... $$M_z = \left[1 - \frac{1}{e^{a_0 z} + 1}\right]\left(a_1 + a_2 z + a_3 z^2 + a_4 z^3 + a_5 z^4 + ... + a_i z^{i-1}\right)$$

---

[2] Validation of the curves fitted using Eq. 8-1 and Eq. 8-2 was undertaken prior to analysing the test data. The bending moment fits were assessed by comparing values (predicted from elastic beam theory) for a propped cantilever subjected to uniform loading with the values predicted by Eq. 8-1. For the fitting of slope data, a transverse point load was applied at the free end of a simple cantilever and the quality of fit to the theoretical slope profile was assessed using Eq. 8-2. The findings indicate the equation, subject to appropriate boundary conditions, provides excellent results. Details of this exercise are provided in appendix 8a. The curve fitting procedures adopted for the bending moment and displacement data will now be presented.

To assess the influence of the curve fitting procedure on the shear and reaction profiles, an alternative curve fitting procedure involving cubic splines was employed to pass a smooth curve through the measured moment profiles. The resulting moment profiles were differentiated as before to provide the shear and soil reaction distributions. The cubic splines provided excellent agreement with the measured moments but after double differentiation provided very erratic soil reaction profiles that were inconsistent with the measured pile displacement profiles.

CLT1

Case 1: pile L1

Pile L1 was free to rotate at the pile head and therefore the following boundary conditions at the pit level (z=0) are known:

1. At z=0 the shear force is equal to the applied lateral load.
2. The bending moment at z=0 can be calculated as the applied lateral load multiplied by the height of the load above z = 0m (pit level).
3. At z=0 the soil reaction $p\ (=\frac{d^2M}{dz^2})$ is also equal to zero.

These constraints fix the following coefficients[3] in Eq. 8-1:

$$a_1 = 2M$$
$$a_2 = 2H + a_0a_1/2$$
$$a_3 = a_0a_2/2$$

where a_0, a_1 etc. are curve fitting coefficients
H =the applied lateral load (kN)
M = bending moment (kNm) at z = 0

The remaining coefficients in equation (Eq. 8-1) were determined by iteration until the best-fit curve through the measured points was obtained. A least squares procedure was used to assess the best fit. The procedure was then repeated for each lateral load applied to the pile to obtain best-fit coefficients for the measured bending moment profiles. Typical fitted bending moment profiles to the data are shown in Figure 8-3a with the computed shear, soil reaction and displaced profile for the 47kN load increment shown in Figure 8-3b.

[3] See Appendix 8b for derivation of coefficients

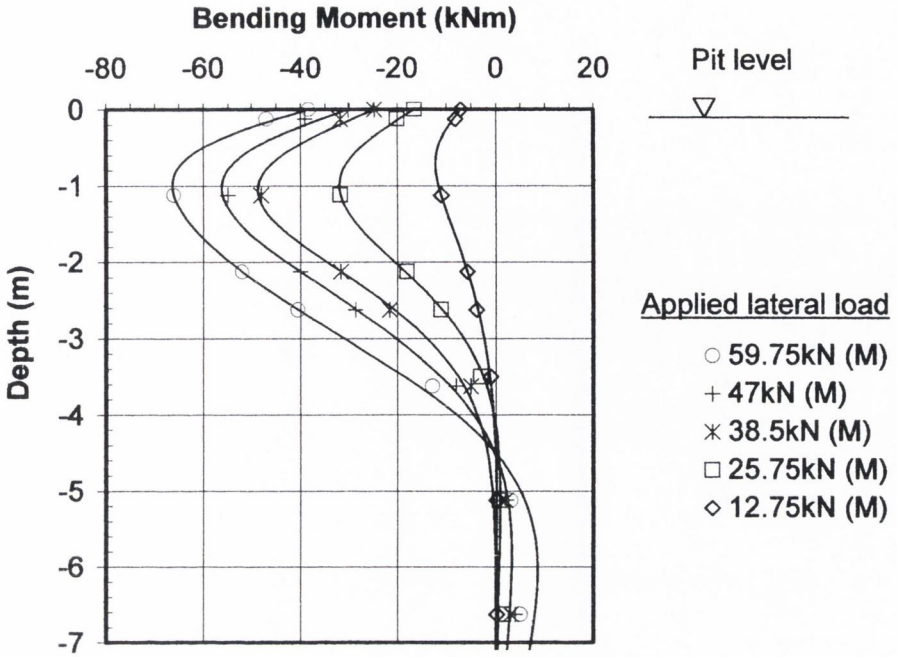

(a) Curves fitted to measured bending moments

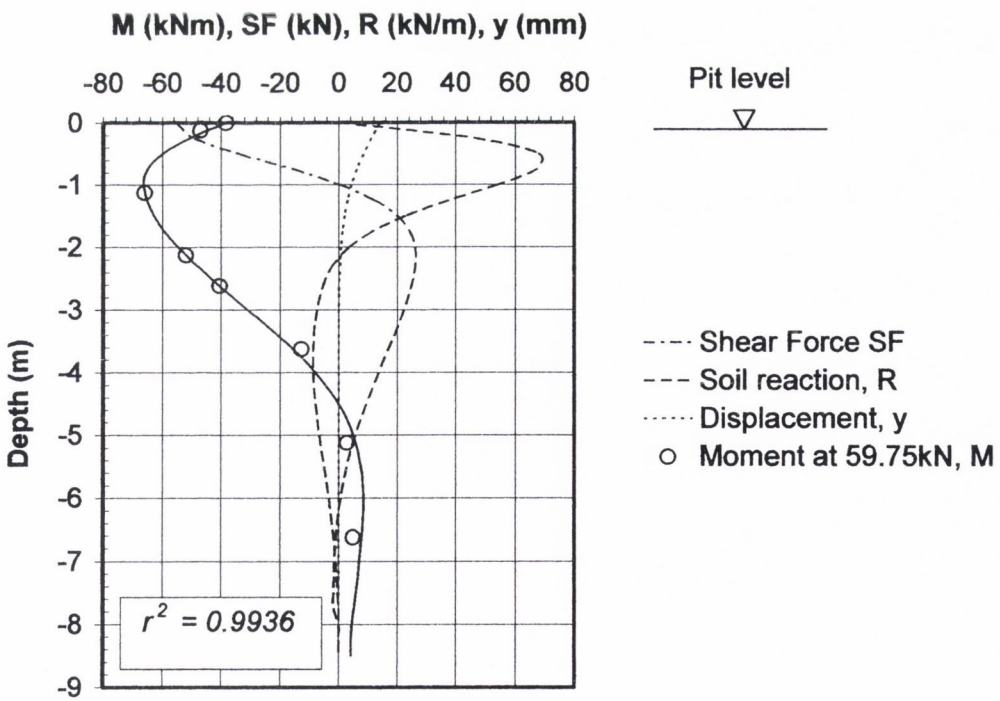

(b) Computed profiles for the 59.75kN load increment

Figure 8-3: Typical curve fitting results for pile L1 (CLT1)

Case 2: pile AL1

A variable restraining moment existed at the head of AL1 (see Fig 6-8) due to the load test setup. As described in section 6.3 (chapter 6) the magnitude of the net applied lateral load and the rotational restraint was derived from the instrumentation. These values permitted the determination of the moment (M_{pit}) and shear (H_R) at pit level (z=0) and were used to derive best-fit equations to M_{meas} employing the same procedure outlined for pile L1 but with a modified a_2 coefficient:

$$a_2 = 2H_R + a_0 a_1/2$$

where H_R =the resultant lateral load (kN) given by Eq. 6-2 in chapter 6.

Typical bending moment profiles for pile AL1 established from the curve fitting procedure are shown in Figure 8-4a with the computed shear, soil reaction and displaced profile for the 59.75kN load increment shown in Figure 8-4b.

CLT2

A similar procedure was adopted for the results from CLT2 with the corresponding results for pile L1 and AL1 shown in Figure 8-5 and Figure 8-6 respectively. Again a good fit was obtained by passing a sixth order polynomial through the measured data points.

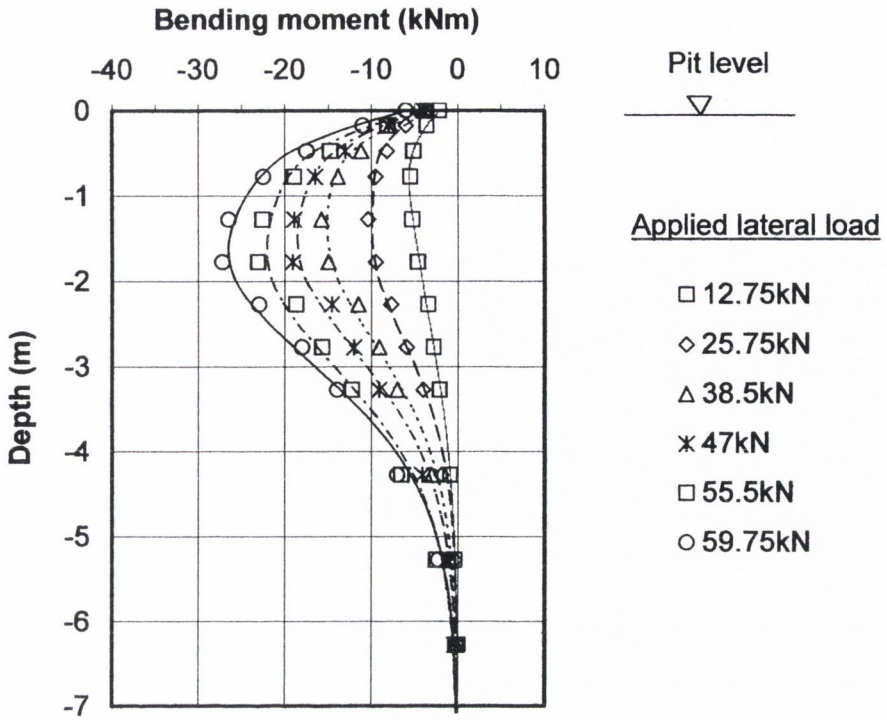

(a) Curves fitted to measured bending moments

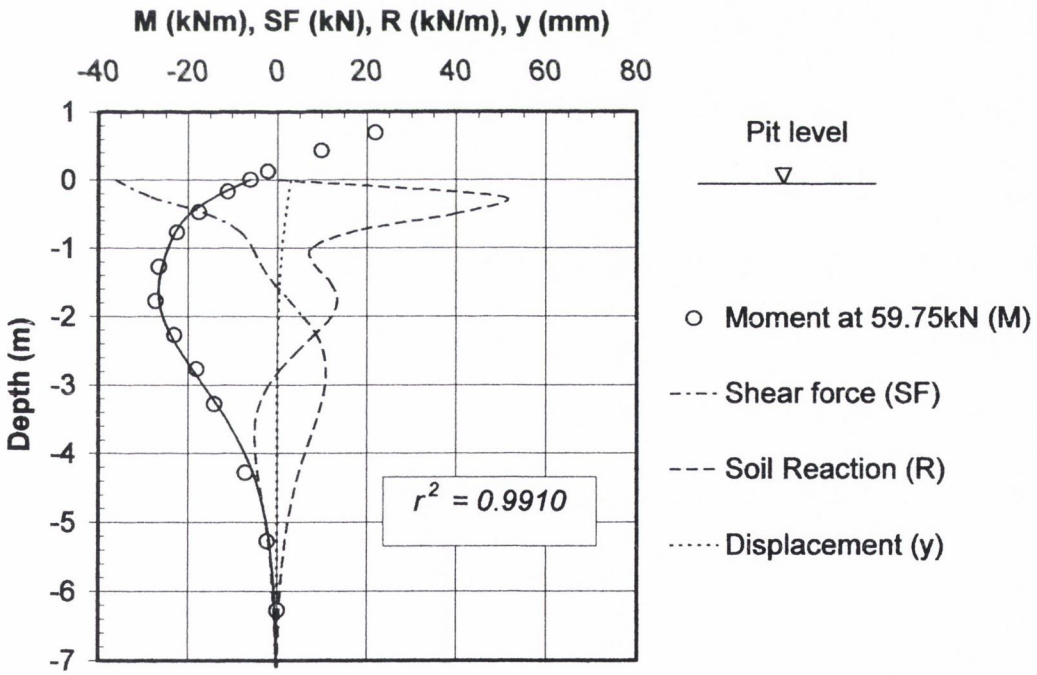

(b) Computed profiles for the 59.75kN load increment

Figure 8-4: Typical curve fitting results for pile AL1 (CLT1)

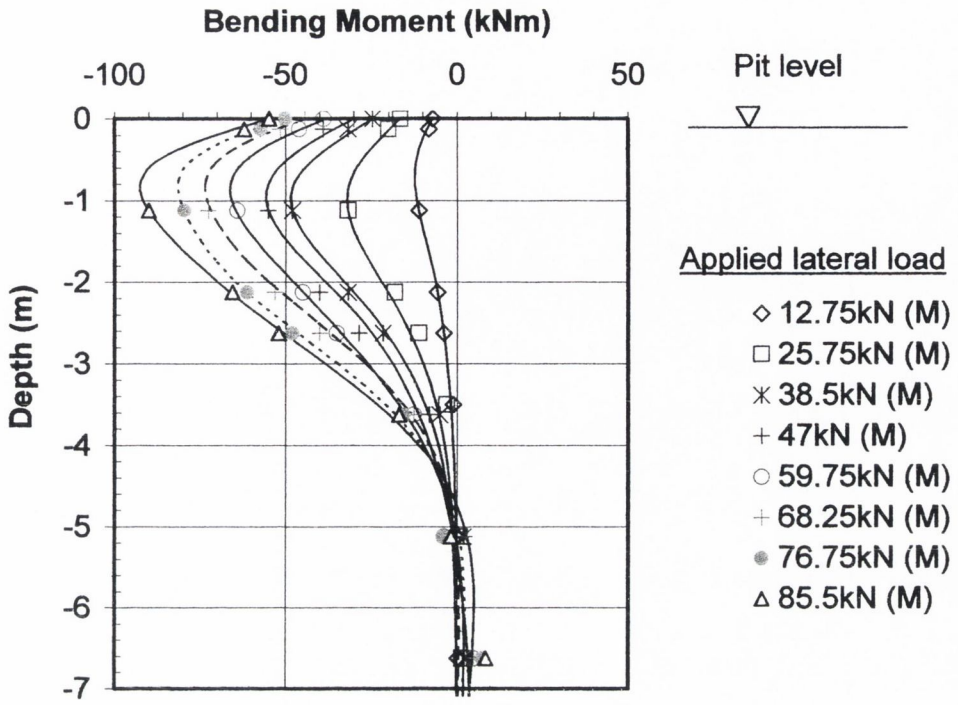

(a) Curves fitted to measured bending moments

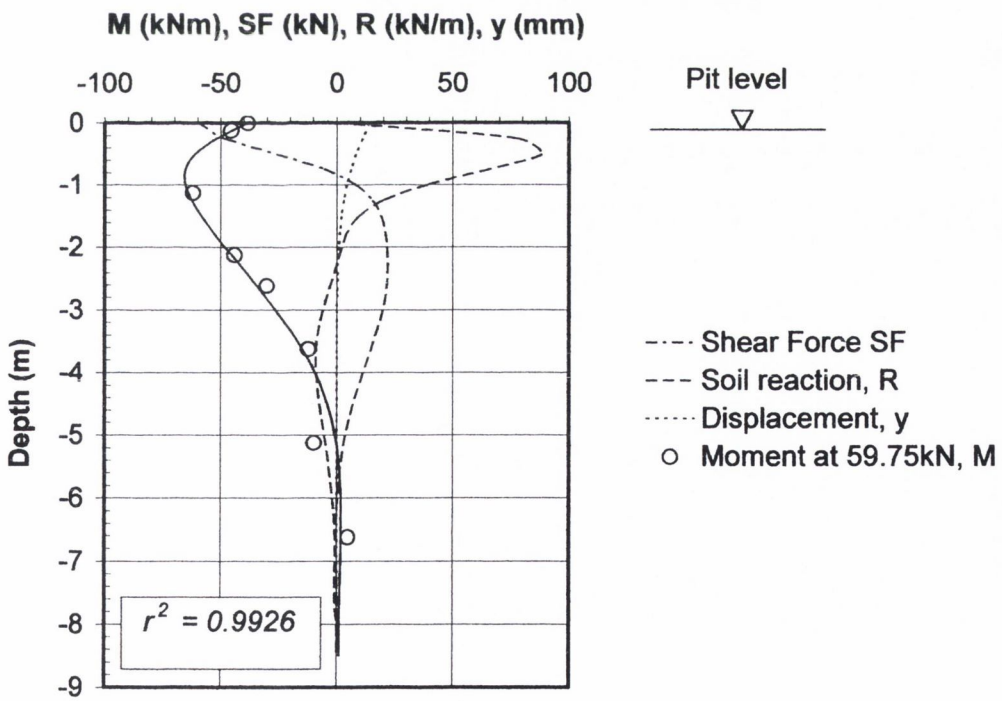

(b) Computed profiles for the 59.75kN load increment

Figure 8-5: Measured and Fitted Moments in pile L1 CLT2

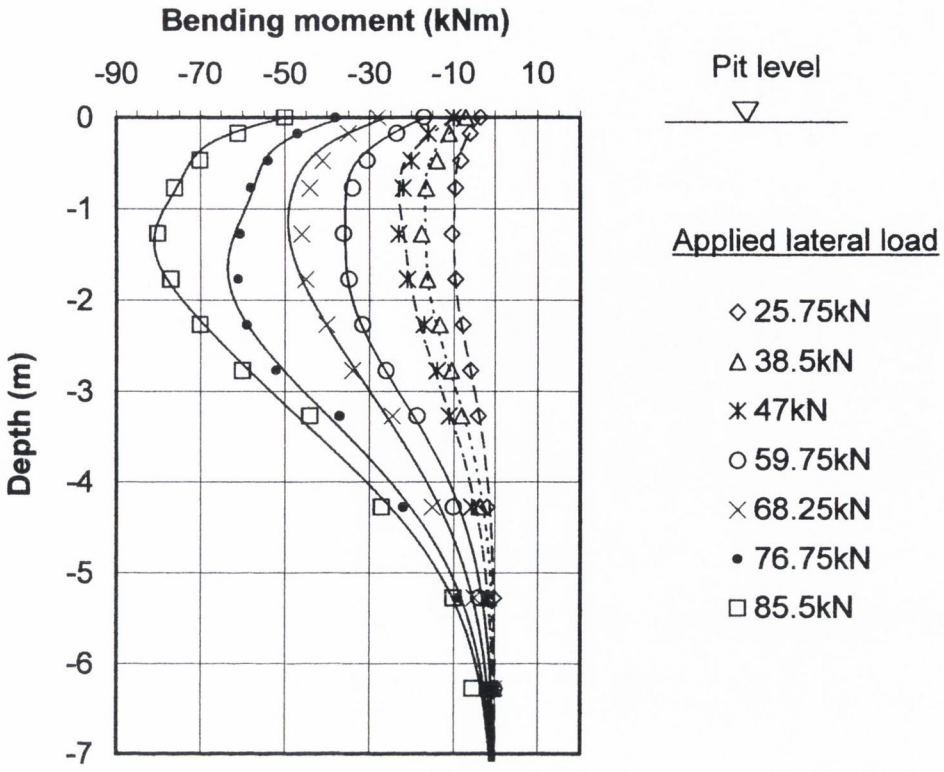

Figure 8-6: Measured and Fitted Moments in pile AL1 CLT2

8.3.1 General comment

Although minor errors in the strain gauge data may have influenced the resultant soil reactions, these are not considered to be significant given the accuracy of the strain gauge data illustrated via a number of independent approaches in chapter 6. The miscellaneous nature of the stiff upper stratum appears to be the principal cause for the soil reaction distributions computed in the tests (Figure 8-4).

8.3.2 Derivation of Pile Displacement Profiles from Measured Slopes

The same form of algebraic equation used to fit a curve to the measured moments was also employed to obtain the displacement profiles i.e.

$$\text{Eq. 8-2...} \qquad \theta_z = \left[1 - \frac{1}{e^{a_0 z} + 1}\right]\left(a_1 + a_2 z + a_3 z^2 + a_4 z^3 + a_5 z^4 + ... + a_i z^{i-1}\right)$$

To analyse the EL results, the measured slopes were fitted to the expression given in Eq. 8-2. A fifth order polynomial component was found to provide the best fit to the data. The errors associated with the fitting procedure were greatest at the top of the pile, so to improve the fit, an additional point was included above the level of the top EL in the curve-fitting exercise; the data for this point was obtained by applying Mohr's Moment Area Theorem for slopes[4] between the top EL and the point of loading. At the point of load application, the moment is equal to zero in the case of pile L1 and is measured by the strain gauges in the case of pile AL1. The additional point made a marked improvement in the fit at the top of the pile.

Both piles were free to rotate at the pile head and therefore the following boundary conditions at the level of the applied lateral load (x = 0) were known:

1. At x = 0 the slope, θ can be calculated as the sum of the slope measured by the EL at pit level ($z = 0$) and the change in slope between the EL and the point of load application as calculated from Mohr's Moment Area Theorem. The lateral load multiplied by the distance from the load to the EL gives the bending moment at the EL for pile L1.
2. At x = 0, M/EI is equal to zero for pile L1 ($\frac{d\theta}{dx} = \frac{M}{EI} = 0$)
3. At x = 0 the shear force is equal to the applied lateral load ($\frac{d^2\theta}{dx^2} = \frac{V}{EI}$).
4. The EL located at pit level ($z = 0$) in each pile provided the pile slope at this point.

These constraints fix the following coefficients[5] in Eq. 8-2:

$$a_1 = 2\theta$$
$$a_2 = a_0 a_1/2$$
$$a_3 = V/EI + a_0 a_2/2$$

[4] Mohr's Moment Area Theorem states that the change in slope between two points is given by the area under the M/EI diagram between the points.
[5] See appendix 8b for derivation of coefficients

where a_0, a_1 etc. are curve fitting coefficients

V = the applied lateral load (kN)

θ = pile slope (radians) at $x = 0$

EI = flexural rigidity of the pile

In the case of pile AL1, the coefficient a_2 is modified due to the presence of a bending moment acting on the pile at the point of loading. Therefore, a_2 is represented by the following expression:

$$a_2 = 2M/EI + a_0a_1/2$$

The remaining curve fitting coefficients a_0, a_4 etc. were optimised using a least squares procedure (see appendix 8b) and iteration until the best-fit curve through the measured points was obtained. Eq. 8-2 was then integrated numerically to give the displacement profile. The agreement between displacement profiles and the measured pile head displacement (as shown in Figure 8-7 to Figure 8-10) confirms the quality of the results.

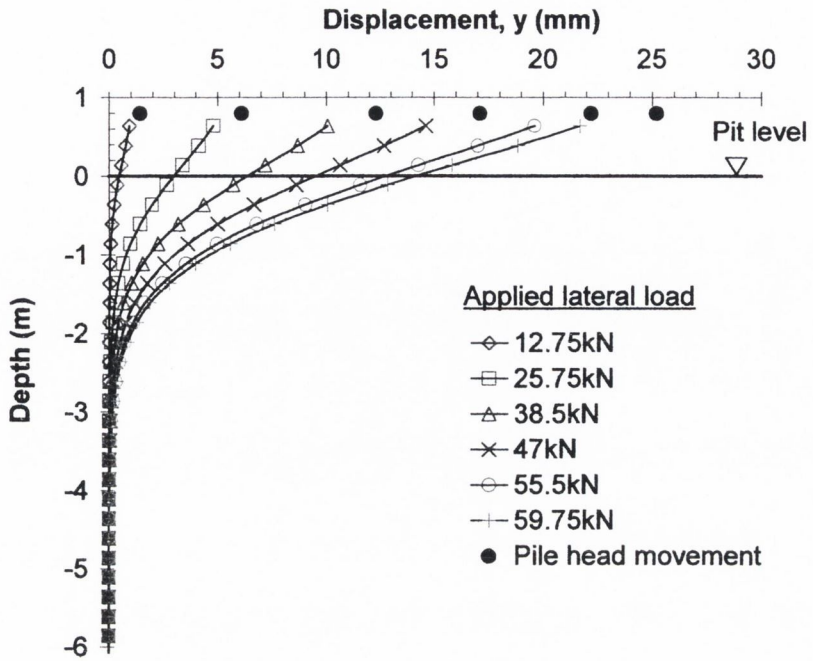

Figure 8-7: Curves fitted to measured pile displacement profile for pile L1 (CLT1)

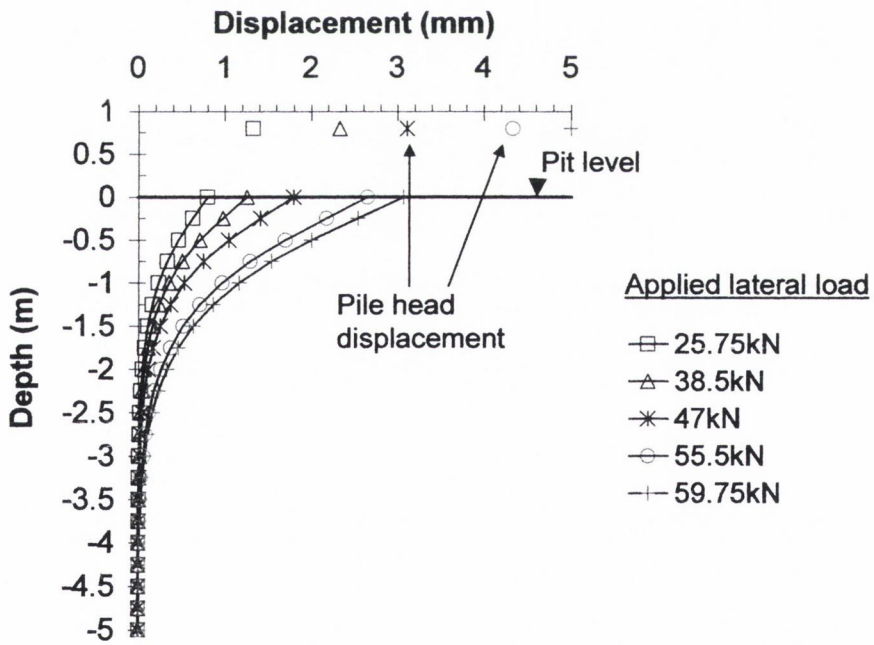

Figure 8-8: Curves fitted to measured pile displacement profile for pile AL1 (CLT1)

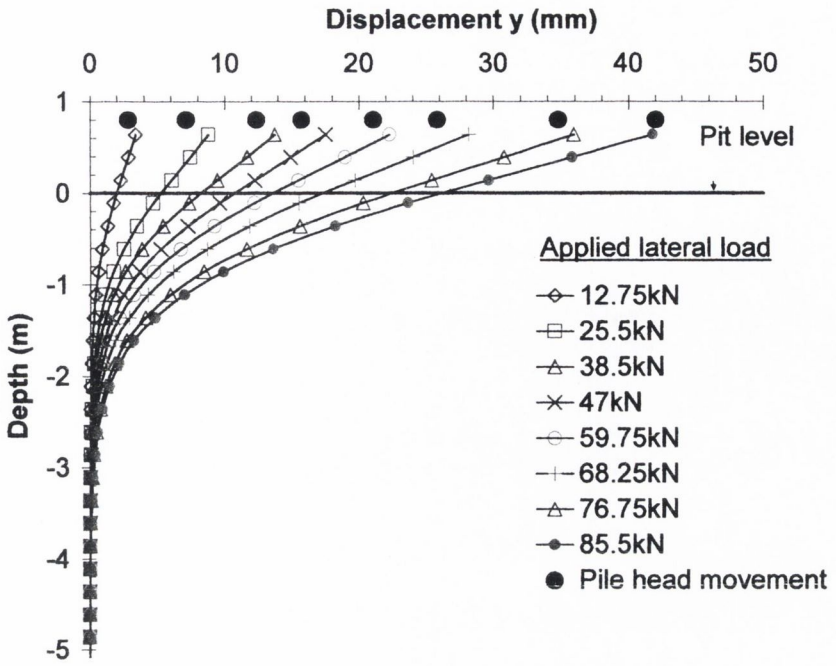

Figure 8-9: Curves fitted to measured pile displacement profile for pile L1 (CLT2)

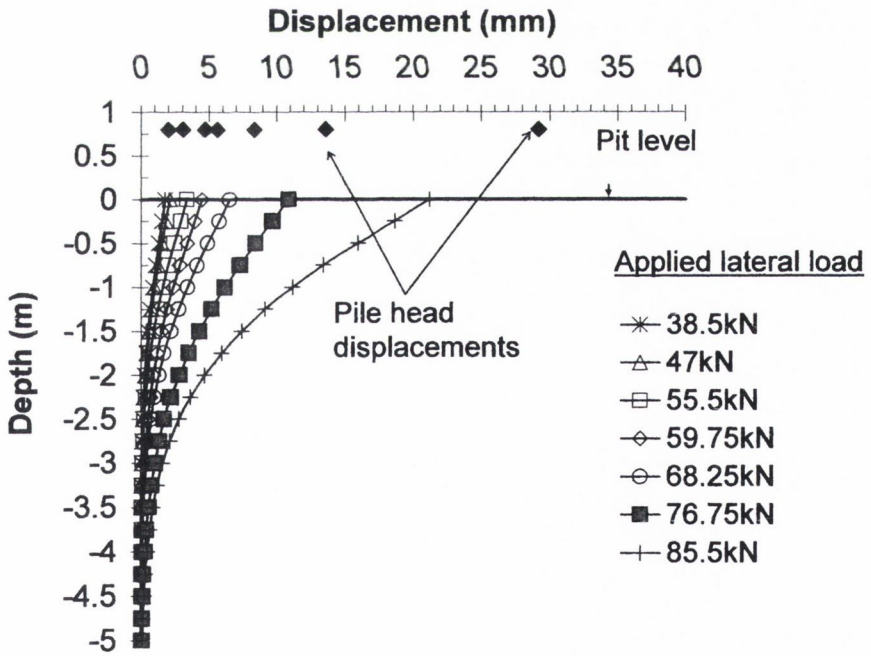

Figure 8-10: Curves fitted to measured pile displacement profile for pile AL1 (CLT2)

8.4 Bending Moment Distributions from Slopes

To assess the consistency of the electro-level results, the bending moment distribution calculated from the differential of the measured slopes was compared with the bending moments derived from the strain gauges. Typical slope fitting results for pile AL1 are shown in Figure 8-11 while Figure 8-12 shows that reasonable agreement between the EL's and the strain gauge bending moment distributions. It is considered that the bending distributions from the strain gauges are more accurate than the electro-level results given the inherent errors associated with the differentiation of the slopes. However, better agreement between the results could be achieved by increasing the number and resolution of electro-levels employed.

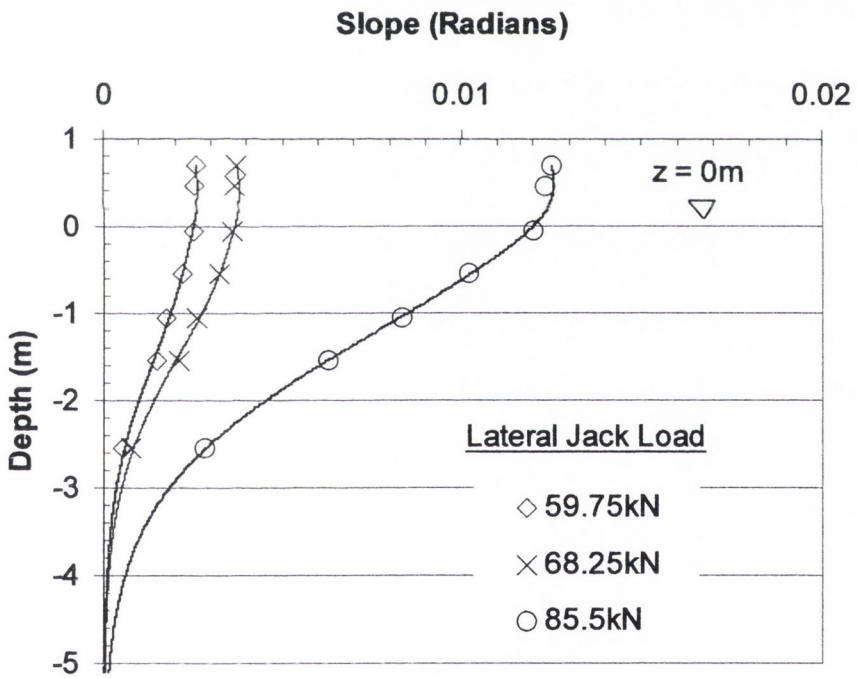

Figure 8-11: Curve fitting to measured slopes for pile AL1, CLT2

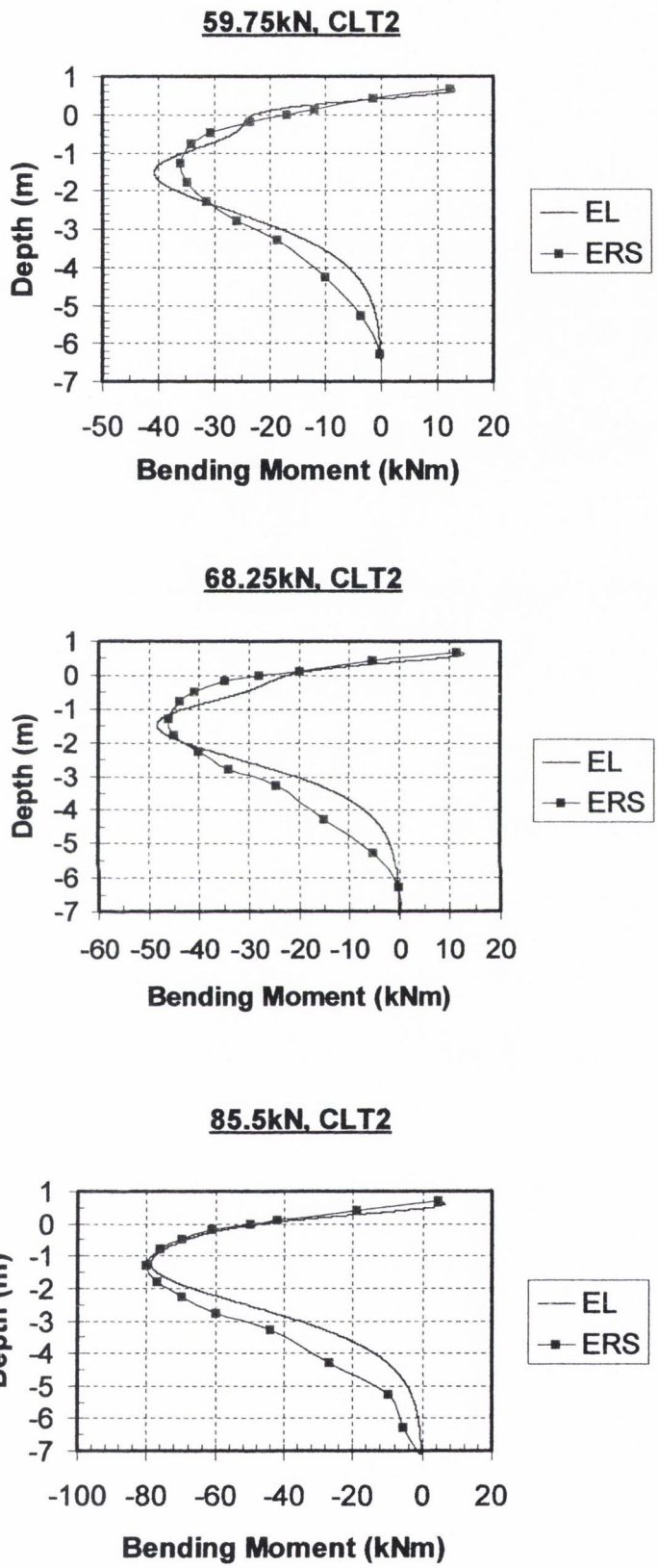

Figure 8-12: Comparison of ERS and EL derived bending moments for AL1 during CLT2

8.5 *p-y* Curves for CLT1 and CLT2

The results of the curve fitting exercise were subsequently used to produce site-specific soil reaction (*p*) versus pile displacement (*y*) curves; the so-called *p-y* curves used in the analysis of laterally loaded piles. These curves are used in practice[6] to calculate the bending moment and displacement profiles for pile design and therefore form the basis for the assessment of the pile test results in this thesis. The *p-y* relationships are discussed in the order in which the tests were conducted while comparisons and trends between the measured *p-y* curves and those published by the API in RP 2A-LRFD (1993) will be presented in chapter 9.

8.5.1 *p-y* Curves for Pile L1

Figure 8-13a and Figure 8-13b present the *p-y* and normalised *p-y* curves respectively for pile L1. The curves clearly indicate the difference in stiffness between the fill and the sleech. There is a notable drop in resistance observed above displacements of ≈1mm at depths greater than z = 1.0m. For example, the equivalent spring stiffness ($K=p/y$) measured at a displacement of 2mm falls from 14.5 MN/m^2 at z = 0.4m to 7.5MN/m^2 at z = 1.6m. This result is consistent with the change in strata observed during the trial pit exploration (TP1). The normalised plots give an indication of the high levels of strain imposed on the soil near the ground surface.

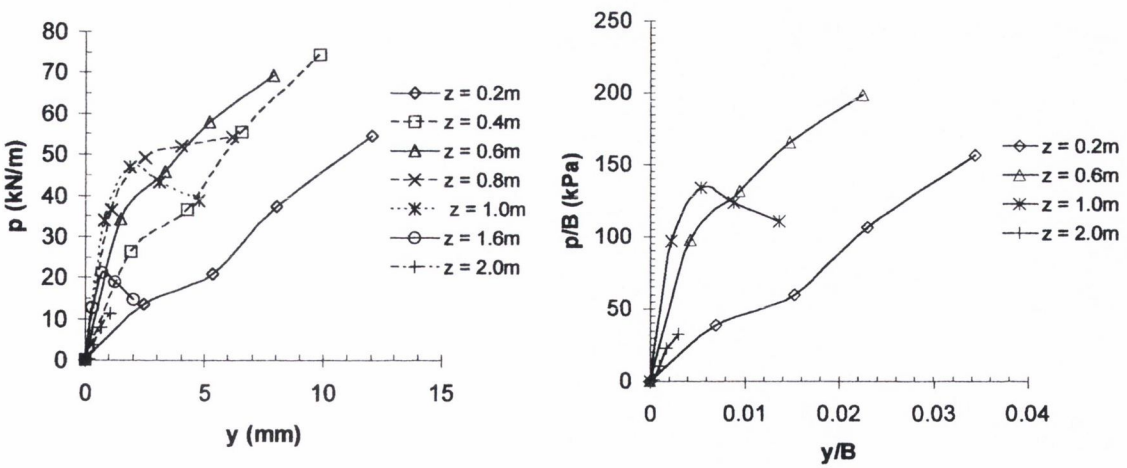

(a) *p-y* curves (b) Normalised *p-y* curves

Figure 8-13: Load transfer curves for L1 (CLT1)

[6] See Chapter 2, section 2.4

The interpreted *p-y* curves suggest that the fill stratum continues to provide resistance while the sleech between z = 1.0m and 2.0m exhibits strain softening. On the basis of the measured soil properties, the sleech would be expected to reach ultimate (maximum) resistance at P between 60kPa to 100kPa or *p* between 21kN/m and 35 kN/m ($\equiv 3c_u$ and $\approx 5c_u$) at these shallow depths. These values are somewhat lower than the peak mobilised resistance (≈134kPa for z = 1.0m). The *p-y* curve at z = 2.0m has not reached its peak resistance but it can be observed that the soil response at this depth is significantly less stiff than the *p-y* curve at z = 1.0m. This variation reflects the change of stratum indicated by the CPT q_c profile in the vicinity of pile L1 (see Figure 4-17 in chapter 4).

8.5.2 *p-y* Curves for Pile AL1

Figure 8-14a and Figure 8-14b present the *p-y* and normalised *p-y* curves for pile AL1 respectively. Once again the curves clearly indicate the difference in stiffness between the upper stiff material and the sleech. There is a notable drop in resistance observed at depths greater than z = 0.5m which is consistent with the change in strata observed during the trial pit exploration (TP2).

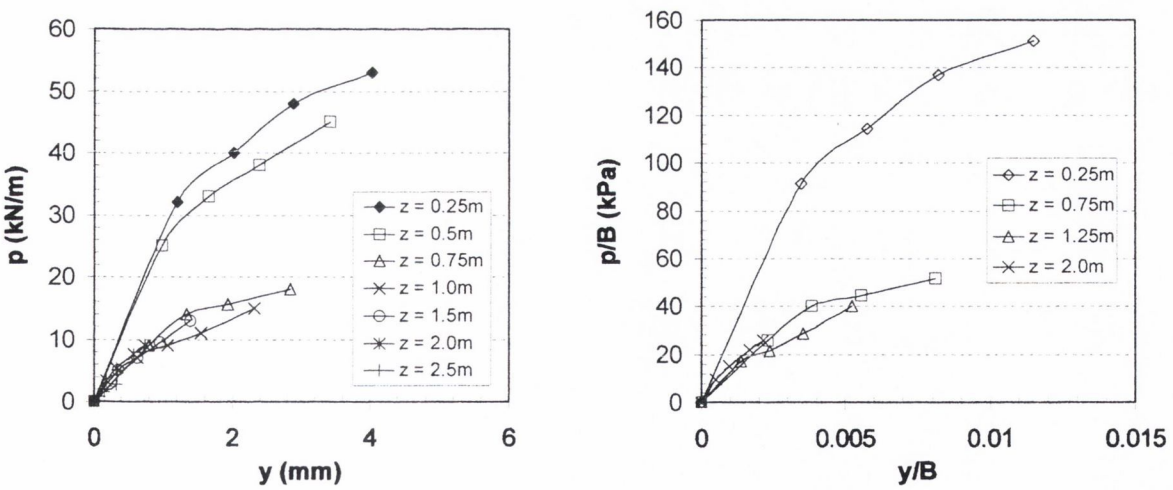

(a) *p-y* curves (b) Normalised *p-y* curves

Figure 8-14: Load transfer curves for AL1 during CLT1

It is apparent from the normalised plot (Figure 8-14b) that the maximum strain in the soil is significantly less than that measured at L1. This difference is due to the reduced shear

force and the restraining moment applied at the pile head as a result of the test setup (used to apply the combined loading) rather than a change in soil behaviour between the piles.

8.5.3 Comparison of *p-y* Curves for Pile L1 and AL1 during CLT1

One of the principal objectives of this research was to determine if piles subjected to combined loading produced different *p-y* responses to those measured by piles subjected to pure lateral load. However, a simple comparison of the *p-y* curves from each pile was complicated by the presence of a miscellaneous fill stratum whose thickness doubled over the short distance between the piles. Fill was present to a depth below pit level (z) of 0.5m adjacent to pile L1 and 0.94m adjacent to pile AL1. Comparisons of the *p-y* curves during CLT1 are shown in Figure 8-15. The following observations can be made:

- At z = 0.25m, the soil adjacent to AL1 exhibits a stiffness that is almost an order of magnitude greater than that at pile L1. For reasons provided in the following and in keeping with the trial pit observations, this difference is attributed to variability within the fill rather than an increased stiffness at AL1 due to combined loading. The following comments substantiate this conclusion.

- The similarity between the *p-y* curves at z = 0.5m suggests that neither combined loading nor pile head fixity is a factor in the *p-y* response of the soil.

- The significantly softer *p-y* response measured for pile AL1 at z = 0.75m reflects the change in stratum at AL1. The measured soil resistances at this depth are in keeping with a typical soft clay response. The *p-y* response for pile L1 reflects the fact that the stiffer material is still present at this depth at L1.

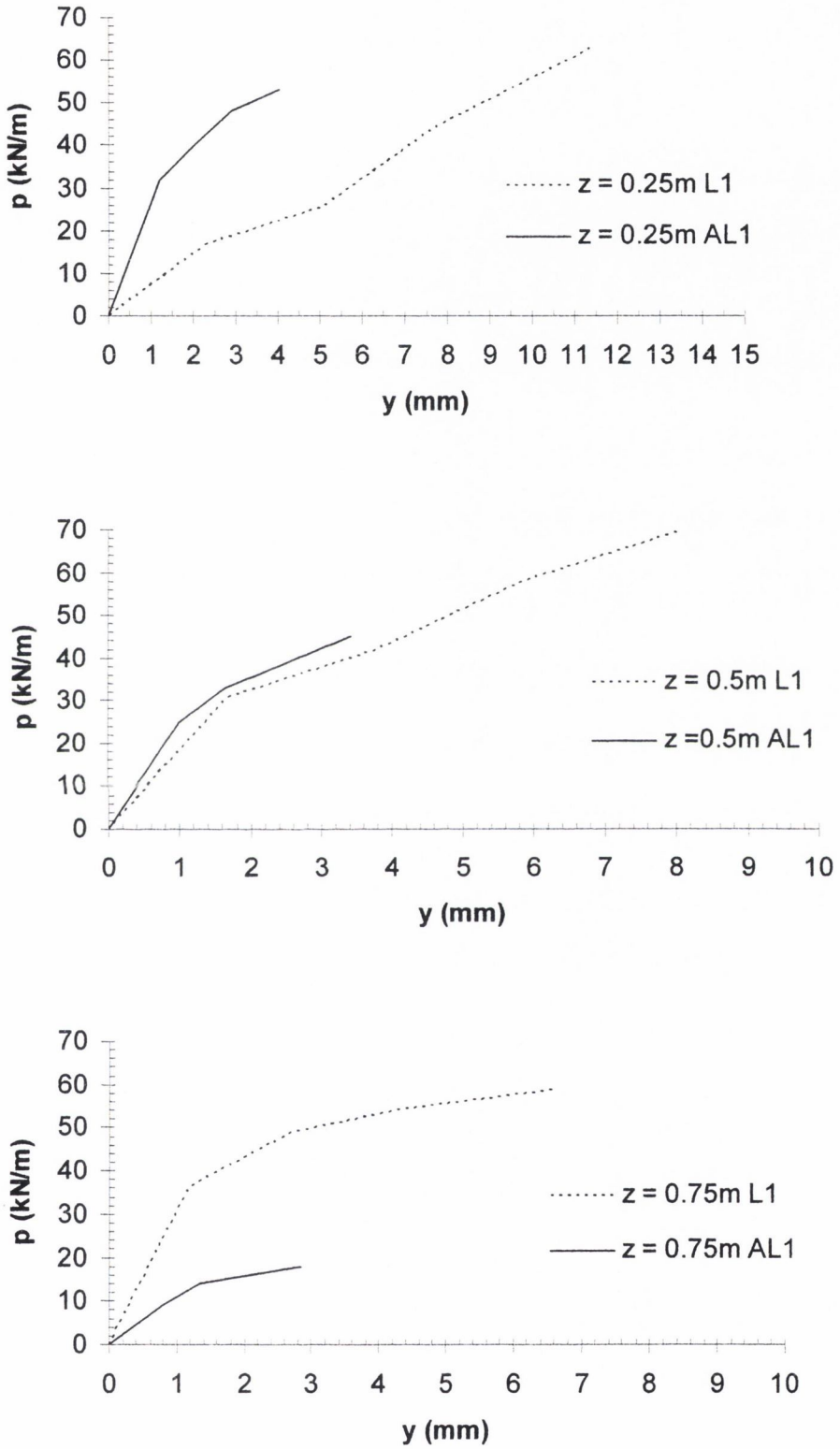

Figure 8-15: *p-y* curves compared for CLT1

8.6 *p-y* Curves for CLT2

The *p-y* relationships derived from CLT2 are important in that they confirm the validity of the relationships measured in CLT1 in addition to extending the relations for higher loads and displacements. As in the case of CLT1 the *p-y* curves are initially presented for each pile and are followed by a review of the results.

8.6.1 *p-y* Curves for Pile L1 (CLT2)

The *p-y* curves for pile L1 (Figure 8-16) show that the fill stratum continues to provide resistance up to the maximum loads applied during the CLT2. The initial *p-y* response in the fill is softer than that measured during CLT1 and may be a consequence of a post-hole that developed during the initial load test[7]. The latter section of the *p-y* curves shows an increase in resistance brought about by the pile re-engaging with the soil at the higher load levels. The *p-y* curve at z = 1.0m again illustrates the transition between the dense upper stratum and the sandy sleech.

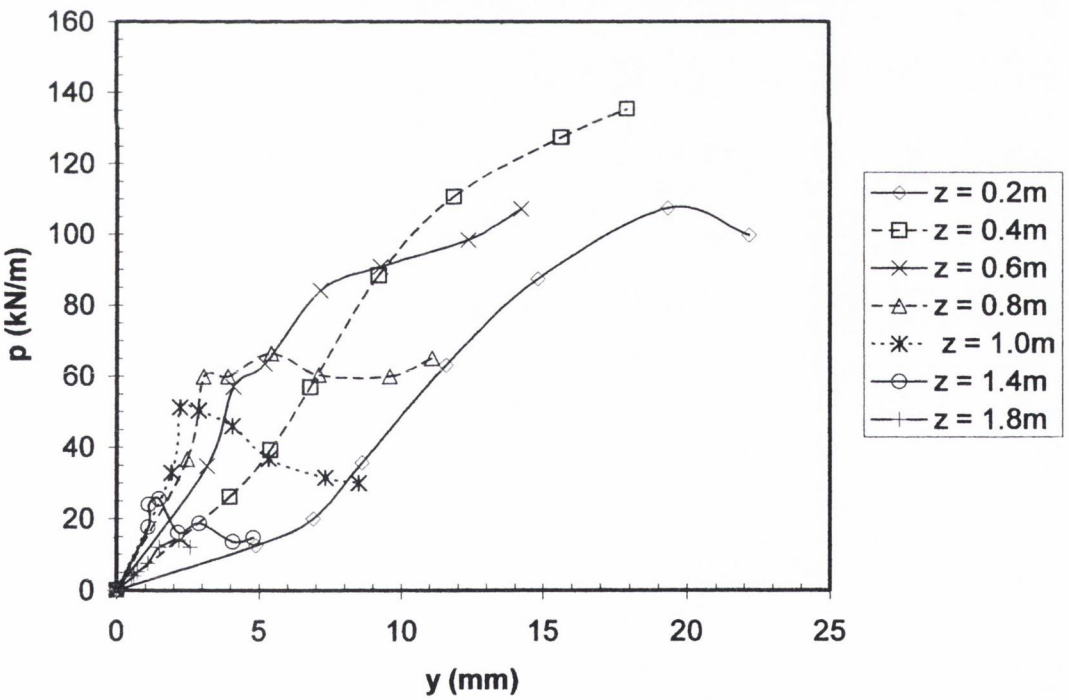

Figure 8-16: *p-y* curves for L1 measured during CLT2

[7] Recall that residual displacements of ≈5mm were recorded at pit level (z = 0m) at the end of CLT1; see Figure 5-11. Note that residual displacements for pile AL1 (see Figure 5-10) were insignificant and therefore did not influence the initial *p-y* response for CLT2.

8.6.2 *p-y* Curves for Pile AL1

Soil failure at the end of CLT2 is clearly evident from the *p-y* curves shown in Figure 8-17, although no strain-softening/brittleness such as indicated on Figure 8-16 was observed. The large strains in the soil following yield obviously resulted in the rotation of the pin joint discussed in chapter 6. The marked difference in the stiffness and the resistances offered by the fill and the sleech is again apparent.

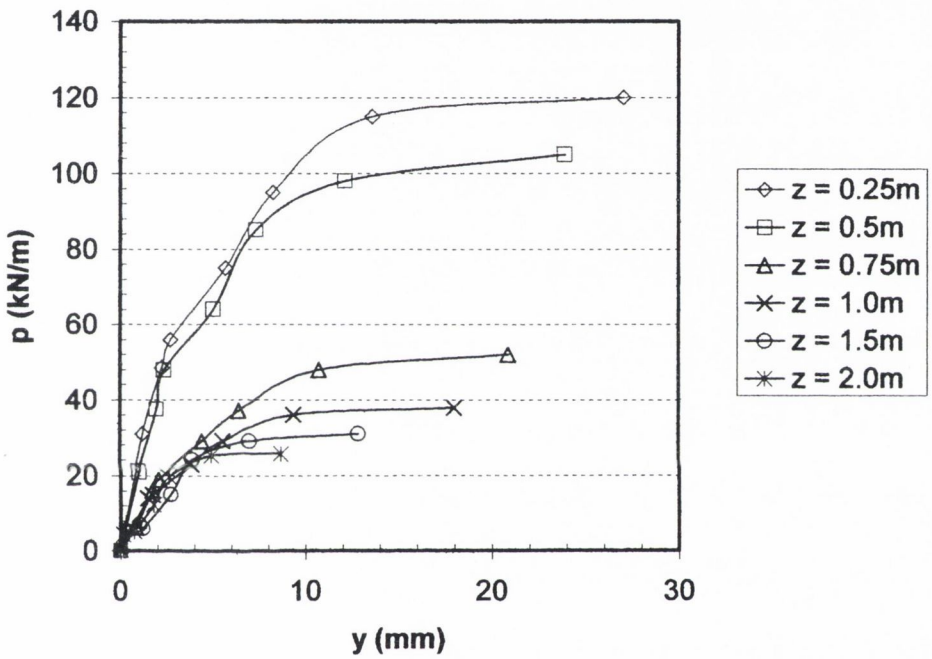

Figure 8-17: *p-y* curves for pile AL1 for CLT2

8.7 Difference in p-y Response between CLT1 and CLT2

Pile AL1

The initial *p-y* responses during CLT1 and CLT2 are compared in Figure 8-18. The curves illustrate that the initial stiffness of the re-load curves (i.e. measured during CLT2) is similar to that measured during first-time loading. The average modulus of subgrade reaction, K ($=p/y$) measured at a displacement of 2mm is $\approx$22MN/m^2 over the initial 0.5m. At the interface with the sandy sleech (z $\approx$0.75m), K (at y=2mm), is 8.7 MN/m^2 and at

z=1m is 7.5MN/m^2. This latter K value is somewhat larger than the K value of 4.5MN/m^2 inferred from cone pressuremeter tests[8] at approximately the same depth.

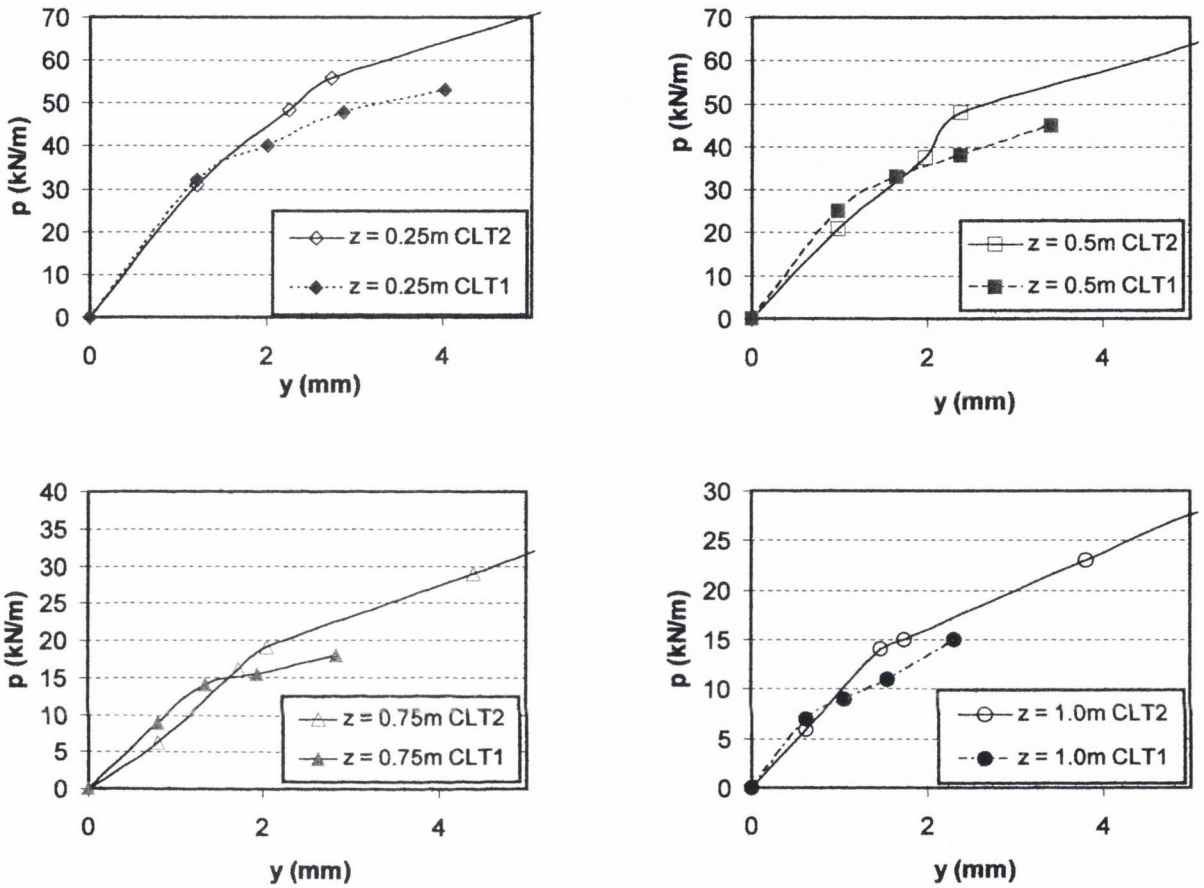

Figure 8-18: Comparison of *p-y* curves derived from CLT1 and CLT2 for pile AL1

Pile L1

The *p-y* curves inferred for the fill adjacent to pile L1 are summarised in Figure 8-19. The *p-y* response on re-loading (i.e. CLT2) is broadly similar to that measured during the initial test. However, the initial portion of the re-load *p-y* curve suggests that a gap or post-hole formed around the pile during CLT1 and extended to a depth greater than those presented in Figure 8-19. This is inferred from the less stiff initial response of the *p-y* curve for displacements up to the residual values measured at the end of CLT1 (see Figure 5-11).

[8] See Figure 8-20 for CPM test at 2.6m bgl.

The coefficient of subgrade reaction, $K = p/y$, measured at a lateral displacement of 9mm (equivalent to 2.5% of the pile 'diameter') ranges from 4MN/m^2 at z = 0.2m to 9MN/m^2 at z = 0.6m before reducing to 6.6MN/m^2 at the interface with the soft sandy sleech (z =0.8m). The latter indicates that the test results were sensitive enough to detect the reduced stiffness of the sleech.

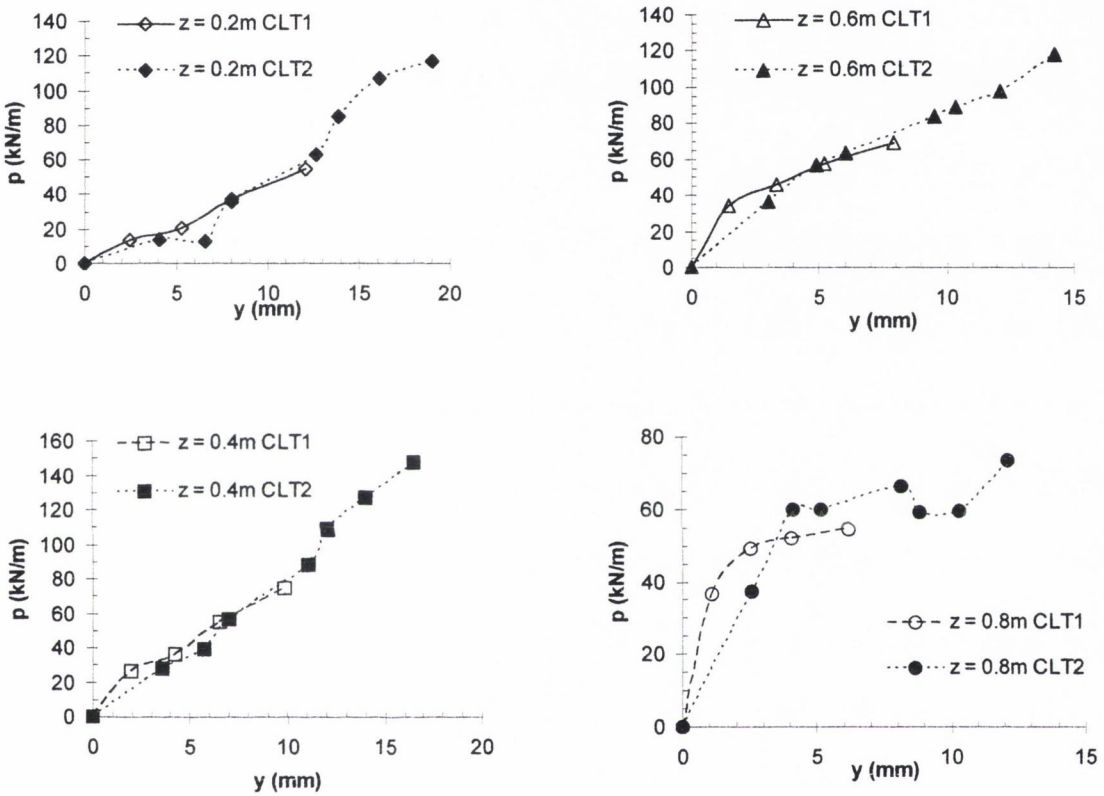

Figure 8-19: Comparison of *p-y* curves derived from CLT1 and CLT2 for pile L1

Once again, comparing the measured K in the sandy sleech (z = 0.8m) at a displacement of 2.5% the pile diameter with the K value determined from the cone pressuremeter test at the same displacement, 2.6m bgl (Figure 8-20), indicates that a lower K value (3.3MN/m^2) was recorded by the pressuremeter. Note that the locations of the pressuremeter tests are related to their depth below ground level (bgl) and the test at 2.6m bgl equates to z ≈ 1.35m at pile L1.

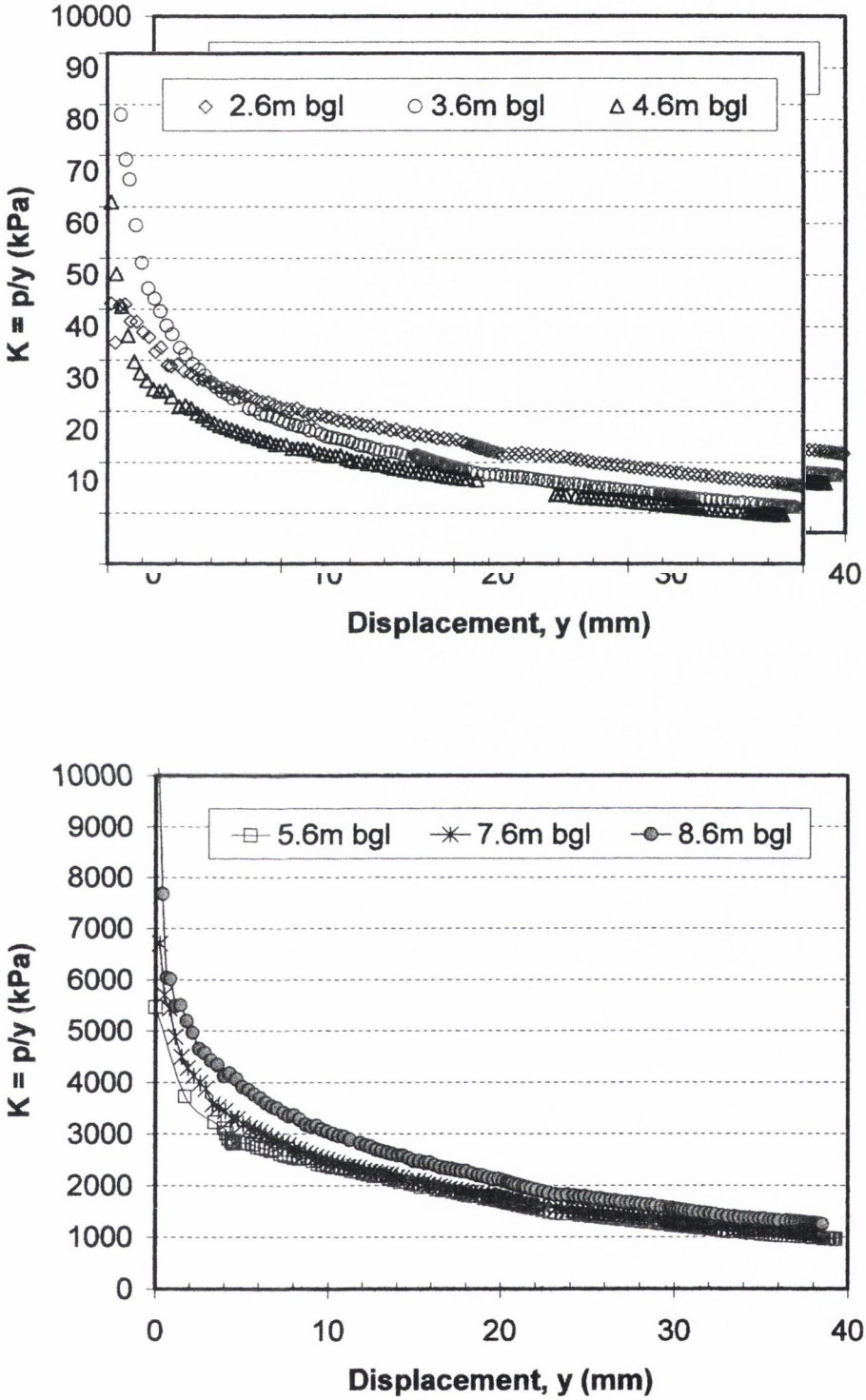

Figure 8-20: Variation in modulus of subgrade reaction, *K* with soil displacement from CPM tests

8.8 Interpretation of Re-tests on Piles Subjected to Lateral Load.

As outlined in chapter 5[9], the purpose of the re-test was to assess if a previously axially loaded pile (AL1) had caused an increase in the stiffness of the soil surrounding the pile. In addition the simultaneous re-testing of an adjacent pile (that was previously unloaded axially; pile L1) provided information on the effects of ageing (after initial loading) in the soil.

Strain gauge prediction of pile bending moment

Only the vibrating wire (VW) strain gauges on pile L1 were monitored during the Re-test. The VW gauges on AL1 were located 9.5m below ground level and therefore would not register measurable strain due to lateral loading above ground level. Of the four VW gauges in L1 only two of the gauges (located 0.375m and 3.625m below the applied load) continued to provide credible data. Therefore, the bending moment profile for pile L1 could not be interpreted on the basis of two VW strain gauge measurements. Nevertheless, the moments[10] at the VW gauges along with the free moments above pit level are compared with the results from the earlier tests in Figure 8-21. The results indicate bending moments consistent with the measurements recorded during CLT1 and CLT2 at the same load level. The slightly larger bending moments registered for the re-test reflect the application of the lateral load at the higher level than in the initial tests. The resistance to load and measured moments indicate that a plastic hinge had not developed as a result of the initial tests

[9] The reader is reminded that only load and displacement instruments (along with a limited number of vibrating wire gauges on pile L1) were monitored during the re-test.

[10] The bending moments at the VW strain gauge locations were inferred from the M-ε relationship in chapter 6.

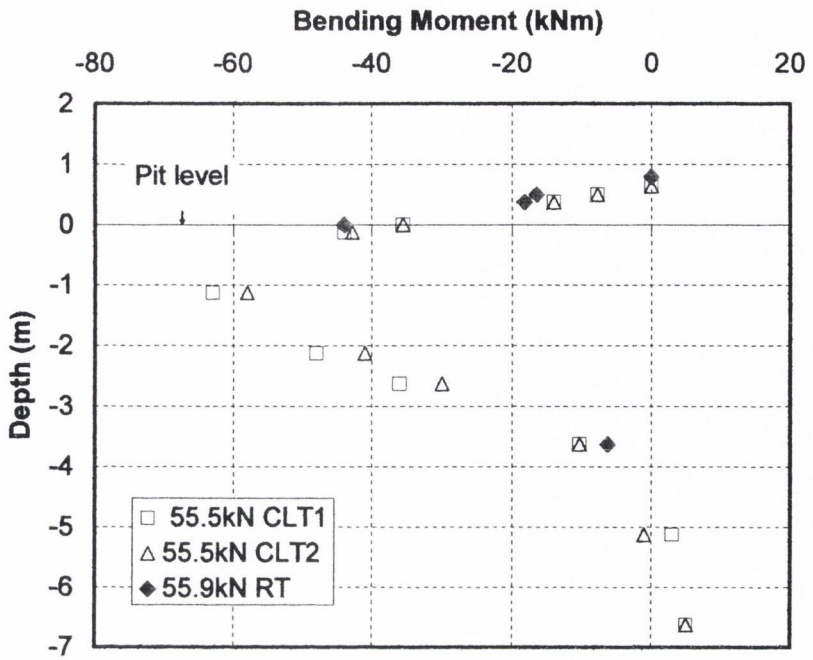

Figure 8-21: Bending moments in pile L1 compared for the three load tests

Figure 8-22 to Figure 8-25 summarise the slopes, displacements and bending moment measurements for the RT.

8.8.1 Findings from the Re-Test

The additional lateral load test provided information that assisted the interpretation of the results from the initial load tests. The results confirmed the bearing capacity failure in the soil around pile AL1. The results also provided information on the influence of an axial load on the lateral performance of a pile (AL1) and an opportunity to assess the effects of ageing[11] in the soil around a previously loaded pile (L1). The main findings of the test are summarised in the following comments:

- The presence of the axial load on pile AL1 did not significantly influence the lateral resistance of the soil. The reason for this may be explained by considering the zone of influence created when a pile is loaded vertically and laterally. Gabr et

[11] According to Atkinson (1993), the principal processes of ageing are compacting, creep, cementing, weathering and changes in the salinity of the pore water.

al. (1994) suggested the zone of influence during lateral loading was about 3 pile diameters based on a study by Price and Wardle (1979) of soil movements around a laterally loaded pile. Contrast this with Burland's (1973) finding that under axial loading, only a narrow zone beyond the soil-pile interface is mobilised in shaft friction. Therefore, any increase in soil stiffness due to an axial load would not significantly influence the far field stiffness of the much larger volume of soil stressed under lateral load particularly within the critical depth.

- The lateral load-pile head displacement response and the displacement profiles for the re-loading of pile L1 revealed that there had been no significant gain in soil strength due to ageing in the intervening nineteen month period since the initial load tests.

- The load-displacement behaviour of pile AL1 shows a flexible response with large plastic strains remaining after unloading. Pre-existing failure planes formed near the ground surface during the initial CLT programme may have contributed to this response. The more elastic response observed for pile L1 indicates that the bearing capacity of the soil had not been exceeded during the initial test programme.

- The displacement profiles for both piles (Figure 8-23) show that the lateral resistance to pile movement is provided by the soil in top 2.6m or ≈7.5 pile diameters below the pit level. This is in keeping with the commonly quoted values of 6 - 10 pile diameters (Dyson and Randolph, 2001; Tomlinson, 1994; Davisson and Gill, 1963 and others).

- The bending moment profiles shown in Figure 8-24 and Figure 8-25 for pile L1 and AL1 respectively are considered reasonable given the difficulty encountered in maintaining the load at the jack.

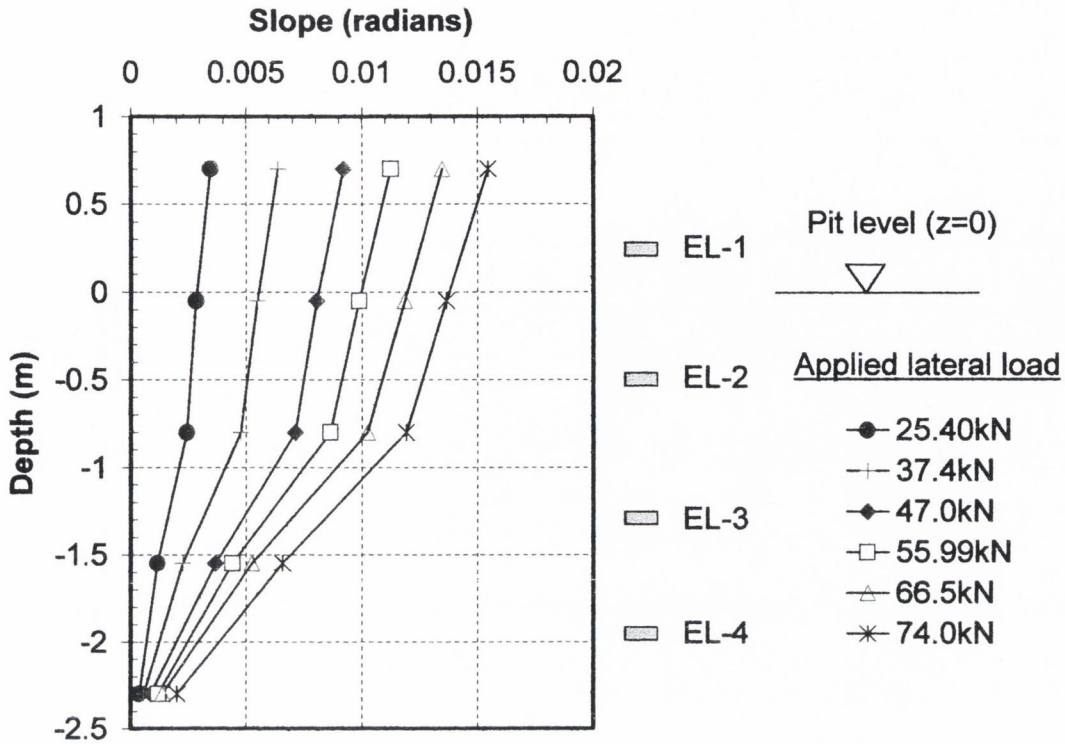

(a) Pile L1

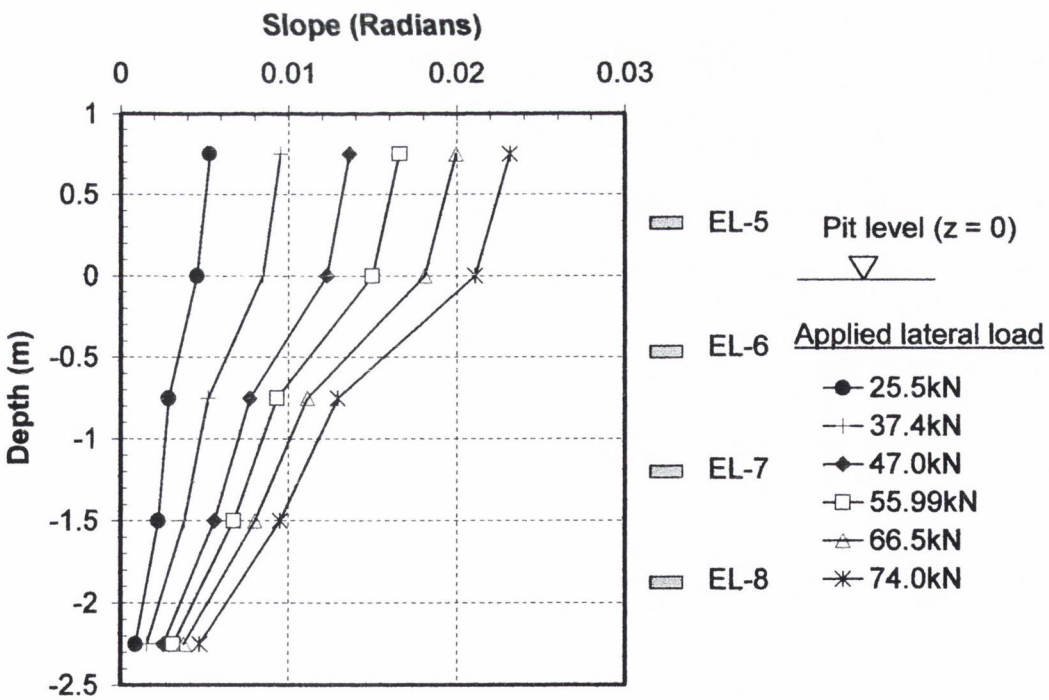

(b) Pile AL1

Figure 8-22: Slope profiles measured during Re-Test

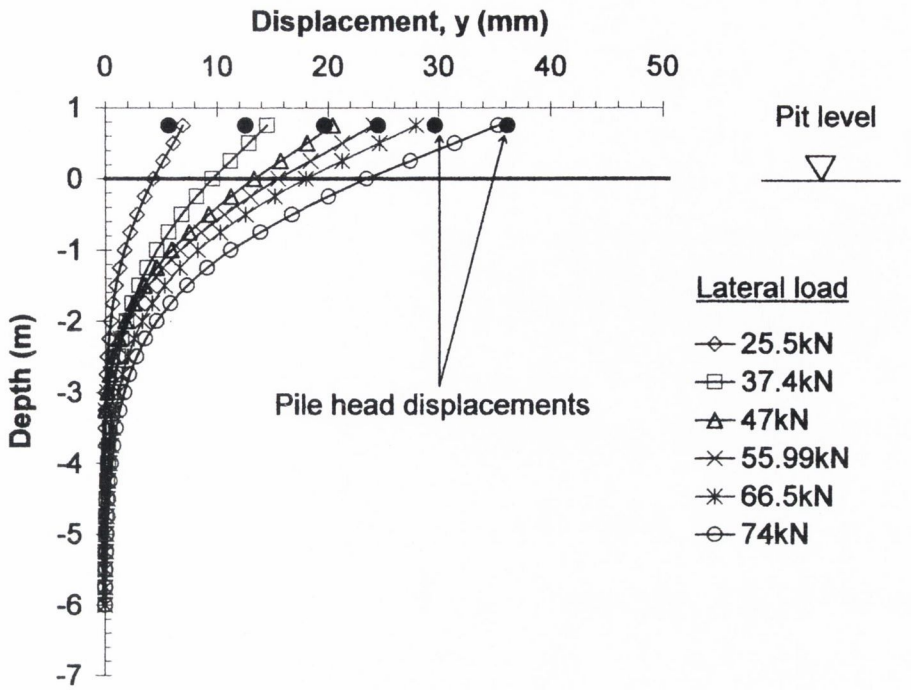

(a) Pile L1

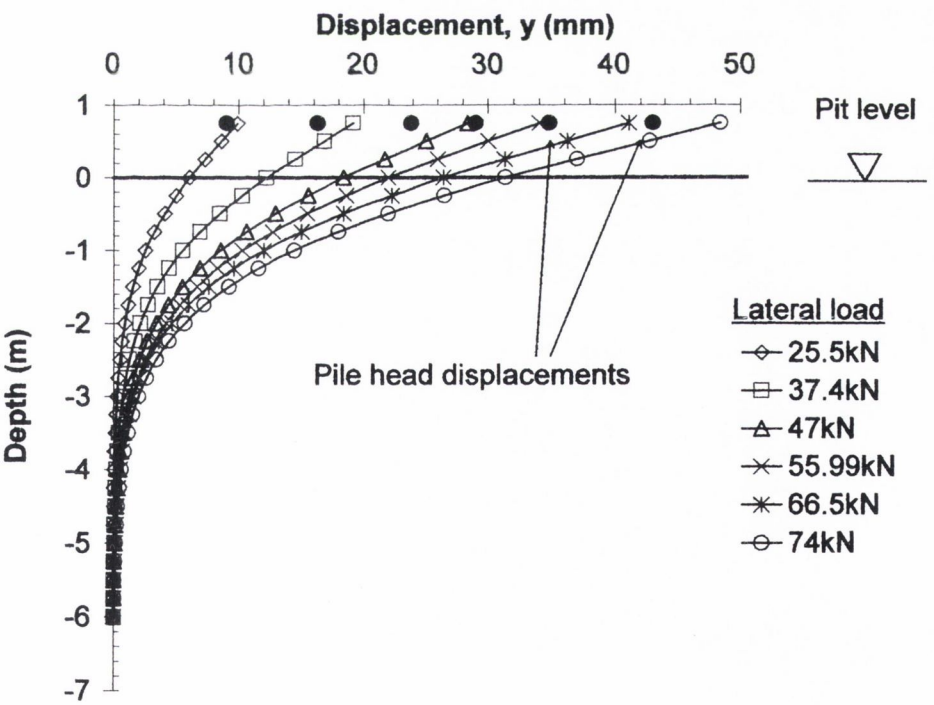

(b) Pile AL1

Figure 8-23: Displacement profiles for RT compared with measured pile head movement

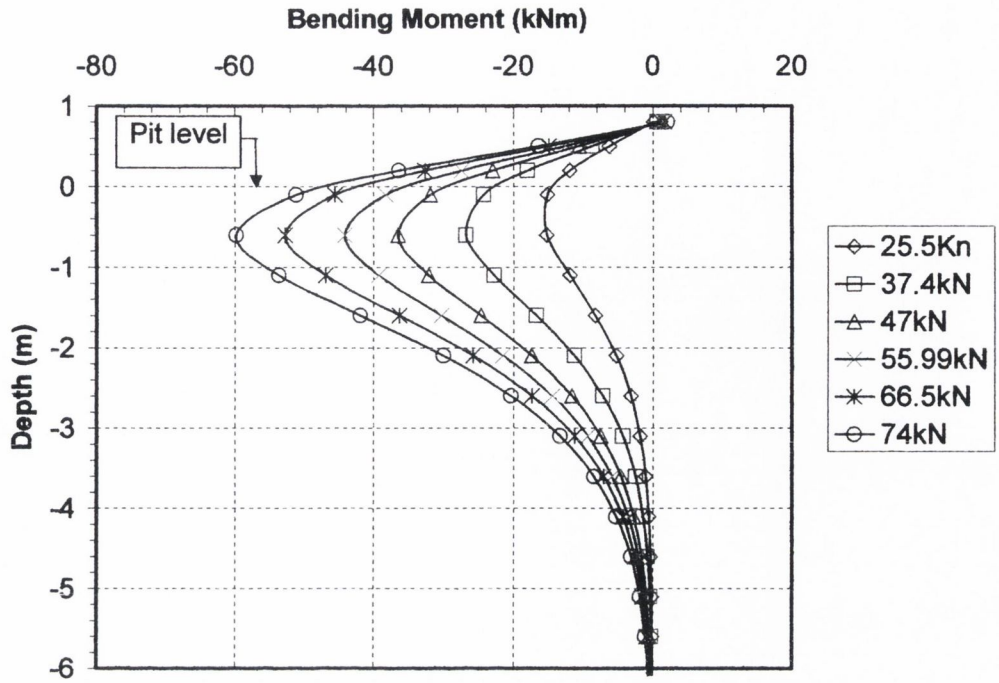

Figure 8-24: Moment profiles for L1 back calculated from EL data

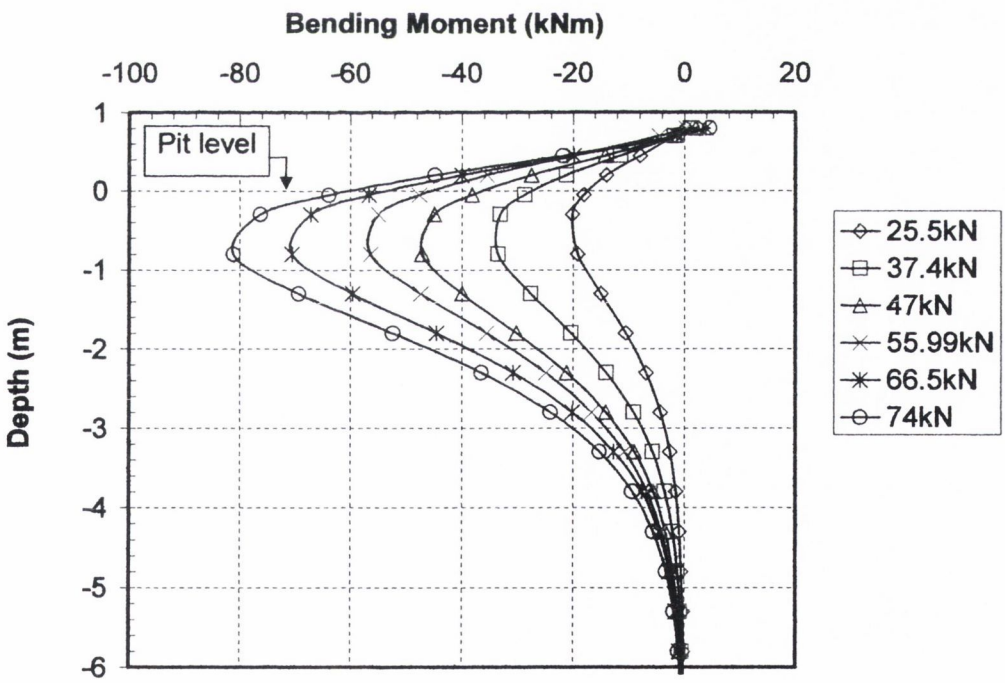

Figure 8-25: Moment profiles for AL1 back calculated from EL data

Chapter 9

Discussion of Research Findings

9. DISCUSSION OF RESEARCH FINDINGS

9.1 Introduction

The instrumented pile load tests in Belfast were performed in what can, most simply, be described, as a layered stratigraphy. To assist a more general interpretation of these tests and of the lateral load tests performed in Coolock (Chapter 7), this chapter initially presents the following:

(i) the results from a 2-D (plane strain) finite element analysis for a laterally loaded pile wall in a layered medium (stiff overlying soft)

(ii) an investigation of the applicability of the *p-y* approach for laterally loaded piles in an elastic soil (using integrated forms of Mindlin's equations; see *OASYS* Geotechnical Programs Manual, Ove Arup & Partners, 1997).

(iii) the results from pile lateral load tests conducted in a fixed beam centrifuge performed at the University of Western Australia. These tests were commissioned directly by the author and Trinity College Dublin to investigate the influence of a pile axial load on its response to lateral load.

(iv) a parametric study into the sensitivity of pile bending moments and displacement on specified *p-y* curves

These four components of investigation allow some general conclusions to be made regarding the *p-y* method of analysis and its applicability to the two test sites in Belfast and

Coolock. Subsequently, the usefulness of the Cone Penetration Test (CPT) and the Cone Pressuremeter (CPM) in facilitating the prediction of pile lateral response is assessed using the results from the pile tests conducted in Belfast. These tests are also used to allow a discussion of the combined effects of preloading and ageing on lateral pile stiffness and capacity.

The final section of this Chapter is devoted to a discussion of the two aspects that are at the core this research and have a important practical significance; i.e. influence of (i) pile head condition, and (ii) axial load on the soil response provided to a laterally loaded pile.

9.2 FE Analysis of p-y Response in a Layered Soil

This section examines the effect of a stiff layer near the ground surface on the inferred *p-y* response in the sleech by presenting the results from Finite Element (FE) analyses of a laterally loaded wall in stratigraphy matching that at Kinnegar. The analyses presented in Section 9.3 indicate that there are significant interaction effects between 'spring locations' if the pile breadth (diameter) is large and hence it may be concluded that such interaction effects will be exaggerated significantly in the analyses presented here[1].

The FE mesh had a grid of quadrilateral elements extending 12.65m on the active side of the pile and 21m on the passive side with the 'pile wall' fully embedded in the (10m) layered stratigraphy. The elements were concentrated in a narrow band over the top two metres on either side of the pile. The size and spacing of the elements were subsequently increased at distances remote from the pile (≈4m on either side of the pile) and full restraint was provided along the bottom and side boundaries of the FE grid.

Two drained FE analyses (analysis I and II) were performed; analysis I involved an initial strata comprising a 9m uniform soft clay modelled as an elastic perfectly plastic material with c_u = 10kPa, ϕ = 0°, E = 4000kPa and Poisson ratio ν = 0.2. The second strata represented a medium dense sand layer between 9m and 10m, and was modelled as a linear elastic material with E = 20MPa and ν = 0.2. The pile wall, which was incrementally

[1] Unfortunately, the author did not have access to a 3D soil FE program.

loaded via a transverse pressure (shear) applied at ground level, was also modelled as a linear elastic beam (with an elastic stiffness E_{pile} = 30000MPa and ν =0.2).

Analysis II was similar to Analysis I, the only difference being the incorporation of a stiff layer between 0.5m and 1.5m to simulate the conditions encountered at Kinnegar[2]. The stiff layer, modelled as an elastic perfectly plastic soil, was divided into two 0.5m sublayers having the following properties; c_u = 50kPa, ϕ = 0°, E = 20000kPa and ν = 0.2. The remaining stratigraphy and pile properties were identical to those in the first analysis. The result for one of the load increments is shown in the form of a partial deformed mesh in Figure 9-1.

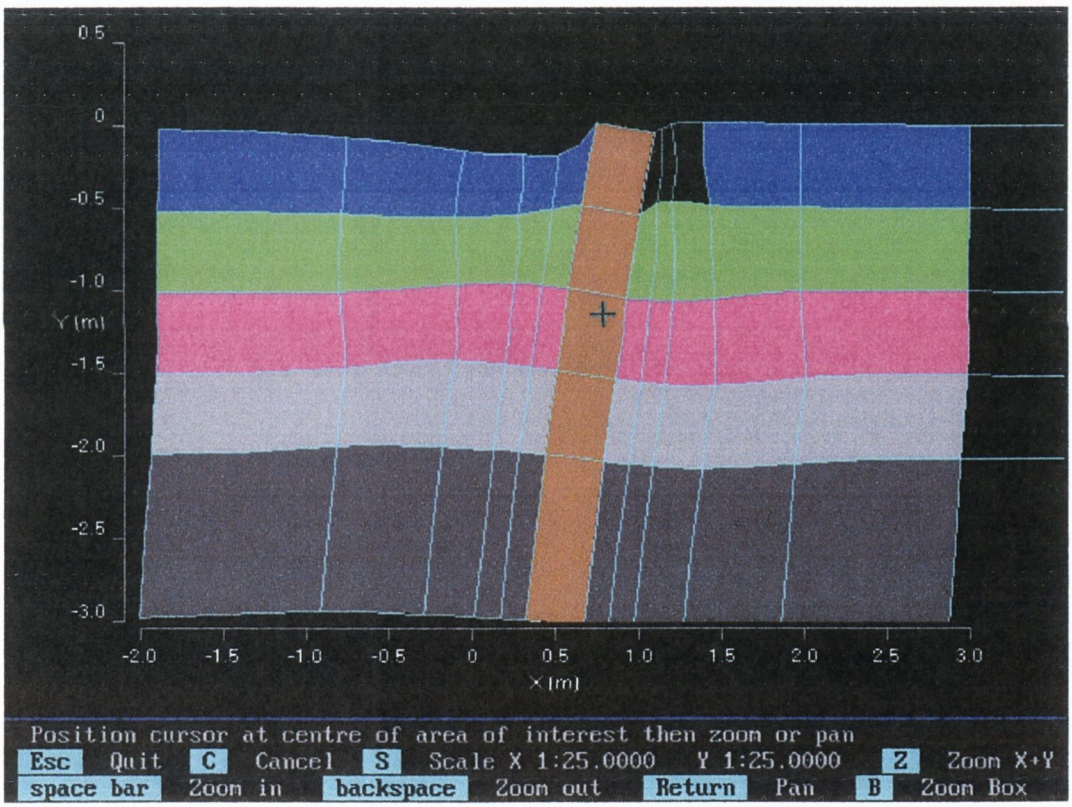

Figure 9-1: Typical deformed mesh

The pressure-lateral displacement response at 1.75m depth is presented on Figure 9-2 for Analysis I and II. Clearly, a dramatically different relationship is obtained in each case, despite the fact that the analyses adopted the same soil properties at 1.75m. It is evident

[2] The initial 0.5m depth on the passive side represented the pit excavated in front of the pile and was modelled as a void in the FE analysis.

that, at a given pile displacement, the higher stresses generated near the surface in the case of the stiff layer induce larger displacements at depth and lead to an *apparently* softer pressure-displacement response for the soil layer at 1.75m i.e. displacements occur at this level that are not associated with the specific lateral stress at this level. The effects of interaction between the various layers of soil are also evident in this figure where, in Analysis I, the spring stiffness (*p/y* or *P/y*) at 20mm movement is only 15% of what might be expected on the basis of the Young's modulus (E=4000 kPa) at this level; the corresponding percentage for Analysis II is just 2.5%.

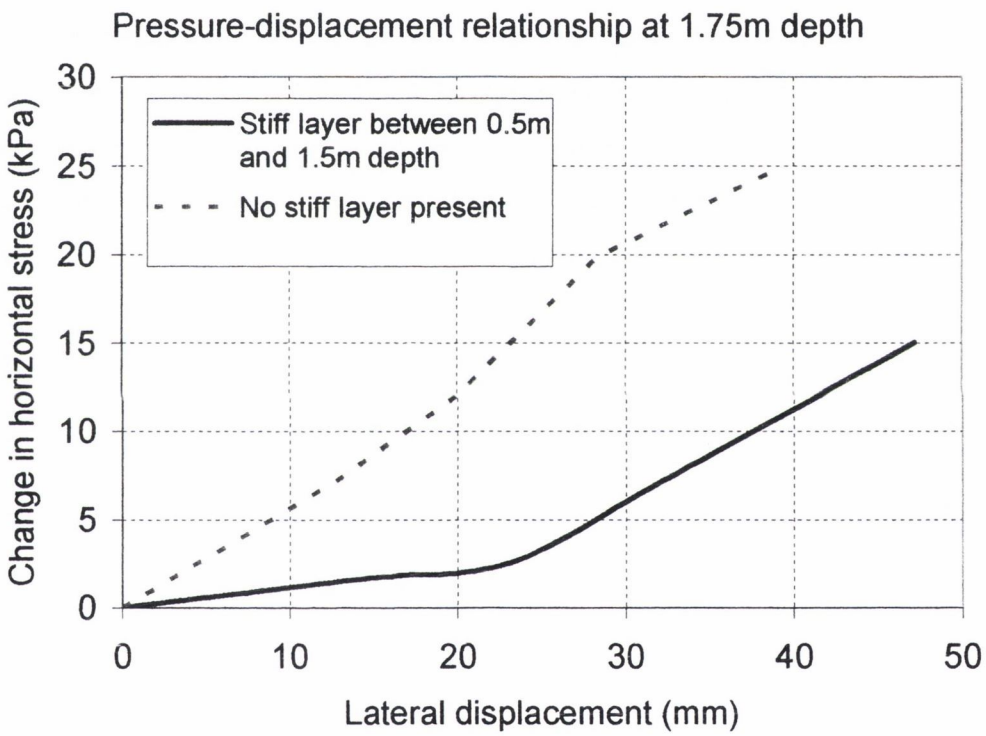

Figure 9-2: Pressure-lateral displacement curves for Analysis I (stiff layer between 0.5m and 1.5m) and Analysis II (no stiff layer)

It would therefore appear that the effect of a stiff layer at shallow depth is such that the stiffness of the *p-y* curves inferred for the sleech will be smaller and possibly significantly smaller than the true stiffness. Evidence for this effect is examined later in this chapter, which also has implications for the modelling assumptions made in the foregoing.

9.3 Influence of Pile Width on p-y Interaction

To examine the applicability of the *p-y* approach for piles, a series of analyses were performed using the OASYS MINLIN program. This program provides solutions for integrated forms of Mindlin's equations and was used to calculate the distribution of lateral displacements induced in an elastic half space due to the application of a lateral stress on a vertically orientated area (of depth D and breadth B).

Figure 9-3 shows the variation in displacement induced in the soil by varying the breadth (B) of the loaded area. It can be seen that, even for small loaded areas, measurable displacements are induced remote from the loaded area e.g. in the case of B = 0.3m normalised displacements (y/y_{max}) of 0.05 were measured at a distances of 2m on either side of the centroid of the loaded area. The movement becomes significant when the width of the loaded area is large as shown by the distribution for B = 3.0m, which gave y/y_{max} = 0.2 at 2m from the centroid. Lower movements may be expected remote from a loaded area in practice because of the non-linearity of soil stiffness.

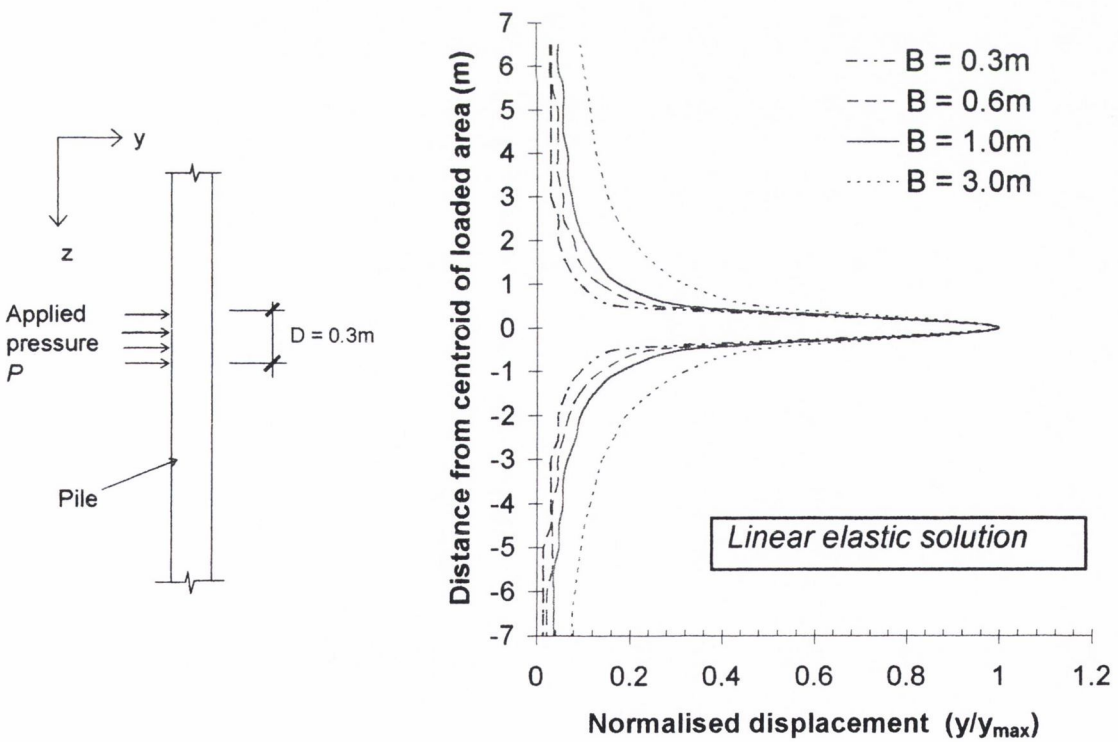

Figure 9-3: Influence of pile width on soil displacement

The implications of the foregoing for a laterally loaded pile are shown in Figure 9-4. The elastic soil model demonstrates the interaction that occurs between two loaded squares (B = D = 0.3m) separated by a distance of 2.0m. The three loading scenarios illustrated in the figure are; the influence of a singly loaded area compared with that of a second area subjected to the same pressure (P). These profiles are contrasted with two loaded areas but with the area closer to ground level being subjected to a greater pressure[3] (2P) than the lower area (P). The effect of the overlapping displacements on the soil movement remote from the 'springs' is evident. Hence, for *p-y* curves specified at relatively close spacing (0.3m being typical in the region of 6 to 10 pile diameters below ground level) the effect on soil displacement would be even more pronounced in this analysis. However, the non-linearity of real soils, while leading to higher displacements at the point of load application would result in a much reduced displacement remote from the load and this is the fundamental justification for the *p-y* method of analysis.

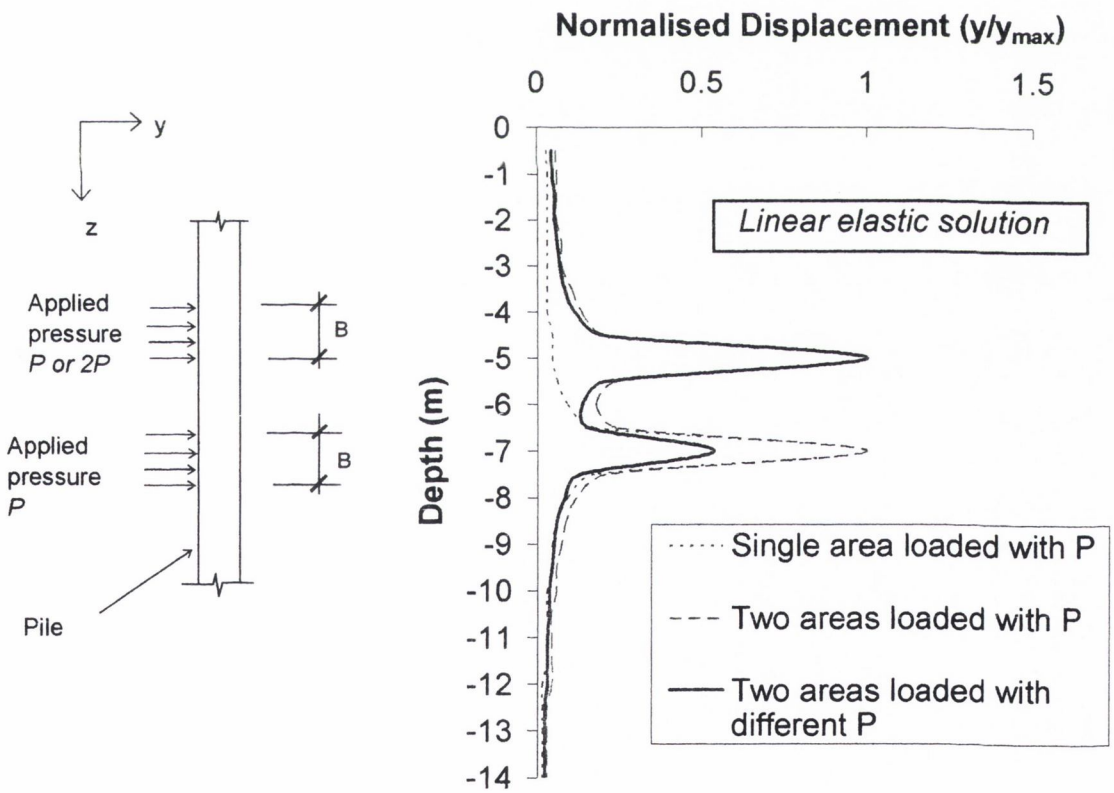

Figure 9-4: Interaction between loaded squares (B x B) in an elastic medium

[3] In keeping with a laterally loaded pile problem

Combining the findings of this Section and the analysis of the laterally loaded pile wall in Section 9.2, it is evident that the relatively small width of a pile compared to a wall provides the justification for the use of the *p-y* approach for piles. Moreover, given that the non-linearity of soil stiffness will lead to lower displacements remote from the loaded area, the *p-y* approach may be expected to lead to reasonable predictions in the absence of more sophisticated 3-D Finite Element analyses incorporating realistic constitutive models for the soils (including soil stiffness non-linearity). Evidence in support of the use of the *p-y* approach is provided in various ways throughout the remainder of this chapter.

9.3.1 Implications of pile width for the analysis of laterally loaded piles

The *p-y* approach for laterally loaded piles implicitly assumes that the application of a unit pressure (P) to a given soil gives rise to a displacement (y) that is in proportion to the width of the loaded area i.e. the pile width B. Such an assumption follows on directly from solutions for 'elastic' soil, e.g.

$$y = \frac{I_f P B (1-\nu^2)}{E} \qquad (1)$$

or

$$\frac{p}{y} = K = \frac{E}{[(1-\nu^2) I_f]} \qquad (2)$$

Soil is not, however, linear elastic and as such many researchers (e.g. Burland & Burbidge 1985) have noted that the drained displacement (y) varies approximately with the foundation width (B) raised to a power of between 0.5 and 0.8, with 0.7 being a typical average. All other things being equal, it follows that there is a width dependency of the coefficient of subgrade reaction (K) and that it varies approximately with $B^{0.3}$. It is therefore apparent that the *p-y* curves derived for the near surface Belfast soils with B=0.35m would need to be stiffened by a factor of ≈1.56 if they were to be applied to a prediction for a pile with B=1.5m. Although such an observation requires thorough

corroboration through experimentation, evidence in its support was observed by the author when examining *p-y* curves derived for 1.5m diameter bored piles in Bangkok clay (Ove Arup & Partners, 1993). The stiffness of these *p-y* curves was almost double those expected on the basis of API recommendations. The effect of pile width should also clearly be considered when transforming CPM data to equivalent *p-y* data for use in predictions.

9.4 Centrifuge Tests on a Model Pile Subjected to Combined Load

To investigate the effect of an axial load on the *p-y* response of the soil, at the request of the author and Trinity College Dublin, Shim (2000) conducted lateral load tests on axially loaded piles at 100g in the fixed beam centrifuge at the University of Western Australia. 13mm diameter (d), 340mm long closed ended steel piles (≡prototype dimensions of 1.3m diameter and 34m length) were jacked (at 1g) into very fine silica sand with a uniform relative density (D_r) of 60%. A steel cube, of side width ≈40mm (≡prototype weight of 47 kN) was then positioned at the head of the pile before increasing the acceleration of the strongbox to 100g and subsequent application of a lateral load. Another identical test was performed without the steel cube in position i.e. with no axial pile load present. Strain gauges positioned at close centres along the pile were used to deduce bending moments from which *p-y* curves (or pressure vs. y/d curves) were derived. It should be noted that centrifuge modelling involves its own rigor which has not been discussed in this thesis. Instead the results of centrifuge tests on model piles subjected to combined lateral and axial loading are presented to complement the findings of the full scale combined load tests reported in chapter 8.

The pile head load-displacement variation with and without the axial load present is shown on Figure 9-5. It is clear that, even from the earliest stages of loading, the pile with no axial load exhibits a response which is ≈20% stiffer then that of the pile with an axial load. This difference is also evident in the $P/\gamma' d$ vs. y/d curves in Figure 9-6 (where γ'= effective unit weight). The highest discrepancies between the responses arise at shallow depths i.e. $z \leq 2d$ where d is the pile diameter. The reduced stiffness exhibited by the pile under axial

load probably reflects an increase in displacement due to the eccentricity of the axial load created by lateral loading.

Although the axial load of 47 kN was a small proportion of the full shaft capacity of the piles used by Shim (2000), the relatively low CPT q_c values at shallow depths in the centrifuge, which increase from zero at z=0 to 5000 kPa at z=4d, as shown in Figure 9-7, are such that one may expect that this load would lead to the mobilisation of a significant proportion of the limiting pile skin friction at these depths. As such, one might also expect that dilation of the sand at the pile interface would lead to higher radial stresses on the pile and therefore a higher lateral stiffness. Such a phenomenon is clearly not evident from Figure 9-5 or Figure 9-6 and it may be concluded that the presence of an axial load is very unlikely to lead to a higher lateral soil stiffness.

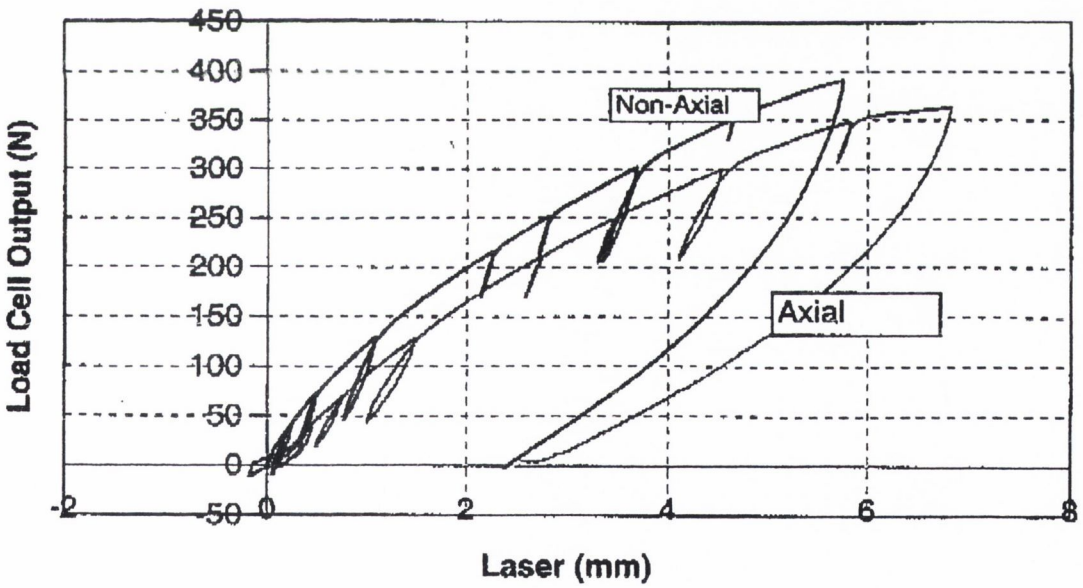

Figure 9-5: Pile head load-displacement response for laterally loaded model piles with and without axial load (Shim 2000).

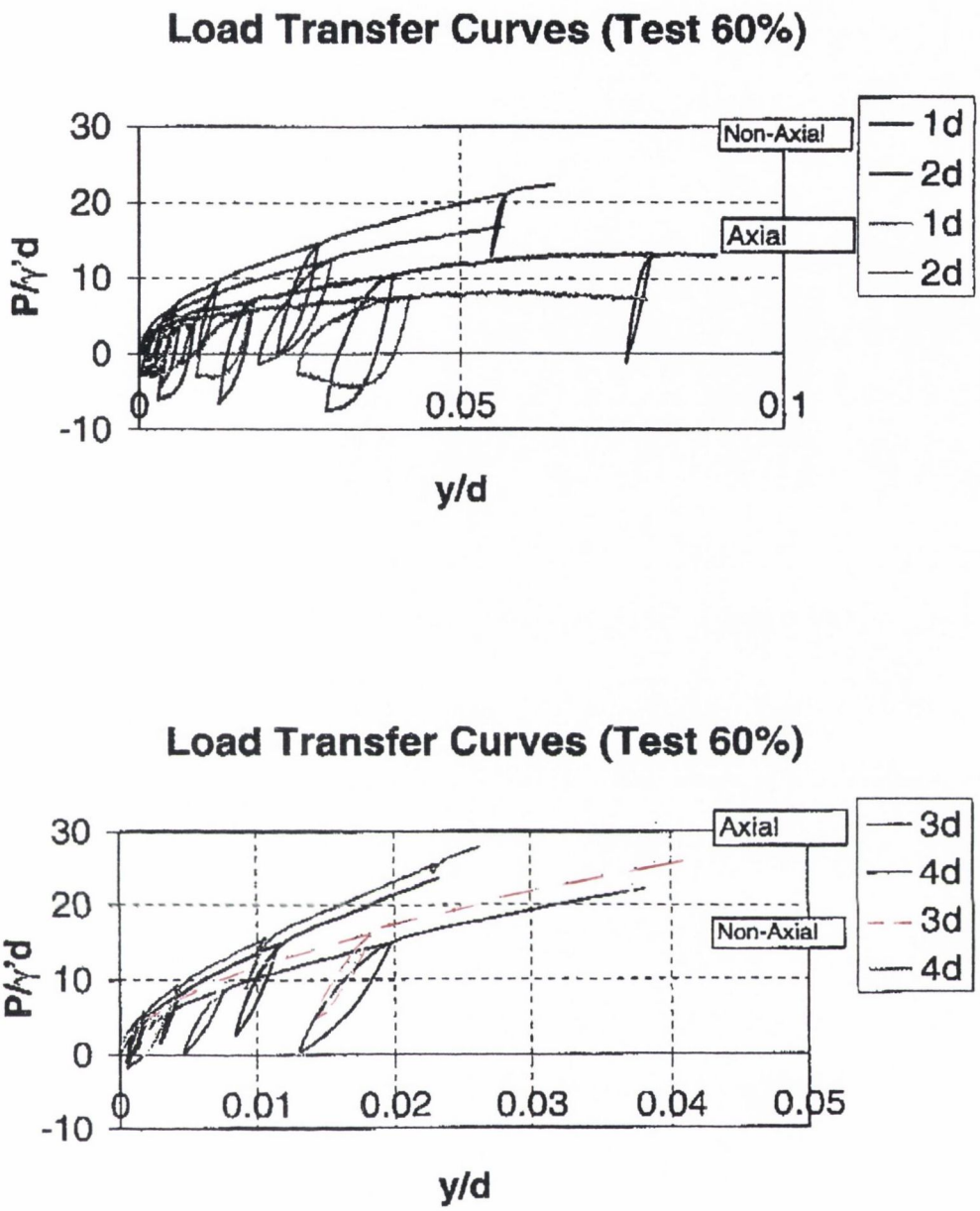

Figure 9-6: Comparison of P/γ'd vs. y/d curves for axial and non-axially loaded pile (from Shim, 2000)

CPT 1

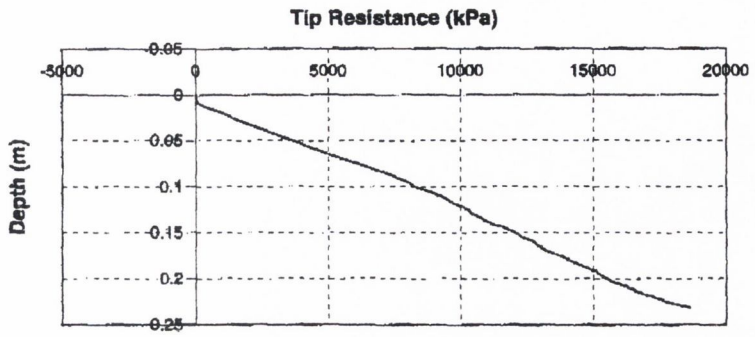

CPT 2

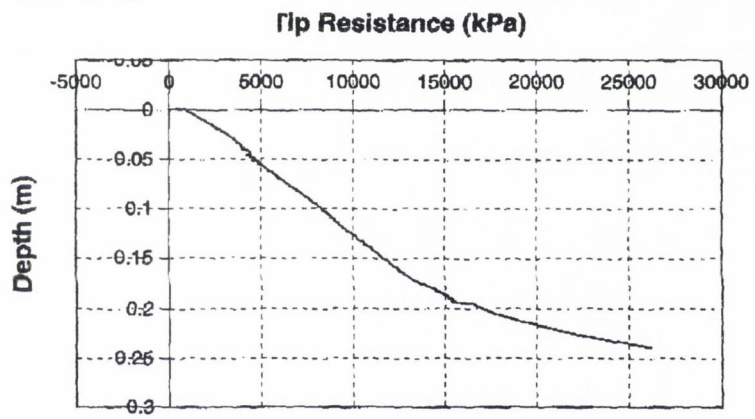

Figure 9-7: CPT results from fine silica sand (with a D_r of 60%) surrounding the pile.

9.5 Parametric Study to Assess the Sensitivity of the Pile Response to Variations in Soil Properties

To further investigate characteristics of the *p-y* approach, a parametric study was undertaken using the OASYS ALP program to assess the sensitivity of predictions of a laterally loaded pile in a layered stratigraphy. The initial *p-y* curves were generated using the soil properties reported in chapter 4 and the generic *p-y* criteria for sand and soft clay specified in API (1993).

9.5.1 Sensitivity of Pile Response to Variations of the Soil Properties within the Critical Depth

The sensitivity of a laterally loaded pile response to minor variations in the soil properties in the top five pile widths (i.e. 5B) was examined using ALP. A pile, given the same properties as the test pile, was embedded 9.6m in a stratigraphy matching that at Kinnegar. The following properties were specified; the upper layer between 0.0m and 1.5m was represented by a dense sand having the following properties; unit weight γ = 19kN/m^3, angle of friction ϕ' = 36°, the initial soil subgrade reaction coefficient k_i = 25MN/m^3 and the coefficient of earth pressure at rest K_0 = 0.5. This was followed by 7.6m of soft clay before being seated 0.5m into a medium dense sand.

In this analysis the properties of the dense granular layer were varied as shown in the following table and the results are shown in Figure 9-8.

Dense Sand Parameter	Variation	Depth
Angle of friction, ϕ'	36° ± 5°	0.0m – 1.5m
Initial coefficient of subgrade k (MN/m^3)	25 ± 10	

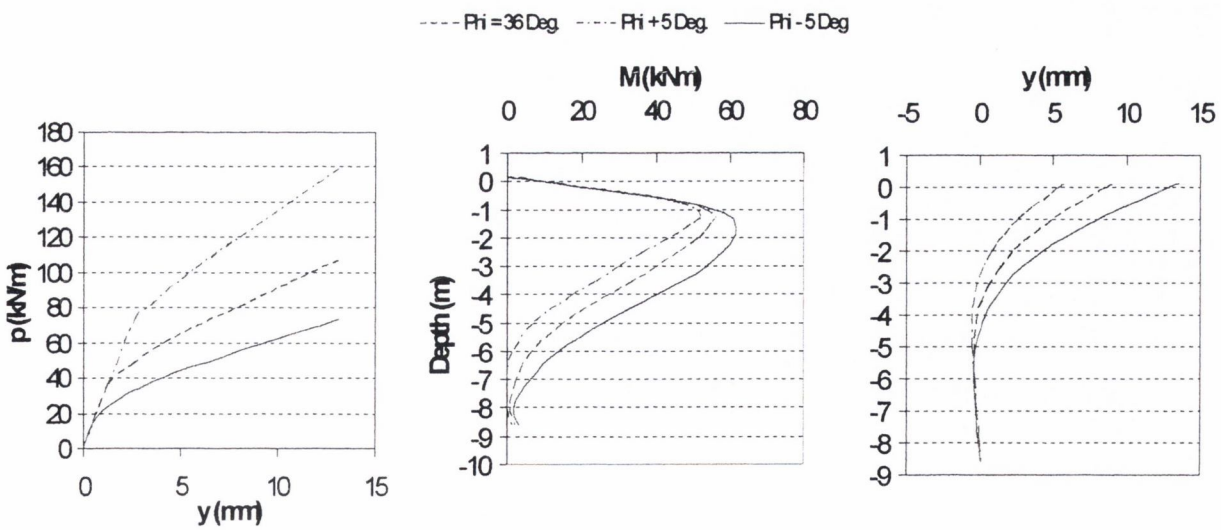

Figure 9-8: Response due to variations in ϕ'.

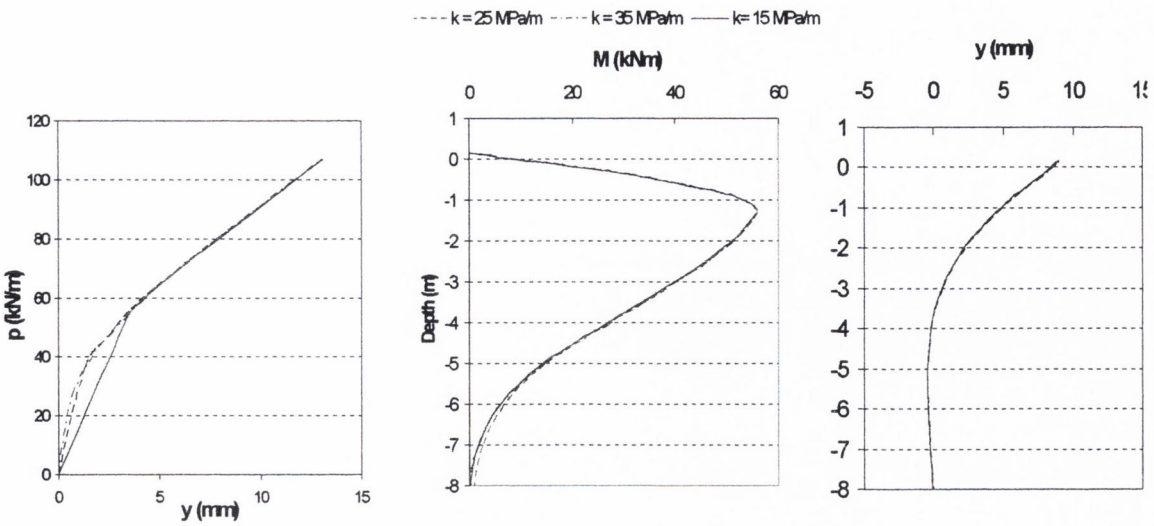

Figure 9-9: Variation in initial coefficient of subgrade (k) within the critical depth.

The foregoing analysis illustrates that variations in the properties of the near surface soils in a stratigraphy similar to Kinnegar can have a significant effect on the *p-y* response of the soil and hence the bending moment and displacement profiles. It is evident from Figure 9-9 that the pile behaviour is not very sensitive to the value selected for the initial coefficient of subgrade i.e. a variation of ±40% in this parameter resulted in no discernible difference in the displacement and moment profiles.

9.5.2 Effect of Varying Soil Properties within a Uniform and Layered Medium

Two ALP analyses were performed, which were similar to FE analyses carried out for a laterally loaded wall in Section 9.2. In both analyses the pile was assumed to behave elastically and given the same properties as the test pile. Analysis I adopted the same stratigraphy as that specified in section 9.5.1.

In Analysis II the same pile was embedded to a depth of 9.6m but on this occasion the initial 9.1m comprised a uniform soft clay that was underlain by a medium dense sand layer as in Analysis I. The purpose of Analysis II was to provide a means of judging the effect a 1m dense granular layer had on the lateral response of the pile. In these analyses, only the properties of the soft clay were varied as shown in the following table:

Soft Clay Parameter	Variation	Depth
Strain at half the maximum deviator stress, ε_{50}	0.03 ± 50%	1.5m – 3.5m
	0.01 ± 50%	3.5m – 7.6m
Undrained shear strength, c_u (kPa)	20 ± 50%	1.5m – 3.5m
	24 ± 50%	3.5m – 7.6m
Unit weight, γ (kN/m^3)	γ = 19± 2 kN/m^3	Sand
	γ = 16± 2 kN/m^3	Soft clay

While the ALP analyses does not account for interaction effects between different strata i.e. the *p-y* curves at the selected depth of 1.8m are the same in analysis I & II, the results for analysis I indicate the pile bending moment and displacement profiles are not particularly sensitive to variations in the *p-y* curves that result from a ±50% variation in c_u (Figure 9-10). However, Figure 9-11 reveals that notable differences exist in these profiles for a uniform soft clay deposit at the same depth.

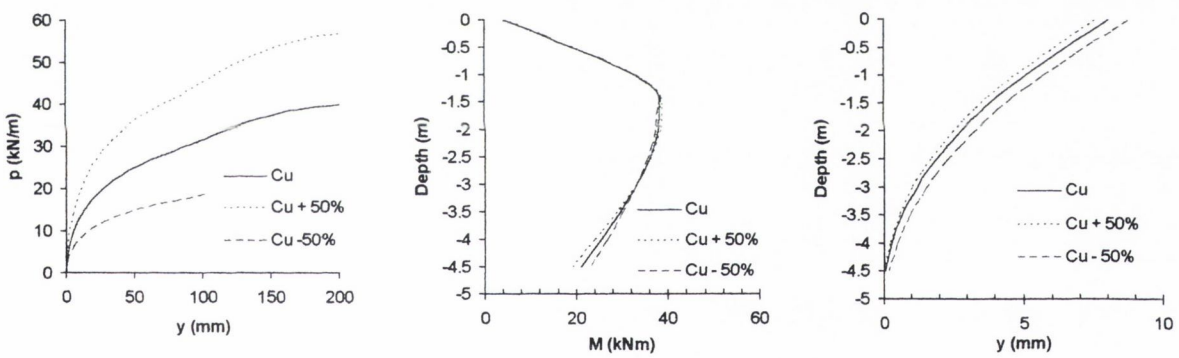

Figure 9-10: Effect of varying c_u in soft clay with an overlying stiff layer (Analysis I)

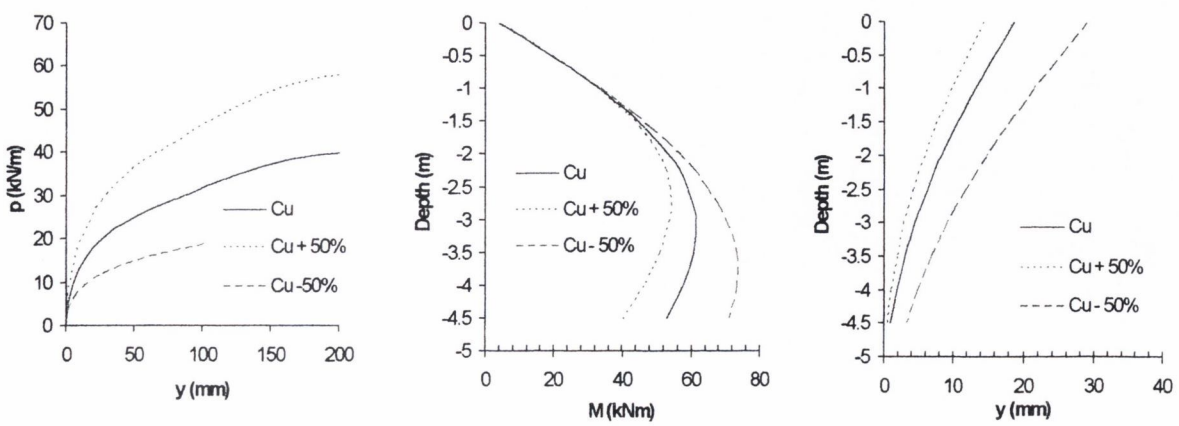

Figure 9-11: Effect of varying c_u in uniform soft clay (Analysis II)

A similar result can be gleaned from Figure 9-12 and Figure 9-13 for variations of ±50% on the reference strain, ε_{50}. The results for analysis I indicate that the displacement profiles are more sensitive than the bending moments to variations in c_u and ε_{50}. The variation in the unit weight γ does show some variation in the bending moment distribution (Figure 9-14) when a dense upper stratum is present but no apparent difference is evident in a uniform soft clay (Figure 9-15).

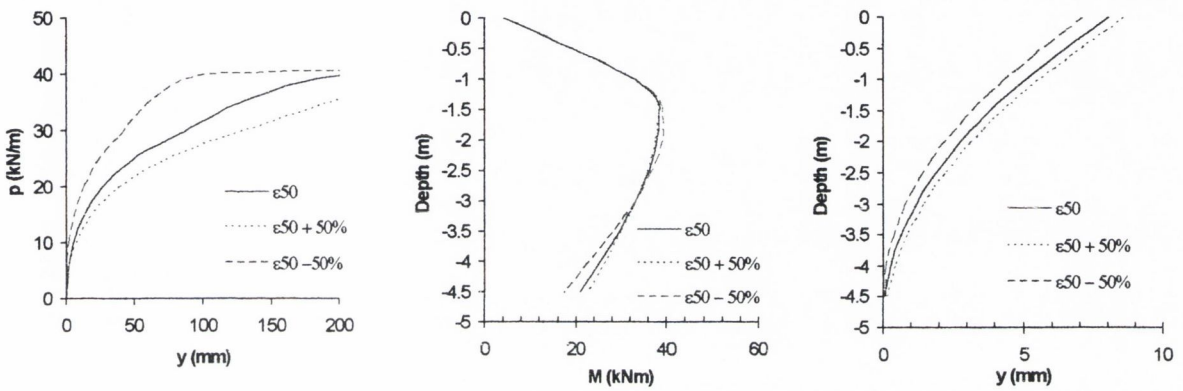

Figure 9-12: Effect of varying ε_{50} in soft clay with an overlying stiff layer (Analysis I)

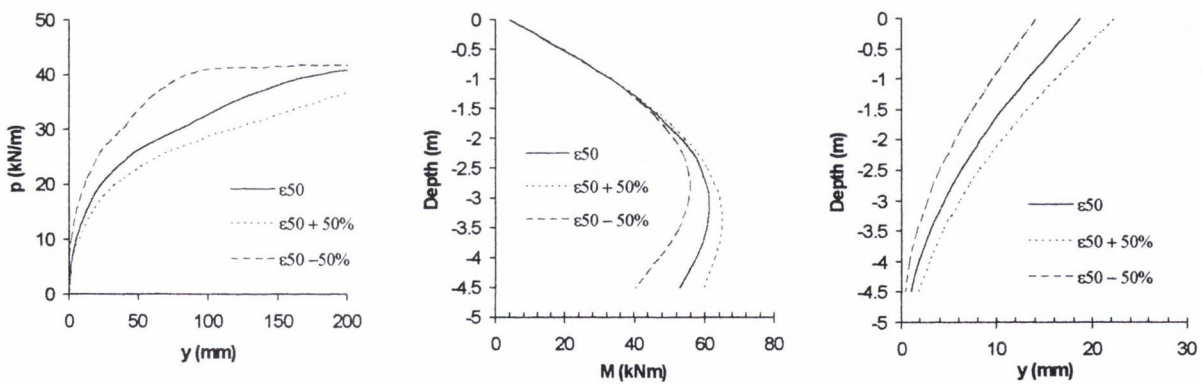

Figure 9-13: Effect of varying ε_{50} in soft uniform clay (Analysis II).

These analyses suggest that the pile response in a layered stratigraphy (similar to that described in chapter 4) is not particularly sensitive to different *p-y* responses generated by varying the soil properties in the soft clay. This confirms Bransby's (1999) finding that the *p-y* method is not particularly sensitive to the exact form of the *p-y* curves used in the

analysis. The results also illustrate the controlling influence that a relatively shallow dense stratum close to ground level exercises on the lateral pile response.

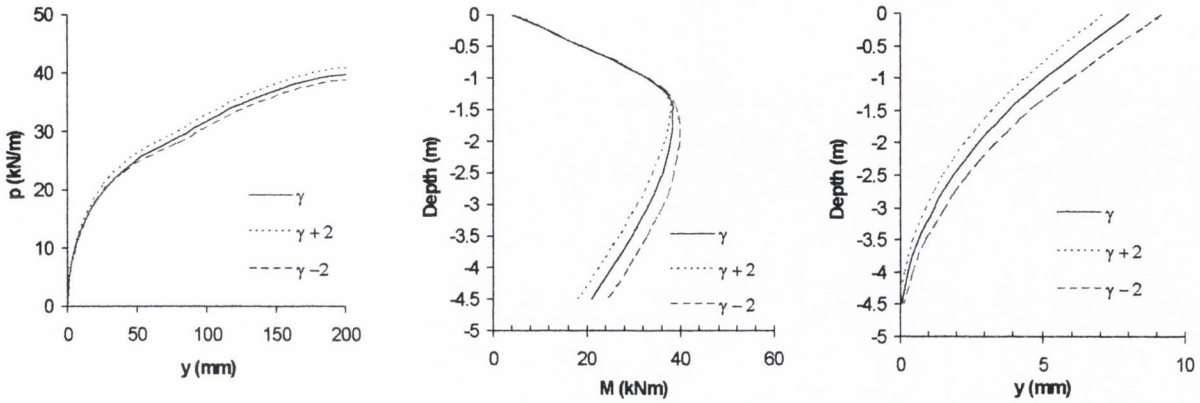

Figure 9-14: Effect of varying γ in soft clay with an overlying stiff layer (Analysis I).

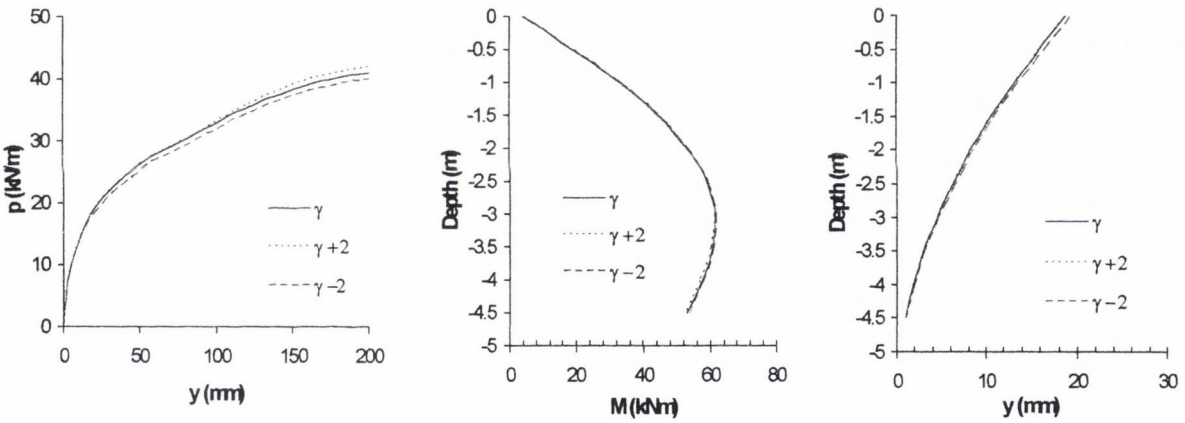

Figure 9-15: Effect of varying γ in uniform soft clay (Analysis II).

9.6 Measured Ultimate Lateral Resistance

The Kinnegar field tests were terminated following the failure of the soil around pile AL1. The layered stratigraphy and the unusual nature of the applied failure load to AL1 necessitated judgment in the application of existing methods for estimating the ultimate lateral resistance of the soil. Broms' (1964a and b) approach was utilised in chapter 5 to estimate the maximum lateral load to be applied during the load tests. The approach was performed assuming a cohesionless material with c'=0 & ϕ' = 38° and an undrained clay

with c_u = 20kPa to yield predicted lateral capacity values (P_u) of between 64kN and 84kN; these compare favourably with the measured failure load of 82kN. The Broms' approach also gave reasonable predictions for the ultimate resistance of piles in stiff Dublin boulder clay. A P_u value of 223kN was estimated (which represents a 3% over prediction of the failure load) based on (a pre-selected) representative average c_u value of 200kPa over the critical pile depth. Although alternative, slightly more complicated, methods for predicting P_u are discussed in Chapter 2 (e.g. Randolph and Houlsby (1984), Briaud (1997)); the tests presented in this thesis confirm the adequacy of Broms' approach.

9.7 Long-term Changes in Pile Lateral Response

The decision to retest the piles under pure horizontal loading nineteen months after the initial tests was twofold:

- Firstly, to assess if the stiffer response of pile AL1 observed during the initial combined loading was due to an increased soil stiffness created by shear stresses developed in response to the axial load. This will be discussed in section 9.12 and secondly,
- To assess the effects of soil ageing on the lateral response of a pile (L1)

In regard to the latter, Jardine et al. (1998) and Chow et al. (1998) have investigated effects of soil ageing on axially loaded open-ended steel piles installed in dense marine sands. The research found that shaft capacities increased by up to 85% over periods of six months to five years after the piles were initially load tested. The possible causes were investigated against a background of previous case histories, laboratory soil testing, pile corrosion and a new effective stress analysis procedure for piles proposed by Lehane and Jardine (1994). The effective stress analysis procedure was amended in Jardine and Overy (1996) to include a site specific correction factor to obtain good predictions for the pile capacity at the second test site involving dense North Sea sands.

The researchers concluded that the increase in capacity was attributed to the relaxation of circumferential arching mechanisms that developed during pile driving and which limited the radial stresses acting on the pile shaft. It was further concluded that creep led to the

breakdown of these arching stresses acting on the pile shaft and hence led to gains in shaft capacity. It was also suggested that micro-rearrangement of sand grains during creep may also result in stronger dilation effects during shearing, producing larger increases in radial stress during pile loading.

Re-testing the Belfast piles after a prolonged period of ageing revealed that no significant change in the lateral soil resistance took place. Both the pile head movement (Figure 5-18 is reproduced in Figure 9-16) and displacement profiles (Figure 5-21) indicate that the soil response to lateral load remained approximately constant after the nineteen month rest period. This result is not altogether surprising given the cohesionless nature of the near surface material. It is noteworthy that any post-holing that developed around the piles during the initial CLT series was absent and full contact between the soil and pile was reinstated over the 19 month rest period. Evidence of this is provided in the pile head load-displacement plot shown in Figure 9-16 and by field observation.

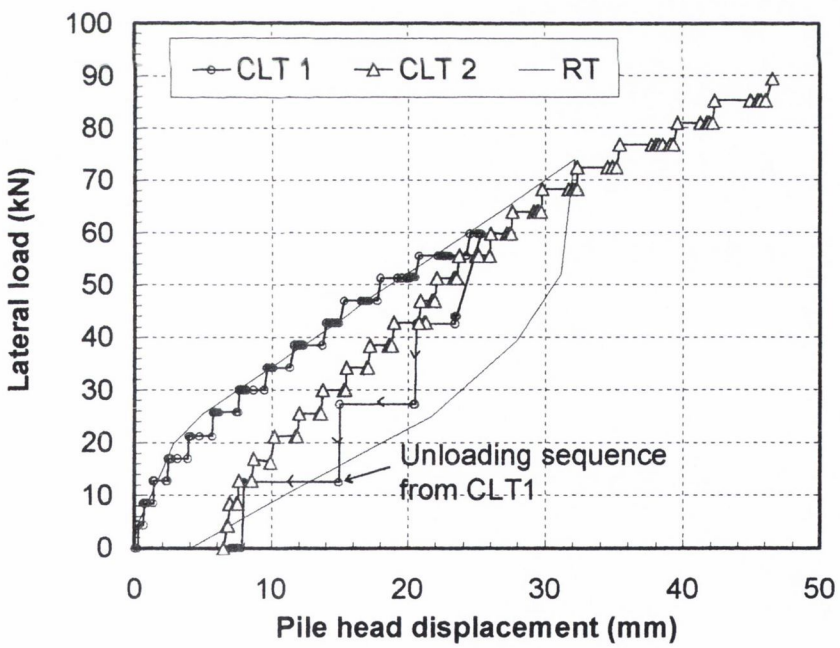

Figure 9-16: Lateral load versus pile head displacements for initial load tests and the retest for pile L1

9.8 Measured p-y Curves Compared with API p-y Guidelines

The measured *p-y* curves from within the critical depth are compared with the API *p-y* guidelines for soft clay and sand. In Figure 9-17, the *p-y* curve for pile L1 at z = 1.0m is typical of that predicted by API for sands at the same depth; in this instance however, the agreement is considered fortuitous given the miscellaneous nature of the fill surrounding L1. Clearly the measured *p-y* curve at z = 1.0m for pile AL1 falls almost midway between the API criteria for sand and soft clay, this is consistent with the silty nature of the sleech observed during the trial pit exploration.

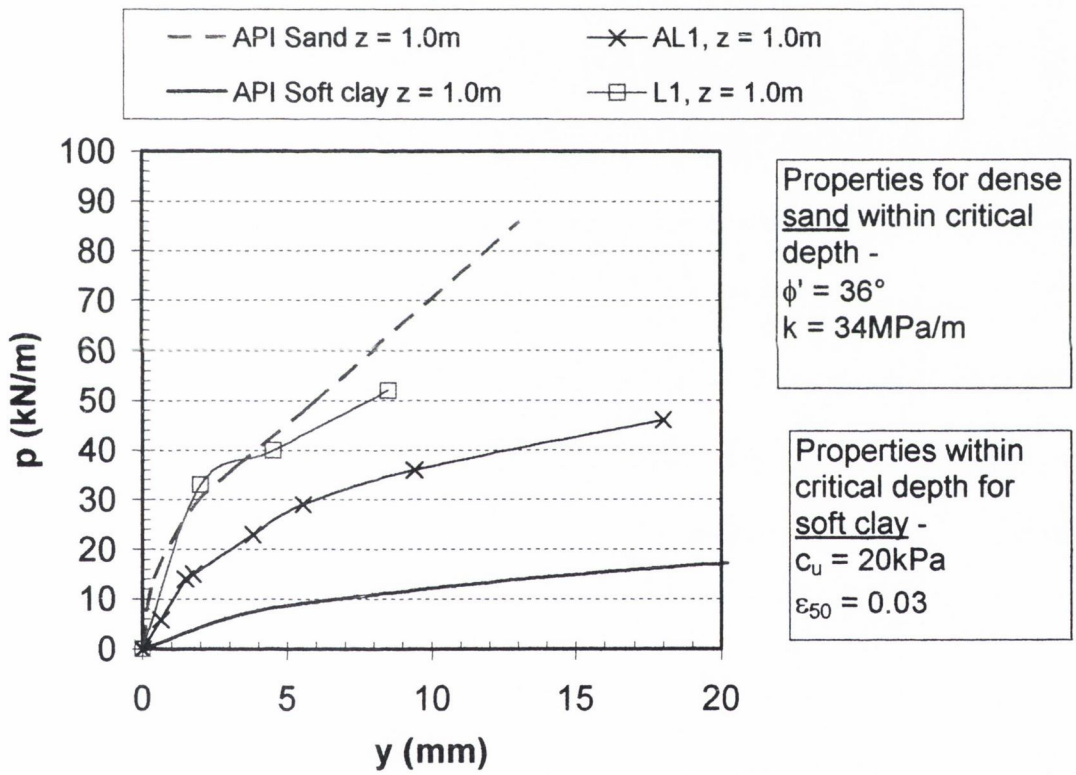

Figure 9-17: Comparison of Kinnegar *p-y* curves and the API recommended soft clay and sand *p-y* curves at z = 1.0m

Similar plots are shown in Figure 9-18 for the granular fill and soft clay at depth. Figure 9-18a illustrates the relationship between the measured *p-y* curves in the granular fill with the API predictions for soft clay and sands. Again the measured response (for each pile) mirrors that predicted by the API criteria for sand but with a much higher resistance after

the initial soil yield. Figure 9-18b shows the *p-y* response at depth is typical of a soft clay but having a significantly higher initial stiffness than predicted using the API criteria.

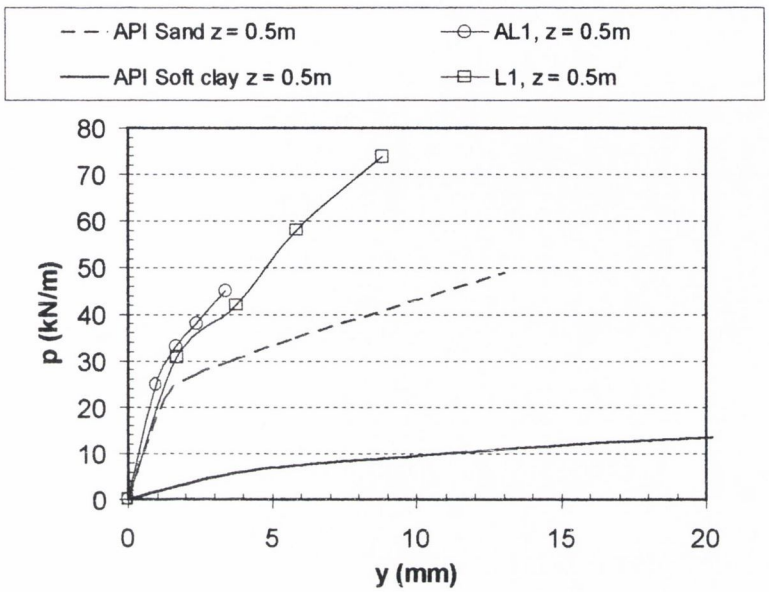

(a) Granular fill

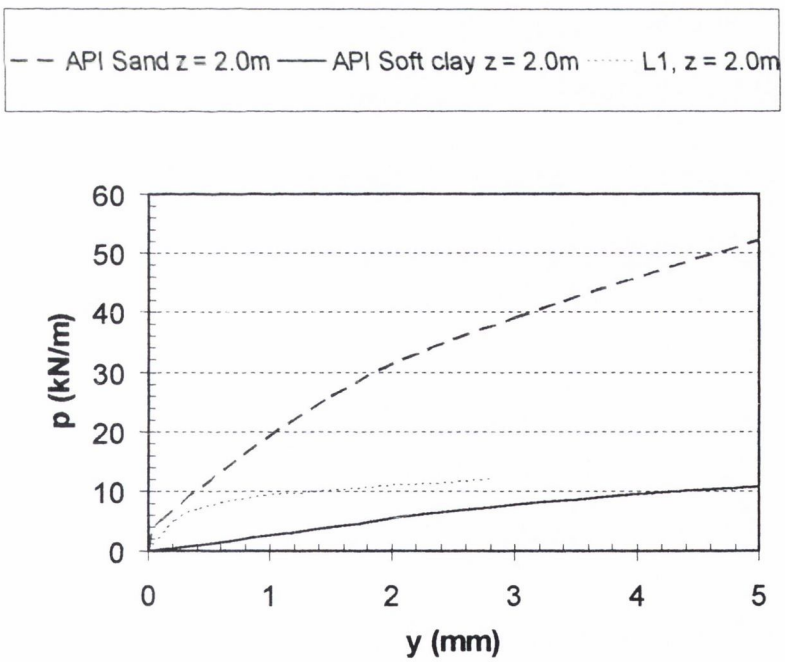

(b) Soft clay at depth

Figure 9-18: Comparison of *p-y* curves in the granular fill & soft clay with API *p-y* curves

9.9 Comparison of Stiff DBC and Belfast Soft Clay p-y Response

The normalised *p-y* curves for the two test sites are compared in Figure 9-19. It is of interest to note the significant plastic behaviour at relatively low soil strain in the soft clay. Contrast this with the almost linear response of the stiff clay despite subjecting the soil to strains of ≈ three times the magnitude experienced by the soft clay. This ductile behaviour of the stiff clay is consistent with the high values for ε_{50} reported in chapter 7 for Dublin boulder clay.

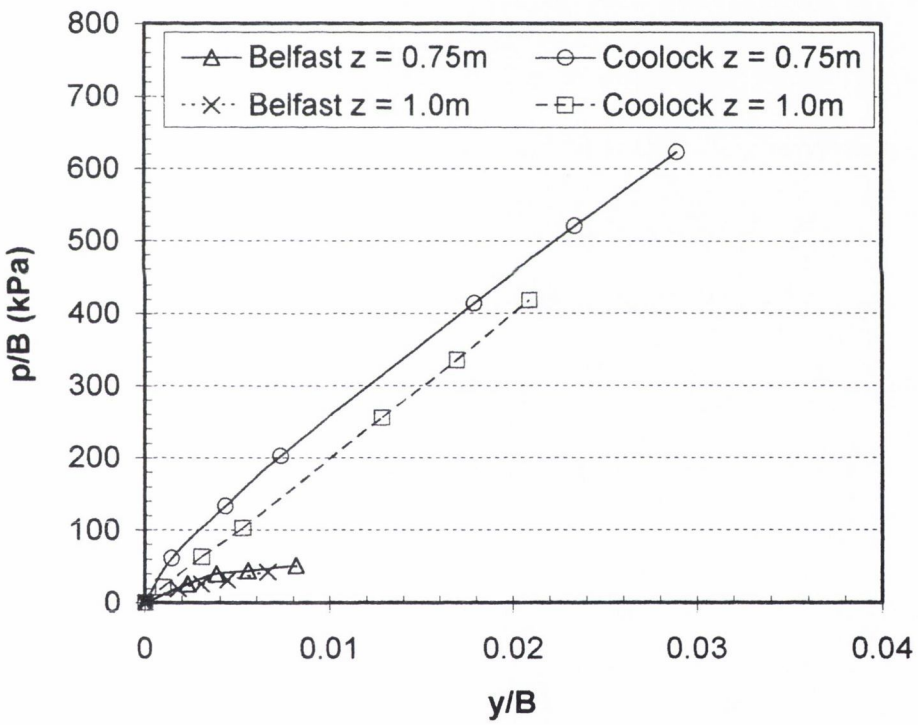

Figure 9-19: Comparison of *p-y* curves in stiff clay and soft clay from the two test sites.

9.10 Application of the CPT to predictions of pile response to lateral load

This section examines the potential of a *p-y* method based on the CPT q_c values for the prediction of pile response to lateral load. A linear dependence of *p* on the CPT q_c profile was assumed and the form of the *p-y* curves adopted was based on that presented by API (1993) for soft and stiff clay i.e. the p/y was assumed to vary approximately with $(y/B)^{0.55\pm0.05}$.

The following best-fit relationships were derived using a simple trial and error procedure which involved comparing the *p-y* curves established for piles L1 and AL1 at Kinnegar with the estimated CPT q_c profile adjacent to each pile.

- *Sleech* (z between 1.75m and 7.6m adjacent to pile L1 and z between 1.0m and 7.6m adjacent to pile AL1):

$$p = 0.19 q_c y \left(\frac{y}{B}\right)^{-0.6}$$

- *Sandy fill* (z between 0.5m and 1.75m adjacent to pile L1 and z between 0.5m and 1.0m for pile AL1)

$$p = 0.44 q_c y \left(\frac{y}{B}\right)^{-0.5}$$

These relationships imply approximate equivalent Young's moduli ($E \approx p/y$) at displacements equal to 1% of the pile width of $3q_c$ for the sleech and 4.4 q_c for the sandy fill. Such multiples of q_c are consistent with those commonly employed for estimating the settlement of shallow foundations (for which the ratio of settlement to foundation width is in the order of 1%); e.g. see Poulos 1989.

9.10.1 Pile L1

The *p-y* relationships established above were used with OASYS ALP to predict bending moments and displacements for pile L1. These predictions are compared with measured moments and displacements at pile head loads of 25.75kN and 60kN (Note that the measurements at these loads are designated as M25.75kN and M60kN).

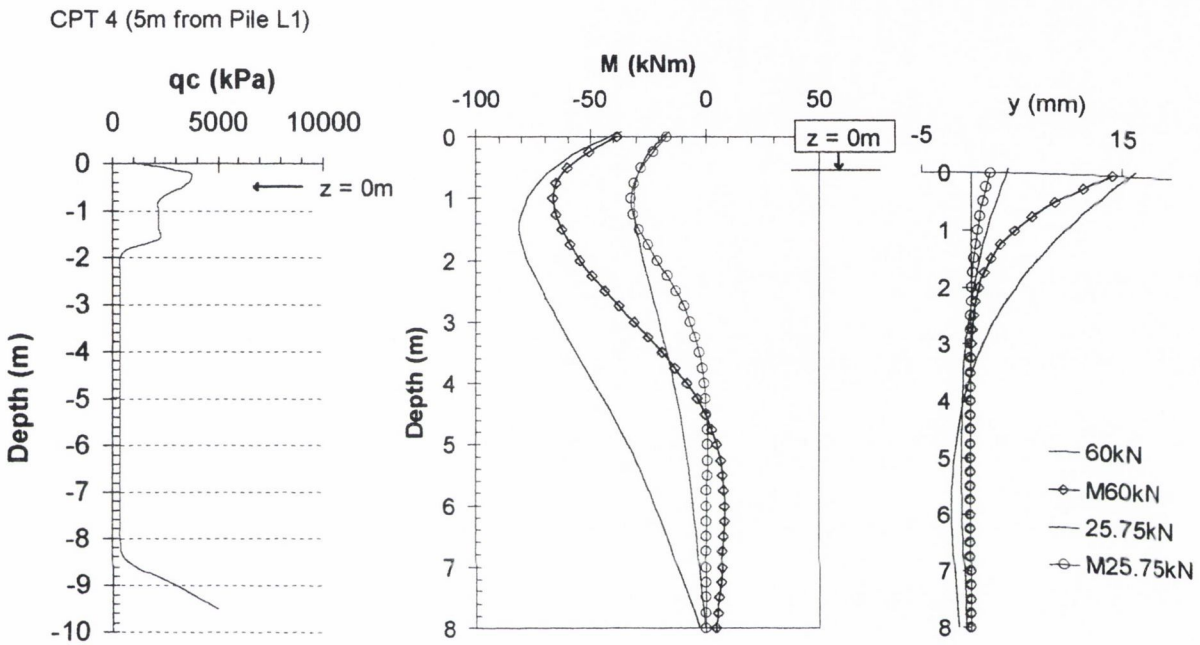

Figure 9-20: Measured and predicted Moment and Displacement profiles for pile L1

As seen on Figure 9-20, the lateral displacements predicted using these equations compare reasonably well with the measured displacements particularly at the lower load level (there is a tendency for some variation at the higher load increment). The profiles also show that the ground level displacements are estimated with reasonable accuracy for both load levels. The bending moment distributions again show some variation with those inferred from the strain measurements but the magnitude of the maximum bending moments are tolerably consistent with the measured values.

9.10.2 Pile AL1

A similar exercise was undertaken for pile AL1 the results, shown in Figure 9-21, again indicate the suitability of CPT q_c data for use in the analysis of laterally loaded piles. The chosen *p-y* relations gave bending moments that correlated well with the measured distribution while conservative estimates of the pile displacement were provided for both load increments.

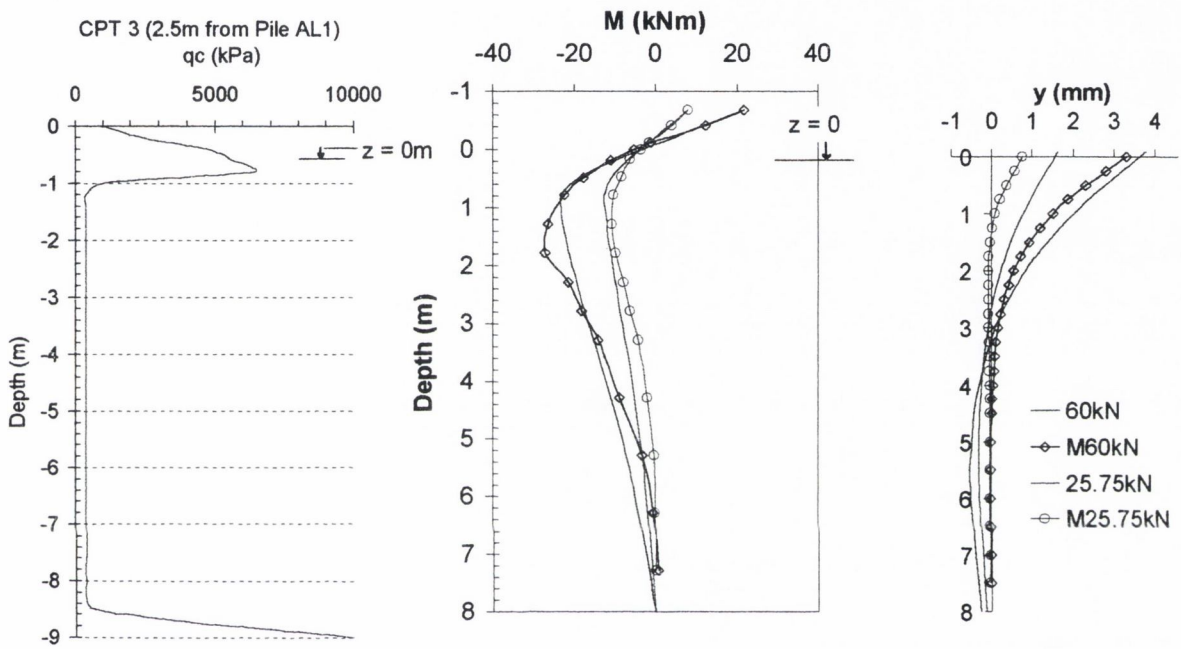

Figure 9-21: Measured and predicted displacement profiles for pile AL1

The foregoing analyses have demonstrated that a relationship can be established between the soil's *p-y* response at a given depth and the CPT q_c value at the corresponding depth. The results are reasonable considering the variability of the fill stratum and the dominant influence this material has on the overall pile behaviour. It is also noteworthy that the results from all the analyses undertaken demonstrate the lack of sensitivity of the solution to the boundary conditions at the pile head.

9.11 Comparison of CPM and Experimental p-y Curves in Soft Clay

A similar type of analysis to that described in section 9.10 could not be performed with the CPM results as there were insufficient tests performed at shallow depths and there were no CPM tests in the fill. The experimental *p-y* curves derived for L1 and AL1 in the soft clay at z = 1.8m could, however, be compared directly with the *p-y* response inferred from the CPM test at approximately the same depth (using the procedure of Robertson et al. (1986)). This comparison is provided on Figure 9-22 where the stiffness of *p-y* curve derived from the CPM is seen to be only approximately 50% of that derived from the pile tests. The softer response of the CPM *p-y* curve may reflect:

- the lower diameter of the pressuremeter device. Based on the hypothesis in Section 9.3.1, the pressuremeter device may be expected to give a stiffness which is only ≈67% of that of the 350mm wide pile.

- differences between the load transfer mechanism of the CPM membrane and that of a laterally loaded reinforced concrete pile; the contribution to resistance provided by the latter is made up of a potentially stiffer side friction resistance component in addition to lateral straining at the front of the pile.

Further comparative exercises of this nature will be required to derive appropriate correction factors to the CPM expansion curve if such curves are to be used routinely to derive *p-y* curves for piles.

The comparison on Figure 9-22 also suggests that the lateral stiffness derived for the sleech in Belfast using the CPM is probably not under-estimated significantly. It may therefore be inferred from the analytical studies conducted in Sections 9.2 and 9.3 that the effects of soil stiffness non-linearity and the relatively small width of the pile combined to lead to a low level of interaction between the respective *p-y* 'springs' located at spacings approximately equivalent to the pile width. The corollary to this observation is that assumptions/approximations implicit in the *p-y* approach are valid for design purposes.

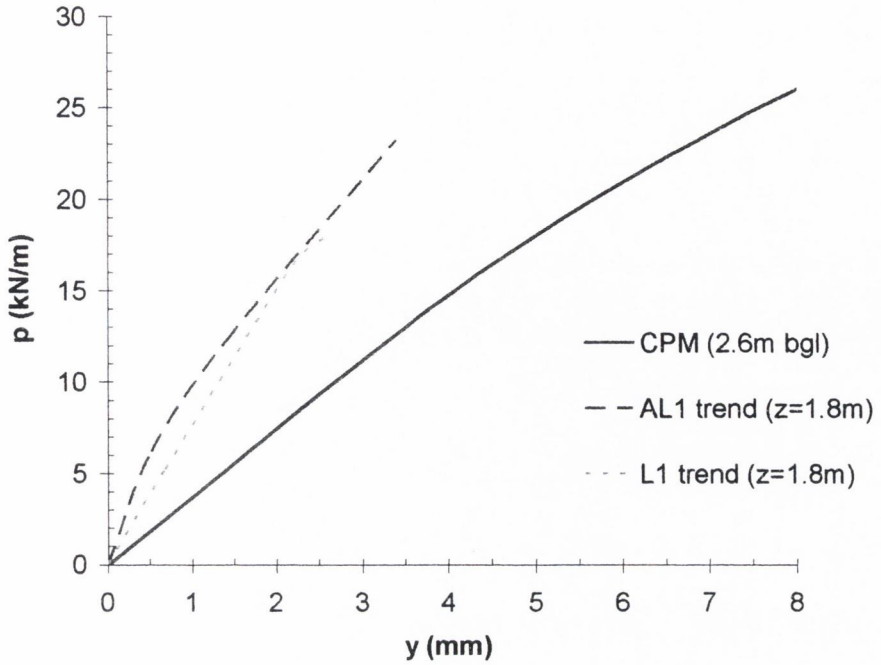

Figure 9-22: Experimental *p-y* curves compared with typical PM *p-y* curves for soft clay

9.12 *Influence of axial load on the pile*

The load-displacement results presented in chapter 5 appear to suggest that an axial load has a significant stiffening influence on the lateral response of the pile (at least up to displacements approximating allowable values for laterally loaded piles[4]). However, the analysis presented in chapter 6 highlights that the stiffer response was most likely attributable to a number of structural factors associated with the load test setup, these are:

1. Pile Head Condition

   As the displacement and rotation increases at the pile head, the bending moment induced by an eccentric axial load requires careful consideration; in particular the method of transferring the axial load to the pile was found to significantly influence

[4] The issue of allowable pile displacement depends on the structure supported by the piles; a value of 20mm is often suggested for conventional land based structures although Tomlinson (1994) states that such practices are unrealistic since pile movement can only be accurately determined by field trials. Long et al. (1984) note that the displacements may be limited to 2.5% of the pile diameter (d) for the design of offshore structures.

the pile head restraint. In the Kinnegar CLT series, significant rotational restraint[5] was measured at the point of lateral loading, which resulted in smaller displacements and bending moments in pile AL1 compared to those measured at L1 under the same loads.

2. Prestressing Effect of an Axial Load on a Reinforced Concrete Pile

   In the case of reinforced concrete piles under vertical working loads, the 'prestressing effect' would enhance the flexural stiffness of the pile and hence its response to lateral load by delaying the on-set of flexural cracking. Thus for a given lateral load, the precompressed pile would be expected to demonstrate an extended elastic response above that experienced by the same pile without a vertical load. The stiffer response of the pile subjected to combined loading is due to the pile operating at its full flexural rigidity (EI) for an extended period until the effect of the prestress has been overcome by the lateral load. This phenomenon may be considered as a beneficial consequence of the construction process but is unlikely to be considered in design due to the difficulty in predicting the minimum axial load acting on the pile along with the reduction in EI as the bending moment is increased[6]. Secondary effects at the pile head due to lateral displacement and rotation (e.g., the P-Δ effect) also requires consideration as these can often be significant (particularly in the case of flexible piles with a small cross sectional area).

3. *p-y* response of the soil

   In the Kinnegar field tests the combined loading of pile AL1 resulted in a significantly stiffer response than the adjacent laterally loaded pile (L1). This prompted the need for further investigation (such as those tests commissioned at the University of Western Australia) to assess the influence of the vertical load on the soil stiffness. For the reasons discussed in section 9.13, a beneficial increase in soil stiffness was unlikely. In fact on re-testing, pile AL1 exhibited greater

[5] Described in section 6.3, page 161.

[6] Given that the compressive stresses applied to the pile in the Kinnegar tests were relatively small (1.37MPa and 1.1MPa for CLT1 and 2 respectively) the effect of the axial load on the bending moment is relatively small (representing an increase of ≈4kNm in the cracking moment).

displacement than pile L1 at the same load level (see Figure 5-16, page 153). This behaviour was attributed to failure in the soil mass resulting from:

- The reduced thickness of dense granular fill surrounding pile AL1 compared to that next to L1 and
- The increased lateral load component experienced by pile AL1 once the rotation of the pin joint became significant.

In support of these findings, analytical analyses by Shahrour and Meimon (1991) also found that the horizontal soil reaction generated by the combined loading was independent of the load inclination i.e., unaffected by the presence of an axial load. Furthermore, Trochanis et al. (1991) and Anagnostopoulos and Georgiadis (1993) found that the lateral load-displacement curve was practically unaffected by the presence of an axial load.

9.13 Overview of Combined Load Tests

The restraint induced at the pile head when the vertical load is applied through a superstructure with a stiffness and rigidity resembling that of a real structure is not evident from the centrifuge tests performed by Shim (2000). In the case of the Kinnegar field tests, the restraint that developed (in the form of an applied moment) resulted in a reduced shear force being applied to the pile. Interestingly, the different loading regimes did not result in a significant change in the *p-y* response of the soil as shown in Figure 9-22.

Support for some of these findings can be seen in 3-D FEA of Trochanis et al. (1991) and Shahrour and Meimon (1991). Bransby (1999) concluded on the basis of the non-linearity of real soils that *p-y* curves obtained from field and laboratory tests are not likely to be dominated by far-field soil displacements (unlike in elastic soil models, see sections 9.2 and 9.3) and so will be almost independent of pile head fixity. Although the current database of tests adopted by the API (1993) for the construction of *p-y* curves have indicated some differences in the soil response when piles are tested with free heads and restrained heads (Matlock, 1970 and Reese et al., 1975), these differences have been adjudged small and accordingly no refinements to the *p-y* formulations have been deemed

necessary. Dyson and Randolph (2001)[7] found the *p-y* response for the fixed head pile exhibited a slightly stiffer initial response before tending to become parallel with the free head curve; the differences were, however, again small and no conclusion was drawn regarding the implications for pile design. Ashour and Norris (2000) found that the effect of pile head fixity on the *p-y* response in soft clay was nominal but the restraint could become significant for dense sands and stiff clays.

The combination of soil layering and pile head restraint[8] in the Kinnegar load tests prevents a direct assessment of the influence of each individual phenomenon. Furthermore the discussion is limited to the response of the soft clay due to the variability that exists within the fill. In any event, it can be concluded that the *p-y* response in the soft clay shows only small variations between the piles and these are just as likely to be due to the approximation inherent in the *p-y* approach as they are to do with pile head restraint. A parametric study to assess the implications of such variations (presented in section 9.5) revealed that the structural response of a laterally loaded pile is not sensitive to variations in the *p-y* response of the magnitude measured in this research. Furthermore, the effect of soil layering appears to be adequately modelled by choosing appropriate *p-y* curves for the various stratigraphies involved.

9.14 Conclusion

The discussion presented on the *p-y* approach for laterally loaded piles provides significant justification for the continued use of the *p-y* approach for predicting pile response to lateral load. The greatest uncertainty lies in the selection of appropriate *p-y* curves. While the API recommendations are generally reasonable, assessment of correlations with CPT and CPM data suggests that improved estimates of *p-y* curves are possible using correlations with in-situ test parameters. Moreover, the availability of CPT and CPM data at the site investigation stage of a project facilitates the early design of piles governed by lateral loading criteria.

---

[7] Dyson and Randolph's findings were based on centrifuge tests on model piles embedded in calcareous sand having free and restrained pile-head conditions.

[8] These effects were assessed individually by Ashour and Norris in their semi-theoretical SW approach.

Chapter 10

Research Conclusions and Implications for Pile Design

10. RESEARCH CONCLUSIONS AND IMPLICATIONS FOR PILE DESIGN

10.1 Introduction

This thesis presented the results of full-scale instrumented field studies on laterally loaded piles. The research centred around tests on (i) 350mm square reinforced concrete piles driven through a surface layer of granular fill into a deep deposit of soft clay and (ii) 203mm wide steel H-piles driven into a stiff glacial till. The piles were subsequently subjected to a series of static loading tests. The thesis has examined a number of topical issues in regard to the design of laterally loaded piles; these include the influence of soil layering, pile head restraint and ageing. The influence of an axial load on the lateral pile response was also examined and additional investigation of the axial load effect was also undertaken via centrifuge tests on a pile embedded in a calcareous sand and subjected to lateral and combined loading.

The results of the field tests were used to derive *p-y* curves or non-linear 'soil springs' that characterise the soils at each test site. These results were compared with the *p-y* response derived from cone pressuremeter tests and cone penetration tests performed in the vicinity of the load tests at the soft clay site. The *p-y* response was also compared with the (widely employed) recommendations of the American Petroleum Institute (API).

For clarity, the main findings of the thesis are presented under two headings. The first deals with the structural aspects of the load tests and emphasises the issues involved in the interpretation of the instrumentation data. The second presents the geotechnical findings and proposes recommendations to improve the lateral performance of piles.

10.2 Structural Aspects in the Interpretation of Laterally Loaded Pile Tests

Instrumentation

The use of instrumented pile load tests to investigate the behaviour of laterally loaded piles was accomplished with success in this research. The following comments summarise the issues regarding the selection and interpretation of the instruments:

- Relatively low cost instrumentation of the nature employed in this research can provide sufficiently accurate data to permit the derivation of site-specific *p-y* curves.

- Electro-levels (EL) permit pile displacement profiles to be determined to a high degree of accuracy. The profiles determined in this research were consistent with the displacements measured (independently) at the pile head and the distributions computed from the strain gauge data. It is also worth noting that ELs provide instantaneous slope data along the monitored length of pile and, in this respect, are also superior to the standard inclinometer, which provides an average over the torpedo gauge length.

- The ELs can be used with any type of pile and can provide a useful means of checking current design methods. However, to obtain *p-y* curves directly from EL data alone requires sensors strategically placed at close centres over the critical length. The sensors must also be set to a sufficiently high resolution such that curves fitted to the measured slopes can undergo multiple differentiations and still result in soil reaction distributions that are in reasonable agreement with expected or measured results. This was achieved with some success by Price & Wardle (1987c). Finally, as the soil

reaction is directly related to the flexural rigidity (EI) of the pile section, an accurate profile of the variation in EI at various stages of loading is paramount in the interpretation of soil reactions using EL data.

- Fixing ERS gauges to the steel reinforcement in concrete piles is time consuming and can have varied success depending on the quality of the installation and the method of pile installation. The use of ERS gauges proved very successful for Belfast tests, but the measurement of a moment-curvature (or moment-strain) relationship using a prototype is recommended to take direct account of the changing flexural rigidity experienced by the pile once the concrete starts to crack. This can be achieved by locating strain gauges on both the compression and tension reinforcement. By positioning these gauges at the same level at various positions along the pile length facilitates the direct derivation of the pile moment-curvature relationship from the prototype.

- The success of all instrumentation relies on careful calibration in advance of the load tests. On site calibration of the instruments is preferable in order to take account of site conditions which may influence the instrument performance. Redundancy in the calibration checks should be incorporated wherever possible.

- Pressure cells strategically positioned along the pile can provide useful corroborative data in the investigation of lateral pile behaviour but full benefit from these instruments can only be obtained if they are located within the critical pile length. Instruments located outside this depth tend to register very small pressures due to the significant lateral resistance developed in side skin friction as the pile moves laterally relative to the soil.

Pile Section Properties

The well-defined flexural rigidity (EI) of a steel pile leads to obvious advantages in its selection as a means of deriving *p-y* relationships. However, if the pile adopted is subject to a reduction in EI as the loading is increased (e.g. a reinforced concrete pile), then the

additional flexibility of the pile requires special consideration when designing the foundations. In such cases, it is recommended that the variation in EI (with respect to the pile bending moment) be measured directly in a field test or via a prototype. Adopting conventional structural engineering approach is not recommended because of the inherent conservatism adopted in 'design' based calculations.

Effect of an Axial Load on the Pile Structural Response

The influence of an axial load on a concrete pile leads to an enhanced section stiffness and hence pile performance under lateral load. However, eccentricities that develop when the pile is loaded laterally necessitate special consideration of the section response e.g. the pile's bending stiffness and secondary P-Δ effects. The combined loading of a pile in the Belfast tests illustrated the non-ductile (rapid) manner in which piles can fail once the beneficial effect of pile head restraint has been overcome by these secondary effects.

10.3 Geotechnical aspects of laterally loaded pile behaviour

Effect of an Axial Load on the Soil *p-y* Response

The structural implications of an axial pile load were summarised above. This research also showed that the presence of an axial load on a pile had no significant effect on the *p-y* response of the soil and therefore its effect (in the vast majority of practical situations[1]) can be ignored when conducting a *p-y* analysis to determine the structural and serviceability parameters for foundation design.

Accuracy of the p-y approach

The discussion presented in chapter 9 on the *p-y* approach for predicting pile response to lateral load provides significant justification for the continued use of the *p-y* method. The greatest uncertainty lies in the selection of appropriate *p-y* curves; this can be assisted

[1] Where the axial load is well below the buckling capacity of the pile

however, by obtaining *p-y* correlations with in-situ tests such as CPT and CPM tests in particular, rather than the traditional correlations based on laboratory tests (e.g. triaxial UU tests).

Effect of an Pile Head Restraint and Soil Layering on the Soil *p-y* Response

It can be concluded from the test results presented for the Belfast tests that the effect of a pile head restraint has very little effect on the *p*-y response in soft clay. The small variations in the *p-y* response observed between the piles are just as likely to be due to the approximation inherent in the *p-y* approach as they are to do with pile head restraint. A parametric study to assess the implications of such variations (presented in section 9.5 of chapter 9) revealed that the structural response of a laterally loaded pile is not sensitive to variations in the *p-y* response of the magnitude measured in this research. Furthermore, the effect of soil layering appears to be adequately modelled by choosing appropriate *p-y* curves for the various stratigraphies involved.

Critical Depth Governing the Lateral Capacity of Piles

In this thesis, the results from instrumented load tests at two test sites, having significantly different ground and pile conditions, were presented. The steel H piles at Coolock were embedded in a hard glacial till with undrained shear strengths of up to 600kPa. In contrast, the piles at Belfast had a flexural rigidity about five times higher than the Coolock piles and were embedded in a layered deposit comprising predominantly soft clay beneath a dense granular crust. In each case however, the lateral response of the piles were dominated by the soil properties within a depth of ≈6B from the ground surface. This suggests that considerable economies in the foundation design may be gained if the soil within this depth is densified in advance of pile construction.

Site Investigation Requirements

Prediction of pile response to lateral load is crucially dependent on the properties of the near surface soils; testing should therefore concentrate on determining the appropriate soil parameters from this zone. While the API recommendations have been shown to be

adequate for many purposes, assessment of correlations with CPT and CPM data suggests that improved estimates of *p-y* curves can be obtained using correlations with in-situ test parameters. This thesis indicates that further work is still, however, required in the refinement of the derivation of *p-y* curves from CPM data, while correlations with the CPT data appear promising. Finally, since the near surface soil controls the lateral response, it is certainly not beyond the bounds of practicality to obtain block samples of soil for appropriate passive testing in the laboratory.

Long Term Soil Performance

Re-testing of the Belfast piles after a prolonged period of ageing revealed that no significant change in the lateral soil resistance took place. This may well be primarily attributable to the relatively loose cohesionless nature of the near surface material and the consequent absence of a post-hole (that had developed around the piles during initial testing) during the re-test. An enhancement in the lateral stiffness and strength of the sleech was not observed.

10.4 Concluding Comment

Instrumented pile test data, such as that presented in this thesis, plays an important role in the advancement of our understanding of the factors affecting the behaviour of piles (and adjacent soil) under lateral load. In addition, current theoretical developments, such as the 'strain wedge' approach for determining *p-y* curves and 3-D Finite Element analyses, have provided useful insights. These theoretical approaches have yet, however, to reach the stage where they may be generally applied to routine design. This thesis has demonstrated that the *p-y* approach is sufficient for most practical purposes - so much so, in the opinion of the author, despite the immense growth in computing power, that the more sophisticated 3-D FE approach will be slow to gain popularity with the practitioner. The main scope for improvement lies in the refinement of existing correlations for *p-y* curves. It is hoped that this thesis has contributed to this goal.

10.5 Recommendations for areas of further research

From a research standpoint, the use of 3-D finite element (FE) analysis to model the soil-pile interaction under combined loading is viewed as the next step forward in the advancement of laterally loaded pile analysis. The results of the field tests presented in this research provide a basis for the development of a realistic FE model. The 3-D FE model can subsequently be utilised to investigate the effect of pile shape and size on *p-y* curves developed from correlations with the cone pressuremeter and cone penetration tests.

References

1. ACI Committee 318. (1989). *Building code requirements for reinforced concrete,* ACI 318-89, *and Commentary*, ACI 318R-89, American Concrete Institute, Detroit, USA.
2. Allan, P. G. (1994). *A brief description of the Cambridge self-boring pressuremeter and the interpretation of tests in clays and sands,* Cambridge SBP Description, PGA, Cambridge University, England.
3. American Petroleum Institute. (1993). *Recommended Practice for Planning, Designing and Constructing Fixed Offshore Platforms - Load and Resistance Factor Design*, API RP 2A - LRFD, 1st Edition, American Petroleum Institute.
4. Anagnostopoulos, C. and Georgiadis, M. (1993*). Interaction of Axial and Lateral Pile Responses*, J. of Geotechnical Engineering, ASCE, Vol. 119, No. 4, pp.793-798.
5. Anderson, J. B., and Townsend, F. C. (1999). *Validation of p-y curves from pressuremeter tests at Pascagoula, Mississippi,* Proc., XI Panamerican Conf. on Soil Mechanics and Geotechnical Engineering.
6. Anderson, J. B., Grajales, B., Townsend, F. C. and Brown. (1999). *Validation of p-y curves from pressuremeter and dilatometer tests at Auburn, Alabama,* ASCE GSP No. 92 Behavioral Characteristics of Residual Soils, Charlotte, N.C.
7. Arman, A. and McManis, K. L. (1975). *Effects of storage and extrusion on sample properties,* ASTM V. STP599, pp. 66-87.
8. Ashour, M. and Norris, G. (2000). *Modelling lateral soil-pile response based on soil-pile interaction*, J. of Geotechnical and Geoenvironmental Engineering, American Society of Civil Engineers, Vol. 126, No. 5, pp. 420-428.
9. Ashour, M., Norris, G. and Pilling, P. (1998). *Lateral loading of a pile in layered soil using the strain wedge mode*l, J. of Geotechnical and Geoenvironmental Engineering, American Society of Civil Engineers, Vol. 124, No.4, pp. 303-315.
10. Atkinson, J., (1993). *An introduction to the mechanics of soils and foundations*, McGraw Hill.
11. Baguelin, F., Jezequel, J. F., Shields, D. H. (1978). *The pressuremeter and foundation engineering*, Trans. Tech. Publications, Clausthal-Zellerfield, W. Germany.
12. Baguelin, F.J., Frank, R.A. and Said, Y. (1977). *Theoretical study of lateral reaction mechanism of piles*, Géotechnique, Vol. 27, No. 3, pp 405-434.

13. Baguelin, F.J., Jezequel, J. F. and Shields, D. H. (1978). *The pressuremeter and foundation engineering*, Trans Tech Publications, Clausthal-Zelerfeld, Germany.
14. Baguelin, F.J., Frank, R.A. (1980). "*Theoretical studies of piles using finite element methods*," Numerical methods in offshore piling, ICE, London, pp 83-91.
15. Banerjee P. K., Davies, T. G. (1978). *The behaviour of axially and laterally loaded single piles embedded in non-homogeneous soils*, Géotechnique 28, No 3, pp. 309-326.
16. Bell, A. (1977). *A geotechnical investigation of post-glacial estuarine deposits at Kinnegar, Belfast Lough*, PhD. Thesis, Queen's University Belfast.
17. Bowles J. E. (1996). *Foundation Analysis and Design*, 5th Ed., McGraw Hill, New York.
18. Bransby, M. F. (1996). *Difference between load-transfer relationships for laterally loaded pile groups: Active p-y or Passive p-δ*, J. Geotech. Egng., ASCE, Vol. 122, No. 12, pp. 1015-1018.
19. Bransby, M. F. (1999). *Selection of p-y curves for the design of single laterally loaded piles*, Int. J. for Numerical and Analytical Methods in Geomechanics, 23, 1909-1926.
20. Briaud, J. L. (1992). *The Pressuremeter,* A. A. Balkema, Rotterdam, The Netherlands.
21. Briaud, J. L. (1997). *SALLOP: Simple Approach for Lateral Loads on Piles*, J. Geotechnical and Geoenvironmental Engineering, Vol. 123, No. 10, pp. 958-964.
22. Briaud, J. L., Smith, T. and Meyer B. (1984). *Laterally loaded piles and the pressuremeter: comparison of existing methods*, American Society for Testing and Materials, West Conshohocken, Pa. pp 97-111.
23. Briaud, J. L., Smith, T.D. and Tucker, L. M. (1985). *A pressuremeter method for laterally loaded piles*, Proc. 11th Int. Conf. On Soil Mechanics and Foundation Engineering, V3, pp 1353-1356.
24. Brinch Hansen, J. B. (1961). *The ultimate resistance of rigid poles against transversal forces*, Danish Geotechnical Institute, V.12, pp. 5-9.
25. Broms, B. B. (1964a). *The lateral resistance of piles in cohesive soils*, Journal of the Soil Mechanics Division, Am. Soc. Civ. Engrs., Vol 90, No. SM2, pp. 27-63.
26. Broms, B. B. (1964b). *The lateral resistance of piles in cohesionless soils*, J.S.M.F.D., Am. Soc. Civ. Engrs., Vol. 90, SM3, pp123-156.

27. Broms, B. B. (1965). *Design of laterally-loaded piles*, Proc. Am. Soc. Civ. Engrs., J. Soil Mech. Found. Div., 91 (SM3), 79 to 99.
28. Burland, J. B. (1973). *Shaft friction of piles in clay – a simple fundamental approach*, Ground Engineering, Vol. 7, pp. 30-42.
29. Burland, J. B. (1990). *On the Compressibility and Shear Strength of Natural Clays*, *Géotechnique*, 40, No.3, 327-378.
30. Burland, J. B. and Burbidge, M. C. (1985). *Settlement of foundations on sand and gravel,* Proc. ICE, Part 1, 78, pp. 1325-1381.
31. Burland, J. B. and Cooke, R. W. (1974). *The design of bored piles in stiff clays,* Ground Engineering 7, 4, pp. 28-35.
32. Burland, J. B., and Starke, W. (1994). *Review of measured negative pile friction in terms of effective stress*, XIII ICSMFE, New Delhi, India, pp. 493–496.
33. Burland, J. B., Butler, F. G. and Dunican, P. (1966). *The behaviour and design of large diameter bored piles in stiff clay*, Proc. Symp. on Large Bored Piles, 51-57. ICE, London.
34. Bustmante, M. and Gianeselli, L. (1982). *Pile bearing capacity prediction by means of static penetrometer CPT,* Proceedings of the 2nd European Symposium on Penetration Testing, Amsterdam, Vol. 2, pp 493-500.
35. Byrne, P. M. and Atukorala, U. (1983). *Prediction of p-y curves from pressuremeter tests and finite element analyses,* University of B.C., Civil Eng. Dept., Soil Mechanics Series No. 66.
36. Carney, M. (2002). Trinity College Dublin – Personal Communication.
37. Chow, F. C., Jardine, R. J., Brucy, F. and Nauroy, J. F. (1998). *Effects of time on capacity of pipe piles in dense marine sand,* J. of Geotechnical and Geoenvironmental Eng., Vol. 124, No. 3, ASCE, pp 254-264.
38. Clarke, B. G. (1995). *The pressuremeter in Geotechnical Design,* Blackie, Glasgow.
39. Clarke, B. G. (1997). *Pressuremeter testing in ground investigation – Part II – interpretation,* Proc. Instn. Civ. Engrs, Geoth. Engng., 125, pp. 42-52.
40. Craig, R. F. (1987). *Soil Mechanics,* 4th Ed., Van Nostrand Reinhold (UK).
41. Crooks, J.H.A. and Graham, J. (1972). *Stress-strain properties of Belfast estuarine clay.* Engineering Geology, 6, pp. 275-288.

42. Crooks, J. H. A. & Graham, J. (1976). *Geotechnical properties of the Belfast estuarine deposits.* Géotechnique 26, No. 2, 293-315.

43. Dalton, C. (1997). *Developments in site investigation,* Ground Engineering, Vol. 30, No. 9, pp 22-23.

44. Davies, T. G. and Budhu M. (1986). *Non-linear analysis of laterally loaded piles in heavily overconsolidated clays*, Geotechnique 36, No. 4, pp. 527-538.

45. Davisson, M. T. and Gill, H. T. (1963). *Laterally loaded piles in a layered soil system*, J. of Soil Mechanics and Foundation Division, Proc. Of the American Society of Civil Engineers, Vol. 89, No. SM3, pp. 63-94.

46. Davisson, M. T. and Robinson, K. E. (1965). *Bending and buckling of partially embedded piles*, Proc. 6th Int. Conf. ISSMFE, Vol. 2, pp. 243-6.

47. Davisson, M. T. (1970). *Lateral load capacity of piles,* Hwy. Res. Rec. – National Academy of Science, V. 333, pp. 104-112.

48. Doran, I. G. (1992). *Soils of Northern Ireland.* The Structural Engineer, Vol. 70, No. 77, pp. 135-138.

49. Douglas, D. J., Davil, E. H. (1964). *The movement of buried footings due to moment an horizontal load and the movement of anchor plates*, Géotechnique, Vol. 14, pp. 115-132.

50. Dunnavant, T. W., and O'Neill, M. W. (1989). *Experimental p-y model for submerged stiff clay,* J. of Geotechnical Engineering, Vol. 115, No. 1, pp. 95-114.

51. Dunnicliff. J. and Green, G. E. (1988). *Geotechnical Instrumentation for monitoring field performance*, Wiley, N.Y.

52. Dyson, G. J. and Randolph, M. F. (2001). *Monotonic lateral loading of piling calcareous sand*, J. of Geotechnical and Geoenviromental Engineering, ASCE, Vol. 127, No. 4, pp. 346-352.

53. Elson, W. K., (1984), *Design of laterally loaded piles*, CIRIA Report 103, London.

54. Evans, L. T. (1982), *Simplified analysis of laterally loaded piles*, Ph.D. Dissertation, University of California at Berkley.

55. Farrell, E. R. (1989). *Settlement parameters of Dublin Black Boulder Clay,* Ground Engineering, Ground Engineering, July, pp. 30 - 32.

56. Farrell, E. R. and Wall, D. (1990). *Soils of Dublin,* Proc. of the Institution of Engineers of Ireland.

57. Fleming W. G. K., Weltman A. J., Randolph M.F. and Elson W. K. (1992). *Piling Engineering*, 2nd Ed., E & F N Spon, London.
58. Fugro Limited. (1997). *Field Report for Kinnegar STW outfall extension, Kinnegar sewage treatment works*, Site Investigations, Report No. 65137-1.
59. Gabr, M. A., Lunne, T. and Powell, J. J. (1994). *P-y analysis of laterally loaded piles in clay using DMT,* J. of Geotechnical Engineering, Vol. 120, No. 5, pp 816-837.
60. Gauge Technique Ltd. *Vibrating wire product literature.*
61. Georgiadis, M., Butterfield, R. (1982). *Laterally loaded pile behaviour*, J. of the Geotechnical Engineering Division, ASCE, Vol. 108, No. GT1, pp. 155-165.
62. *Geotechnical Report on behalf of Trinity College*, Pile group research project, Kinnegar sewerage treatment works, Report No. SI98041. Department of the Environment N.I., Construction Services (1998).
63. Gibson, R. E. and Anderson, W. F. (1961). *In situ measurement of soil properties with the pressuremeter,* Civil Engng. Public Works Rev., 56, pp. 615-618.
64. Gieck, K. and Gieck, R. (1990). *Engineering Formulas*, 6th Ed., Mc Graw Hill.
65. Gill, H. G. and Demars, K. R. (1970). *Displacement of laterally loaded structures in nonlinearly responsive soil.* Technical Report R670, Port Hueneme, California; Naval Civil Engineering Laboratory.
66. Glynn, D. (2001). DoE. Northern Ireland – Personal communication.
67. Gottfried, B. S., (1998). *Spreadsheet tools for engineers*, McGraw Hill.
68. Head, K. H. (1998). *Manual of soil laboratory testing*, Vol. 3, Wiley.
69. Hesham EI Naggar, M., Bentlay, K. J. (2000). *Dynamic analysis of laterally loaded piles and dynamic p-y curves*, Canadian Geotechnical Journal, Vol. 37, No. 6, pp. 1166-1183.
70. Hetenyi M. (1946). *Beams on Elastic Foundation*, The University of Michigan Press, Ann Arbor, Michigan.
71. Hight, D. W., Bond, A. J. and Legge, J. D. (1992). *Characterization of the Bothkennar clay: an overview*. Géotechnique, Vol. 42, No. 2, 303-347.
72. Houlsby, G. T. and Teh C. I. (1988). *Analysis of the Piezocone in Clay*, Conference on Penetration Testing, Balkema, Rotterdam, pp. 777-783.
73. Houlsby, G. T. and Withers, N. J. (1988). *Analysis of the cone pressuremeter test in clay,* Géotechnique, 38, No. 4, pp. 575-587.

74. Hsiung, Y. and Chen, Y. (1997). *Simplified method for analysing laterally loaded single piles in clays*, J. of Geotechnical and Geoenvironmental Engineering, ASCE, Vol. 123, No. 11, pp. 1108-1029.

75. Hunt E. R. (1986). *Geotechnical Engineering Techniques and Practices*, McGraw Hill, New York.

76. Jardine R. J. and Chow F. C. (1996). *New Design Methods for Offshore Piles*, MTD Publication 96/103.

77. Jardine R. J. and Overy, R. F., (1996). *Axial capacity of offshore driven piles in dense sand,* Proc., 28th Offshore Technology Conf., Rep. No. OTC 7973, Houston, Texas, pp. 161-170.

78. Jardine, R. J., Chow, F. C., Matsumoto, T. and Lehane, B. M. (1998). *A New Design Procedure for Driven Piles and its Application to Two Japanese Clays.* Soils and Foundations, Vol. 38, No. 1, pp. 207-219.

79. Lehane, B. M. (1992). *Experimental investigations of pile behaviour using instrumented field piles*, Ph.D. Thesis, University of London (Imperial College).

80. Lehane, B. M. and Jardine, R. J. (1994). *Shaft capacity of driven piles in sand: a new design approach,* Proc., Conf. Behaviour of Offshore Struct. (BOSS), Boston, Mass., Pergamon Press, Inc., Oxford, U.K., pp. 23-36.

81. Lehane, B. M., McCabe, B, Phillips, D. T., Jardine, R, Paul, T. and Horkan, E. (1999). *Piling Research in Belfast's Soft Clay*, Trans. Inst. of Engrs. of Ireland 1998-99.

82. Lehane, B. M., and Cosgrove, E. (2000). *Applying triaxial compression stiffness data to settlement prediction of shallow foundations on cohesionless soil*, Geotechnical Engineering, Paper 12156, Proc. Instn. Civ. Engrs. Vol. 143, pp. 191-200.

83. Lehane, B. M., and Simpson, B. (2000). *Modelling glacial till under triaxial conditions using a BRICK soil model,* Can. Geotech. J. Vol 37, pp. 1078-1088.

84. Lehane, B. M., Chow, F. C., McCabe, B. A. and Jardine, R. J. (2000). *Relationship between shaft capacity of driven piles and CPT end resistance*, Geotechnical Engineering, Paper 11973, Proc. Instn. Civ. Engrs. Vol. 143, pp. 93-101.

85. Long, M. M., Lambson, M. D., Clarke, J. and Hamilton, J. (1984). *Cyclic lateral loading of an instrumented pile in overconsolidated clay at Tillbrook Grange,*

Paper 16, Proc. Recent Large Scale Fully Instrumented Pile Tests in Clay, ICE, London.

86. Lunne, T., Robertson. P. K. and Powell, J. J. M. (1997). *Cone penetration testing in geotechnical practice,* Spon Press.
87. Luttenegger, A. J. and Cerato, A. B. (2000). *Surface area and engineering properties of fine grained soils,* Proc. 15th International Conf. on Soil Mechanics and Geotechnical Engineering, Istanbul, 1, pp. 603-606, Balkema.
88. MacGregor J. G. (1992), *Reinforced Concrete Mechanics and Design*, 2nd Ed. Prentice Hall, N.J., USA.
89. Manning, P.I., Robbie, J.A. and Wilson, H.E. (1972). *Geology of Belfast and the Lagan Valley*, HMSO, Belfast.
90. Matlock, H. (1963). *Applications of numerical methods to some structural problems in offshore operations*, Proc. 1st. Conf. On Drilling and Rock Mechanics, V. XV, No. 9, pp. 1040-1046.
91. Matlock, H. (1970). *Correlations for the design of laterally loaded piles in soft clay*, Proc. 2nd Annual Offshore Technology Conference, V.1204, pp. 577-594.
92. Matlock, H. and Reese, L.C. (1960). *Generalised solutions for laterally loaded piles*, J. of the Soil Mechanics and Foundation Division, Proc. ASCE, Vol. 86, No. SM5, pp. 63-91.
93. McCabe, B. A. (2002). *Experimental investigation of driven pile group behaviour in Belfast soft clay,* PhD. Thesis, Trinity College, Dublin.
94. McCabe, B. A. (2002). NUI Galway – Personal communication.
95. McClelland, B. and Focht, J. A. Jr. (1958). *Soil Modulus for Laterally Loaded Piles*, Trans. American Society of Civil Engineers, Vol. 123, pp.1049-1074.
96. Measurements Group Inc. (1992). *Student manual for gage technology*, Bulletin 309D.
97. Meyer, B. J. and Reese, L. C. (1979). *Analysis of single piles under lateral loading*, Center for Transportation Research, Research Report 244-1, Bureau of Engineering Research, University of Texas, Austin, Texas.
98. Meyerhof, G. G. & Ghosh, D. P. (1989). *Ultimate capacity of flexible piles under eccentric and inclined loads*, Canadian Geotechnical Journal, V.26, pp. 34-42.

99. Meyerhof, G. G. & Sastry, V. V. R. N. (1985). *Bearing capacity of rigid piles under eccentric and inclined loads*, Canadian Geotechnical Journal, V.22, pp. 267-276.

100. Mindlin, R. D. (1936). *Forces at a point in the interior of a semi-infinite solid*, Physics, V.7, pp. 195-202.

101. Nash, W. A. (1992). *Statics and Mechanics of Materials,* Schaum's Outline Series, McGraw-Hill.

102. Neville, A. M. (1981). *Properties of Concrete*, Longman Scientific, London.

103. Norris, G. N. (1986). *Theoretically based BEF Laterally Loaded pile analysis,* Proc. 3rd Int. Conf. On Numerical Methods in offshore piling, Technip, Paris, pp 361-386.

104. O'Brien, E. J. and Dixon, A. S. (1995). *Reinforced and Prestressed Concrete – The Complete Process,* Longman, London.

105. Ove Arup & Partners. (1993). *Bangkok Elevated Road and Train System – Report on lateral pile load tests made at Bangsue Junction – Bangkok,* Report 20890/1/RE-032.

106. Ove Arup & Partners. (1997). *Oasys: geotechnical programs manual,* Ove Arup and Partners, London, England.

107. Phillips, D. T. (1995). *An investigation of laterally loaded piles in Dublin Boulder Clay,* M.Sc. Dissertation, University of Dublin (Trinity College), Dublin.

108. Phillips, D. T. and Lehane, B. M. (1998). Laterally Loaded Piles in Stiff Boulder Clay, Proc. of the 7th Int. Conf. on Piling and Deep Foundations, DFI. Vienna, Paper 5.13, pp. 1-6.

109. Portland Cement Association (1988). *Design and Control of Concrete Mixtures*, 13th Ed. IL. USA.

110. Poulos, H. G. (1971). *Behaviour of laterally loaded piles: I- Single piles*, Proc. Am. Soc. Civ. Engrs., Vol. SM5, pp. 711-31.

111. Poulos, H. G. (1971). *Behaviour of laterally loaded piles: II- Pile groups*, Proc. Am. Soc. Civ. Engrs., Vol. SM5, pp. 733-751.

112. Poulos, H. G. (1989). *Pile behaviour – theory and application*, Géotechnique, London, England, 39, No.3, pp. 365-415.

113. Poulos H.G., and Davis, E.H. (1980). *Pile Foundation Analysis and Design*, John Wiley and Sons, New York.

114. Powell, J. M. and Uglow, I. M. (1988). *Dilatometer test results at five UK sites,* Rpt. No. 521610, Building Research Establishment, London, England.

115. Price, G, Wardle, I. F. and Jennings, D. (1985). *The use of slope measuring devices for monitoring bending strains in piles*, Proc. 21st Annual Conf. of the British Society for Strain Measurement, Cambridge.

116. Price, G. and Wardle, I. F. (1979). *The deformation of vertical piles in London clay under static and cyclic horizontal working loads*, Proc., Conf., in Recent Development in the Design and Const. Of Piles, London, England, pp. 87 – 94.

117. Price, G. and Wardle, I. F. (1987a). *The use of electro-levels in laterally loaded precast driven piles at Stretton*, Contract Report 48, Transport and Road Research Laboratory, Berkshire, England.

118. Price, G. and Wardle, I. F. (1987b). *Lateral load tests on large diameter bored piles*, Contract Report 46, Transport and Road Research Laboratory, Berkshire, England.

119. Price, G. and Wardle, I. F. (1987c). *Vertical and lateral load tests on driven cast in place piles at Yarmouth*, Contract Report 47, Transport and Road Research Laboratory, Berkshire, England.

120. Price, G. and Wardle, I. F. (1988). *Comparison of vertical and shallow angled raked piles under lateral load*, Contract Report 45, Transport and Road Research Laboratory, Berkshire, England.

121. Randolph, M. F. (1981). *The response of flexible piles to lateral load*, Géotechnique, Vol. 31, No. 2, pp. 247-259.

122. Randolph, M. F. and Houlsby, G. T. (1984). *The limiting pressure on a circular pile loaded laterally in a cohesive soil*, Géotechnique, Vol. 34, No. 4, pp. 613-623.

123. Reese, L. C. (1977). *Laterally loaded piles: Program documentation*, J. of the Geotechnical Engineering Division, Proc. ASCE, Vol. 103, No. GT4, pp. 287-305.

124. Reese, L. C. (1997). *Analysis of laterally loaded piles in weak rock*, J. Geotechnical and Geoenvironmental Engineering, Vol. 123, No. 11, pp. 1010-1017.

125. Reese, L. C. and Wang, S. H. (1994). *Analysis of piles under lateral loading with non-linear flexural rigidity*, Proc. U.S. FHWA Int. Conf. on Design and Construction of Deep Foundations, Fed. Hwy. Admin., U.S. Dept. of Transport, Washington D.C.

126. Reese, L. C., Cooley, L. A. and Radhakrishnan, N. (1984). *Laterally loaded piles and computer program COM624B*, Technical report K-84-2, US Army Engineer Waterways Experiment Station, Vicksburg, MS.

127. Reese, L. C., Cox, W. R. and Koop, F. D. (1975). *Field testing and analysis of laterally loaded piles in stiff clay*, Proc. 7th Offshore Technology Conference, V.12, No. 2954, pp. 671-690.

128. Reese, L. C. and Welch, R. C. (1975). *Lateral loading of deep foundations in stiff clay*, J. Geotechnical Engineering Division, American Society of Civil Engineer, Vol. 101 No. GT7, pp. 633-649.

129. Reese, L. C., Cox, W. R. and Koop, F. D. (1974). *Analysis of laterally loaded piles in sand*, Proc. 6th Offshore Technology Conference, V.2080, pp. 473-485.

130. Robertson, P. K., Hughes, J. M. O., Campanella, R. G., and Sy. A. (1982). *Design of laterally loaded displacement piles using a driven pressuremeter,* Laterally loaded deep foundations, ASTM STP 835, Kansas City, June 1982.

131. Robertson, P. K., Hughes, J. M.O, Campanella, R. G., Brown, P and McKeown, S. (1986). *Design of laterally loaded piles using the pressuremeter,* The pressuremeter and its marine applications, Second Int. Symp., ASTM STP 950.

132. Sastry V. V. R. N. and Meyerhof, G. G. (1990). *Behaviour of flexible piles under inclined loads,* Canadian Geotechnical Journal, V. 27, pp. 19-28.

133. Schmertmann, J. H. (1975). *Measurement of in situ shear strength,* Proc. Of the ASCE Specialty Conf. On In Situ Measurement of Soil Properties, Raleigh, North Carolina, 2, pp. 57-138.

134. Scott, R. F. (1981). *Foundation Analysis*, Prentice-Hall, New Jersey, USA.

135. Shahrour, I. and Meimon, Y. (1991). *Analysis of the behaviour of offshore piles under inclined loads*, Proc. Int. Conf. on Deep Foundations, pp. 277-284.

136. Shim, X. M., (2000). *Centrifuge tests on model piles subjected to lateral and axial loads,* M.Sc. Thesis, University of Western Australia.

137. Skempton, A. W. (1951). *The bearing capacity of Clays*, Proceedings, Building Research Congress, England.

138. Skempton, A. W. (1954). *The pore pressure coefficients A and B,* Géotechnique, London, 4, pp. 143-148.

139. Smith, T. D. (1983). *Pressuremeter design method for single piles subjected to static lateral load,* Ph.D. Dissertation, Civil Engineering, Texas A. & M University.

140. *Specification for Piling*, The Institution of Civil Engineers, Thomas Telford Ltd., London, 1988.

141. Sullivan, W. R. (1977). *Development and evaluation of a unified method for the analysis of laterally loaded piles in clay*, M.S. Thesis, Graduate School of the University of Texas at Austin, Austin, Texas.

142. Sullivan, W.R., Reese, L. C. and Fenske, C. W. (1980). *Unified method for analysis of laterally loaded piles in clay*, Numerical methods in offshore piling, ICE, London, 135-146.

143. Terzaghi, K. (1955). *Evaluation of coefficients of subgrade reaction*, Geotechnique, Vol. 5, No. 4, pp. 297-326.

144. The Fredericks Company, *Electrolytic Tilt Sensors,* Product Literature, Huntingdon Valley, Pa., USA.

145. Tomlinson M. J. (1994). *Pile Design and Construction Practice*, 4th Ed., E & F N Spon, London.

146. Treacy, P. (1996). *Movement of vertical cuts in Dublin Boulder clay,* M.Sc. Dissertation, University of Dublin (Trinity College), Dublin.

147. Trochanis, A. M., Bielak, J. and Christiano, P. (1991). *Three dimensional non-linear study of piles*, J. Geotech. Engrg., ASCE, Vol. 117, No. 3, pp. 429-447.

148. Tyler, R. G. (1968). *Developments in the measurement of strain and stress in concrete bridge structures*, RRL Report 189, Crowthorne, Berkshire, England.

149. Vesic, A. (1961). *Bending of beams resting on isotropic elastic solid*, J. Engrg. Mech. Div., ASCE, 87(2), 35-53.

150. Window A. L. (1984). *An Introduction to strain gauges*, Welwyn Strain Measurement.

151. Window A. L. (1992). *Strain gauge technology*, 2nd Ed., Elsevier Applied Science.

152. Winkler, E. (1867). *Die lehre von elastizität und festigkeit (On elasticity and Fixity),* Prague.

153. Woodward, R. W., Gardner, W. S. and Greer, D. M. (1972). *Drilled pier foundations,* McGraw-Hill Book Company, New York.

154. Yegian, M. and Wright, S.G. (1973). *Lateral soil resistance-displacement relationship for pile foundations in soft clays*, 5th Annual Offshore Technology Conf. Houston, Paper OTC 1893, Vol. 2, pp. 663-676.

Appendix 2a

Relationship between K and E

APPENDIX 2a

2.1 Relationship between the Subgrade Reaction Modulus, K and Young's Modulus, E

In the analysis of laterally loaded piles, the relationship between the soil's elastic modulus (E) and the modulus of subgrade reaction (K) is often unclear and frequently a source of confusion within the industry. E can be related to K but the user must be aware that both terms have a totally different meaning. E represents the elastic stiffness of a soil mass and is obtained by dividing the stress by some reference strain giving units of stress or modulus. K on the other hand can be considered as the soil stiffness at a discrete depth; this can be conveniently visualised using a spring analogy. When loaded, a spring undergoes displacement until sufficient reaction is mobilised to restore equilibrium; the relationship between the applied load and the resulting spring displacement is known as the spring stiffness, K_{spring}. In foundation engineering, K represents the secant slope at any point on the p-y curve and by convention is defined as the soil reaction p (in units of force/length) divided by the soil movement y under the applied load i.e., $K = p/y$ and hence the spring analogy. Thus the units for the subgrade reaction modulus are also that of stress – and so the confusion.

It was illustrated in Figure 2-16 (chapter 2) that the subgrade reaction modulus is not a constant except for a small range of displacements. In non-linear problems, the ability of the spring model to predict accurately the lateral pile behaviour relies on calculating the modulus of subgrade reaction (a measure of the soil-pile interaction) at any depth during pile loading. Therefore, in a non-linear spring analysis the value of K is not a fundamental soil property but varies with p and y at any given load. This contrasts with a continuum analysis which employs a reference E value to represent the overall elastic response of the soil mass. Relationships between E and K for working stress (elastic) conditions have been provided by Vesic (1961), Broms (1964a), Poulos and Davis (1980) and more recently by Hsiung and Chen (1997). In Broms (1964a) analysis of the relationship between E and the horizontal modulus of subgrade[1] reaction, a secant modulus, E_{50}, corresponding to one-half the ultimate strength of the soil was assumed to govern the lateral displacements at working loads[2]. Broms showed the vertical deflection, y_o, of a circular plate could be calculated from the equation

$$y_0 = \frac{0.8BP(1-\nu^2)}{E_{50}}$$

in which B is the diameter of the loaded area, P, denotes the resulting pressure from the applied load and ν is the Poisson's ratio of the soil. Since PB/y_0 is equal to the coefficient of subgrade reaction, K and if ν is taken as 0.5 then

$$K = 1.67\,E_{50}$$

Poulos (1971) found the most accurate relationship between E and K was obtained by equating the elastic (continuum) and subgrade reaction solutions for the displacement of a stiff fixed-head pile. Assuming a υ of 0.5 and using an influence factor for pile

[1] Broms (1964a) and Terzaghi (1955) assumed that the horizontal modulus of subgrade reaction was the same as the vertical modulus of subgrade reaction measured in clays. Broms (1964a) argues that any differences between the two orientations tend to cancel each other. For example, due to edge effects, the subgrade reaction modulus at the head of a vertical pile will be less than the average modulus of subgrade reaction for a horizontal member. Furthermore, since the vertical member is surrounded on all sides by the elastic medium, the average modulus of subgrade reaction will be larger than that of the horizontal member.

[2] Broms noted that the secant modulus may be considerably less than the initial tangent modulus of elasticity of the soil.

displacement, the following relationship was obtained for a pile with a length (L) to diameter (d) ratio of 25:

$$K = 0.82E$$

The Poulos (1971) relationship was adopted as the default value for clays in the elastic-plastic soil model employed in the computer programme ALP.

Poulos and Davis (1980) investigated the results from laterally loaded piles analysed using both the linear elastic subgrade reaction model and a continuum models. Typical results for the displacements and rotations calculated by each method are illustrated in Figure 2-1 (assuming L/d ratio of 25 and $\upsilon = 0.5$). The results are presented in terms rotational (θ) and displacement (ρ) influence factors (I) for horizontal (H) and moment (M) loading at the pile head. The various I factors are determined on the basis of the soil-pile interaction factor[3] K_R. The results indicate that in all cases, the values from the elastic spring theory are greater than those from elastic theory. Poulos and Davies (1980) found the differences were even more pronounced at L/d ratios < 25. The discrepancy between the predictions is due to inaccuracies in the spring model which ignores the continuity that exists within the soil mass.

[3] $K_R = E_pI_p/E_sL^4$ where E_pI_p is the pile's flexural rigidity, E_s is Young's modulus for the soil and L is the embedded length of pile.

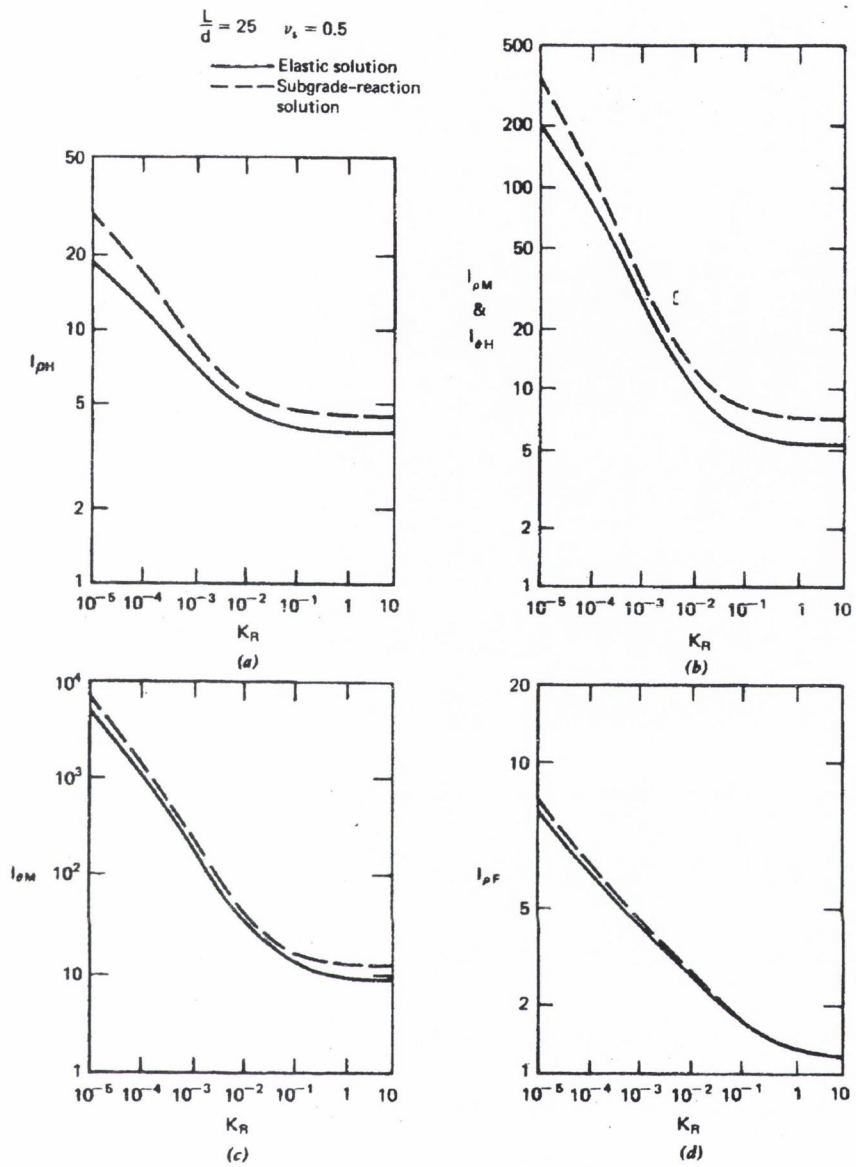

Figure 2-1: Comparison of elastic and subgrade reaction solutions for displacements and rotations, E_s constant. [from Poulos and Davis (1980)]

Elson (1984) quoting the results from a similar comparative study between the coefficient of subgrade reaction and Young's modulus found

$$K = 0.8 \text{ to } 1.8E$$

depending on the method of comparison (deflection or moment) and the pile conditions adopted

Ashour et al. (1998) provides a relationship which empirically links the horizontal modulus of subgrade reaction to the Young's modulus of the soil using the 'Strain-Wedge' (SW) model. In the SW model the parameter K varies in a non-linear fashion with the change in soil strain because K was established from an equivalent linear Young's modulus E of the strained soil i.e. for any depth i:

$$K_i = N_i E_i$$

where N is a derived function that relates stress-strain in the soil (i.e., E) to the corresponding size (depth) and shape of the mobilised wedge.

Appendix 2b

Traditional p-y formulations

APPENDIX 2b

2.1 Criteria for formulating p-y curves in clays

The methods for constructing *p-y* curves were derived largely from the results of field tests on laterally loaded piles. By combining soil mechanics theory with experimental results, correlations were made between soil properties, pile diameter and depth. Such correlation was seen as giving generality to the methods used in construction of *p-y* curves.

McClelland and Focht (1956) are credited with the initial development of the *p-y* concept. They proposed a linear conversion of the scales from non-linear laboratory stress-strain curves to produce correspondingly shaped *p-y* curves for laterally loaded piles. Although the method employed empirically determined correlation constants, their work represented the first significant attempt to deal with the non-linear response of soil to lateral pile displacement. The findings of McClelland and Focht have since been superseded by results from instrumented pile tests at five research sites involving four different soil conditions; these projects are:

1. Soft clay below the water table (Matlock 1970).

2. Stiff clay above the water table (Reese and Welch 1975)
3. Stiff clay below the water table (Reese, Cox and Koop 1975)
4. Unified clay criteria developed for combined soft and stiff clays below the water table (Sullivan, Reese and Fenske 1980)
5. Sands (Reese, Cox and Koop 1974)

These references describe the field tests and the soil conditions at each site. The findings of each test is summarised as a set of guidelines for establishing *p-y* curves which may be used for the design of laterally loaded piles in similar soil conditions. However, the user of these criteria are cautioned that any one set of *p-y* curves is strongly related to only one or two lateral load tests, this fact should be borne in mind when using the curves for design.

In each case, *p-y* curves for static short-term loading are presented initially; these are followed by recommendations for the construction of cyclic *p-y* curves to be used for piles subjected to repeated loading. Therefore, in most cases, particularly in offshore applications the cyclic curves will dictate the pile design. Consequently, the only purpose for studying the short-term static *p-y* curves is to furnish the basis for judging the effects of cyclic loading. Because this thesis concentrates on tests performed in soft and stiff clays, the criterion for sands is not discussed in this review. The following sections summarises the findings from the tests conducted in cohesive soils.

Soft clay below the water table (Matlock 1970).

Matlock (1970) developed a procedure for predicting *p-y* curves in soft, submerged clay; the research programme involved extensive field-testing with an instrumented pile, experiments with laboratory models, and parallel development of analytical methods and correlations.

A flexible 0.32m diameter heavily instrumented pipe pile was used on two separate on shore test sites; the pile was initially driven at Lake Austin and two complete series of free-head loading; one static and one cyclic load tests were performed. The pile was subsequently extracted and re-driven at a site near the mouth of the Sabine River on the Texas-Louisiana border and subjected to a series of static and cyclic tests under both free and fixed head conditions. The soil at Lake Austin was deposited during the last century

behind the Lake Austin dam and had been subjected to desiccation during periods of prolonged drawdown. The clays were therefore somewhat jointed and fissured with vane shear strengths c_u averaging 800 psf ($\approx$ 38kPa). At the Sabine site the clay was more typical of slightly overconsolidated marine deposits. Vane shear strengths c_u averaged about 300 psf ($\approx$ 15 kPa) in the significant upper zone; both sites were submerged to develop design criteria for of offshore piles.

The criteria for obtaining *p-y* curves for static loading consist of two parts. The first is to obtain an expression to describe the variation of the ultimate soil resistance, p_u, with depth. The second is to obtain an expression to describe the variation of the soil resistance with lateral deflection at any particular depth along the pile. The basic difference in these parts is that theory can generally be used to describe the variation of p_u with depth, but empiricism must be employed to describe the actual shape of the *p-y* curve.

The ultimate resistance (p_u) of soft clay increases from $3c_u$ to $9c_u$ as the depth z increases from 0 to z_R according to:

Eq. 0-1... $p_u = c_u B N_p$ for $z \leq z_R$

and

Eq. 0-2... $p_u = 9c_u B$ for $z \geq z_R$

Where p_u = ultimate soil resistance per unit length (kN/m)

N_p = lateral bearing capacity factor $= \left\{ 3 + \frac{\gamma' z}{c_u} + J\frac{z}{B} \right\}$

c_u = undrained shear strength (kN/m²)

B = pile diameter (m)

γ' = effective unit weight (kN/m²)

J = dimensionless empirical constant (0.5 for soft clays)

z = depth below soil surface (m)

z_R = depth below soil surface to bottom of reduced resistance zone (m)

If c_u is constant with depth, equations Eq. 0-1 and Eq. 0-2 are solved simultaneously to give:

$$z_R = \frac{6B}{\frac{\gamma' B}{c_u} + J}$$

If c_u varies with depth, equations Eq. 0-1 and Eq. 0-2 are both solved at each depth, until equation Eq. 0-2 is less than equation Eq. 0-1 to give z_R[1].

The first term in N_p expresses the resistance at the surface, the second term gives the increase with depth due to overburden pressure and the third term may be thought of as the geometrically related restraint that even a weightless soil around a pile would provide against upward flow of the soil. The equation corresponds closely to the theoretical expression developed by Reese (1958).

To define the shape of the *p-y* curve, Matlock selected the following equation based on semi-logarithmic plots of the experimental *p-y* curves, which fell roughly along straight lines the slopes of which yielded the exponent 1/3;

Eq. 0-3... $$\frac{p}{p_u} = 0.5\left(\frac{y}{y_c}\right)^{\frac{1}{3}}$$

where

Eq. 0-4... $$y_c = 2.5\varepsilon_{50}B$$

and ε_{50} is the strain at 50% of the maximum stress difference, determined from UU triaxial compression tests (based on the work of Skempton, 1951).

Hence, from Eq. 0-3 the point of intersection with the plastic branch of the curve (point e where $p/p_u = 1$) will always occur at a horizontal coordinate of 8.

[1] However, at the time of Matlock's work, soils with c_u varying with depth had not been tested physically.

The API (1993) recommends Eq. 0-3 for the construction of short-term *p-y* curves using the following points (see Figure 0-1)

p/p_u	y/y_c
0	0
0.24	0.2
0.50	1.0
0.72	3.0
1.00	8.0
1.00	∞ (2.5B)

where p = soil resistance per unit length (kN/m)

y = lateral deflection (mm)

If no direct laboratory data is available, suggested values of ε_{50} for soft to firm clays are as follows (after Sullivan et al. 1980).

Consistency	ε_{50}
Soft	0.020
Firm	0.010

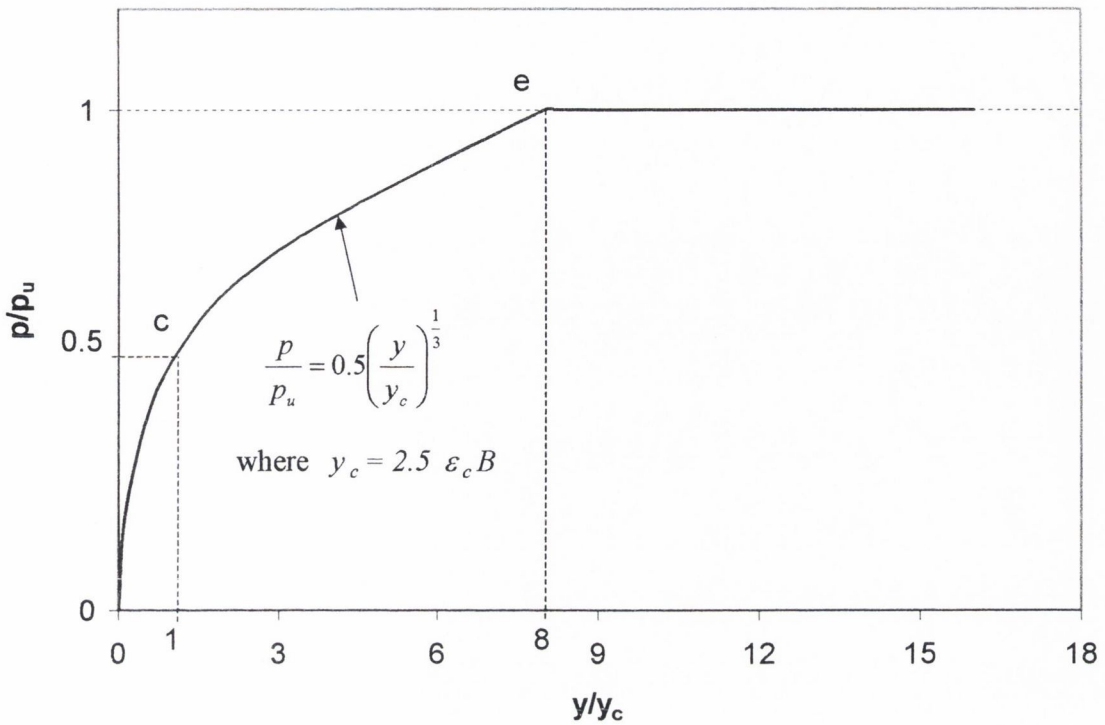

Figure 0-1: *p-y* curve for soft clay (Static)

Cyclic loading

The effects of cyclic loading were found to decrease the ultimate soil resistance to $0.72p_u$ at a displacement of $3y_c$ and further reductions in the soil resistance took place at displacements greater than $3y_c$ for depths less than z_R. A cyclic *p-y* curve using the Matlock (1970) *p-y* criteria is shown in Figure 0-2. The shape of the cyclic curve was based on the results of the field tests at Sabine and on laboratory model tests. During the cyclic tests, a load of given magnitude was repeated until the displacements and bending moment reached an equilibrium condition. It was demonstrated at Lake Austin and confirmed at Sabine Pass that a period of rest does not provide any restoration of the soil resistance since there are no significant forces that would tend to close the cavity at the top of the pile. The API (1993) recommends *p-y* curves for cyclic loading in homogeneous marine clay be generated from the points[2] given in Figure 0-2.

[2] Matlock (1970) recommended a more conservative cyclic *p-y* curve be adopted for cyclic loading in jointed or fissured clays because of the highly concentrated shear deformation and slip along the planes of weakness.

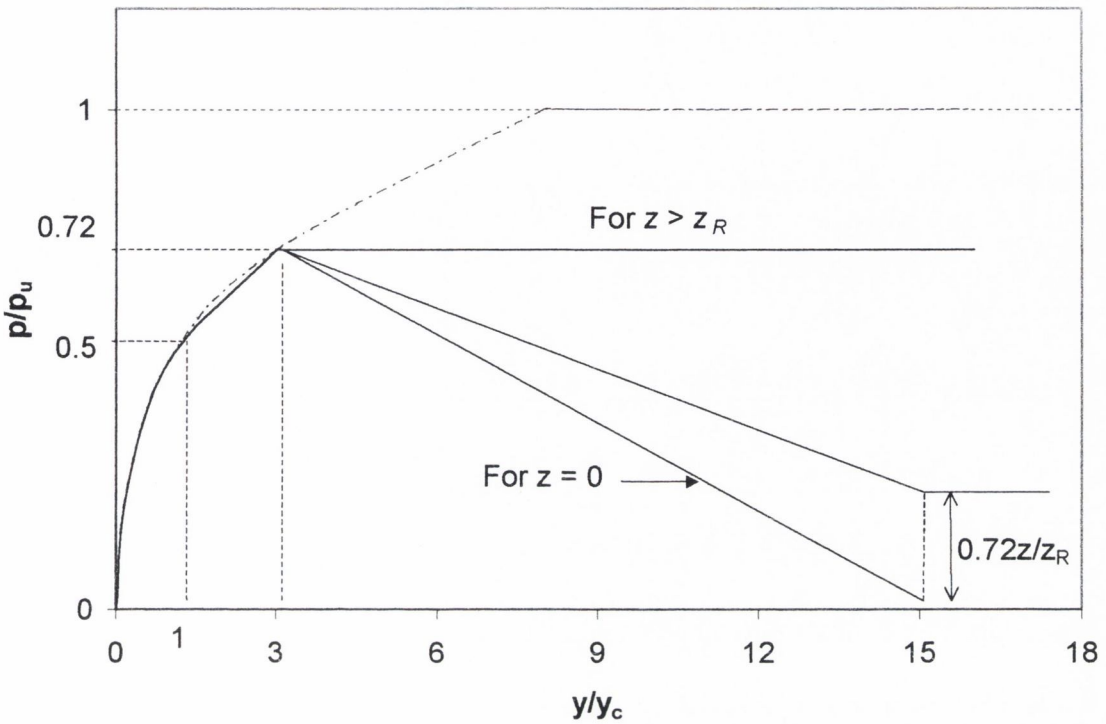

Figure 0-2: *p-y* curve for soft clay (Cyclic)

Stiff clay above the water table (Reese and Welch 1975)

Reese and Welch (1975) proposed criteria for predicting the behaviour of flexible piles in stiff clays ($c_{u\ (avg)} \approx$ 100kPa) above the water table[3]. The field tests were performed on a 914mm (36-inch) diameter bored concrete pile at a site in Houston, Texas. Procedures were recommended for constructing *p-y* curves for the cases of short-term static loading and for cyclic loading.

The criteria that were proposed for static loading are similar to those proposed by Matlock (1970). The equations describing the variation of p_u with depth are nearly the same, except for the manner in which the undrained shear strength is defined. Matlock (1970) defined $c_{u(z)}$ as the undrained shear strength at a depth z; Reese and Welch defined the undrained shear strength as $c_{u(avg)}$, which is the average undrained shear strength from the ground surface to the depth where p_u is being calculated. Another difference between the two

[3] The water table was located 5.5m below ground level during the test.

criteria is the exponent describing the shape of the *p-y* curve. Reese and Welch suggest the expression shown in Eq. 0-5 for stiff clays above the water table.

Eq. 0-5...
$$\frac{p}{p_u} = 0.5\left(\frac{y}{y_{50}}\right)^{\frac{1}{4}}$$

The experimental *p-y* curves (Eq. 0-5) were correlated with the laboratory stress-strain curves described by Eq. 0-6 for UU triaxial tests:

Eq. 0-6...
$$\frac{q}{q_{max}} = 0.5\left(\frac{\varepsilon}{\varepsilon_{50}}\right)^{0.5}$$

where $q = (\sigma_1 - \sigma_3)$ = deviator stress.

Reese and Welch (1975) assumed that the field and laboratory curves were similar in shape and thus could be related as follows

$$\left(\frac{y}{y_{50}}\right)^{1/4} = \left(\frac{\varepsilon}{\varepsilon_{50}}\right)^{1/2}$$

Hence using Eq. 0-4 the soil displacement was calculated from the expression given in Eq. 0-7:

Eq. 0-7...
$$y = \left(\frac{2.5B}{\varepsilon_{50}}\right)\varepsilon^2$$

Therefore, Reese and Welch (1975) concluded that if the laboratory stress-strain curve for a soil is known, then Matlock's expressions for soil resistance given in Eq. 0-1 and Eq. 0-2 can be combined with Eq. 0-4, Eq. 0-5 and Eq. 0-7 to predict short term static *p-y* curves for a deep foundation (with any diameter) in stiff clays above the water table.

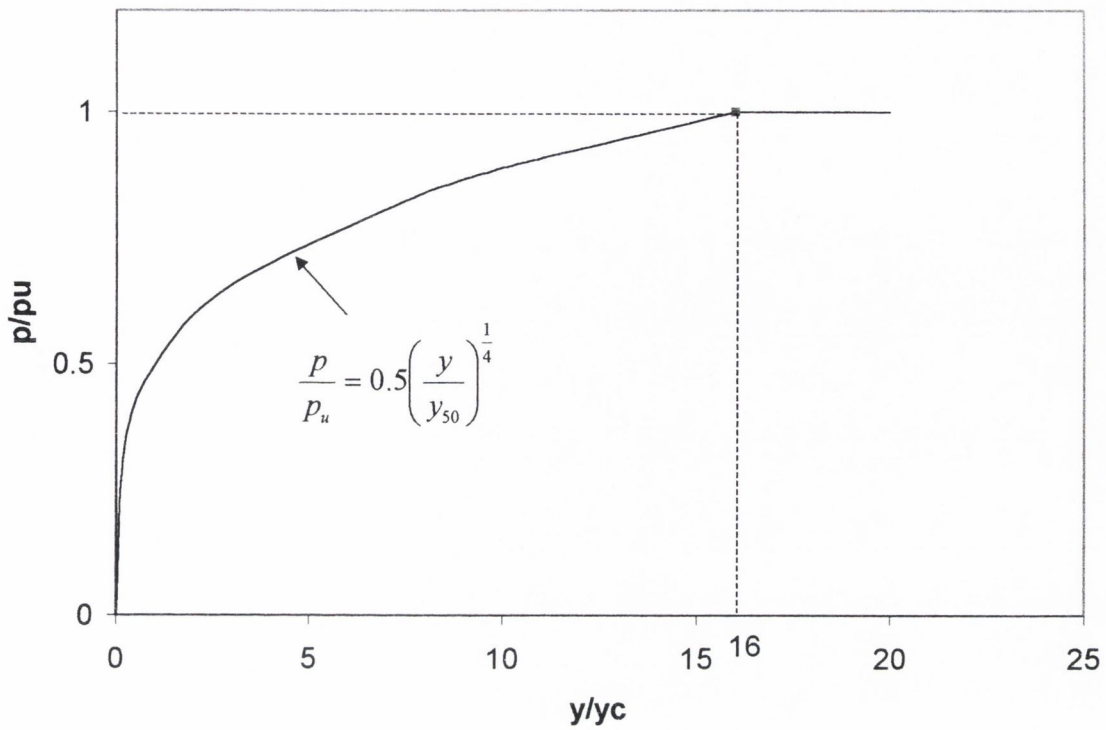

Figure 0-3: Characteristic shape of the static *p-y* curves for stiff clay above the water table (from Reese and Welch, 1975)

Cyclic loading in stiff clay above the water table

The procedure for accounting for the effects of cyclic loading using the Reese and Welch criteria are different than that proposed by Matlock (1970). Reese and Welch found that for clay above the water table repeated load applications do not affect the ultimate soil resistance but do increase the deflection at which p_u occurs. The cyclic deflection, y_c, is computed using Eq. 0-8:

Eq. 0-8... $$y_c = y_s + y_{50} C \log N$$

where

y_s = static deflection

$C = 9.6R^4$

N = number of cycles

and

$$R = \frac{p}{p_u} = \frac{q}{q_{max}} = \text{stress ratio}$$

It can be seen from Eq. 0-8, that the increase in deflection is not only a function of the number of cycles but also the stress level.

The use of these guidelines for developing *p-y* curves in stiff clays above the water table are not recommended for the design of offshore structures because of the effect cyclic loading would have on the resistance of the submerged soil. The recommendations adopted by the API for offshore design in submerged stiff clay are discussed in the following section.

Stiff clay below the water table (Reese, Cox and Koop 1975).

Reese et al. (1975) performed tests on 24-inch (610 mm) diameter instrumented pipe piles embedded 15.2m in a submerged, heavily overconsolidated clay deposit, at a site near Manor, Texas. The clay had undrained (UU) shear strength ranging from about 1ton/ft^2 (≈100kPa) at the ground surface to 3 ton/ft^2 (300kPa) at a depth of 3.66m. The purpose of the tests was to develop criteria that could be used to predict the behaviour of piles under short-term static and cyclic loading in offshore applications. The variation of the ultimate soil resistance with depth was based on the wedge-type failure and the flow-around failure theories discussed in chapter 2. The two theoretical expressions derived for each failure condition were:

For wedge failure:

Eq. 0-9... $$p_u = 2c_uB + \gamma'Bz + 2.83c_uz$$

where

p_u = ultimate soil resistance at depth z

c_u = average undrained shear strength of clay over depth z

γ' = submerged unit weight of soil (assuming water surface to be above ground surface)

For flow around failure:

Eq. 0-10... $p_u = 11 c_u B$

where

c_u = the undrained shear strength of the clay at depth of the *p-y* curve.

Poor agreement was obtained when the ultimate soil resistances using Eq. 0-9 and Eq. 0-10 were compared to the ultimate soil resistances from the experiments. Therefore, the larger theoretical values were adjusted by dividing the observed ultimate soil resistance by the computed ultimate soil resistance using the following empirical adjustment factors:

$$A = (p_u)_s / p_c$$

$$B = (p_u)_c / p_c$$

where

A = empirical adjustment factor for static loading
B = empirical adjustment factor for cyclic loading
p_c = ultimate resistance from theory
$(p_u)_s$ = ultimate resistance measured for static loading
$(p_u)_c$ = ultimate resistance measured for cyclic loading

The experimentally determined values for coefficients A and B are shown in Figure 0-4.

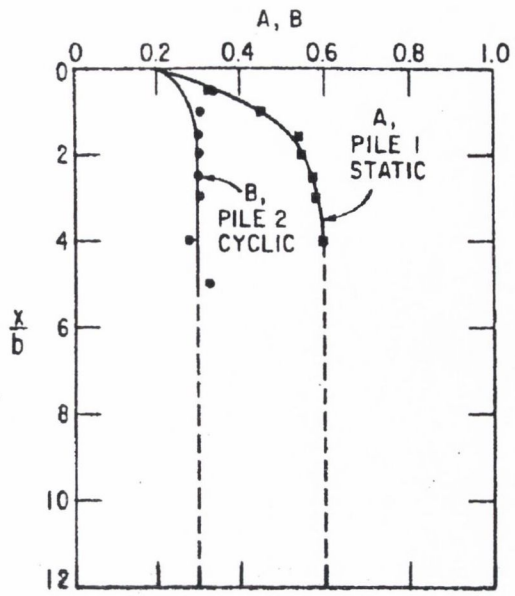

Figure 0-4: Values for coefficients A and B

The construction of the *p-y* curves for the static case involves the use of four functions; an initial straight portion, shown in Figure 0-5 from the origin to point 1; two parabolic sections, from point 1 to point 2 and from point 2 to point 3: and two straight portions, from point 3 to point 4 and a horizontal line beyond point 4. The complex definition of the *p-y* curve is necessitated due to the irregular shape of the experimental *p-y* curves shown in Figure 0-6.

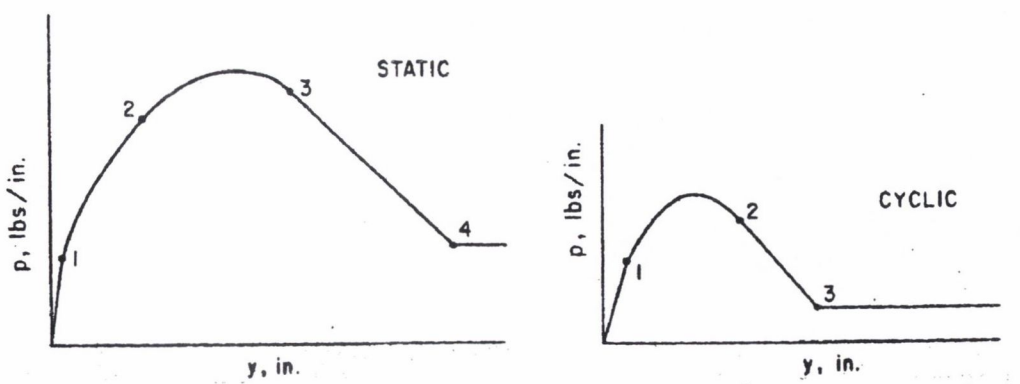

(a) Static (b) Cyclic

Figure 0-5: Characteristic shape of proposed *p-y* criteria for stiff submerged clay

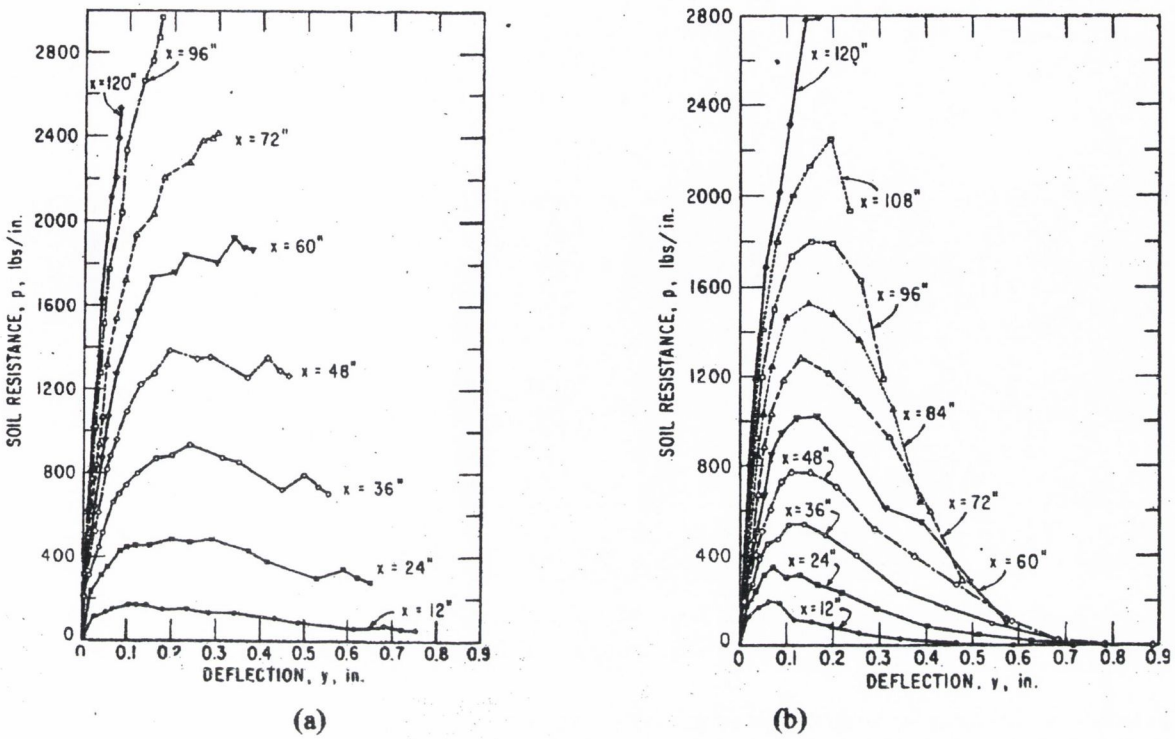

Figure 0-6: Experimental *p-y* curves for (a) static and (b) cyclic loads on 24inch (610mm) diameter pile[4].

The initial slope of a *p-y* curve was defined by:

Eq. 0-11... $K_{si} = k_s z$

where k_s is a constant for static loading and z is the depth under consideration.

Therefore the initial straight-line portion of the *p*-y curve is given by
Eq. 0-12.

Eq. 0-12... $p = K_{si} y$

Values for k suggested by Reese and Welch (1975) are given in Table 0-1.

[4] Note; x represents the depth below ground level.

	Average undrained shear strength (tons/ft^2)		
	0.5-1.0	1-2	2-4
k_s (static) lb/in^3	500	1000	2000
k_c (cyclic) lb/in^3	200	400	800

Note: 1 ton/ft^2 ≈ 100kPa, 1 lb/in^3 ≈ 272 kN/m^3

Table 0-1: Recommended values for k_s for stiff clay

To define the next portion of the curve, the parameter ε_{50} was used to define y_c in Eq. 0-13.

Eq. 0-13... $$p = 0.5 p_c \left(\frac{y}{y_c} \right)^{0.5}$$

where $$y_c = \varepsilon_{50} B$$

The parabolic portion of the curve goes through the origin, but the actual *p-y* curve starts at the intersection of the straight line, defined by the slope, K_{si} in Eq. 0-11, and the parabola, defined by Eq. 0-13[5]. Eq. 0-13 continues to the displacement Ay_c where A is obtained from Figure 0-4 for the nondimensional depth *z/B*. Beyond this point, the parabola is modified by an offset defined by Eq. 0-14.

Eq. 0-14... $$p_{offset} = 0.055 p_c \left(\frac{y - Ay_c}{Ay_c} \right)^{1.25}$$

Thus the shape of the second parabola is obtained by combining Eq. 0-13 and Eq. 0-14 to give;

[5] The characteristic *p-y* curve is drawn as if there is an intersection between Eq. 0-12 and Eq. 0-13. However, there may be no intersection of Eq. 0-12 with any of the other equations defining the *p-y* curve. Eq. 0-12 defines the *p-y* curve until it intersects with one of the other equations or, if no intersection occurs, Eq. 0-12 defines the complete *p-y* curve.

$$p = 0.5p_c\left(\frac{y}{y_c}\right)^{0.5} - 0.055p_c\left(\frac{y - Ay_c}{Ay_c}\right)^{1.25}$$

The offset correction to the *p-y* curve continues to a displacement corresponding to $6Ay_c$. At this point, the *p-y* curve assumes a straight line with a slope defined by the Eq. 0-15.

Eq. 0-15... $$E_{ss} = -\frac{0.0625p_c}{y_c}$$

The straight line defined by Eq. 0-15 continues to a displacement of $18Ay_c$, where the soil resistance remains constant for further increases in displacement. A *p-y* curve for static loading is shown in Figure 0-7a.

Cyclic loading in stiff submerged clay

The effects of cyclic loading in stiff submerged clay are to reduce the ultimate soil resistance and to reduce the deflection at which this ultimate resistance occurs. Three functions are used to describe the cyclic *p-y* curve. The first function is;

Eq. 0-16... $$K_{si} = k_c z$$

Values for k_c are given in Table 0-1. The parabolic portion of the cyclic *p-y* curve starts at the intersection of the straight line defined by Eq. 0-12 (but with the slope given in Eq. 0-16)[6] and is described by the curve given in Eq. 0-17.

[6] The characteristic *p-y* curve is drawn as if there is an intersection between Eq. 0-12 and Eq. 0-17. However, there may be no intersection of those two equations, and there may be no intersection of Eq. 0-12 with any of the other equations defining the *p-y* curve. If there is no intersection, the equation should be employed that gives the smallest value of *p* for any value of *y*.

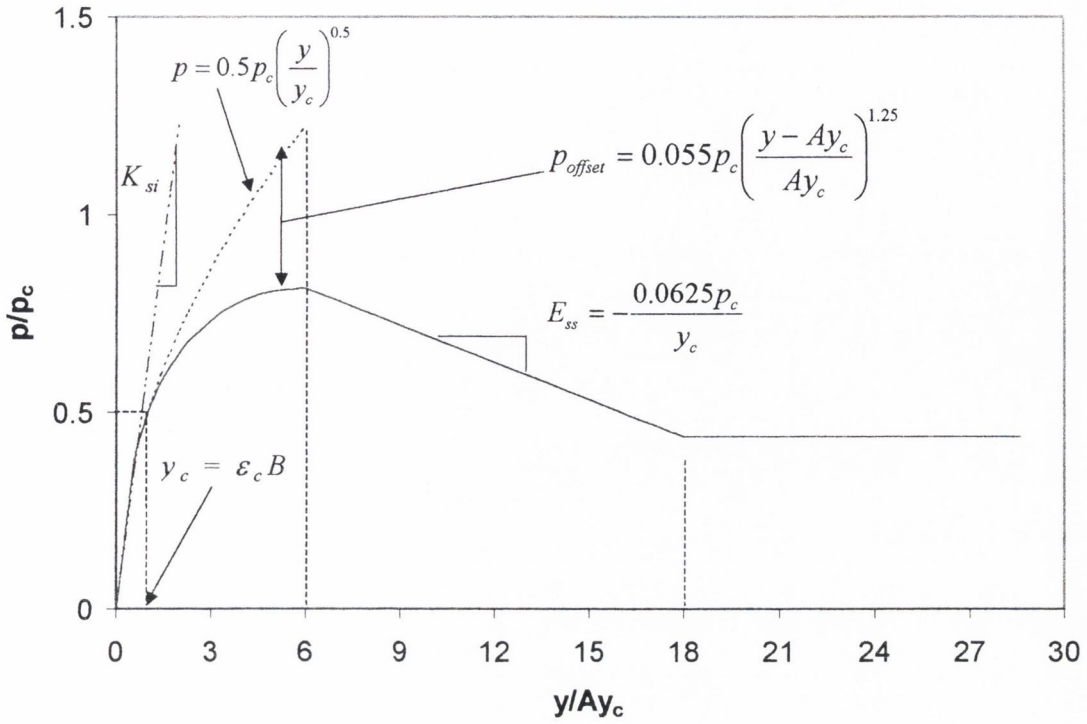

(a) Static loading

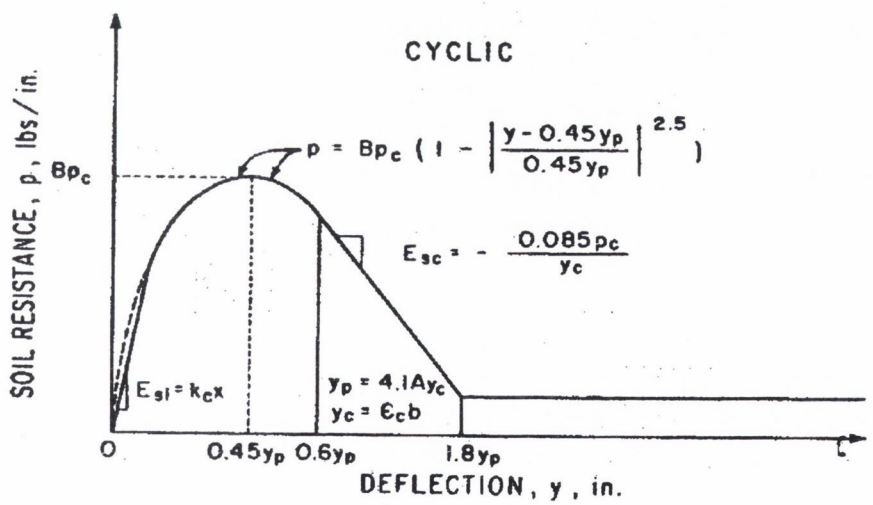

(b) Cyclic loading

Figure 0-7:Characteristic shape of *p-y* curves for stiff clay below the water table

Eq. 0-17... $$p = Bp_c\left[1-\left(\frac{y-0.45y_p}{0.45y_p}\right)^{2.5}\right]$$

where $y_p = 4.1\,Ay_c$

The parabola continues to a deflection corresponding to $0.6y_p$. At this point the *p-y* curves assumes a straight line with a slope defined by Eq. 0-18.

Eq. 0-18... $$E_{sc} = -\frac{0.085p_c}{y_c}$$

The straight line defined by the slope E_{sc} continues to a displacement of $1.8y_p$ at which point the *p-y* curve becomes horizontal. A *p-y* curve for cyclic loading is shown in Figure 0-7b.

Unified clay criteria developed for combined soft and stiff clays below the water table (Sullivan et al., 1980)

In an attempt to provide a link between the soft clay and stiff clay *p*-y criteria for submerged soils, Sullivan et al. (1980) provided recommendations for ascertaining the range of undrained shear strength in which the criteria for soft clay versus those for stiff clay should be used. Sullivan et al. examined the original experiments in soft clay at Sabine and the tests in stiff clay at Manor. The analysis was used to establish a set of recommendations that yield computed behaviours in reasonably good agreement with the experimental results. However, the unifying criteria was generalised by introducing empirical factors obtained from correlations with the test data. The empirical factors depend mainly on the stress-strain properties of the clay and necessitate judgement when selecting appropriate parameters for use in the prediction equations. The expressions proposed by Sullivan (1977) for N_p as a function of depth are plotted in nondimensional form in Figure 0-8.

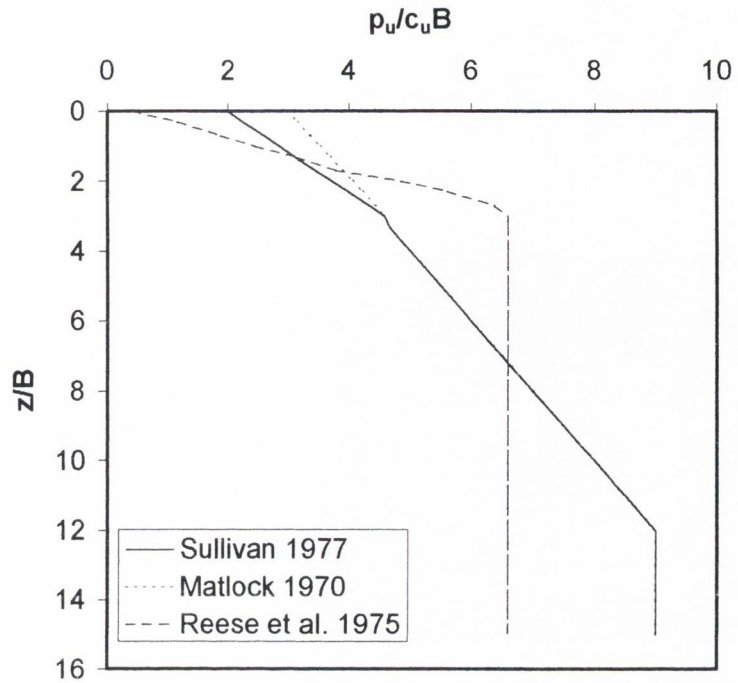

Figure 0-8: Variation of N_p with depth for a soil deposit with a uniform shear strength

The variation in N_p differs from both Matlock (1970) and Reese et al. (1975) because three equations were used to describe the variation of p_u with depth. Sullivan's expression for N_p for z/B greater than 3, is the same as Matlock's for a constant shear strength deposit (Figure 0-8). The equations proposed for describing the variation of the ultimate soil resistance with depth are again based on a wedge type failure near the ground surface and flow around failure of the soil at depth. Both types of behaviour were discussed in detail in chapter 2. Eq. 0-19 and Eq. 0-20 were proposed for the ultimate soil resistance near the ground surface and Eq. 0-21 for the ultimate resistance at great depth.

Eq. 0-19... $$p = \left(2 + \frac{\gamma' z}{c_u} + 0.833\frac{z}{B}\right) c_{u\,avg} B \qquad \text{for } 0 < z < 3B$$

Eq. 0-20... $$p = \left(3 + 0.5\frac{z}{B}\right) c_u B \qquad \text{for } 3B < z < 12B$$

Eq. 0-21... $p_u = 9c_uB$ for $z > 12B$

The average undrained shear strength was employed in Eq. 0-19 because of the assumption of a wedge type failure near the ground surface. The transition depths are for clay with constant shear strength, if $(c_u)_{avg}$ is not constant, the smallest value of p_u for the three equations should be selected corresponding to a particular depth.

The shape of the *p-y* curve was generalised, and correlations were made with the results of both the Sabine tests and Manor tests. To account for the large differences in behaviour of the test piles at the two sites, mathematical expressions and empirical factors were applied to the generalised *p-y* curves. A characteristic *p-y* curve using the unified criteria is shown in Figure 0-9. The curve is similar to that proposed by Matlock (1970) with the exception that the Matlock criterion produces a slope approaching infinity as the displacement approaches zero. Sullivan (1977) chose to use a linear function to define the initial portion of the *p-y* curve:

Eq. 0-22... $p = (K_s)_{max}y$ where $(K_s)_{max} = kz$

The parameter k is a constant whose magnitude depends only on the shear strength of the clay; typical values for the unified criteria are given in Table 0-2.

c_u (kPa)	k (MN/m^3)
12 - 25	8
25 – 50	27
50 – 100	80
100 – 200	270
200 - 400	800

Table 0-2: Representative values for k

Except for the initial slope, the shape of the static *p-y* curve, up to a deflection of $8y/y_c$, is the same as the shape suggested by Matlock (1970) given in Eq. 0-3. However, Sullivan redefined y_c as;

Eq. 0-23... $$y_c = A\varepsilon_{50}B$$

The soil resistance after large deformation ($y/y_{50} > 30$) is given by Eq. 0-24 and Eq. 0-25. The smaller of the values computed by the two equations should be employed.

Eq. 0-24... $$p_R = p_u\left(F + \{1-F\}\frac{z}{12B}\right) \qquad \text{for } z < 12B$$

Eq. 0-25... $$p_R = p_u \qquad \text{for } z > 12B$$

where p_R is the residual shear resistance.

Eq. 0-23 and Eq. 0-24 used to define the *p-y* curve contain the coefficients A and F[7]. Table 0-3 gives the determined empirically coefficients from the results of the Sabine and Manor tests. For soils which are different than those at Sabine and Manor, Sullivan et al. (1980) suggests measuring the soil properties listed in Table 0-3 and comparing the results obtained with those at Sabine or Manor, judgement must then be used to select appropriate values for A and F.

[7] F is a function of the stress-strain characteristics of the soil.

Site	Sabine River	Manor
Clay description	Inorganic, intact	Inorganic, very fissured
	$(c_u)_{avg.} \approx 15$kPa	$(c_u)_{avg.} \approx 115$kPa
	OCR ≈ 1	OCR > 10
	$S_t \approx 2$	$S_t \approx 1$
	$\varepsilon_{50} = 0.007$	$\varepsilon_{50} = 0.005$
	$w_L = 92$	$w_L = 77$
	PI = 68	PI = 60
	LI= 1	LI ≈ 0.2
A	2.5	0.35
F	1.0	0.5

Table 0-3: Curve parameters for unified criteria

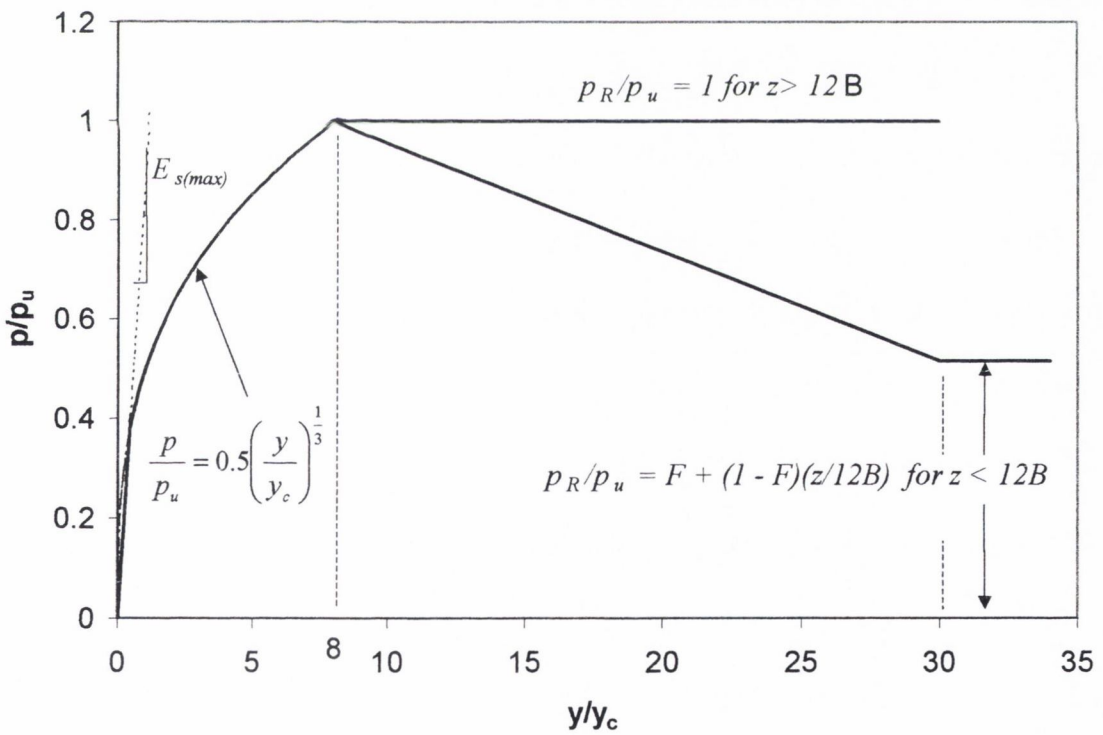

Figure 0-9: Characteristic shape of *p-y* curve for unified clay criteria for short term static loading (from Sullivan et al., 1980)

For static loading, the residual soil resistance is reached at a displacement of $30y_c$. The selection of $30y_{50}$, and the increase of p_R/p_u with depth are arbitrary. However, the shape of the curve shown in Figure 0-9 for the residual portion of the curve gave good agreement between the measured and computed values when compared with experimental values.

Unified p-y curve for cyclic loading.

The *p-y* curve for cyclic loading shown in Figure 0-10 is completely empirical, and is similar in shape to the curve for static loading, but the ultimate soil resistance is reduced. Matlock (1970) found that p_u was reduced to about 72% of the static value; however, Reese et al. (1975) found that p_u reduced to about 50% of the static value for their tests. Sullivan therefore used a 50% reduction in p_u for the unified cyclic criteria. The reduction in p_u and the use of 2 for N_p at the ground surface would lead to a conservative estimate of p_u for the Sabine tests. In Figure 0-10, it can be seen that the soil resistance at deflections larger than $20y/y_{50}$ is zero at the ground surface and increases to $0.5p_u$ at a depth of 12B.

The shapes of the static and cyclic *p-y* curves for the unified method are based on the assumption that Eq. 0-22 and Eq. 0-3 intersect. If intersection does not occur, the *p-y* curve is defined by Eq. 0-22 until there are an intersection between Eq. 0-22 and the curves defining the *p-y* curve at greater pile displacements.

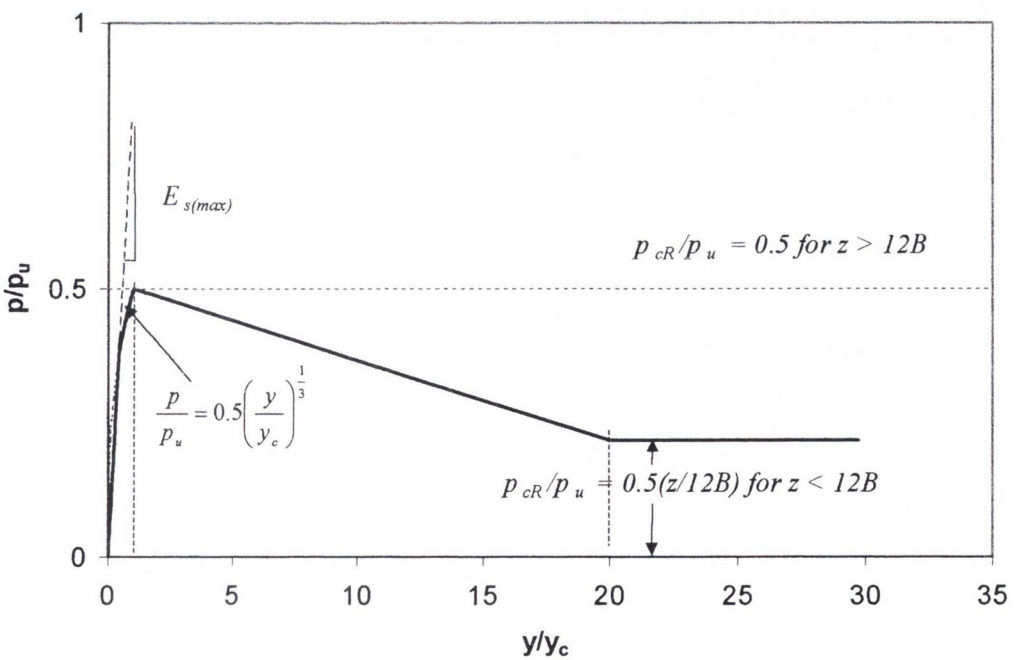

Figure 0-10: Characteristic shape of *p-y* curve for unified clay criteria for cyclic loading (from Sullivan et al., 1980)

Appendix 3

Calibration and Performance of Instruments

Electro-level calibration.

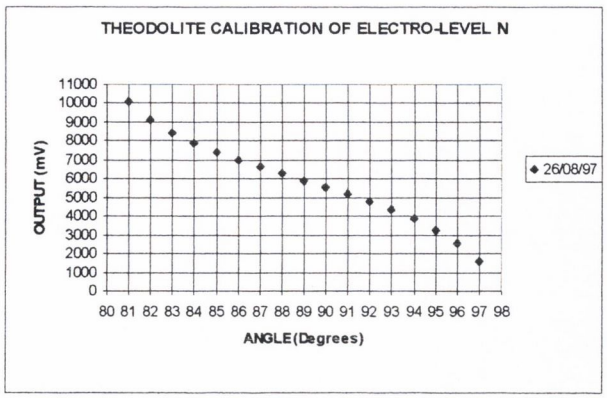

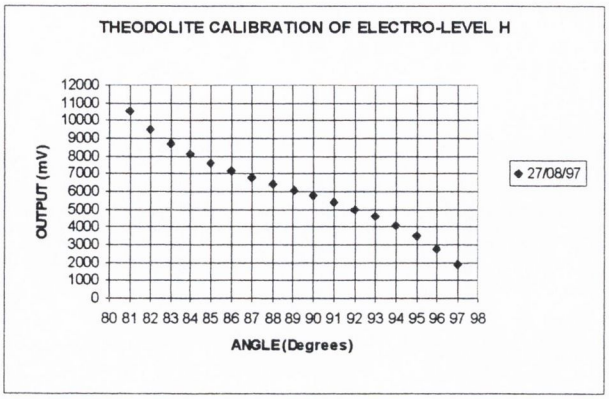

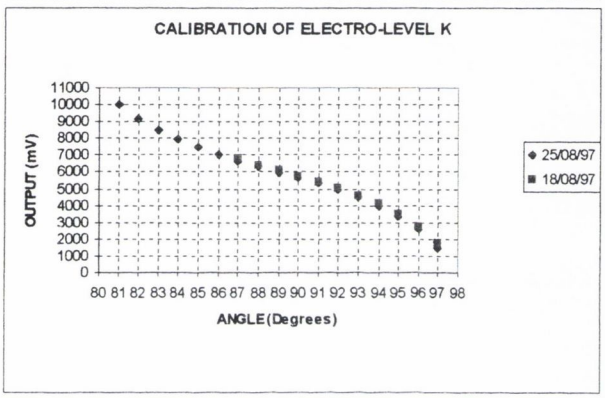

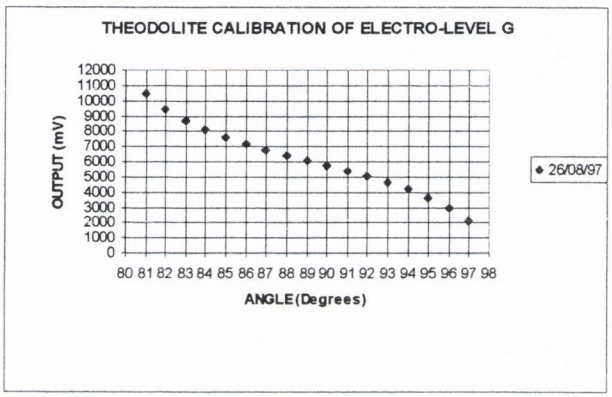

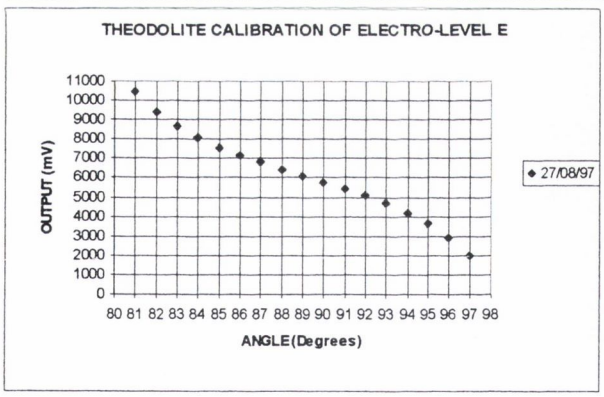

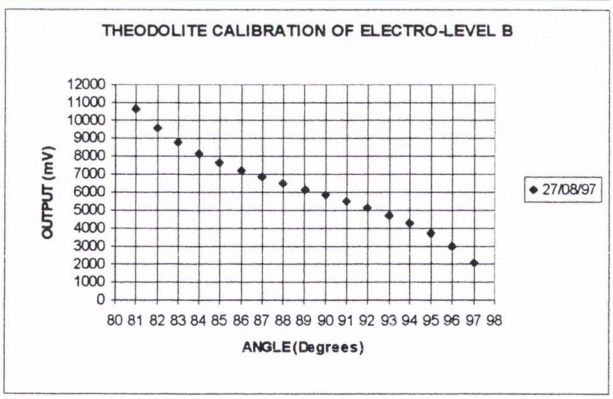

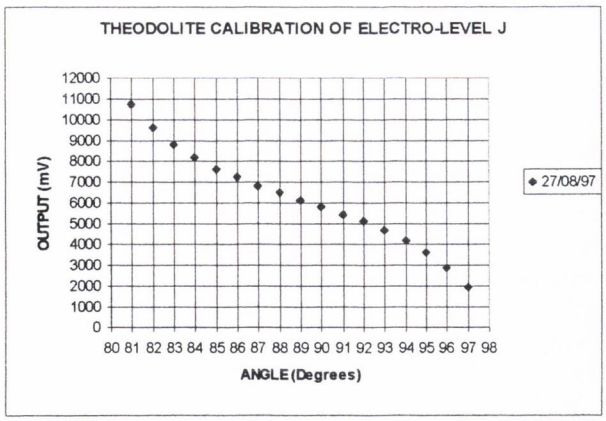
THEODOLITE CALIBRATION OF ELECTRO-LEVEL J
OUTPUT (mV)
12000
11000
10000
9000
8000
7000
6000
5000
4000
3000
2000
1000
0
80 81 82 83 84 85 86 87 88 89 90 91 92 93 94 95 96 97 98
ANGLE (Degrees)
27/08/97

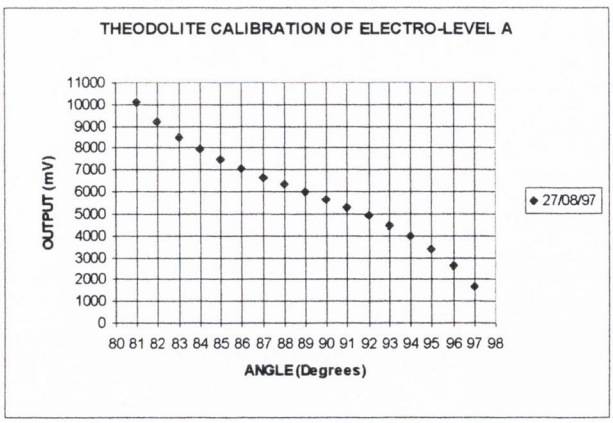
THEODOLITE CALIBRATION OF ELECTRO-LEVEL A
OUTPUT (mV)
11000
10000
9000
8000
7000
6000
5000
4000
3000
2000
1000
0
80 81 82 83 84 85 86 87 88 89 90 91 92 93 94 95 96 97 98
ANGLE (Degrees)
27/08/97

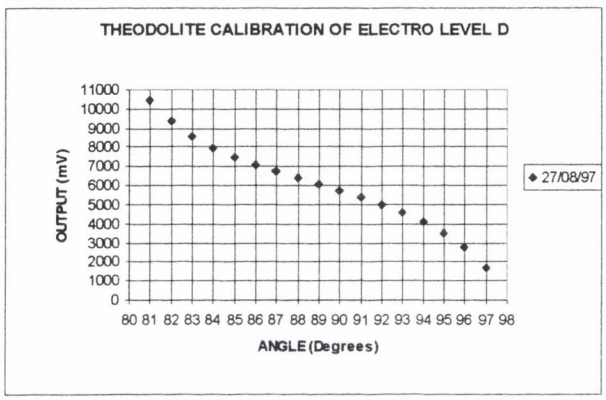
THEODOLITE CALIBRATION OF ELECTRO LEVEL D
OUTPUT (mV)
11000
10000
9000
8000
7000
6000
5000
4000
3000
2000
1000
0
80 81 82 83 84 85 86 87 88 89 90 91 92 93 94 95 96 97 98
ANGLE (Degrees)
27/08/97

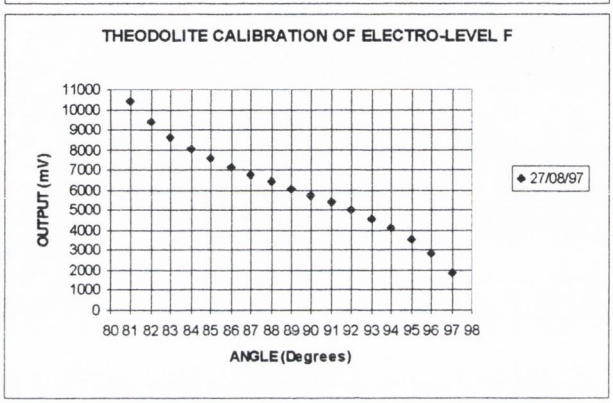
THEODOLITE CALIBRATION OF ELECTRO-LEVEL F
OUTPUT (mV)
11000
10000
9000
8000
7000
6000
5000
4000
3000
2000
1000
0
80 81 82 83 84 85 86 87 88 89 90 91 92 93 94 95 96 97 98
ANGLE (Degrees)
27/08/97

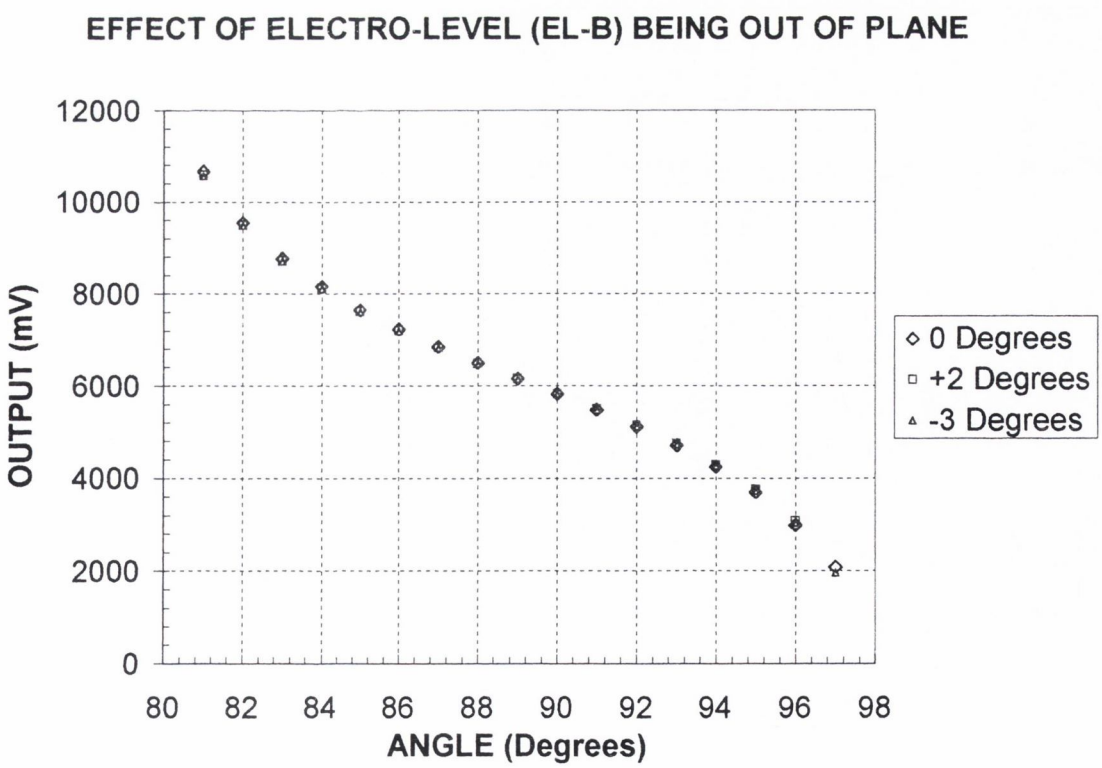
EFFECT OF ELECTRO-LEVEL (EL-B) BEING OUT OF PLANE
OUTPUT (mV)
12000
10000
8000
6000
4000
2000
0
80
82
84
86
88
90
92
94
96
98
ANGLE (Degrees)
0 Degrees
+2 Degrees
-3 Degrees

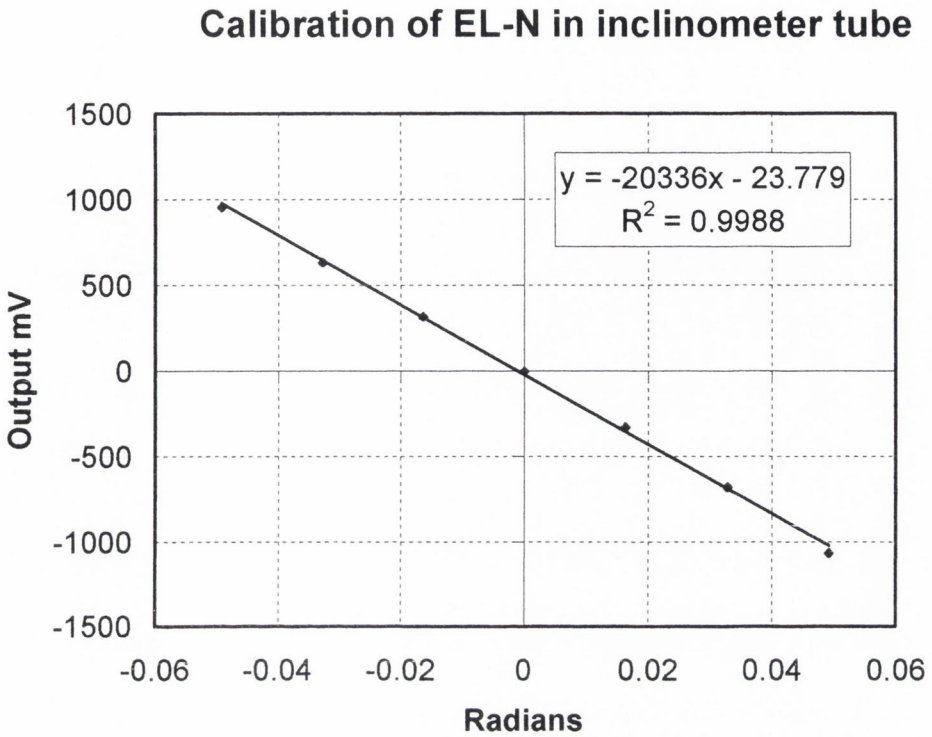

Typical Calibration curve and best fit line for linear operating range

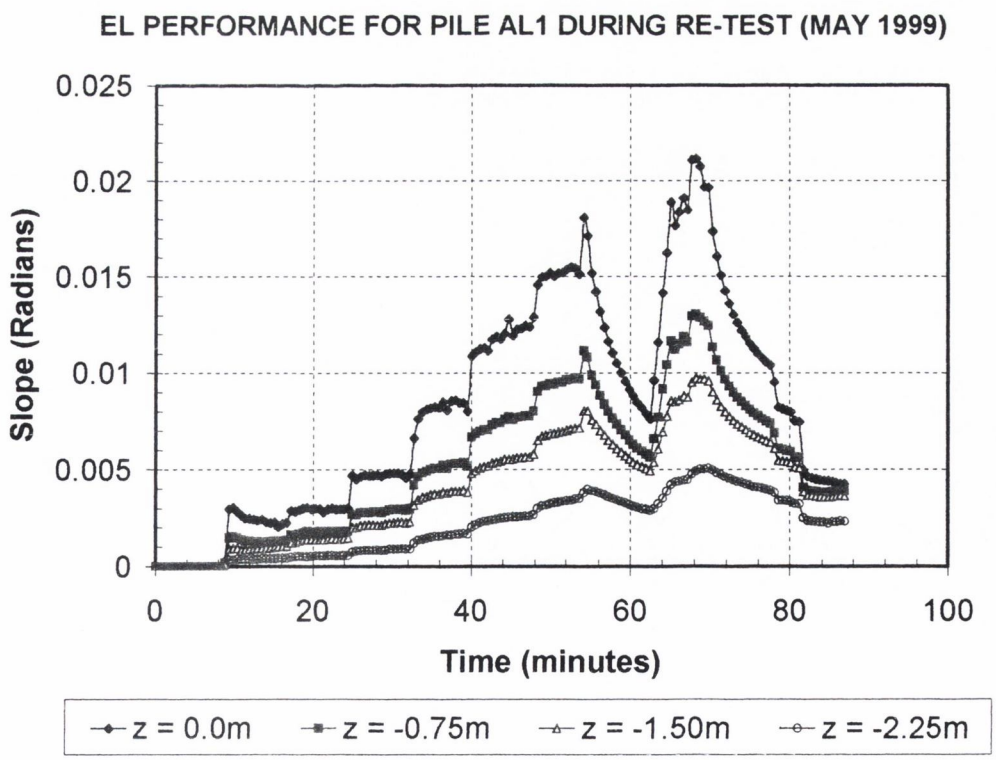

Typical EL output versus Time profiles recorded during the load tests

Pressure Cell Calibration

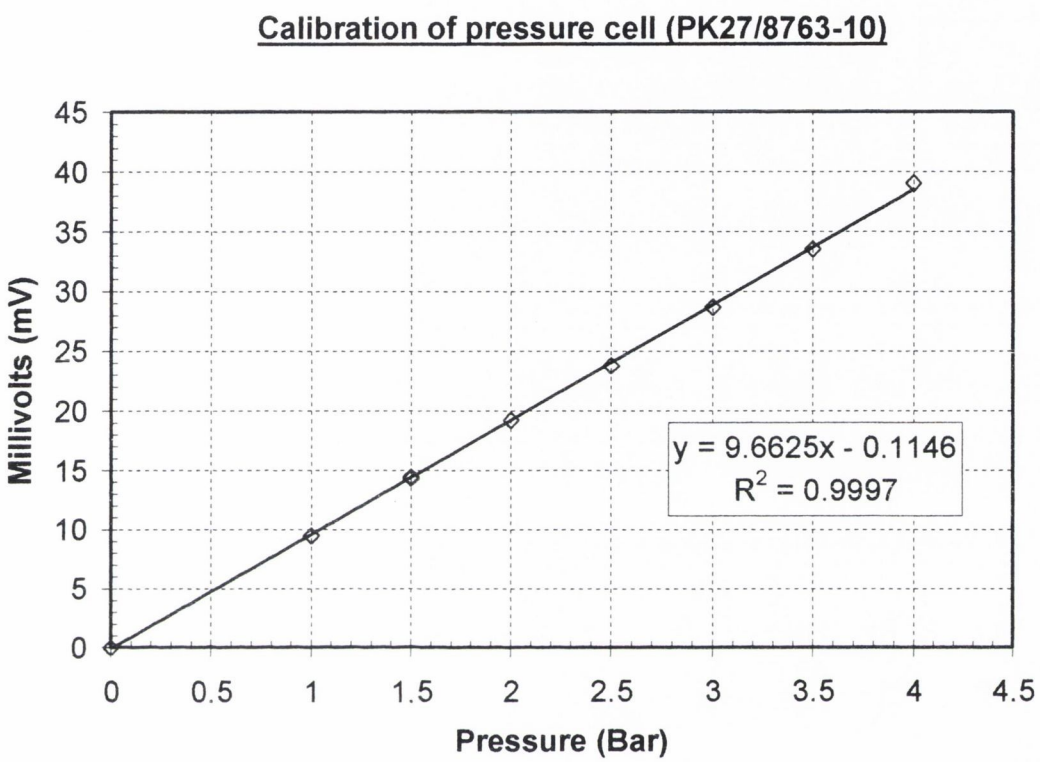

Strain Gauge Calibration

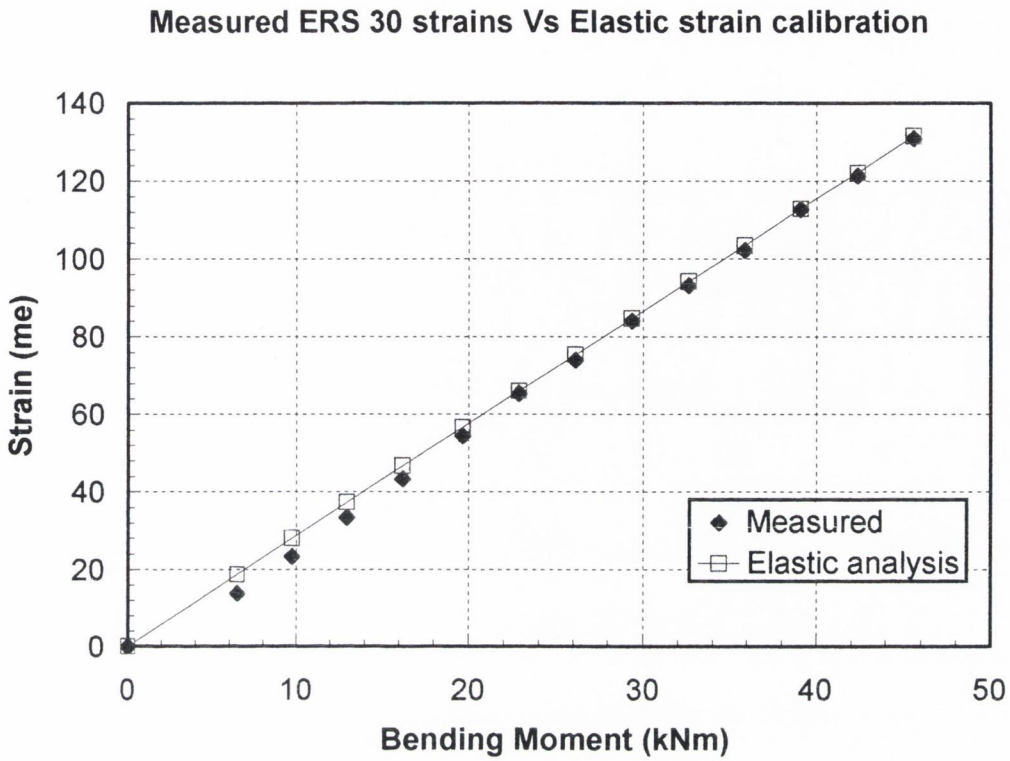

Calibration of field strain for ERS 30 against strain prediction using elastic theory

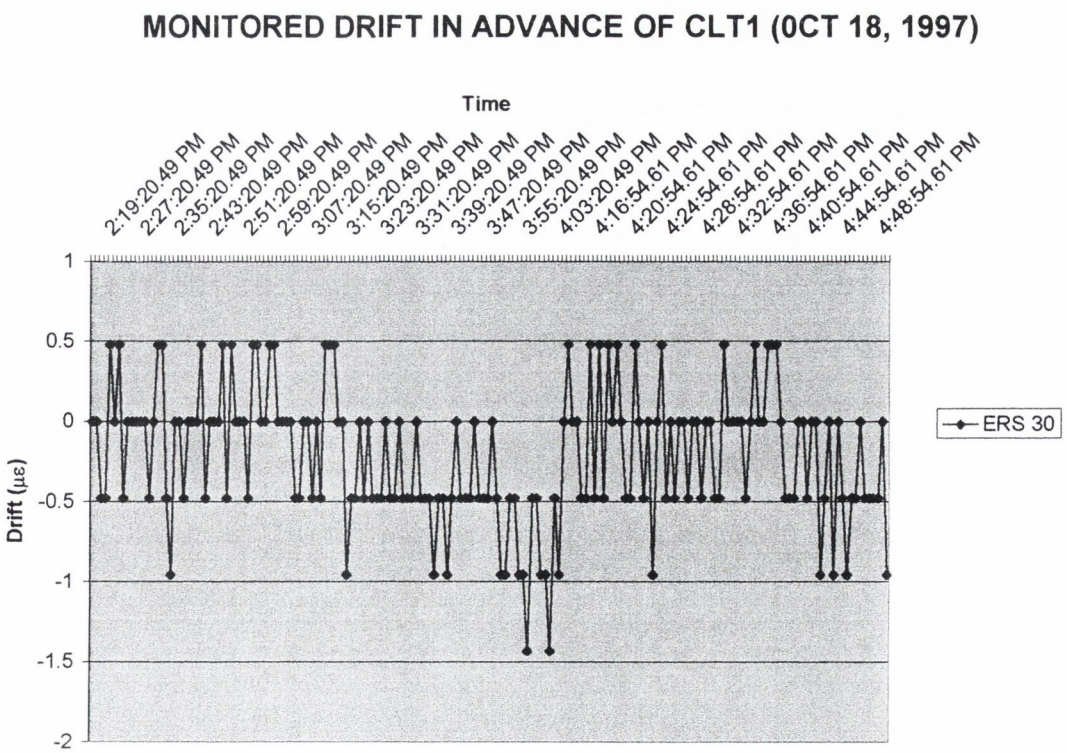

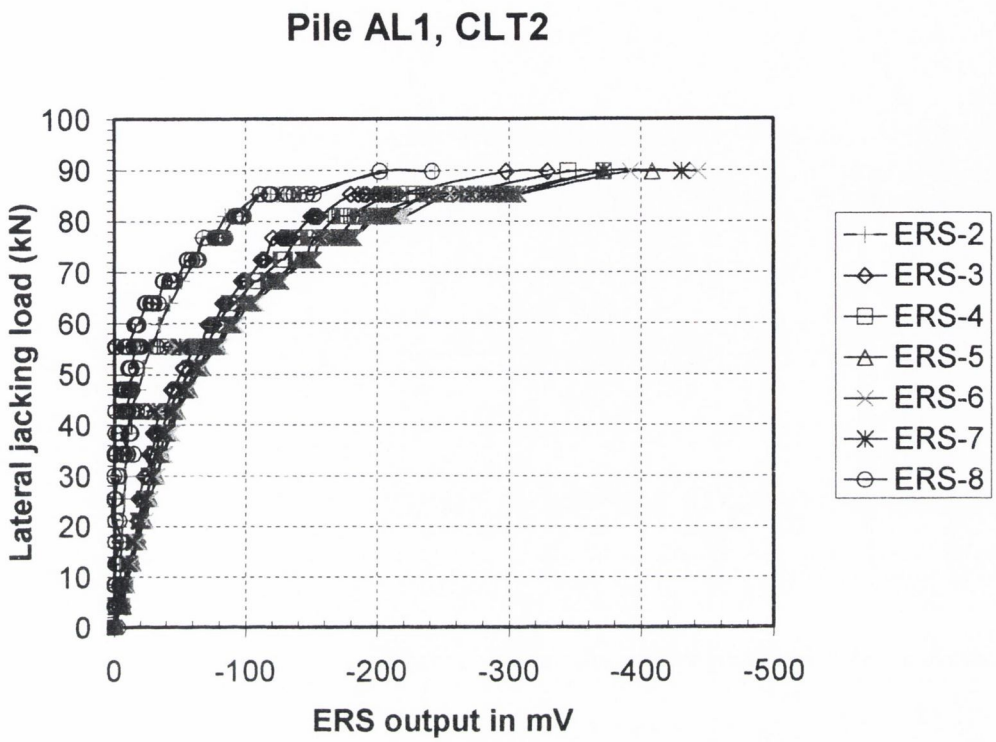

Strain gauge output versus load for CLT2

Load Cell Calibration

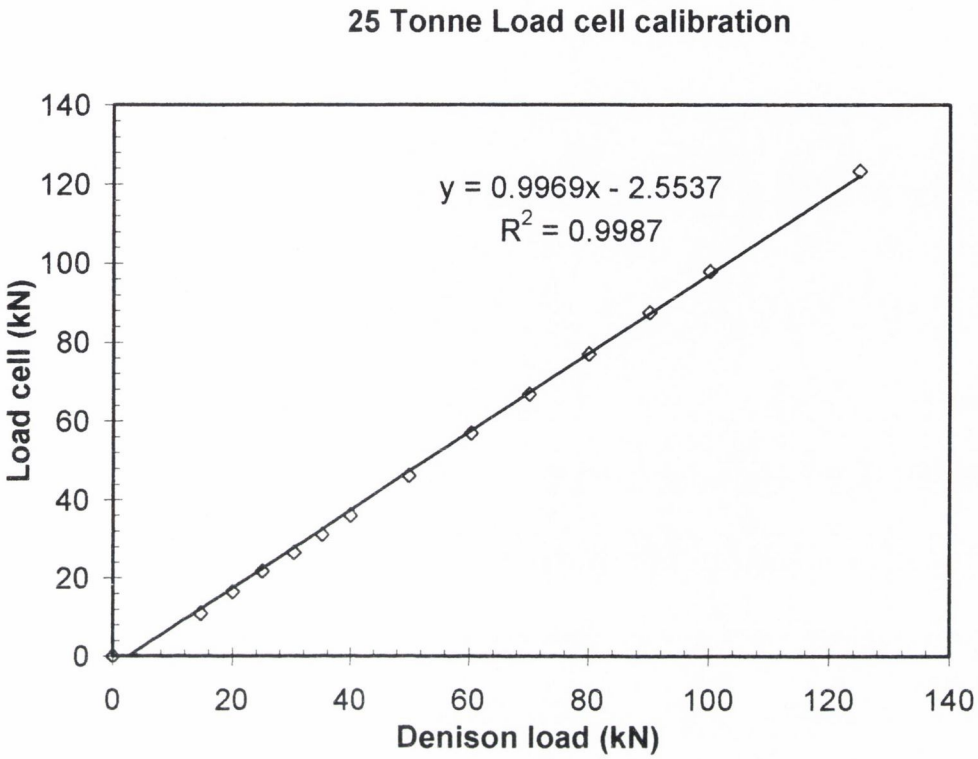

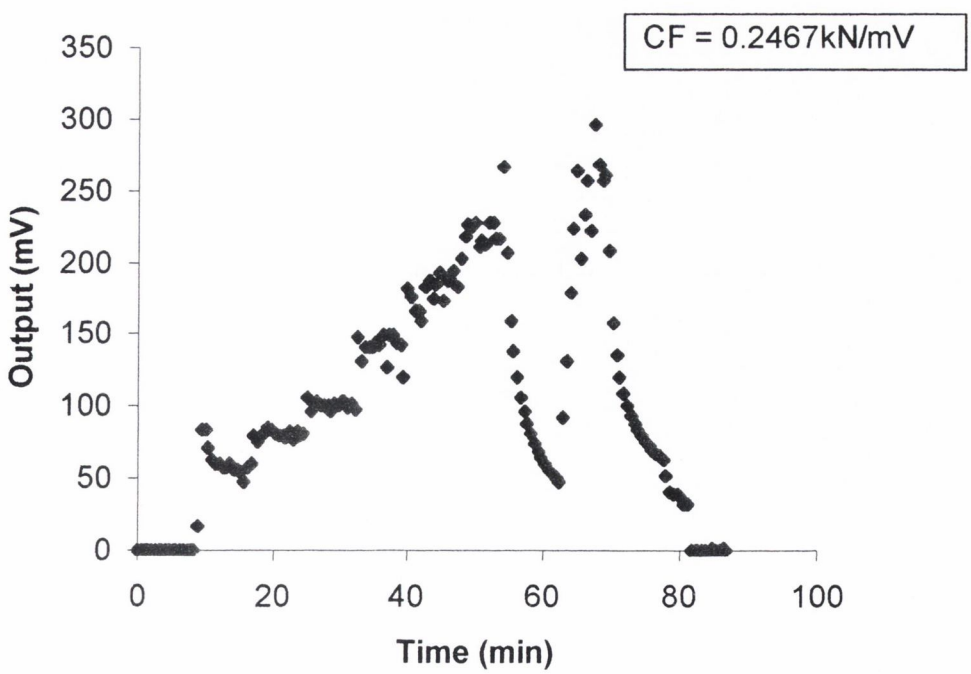

LVDT Performance

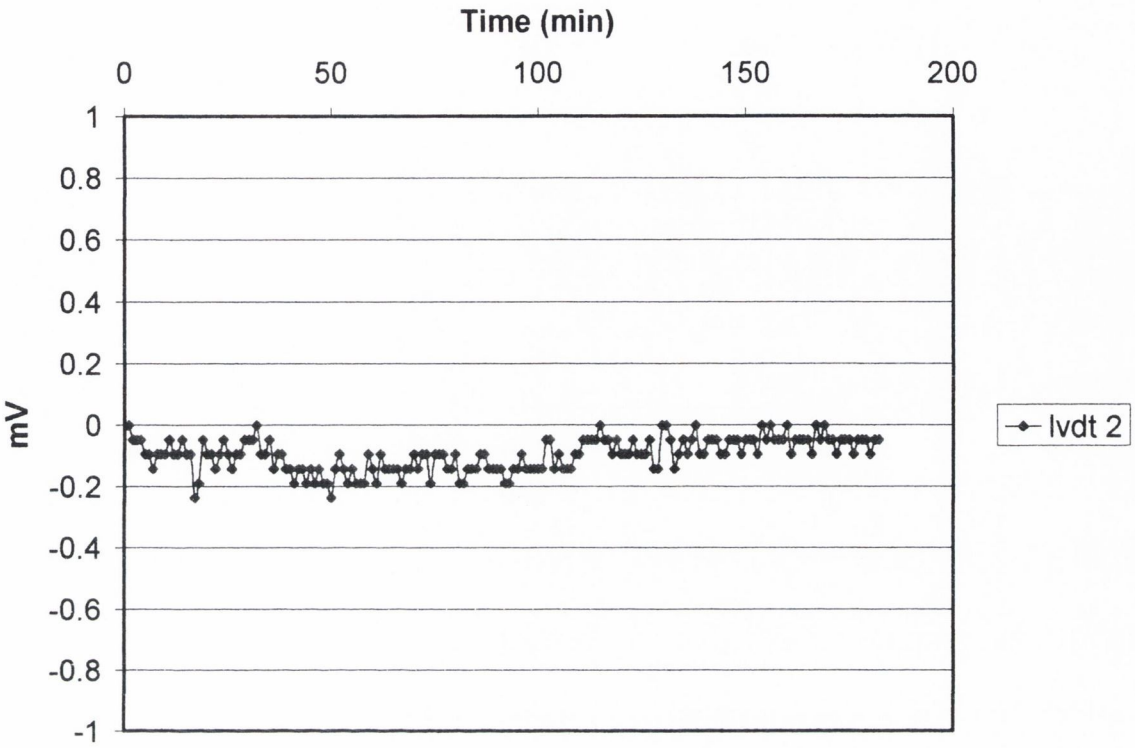

Monitoring drift in LVDT in advance of CLT1

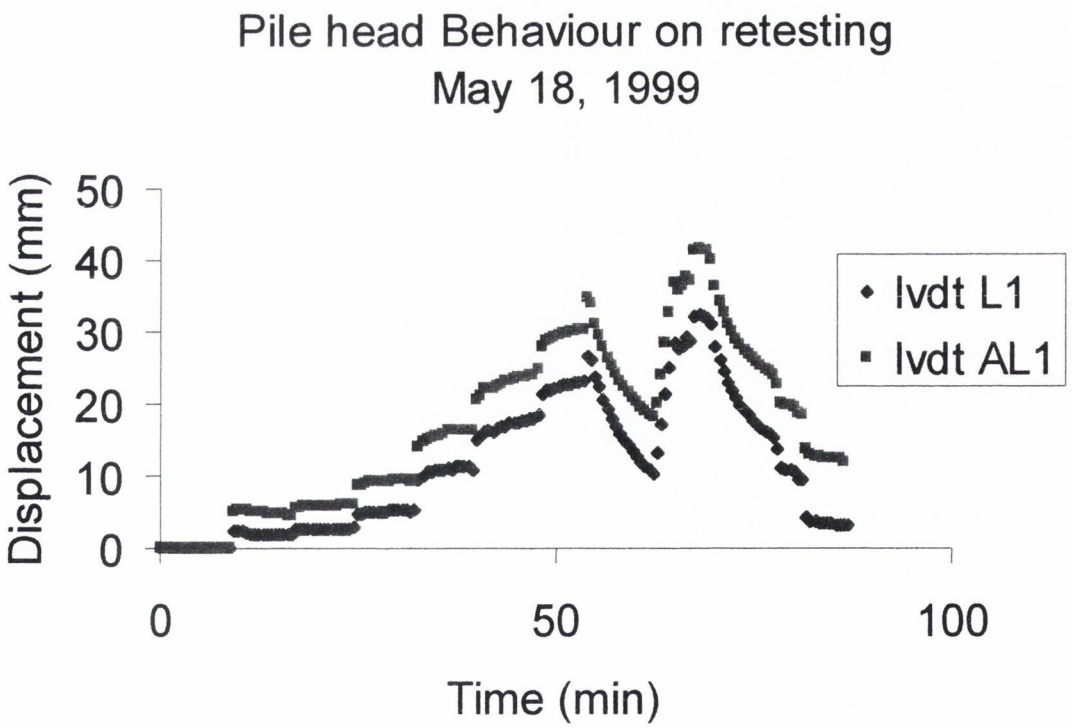

Appendix 4

Cone Pressuremeter Test Results

Note: The interpretation in this appendix is based on the method proposed by Houlsby and Withers (1988) for 'pushed in' pressuremeters.

RESULTS FOR CPM TEST AT 2.6m bgl

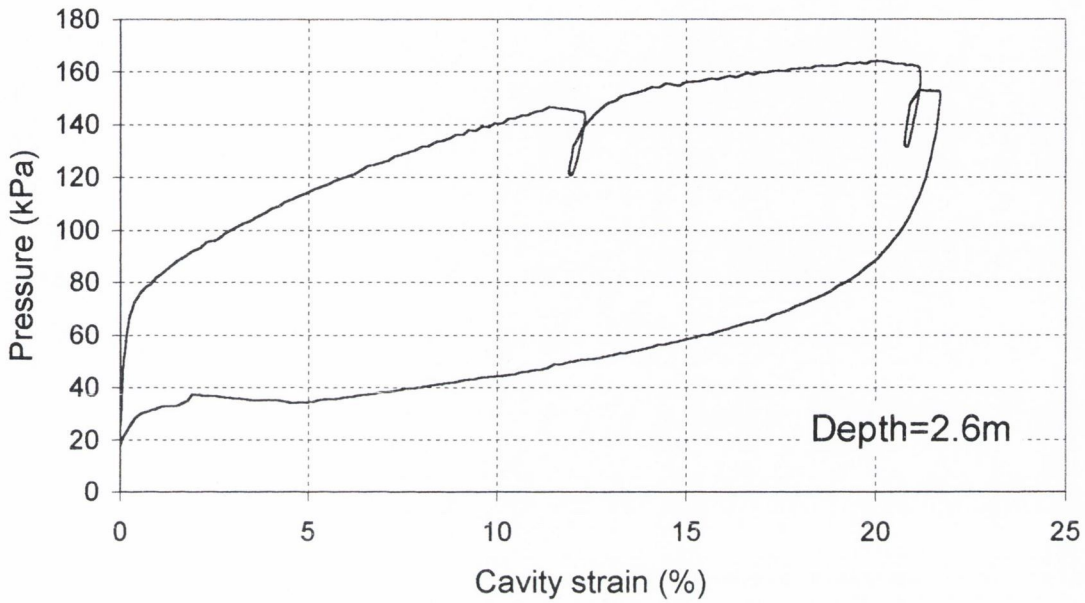

Cone Pressuremeter Curve at 2.6m bgl

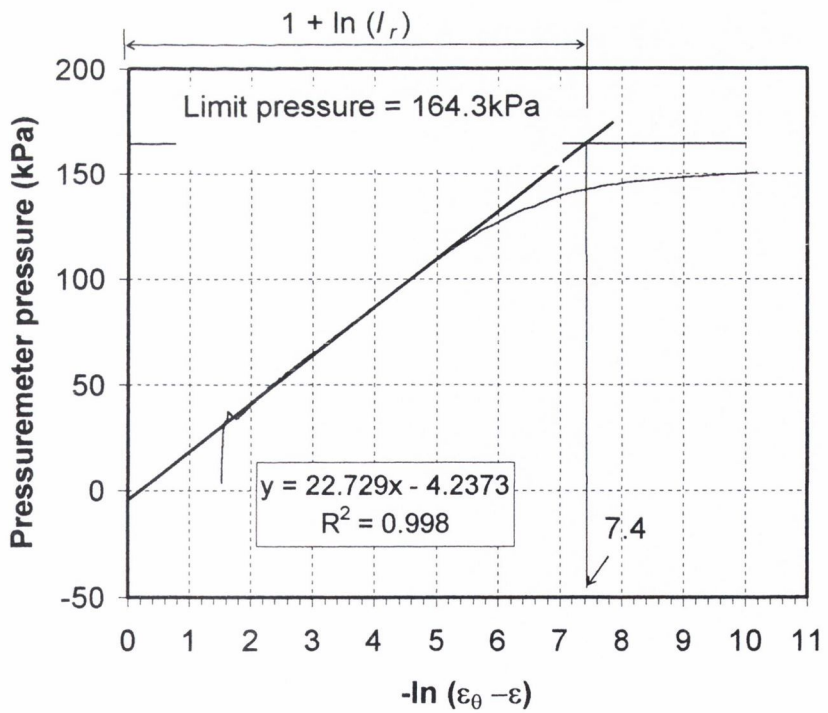

Determination of Limit Pressure for CPM at 2.6m bgl

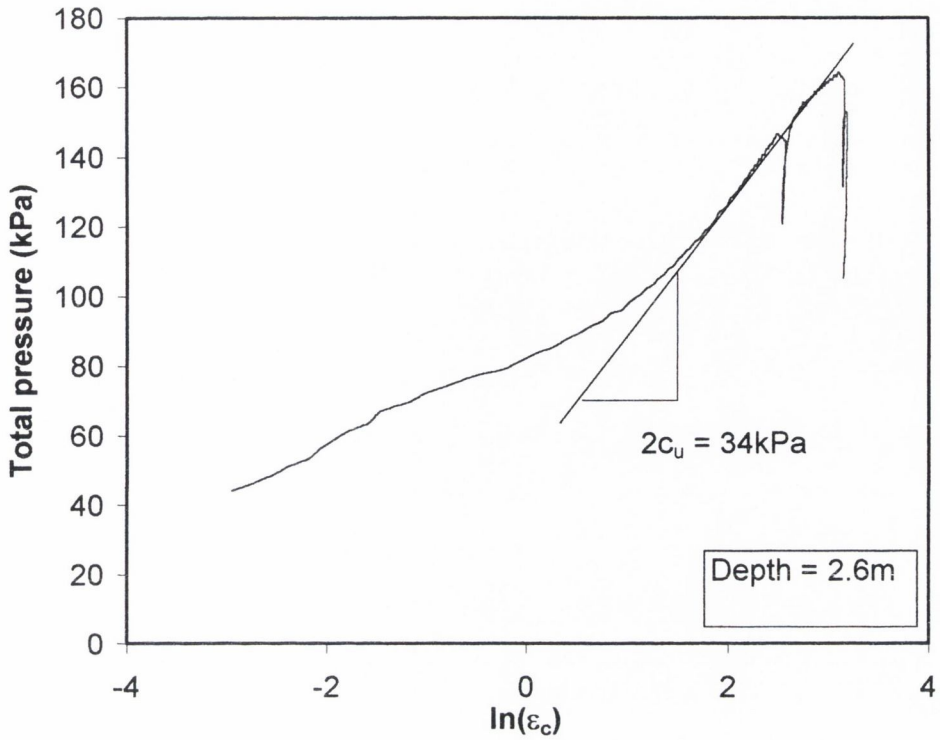

Estimated Undrained Shear Strength for CPM at 2.6m bgl from unload curve

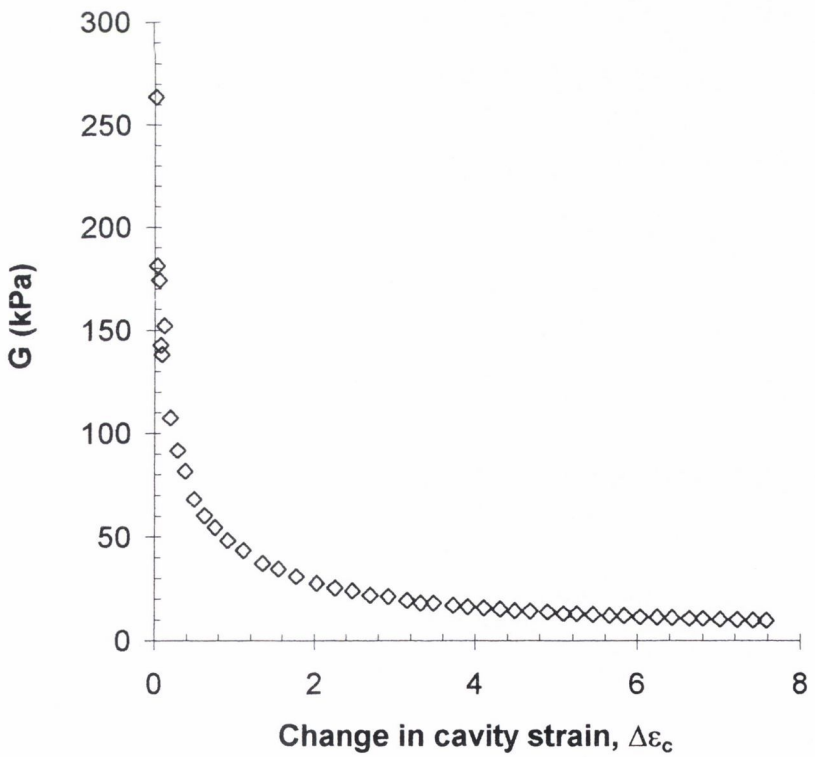

Shear modulus versus Cavity Strain at 2.6m bgl

RESULTS FOR CPM TEST AT 3.6m bgl

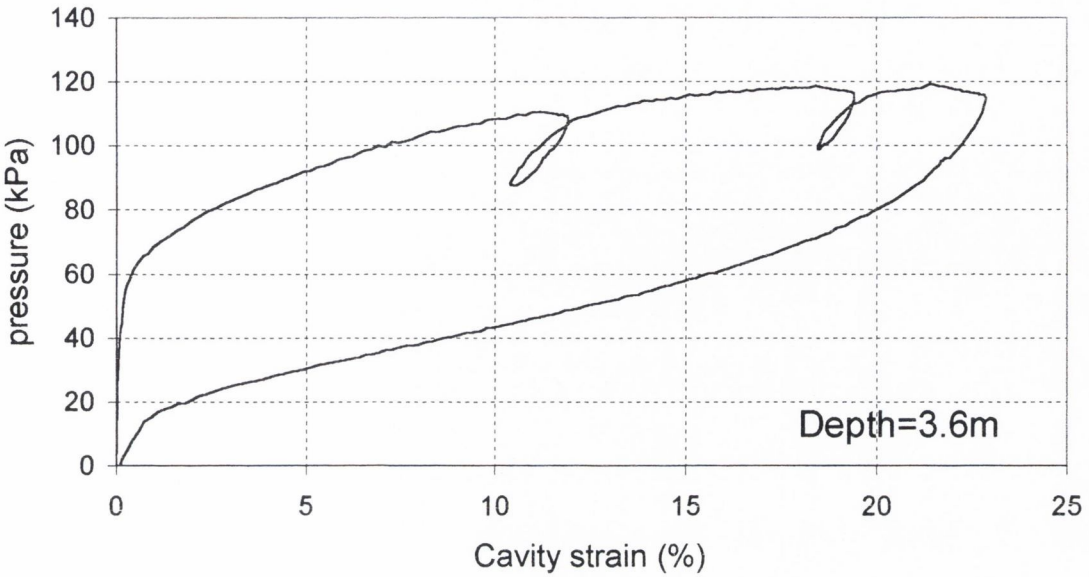

Cone Pressuremeter Curve at 3.6m bgl

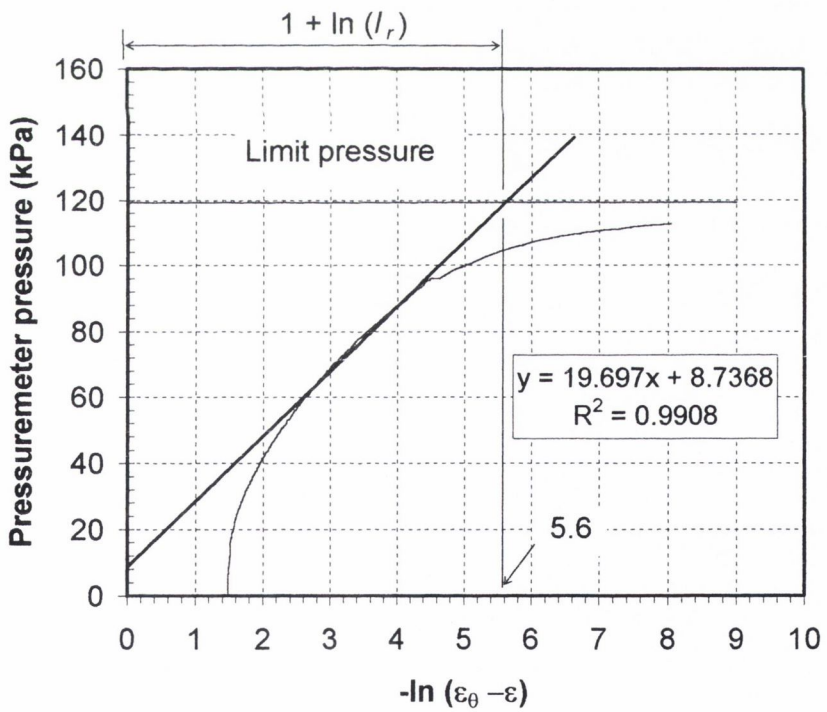

Determination of Limit Pressure for CPM at 3.6m bgl

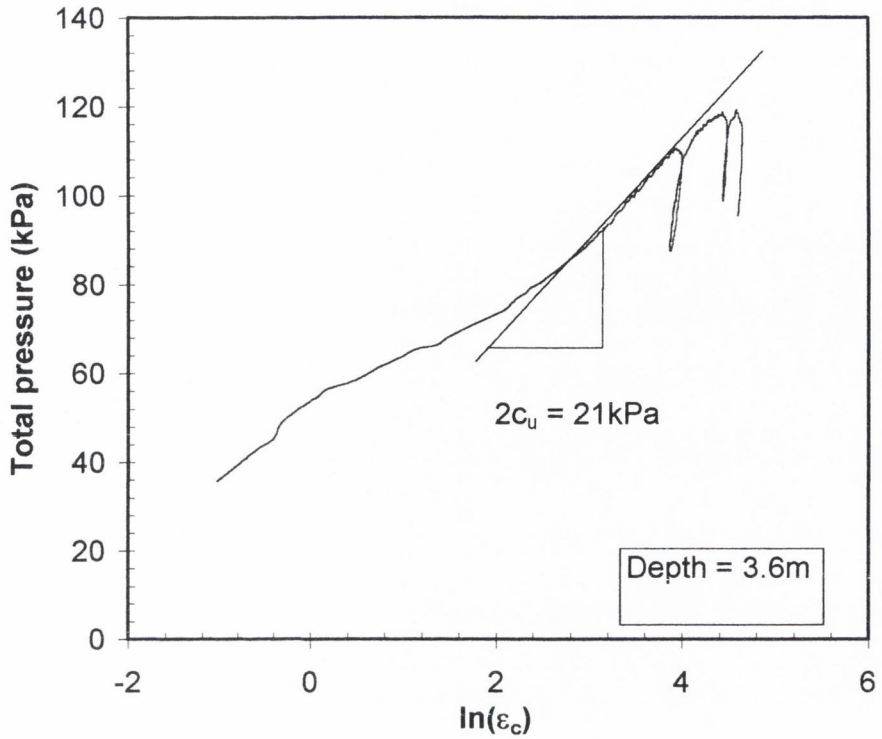

Estimated Undrained Shear Strength for CPM at 3.6m bgl from unload curve

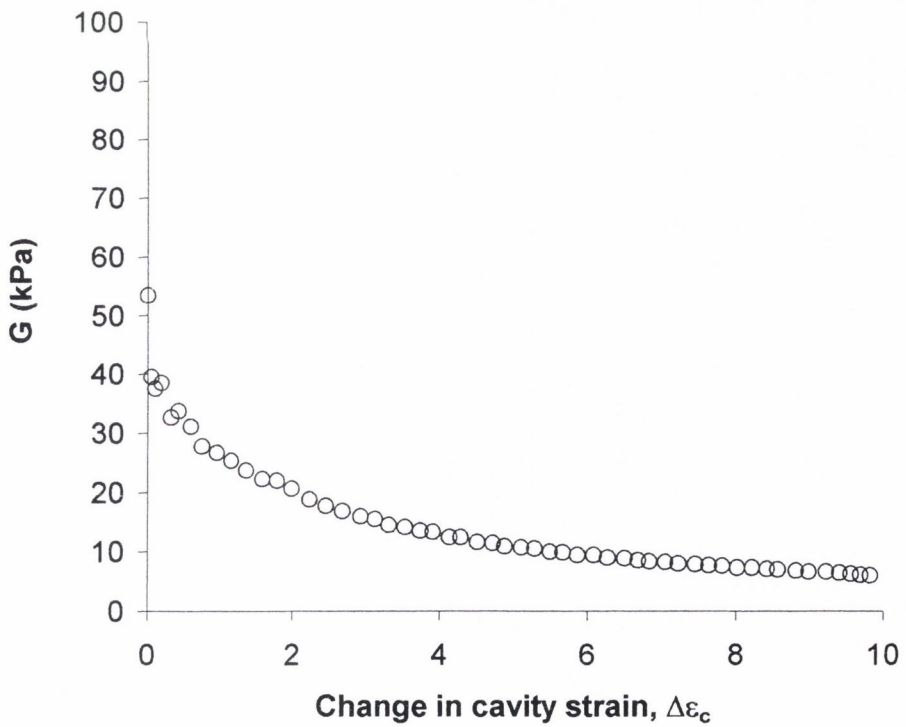

Shear modulus versus Cavity Strain at 3.6m bgl

RESULTS FOR CPM TEST AT 4.6m bgl

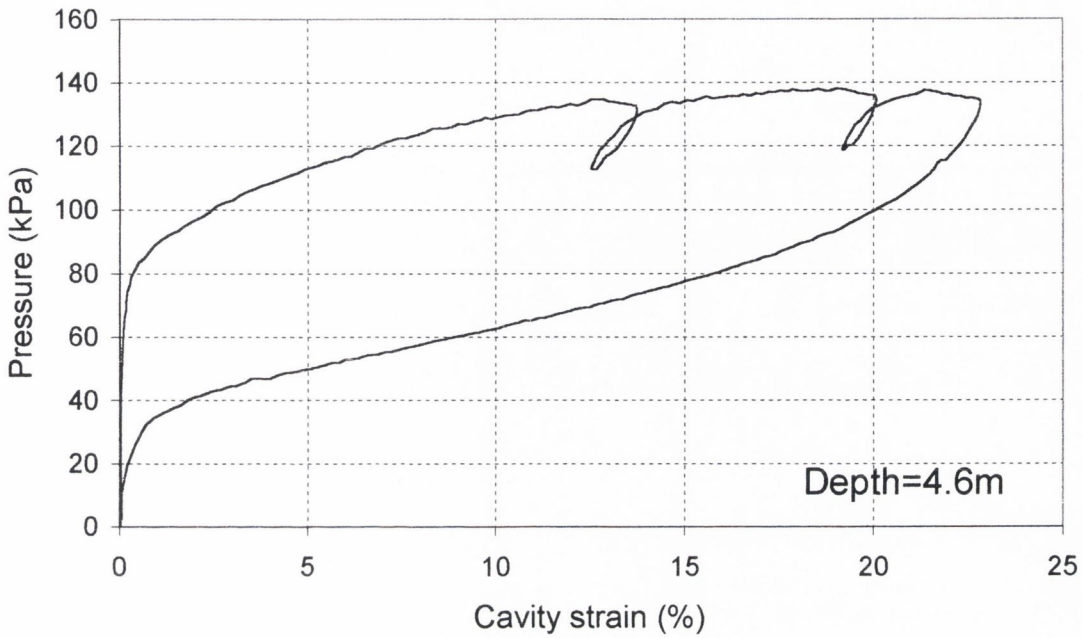

Cone Pressuremeter Curve at 4.6m bgl

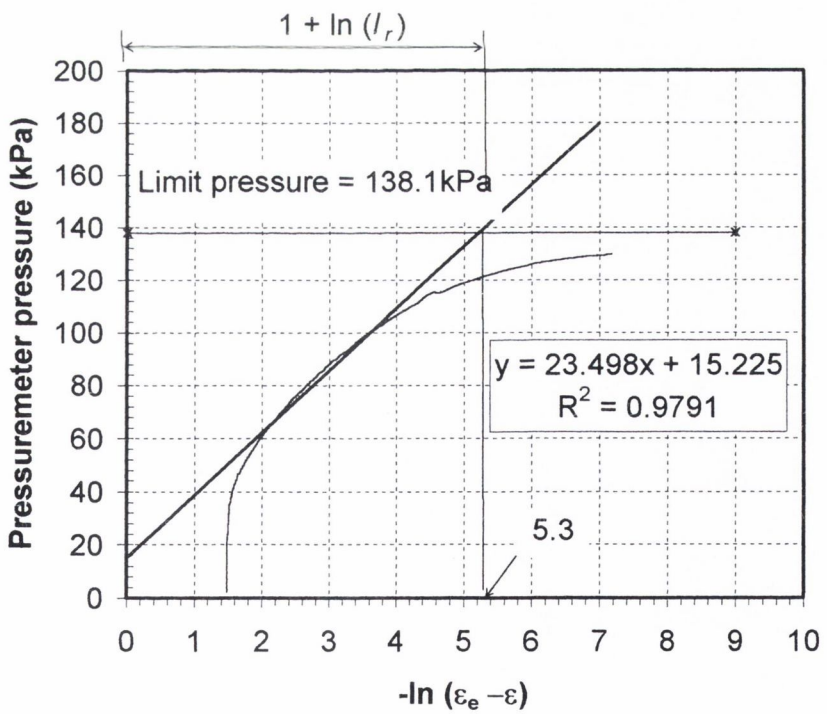

Determination of Limit Pressure for CPM at 4.6m bgl

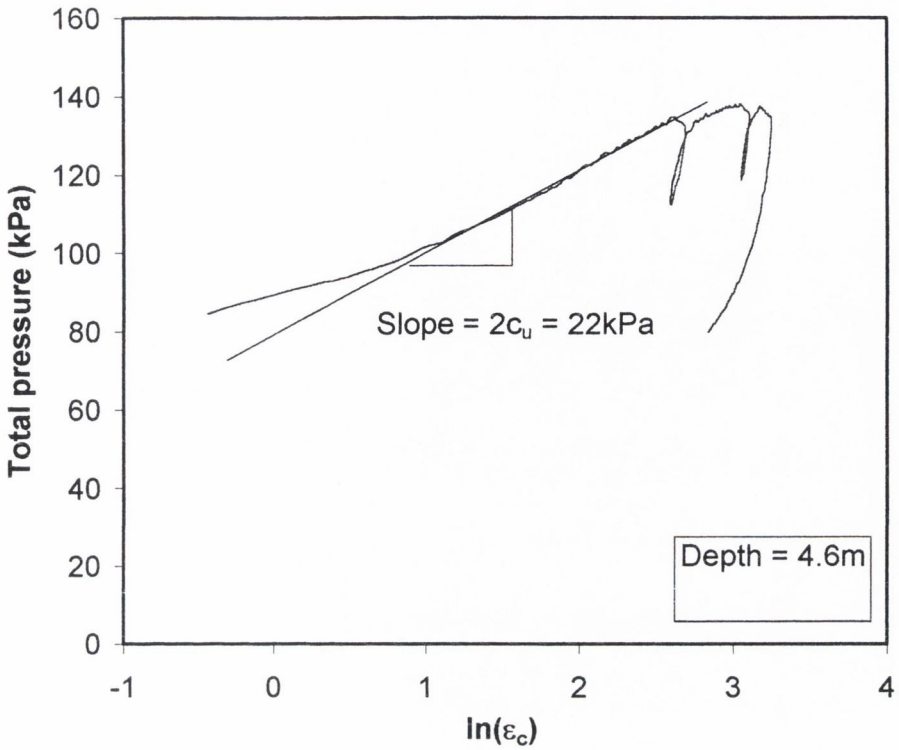

Estimated Undrained Shear Strength for CPM at 4.6m bgl from unload curve

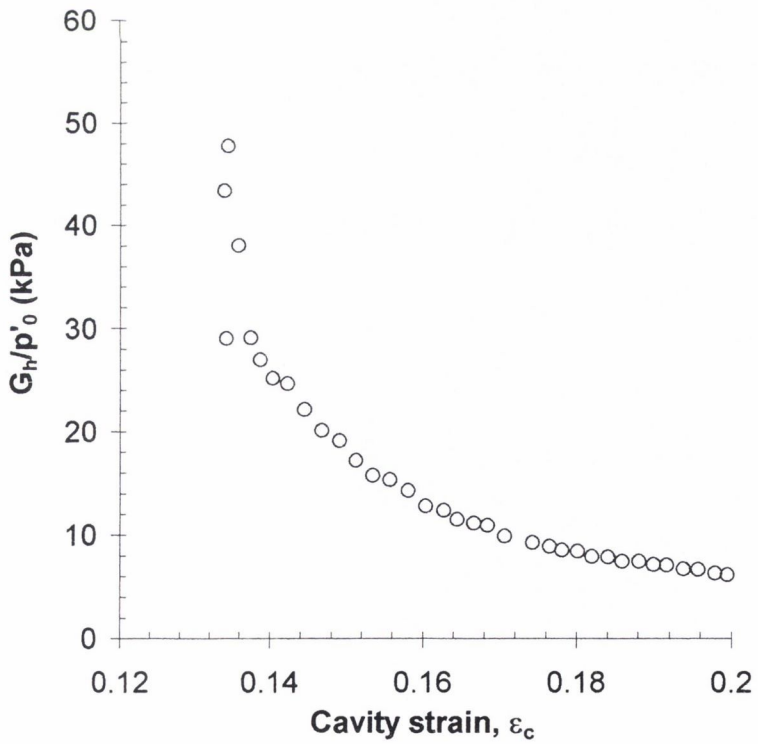

Shear modulus versus Cavity Strain at 4.6m bgl

RESULTS FOR CPM TEST AT 5.6m bgl

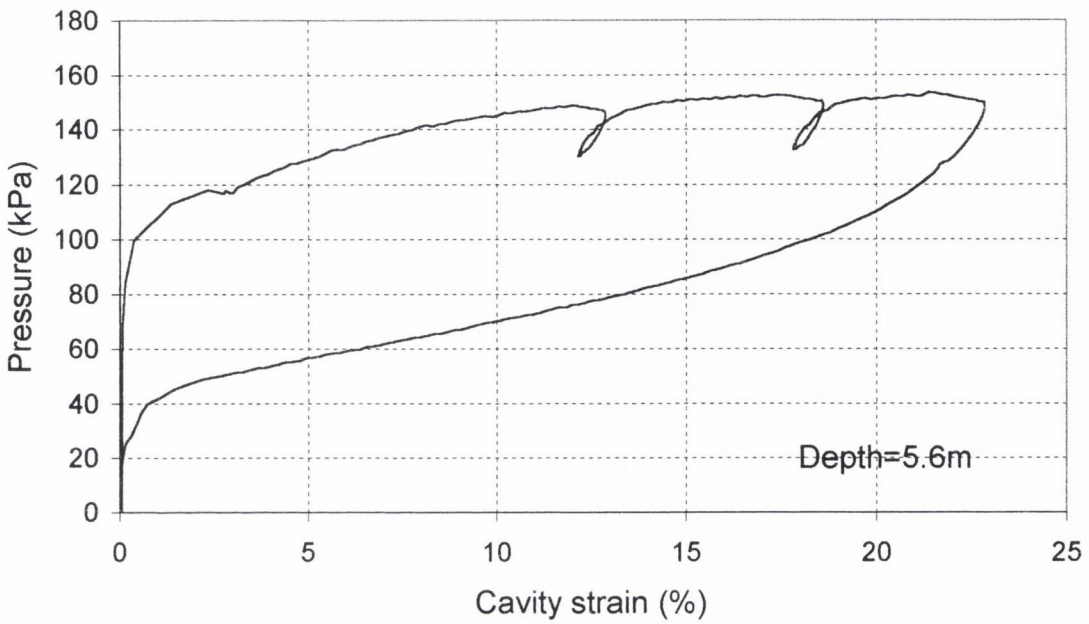

Cone Pressuremeter Curve at 5.6m bgl

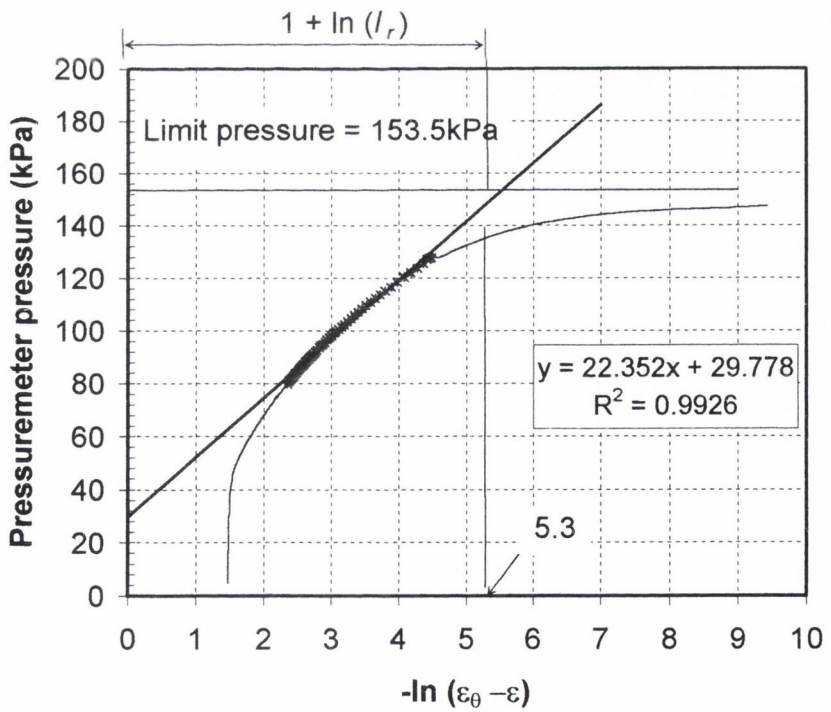

Test depth
5.6m

Determination of Limit Pressure for CPM at 5.6m bgl

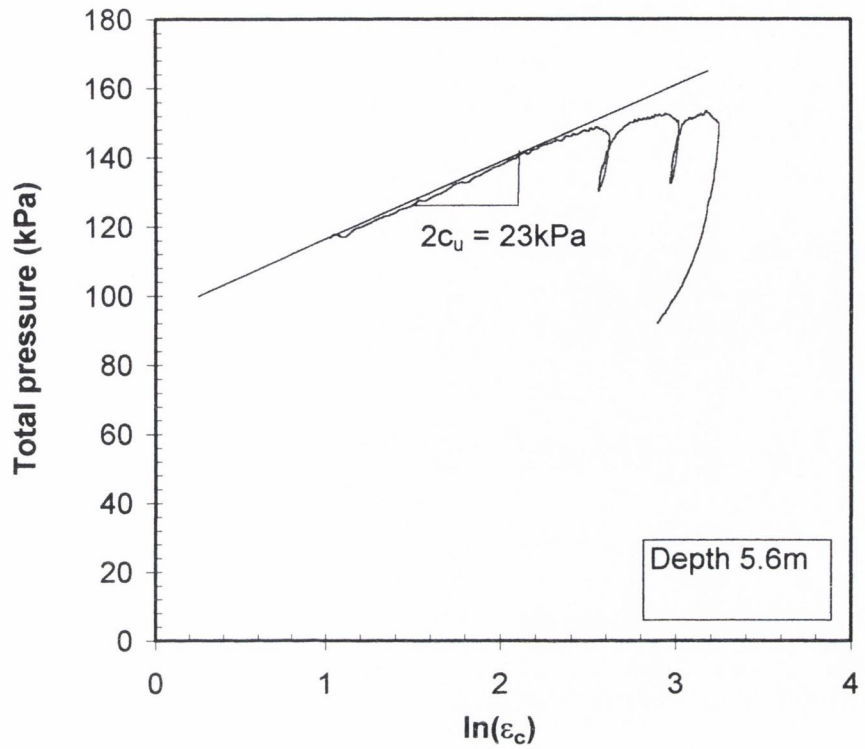

Estimated Undrained Shear Strength for CPM at 5.6m bgl from unload curve

RESULTS FOR CPM TEST AT 6.6m bgl

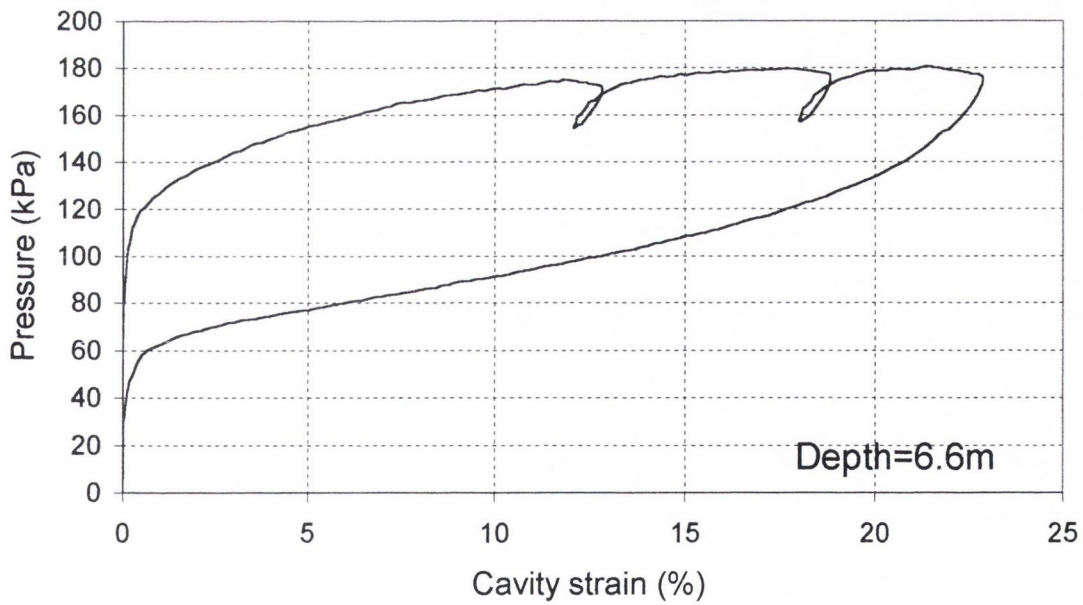

Cone Pressuremeter Curve at 6.6m bgl

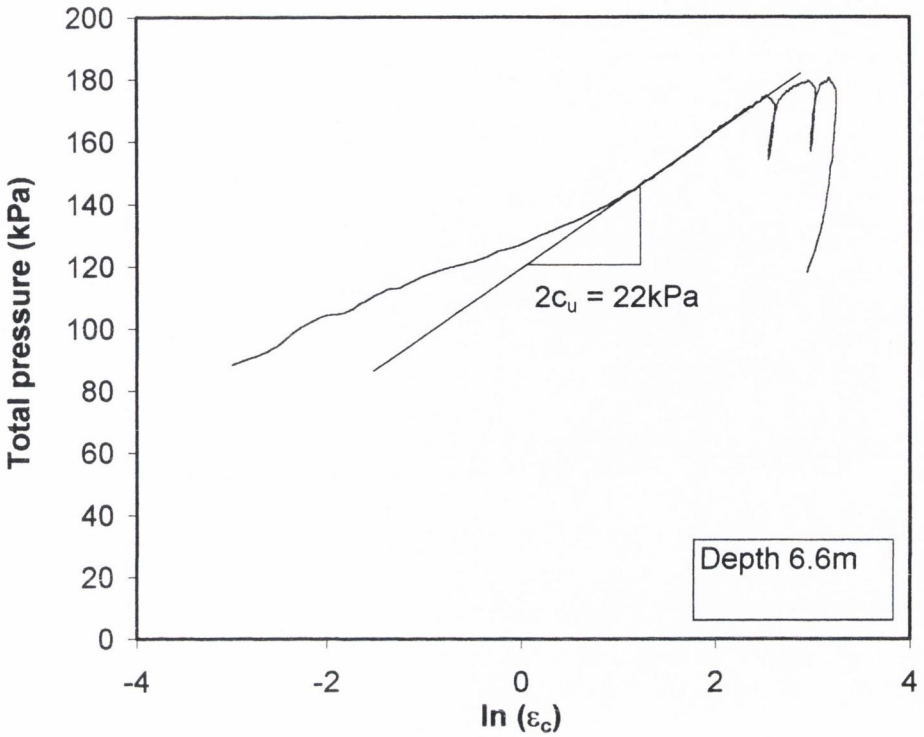

Estimated Undrained Shear Strength for CPM at 6.6m bgl from unload curve

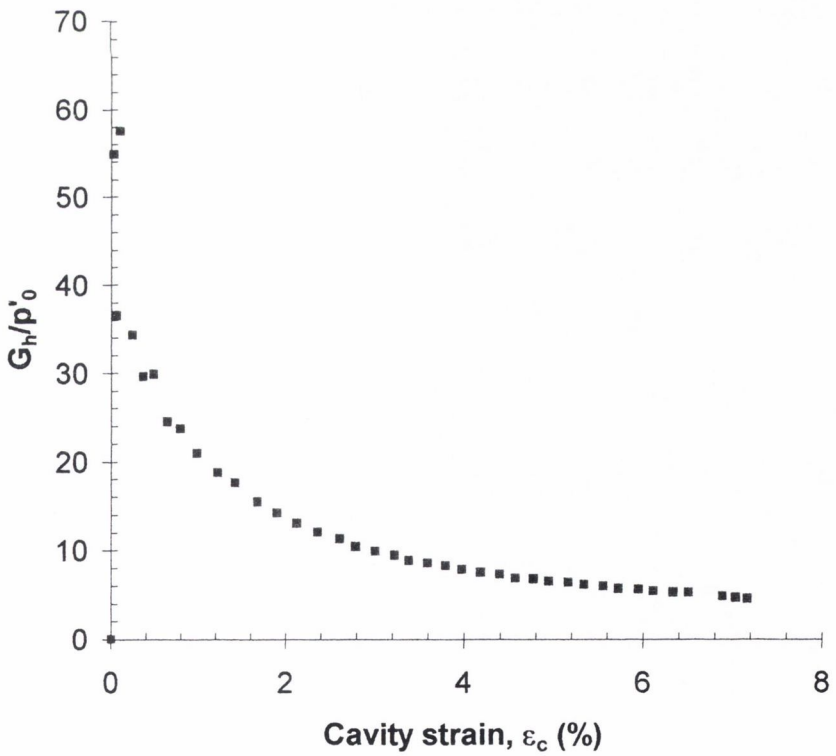

Shear modulus versus Cavity Strain at 6.6m bgl

RESULTS FOR CPM TEST AT 7.6m bgl

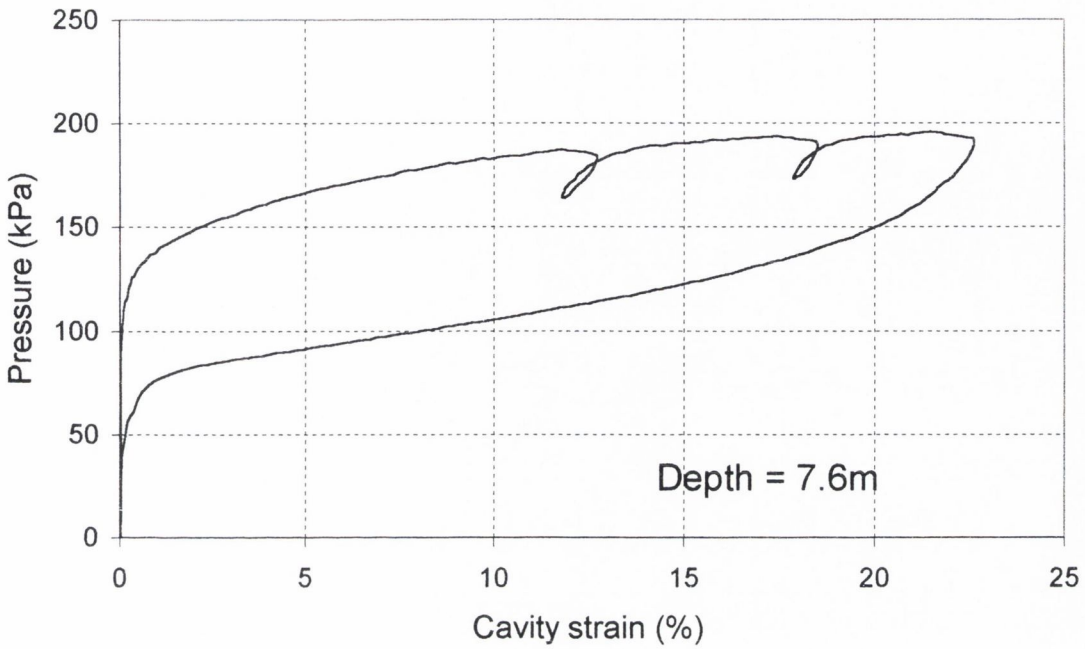

Cone Pressuremeter Curve at 7.6m bgl

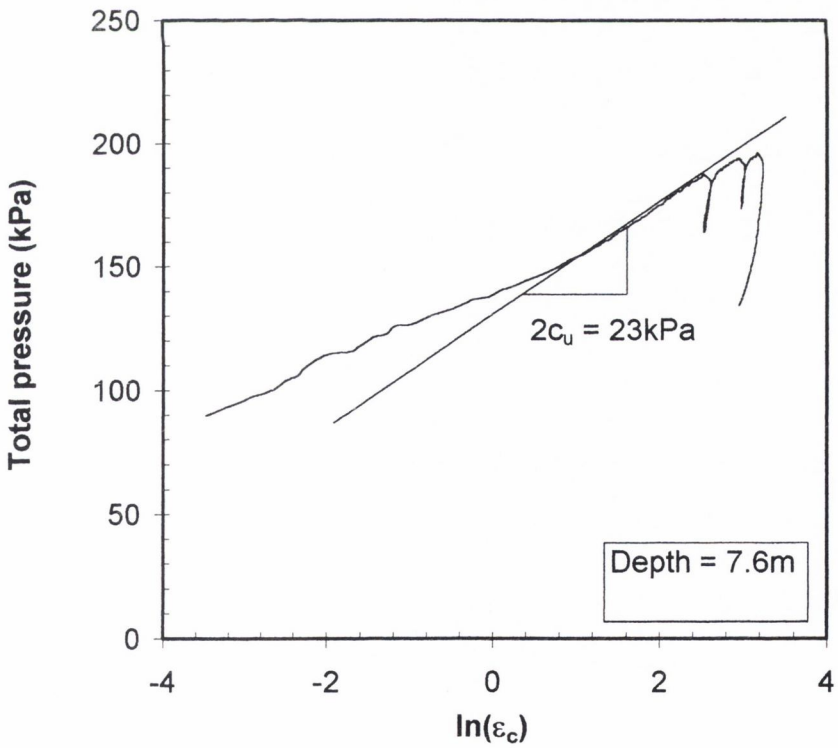

Estimated Undrained Shear Strength for CPM at 7.6m bgl from unload curve

RESULTS FOR CPM TEST AT 8.6m bgl

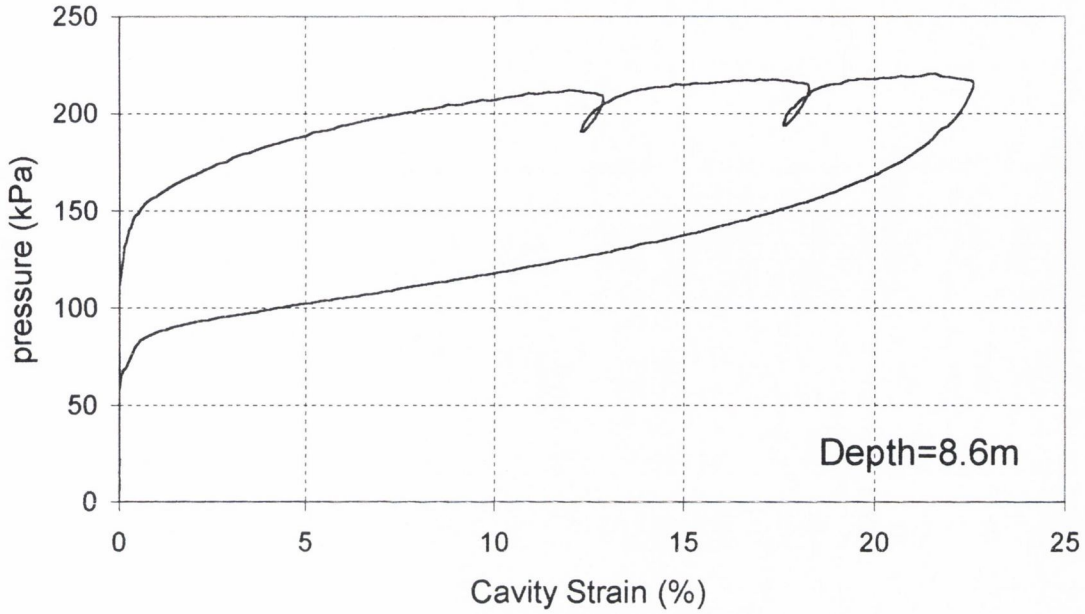

Cone Pressuremeter Curve at 8.6m bgl

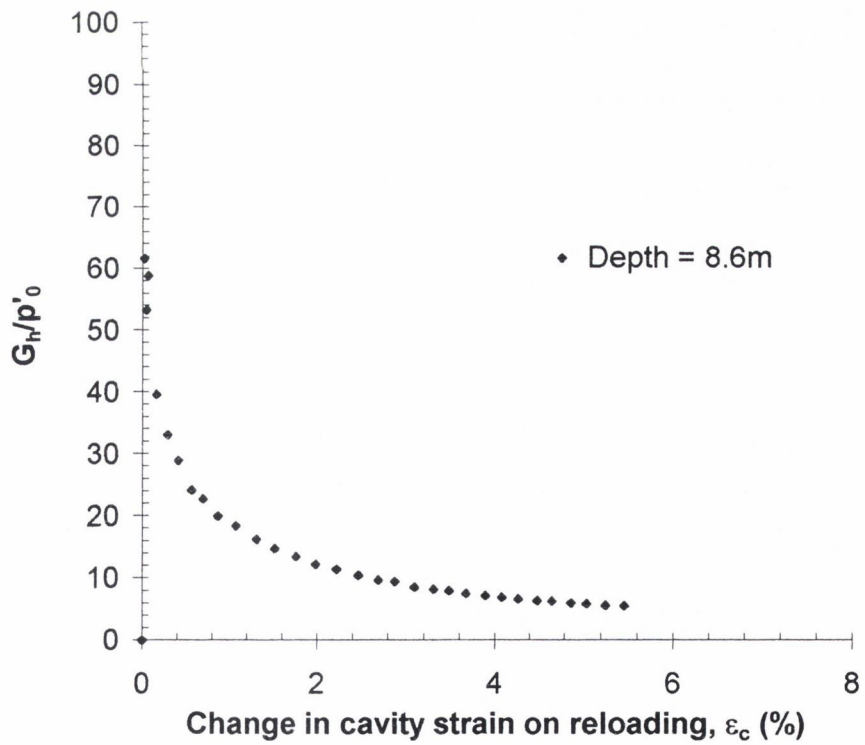

Normalised shear modulus versus Cavity Strain at 8.6m bgl

Appendix 5a

Estimates of Axial Pile Resistance

ESTIMATE OF AXIAL PILE RESISTANCE

LCPC METHOD

Bustamante and Gianeselli Method (1982) - Using CPT results.

$Q_{ult} = Q_s + Q_b$

$Q_{ult} = f_p A_s + q_p A_p =$	168 + 1007 =	1175 kN

$Q_a = Q_{ult}/3$	392 kN

where	Q_{ult} =	Total ultimate axial pile capacity	
	Q_s =	Shaft resistance	
	Q_b =	Base resistance	
	f_p =	Unit side friction	$f_p = q_c/\alpha_{(LCPC)}$
	A_s =	Shaft area	
	q_p =	Unit end bearing*	$q_p = k_c q_{ca}$
	A_p	Pile end area	

Use the results from CPT4 - Located within 3m of the test pile.

*The equivalent average cone resistance, q_{ca}, at the base of the pile is used to calculate the unit end bearing resistance q_p.

Mean q_c measured between -a and +a below and above the pile base respectively where a = 1.5D

D is the pile diameter

Pile detail	L (bgl)	9.6	m
	D =	0.35	m square PC concrete
	1.5D =	0.525	m

Friction coefficien	α =	90	for soft clay (q_c < 1) Table 6.5
	α =	150	for comp to v. comp S and G (q_c > 12 MPa) Table 6.4
Bearing capacity factor	k_c =	0.4	for comp to v comp S and G (q_c > 12 MPa) Table 6.4

Note: Ignore skin friction over the top 1m due to pit excavation and disturbance due to pile driving

	SHAFT RESISTANCE			*BASE RESISTANCE*		
Depth	**qc (MPa)**	**f_p**	**Qs segment**	***Average q_{ca} (MPa)***	***$q_p = k_c q_{ca}$***	**Remarks**
-1	1.93	0.02				Fill
-1.26	1	0.01				Fill
-1.5	1.25	0.01				Fill
-1.76	1.15	0.01				Fill
-2	0.25	0.00	0.97			Sandy silt
-2.26	0.25	0.00	0.97			Sleech
-2.5	0.2	0.00	0.78			Sleech
-2.76	0.25	0.00	0.97			Sleech
-3	0.25	0.00	0.97			Sleech
-3.26	0.25	0.00	0.97			Sleech
-3.5	0.3	0.00	1.17			Sleech
-3.76	0.25	0.00	0.97			Sleech
-4	0.25	0.00	0.97			Sleech
-4.26	0.3	0.00	1.17			Sleech
-4.5	0.3	0.00	1.17			Sleech
-4.76	0.3	0.00	1.17			Sleech
-5	0.3	0.00	1.17			Sleech
-5.26	0.3	0.00	1.17			Sleech
-5.5	0.35	0.00	1.36			Sleech
-5.76	0.3	0.00	1.17			Sleech
-6	0.3	0.00	1.17			Sleech
-6.26	0.3	0.00	1.17			Sleech
-6.5	0.3	0.00	1.17			Sleech
-6.76	0.3	0.00	1.17			Sleech
-7	0.35	0.00	1.36			Sleech
-7.26	0.35	0.00	1.36			Sleech
-7.5	0.35	0.00	1.36			Sleech
-7.76	0.35	0.00	1.36	q_{ca} →		Sleech
-8	0.35	0.00	1.36	**20.56**		Sleech
-8.26	0.5	0.01	1.94	q_{ca}' →		Sleech
-8.5	0.7	0.01	2.72	***17.99***		Sleech
-8.76	2.2	0.01	5.13	0.00		top of Sand
-9	6.65	0.04	15.52	15.52		
-9.26	8.65	0.06	20.18	20.18		
-9.5	9.5	0.06	22.17	22.17		End of pile
-9.76	9.5	0.06	22.17	22.17		
-10	9.75	0.07	22.75	22.75		
-10.26	11.5	0.08	26.83	0.00		
		Q_s =	**168 kN**	**Q_b =**	**1007 kN**	

∴ Total resistance $Q_u = Q_s + Q_b = 168 + 1007 = 1175$ kN

Jardine and Chow Method (1996)

Ref: New Design Methods for Offshore Piles, MTD Publications 96/103

Pile Resistance $\boxed{Qt = Qb + Qs}$ where Qt = Total Resistance

Qb = Base Resistance

Qs = Shaft Resistance

SHAFT RESISTANCE, Qs

$\text{Log}_{10} S_t =$ 0.84509804

9.5 m Tip upwards

z (m)	h from tip	h/R	YSR	$Kc = [2.2 + 0.016 YSR^{-0.67} \Delta Ivy] YSR^{0.42} (h/R)^{-0.2}$	σ_{vo}'	$\sigma_{rf}' = 0.8\sigma_{vo}' K_c$	$\tau_f = \sigma_{fr} \tan \delta_f$
9	0.5	0.7143	1.2	2.553737082	81	165.4821629	22.0962386
8.75	0.75	1.0714	1.2	2.354821167	79.5	149.7666262	19.9977995
8.5	1	1.4286	1.2	2.223157255	78	138.7250127	18.5234525
8.25	1.25	1.7857	1.2	2.126121998	76.5	130.1186663	17.374278
8	1.5	2.1429	1.2	2.049990894	75	122.9994536	16.4236751
7.75	1.75	2.5	1.2	1.987753715	73.5	116.8799185	15.6065556
7.5	2	2.8571	1.2	1.935370801	72	111.4773581	14.8851711
7.25	2.25	3.2143	1.2	1.890312821	70.5	106.6136431	14.2357367
7	2.5	3.5714	1.35	1.943772805	69	107.2962588	14.3268839
6.75	2.75	3.9286	1.35	1.907071451	67.5	102.9818583	13.7507975
6.5	3	4.2857	1.35	1.874171168	66	98.95623768	13.2132709
6.25	3.25	4.6429	1.35	1.844407295	64.5	95.17141642	12.7078973
6	3.5	5	1.35	1.81727183	63	91.59050025	12.2297504
5.75	3.75	5.3571	1.35	1.792368282	61.5	88.18451946	11.774962
5.5	4	5.7143	1.35	1.769381594	60	84.93031651	11.34044
5.25	4.25	6.0714	1.35	1.748057514	58.5	81.80909164	10.9236741
5	4.5	6.4286	1.35	1.728188062	57	78.80537561	10.5225987
4.75	4.75	6.7857	1.45	1.761188355	55.5	78.19676296	10.4413328
4.5	5	7.1429	1.45	1.743213282	54	75.30681379	10.0554483
4.25	5.25	7.5	1.45	1.726285674	52.5	72.50399831	9.68119839
4	5.5	7.8571	1.45	1.710298793	51	69.78019076	9.31749815
3.75	5.75	8.2143	1.45	1.695161024	49.5	67.12837654	8.96341093
3.5	6	8.5714	1.45	1.680793179	48	64.54245809	8.61812253
3.25	6.25	8.9286	1.45	1.66712638	46.5	62.01710134	8.28092072
3	6.5	9.2857	1.45	1.654100359	45	59.54761291	7.9511788
2.75	6.75	9.6429	1.45	1.641662102	43.5	57.12984115	7.62834242
2.5	7	10	1.45	1.629764746	42	54.76009546	7.31191879

Equiv. Pile Dia., D = 0.39493271 m

$\Sigma\tau_f =$ 338.182554

SHAFT RESISTANCE IN SLEECH

$Qs = \pi D \sum \tau_f \, dz =$ 419.55 kN

BASE RESISTANCE (IN SAND)

$Q_b = q_b A_{base}$ where $q_b = q_{c(avg)} [\, 1 - 0.5 \log(D/D_{CPT})]$

Qb = 841.72 kN

TOTAL RESISTANCE

Qt = 1261.27 kN

AXIAL PILE RESISTANCE USING CONVENTIONAL APPROACH

$Q_{ult} = Q_s + Q_b$

Q_{ult} = Ultimate Resistance (kN)

Q_s = Shaft Resistance determined usin the α-Method

Q_b = Base Resistance using Berezantsev el al's N_q Factor

SHAFT RESISTANCE IN SLEECH

$Q_s = \alpha\ c_u\ A_s$

c_u = Average undrained shear strength along shaft = 20 kPa

and α is the 'shaft adhesion factor'

$\alpha = 0.5/(c_u/\sigma_v')^{0.5}$ for $c_u/\sigma_v' < 1.0$ (API 1993)

where σ_v' = Effective vertical stress at mid depth of sleech

$\sigma_v' = 19 \times 2 + (16-10)(7.6/2) =$ 60.8 kPa

$\alpha = 0.5/(c_u/\sigma_v')^{0.5} = 0.5/(20/60.8)^{0.5} =$ 0.9

$A_s = 4 \times L \times B =$ 10.64 m^2

$Q_s = \alpha\ c_u\ A_s$ $0.9 \times 20 \times 10.64 =$ 191.52 kN

BASE AND SHAFT RESISTANCE IN SAND

End bearing in medium dense sand

SPT N = 15
q_c = 12.5 MPa

Estimate ϕ'

From q_c = 12.5MPa
σ_v' = 19 x 2 + (16-10)(7.6) = 83.6 kPa

ϕ' = 40° from Tomlinson (1994) Fig 4-14 p115

From N = 15
ϕ' = 38° After Schmertmann (1975) from Fig 8-9 in Craig (1987). P306

Taking ϕ' = 38°

$Q_{ult} = Q_s + Q_b$

$Q_{ult} = 0.5K_s\sigma_v' \tan\delta A_s + N_q \sigma_v' A_b$

$\delta \sim 0.8\phi'$ = 30° T4.2 p119 Tomlinson (1994)
For small displacement piles $K_s/K_0 \sim 1.0$
hence $K_s = 1 - \sin\phi'$ = 0.38

Q_{ult} = 921.0782 kN

Total Pile Resistance = 191.52 + 921.1 = **1113 kN**

Soil Model

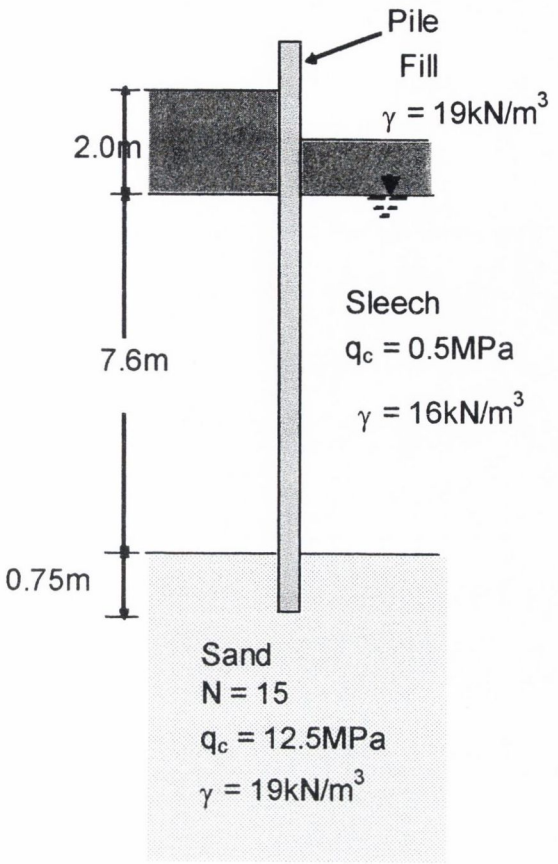
Pile
Fill
γ = 19kN/m3
2.0m
Sleech
qc = 0.5MPa
γ = 16kN/m3
7.6m
0.75m
Sand
N = 15
qc = 12.5MPa
γ = 19kN/m3

Appendix 5b

Load Shedding & Downdrag Calculations

CALCULATIONS

Area of steel = 1608 mm^2

Area of conc = bd - As 120892 mm^2

Ec = 36 kN/mm^2

Es = 205 kN/mm^2

$$F = A_cE_c\varepsilon + A_sE_s\varepsilon$$

$$F = (AcEc + AsEs)\varepsilon$$

AXIAL LOAD DISTRIBUTION ALONG PILE SHAFT (kN)

	Depths						
Load (kN)	**0.125**	**0.525**	**1.075**	**2.475**	**4.02**	**5.725**	**9.5**
3.3kN	3.3	3.3	2.2	5.6	3.4	1.1	0.0
11kN	11.2	11.1	15.6	13.5	13.4	7.8	0.0
135kN	132.9	135.2	134.3	125.5	114.4	97.5	84.2
168kN	167.6	167.7	167.8	158.9	144.6	124.7	107.1
164kN	161.9	164.2	164.5	156.6	145.8	122.3	107.1
161kN	161.9	160.7	161.2	153.6	141.1	118.8	107.1
DEPTH	**-0.125**	**-0.525**	**-1.075**	**-2.475**	**-4.02**	**-5.725**	**-9.5**

LOAD SHEDDING DISTRIBUTION

The following data is obtained from the average strain distribution profile at 1.5m intervals

Depth (m)	Measured microstrain				Axial load (kN)			
	3.3kN	11kN	135kN	168kN	3.3kN	11kN	135kN	169kN
0	0.75	2.4	28.4	36	4	11	133	169
1.5	0.48	2.4	27.7	36	2	11	130	169
3	0.32	2.4	25.5	32	1	11	119	150
4.5	0.3	2.4	22.3	28	1	11	104	131
6	0.24	1.5	20.5	26	1	7	96	122
7.5	0.12	0.75	19.2	24	1	4	90	112
9	0	0	18	22.87	0	0	84	107

ESTIMATE OF PILE DOWNDRAG

The change in strain, $\Delta\varepsilon$ after pile installation and before the axial load was applied = 30.55 $\mu\varepsilon$

L_{shaft} = 7.6 m

B = 0.35 m

Area of steel, A_s = 1608 mm^2

Area of conc = BD - (A_s) = 120892 mm^2

Area of shaft, $A_{shaft} = 4BL_{shaft}$ = 10.64 m^2

E_c = 36 kN/mm^2

E_s = 205 kN/mm^2

The downdrag force, F_{NSF} can be determined from the measured strains and the properties of the pile materials as follows:

$$F_{NSF} = A_cE_c\Delta\varepsilon + A_sE_s\Delta\varepsilon$$

$$F_{NSF} = (A_cE_c + A_sE_s)\Delta\varepsilon$$ 143 kN

Downdrag, $F_{NSF} = \beta\sigma'_{v0}A_{shaft}$

$\beta = \tau_{sf}/\sigma'_{vo} = \{F_{NSF}/[A_{shaft}]/\sigma'_{v0}\}$ = 0.3

where β = Effective stress shaft adhesion factor

τ_{sf} = $F_{NSF}/[A_{shaft}]$

σ'_{vo} = $(\gamma_{fill} \times 1) + (\gamma'_{sleech} \times L_{shaft}/2) = (19 \times 1) + (6 \times 3.8)$ = 41.8 kPa

The calculated value of β is consistent with the value of 0.25 - 0.35 determined by Burland (1973) and Burland and Starke (1994)

Appendix 6a

Structural Analysis of Pile Section

&

Cracked and Uncracked Flexural Rigidity

PILE MOMENT CAPACITY

Introduction

This analysis calculates the theoretical moment capacity for the test pile used in Belfast. This is not a design exercise therefore the traditional factors of safety on materials have been omitted in order to obtain the best estimate of the pile's moment of resistance The 58 mm diameter inclinometer tube located in the centre of the pile has been ignored in these calculations.

These calculations check the capacity of the pile section as the neutral axis is varied throughout the section. In each calculation the strain in the steel is checked against the yield strain and the appropriate resulting value (elastic or yield) for strain is employed when calculating the force in the steel.

MATERIAL PROPERTIES

Concrete compressive strength, f_{cu} =	54 MPa	Cube tests	
Steel yield stress f_y =	500 MPa	Mill report	
36 kN/mm^2	Area of steel = 8T16 :	1608 mm^2	
205 kN/mm^2			

SECTION PROPERTIES

Width b =	350 mm	Cover to all steel =	35 mm
Depth h =	350 mm	Link steel (helical) =	5 mm
Pile Area A_g =	122500 mm^2		
Second Moment of Area, I_g =	0.0012505 m^4		

where A_g and I_g represent the gross area and second moment of area respectively.

CALCULATE THE POSITION OF THE NEUTRAL AXIS, x

The pile is reinforced with 3T16 bars tension and compression sides with 2T16 in the centre Assume static equilibrium of forces along the axis of the pile and use the properties of similar triangles to determine the strain distribution in the steel. The following calculations are for a balanced section, i.e. the steel and the concrete fail simultaneously.

Depths from the tensile edge of the pile		Area mm^2		
A_{s1}	48	603	At yield, the following strains apply	
A_{s2}	175	402	$\varepsilon_{conc.}$	0.0035
A_{s3}	302	603	ε_{steel}	0.002439

A_{s1}, A_{s2} and A_{s3} represent the different layers of steel bars in the pile

Initial trial depth for Neutral Axis (NA), x= 45.86 mm

Note

ultimate concrete design stress = $0.67f_{cu}$, research has shown that a factor of 0.67 is required to adjust for the difference between the cube compressive strength and its bending strength

Table 1

Element	Strain (st)	Force steel = $E_{st}\ \varepsilon_s\ A_s$	Force conc = $E_c\ \varepsilon_c\ A_c$
A_{s1}	-0.00016318	-20.172 kN	522.6725 kN
A_{s2}	-0.00985536	-201 kN	
A_{s3}	-0.01954753	-301.5 kN	

Sum Forces Σ = 0.00044 kN approximately = 0

Therefore the neutral axis is located at 45.86mm from the compression face of the pile, see Figure 1 below.

MOMENT CAPACITY

Calculate the ultimate moment capacity of the section
by summing moments of the forces in table 1 about the centroid

M : 116 kNm

Check

As a check on the above, the moments of the steel and concrete forces are summed about tension steel

M 116 kNm okay

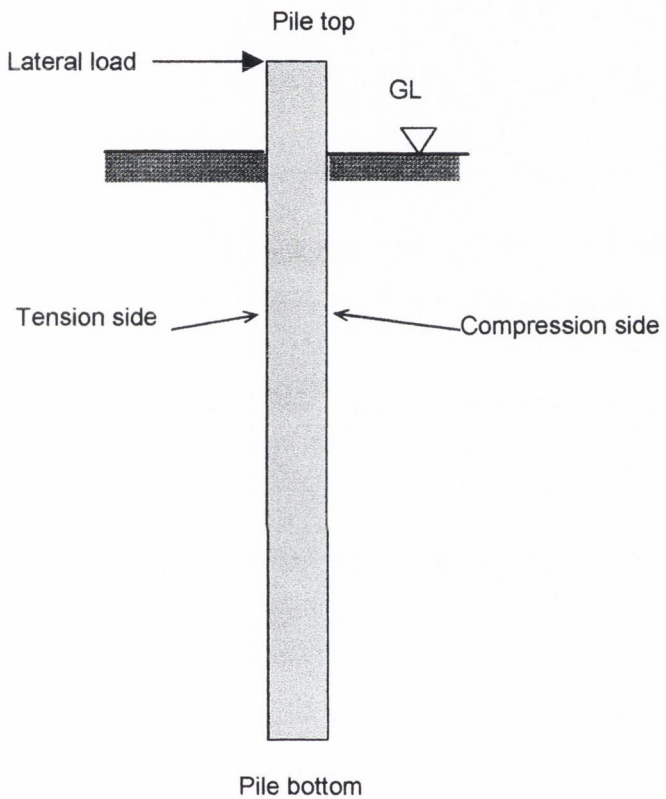

FIGURE 1

Note that the above result is the moment capacity of the pile (ignoring any material safety factors) when subjected to pure bending. If the pile carries an axial load the moment capacity will be increased due to the prestressing effect of the axial load. Therefore the following beam column calculations are performed to calculate the interaction diagram for the pile under combined loading.

Tensile capacity of section

Making an allowance for the tensile strength of the concrete equal to 7% of f_{cu}

The ultimate tensile capacity of the pile can be approximated as follows;

$P_{ten} = f_{cut}A_c+f_yA_s =$ -1251 kN -804 kN

(above figure is the tensile capacity of the pile ignoring the tensile strength of the concrete)

Compressive capacity of section

$P_{comp} = 0.67f_{cu}bh + f_yA_s$ 5178 kN

Calculate the Axial capacity, P and the Moment capacity , M of the pile when x is at the centroid of the section

The position of the centroid is determined as follows

$x_{centroid} = d/ (1+\varepsilon_y/0.0035) =$ 178 mm

x = 178 mm

Element	Strain (steel)	Force (steel)	Force concrete	A_s	F_s
As1	0.00255618	301.5 kN	2028.613 kN	603	301.5
As2	5.89888E-05	4.861264 kN		402	4.861264
As3	-0.0024382	-301.5 kN		603	-301.398

$P_{centroid} = F_{As1}+F_{As2}+F_c-F_{As3}$ 2033 kN

$M_{centroid} =$ 275 kNm

Calculate P and M for intermediate values of x

x = 100 mm

Element	*Strain (st)*	*Force (st)*	*Force conc*	A_s	F_s
As1	0.00182	224.9793 kN	1139.67 kN	603	224.9793
As2	-0.002625	-201 kN		402	201
As3	-0.00707	-301.5 kN		603	301.5

$P_{100} = F_{As1}-F_{As2}+F_c-F_{As3} =$ 862 kN

$M_{100} =$ 215 kNm

x = 200 mm

Element	*Strain (st)*	*Force (st)*	*Force conc*	A_s	F_s
As1	0.00266	301.5 kN	2279.34 kN	603	301.5
As2	0.0004375	36.05438 kN		402	36.05438
As3	-0.001785	-220.653 kN		603	-220.653

$P_{200} = F_{As1}+F_{As2}+F_c-F_{As3}$ = 2396 kN

M_{200} = 260 kNm

x = 400 mm

Element	*Strain (st)*	*Force (st)*	*Force conc*	A_s	F_s
As1	0.00308	301.5 kN	4432.05 kN	603	301.5
As2	0.00196875	162.2447 kN		402	162.2447
As3	0.0008575	105.9999 kN		603	105.9999

$P_{400} = F_{As1}+F_{As2}+F_c+F_{As3}$ = 5002 kN

M_{400} = 52 kNm

x = 150

Element	*Strain (st)*	*Force (st)*	*Force conc*	A_s	F_s
As1	0.00238	301.5 kN	1709.505 kN	603	294.2037
As2	-0.00058333	-48.0725 kN		402	-48.0725
As3	-0.00354667	-301.5 kN		603	301.5

$P_{150} = F_{As1}-F_{As2}+F_c-F_{As3}$ = 1661 kN

M_{150}= 260 kNm

x = 75 mm

Element	*Strain (st)*	*Force (st)*	*Force conc*	A_s	F_s
As1	0.00126	155.7549 kN	854.7525 kN	603	155.7549
As2	-0.00466667	-201 kN		402	201
As3	-0.01059333	-301.5 kN		603	301.5

$P_{75} = F_{As1}-F_{As2}+F_c-F_{As3}$ = 508 kN

M_{75} = 179 kNm

x = 350 mm

Element	*Strain (st)*	*Force (st)*	*Force conc*	A_s	F_s
As1	0.00302	301.5 kN	3988.845 kN	603	301.5
As2	0.00175	144.2175 kN		402	144.2175
As3	0.00048	59.3352 kN		603	59.3352

$P_{350} = F_{As1}+F_{As2}+F_c+F_{As3}$ = 4494 kN

M_{350} = 116 kNm 115.6309

x = 35

Element	*Strain (st)*	*Force (st)*	*Force conc*	A_s	F_s
As1	-0.0013	-160.7 kN	398.8845 kN	603	-160.7
As2	-0.014	-201 kN		402	201
As3	-0.0267	-301.5 kN		603	301.5

$P_{35} = -F_{As1}-F_{As2}+F_c-F_{As3}$ = -264 kN

M_{35} = 81 kNm

PLOT DATA FOR INTERACTION DIAGRAM

x	M (kNm)	P (kN)	
tension	0	-804	ignore conc tensile capacity
35	79	-279	
46.799	116	0	
75	174	476	
100	210	820	
150	254	1598	
178(bal)	268	1958	
200	253	2312	
350	113	4346	
400	52	4838	
infinity	0	5016	

INTERACTION DIAGRAM FOR BELFAST TEST PILE

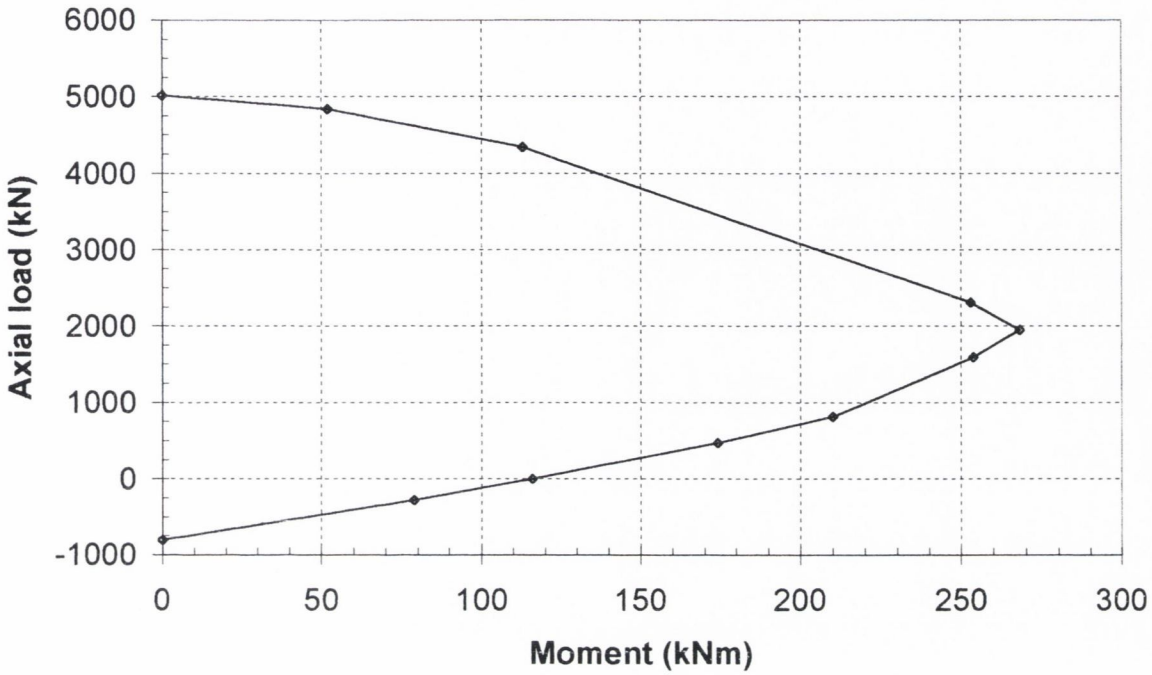

Uncracked Flexural Stiffness (EI)

From ENV 2 (1994), the following formula is given for the Young's Modulus of concrete

$E_c = 9500(f_{cu}+8)^{0.33}$ = 37 kN/mm^2 f_{cu} = 54 MPa

E_{st} = 205 kN/mm^2 f_y = 500 MPa

The relative stiffness between the reinforcing steel and the concrete is expressed as the modular ratio, n

$n = E_{st}/E_c$ = 5.540541

As the pile section is symmetrically reinforced the neutral axis is located at the centroid of the section, i.e., h/2 = 175mm.

Layer	Depths from top of pile	Area mm^2	(n-1)A_s*
A_{s1}	48	603	2737.946
A_{s2}	175	402	1825.297
A_{s3}	302	603	2737.946

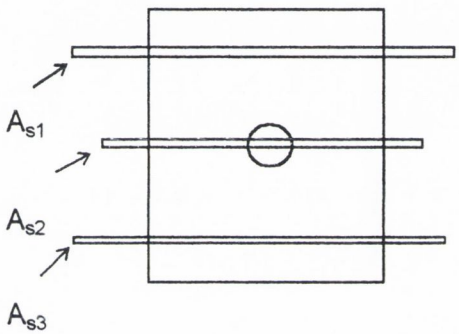

Width b = 350 mm d' = 48
Depth h = 350 mm
Inclin diam 58 mm

FIGURE 2

$I_u = (bh^3/12 - \pi D^4/64) + [(n-1)A_s(h/2-d')^2]$ = 0.001338 m^4 6.52 % >I_{gross} when the reinforcing bars are included in the calculation

$(EI)_u$ = 49517 kNm^2

*Note
When the steel is in the compression zone of an uncracked tension zone, its transformed area is nA_s, but it displaces an area of concrete equal to A_s. As a result, compression steel is transformed into an equivalent concrete area of $(n-1)A_s$.
When the beam is cracked, the steel in the tension zone does not displace any concrete and hence has a transformed area of nA_s.

Note that E_c is known to vary with the strain in the concrete (BRE RPT 46)
This needs to be researched further, but for the purposes of these calculations Ec is assumed to be constant.

Cracked Flexural Stiffness (EI)

From ENV 2 (1994), the following formula is given for the Young's Modulus of concrete

$E_c = 9500(f_{cu}+8)^{0.33}$ =	37 kN/mm^2	f_{cu} =	54 MPa
E_{st} =	205 kN/mm^2	f_y =	500 MPa

The relative stiffness between the reinforcing steel and the concrete is expressed as the modular ratio, n

$$n = E_{st}/E_c = 5.540541$$

Assume that the neutral axis is below than the top steel, A_{s1}. The transformed areas are:

Top steel, A_{s1}	$(n-1)A_s$ =	2737.946 mm^2	(see Figure 2 on previous page)
Mid steel, A_{s2}	nA_s =	2227.297 mm^2	
Bottom steel, A_{s3}	nA_s =	3340.946 mm^2	

Let the depth to the neutral axis be *c*, and sum the moment of the areas about the neutral axis to compute *c*.

Element	Area (mm^2)	y' (mm)	Ay' (mm^3)
Compression zone	350c	c/2	$175c^2$
Top steel, A_{s1}	2738	c-48	2738c-131424
Mid steel, A_{s2}	2227	c-350/2	2227c - 389725
Bottom steel, A_{s3}	3341	c-302	3341c - 1008982
			9.1E-06

c = distance to centroid when $\Sigma Ay' = 0$

$c^2 + 47.46c - 8743.61 = 0$

c = 72.74 mm > 48mm

Since the top steel is in the compression zone the initial assumption is OK

Element	Area	y	$I_{own\ axis}$	Ay^2
Compression zone	25459.5	36.37068	11226154.41	33678495.93
Top steel	2738	24.74136		1676025.067
Mid steel	2227	-102.259		23287360.12
Bottom steel	3341	-229.259		175601372.8
			I_{total} =	0.000245469 m^4

$(EI)_c$ = **9082.4 kNm^2**

$(EI)_c$ is only 18% of the uncracked flexural stiffness

Appendix 6b

Moment-Strain Relationship for Reinforced Concrete Pile Section from Finite Element Analysis

APPENDIX 6b

6.1 Finite element model for moment-strain relationship

As outlined in chapter 6, the field measured moment-strain relationship was limited by the magnitude of the free moment that could be generated at the reference strain gauge level i.e. 0.765m below the applied lateral load. The presence of soil below this level provided passive resistance (of unknown magnitude) to lateral pile movement and thus prevented the use of strain gauges at greater depths to extend the M-ε relationship.

A 2-D[1] finite element analysis (FEA) was therefore performed with three objectives:

(1) To produce predictions that were consistent with those from the measured M-ε relationship

(2) Extend the moment-strain relationship measured by the reference gauge and

[1] Only 2-D FEA was possible with the software employed (which facilitated specification of non-linear stress-strain relationships for the materials).

(3) To establish the influence of an axial load on the M-ε relationship.

The analysis was performed using the multi-linear material option available in the OASYS *SAFE* software. The programme replicated the non-linear behaviour of the reinforced concrete section once cracking occurs. The steel and concrete strength properties adopted for this model are shown in Figure 0-2. The pile was represented as a simple cantilever wall with the steel reinforcement located at the same position within the pile section but distributed *pro rata* over a typical 1m length of wall. The FE mesh (Figure 0-1) was constructed from eight node rectangular elements with four Gauss points per element. The mesh was designed to have a minimum number of rectangular elements, but also to have well-conditioned elements and to ensure the cantilever had sufficient length to replicate beam action. The elements representing the steel in the compression and tension sides of the pile, because of their relatively small area compared to concrete, were specified with the maximum permissible aspect ratio (*l/d*) ratio of 8.[2] To avoid localised stress concentrations that would result if the cantilever (wall) was loaded by a concentrated point load, shear stresses acting at the free end of the pile simulated the 'lateral load' while the axial load was simulated as a compressive stress applied normal to the cantilever section[3].

The program was initially run assuming a linear elastic pile section to predict the pile strains due to known bending moments to validate the accuracy of the FE analysis. The results of the linear elastic analyses (shown in Figure 0-3) confirm the validity of the FE model. It can be seen that the model predicts the M-ε relationship within 1.5% of the theoretical result. Hence, with the model validated, additional computer runs employing the multi-linear material option were performed to extend the M-ε relationship to larger strains. The strain (in the compression steel) close to the fixed end of the cantilever was compared with the increasing bending moment

[2] This ratio was also maintained for the middle steel layer, despite the smaller number of bars at this location; the adjustment was compensated for in the model by reducing the layer stiffness in proportion to the reduced area of steel at that location.

[3] Further details on the *SAFE* programme can be obtained in the user manual OASYS *SAFE*, 1997

Figure 0-4 shows the resulting M-ε relationships plotted in conjunction with the in-situ relationship measured by L1. The FE results predicted bending moments within 5% of the in situ measurements resulting in a good fit between both sets of data. Additional FE analyses involving combined axial and lateral loading were carried out to simulate the conditions at pile AL1. These relationships were subsequently used to interpret the pile bending moments from the measured strains.

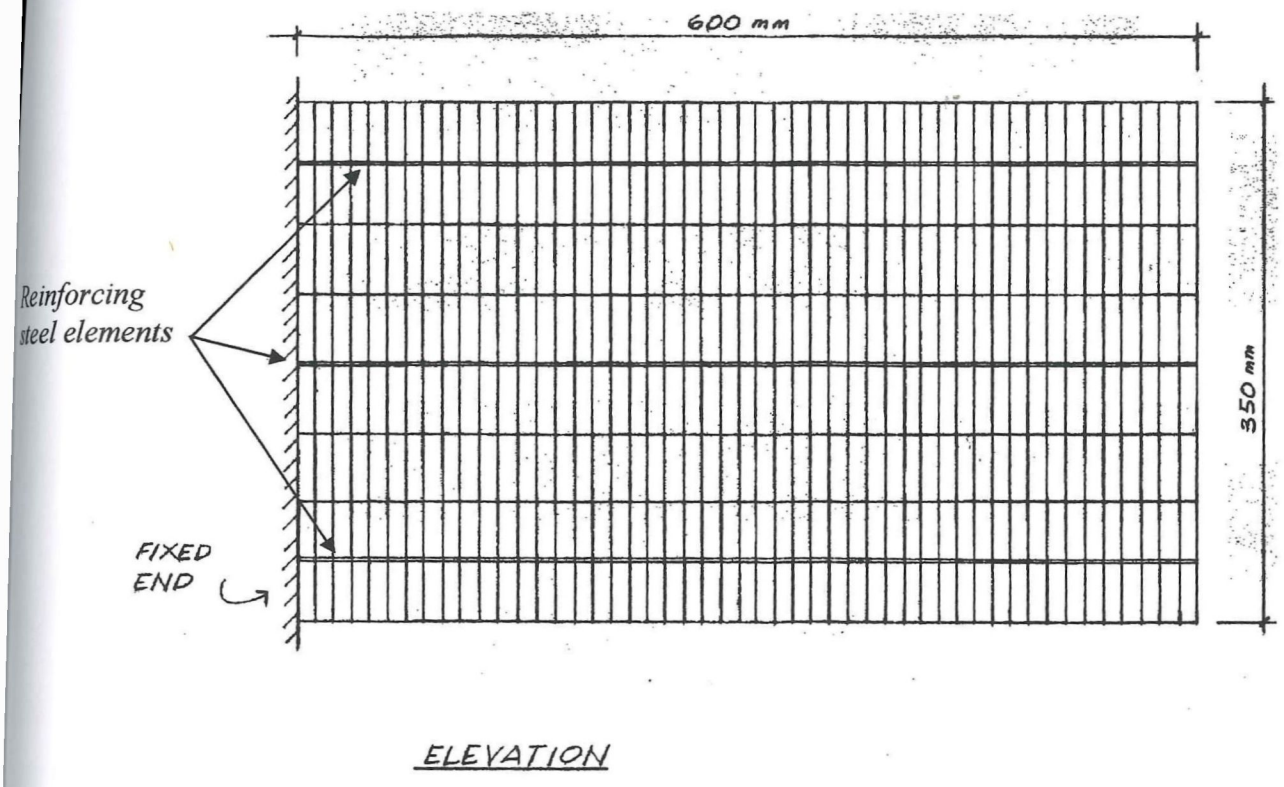

Figure 0-1: Finite Element mesh used to analyse the M-ε relationship for the piles

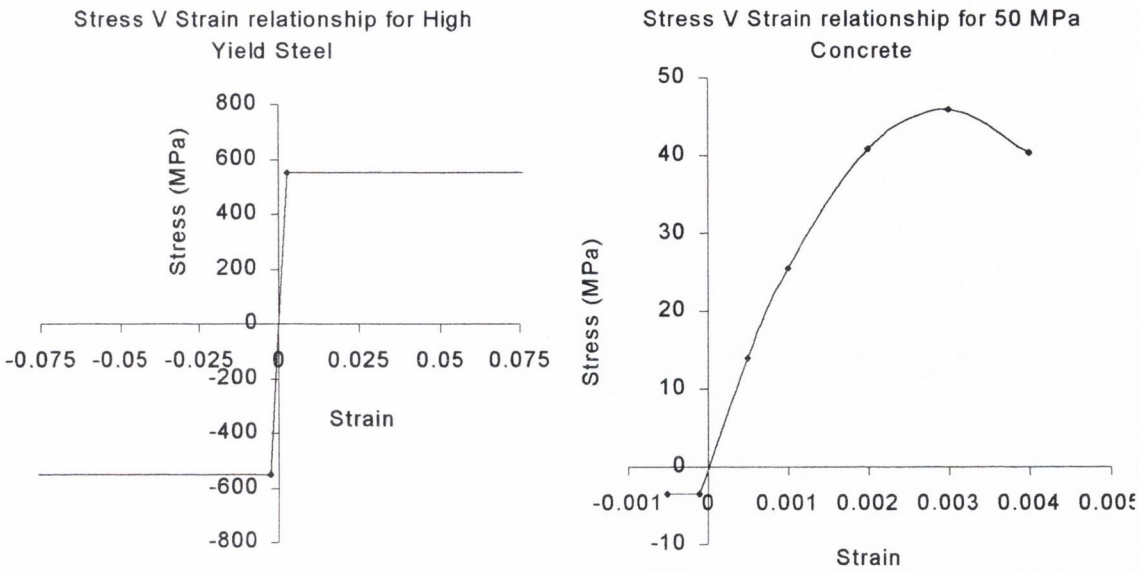

Figure 0-2: Constitutive relationships for steel and concrete

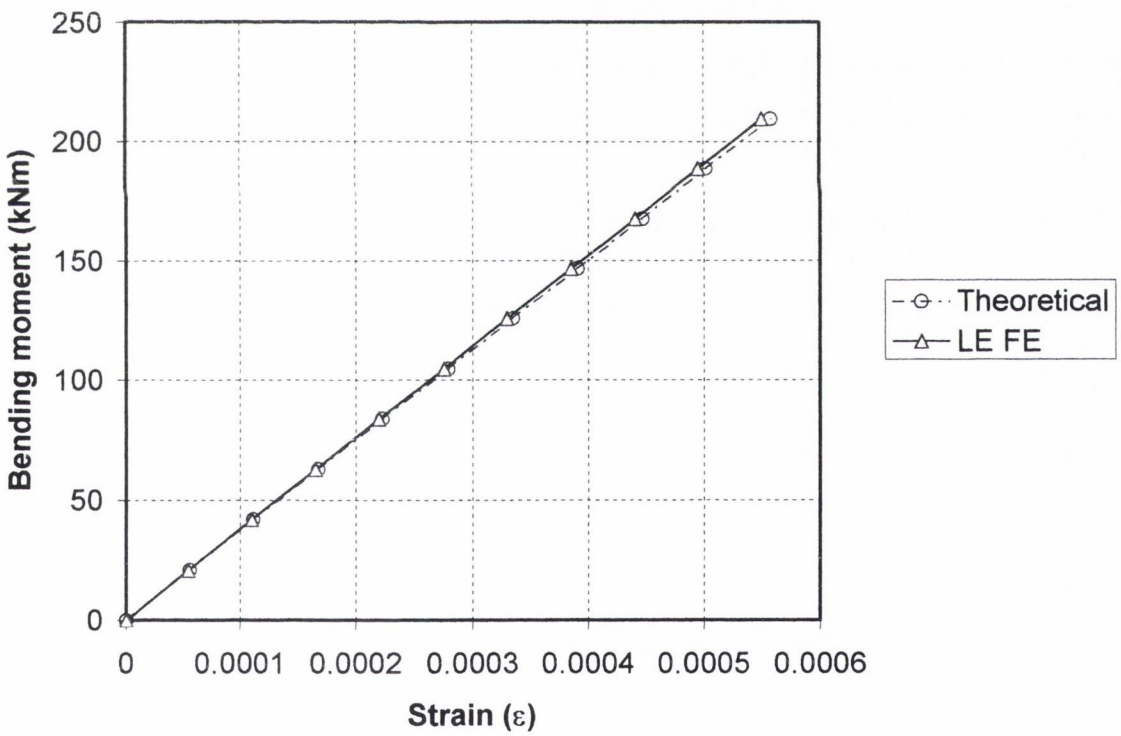

Figure 0-3: Comparison of linear elastic (LE) FE and theoretical elastic Moment-strain predictions

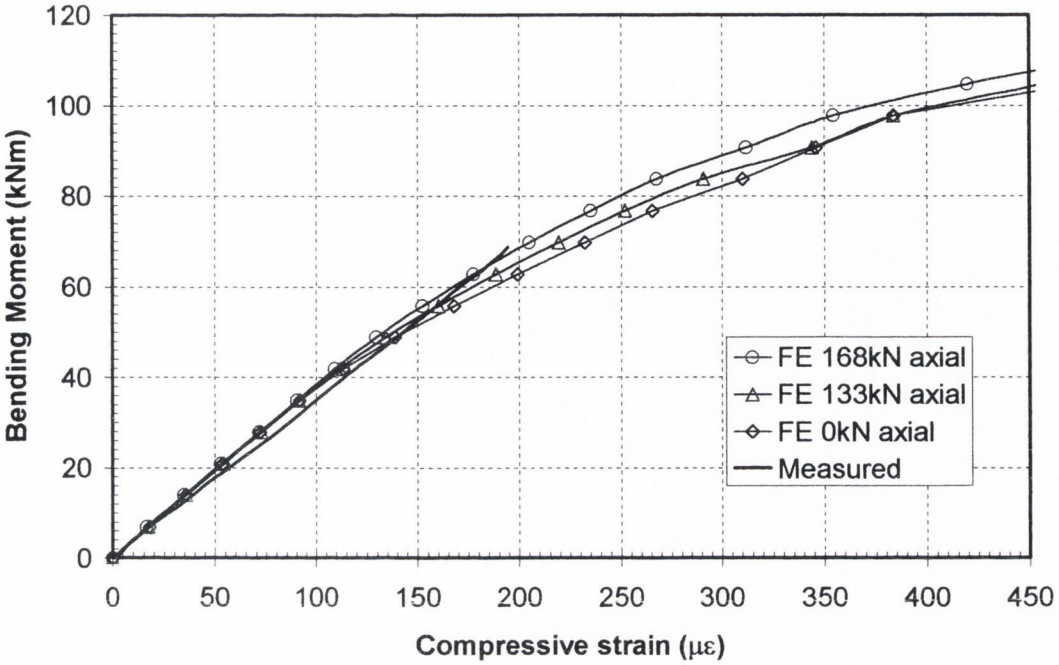

Figure 0-4: Non-linear FE M-ε relationships for various axial loads compared with measured in-situ relationship at pile L1

Appendix 6c

Back-calculated E_c from Lateral Load Tests

APPENDIX 6c

The following calculations back-figure the Young's modulus for the concrete E_c, for three load increments during CLT1. The calculations utilise strain gauge data from pile AL1 and the Moment-ε relationship established in appendix 6b. The maximum bending strain during the test was less than 35με which is well below the strain necessary to induce cracking in the concrete. Therefore, at these low strains, the concrete on the tension side of the pile contributed to the moment of resistance. It is of interest to note that the strain data reveals a reduction in the value of E_c as the applied bending moment is increased, most practitioners would assume E_c as a constant when undertaking design calculations. It is also evident from the calculations that the neutral axis (NA) does not coincide with the centroid of the pile, but remains in approximately the same position over the three load increments. The NA is displaced by approximately 15mm towards the compression face of the pile. There are a number of possible reasons for this result:

1. The axial load applied to the pile may be acting at a small eccentricity.
2. The dimensions assumed from the centroid of the pile to the actual location of the strain gauge may be in error due to minor variations in the position of the reinforcement bars after concrete placement.

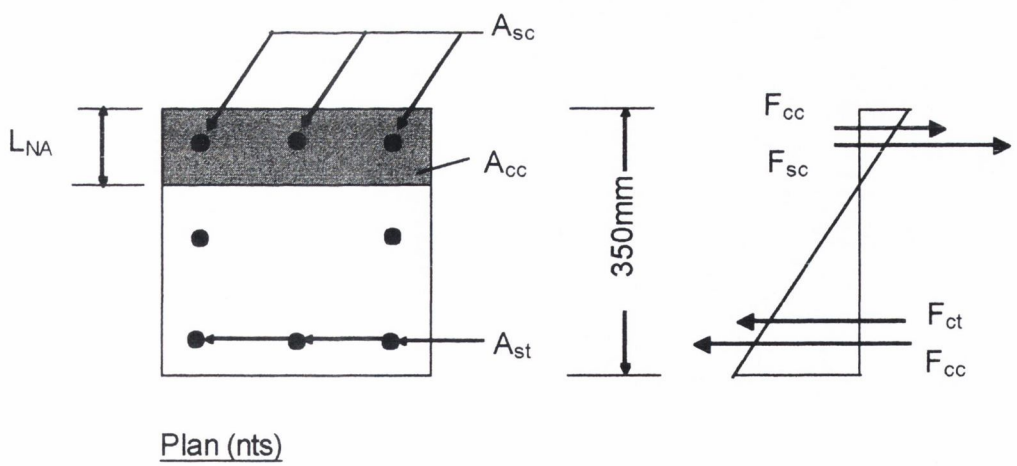

Figure 6c-1: Schematic illustration of pile cross section and component forces

PILE AL1

CLT1 Applied lateral load = 38.5kN

DATA

Distance from centroid, y_{st}	125.00	mm
Distance from centroid to extreme conc fibre, y_c	175.00	mm
Young's modulus for steel, E_{st} =	205.00	kN/mm^2
Strain in tension bar, ε_t	-14.81	με
Strain in compression bar, ε_c	16.24	με
M_{meas} from ERS gauge 1 and FE M-ε relationship =	7.20	kNm

CALCULATED DATA

Strain in concrete at exterme compression fibre, ε_{cc}

$\varepsilon_{cc} = \varepsilon_c L_{NA}/(L_{NA} - y_{st})$ = 2.35646E-05

Strain in concrete at exterme tension fibre, ε_{ct}

$\varepsilon_{st} = \varepsilon_c((350 - L_{NA})/(350 - (L_{NA} + (y_c - y_{st}))$ = -2.0132E-05

Location of neutral axis (NA) from extreme compressive fibre (L_{NA}) such that $\Sigma F = 0$ 160.86 mm

Area of concrete compression, A_{cc}	56300.95	mm^2
Area of concrete tension, A_{ct}	66199.05	mm^2
Area of steel = 3T16	603	mm^2

Forces

Force in conc in compression, F_{cc} =	$0.5E_c\varepsilon_{cc}(A_{cc} - A_{st})$ =	0.66 E_c (kN)	let the constant = k_1
Force in conc in tension, F_{ct} =	$0.5E_c\varepsilon_{ct}(A_{ct} - A_{st})$	-0.66 E_c (kN)	let the constant = k_2
Force in steel in compression, F_{sc} =	$E_{st}\varepsilon_c A_{st}$	2.01 (kN)	
Force in steel in tension, F_{st} =	$E_{st}\varepsilon_t A_{st}$	-1.83 (kN)	

Respective moments about NA of section **Check $\Sigma F = 0$**

M_{cc} =	$F_{cc}(2/3)L_{NA}$ =	0.070376081 E_c	F_{cc} =	28.717454
M_{ct} =	$F_{ct}(2/3)(350 - L_{NA})$	-0.083258086 E_c	F_{ct} =	-28.894242
M_{sc} =	$F_{sc}\{(L_{NA} - (y_c - y_s)\}$ =	0.222552032	F_{sc} =	2.0075076
M_{st} =	$F_{st}\{350 - (L_{NA} + (y_c - y_{st})\}$ =	-0.254729144	F_{st} =	-1.8307382
			ΣF =	-1.879E-05

Sum moments about NA of section and equating with Mmeas

$M_{meas} = M_{cc} + M_{ct} + M_{sc} + M_{st}$

$M_{meas} = (k_1 + k_2)E_c + M_{sc} + M_{st}$

$E_c = [M_{meas} - (M_{sc} + M_{st})]/(k_1 + k_2)$

E_c = **43.76** kN/mm^2

CLT1

CLT1 Applied lateral load = 47kN

DATA

Distance from centroid to steel, y_{st}	125.00	mm
Distance from centroid to extreme conc fibre, y_c	175.00	mm
Young's modulus for steel, E_{st} =	205.00	kN/mm^2
Strain in tension bar, ε_t	-19.51	με
Strain in compression bar, ε_c	21.44	με
M_{meas} from ERS gauge 1 and FE M-ε relationship =	8.50	kNm

CALCULATED DATA

Strain in concrete at exterme compression fibre, ε_{cc}

$\varepsilon_{cc} = \varepsilon_c L_{NA}/(L_{NA} - y_{st})$ = 3.11491E-05

Strain in concrete at exterme tension fibre, ε_{ct}

$\varepsilon_{st} = \varepsilon_c((350 - L_{NA})/(350 - (L_{NA} + (y_c - y_{st}))$ = -2.64984E-05

Location of neutral axis (NA) from extreme compressive fibre (L_{NA}) such that $\Sigma F = 0$ 160.41 mm

Area of concrete compression, A_{cc}	56144.16	mm^2
Area of concrete tension, A_{ct}	66355.84	mm^2
Area of steel = 3T16	603.00	mm^2

Forces

Force in conc in compression, F_{cc} =	$0.5E_c\varepsilon_{cc}(A_{cc} - A_{st})$ =	0.865029 E_c (kN)	let the constant = k_1
Force in conc in tension, F_{ct} =	$0.5E_c\varepsilon_{ct}(A_{ct} - A_{st})$	-0.871173 E_c (kN)	let the constant = k_2
Force in steel in compression, F_{sc} =	$E_{st}\varepsilon_c A_{st}$	2.650306 (kN)	
Force in steel in tension, F_{st} =	$E_{st}\varepsilon_t A_{st}$	-2.411729 (kN)	

Respective moments about NA of section				**Check ΣF = 0**
M_{cc} =	$F_{cc}(2/3)L_{NA}$ =	0.092507 E_c	F_{cc} =	33.60636099
M_{ct} =	$F_{ct}(2/3)(350 - L_{NA})$	-0.110109 E_c	F_{ct} =	-33.84507357
M_{sc} =	$F_{sc}\{(L_{NA} - (y_c - y_s)\}$ =	0.292625	F_{sc} =	2.6503056
M_{st} =	$F_{st}\{350 - (L_{NA} + (y_c - y_{st})\}$ =	-0.336649	F_{st} =	-2.41172865
			ΣF =	-0.000135628

Sum moments about NA of section and equating with Mmeas

$M_{meas} = M_{cc} + M_{ct} + M_{sc} + M_{st}$

$M_{meas} = (k_1 + k_2)E_c + M_{sc} + M_{st}$

$E_c = [M_{meas} - (M_{sc} + M_{st})]/(k_1 + k_2)$

E_c = **38.85 kN/mm^2**

PILE AL1

CLT1 Applied lateral load = 59.75kN

DATA

Distance from centroid to steel, y_{st}	125	mm
Distance from centroid to extreme conc fibre, y_c	175	mm
Young's modulus for steel, E_{st} =	205	kN/mm^2
Strain in tension bar, ε_t	-24.31	με
Strain in compression bar, ε_c	26.24	με
M_{meas} from ERS gauge 1 and FE M-ε relationship =	9.9	kNm

CALCULATED DATA

Strain in concrete at exterme compression fibre, ε_{cc}

$\varepsilon_{cc} = \varepsilon_c L_{NA}/(L_{NA} - y_{st})$ = 3.78359E-05

Strain in concrete at exterme tension fibre, ε_{ct}

$\varepsilon_{ct} = \varepsilon_c((350 - L_{NA})/(350 - (L_{NA} + (y_c - y_{st}))$: -3.31915E-05

Location of neutral axis (NA) from extreme compressive fibre (L_{NA}) such that $\Sigma F = 0$ 163.14 mm

Area of concrete compression, A_{cc}	57100.13	mm^2
Area of concrete tension, A_{ct}	65399.87	mm^2
Area of steel = 3T16	603	mm^2

Forces

Force in conc in compression, F_{cc} =	$0.5E_c\varepsilon_{cc}(A_{cc} - A_{st})$ =	1.06881048 E_c (kN)	let the constant = k_1
Force in conc in tension, F_{ct} =	$0.5E_c\varepsilon_{ct}(A_{ct} - A_{st})$	-1.075354223 E_c (kN)	let the constant = k_2
Force in steel in compression, F_{sc} =	$E_{st}\varepsilon_c A_{st}$	3.2436576 (kN)	
Force in steel in tension, F_{st} =	$E_{st}\varepsilon_t A_{st}$	-3.00508065 (kN)	

Respective moments about NA of section

				Check $\Sigma F = 0$
M_{cc} =	$F_{cc}(2/3)L_{NA}$ =	0.116246127 E_c	F_{cc} =	38.9688301
M_{ct} =	$F_{ct}(2/3)(350 - L_{NA})$	-0.133958147 E_c	F_{ct} =	-39.20741496
M_{sc} =	$F_{sc}\{(L_{NA} - (y_c - y_s)\}$ =	0.366997886	F_{sc} =	3.2436576
M_{st} =	$F_{st}\{350 - (L_{NA} + (y_c - y_{st})\}$ =	-0.411265643	F_{st} =	-3.00508065
			ΣF :	-7.90629E-06

Sum moments about NA of section and equating with Mmeas

$M_{meas} = M_{cc} + M_{ct} + M_{sc} + M_{st}$

$M_{meas} = (k_1 + k_2)E_c + M_{sc} + M_{st}$

$E_c = [M_{meas} - (M_{sc} + M_{st})]/(k_1 + k_2)$

E_c = **36.46** kN/mm^2

Appendix 6d

Analysis of Head Restraint at Pile AL1

APPENDIX 6d

Analysis of Pile Head Restraint at AL1

The following is a summary of the analysis undertaken to assess the magnitude of the restraint induced at the pile head of AL1. The calculations are based on the structural model presented in chapter 6 (section 6.3) which utilises data from the pile head displacement transducers, strain gauges and the electro-level located closest to the applied lateral load. The accuracy of the results are verified by calculating the net lateral load applied to the pile using data from a strain gauge located 0.265m below the lateral load and comparing the result with the load predicted by a second strain gauge (ERS2) positioned 0.565m below the lateral load. The calculations indicate the strain gauges predict a value of applied lateral load within 3% or better of each other at each load increment, the average result was adopted for the analysis of pile AL1.

ANALYSIS OF PIN ROTATION ON THE LATERAL LOAD APPLIED TO PILE AL1 CLT1

Note: The rotation at the pin joint is calaulated on the basis of measurements recorded by LVDT 4 and EL D. Similar triangles are used to calculate the displacement at the pin joint (Δ). With Δ and the vertical distance from the test beam to the pin known, the angle β is determined and hence the horizontal component of the applied axial load can be calculated.

El 5.04E-05 radians/mV

Applied vertical load (kN)		***168.0***	***168.0***	***168.0***	***168.0***	***168.0***	***168.0***
Lateral load, H (kN)		**12.8**	**25.5**	**38.5**	**47.0**	**55.5**	**59.8**
Displacement measured at LVDT		**0.5**	**1.3**	**2.2**	**3.0**	**3.9**	**5.0**
EL-D net output (mV)		11.4	17.5	28.6	39.6	44.4	49.0
EL-D slope (rad)		0.0006	0.0009	0.0014	0.0020	0.0022	0.0025
Back-figured disp at pin (Δ)		0.9	1.9	3.4	4.6	5.6	6.9
Distance from kentledge beam to pin		865.0	865.0	865.0	865.0	865.0	865.0
Slope distance from beam to pin		865.0	865.0	865.0	865.0	865.0	865.0
Angle β = (Δ/865mm)	β rads	0.0011	0.0022	0.0039	0.0053	0.0065	0.0080
	β DEG	0.0622	0.1288	0.2222	0.3015	0.3706	0.4580
Angled vertical load due to pin rotation	V	168.0	168.0	168.0	168.0	168.0	168.0
Vertical component of inclined vertical load, V_{comp} =Vcos β		168.0	168.0	168.0	168.0	168.0	168.0
Horizontal component due to pin rotation, V sin β		**0.2**	**0.4**	**0.7**	**0.9**	**1.1**	**1.3**
p delta = (Vcos β) .Δ (kNm)		0.2	0.3	0.6	0.8	0.9	1.2
M_{horiz} component of V = (Vsinβ)e (kNm) where e = 0.935+0.14+0.125		0.2	0.5	0.8	1.1	1.3	1.6
Dist from lat load to ERS 1& 15 =	0.265						
Dist from pin to ERS 1 & 15 =	1.2						
M inferred from ERS1 and M-ε relationship		**1.3**	**3.3**	**6.8**	**8.6**	**10.1**	**11.1**
M inferred from ERS2 and M-ε relationship		**-1.2**	**-1.9**	**-1.0**	**-0.3**	**0.1**	**0.5**
Friction developed at pin, h =(0.265H+1.2Vtanβ-M_o)/1.2 + PΔ/1.2	**(for ERS1)**	**4.2**	**9.1**	**15.3**	**19.1**	**22.5**	**24.8**
Friction developed at pin, h =(0.565H+1.5Vtanβ-M_o)/1.5 + PΔ/1.5	**(for ERS2)**	**4.3**	**9.0**	**14.9**	**18.9**	**22.7**	**25.0**
Net horiz load applied to pile H_R from ERS 1		**8.7**	**16.8**	**23.9**	**28.8**	**34.0**	**36.3**
Net horiz load applied to pile H_R from ERS 2		**8.6**	**16.9**	**24.3**	**29.0**	**33.9**	**36.1**
Average H_R from ERS 1 & ERS 2 in kN		***8.7***	***16.9***	***24.1***	***28.9***	***34.0***	***36.2***
Moment at point of horiz load application (kNm)		**-3.8**	**-8.1**	**-13.7**	**-17.0**	**-20.1**	**-21.9**

ANALYSIS OF PIN ROTATION ON THE LATERAL LOAD APPLIED TO PILE AL1 CLT2

Electro-level cali EL CF = 5.04E-05 rads/mV

Applied vertical load (kN)		***133.0***	***133.0***	***133.0***	***133.0***	***133.0***	***133.0***	***133.0***	***133.0***	***133.0***
Lateral load, H (kN)		**12.8**	**25.5**	**38.5**	**47.0**	**55.5**	**59.8**	**68.3**	**76.8**	**85.3**
Displacement measured at lvdt		**1.7**	**2.5**	**3.4**	**4.5**	**5.9**	**7.0**	**9.7**	**14.8**	**27.8**
EL-D net output (mV)		2.6	5.2	12.6	19.5	26.3	32.4	42.2	81.8	131.4
EL-D slope (rad)		0.0001	0.0003	0.0006	0.0010	0.0013	0.0016	0.0021	0.0041	0.0066
Back-figured disp at pin (Δ)		1.8	2.7	3.9	5.2	6.9	8.2	11.3	18.0	33.0
Distance from kentledge beam to pin		865.0	865.0	865.0	865.0	865.0	865.0	865.0	865.0	865.0
Slope distance from beam to pin		865.0	865.0	865.0	865.0	865.0	865.0	865.1	865.2	865.6
Angle β = (Δ/865mm)	β rads	0.0021	0.0031	0.0045	0.0060	0.0080	0.0095	0.0131	0.0208	0.0381
Check on β		0.0021	0.0031	0.0045	0.0060	0.0080	0.0095	0.0131	0.0208	0.0381
β degrees		0.1	0.2	0.3	0.3	0.5	0.5	0.7	1.2	2.2
Angled vert. load due to pin rotation	V	133.0	133.0	133.0	133.0	133.0	133.0	133.0	133.0	133.0
Vertical component of inclined vertical load, V	Vcomp = V cos β	133.0	133.0	133.0	133.0	133.0	133.0	133.0	133.0	132.9
Horizontal compponent due to pin rotation	**V sin β (kN)**	**0.3**	**0.4**	**0.6**	**0.8**	**1.1**	**1.3**	**1.7**	**2.8**	**5.1**
p delta = (Vcos β) .Δ (kNm)		0.2	0.4	0.5	0.7	0.9	1.1	1.5	2.4	4.4
M_{horiz} component of V = (Vtanβ)e (kNm)		0.3	0.5	0.7	1.0	1.3	1.5	2.1	3.3	6.1
Distance from lat load to ERS 1& 15 (m) =	0.265									
e = Distance from pin to ERS 1 & 15 = (0.935 + 0.14 + 0.125) m	1.2									
Moment measured at ERS 1 & 15 =										
M inferred from ERS1 and M-ε relationship		**0.8**	**2.3**	**4.0**	**2.3**	**-0.1**	**-1.2**	**-5.1**	**-9.8**	**-22.5**
M inferred from ERS2 and M-ε relationship		**-2.1**	**-3.0**	**-4.1**	**-6.4**	**-11.3**	**-14.0**	**-20.8**	**-28.6**	**-47.5**
Friction developed at pin, h =(0.265H+1.2Vsinβ-M_o)/1.2 + PΔ/1.2	**(for ERS1)**	**4.0**	**8.3**	**12.9**	**13.7**	**14.0**	**14.4**	**13.8**	**13.5**	**8.8**
Friction developed at pin, h =(0.565H+1.5Vsinβ-M_o)/1.5 + PΔ/1.5	**(for ERS2)**	**3.8**	**8.3**	**12.7**	**14.7**	**15.1**	**15.2**	**14.6**	**14.2**	**8.4**
% difference in above results		***3.0***	***0.0***	***1.2***	***-7.5***	***-7.5***	***-5.5***	***-5.6***	***-4.9***	***4.1***
Net horiz load applied to pile H_R from ERS 1		**9.1**	**17.7**	**26.2**	**34.1**	**42.6**	**46.6**	**56.2**	**66.0**	**81.5**
Net horiz load applied to pile H_R from ERS 2		**9.2**	**17.7**	**26.4**	**33.1**	**41.5**	**45.8**	**55.4**	**65.3**	**81.9**
% difference in above results		**-1.3**	**0.0**	**-0.6**	**3.0**	**2.5**	**1.7**	**1.4**	**1.0**	**-0.4**
Average H_R from ERS 1 & ERS 2		***9.1***	***17.7***	***26.3***	***33.6***	***42.0***	***46.2***	***55.8***	***65.6***	***81.7***
Moment at point of horiz load application		**-3.4**	**-7.3**	**-11.5**	**-12.0**	**-12.1**	**-12.3**	**-11.3**	**-10.1**	**-3.5**

Appendix 8a

Validation of curve fitting equation

Appendix 8a - Validation of Curve Fitting Equation

8.1 Bending Moments

The curve fitting procedure was validated by analysing a propped cantilever having the same flexural rigidity as the test piles, see structural model in Figure 0-1a. The bending moment at twenty-two points along the cantilever was calculated using elastic beam theory, and Eq. 8-1 was employed to fit a smooth curve to this data. The fitted bending moments were then treated in the same way as the experimental data. Figure 0-1b shows the calculated bending moments in addition to the shear force and reaction profiles calculated from the first and second differentials of Eq 8.1 respectively. The results show very good agreement between the theoretical and fitted bending moment profiles (r^2 = 0.9938). The location and magnitude of the maximum span moment predicted was within 7% and 1% respectively of the theoretical values.

Eq. 0-1... $$M_z = \left[1 - \frac{1}{e^{a_0 z} + 1}\right]\left(a_1 + a_2 z + a_3 z^2 + a_4 z^3 + a_5 z^4 + ... + a_i z^{i-1}\right)$$

The derived shear and reaction profiles are in keeping with the theoretical profiles, the deviation from the theoretical results is due to the influence of the polynomial and exponential components in the curve fitting equation preventing a sloping straight line in the shear force distribution. However, the method is well suited to the non-linear soil reaction and shear distributions typically encountered in the analysis of laterally loaded piles.

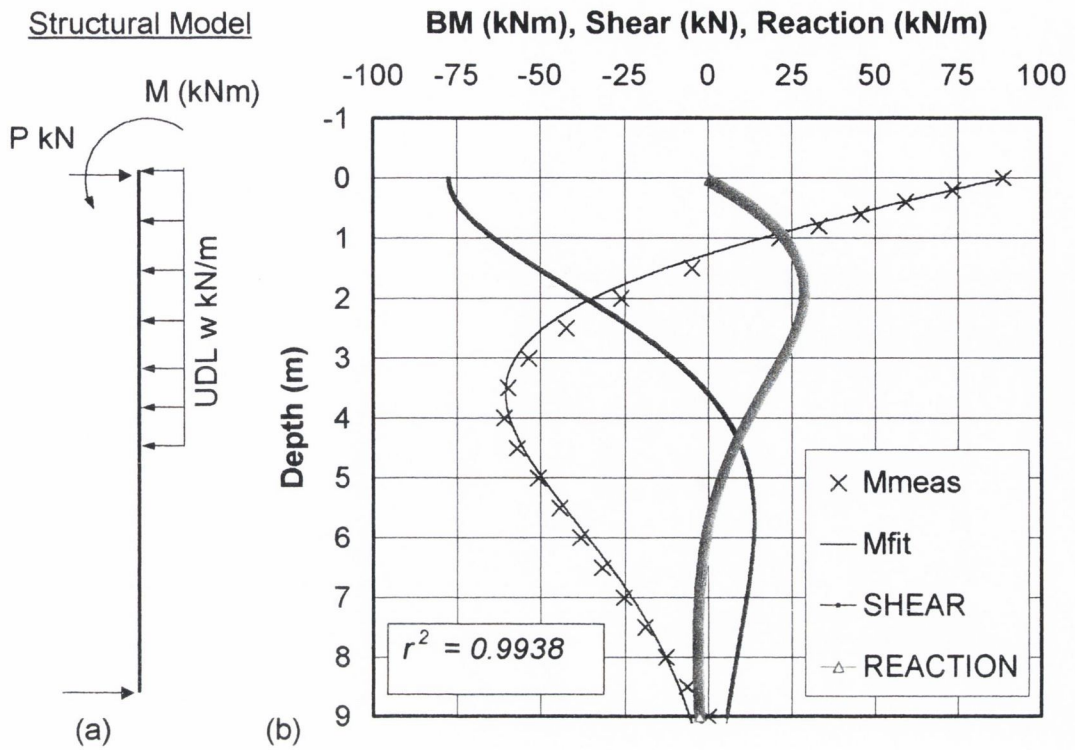

Figure 0-1: Validation of curve fitting procedure for a propped cantilever subjected to a lateral load of 77kN and a moment of 89kNm at the fixed end.

8.2 Slope Profile

The curve fitting approach for measured slopes was again validated by analysing a cantilever having the same flexural rigidity as the test piles. The structural model used is shown in Figure 0-2a. The slope at thirteen points along the cantilever was calculated using elastic beam theory. Eq. 0-2 was then employed to fit a smooth curve to the thirteen data points. Figure 0-2b shows the slopes calculated from beam theory along with the fit obtained. The curve fitting provides satisfactory agreement between the theoretical and fitted slopes (r^2 = 0.9932). The slope equation was then integrated to give the deflected profile of the cantilever and the result is compared with the theoretical displaced profile in Figure 0-3. The method predicted the deflection at the free end within 2% of the theoretical value.

Eq. 0-2... $$\theta_z = \left[1 - \frac{1}{e^{a_0 z} + 1}\right]\left(a_1 + a_2 z + a_3 z^2 + a_4 z^3 + a_5 z^4 + ... + a_i z^{i-1}\right)$$

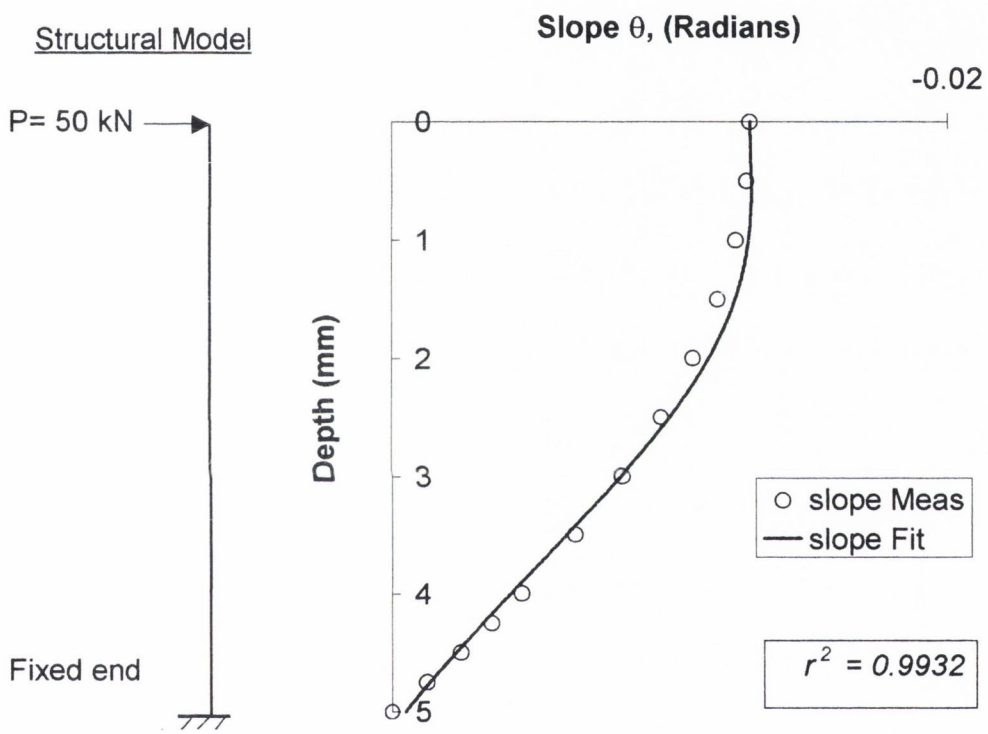

Figure 0-2: Validation of curve fitting procedure for a cantilever subjected to a lateral load of 50kN at the free end.

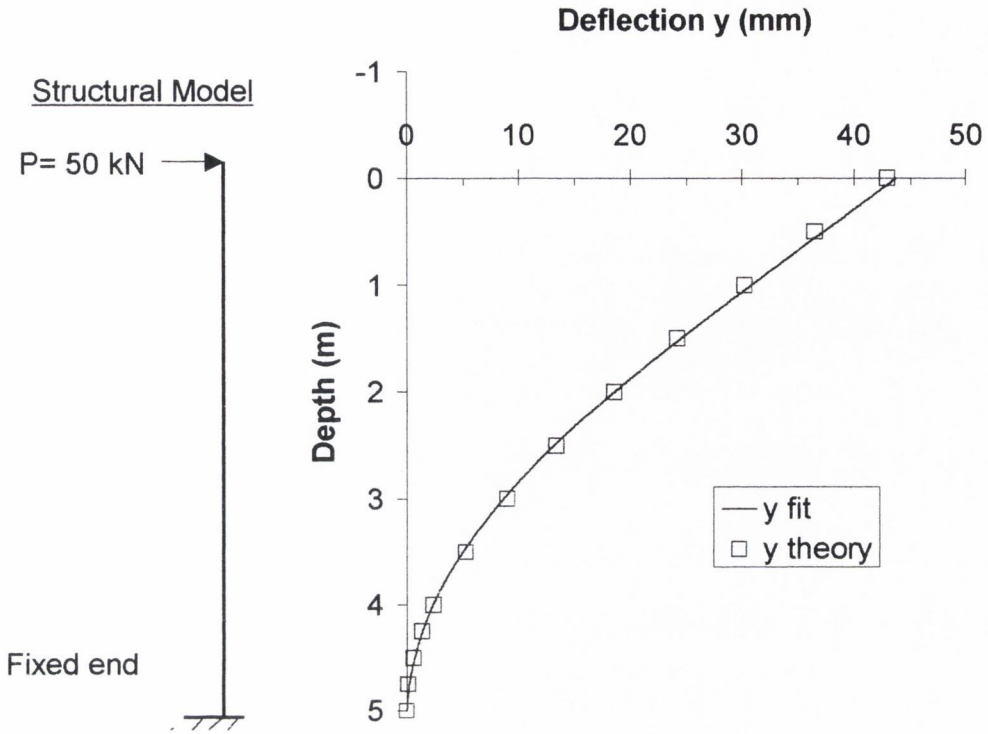

Figure 0-3: Theoretical deflection profile compared with curve fitting prediction

Appendix 8b

Derivation of Curve Fitting Coefficients and Least Squares Optimisation

APPENDIX 8b: CURVE FITTING OF MEASURED SLOPES AND BENDING MOMENTS

CURVE FITTING - SLOPES

$$= \left(1 - \frac{1}{e^{-a_0 x} + 1}\right)\left(a_1 + a_2 x + a_3 x^2 + \ldots + a_n x^{n-1}\right)$$

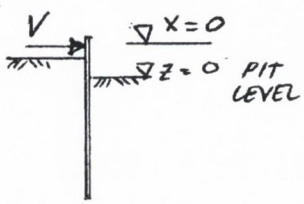

BOUNDARY CONDITIONS

1. AT $X = 0$ θ = MEASURED SLOPE AT PT OF LOAD APPLICATION

2. $X = 0$ $\frac{M}{EI} = \frac{d\theta}{dx} = 0$

3. $X = 0$ $\frac{V}{EI} = \frac{d^2\theta}{dx^2}$ = APPLIED LATERAL LOAD

$$\frac{d\theta}{dx} = \left(1 - \frac{1}{e^{-a_0 x} + 1}\right)\left(a_2 + 2a_3 x + \ldots\right) + \left(a_1 + a_2 x + a_3 x^2 + \ldots\right)\left(\frac{-a_0 e^{-a_0 x}}{(e^{-a_0 x} + 1)^2}\right)$$

AT $X = 0$ $\quad \frac{M}{EI} = 0 = \frac{a_2}{2} + (a_1)\left(-\frac{a_0}{4}\right)$

$$\Rightarrow \boxed{a_2 = \frac{a_0 a_1}{2}}$$

$$\theta = \left(1 - \frac{1}{e^{a_0 x} + 1}\right)\left(a_1 + a_2 x + a_3 x^2 + \ldots + a_n x^{n-1}\right)$$

AT $X = 0$ $\quad \theta = \frac{a_1}{2}$

$$\Rightarrow \boxed{a_1 = 2\theta}$$

$$\frac{d^2\theta}{dx^2} = \left(1 - \frac{1}{e^{-a_0x}+1}\right)(2a_3) + (a_2 + 2a_3x)\left(\frac{-a_0 e^{-a_0x}}{(e^{-a_0x}+1)^2}\right)$$

$$+ (a_1 + a_2x + \ldots)\left[(-a_0e^{-a_0x})\left(\frac{2a_0e^{-a_0x}}{(e^{-a_0x}+1)^3}\right) + \frac{a_0^2 e^{-a_0x}}{(e^{-a_0x}+1)^2}\right]$$

$$+ \left(\frac{-a_0 e^{-a_0x}}{(e^{-a_0x}+1)^2}\right)(a_2 + 2a_3x + \ldots)$$

AT $x = 0$ $\quad \frac{V}{EI} = a_3 + (a_2)\left(-\frac{a_0}{4}\right) + a_1\left[(-a_0)\left(\frac{2a_0}{8}\right) + \frac{a_0^2}{4}\right] + \left(-\frac{a_0}{4}\right)(a_2)$

$$a_3 - \frac{a_0a_2}{4} + a_1\left[-\frac{a_0^2}{4} + \frac{a_0^2}{4}\right] - \frac{a_0a_2}{4}$$

$$\frac{V}{EI} = a_3 - \frac{a_0a_2}{2}$$

$$\Rightarrow \boxed{a_3 = \frac{V}{EI} + \frac{a_0a_2}{2}}$$

NOTE

FOR PILE AC1 $\div$ THE COEFFICIENT a_2 HAS TO BE MODIFIED DUE TO THE PRESENCE OF A BENDING MOMENT AT $x = 0$

$$\frac{M}{EI} = \frac{a_2}{2} - \frac{a_1a_0}{4}$$

$$\Rightarrow \boxed{a_2 = \frac{2M}{EI} + \frac{a_1a_0}{2}}$$

CURVE FITTING – MOMENTS

$$M = \left(1 - \frac{1}{e^{-a_0 z} + 1}\right)\left(a_1 + a_2 z + a_3 z^2 + \ldots + a_n z^{n-1}\right)$$

BOUNDARY CONDITIONS – PILE L1

1. AT $z = 0$ THE M CAN BE CALCULATED AS THE APPLIED LOAD MULTIPLIED BY THE HEIGHT OF THE LOAD ABOVE P/T LEVEL

2. AT $z = 0$ THE SHEAR FORCE IS EQUAL TO THE APPLIED LATERAL LOAD.

3. AT $z = 0$ THE SOIL REACTION p IS ALSO EQUAL TO ZERO

FROM BOUNDARY CONDITION 1

$$M = \left(1 - \tfrac{1}{2}\right)(a_1)$$

$$M = \frac{a_1}{2}$$

$$\Rightarrow \quad \boxed{a_1 = 2M}$$

FROM BOUNDARY CONDITION 2

$$= \frac{dM}{dz}$$

$$M = \left(1 - \frac{1}{e^{-a_0 z}+1}\right)\left(a_1 + a_2 z + a_3 z^2 + \ldots + a_n z^{n-1}\right)$$

$$u \qquad\qquad v$$

$$M = u.v \Rightarrow \frac{dM}{dz} = u\frac{dv}{dz} + v\frac{du}{dz}$$

$$\frac{dv}{dz} = a_2 + 2a_3 z +$$

$$\frac{du}{dz} = \frac{d}{dz}\left[-(e^{-a_0 z}+1)^{-1}\right]$$

$$= (e^{-a_0 z}+1)^{-2}(-a_0 e^{-a_0 z})$$

$$\frac{du}{dz} = \frac{-a_0 e^{-a_0 z}}{(e^{-a_0 z}+1)^2}$$

$$SF = \frac{dM}{dz} = \left(1 - \frac{1}{e^{-a_0 z}+1}\right)(a_2 + 2a_2 z + ..) + (a_1 + a_2 z + ...)\left(\frac{-a_0 e^{-a_0 z}}{(e^{-a_0 z}+1)^2}\right)$$

For $z = 0$

$$= \left(\tfrac{1}{2}\right)(a_2) + (a_1)\left(\frac{-a_0}{2^2}\right)$$

$$= \frac{a_2}{2} \quad \frac{a_0 a_1}{4} \Rightarrow 4SF = 2a_2 - a_0 a_1$$

$$\Rightarrow \boxed{a_2 = 2SF + \frac{a_0 a_1}{2}}$$

FROM BOUNDARY CONDITION 3

$$= \frac{d^2M}{dz^2} = \frac{d(SF)}{dz}$$

$$SF = \left(1 - \frac{1}{e^{-a_0 z}+1}\right)(a_2 + 2a_3 z + \ldots) + (a_1 + a_2 z \ldots)\left(\frac{-a_0 e^{-a_0 z}}{(e^{-a_0 z}+1)^2}\right)$$

SF CAN BE DIFFERENTIATED AS A DOUBLE PRODUCT

OBTAINING THE DIFFERENTIAL FOR THE LAST TERM

I.E. $\frac{d}{dz}\left(\frac{-a_0 e^{-a_0 z}}{(e^{-a_0 z}+1)^2}\right) \equiv \underset{u}{(-a_0 e^{-a_0 z})}\underset{v}{(e^{-a_0 z}+1)^{-2}}$

$$= (-a_0 e^{-a_0 z})\left[(-2(e^{-a_0 z}+1)^{-3}(-a_0 e^{-a_0 z}))\right] + (e^{-a_0 z}+1)^{-2}(a_0^2 e^{-a_0 z})$$

$$= (-a_0 e^{-a_0 z})\left(\frac{2a_0 e^{-a_0 z}}{(e^{-a_0 z}+1)^3}\right) + \frac{a_0^2 e^{-a_0 z}}{(e^{-a_0 z}+1)^2}$$

$$\frac{d(SF)}{dz} = \left(1 - \frac{1}{e^{-a_0 z}+1}\right)(2a_3) + (a_2 + 2a_3 z + \ldots)\left(\frac{-a_0 e^{-a_0 z}}{(e^{-a_0 z}+1)^2}\right) +$$

$$(a_1 + a_2 z + \ldots)\left[(-a_0 e^{-a_0 z})\left(\frac{2a_0 e^{-a_0 z}}{(e^{-a_0 z}+1)^3}\right) + \frac{a_0^2 e^{-a_0 z}}{(e^{-a_0 z}+1)^2}\right] + \left(\frac{-a_0 e^{-a_0 z}}{(e^{-a_0 z}+1)^2}\right)(a_2)$$

WHEN $z = 0 \quad P = \frac{d(SF)}{dz} = 0$

$$a_3 + (a_2)\left(-\frac{a_0}{4}\right) - \left(\frac{a_0}{4}\right)a_2 = 0$$

$$\boxed{a_3 = \frac{a_0 a_2}{2}}$$

8.1 Least squares curve fitting and error analysis

A least squares curve fitting procedure (similar to that described in Gottfried, 1998) using the algebraic expressions given in chapter 8 was used to optimise the fit to the measured moment and slope data.

In the curve fitting procedure both the r-squared value (r^2) and the sums of the squares of the errors (SSE) and the coefficient of variation (COV) are provided. The r^2 value always remains between 0 and 1 and assessing the quality of the fit over such a small range can be difficult. A better prediction can be made from the SSE since in gives a much greater variation than r^2 values.

In the case of the pile slope, θ for example; $r^2 = 1 - (SSE/SST)$ where $SSE = \Sigma[\theta_i - f(x_i)]^2$ and $SST = \Sigma[\theta_i - \theta_{mean})]^2$. SST represents the sum of the squares of the deviations about the mean value, θ_{mean}. The coefficient of variation $COV = SD/\theta_{mean}$ where SD represents the standard deviation of the data.

Table 8-1 illustrate the typical least squares calculations involved in fitting the bending moment profiles and Table 8-2 presents the same for the measured slopes. The column headed W-SSE represents an alternative curve fitting option than maximising r^2. This procedure involved weighting the sum of the squares of the errors (SSE) terms in accordance with the perceived importance of the measured data points. The sum of this column can then be minimised to give the best fit to the data. In general maximising the r^2 value provided the best overall fit to the data.

Depth from pit	Mfit	M meas	Weight	SD	COV	W-SSE	SSE	SST	r2=1-[SSE/SST]
0	-30.08	-30.08	1	7.1876	-0.2942	0	0	31.866	
0.125	-35.67183	-39	100000			1E+06	11.077	212.14	
1.125	-58.43506	-56	100000			592954	5.9295	996.35	
2.125	-39.46049	-40	100000			29107	0.2911	242.27	
2.625	-27.15831	-28.6	100000			207846	2.0785	17.347	
3.625	-9.231222	-8	40			60.636	1.5159	270.11	
5.125	2.1096701	2.2	30			0.2448	0.0082	709.42	
6.625	4.257746	4	30			1.993	0.0664	808.55	
		-24.435				**2E+06**	**20.966**	**3288.1**	**0.993623491**

Table 8-1: Typical calculation for optimisation bending moment fit at 47kN for pile L1 (CLT1)

Depth from pit	θ fit	θ meas	Weight	SD	COV	W-SSE	SSE	SST	r2=1-[SSE/SST]
0	0.0080	0.0080	1	0.0012	0.2535	0	0	1.12E-05	
0.768	0.0080	0.0076	5000			0.0005	1.08E-07	8.91E-06	
1.29	0.0060	0.0062	100000			0.0069	6.89E-08	2.45E-06	
1.79	0.0035	0.0036	10000			0.0001	9.22E-09	1.01E-06	
2.17	0.0021	0.0016	60000			0.0168	2.79E-07	9.34E-06	
3.29	0.0003	0.0008	40			0.0000	2.12E-07	1.47E-05	
		0.0046				**0.0243**	**6.78E-07**	**4.77E-05**	**0.9858**

Table 8-2: Typical calculation for optimisation slope fit at 47kN for pile L1 (CLT1)

Appendix 8c

Test Results

APPENDIX 8c: TEST RESULTS

PILE L1, CLT1 - 55.5kN LOAD INCREMENT

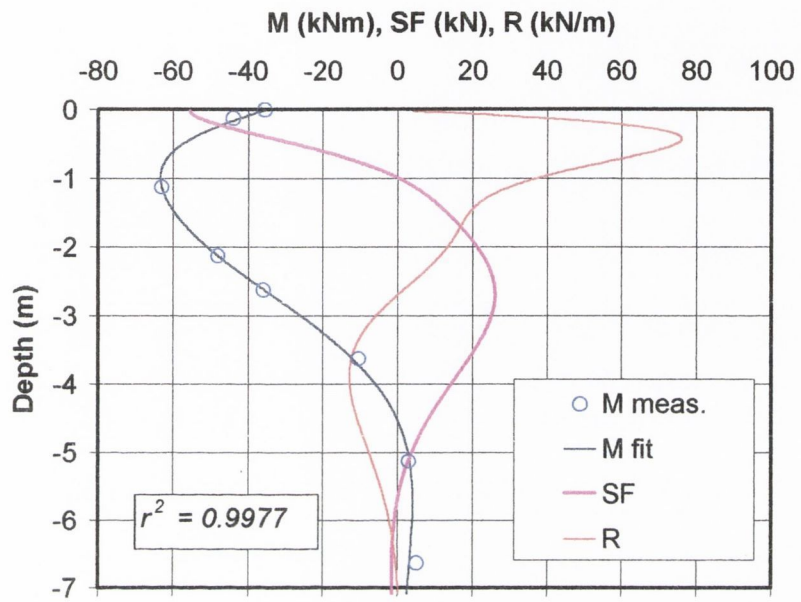

PILE L1, CLT1 - 47kN LOAD INCREMENT

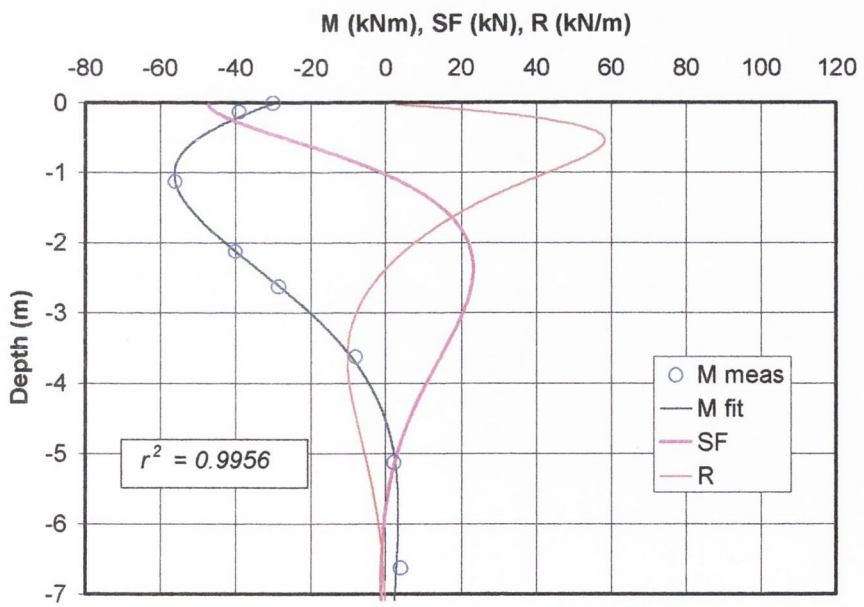

PILE L1, CLT1 - 38.5kN LOAD INCREMENT

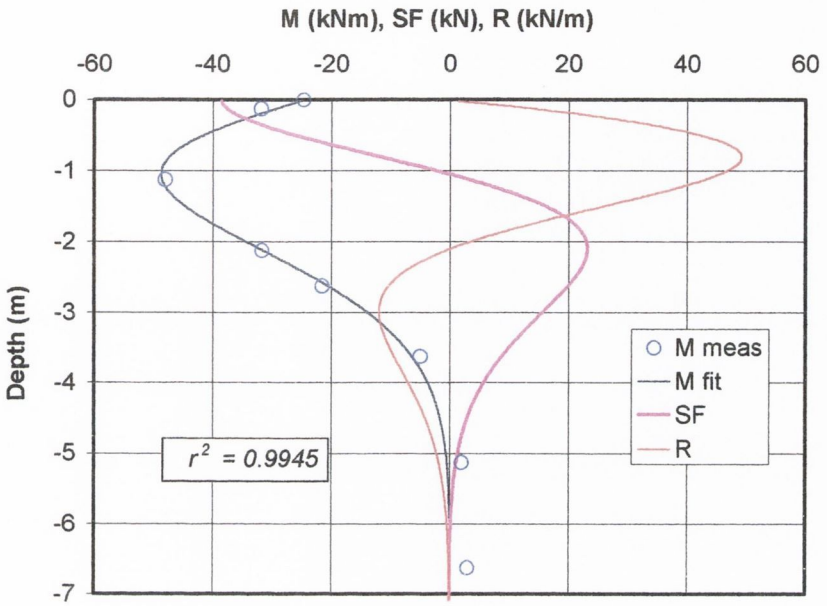

PILE L1, CLT1 - LOAD INCREMENT 25.75kN

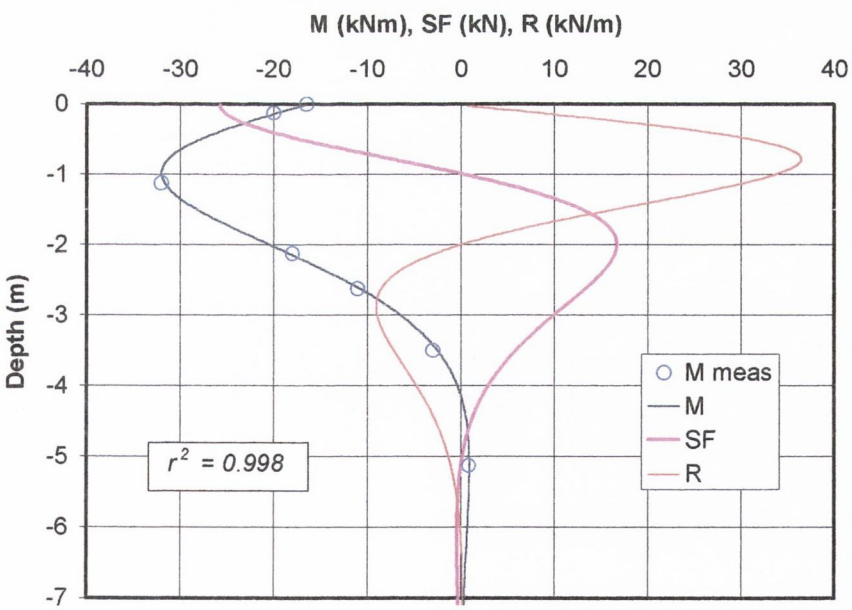

PILE AL1, CLT1 - LOAD INCREMENT 25.75 kN

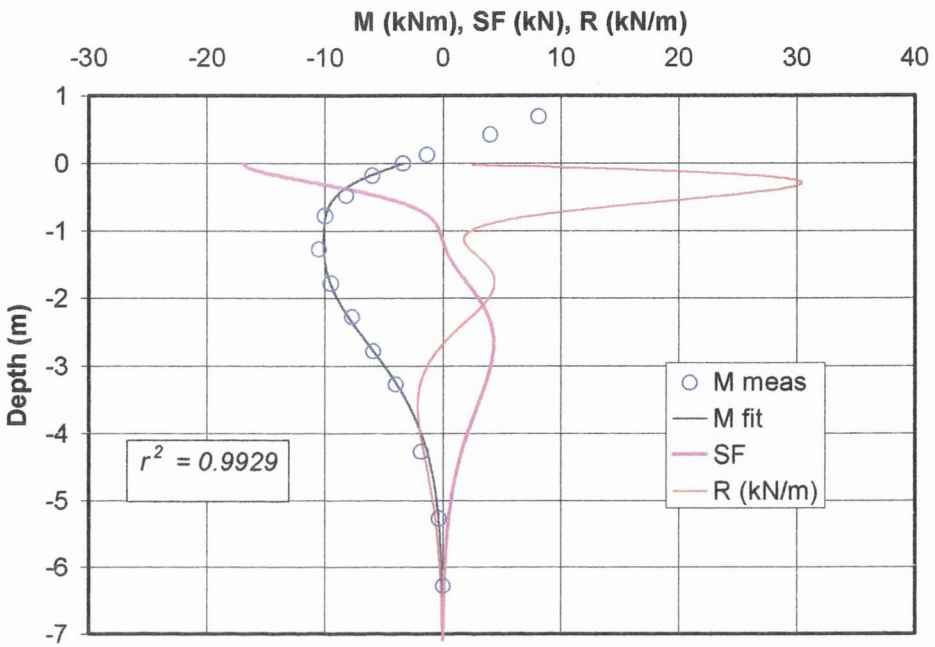

PILE AL1, CLT1 - LOAD INCREMENT 38.5kN

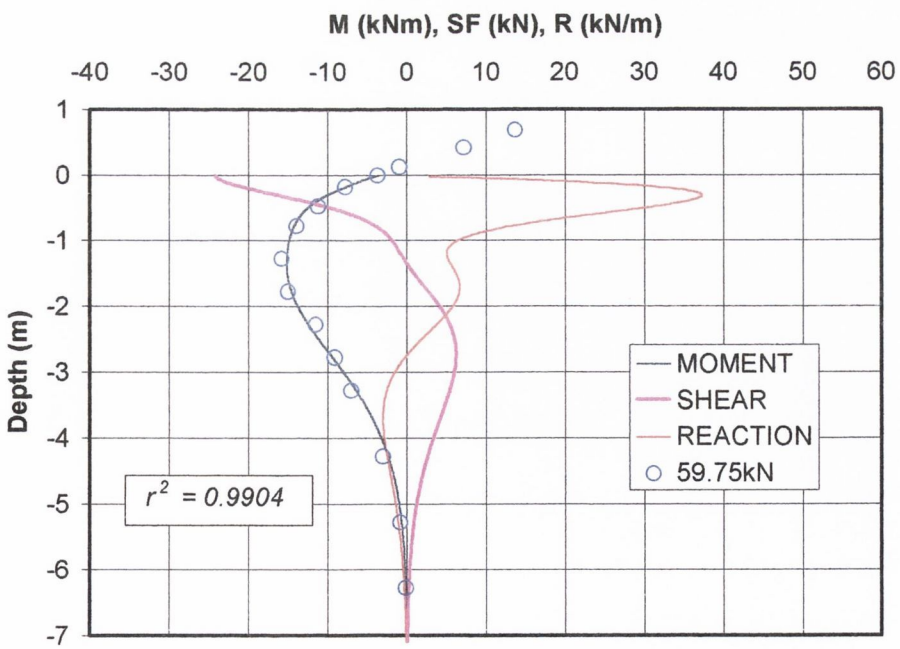

PILE AL1, CLT1 - LOAD INCREMENT 47kN

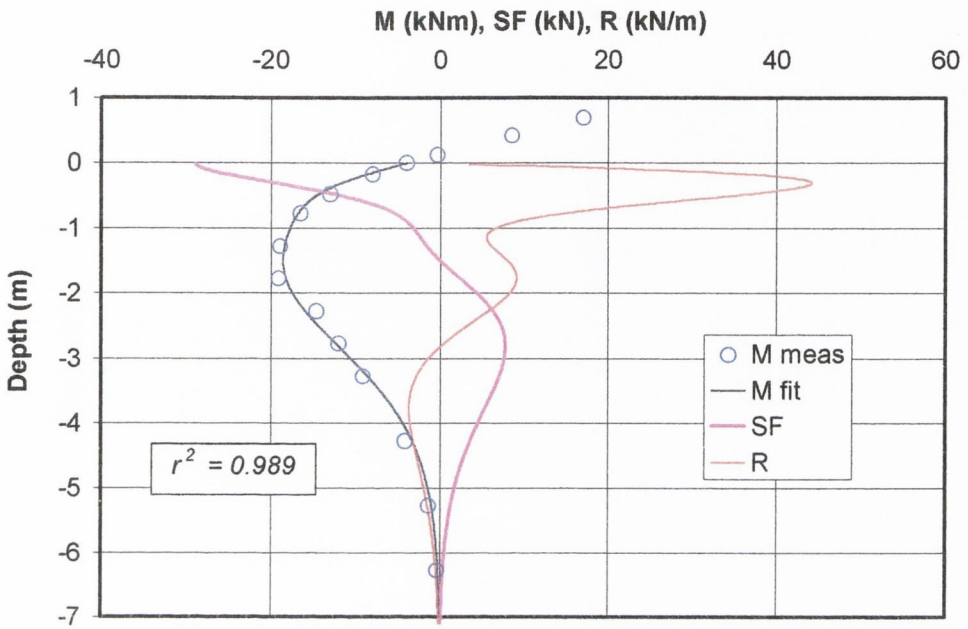

PILE AL1, CLT1 - LOAD INCREMENT 55.5kN

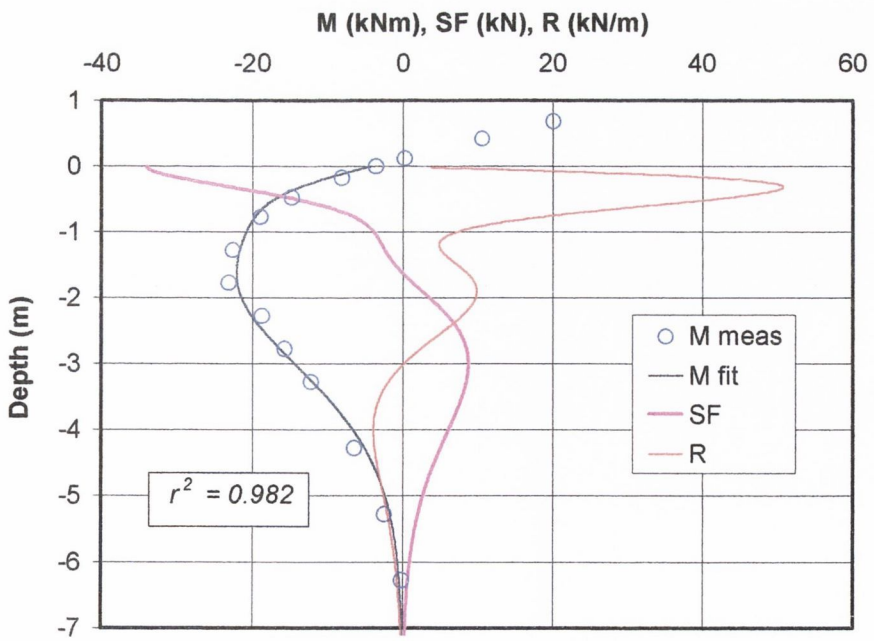

PILE L1, CLT2 - LOAD INCREMENT 85.5 kN

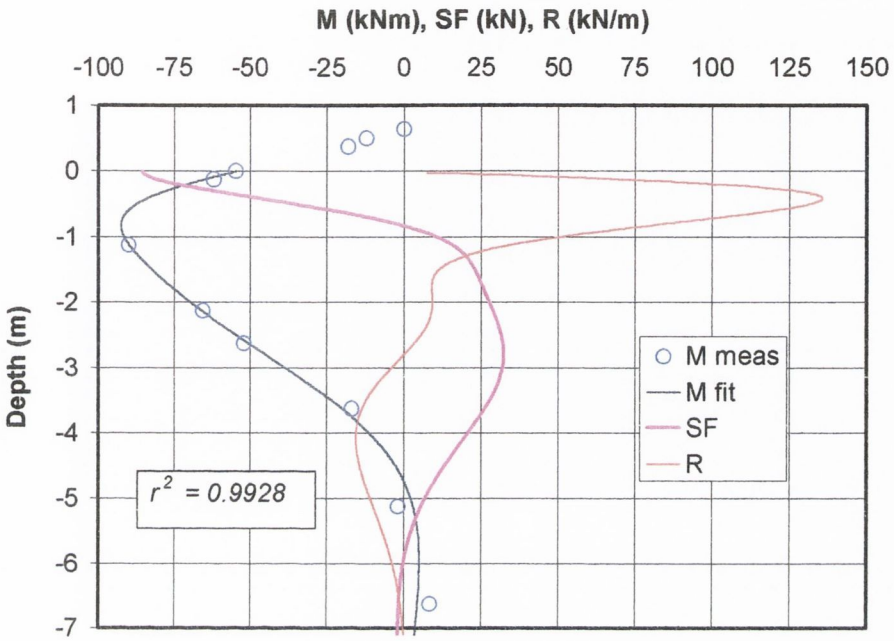

PILE L1, CLT2 - LOAD INCREMENT 76.75kN

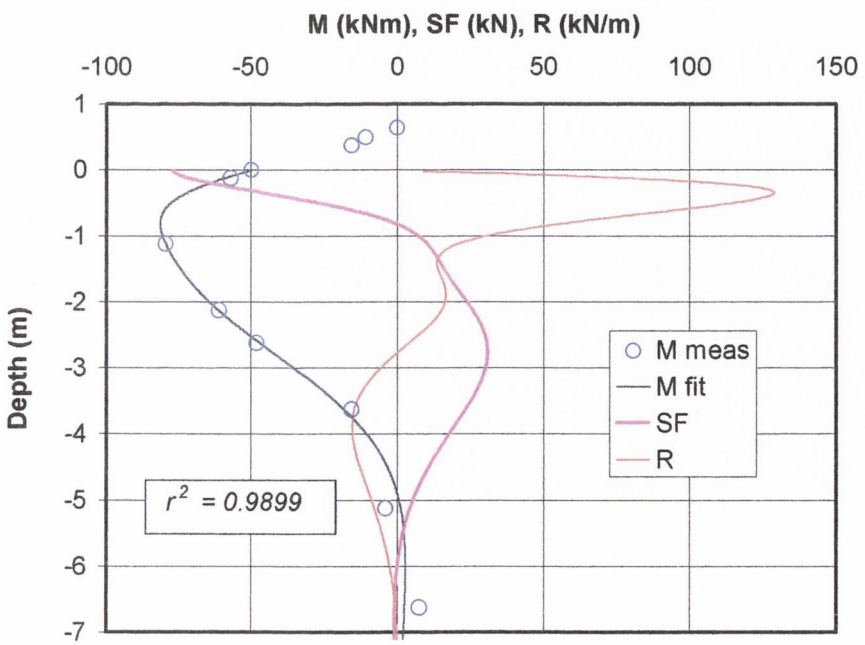

PILE L1, CLT2 - LOAD INCREMENT 68.25kN

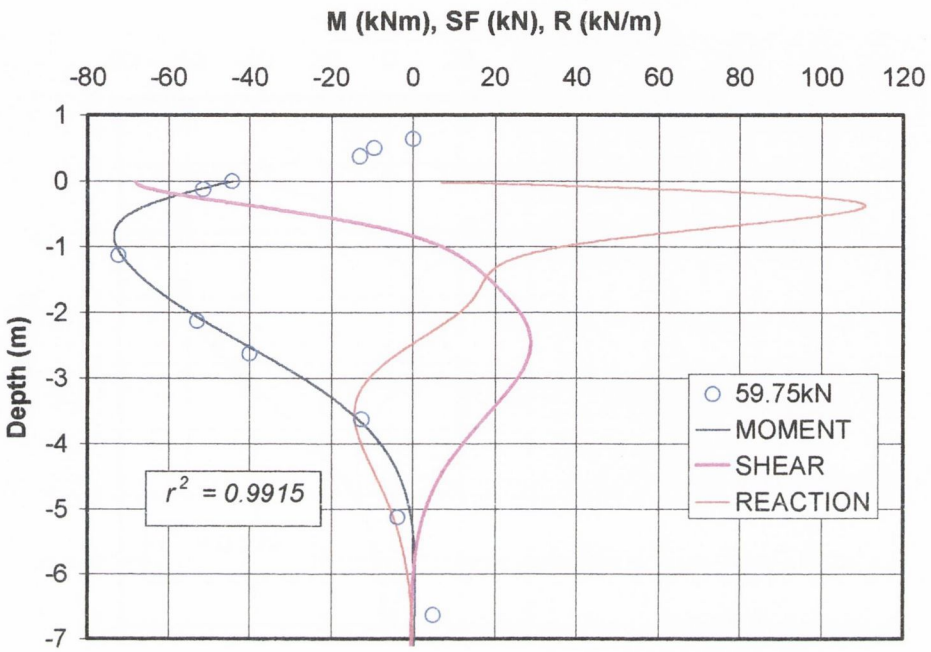

PILE AL1, CLT2 - LOAD INCREMENT 68.25kN

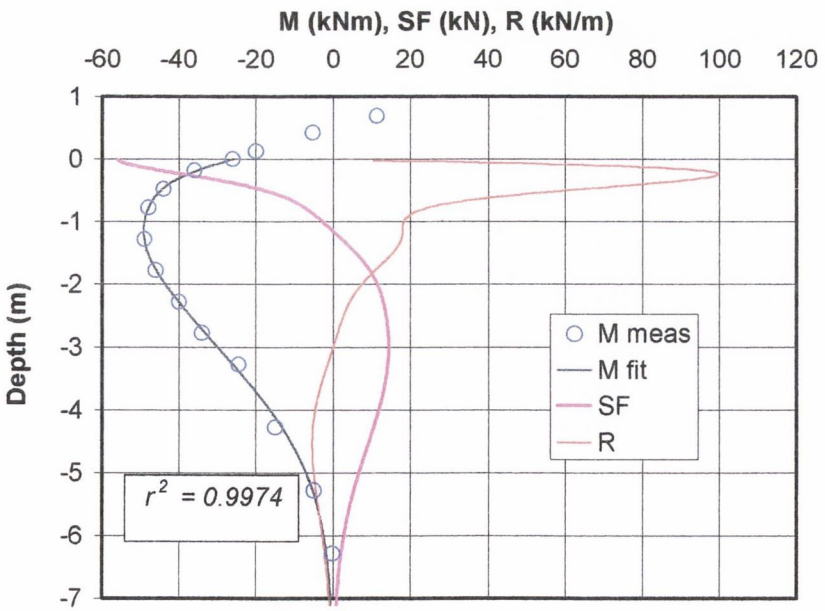

PILE AL1, CLT2 - LOAD INCREMENT 76.75kN

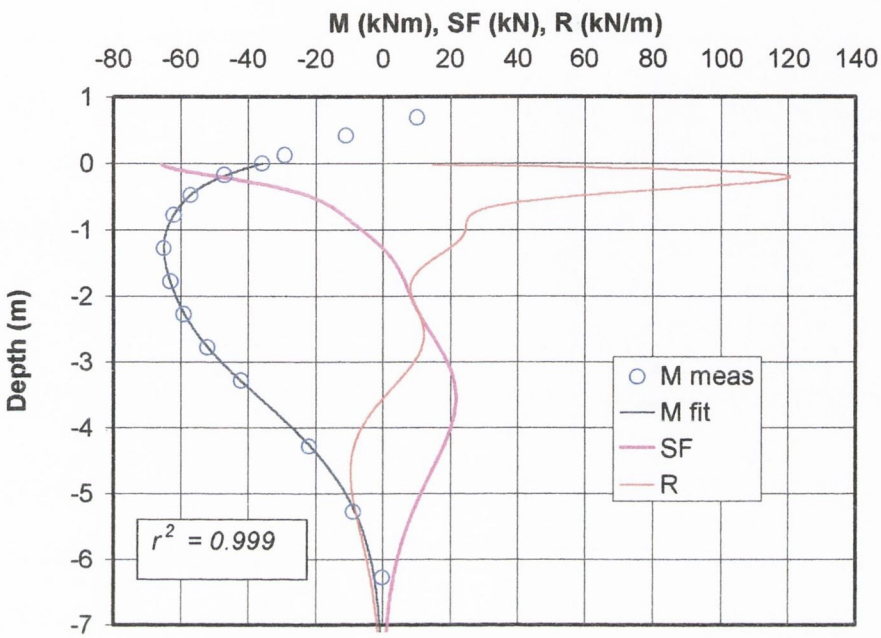

Appendix 9

Interpretation of Instrumentation Data

APPENDIX 9

Interpretation of Instrumentation Data

The success of the electro-levels (EL) in accurately predicting the pile displacement profiles must be gauged against difficulties encountered determining bending moment distributions from EL data at low stress levels. To assist in the interpretation of the EL data, the ELs were energised two and a half hours before the first combined load test (CLT1) commenced, this permitted the effect of temperature and/or drift in the instruments to be assessed. A small but constant increase in the output of the ELs was measured during this period; a correction for this drift was applied when deriving the slope profile for each load increment during the load tests. Comparing the EL moment profiles with the strain gauge moment profiles at the same load increments indicated the EL predictions only fell within an order of magnitude of the strain gauge profiles. This was particularly the case at the lower load increments (during CLT1) where the exact value of the flexural rigidity of the pile is difficult to establish accurately once the cracking moment of the pile was exceeded. The agreement between the moment profiles improved significantly at the higher load levels (>59.75kN) during CLT2 and suggests that the resolution of the slopes at low load increments may have been insufficient to permit the bending moments to be derived accurately. The predicted moment profiles established from the re-test EL data were considerably more realistic given that the flexural rigidity of the piles remained approximately constant (and close to their fully cracked value) following the large strains induced at the end of CLT2.

The pile stiffness is not the only factor influencing the accuracy of the EL bending moment profiles. Price and Wardle (1987a) found that the sensitivity of curves fitted[1] to known slopes depended on the accuracy of the input data and the number of points considered in the analysis. By fitting a curve to a series of slopes, calculated using elastic beam theory along a propped cantilever, Price and Wardle (1987a) concluded that a minimum of eight slopes at resolutions of one second of arc were required to give good overall agreement with theoretical predictions for the beam bending moment, shear and reaction profiles. In

[1] The curve fitting procedure employed by Price et al. (1985) was similar to the method employed in this thesis.

the pile load tests conducted for this thesis, the ELs were operating at a resolution of ten seconds of arc and only six ELs were incorporated in pile AL1 and five ELs in the case of pile L1. These factors in addition to the inherent errors associated with the differentiation of slope equation may explain the over prediction in bending moment during the initial tests. The pile displacement profiles determined by integrating the best fit curves to the measured slopes was considerably more successful and provided displacement profiles that were in good agreement with the measured displacements at the pile head. The success of this procedure is attributed to 'smoothening' associated with the integration of the slope profiles.

It is therefore concluded that ELs if employed in the correct quantity and set to a high resolution may provide a cheap and efficient means of monitoring and obtaining design data for laterally loaded piles. The fact that the instruments are inserted after the piles have been installed eliminates one of the major risks associated with pile instrumentation. Furthermore, the removal and re-use of the ELs on subsequent tests is likely to find favour with test engineers and piling contractors. If the ELs are employed with piles having well defined physical properties e.g. steel pipe piles, the difficulties encountered in estimating the flexural rigidity (as in the case of reinforced concrete piles) is eliminated and thus adds to the attractiveness of EL instrumented piles.

The interpretation of strain gauge data from reinforced concrete piles requires the establishment of an accurate moment-strain (or moment-curvature) relationship in order to determine the bending moment distribution within the member. This relationship can be measured directly by incorporating strain gauges at the same level on diametrically opposite reinforcing bars and applying a known bending to the member. The measured relationship can be compared analytically using for example, a FE analysis based on the stress-strain relationships for the structural material. Both techniques were employed for the pile sections employed in the field load tests and the results were in excellent agreement. However, for future strain gauging of reinforced concrete members, the author recommends that strain gauges, located as described above, be extended along the member to facilitate the development of a moment-curvature relationship and in the case of a laterally loaded pile, the pairs of gauges should extend to a depth beyond the critical length of the pile.